



Terms and Conditions of Use of Digitised Theses from Trinity College Library Dublin

Copyright statement

All material supplied by Trinity College Library is protected by copyright (under the Copyright and Related Rights Act, 2000 as amended) and other relevant Intellectual Property Rights. By accessing and using a Digitised Thesis from Trinity College Library you acknowledge that all Intellectual Property Rights in any Works supplied are the sole and exclusive property of the copyright and/or other IPR holder. Specific copyright holders may not be explicitly identified. Use of materials from other sources within a thesis should not be construed as a claim over them.

A non-exclusive, non-transferable licence is hereby granted to those using or reproducing, in whole or in part, the material for valid purposes, providing the copyright owners are acknowledged using the normal conventions. Where specific permission to use material is required, this is identified and such permission must be sought from the copyright holder or agency cited.

Liability statement

By using a Digitised Thesis, I accept that Trinity College Dublin bears no legal responsibility for the accuracy, legality or comprehensiveness of materials contained within the thesis, and that Trinity College Dublin accepts no liability for indirect, consequential, or incidental, damages or losses arising from use of the thesis for whatever reason. Information located in a thesis may be subject to specific use constraints, details of which may not be explicitly described. It is the responsibility of potential and actual users to be aware of such constraints and to abide by them. By making use of material from a digitised thesis, you accept these copyright and disclaimer provisions. Where it is brought to the attention of Trinity College Library that there may be a breach of copyright or other restraint, it is the policy to withdraw or take down access to a thesis while the issue is being resolved.

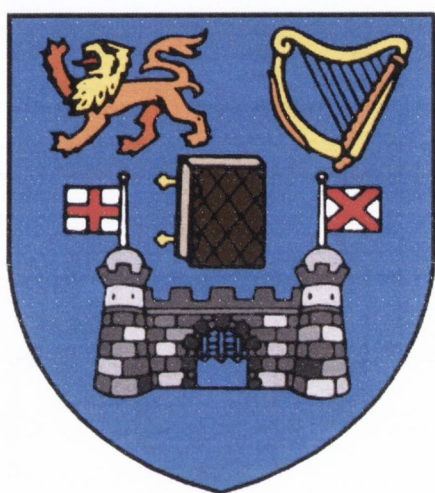
Access Agreement

By using a Digitised Thesis from Trinity College Library you are bound by the following Terms & Conditions. Please read them carefully.

I have read and I understand the following statement: All material supplied via a Digitised Thesis from Trinity College Library is protected by copyright and other intellectual property rights, and duplication or sale of all or part of any of a thesis is not permitted, except that material may be duplicated by you for your research use or for educational purposes in electronic or print form providing the copyright owners are acknowledged using the normal conventions. You must obtain permission for any other use. Electronic or print copies may not be offered, whether for sale or otherwise to anyone. This copy has been supplied on the understanding that it is copyright material and that no quotation from the thesis may be published without proper acknowledgement.

Design, Synthesis and Photophysical Evaluation of Novel Luminescent Sensing Devices: From Anion Sensors to Heteroditopic Receptors

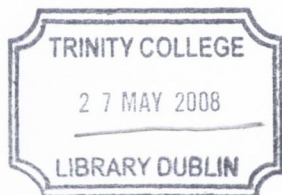
Cidália Maria Gomes dos Santos
October 2007



University of Dublin Trinity College

Based on research carried out under the direction of
Prof. Thorfinnur Gunnlaugsson

*A thesis submitted to the School of Chemistry,
University of Dublin, Trinity College for the degree of
Doctor of Philosophy*



THESIS
8440

Declaration

This thesis is submitted for the degree of Doctor of Philosophy to the University of Dublin, Trinity College, and has not been previously submitted for any degree or examination to this, or any other University. Except where acknowledged, all work described herein is original and has been carried out by the author. Permission is granted so that the Library may lend or copy this thesis upon request. This permission covers only single copies made for study purposes, subject to normal conditions of acknowledgement.

Cidália Maria Gomes dos Santos

Cidália Maria Gomes dos Santos

Acknowledgements

First of all I would like to thank Prof. Thorfinnur Gunnlaugsson for giving me the opportunity to undertake this project. I am grateful for his guidance and encouragement during the course of this research. Not less important was his support and friendship during the long years that I have known him.

I would also like to thank the entire group, Andrew, Ann-Marie, Célia, Celine, Christophe, Claire, Danny, Debbie, Doireann, Emma, Eoin, Flo, Fred, Gary, Jennifer, Jilly, Joe, Julie, Julien, Katell, Lin, Lisa, Niamh, Raman, Rebecca, Sally and Susan for all their support, friendship, and helpful discussions. Thank you “guys”.

I would also like to thank all the staff in the Chemistry department, including Dr. John O’Brien and Dr. Manuel Ruether for all their help with the countless NMRs. Thanks to Dr. Martin Feeney and Dr. Dilip Rai (UCD) for all the assistance with the mass spectrometry. Thanks to the School technical staff Fred, Ed, Patsy, Brendan, Mark, Peggy and Theresa for all their help. And thank you to the secretaries Corrine, Tess, Helen and Maria. I am very grateful to Dr. Tom McCabe for the crystal structures.

To Leonor, her husband António and all my family and friends in general, I thank the everyday encouragement, support and all the “prayers” and thoughts.

To António Sousa and Maria Helena Sousa, a big thank you for welcoming me to their lives with an open heart, by helping me with their valuable advice and friendship.

I am forever grateful to my mother, Lídia Gomes, and my late father Diamantino Santos, for everything including their love and support. I am sure that without both of you I would be somewhat lost. O meu coração está cheio de saudade, mas a certeza do vosso amor dá-me força para ultrapassar os diversos obstáculos da vida. Amo-vos.

Finally, to my other half, my wonderful husband Carlos Sousa for his incentive, dedication and so many other things. His patience and constant encouragement gave me the strength to overcome the everyday problems throughout this long journey. To him I owe so many things, and to him I dedicate this work.

Chapter 4 deals with the design, synthesis, and characterisation of a urea functionalised *phen* based heteroditopic receptor. This chapter is divided into three parts. In the first part, the ability of such a urea functionalised receptor to work as a selective fluorescent sensor for chloride is demonstrated. Spectrophotometric studies (absorption and fluorescence) showed that, while only minor changes were observed in the ground state upon anion recognition, the fluorescence emission was significantly affected. Nevertheless, only in the presence of chloride was the emission intensity enhanced, while for the other competitive anions the emission was quenched. In the second part of this chapter, we demonstrate the binding of the *phen* based receptor with transition metals such as Cu(II) and Fe(II). Binding studies in solution revealed strong interaction between the metal ions and the *phen* moiety of two receptors, giving rise to the formation of the 1:2 (metal:receptor) stoichiometry. In the solid state, the Cu(II) ion was shown to form a binuclear complex, through interaction of two copper ions with four receptor molecules. Each Cu(II) ion was found to be in a distorted square-pyramidal geometry, coordinated to four nitrogen atoms from the two *phen* receptors and one oxygen atom from the urea moiety of a neighbour receptor. Finally, in the third part of this chapter, the influence of the metal ion on the binding affinity towards anions is examined. The metal was found to induce enhancements in the anion binding affinity, resulting in higher binding constants than those observed for the simple urea based receptor. In addition, a new method for discriminating the nature of the bound anion was devised, as only the addition of phosphates, H_2PO_4^- and $\text{H}_2\text{P}_2\text{O}_7^{2-}$, quenched the emission intensity of both the Cu(II) and the Fe(II) *phen* coordinated complexes.

Chapter 5 examines the formation, characterisation, and photophysical studies of a novel supramolecular self-assembly complex, between Eu(III) and the heteroditopic receptor described in Chapter 4. The lanthanide luminescence of the Eu(III) was 'enhanced in the presence of the *phen* based receptor, demonstrating the sensitisation of the metal ion by this receptor. It is also shown that the presence of the Eu(III) ion induces the formation of a self-assembly complex in a 1:3 (metal:receptor) stoichiometry. Furthermore, the ability of such a self-assembly architecture to signal the presence of anions is demonstrated, as the lanthanide luminescence intensity of this system was observed to change drastically in the presence of anions.

Chapter 6, the final chapter, outlines the experimental procedures for the synthesis and evaluation of the compounds discussed in Chapters 2, 3, 4, and 5.

Abstract

This thesis entitled “*Design, Synthesis and Photophysical Evaluation of Novel Luminescent Sensing Devices: From Anion Sensors to Heteroditopic Receptors*” is divided into six chapters. Chapter 1, the introduction, is divided into two parts. The first part provides an insight into the field of anion recognition based on the use of optical chemosensors, followed by a brief overview of the fluorescent based sensors that have been developed in the past. The principles and advantages of lanthanide luminescent sensing are illustrated and a review of lanthanide complexes used in anion sensing is presented. The second part of this chapter highlights the recognition of both cations and anions by using heteroditopic receptors. A review on the advances of synthetic heteroditopic receptors reported in the literature is presented. Their mode of action, as well as their relevance on the detection and extraction of toxic ions from aqueous environments, and their use as artificial carriers and channels for the transport of inorganic and organic salts across membranes is also described.

Chapter 2 details the synthesis and characterisation of a novel cyclen based lanthanide luminescent sensor, designed for the recognition of anions by incorporating hydrogen bonding receptor moieties into a covalently attached antenna. The synthesis of cyclen based Tb(III) and Eu(III) diaryl-urea complexes and their photophysical properties is described. Analysis of the ground state, the emission from the singlet and the Tb(III) excited states, clearly shows the ability of the Tb(III) complex to signal the presence of anions in solution, through multiple binding interactions. The long-lived lanthanide luminescence from the Tb(III) diaryl-urea complex was significantly enhanced only upon recognition of H_2PO_4^- . Furthermore, this complex displays good selectivity for H_2PO_4^- over other competitive anions such as CH_3COO^- .

Chapter 3 describes the synthesis and characterisation of three new and structurally simple anion receptors, based on the use of combined aryl amide and urea moieties as hydrogen bonding sites. These receptors differ only in the relative position of the amide moiety to that of the urea functionality. Such a difference was observed to play a major role in the ability of these receptors to form large solid state networks through the formation of either intra or intermolecular hydrogen bonding interactions. Furthermore, all three receptors revealed different binding interactions with the various anions studied, which demonstrates that by changing the position of the amide moiety on the aromatic ring, and hence by introducing small changes to the structure of the receptor, different binding interactions and binding affinities can be induced.

Abbreviations

Å	ångström (1×10^{-10} m)
Abs	absorbance
bipy	bipyridine
br	broad (NMR)
CDCl ₃	deuterated chloroform
CD ₃ CN	deuterated acetonitrile
CD ₃ OD	deuterated methanol
CHCl ₃	chloroform
CH ₂ Cl ₂	dichloromethane
CH ₃ CN	acetonitrile
Cyclen	1,4,7,10-tetraazacyclododecane
δ	chemical shift
d	doublet (NMR)
DCM	dichloromethane
DMSO	dimethyl sulfoxide
DO3A	1,4,7,10-tetraazacyclododecane-1,4,7-triacetic acid
eq	equivalents
ES-MS	electrospray mass spectrometry
eT	electron transfer
ET	energy transfer
EtOH	ethanol
G	unspecified guest
H	unspecified host
HCl	hydrochloric acid
HOMO	highest occupied molecular orbital
HPLC	high performance liquid chromatography
ICT	internal charge transfer
IR	infra red
ISC	inter system crossing
<i>J</i>	coupling constant
<i>K</i>	apparent stability constant
L	unspecified ligand

Lit.	literature
Ln	lanthanide
Ln*	lanthanide excited state
log	logarithm (base 10)
LUMO	lowest unoccupied molecular orbital
m	multiplet (NMR)
mL	millilitre
m.p.	melting point
M ⁿ⁺	unspecified metal ion
m/z	mass to charge ratio
MeCN	acetonitrile
MeOH	methanol
MLCT	metal to ligand charge transfer
MRI	magnetic resonance imaging
nm	nanometer
ns	nanosecond
NEt ₃	triethylamine
NMR	nuclear magnetic resonance
PET	photo induced electron transfer
pH	$-\log[\text{H}_3\text{O}^+]$
phen	phenanthroline
ppm	parts per million
S ₀	singlet ground state
S ₁	first excited singlet state
SSD	squared standard deviation
T ₁	lowest energy triplet state
TBA ⁺	tetrabutylammonium cation
terpy	terpyridine
THF	tetrahydrofuran
Trif	triflate (trifluoromethanesulfonate)
UV-vis	ultraviolet-visible (spectroscopy)
ε	molar extinction coefficient
λ	wavelength
ν	frequency

μ	micro (1×10^{-6})
μM	micromolar
τ	lifetime

Table of contents

Chapter 1:	Introduction	
1.1	Introduction	1
1.2	Molecular sensors	1
1.3	Anion receptors	2
1.3.1	Nature of anion receptors	4
1.4	Signaling units	5
1.4.1	Fluorescence based signaling	5
1.4.1.1	Fluorescent sensors	6
1.4.2	Lanthanide luminescence based signaling	13
1.4.2.1	Quenching of the lanthanide excited state (Ln(III) [*])	15
1.4.2.2	Lanthanide complexes	17
1.5	Lanthanide complexes as sensing devices	20
1.5.1	Lanthanide complexes as anion sensors	20
1.6	Heteroditopic Receptors	26
1.7	Conclusion	38
Chapter 2:	Cyclen based lanthanide luminescent devices for anion sensing	
2.1	Introduction	39
2.1.1	Lanthanide luminescent sensors	39
2.2	Synthesis and characterisation of ligand 61	42
2.3	Synthesis and characterisation of the lanthanide complexes of 61, Ln.61	45
2.3.1	Determination of metal bound water molecules	48
2.4	Photophysical properties of Tb.61 and Eu.61 complexes	49
2.5	Photophysical studies of Tb.61 towards the binding with anions	51
2.5.1	Photophysical studies of Ln.61 towards binding with CH ₃ COO ⁻	52
2.5.2	Photophysical studies of Tb.61 towards binding with H ₂ PO ₄ ⁻	60
2.5.3	Photophysical studies of Tb.61 towards binding with H ₂ P ₂ O ₇ ²⁻	71
2.5.4	Photophysical studies of Tb.61 towards binding with F ⁻	79
2.5.5	Photophysical studies of Tb.61 towards binding with Cl ⁻	89
2.6	Selectivity of Tb.61 towards H ₂ PO ₄ ⁻ over CH ₃ COO ⁻	91
2.7	Conclusions	92
Chapter 3:	Simple urea-amide receptors for anion recognition	
3.1	Introduction	94
3.2	Synthesis of receptors 71, 72 and 73	95

3.3	Characterization of receptors 71, 72, and 73	97
3.4	Crystal structure analysis of receptors 71, 72, and 73	100
3.5	Absorption properties of receptors 71-73	105
3.6	Absorption studies upon addition of anions	106
3.6.1	Absorption studies performed on 71	107
3.6.2	Absorption studies performed on 72	111
3.6.3	Absorption studies performed on 73	118
3.7	Conclusions	122

Chapter 4: Sensing based on a fluorescent heteroditopic receptor

4.1	Introduction	124
4.2	Design and synthesis of heteroditopic receptor 87	126
4.2.1	Synthesis and characterisation of 87	126
4.3	Photophysical properties of receptor 87	131
4.4	Photophysical studies of 87 with anions	131
4.5	Photophysical studies of 87 with Cu(II) and Fe(II)	143
4.5.1	Binding studies carried out on Cu(II)	144
4.5.2	Binding studies carried out on Fe(II)	152
4.6	Photophysical studies on the metal complexes towards binding with anions	156
4.6.1	Ground state investigations	157
4.6.1.1	Interaction of Fe:87 ₂ with anions	157
4.6.1.2	Interaction of Cu:87 ₂ with anions	160
4.6.2	Excited state investigations	161
4.7	Conclusions	166

Chapter 5: Anion sensing using a Eu(III) induced supramolecular self-assembly architecture

5.1	Introduction	168
5.2	Design of a Eu(III) self-assembly system	168
5.3	Synthesis and characterisation of the europium complex, Eu:87 ₃	171
5.4	Determination of bound water molecules of the lanthanide complex, Eu:87 ₃	173
5.5	Job's Method for stoichiometry determination	174
5.6	Photophysical studies of receptor 87 with Eu(III)	175
5.6.1	UV-Visible absorption studies	175
5.6.2	Fluorescence studies	177
5.6.3	Lanthanide luminescence studies	178
5.6.4	Stability constants, log <i>K</i> , for the formation of Eu:87 ₃	179
5.7	Anion sensing by Eu:87 ₃	180
5.7.1	Photophysical studies of Eu:87 ₃ complex towards binding with anions	182
5.7.2	Changes in the absorption spectra of Eu:87 ₃ upon anion	183

	recognition	
5.7.3	Changes in the fluorescence emission spectra of Eu:87 ₃ upon anion recognition	192
5.7.4	Changes in the lanthanide luminescence of Eu:87 ₃ upon anion recognition	200
5.8	Conclusions	210

Chapter 6: Experimental procedures

6.1	General experimental details	214
6.2	Ultraviolet-Visible and Luminescence spectroscopy	215
6.3	Lifetime measurements for Tb(III) and Eu(III) complexes	218
6.4	Experimental details for Chapter 2	219
6.5	Experimental details for Chapter 3	223
6.5.1	Procedure 1: General experimental procedure for compounds 77, 78, and 79	223
6.5.2	Procedure 2: General experimental procedure for compounds 80, 81, and 82	224
6.5.3	Procedure 3: General experimental procedure for compounds 71, 72, and 73	226
6.6	Synthetic procedures for Chapter 4 and Chapter 5	228

General Conclusion

	General Conclusion	230
--	--------------------	-----

References

	References	232
--	------------	-----

Appendix

Appendix 0	Binding Constants (log <i>K</i>) determination	241
Appendix 1	Crystallographic data	243
A1 1	Crystallographic data for 71	243
A1.1.1	CIF file for 71	244
A1 2	Crystallographic data for 72.CH ₃ OH	250
A1.2.1	CIF file for 72.CH ₃ OH	251
A1 3	Crystallographic data for 73	258
A1.3.1	CIF file for 73	259
A1 4	Crystallographic data for 87	266
A1.4.1	CIF file for 87	267
A1 5	Crystallographic data for (Cu ₂ :87 ₄). (ClO ₄) ₄ . (CH ₃ CN) ₂	274
A1.5.1	CIF file for (Cu ₂ :87 ₄). (ClO ₄) ₄ . (CH ₃ CN) ₂	275
Appendix 2	UV-Vis titration and speciation data for Chapter 3	288
Appendix 3	Absorption, fluorescence, and speciation data for Chapter 4	305

A3.1	Titration of 87 with anions	305
A3.2	Speciation diagrams for the titration of 87 with Cu(II)	307
A3.3	Titration of Fe:87 ₂ with anions	308
A3.3.1	Absorption titrations of Fe:87 ₂ with anions	308
A3.3.2	Fluorescence emission titrations of Fe:87 ₂ with anions	310
A3.4	Titration of Cu:87 ₂ with anions	311
A3.4.1	Absorption titrations of Cu:87 ₂ with anions	311
A3.4.2	Fluorescence emission titrations of Cu:87 ₂ with anions	313

Publications

pH driven self-assembly of a ternary lanthanide luminescence complex: the sensing of anions using a β -diketonate-Eu(III) displacement assay

Chem. Commun., **2007**, 129-131

Selective fluorescent sensing of chloride

Tetrahedron Lett., **2007**, 48, 3135-3139

Lanthanide luminescent anion sensing: evidence of multiple anion recognition through hydrogen bonding and metal ion coordination

Chem. Commun., **2007**, 3389-3391

“When nature finishes to produce its own species, man begins (...) to create an infinity of species.”

Leonardo da Vinci

Chapter 1

Introduction

1.1 Introduction

Supramolecular chemistry has become one of the fastest growing areas of chemistry.¹ A fundamental concept associated with supramolecular chemistry is that of molecular recognition, which has been defined by biologists and chemists as a process involving both binding and selection of guest(s) by a given receptor (host) molecule. Mere binding is not recognition, since it is a specific function belonging to the host-guest complex, one may say that recognition is binding with a purpose. The recognition process must be fast and reversible. Selectivity is ultimately the result of strong binding by species of interest and lesser binding by species of non interest.^{2,3} Supramolecular chemistry in combination with advances in photochemistry are the basis for a novel and powerful area of current research in the field of host-guest interactions, contributing to the progress on the systematic design and synthesis of novel sensing systems.

The following sections of this chapter will be used to discuss and provide detailed examples on the sensing process by means of optical recognition. A major part of this discussion will be focused on the binding of anionic species. This will then be followed by a detailed discussion into the development of lanthanide complexes as sensors. Finally, detailed examples of the simultaneous binding of anions and cations by the use of heteroditopic receptors will be provided.

1.2 Molecular sensors

A sensor is an entity that responds to chemical or physical stimulus by generating a signal measurable by an external operator. Therefore, a chemosensor (chemical sensor) has to be equipped with two basic components: a **receptor** and a **signaling entity**. The receptor must be able to selectively interact and recognise the desired analyte, such as ions and molecules, while the role of the signaling system is to act as a signal transducer. That is, to translate the chemical changes taking place at a molecular level (recognition process) into a visible or measurable output. The output can have different instrumental nature, such as being a shift in a NMR peak, the displacement of a voltammetric wave, a color change associated with the modified absorption spectrum, or a change in luminescent properties. Nevertheless, optical responses such as colorimetric, fluorescent (photoinduced electron transfer, PET) and luminescent (metal centred) are among the most common.⁴⁻⁶ The sensor

can be constructed by combining these two components in different ways, as shown in **Figure 1.2.**⁴

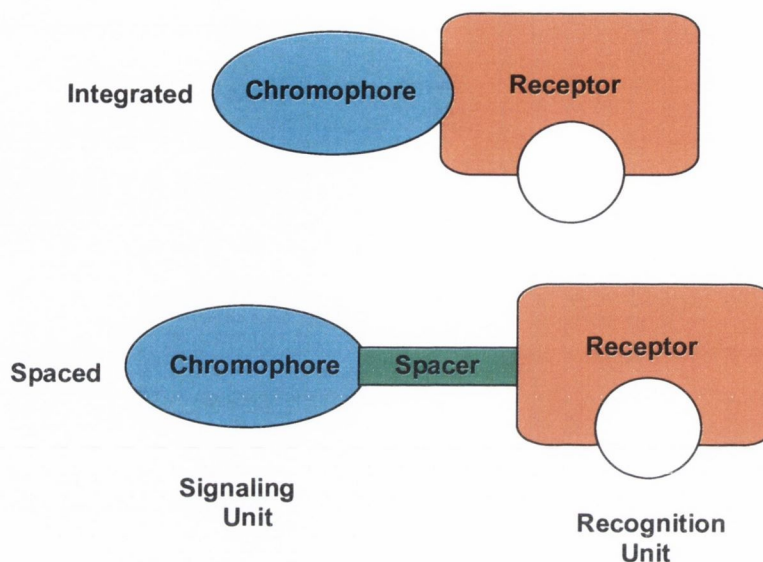


Figure 1.2 Schematic representation of the basic components of a chemosensor.⁴

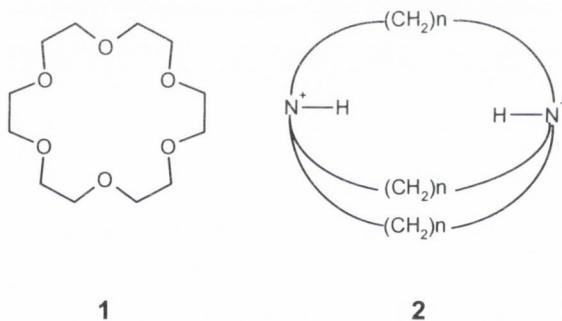
The way in which the receptor (recognition unit) and the chromophore (signaling unit) are connected depends on the photophysical property employed. Sensors where the signaling moiety and the receptor are attached in an integrated manner involve photophysical processes in which an internal charge transfer (ICT) is required in the communication process.⁴ The method of communication between the receptor and the chromophore in spaced systems occurs *via* electron transfer (eT) or energy transfer (ET). In such systems the spacer is used to prevent any π - π or σ - π interactions between the two components.^{7,8}

The following sections will look briefly at the history of anion sensing, and discuss the factors which may affect the development of anion receptors and sensors.

1.3 Anion receptors

Monitoring the concentration of ions and molecules *in vivo* is of critical importance as many of these ions and molecules are involved in crucial biological and chemical processes. Anions, in particular, are essential to life, as many biological processes depend

on the presence or transport of these negatively charged species, or use them to carry out chemical transformations.⁹ They have also become progressively more used in industrial processes as well as in agriculture, which consequently puts them in the class of pollutants.¹⁰ It has thus become evident that there is significant need for the development of synthetic receptors able to report the presence of anions. Nevertheless, sensors for selective detection of anionic species are still relatively rare, when compared to the development of sensors for selective detection of cations.¹¹⁻¹⁵ Interestingly, both receptors for the binding of cations as well as anions were first reported in the same year. In 1967, two papers were submitted for publication by Pedersen and by Park and Simmons, respectively. Pedersen's paper dealt with the synthesis of the first series of crown ethers, including the well known 18-crown-6, **1**, and their ability to bind cations.¹⁶ The manuscript by the other two authors reported the first synthetic receptor, **2**, able to bind halide anions.¹⁷ In this case the halide was held by the array of hydrogen bonds within the bicyclic framework as well as by electrostatic interactions.



Whereas the coordination chemistry of cations has been extensively studied, anion coordination still remains relatively unexplored. In fact, while cation coordination flourished instantaneously after Pedersen's publication, the field of anion binding only started to develop around eight years after the first example provided by Park and Simmons. In 1976 Graf and Lehn reported a protonated cryptand, which demonstrated high binding affinity towards halide ions such as Br⁻ and Cl⁻.¹⁸ Although this ligand was designed to bind alkali (K⁺, Rb⁺, Cs⁺) and ammonium (NH₄⁺) cations,¹⁹ it was observed that the protonated tetraammonium was able to bind halides selectively.¹⁸ Ever since, the

synthesis of anionic receptors has been a tremendous challenge for chemists mainly due to some inherent features of anions, in comparison with other species such as cations.

Anions are larger than their isoelectronic cations, and therefore have a lower charge to radius ratio. This decreases the effectiveness of electrostatic binding.²⁰ Anionic species display a wide range of shapes, sizes and geometries, and therefore a higher degree of receptor design is required for host-guest complementarity.^{9,20}

The halides, F^- , Cl^- , Br^- and I^- are all mono-atomic and spherical. Their lone pair of electrons does not introduce directionality to the system and are thus difficult to exploit when designing receptors. Oxoanions such as phosphates and sulfates display tetrahedral geometries, while carboxylate and nitrate anions are flat trigonal planar in structure. Another feature to have in consideration is that anions are pH sensitive, and so receptors must function within the pH window of the target anion. Also of detrimental importance is the nature of solvent, given that solvent effects play a crucial role in controlling anion binding strength and selectivity. As anions are usually highly solvated, competitive solvents particularly hydroxylic solvents such as water, can effectively compete with the receptor binding sites as they can form strong hydrogen bonds with the anions.^{20,21} Hydrophobicity is yet another factor that can be of significance in anion selectivity. The particular interactions between anions and water were first noticed by Hofmeister more than one century ago, leading to the ordering of anions by their degree of hydrophobicity (degree of aqueous solvation) known as the Hofmeister series. The establishment of this series was achieved through studies on the effect of salts on the solubility of proteins.^{13,22}

1.3.1 Nature of anion receptors

Throughout the literature it can be observed that all the mentioned factors, such as geometry and basicity of the anions as well as the nature of the solvent, have to be taken into account when designing selective anion receptors. There are two main types of anion receptors: positively charged and charge neutral receptors.²³ These receptors usually use different types of non-covalent interactions in order to bind the anionic species. Among the most common type of interactions employed by the receptors are: electrostatic interactions, hydrogen bonding, interactions with metal centers, and a combination of these interactions. In order to be able to exploit such interactions with the negatively charged species

(recognition phenomena), receptor binding sites are usually designed by taking advantage of different groups such as amides²⁴⁻²⁷, urea/thioureas^{25,26,28,29}, pyrroles³⁰, Lewis acids,³¹ guanidinium derivatives,^{32,33} and ammonium centers³⁴.

1.4 Signaling units

The role of the signaling unit is as previously stated to act as a signal transducer. That is, to translate the chemical changes taking place at a molecular level (the anion binding process) into a signal.¹⁴ Optical responses such as colorimetric, fluorescent (photoinduced electron transfer, PET) and luminescent (metal centred) are among the most common. In the following sections the use of fluorescence and luminescence as the signaling mode of the recognition event will be discussed.

1.4.1 Fluorescence based signaling

The general phenomenon of light emission from electronically excited species is known as luminescence. There are two main types of luminescence: fluorescence and phosphorescence. Fluorescence is a radiative process between states of the same multiplicity. It occurs for instance when the molecule emits light as it transits from the singlet excited state (S_1) to its ground state (S_0). During the time that the molecule spends in the excited state, energy is dissipated non-radiatively from the higher vibrational levels to form the lowest vibrational level of S_1 . Nevertheless, fluorescence is not the only way of releasing the energy stored in the excited state (S_1). The molecule may return to the electronic ground state (S_0) with only the release of heat (radiationless relaxation), or the molecule may undergo a change of spin state (intersystem crossing) accessing a lower energy triplet state (T_1). Relaxation from the T_1 state to the S_0 state can also occur with light emission (phosphorescence). The process is illustrated by the simplified Jablonski diagram shown in **Figure 1.4.1**. Phosphorescence is longer-lived than fluorescence, as a direct consequence of the forbidden nature of a transition from a triplet to a singlet state.^{35,36}

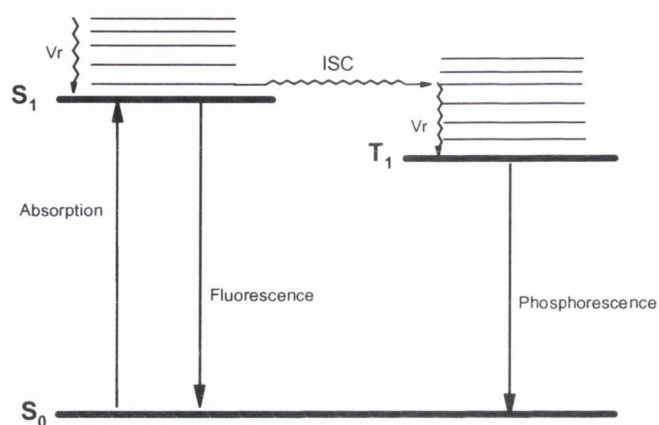


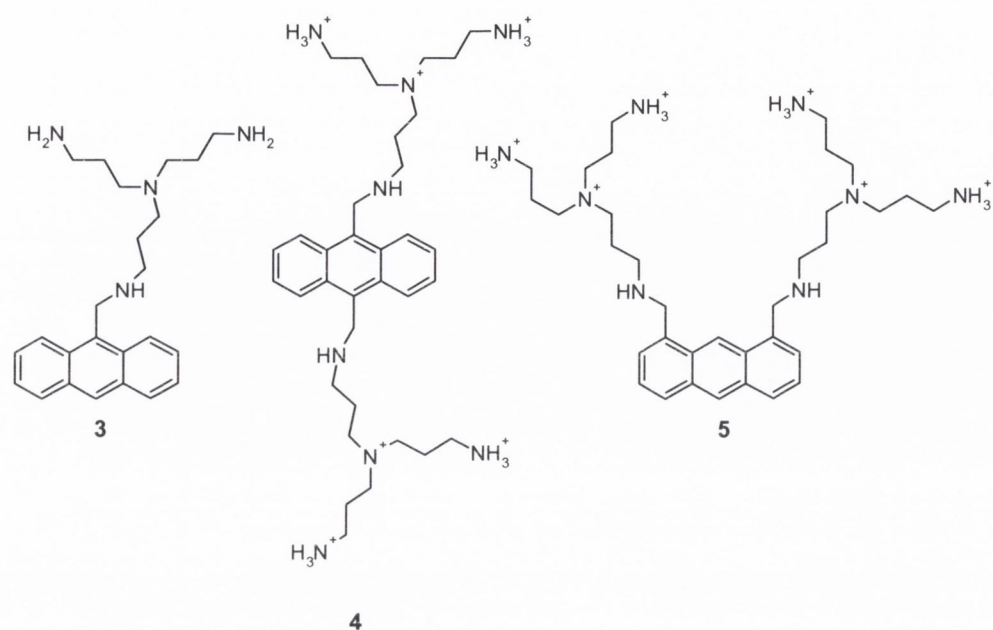
Figure 1.4.1 Simplified Jablonski diagram showing the sequence of events leading to fluorescence and phosphorescence.

Also important are quenching processes. In the presence of an external acceptor, quenching is also able to compete with emission. These processes can be classified into two general pathways: electron transfer and energy transfer. Quenching by electron transfer is a one-electron reaction, in which an electron changes from an occupied orbital of one component to an unoccupied orbital of the other. Quenching by energy transfer can take place by two different mechanisms: the electron-exchange mechanism (Dexter mechanism) and the dipole-dipole mechanism (Förster mechanism).³⁷

1.4.1.1 Fluorescent sensors

Over the years fluorescence has become one of the most used modes of detection, since it offers some advantages including high sensitivity, simplicity, and relatively inexpensive instruments.^{3,7,13,38,39} In particular, photoinduced electron transfer (PET) based fluorescent sensors have been extensively studied and widely used for sensing purposes.^{4,6,21,29}

Czarnik and co-workers developed the anthrylpolyamine conjugates **3**, **4**, and **5** for the recognition of phosphate, citrate and pyrophosphate, respectively.^{3,40,41} It was found that in aqueous solution, at pH 6, all the amine groups in **3** were protonated except the one linked to the anthracenyl fragment.



The binding process taking place between the protonated form of **3** and phosphate is depicted in **Figure 1.4.1.1.1** and **Figure 1.4.1.1.2**. The tetraamine in its protonated form, **6**, displayed only a weak fluorescence (**Figure 1.4.1.1.1**).⁴⁰ In the absence of anions, the system is only weakly fluorescent, as the anthracene fluorescence is switched “off” due to photoinduced electron transfer (PET) from the lone pair of the nitrogen of the benzylic amine to the excited state of the anthracene. Illustration of the PET mechanism is shown in **Figure 1.4.1.1.1**. In the presence of phosphate, the three positive charges on the ammonium ions interact with the three oxygen atoms of the anion leaving the remaining OH group in close proximity to the free amine as shown in structure **7** (**Figure 1.4.1.1.1**). This species (**7**) was expected to show low fluorescence due to quenching by the free amine group.⁴⁰

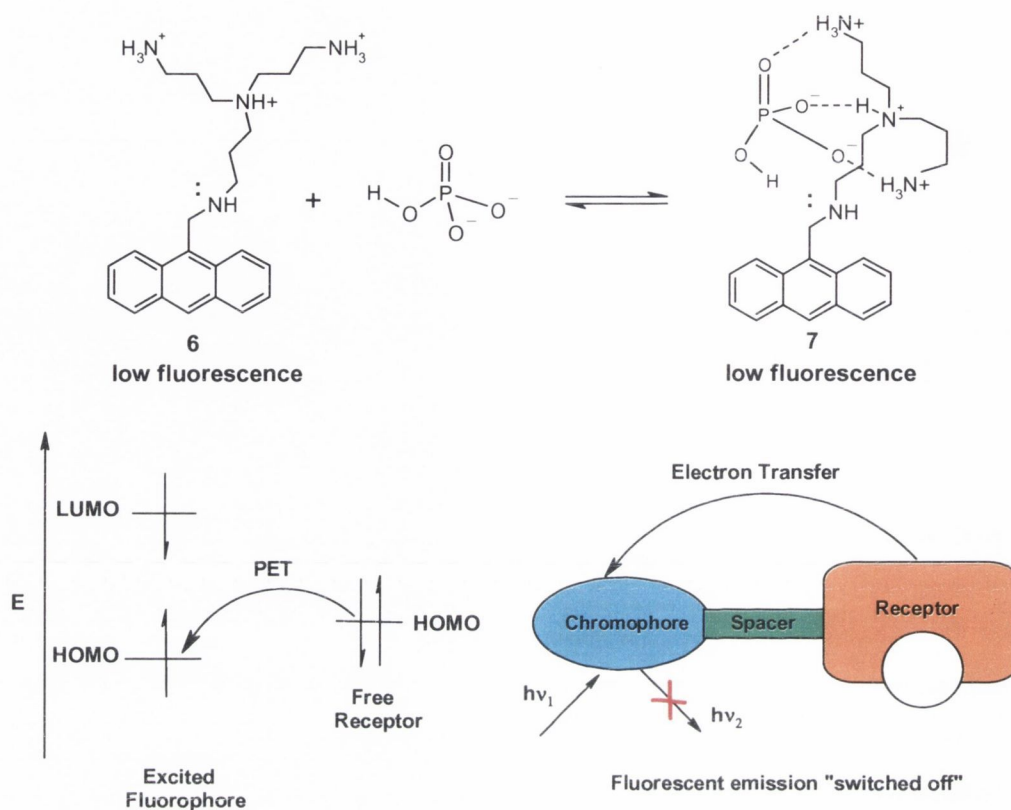


Figure 1.4.1.1.1 Illustration of PET mechanism for **3**. When the receptor is unbound (**6**) or partially bound (**7**) electron transfer from the lone pair of the benzylic nitrogen of the receptor can occur, preventing the deactivation of the fluorophore excited state. Consequently, low fluorescence emission is observed for **6** and **7**.

The close proximity of the OH group to the benzylic amine (**7**) leads to a favourable intracomplex proton transfer to the benzylic nitrogen, giving rise to **8**. This proton transfer suppresses the PET process, and therefore anion binding is accompanied by an increase in the fluorescence emission intensity.⁴⁰ The switching “on” of the fluorescence upon anion binding is illustrated in **Figure 1.4.1.1.2**. Binding of **3** to adenosine triphosphate, citrate, sulphate, and acetate also lead to fluorescence enhancements, although to a smaller degree than those observed for the phosphate. Structural modification of conjugated probes gave rise to even larger fluorescence enhancements for the binding of citrate to the anthrylbispolymine **4**.⁴⁰ Compound **5** was designed to discriminate between phosphate and pyrophosphate ions on the basis of size. It was found that **5** binds pyrophosphate over 2000 times more strongly than phosphate.⁴¹

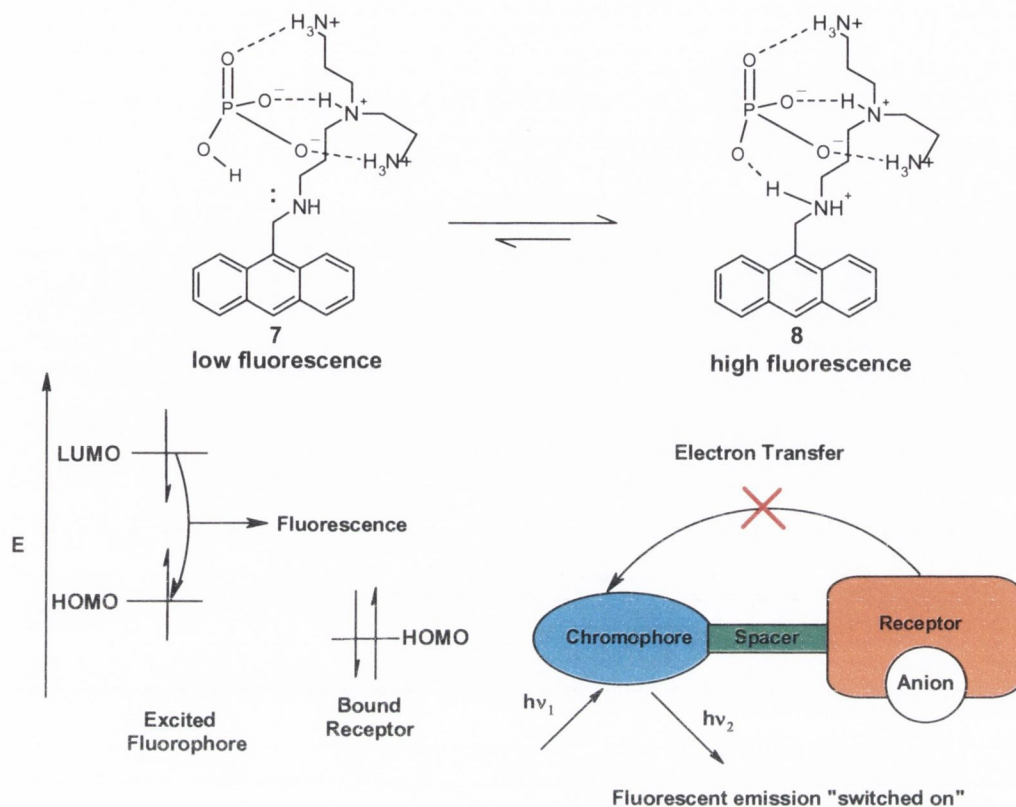
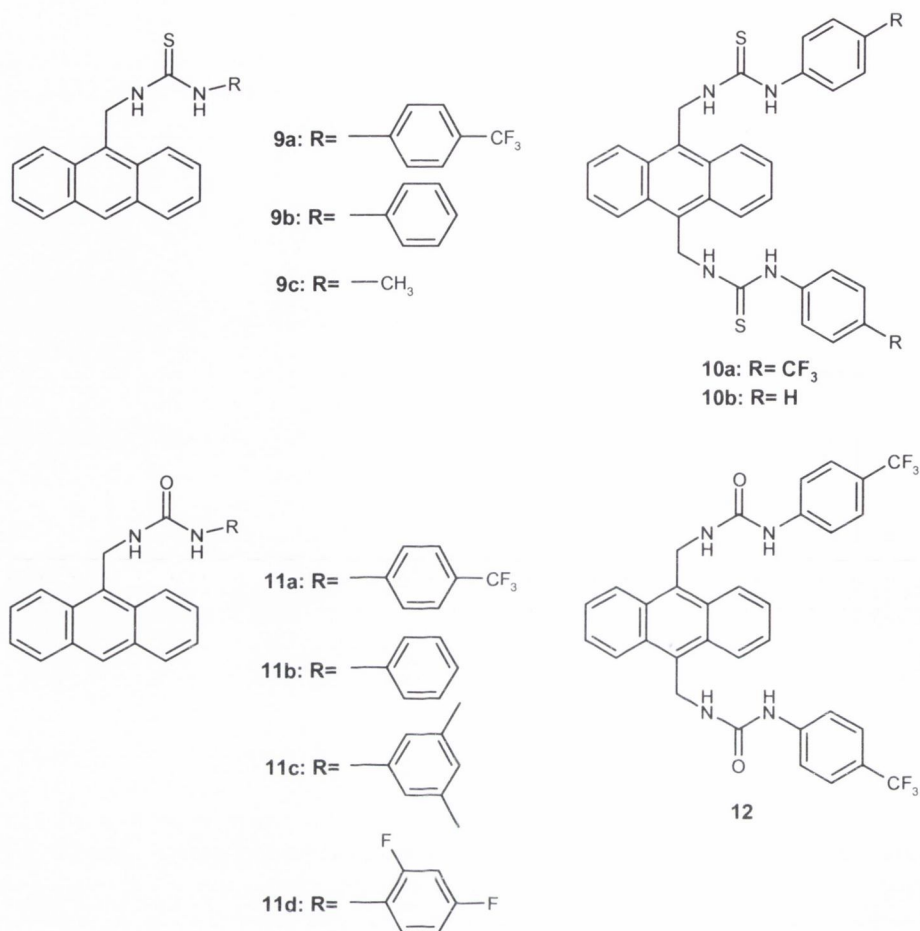


Figure 1.4.1.1.2 Illustration of PET mechanism for **3** upon binding with phosphate. In this case, when the receptor is fully bound to the anion (**8**) the lone pair of the benzylic nitrogen is not available hence the PET quenching mechanism is suppressed. As a consequence the fluorescence is “switched on”.

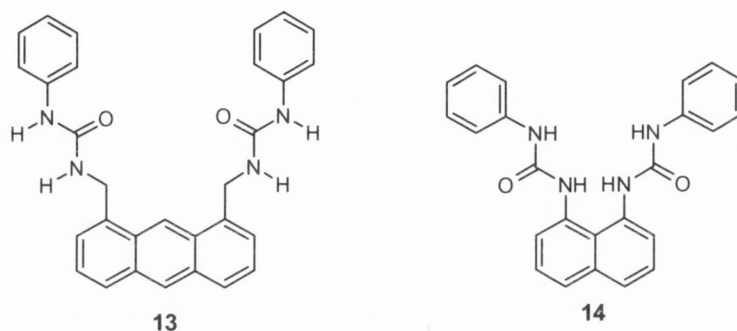
Gunnlaugsson and co-workers have reported several elegant examples, **9-12**, based on urea and thiourea charge-neutral fluorescent sensors. These compounds behave as PET sensors in which the anthracene fluorescence emission was quenched in DMSO in the presence of anions. Chemosensors **9 (a-c)** and **11 (a-d)** contain a thiourea and a urea group, respectively, linked to an anthracene fluorophore *via* a methylene spacer. The recognition process took place through hydrogen bonding interactions between the thiourea/urea NH groups and the anion. The fluorescence emission was quenched in the presence of anions such as F^- , CH_3COO^- , and $H_2PO_4^-$. Furthermore, anions such as Cl^- and Br^- did not induce any changes on the fluorescence spectra.^{21,29,42,43}



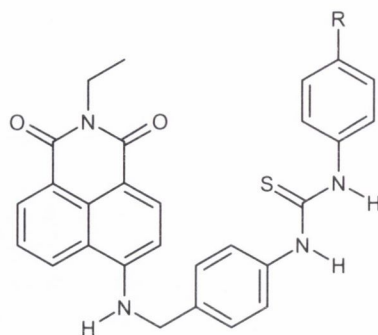
Substitution at the 10-position of anthracene gave rise to the development of the bis-systems **10 (a-b)** and **12**.⁴⁴ These chemosensors were designed for the recognition of bis-carboxylates and pyrophosphate. They showed good affinity for biologically important ions such as glutarate, malonate, and pyrophosphate with 1:1 (host:guest) stoichiometries. The recognition event takes place through the two charge neutral thiourea/urea receptor sites with concomitant PET quenching of the fluorescence emission.⁴⁴ After the pioneering work of Gunnlaugsson, several groups reported the use of simple urea/thiourea based charge-neutral fluorescent sensors for the recognition of anions.

Yoon *et al.* reported a new anthracene derivative bearing two phenylurea groups, **13**. This sensor shows a selective fluorescent quenching effect with F⁻ in acetonitrile-DMSO

(9:1, v/v) via a PET mechanism.^{45,46} The binding selectivity for F^- was found to be almost 120 times higher when compared to Cl^- ions.



Receptor **14** was studied independently by two different research groups. Tarr *et al.* found a fluorescence enhancement upon recognition of F^- in DMSO-acetonitrile (4:6, v/v). In contrast, Cl^- , Br^- , and I^- gave rise to small decreases in the fluorescence emission.⁴⁷ Computer modelling indicated that binding of F^- induced an increase in the planarity of the complex, which might contribute to the fluorescence enhancement. The remaining halides did not induce the same degree of planarity and showed weaker binding constants. Lee *et al.* studied the same receptor **14** in a somewhat different solvent mixture, acetonitrile-DMSO (9:1, v/v).^{48,49} In this medium, additionally to the fluorescence enhancement of the 379 nm band upon addition of F^- a new intense emission band at 445 nm was also observed. This new fluorescence peak was found to be absent upon addition of Cl^- , Br^- , and I^- . Calculations suggested that the new peak was attributed to the increased anionic character of the urea nitrogen due to the strongly charged hydrogen bonding between fluoride and amide protons of the urea moiety. The selectivity towards F^- was attributed to the smaller size of this anion when compared with other halides (Cl^- , Br^- , I^-), which enables fluoride ions to approach the amine protons much closer than other halides.⁴⁹



15 R = H

16 R = CF₃

Recently, Gunlaugsson and co-workers reported two novel fluorescent anion sensors, **15** and **16**, based on the principle of “*chromophore-spacer-receptor*”, as discussed previously (Section 1.2).⁵⁰ These sensors, bearing the ICT (internal charge transfer) naphthalimide chromophore, display a emission band centred at 525 nm in DMSO upon excitation at 444 nm. Upon addition of anions such as F⁻, CH₃COO⁻, and H₂PO₄⁻ the fluorescence emission was quenched, whereas addition of Cl⁻ and Br⁻ induced no changes. This quenching of the fluorescence was assigned to a PET process from the anion-receptor complex to the chromophore. CH₃COO⁻, and H₂PO₄⁻ were observed to form 1:1 (anion:receptor) complexes with the receptor. The quenching was more pronounced for F⁻. In addition, at higher concentrations of F⁻ a new band centred at 536 nm was observed in the absorption spectra, which induced a colour change from yellow to deep purple. These compounds were then described as dual fluorescent-colorimetric anion sensors. These changes in the absorption spectra were assigned to the deprotonation of the 4-amino moiety of the naphthalimide chromophore (enhancement of the push-pull character of the ICT chromophore), giving rise to the formation of bifluoride anion (HF₂⁻).

The examples given in this section are just a very small fraction of the variety of fluorescent anion sensors developed to date. Several reviews have been published, which provide a good account on the development of fluorescent anion sensing.^{14,15,21,29}

Although fluorescence based sensors possess some advantages over other types of sensors, namely high sensitivity, there are also a number of drawbacks when using

fluorescent sensors for *in vivo* applications, such as background emission or auto-fluorescence and light scattering from the surrounding biological environment. Consequently, the emission of many fluorescent systems, characterised by short lifetimes (in the nanosecond range), cannot be distinguished from the emission caused by auto-fluorescence.⁵¹ Such problems have directed research towards the search for a better alternative. One way of overcoming these drawbacks is the use of delayed lanthanide luminescence.⁵²

1.4.2 Lanthanide luminescence based signaling

Over the past number of years, there has been a growing interest in the chemistry of lanthanide complexes. The multidisciplinary character of lanthanide research is patent on the several types of lanthanide complexes that have successfully been developed as functional molecular devices in the fields of chemistry, biology, medicine and materials science.⁵³ For example, (a) luminescent sensors and light converters, (b) contrast agents used in magnetic resonance imaging (MRI) and (c) catalysts in organic and biological reactions.⁵⁴ In all these examples, it is obvious that careful design of the ligands, and hence a precise structural control of the lanthanide ion (Ln(III)) coordination sites, allow the construction of programmed functional devices by taking advantage of the different properties (electronic, spectroscopic and magnetic) of these metal ions.

Due to the unique luminescence properties of the lanthanide ions, lanthanide complexes possess a number of advantages that make them attractive for signalling purposes. These advantages include large Stokes shifts (>200nm), narrow emission bands and long excited state lifetimes, provided that deactivations by non-radiative pathways are minimised. The lifetime of emission from the excited state of the lanthanide ions falls in the range of microseconds (*e.g.* Yb(III), Nd(III)) to milliseconds (for the visible light emitting Eu(III) and Tb(III)).⁵² Such long-lived emissions have led to numerous applications of lanthanide-based systems as luminescent probes and sensors.^{55,56} This is due to the use of time resolved techniques, which allow an easy distinction of the luminescence signal from the shorter-lived (ns time frame) background fluorescence, present in most biological systems, overcoming the problems associated with auto-fluorescence and Rayleigh scattering.^{52,55-58}

The main drawback related to lanthanide ions is their low extinction coefficients associated with Laporte-forbidden $f-f$ transitions. As a result of being such a poor light absorbers, the population of their excited states by direct excitation is inefficient, unless a very intense light source is used such as laser excitation. This disadvantage can be overcome by means of indirect excitation using a sensitising chromophore (also known as antenna).⁵⁹⁻⁶¹ The antenna effect is illustrated in **Figure 1.4.2**. The sensitising antenna, by the absorption of light, is excited to a singlet state ($^1\pi\pi^*$). The energy can then be transferred to its triplet state ($^3\pi\pi^*$), by means of intersystem crossing (ISC), and eventually transmitted to the lanthanide excited state, Ln(III)^* , through an intramolecular energy transfer (ET), k_1 . The excited energy can now be lost through emission of light, leading to the characteristic lanthanide luminescence.^{58,62,63}

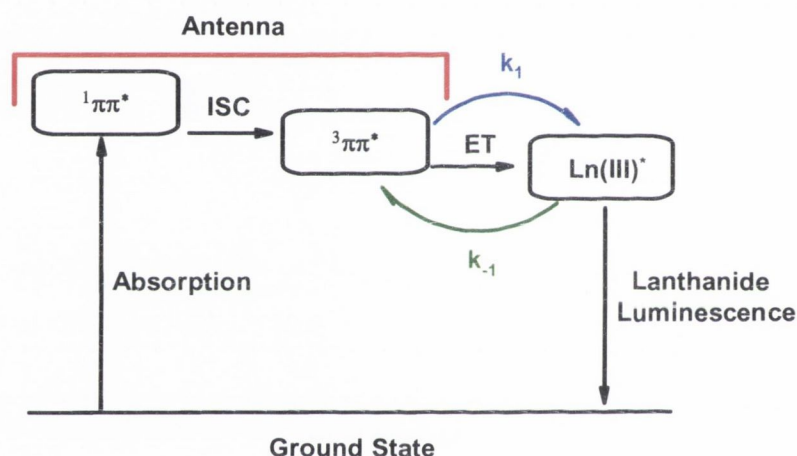


Figure 1.4.2: Simplified schematic representation of the antenna effect occurring in Ln(III) complexes possessing aromatic chromophores. The diagram shows the process of energy transfer (ET), *via* intersystem crossing (ISC), from the antenna to the metal centre leading to lanthanide emission.^{58,62,63}

The intramolecular energy transfer (ET), from the triplet state of the antenna to the lanthanide centre ($^3\pi\pi^* \rightarrow \text{Ln(III)}^*$), can occur *via* two possible mechanisms. The Förster energy transfer mechanism⁶⁴ and the Dexter mechanism⁶⁵. The Förster mechanism involves the overlap of energy levels and it is described in terms of an interaction between the transition dipole moments (a dipolar mechanism). The energy transfer occurs through space and is r^{-6} distance dependent, where r is the distance between the metal ion and the excited chromophore/antenna. Consequently, the energy transfer process can be made more

efficient by minimising the distance between the lanthanide ion and the antenna. In the Dexter mechanism, the energy transfer occurs as a result of an electron exchange between the excited chromophore and the metal ion in a through-bond interaction with an e^{-r} dependency. Again the process can be made more efficient by minimising the distance r .⁶⁶

The sensitisation process is highly dependent on the choice of chromophore, which in turn is generally dictated by the energy of the emissive state of the metal. The sensitizer must possess an excited state with energy similar or higher to that of the metal emissive state in order to allow sensitisation to occur. The use of antennae possessing too small an energy gap ($< 1700 \text{ cm}^{-1}$) is disadvantageous since thermally activated back energy transfer from the metal (Ln(III)^*) to the sensitizer ($^3\pi\pi^*$) can then compete with emission, k_{-1} (**Figure 1.4.2**)^{63,67} Among the lanthanide ions, the two most used visible emitters, Eu(III) (red emission) and Tb(III) (green emission) have the largest energy gaps between their emissive and ground states, being therefore the least sensitive to vibrational quenching by solvent water molecules or by N-H and C-H oscillators. Their emissive states, 5D_0 and 5D_4 , lie at $17\,200 \text{ cm}^{-1}$ and $20\,500 \text{ cm}^{-1}$ for Eu(III) and Tb(III) respectively. Taking this into consideration, a diverse range of aromatic chromophores have been proposed including bipyridines, terpyridines, triphenylenes, quinolines, substituted phenyl and naphthyl groups, all possessing an energy of their triplet excited state lying at least 1700 cm^{-1} above the emissive state of the lanthanide.^{52,58} Another desirable feature of the sensitizer is to possess a relatively low singlet excited state energy (small energy gap between $^1\pi\pi^*$ and $^3\pi\pi^*$) to allow excitation at long wavelengths (300 – 400 nm) avoiding this way the competitive absorption of common biomolecules, such as proteins and nucleic acids. Therefore, the overall efficiency of Ln(III) sensitised emission is regulated by the use of chromophores possessing high extinction coefficients, a fast intersystem crossing step to ensure an efficient population of the triplet state, $^3\pi\pi^*$, and a fast energy transfer step leading to efficient population of the lanthanide excited state.

1.4.2.1 Quenching of the lanthanide excited state (Ln(III)^*)

As mentioned, luminescence from the lanthanide excited states can be quenched by non-radiative processes. Non-radiative deactivation may occur through energy transfer to vibrational modes which match the energy of the excited state of the lanthanide ion.⁶⁸ In

aqueous solution, the main quenching process involves energy transfer into O-H stretching vibrations of solvent water molecules. This process is strongly dependent on the distance between the lanthanide and the O-H oscillator, such that directly coordinated water molecules have a much larger effect than closely diffusing waters. The energy transfer from the Ln(III) to bound or proximate O-H oscillators occurs *via* a Förster⁶⁴ mechanism in which dipole-dipole interactions dominate. This process is distance dependent, following an r^{-6} dependence (r being the distance between the metal centre and the O-H oscillator).⁶⁹ Variations in the number of bound water molecules may therefore lead to significant changes in both the intensity and lifetime of emission.⁶⁸ The extent of this quenching was found to be inversely proportional to the energy gap between the emissive and the ground states of the metal, Tb(III) being the less readily quenched by these oscillators. Although not to the same extent as O-H oscillators, other de-activating vibrations such as from N-H and C-H oscillators can quench the luminescence of a lanthanide ion.⁷⁰

Based on the assumption that moving from H₂O to D₂O changes only the nature of the solvent oscillator, and that all the other quenching paths are the same in water and in deuterated water, the number of water molecules bound to the lanthanide can be assessed by measuring the luminescent lifetimes (τ) of the lanthanide excited states in H₂O ($\tau_{\text{H}_2\text{O}}$) and D₂O ($\tau_{\text{D}_2\text{O}}$) respectively. Determination of q values, number of water-bound molecules, can be made using the equations derived by Horrocks *et al.*⁷¹⁻⁷³ Studies carried out by the Parker group lead to a refinement of these equations by taking into account not only the deactivation by O-H oscillators, but also deactivation by N-H and C-H oscillators, **Equation 1** and **Equation 2**. In these equations, A are proportionality constants that mirror the sensitivity of the corresponding ions to quenching by metal-bound water molecules. These constants, being specific to a given lanthanide ion, are 5.0 and 1.2 ms for Tb(III) and Eu(III) respectively.^{68,74}

$$q^{\text{Tb(III)}} = A [(1/\tau_{\text{H}_2\text{O}} - 1/\tau_{\text{D}_2\text{O}}) - 0.06] \quad \text{Equation 1}$$

$$q^{\text{Eu(III)}} = A [(1/\tau_{\text{H}_2\text{O}} - 1/\tau_{\text{D}_2\text{O}}) - 0.25 - 0.075x] \quad \text{Equation 2}$$

The correction terms -0.25 and -0.06 represent quenching by second sphere water molecules, whereas $-0.075x$ represents the quenching by N-H oscillators, where x is the number of such oscillators directly bound to a given complex.⁶⁸

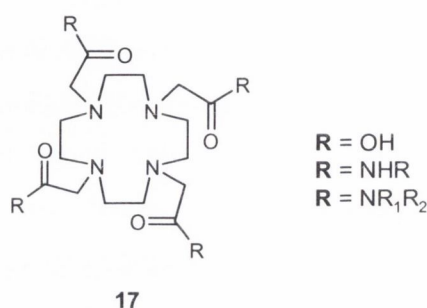
In order to minimise vibration-induced deactivation processes, a rigid metal-ion environment is needed which is free of high energy vibrations and which can protect the Ln^{III} ion from solvent coordination. The next sections shall detail some examples of macrocyclic ligands, which have been employed in lanthanide complexation.

1.4.2.2 Lanthanide complexes

Lanthanide ions are inherently toxic to biological systems as they can displace Ca(II) in proteins, due to the size similarity with this cation.^{75,76} So in order to use these ions for *in vivo* sensing, thermodynamically and kinetically stable complexes are required.^{75,77,78} This can be obtained by designing ligands able to encapsulate the lanthanide ions by satisfying the coordination requirements of these ions, within which the metal centre can be shielded from quenching moieties previously discussed. So, in order to successfully design these ligands several lanthanide characteristics have to be considered. Ln(III) ions possess relatively high charge densities and have strong electrostatic nature in their binding as well as a variety of coordination numbers, most frequently between eight and ten. Their Lewis acidity favours binding to nitrogen and oxygen atoms, and hence combinations of amide and carboxylic groups are usually used in lanthanide complexation. The idea behind the design of such ligands is to build a pre-organised system bearing several donor atoms generating suitable interactions with the metal ion. Amongst the most commonly used frameworks are multidentate ligands such as podands⁷⁹, polyaminocarboxylates, β -diketonates, macrocycles; either pre-disposed (*e.g.* cyclen derivatives and calixarenes fitted with functionalised pendant arms), or pre-organised (*e.g.* crown ethers or cryptands).^{56,80} Of special interest for our research are macrocyclic receptors based on cyclen (1,4,7,10-tetraazacyclododecane). Below will be detailed some examples of such cyclen based ligands.

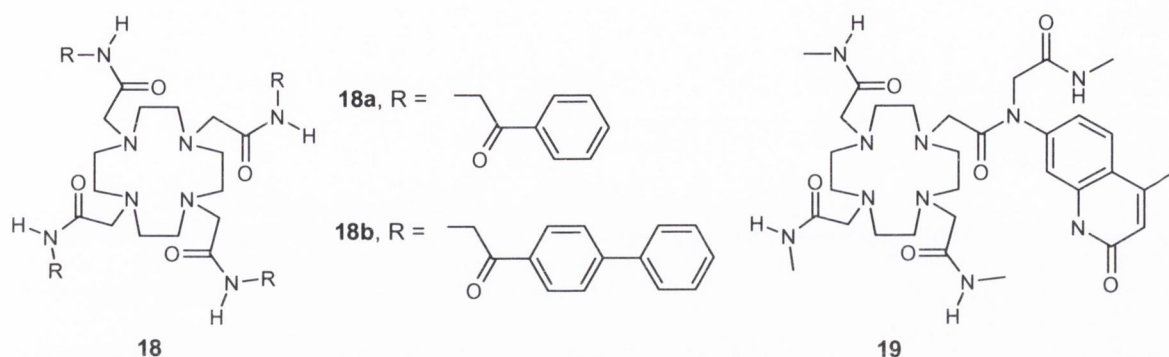
Tetra-substituted cyclen ligands such as **17**, possessing coordinated carboxylates (DOTA), phosphinates, or amide pendant arms, by providing eight coordinating atoms, four by the macrocyclic nitrogens and four by the pendant arms, these ligands provide a

good base for the design of kinetically inert and thermodynamically stable lanthanide complexes. Such functionalisation also offers the possibility to easily incorporate aromatic chromophores as sensitisers, thus giving rise to responsive lanthanide luminescent complexes.^{61,67,69,81}

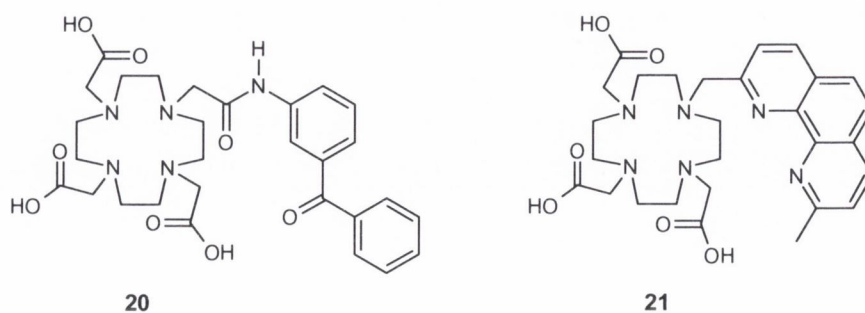


Bünzli *et al.* reported tetraamide cyclen frameworks bearing the aromatic phenacyl (**18a**) and 4-phenylphenacyl (**18b**) chromophores, which were able to efficiently sensitise the luminescence of Tb(III) and Eu(III) ions in water.⁸² These ligands form stable 1:1 complexes with lanthanide ions in water. The crystal structure obtained for **Tb.18a** showed the metal ion lying on a C_4 axis and being nine coordinate, with one water molecule in its inner coordination sphere. The absolute quantum yields were determined for the complexes, of both **18a** and **18b**, formed with Sm(III), Eu(III), Tb(III), and Dy(III). Large values of 23.1% for $[\text{Tb}(\text{H}_2\text{O})\mathbf{18a}]^{3+}$ and 24.7% for $[\text{Eu}(\text{H}_2\text{O})\mathbf{18b}]^{3+}$ were found upon excitation of the phenacyl and 4-phenylphenacyl chromophores, respectively.

Parker and co-workers reported a cyclen based ligand with three acetamide pendant arms and a quinoline based chromophore sensitiser linked via an amide, **19**.⁵⁹ In this case, measurement of the luminescence quantum yields showed that sensitisation of **Tb.19** was more efficient than for the **Eu.19** complex, with values of 0.044 and 0.018 respectively. Both the intensity and lifetime of the terbium emission were significantly reduced through a thermally activated back energy transfer process of deactivation, due to a low-lying triplet state. The low quantum yield of **Eu.19** was attributed to a competitive charge transfer de-excitation pathway, hence limiting the efficiency of sensitisation.



Beeby *et al.* have reported a cyclen based ligand functionalised with three carboxylic pendant arms and a benzophenone chromophore attached to the fourth cyclen nitrogen through an amide bridging group, **20**.⁸³ This ligand (**20**) gave rise to charge neutral Eu(III) and Tb(III) complexes, exhibiting quantum yields of 0.095 and 0.27 for **Eu.20** and **Tb.20** respectively when measured in water.⁸⁴ Quici and co-workers reported ligand **21**.⁸⁵ Similarly to the previous ligand (**20**) discussed, ligand **21** is also based on the 1,4,7,10-tetraazacyclododecane-1,4,7-triacetic acid (DO3A) as the receptor unit for the lanthanide ions. Nevertheless, the chromophore is now an appended functionalised 1,10-phenanthroline (*phen*). In the Ln(III) complexes of **21**, the *phen* moiety was found to be directly involved in the coordination process of the lanthanide ions. Furthermore, the rigidity of the *phen* chromophore and its spatial arrangement within the complex was found to prevent the access of any water molecule into the first coordination sphere of the metal, hence resulting in good shielding of the lanthanide centre ($q = 0$ and $q = 0.2$ for **Eu.21** and **Tb.21** respectively). The complexes showed high luminescence efficiencies in water, with an increase in the quantum yield for **Eu.21** of 0.21, when compared to the quantum yield of 0.095 for **Eu.20**.



The examples given above were selected to show that the photophysical properties of lanthanide complexes vary greatly depending on the properties of the sensitising chromophore. The following section will detail some examples regarding the application of lanthanide complexes as sensing devices.

1.5. Lanthanide complexes as sensing devices

Taking into account all the requirements discussed in the previous sections, in order to use lanthanide complexes as signaling devices or sensors, the detection of any changes in the photophysical properties of the complexes as a direct consequence of the presence of an analyte is of crucial importance. As already mentioned (**Section 1.4.2**), the presence of a chromophore or an antenna able to sensitise the lanthanide luminescence is of crucial importance. There are a number of different methods for modulating the emission properties by external sources (ions or molecules).

The sensitisation process can be modulated by the incorporation of a recognition unit into the antenna.⁶⁷ Upon analyte recognition, the physical properties of the antenna, such as the excited state energy, the redox properties, or even structural changes are modulated. This in turn affects the photophysical properties of the lanthanide ion (excited state lifetimes, emission intensity).

The recognition process can also take place directly at the metal ion centre, provided that weakly bound ligands, such as solvents, can be displaced by the targeting analyte.^{67,86,87}

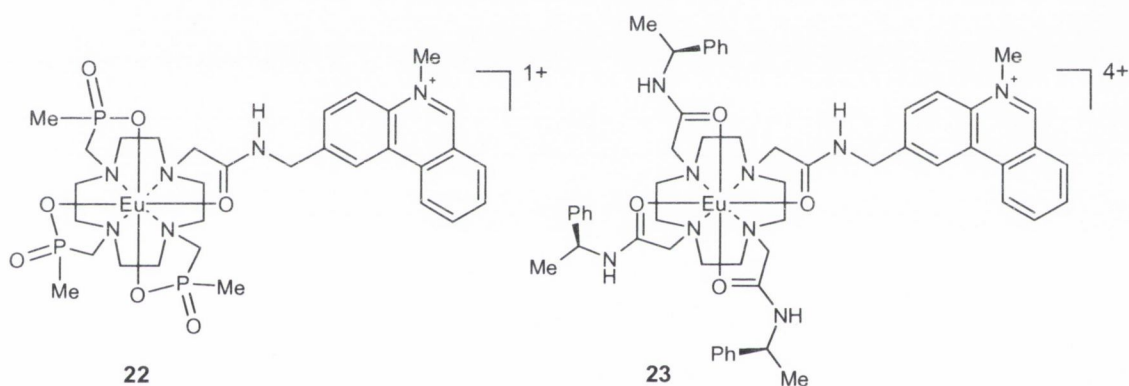
In the following section examples of cyclen based lanthanide complexes for the sensing of anions will be presented and their mode of action discussed. Several reviews have been published, which provide a good account of the development of lanthanide complexes for sensing purposes in general, including anions, cations, and neutral molecules.^{58,61,62,66,67,88}

1.5.1. Lanthanide complexes as anion sensors

In principle, anions may perturb the excited state of the chromophore, or may affect the rate of quenching of the lanthanide excited state.⁵² In the latter case, anion binding to the lanthanide ion can lead to large changes in the lanthanide emission lifetime as well as

emission intensity, as bound water molecules are displaced.^{67,89} Examples of both cases will be presented below.

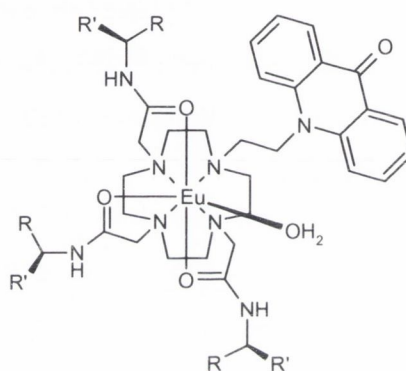
Addition of halide ions to the Eu(III) complexes **22** and **23**, lead to a decrease in the intensity of the phenanthridinium fluorescence (405 nm) and an associated decrease in the Eu(III) luminescence intensity. A reduction in the emission intensity of a factor of four was observed.⁶⁰ The Cl⁻ quenching effect was independent of added lactate, phosphate, citrate, and hydrogencarbonate. The efficiency of quenching followed the order I⁻ > Br⁻ > Cl⁻ and was supposed to involve charge transfer from the halide ion to the excited singlet of the chromophore. The fluorescence of *N*-alkylated phenanthridinium ions is known to be quenched by halide anions in aqueous media.⁹⁰ This phenomenon has been employed in the development of assays for chloride ion in biological media.⁹¹



As previously mentioned, water molecules can bind to the lanthanide ions in unsaturated ligands to fulfill the coordination requirements of these metal ions. Since, water molecules are able to quench the excited state of lanthanide ions such as Eu(III) and Tb(III), displacement of these quenchers would lead to changes in the luminescence properties of the lanthanide. Therefore, this enables the detection of the direct coordination of an analyte to the metal centre.

A series of cationic, zwitterionic, and anionic Eu(III) complexes, such as **24** – **26**, have been developed by Parker *et al.* for the detection of bicarbonate (HCO₃⁻).^{92,93} An acridone was used as the chromophore, which allowed sensitisation of the Eu(III) emission following excitation at 390–410 nm. The advantages of using such an antenna as a sensitizer

had been previously reported by Faulkner *et al.*⁸⁴ Each of these complexes was found to selectively bind bicarbonate at physiological pH. The binding process was signaled by changes of the luminescence lifetimes and of the Eu(III) emission intensities, where q changed from 1 to 0. This supported the displacement of the metal bound inner sphere water molecule. By monitoring the ratio of the emission intensity of Eu(III) of the 618/588 or 618/702 nm emission bands, the solution concentration of bicarbonate could be assessed in a background of competing anions such as lactate, citrate, and phosphate.⁹³

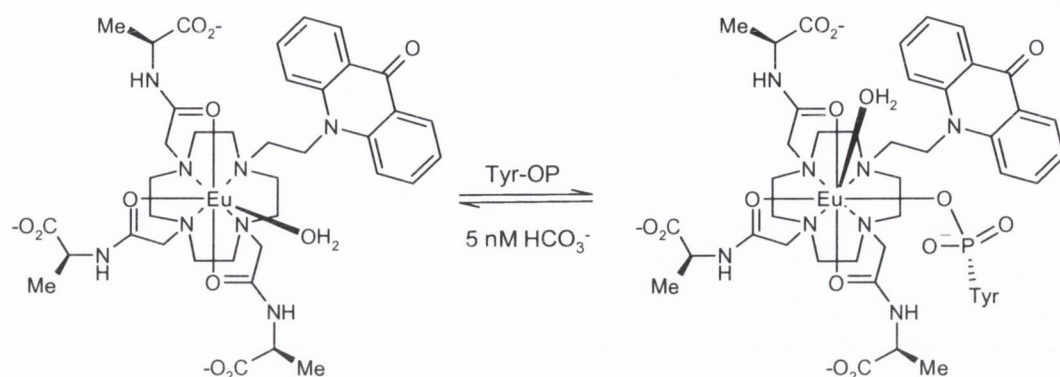


24 R = CO₂Et, R' = Me

25 R = CO₂⁻, R' = Me

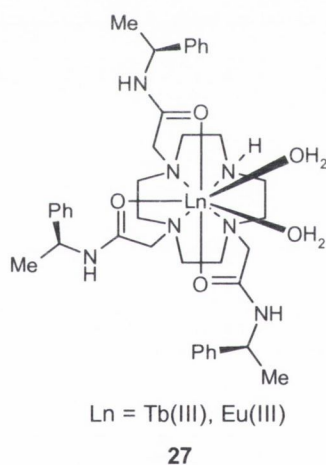
26 R = CO₂⁻, R' = (CH₂)₂CO₂⁻

The use of such acridone Eu(III) complexes (**25**) has been extended to the sensing of phosphate.⁹⁴ The binding of selected phosphates, as well as phosphorylated amino acids such as Ser-OP and Tyr-OP was investigated by observing the emission spectra of the complexes. Job plot analysis revealed the formation of 1:1 adducts, which displayed subtly different emission spectra with Tyr-OP showing the lowest $\Delta J = 2 / \Delta J = 1$ intensity ratio. In each case, the obtained data was consistent with formation of mono-aqua species with phosphate anion acting as a monodentate ligand, as depicted in **Scheme 1.5.1**.

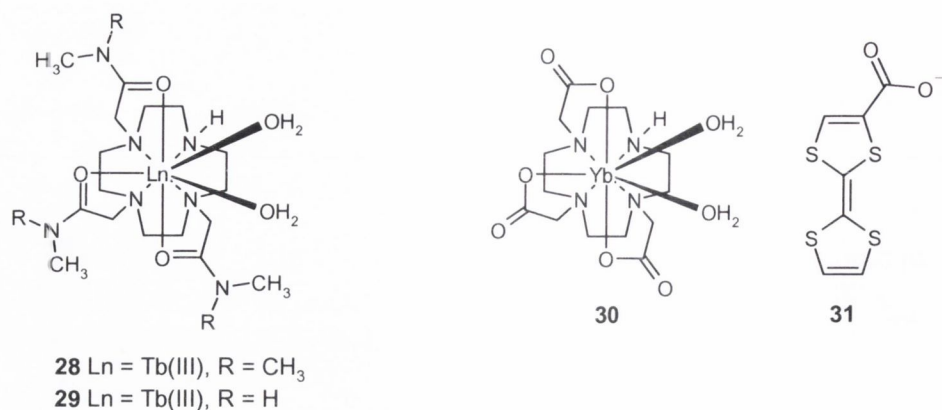


Scheme 1.5.1 Binding of Tyr-OP to the mono-aqua Eu(III) complex **25**.⁹⁴

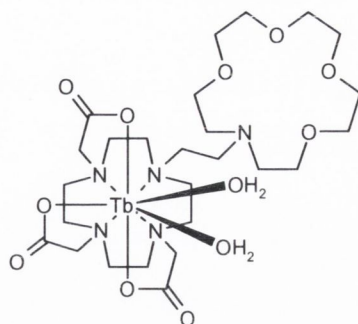
In aqueous media, the heptadentate **Tb.27** and **Eu.27** complexes developed by Parker and co-workers^{89,95} gave rise to weak lanthanide emission, due to the presence of two bound water molecules.



In aqueous solution it was observed that both water molecules could be displaced by anionic species such as phosphate, lactate, and carbonate, resulting in the formation of a 1:1 adduct. This ternary complex was signaled by large changes in the lifetime of the Eu(III) and Tb(III) excited state. In contrast, the lifetimes remained unchanged for ions such as Br⁻ and Cl⁻. In the case of CH₃COO⁻, F⁻, and H₂PO₄⁻, *q* was determined to be *ca.* 1, implying the loss of a single bound water molecule upon coordination of these anions to the lanthanide ions.

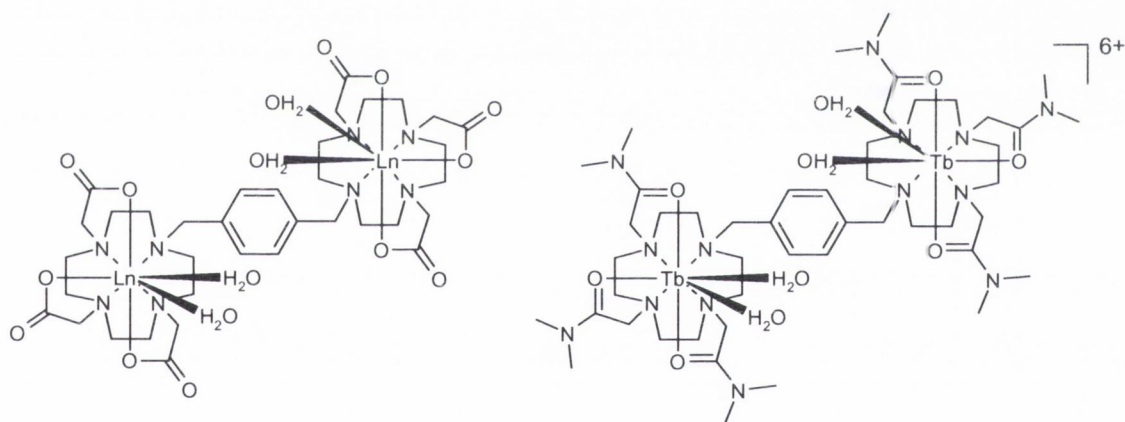


Gunnlaugsson *et al.* have developed similar systems, **28** and **29**, for the binding of aromatic carboxylates.^{86,87} The coordinatively unsaturated Tb(III) complexes **28** and **29** were found to bind aromatic carboxylic anions such as *N,N*-dimethylaminobenzoic acid and salicylic acid in water. The coordination of these aromatic anions to the non-luminescent Tb(III) complexes **28** and **29** occur *via* displacement of the two bound water molecules, giving rise to large enhancements in the Tb(III) luminescence. A similar design was reported by Faulkner *et al.* for the sensing of tetrathiafulvalene carboxylate (**31**), by using the charge neutral IR-emitting Yb(III) complex **30**.⁹⁶ In methanolic solution, the carboxylate coordinates to **30** through displacement of the two bound water molecules. The tetrathiafulvalene antenna was then able to transfer energy to the metal, causing the observed luminescence from the Yb(III) ion. More recently, this research group demonstrated the sensitisation of the Nd(III) analog of **30**, using pyrene carboxylate as the sensitising antenna.⁹⁷ Upon coordination of the pyrene carboxylate in water, intense characteristic Nd(III) emission bands at 1055 and 1350 nm were observed. These results are of extreme importance for the development of lanthanide based sensors and probes for biological applications. These near infrared emitting lanthanides [(Yb(III) and Nd(III)] possess lower energy emissive states, and hence are able to make use of chromophores with longer absorption wavelengths (> 400 nm). This renders them a great advantage over other lanthanide ions such as Tb(III) and Eu(III), when regarding *in vivo* applications.⁹⁸ Nevertheless, since these ions emit at wavelengths greater than 800 nm, specialised instruments are required.



32

Li and Wong reported the cyclen based Tb(III) complex **32**, which was able to signal the presence of anions such as lactate and salicylate in physiological conditions.⁹⁹ Similarly to previous examples, **32** lack the presence of a chromophore, hence was found to be non-luminescent. However, the luminescence lifetime and intensity were observed to vary greatly upon addition of lactate and salicylate.

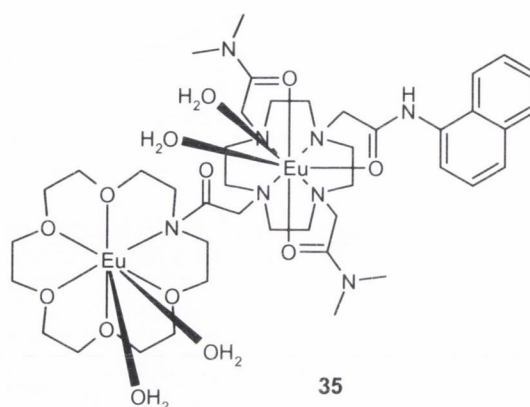


33

34

Faulkner *et al.* reported the elegant xylyl bridged bis-cyclen system **33**, able to accommodate two lanthanide ions. Excitation of the bridging antenna of the various lanthanide complexes gave rise to the typical lanthanide emission.¹⁰⁰ The similar cationic coordinatively unsaturated terbium dinuclear analogue, **34**, was reported by Gunnlaugsson *et al.*¹⁰¹ This complex showed the ability to detect the presence of mono- or bis- aromatic carboxylates, such as *N,N*-dimethylaminobenzoic acid and terephthalic acid respectively, in buffered aqueous solution at physiological pH. The recognition of these ions was found to

occur through the binding of the carboxylates to the metal center, *via* the displacement of the metal bound water molecules. This gave rise to significant enhancements in the Tb(III) emission. In the presence of tartaric acid, the recognition process gave rise to quenching of the Tb(III) emission intensity.



Very recently, Gunnlaugsson and co-workers reported the dinuclear-Eu(III)-bismacrocyclic conjugate **35** as a delayed luminescent lanthanide sensor for dicarboxylates.¹⁰² The sensor was shown to bind small dicarboxylic acids such as aspartic, malonic, succinic, and glutaric acid in pH 6.5 solutions. Nevertheless, only malonic acid gave rise to selective Eu(III) luminescence enhancements, as the emission intensity was reduced for the other acids.

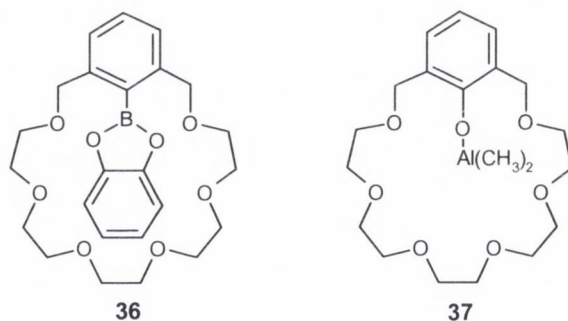
So far this chapter has focused on the sensing of anionic species. However, in our research, we have also been concerned with the development of heteroditopic receptors for the binding of both anions and cations. Consequently, the following section will detail some examples of this kind of receptors and their applicability.

1.6. Heteroditopic Receptors

Although challenging and pertinent, the simultaneous recognition of both cations and anions is still in its infancy. There are only a few examples of these synthetic heteroditopic receptors.¹⁰³ Research in this field is relevant to the detection and extraction of toxic ions from aqueous environments, as well as to the design of artificial carriers and channels for the transport of inorganic and organic salts across membranes.¹⁰⁴

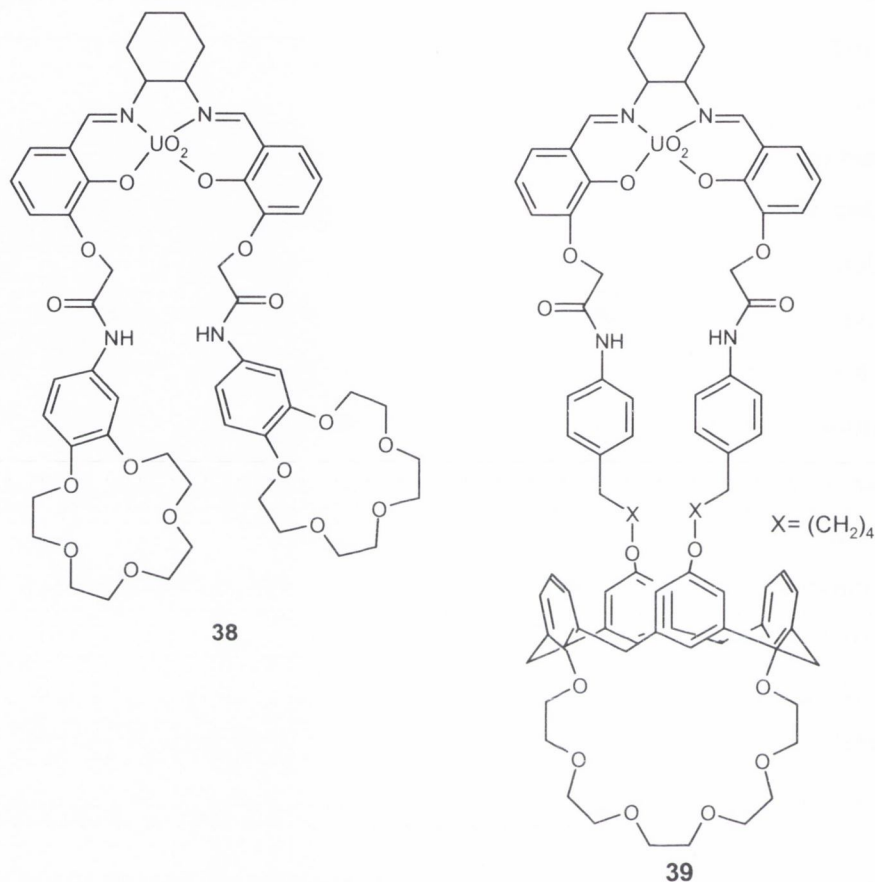
In general, heteroditopic receptors have been designed by combining functionalities such as cation binding crown ethers and modified calixarenes, with anion binding Lewis-acidic metal centres such as pyrroles, amido, and urea groups.^{104,105} This kind of receptors may exhibit interesting cooperative and allosteric binding behaviours. The binding affinity of one ion can be facilitated by the coordination of the other ion due to electrostatic interactions and conformational effects.^{106,107}

One of the first examples of such receptors was provided by Reetz and co-workers who covalently linked a crown ether with a Lewis-acid boron moiety, **36**.¹⁰⁸ Host **36** was found to bind simultaneously with potassium and fluoride ions. Here boron acts as a Lewis-acid site for F^- while the polyoxyethylene chain binds the potassium cation. Under the conditions used no interaction was observed between this host and the salts KCl and KBr. On the other hand, the same host affords monotopic cation binding with KI and KSCN. The same researchers also showed that the phenolic analogue of **36** can be conveniently metalated with Me_3Al to form the aluminium containing compound **37**, which was expected to bind alkali metal salts, due to the presence of a free aluminium coordination site. The complex between **37** with LiCl was confirmed both in solution and in the solid state.¹⁰⁹



Reinhoudt and co-workers have elegantly illustrated the use of UO_2 based crown ether, **38**, as a receptor capable of simultaneously recognise potassium and dihydrogen phosphate. The anion binds the Lewis acidic uranyl (UO_2^{2+}) while the cation attaches to the two benzo[15]crown-5 moieties.¹¹⁰ Receptor **38** was shown to be an efficient carrier for the transport of the hydrophilic salt KH_2PO_4 through liquid membranes.¹¹⁰ By replacing the benzo[15]crown-5 functionalities with a rigid Cs^+ selective calix[4]arene crown-6 moiety,

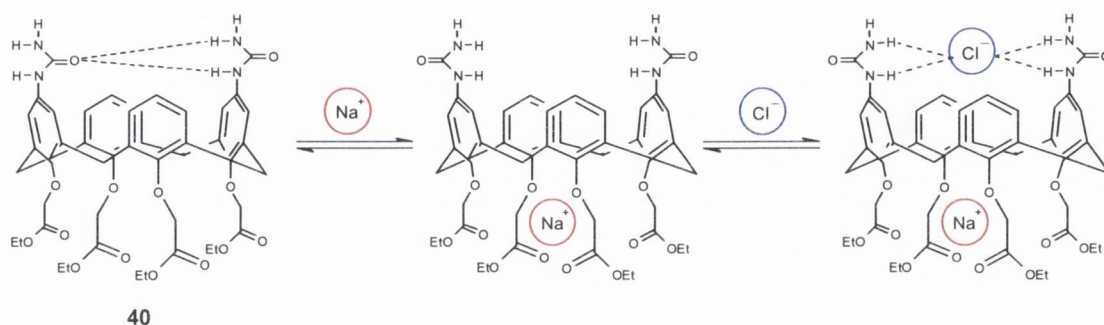
39, Reinhoudt and co-workers demonstrated the ability of this bifunctional receptor to transport CsCl and CsNO₃ through a supported liquid membrane.¹¹¹



Although Cl⁻ is much more hydrophilic than NO₃⁻, a higher rate of flux was observed through the hydrophobic membrane for CsCl than for CsNO₃ in the presence of receptor **39** demonstrating in this way substrate selectivity. More significantly they found that this rate has largely exceeded the one observed when monofunctional analogues were used.^{111,112} This fact was seen as consistent with both binding sites being necessary to accomplish efficient complexation and transport.

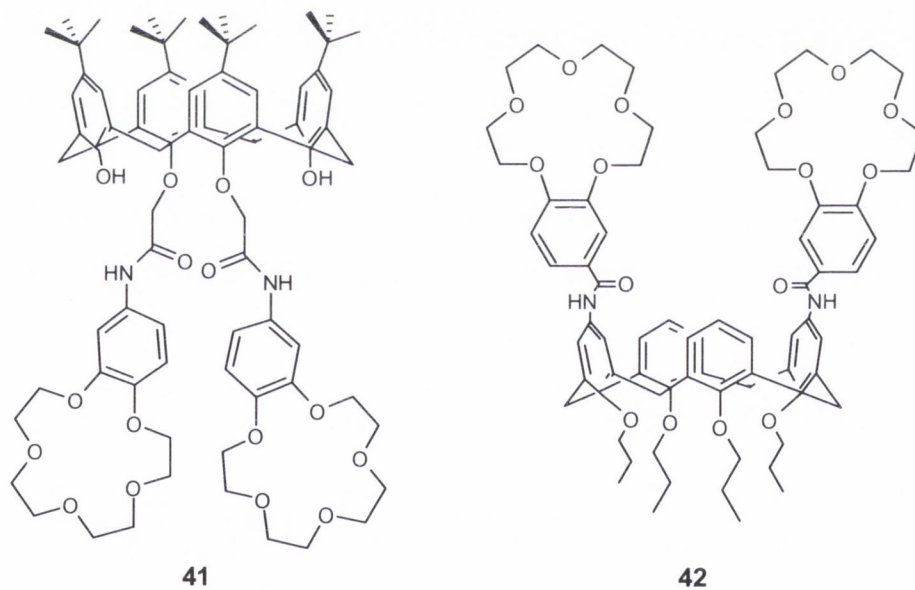
The continued research work by the Reinhoudt group, in the field of heteroditopic receptor design, gave rise to the calix[4]arene scaffold possessing a cation binding site, formed by ester groups, on the lower rim and anion binding urea groups on the upper rim.¹¹³ The resulting receptor, **40**, in CDCl₃ adopts a pinched conformation due to intramolecular hydrogen bonding between the urea groups, thus preventing anion binding.

However, upon addition of sodium ions, cation complexation at the lower rim alters the calyx conformation, breaking the hydrogen bonds between the urea groups as shown in **Scheme 1.6**. As a result, ions such as Cl^- and Br^- can be recognized at the upper rim.



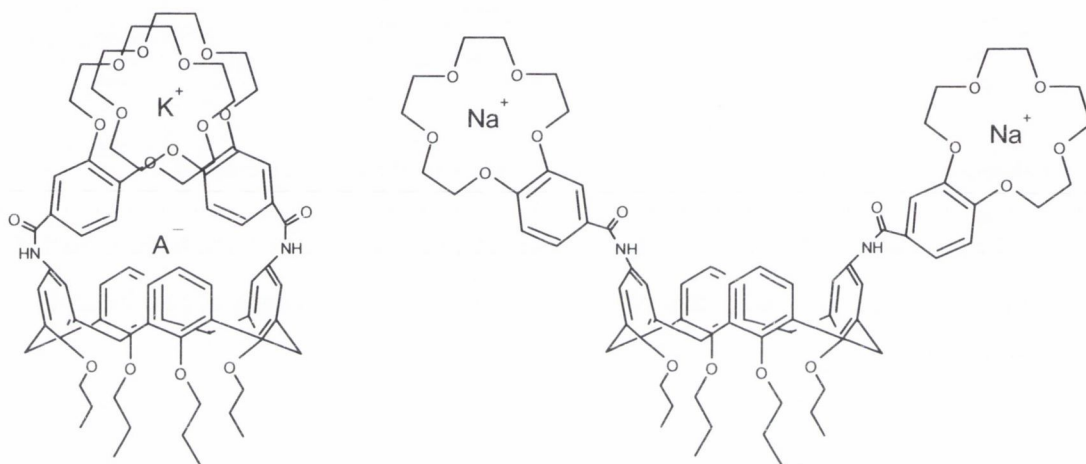
Scheme 1.6: Proposed binding mechanism of Na^+ and Cl^- by the ditopic receptor **40**.¹¹³

Further examples of calix[4]arene based ditopic receptors have been reported by Beer and co-workers. An early example is receptor **41**, which consists of two benzo[15]crown-5 groups attached to the calixarene through amide linkers.¹¹⁴



This compound on its own showed very little affinity for anions. However, in the presence of K^+ and NH_4^+ ions a sandwich complex is formed between the two benzo-crown units, which in turn bring the amide groups into closer mutual proximity. These conformational changes, coupled with the increased electrostatic attraction provided by the

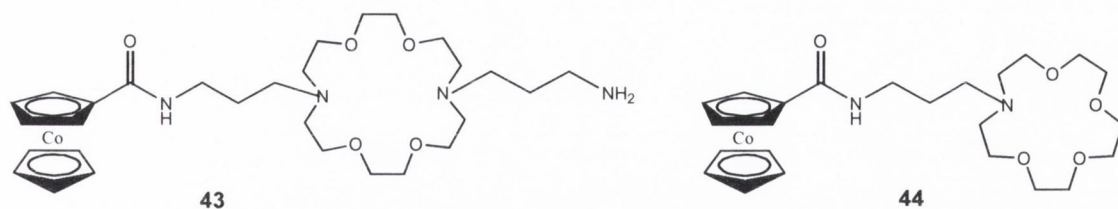
co-bound cation, led to a particularly strong binding of H_2PO_4^- . Structure **42** is a more recent example, coming from the Beer group, of this kind of molecule.¹¹⁵ Using ^1H NMR titration studies, in a 1:1 mixture of $\text{CDCl}_3:d_6$ -DMSO, revealed that the bis crown ether calix[4]arene, **42**, in the presence of one equivalent of K^+ enhances significantly the binding strength of chloride, benzoate, and dihydrogen phosphate anions, *via* favourable pre-organisation and electrostatic effects. In contrast, with two equivalents of sodium a decrease in the strength of anion binding was observed.



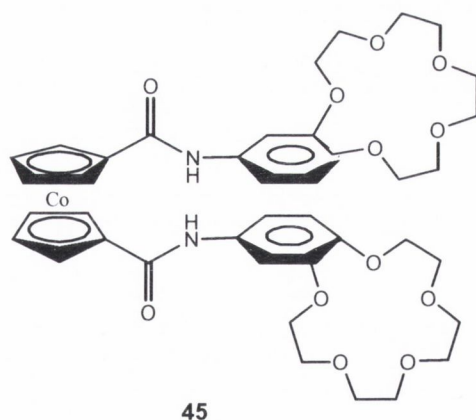
Scheme 1.6.1: Schematic illustration of a 1:1 binding between K^+ and **42** favouring anion complexation, and the $2\text{Na}^+:\text{42}$ complex which is unable to cooperatively bind an anion.¹¹⁵

The observed results were explained by the fact that K^+ forms an intramolecular sandwich complex with the crown ether moieties of **42** leading to a pre-organisation of the amide groups. These conformational changes, allied with mutual electrostatic cation-anion attractions and through bond inductive electrostatic effects of the complexed metal cation, may enhance the relative acidity of the receptor amide protons, leading to stronger hydrogen bonding with the guest anion. On the other hand, each crown ether complexes with one Na^+ , resulting in a $2\text{Na}^+:\text{42}$ complex where the amides are unable to cooperatively complex an anion due to repulsive electrostatic effects (**Scheme 1.6.1**).

The concept of using hosts composed of Lewis acidic metal centres and crown ether moieties has been further extended to cobalt-containing aza crown ethers such as **43** and **44**.¹¹⁶

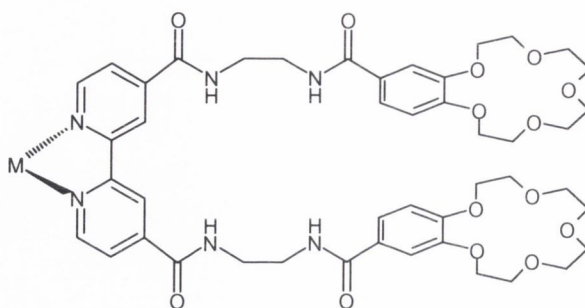


In both cases interaction with TBACl and TBABr, in MeCN, was observed by the downfield shifts of the amide protons. These results have been explained by the researchers to be due to anion interaction with the hydrogen atom of the amide, to the cobalt and to the sodium ions in the crown ether moiety. Beer and co-workers further reported the synthesis of a new cobalticinium bis crown ether receptor, **45**, whose halide anion recognition properties were “switched off” *via* conformational changes induced by the presence of crown ether complexed potassium cations.¹⁰⁶ It was found that receptor **45** forms 1:2 ligand to metal complex with sodium cations, indicating that the two benzo crown ether moieties are individually complexing a Na^+ . In contrast, the larger potassium cation forms a 1:1 intramolecular sandwich complex leading to a spatial arrangement of the anion binding site within the receptor contributing to the inhibition of anion binding. Therefore, the binding of halide anionic species can be switched on or off via the absence or presence of potassium cations.¹⁰⁶



The use of heteroditopic Ru(II) and Re(I)-bipyridyl-bis(benzocrown) receptors **46** and **47** exemplify how K^+ binding can not only give an allosteric effect but also induce a switch in anion selectivity. In the absence of cation the ligands show to be selective for H_2PO_4^-

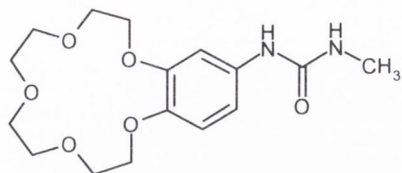
over Cl^- . However, after the formation of the intramolecular K^+ -biscrown sandwich complex the selectivity was reversed.¹¹⁷



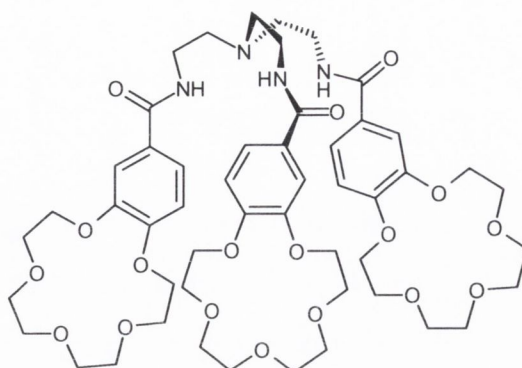
46; M = Ru(II)(bipy)₂

47; M = Re(I)(CO)₃Br

Also reported were a series of calix[4]arene esters linked to Ru(II) or Re(I)-bipyridyl metal sites.¹¹⁸ In the presence of one equivalent of the alkali metal cations (Na^+ and Li^+), an increase in the association constants for Br^- and I^- was observed. The enhanced affinities for the anions, in the presence of the metal cations, were described by the authors to arise from mutual cation-anion attraction, pre-organizational effects and increased strength in hydrogen bonding to the anion, due to disruption of an intramolecular bond between the amide NH proton and calixarene ester moiety promoted by cation complexation. Throughout the literature, other examples of systems making use of the already mentioned benzo-15-crown-5 groups can be found. For instance, Nishizawa *et al.* have used the thiourea functionalised benzo-15-crown-5, **48**, to demonstrate the positive cooperative binding affinity for several anions, such as NO_3^- , Br^- and I^- , in the presence of two equivalents of sodium cations.¹¹⁹ Beer and co-workers have synthesised a tripodal tris(amido benzo-15-crown-5), **49**. In the presence of one equivalent of sodium picrate the receptor shows enhanced anion binding for Cl^- , I^- and ReO_4^- ions. Receptor **49** was shown to efficiently extract NaTcO_4 (sodium pertechnetate) under conditions designed to simulate aqueous waste solutions containing this radioactive waste material.¹²⁰

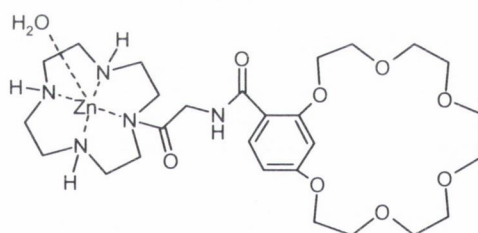


48



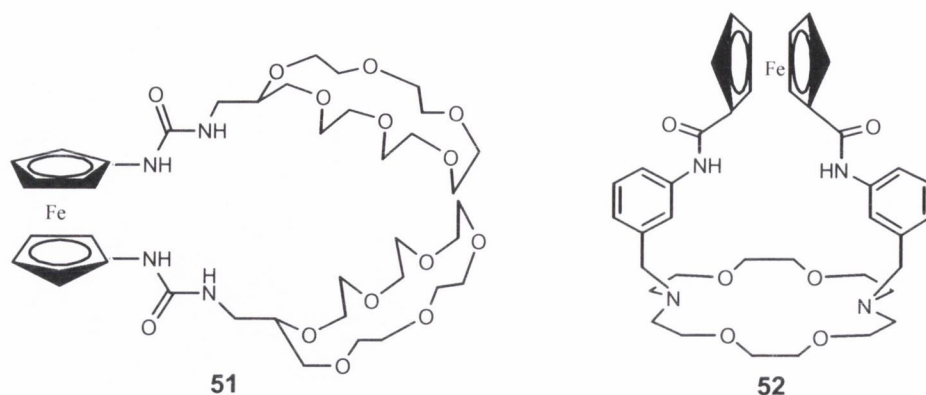
49

Making use of a bigger crown ether moiety, benzo-19-crown-6, Gunning reported a synthetic hetero-receptor, **50**, which exhibits positive cooperativity for the binding of phosphate ion pairs in an aqueous environment, under physiological conditions.¹²¹ The ligand was tested with XH_2PO_4^- , where X was either Na^+ , K^+ or Li^+ . The experimental results confirm that the KH_2PO_4 species is more tightly bound, exhibiting higher binding constants.

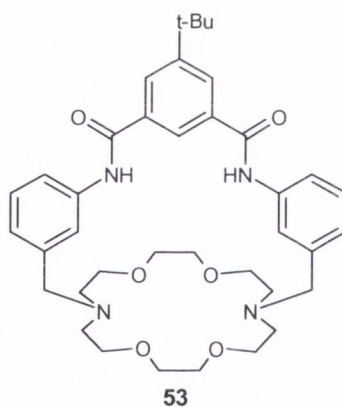


50

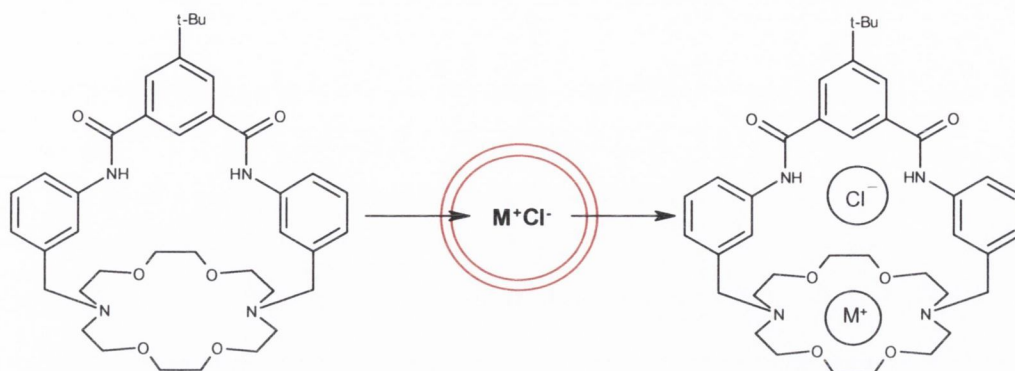
The research has been further extended to ferrocene based receptors. Beer and co-workers reported a receptor that binds alkali metal cations at the lower rim of the calix[4]arene moieties while, the anion binds the amide cleft of the ferrocene unit.¹²² More recent examples are for instance receptors **51**¹²³ and **52**¹²⁴. The former receptor was designed by combining the redox activity of the ferrocene moiety with both the anion binding ability of the urea group and the crown ether as the alkaline binding site.



Electrochemical responses were observed in the presence of dihydrogenphosphate (H_2PO_4^-) and fluoride (F^-) anions. Potassium cations were only detected in the presence of H_2PO_4^- anions. Receptor **52**, based on a diaza crown ether as the cationic binding site, covalently linked to an amido-ferrocene as the anion binding unit, was found to be selective for bromide ion in the presence of sodium cation in 5% $\text{CD}_3\text{CN}/\text{CHCl}_3$ mixture. A similar neutral receptor had already been reported by Smith and co-workers, **53**, which shows the ability to bind sodium and potassium chloride as a contact ion-pair leading to an effective transport of either salt across vesicle membranes.^{125,126}

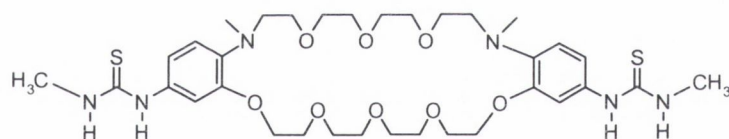


Chloride efflux from unilamellar vesicles was monitored using a chloride selective electrode. Mechanistic studies indicate that the facilitated chloride efflux is due to the uncomplexed macrobicycle receptor-transporter, **53**, diffusing into the vesicle and the complexed transporter-salt diffusing out, **Scheme 1.6.2**.



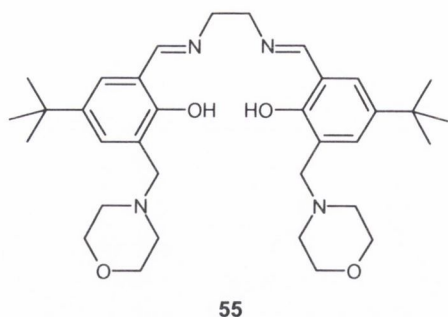
Scheme 1.6.2: Proposed mechanistic pathway for the facilitated Cl^- efflux from vesicles, mediated by transporter **53**.¹²⁶

By attaching two thiourea groups to dibenzo-diaza-30-crown-10, Kubo and co-workers have designed an ion-pair receptor, **54**.¹²⁷ The addition of potassium ions causes the crown ether to wrap around the metal, bringing in this way the two thiourea groups closer together forming a binding site for oxoanions such as $(\text{PhO})_2\text{P}(\text{O})\text{O}^-$. In fact, the binding affinity of the receptor for the phosphate ions, at the two thiourea units, was enhanced by the presence of K^+ in acetonitrile- d_3 .

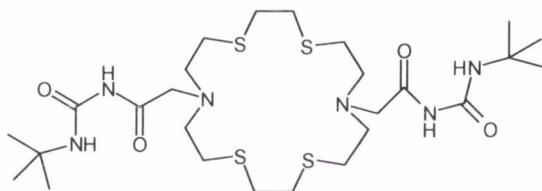


54

With regards to ditopic receptors for transition metal salts, compounds such as **55**¹²⁸ and **56**¹²⁹ have been reported. The later was achieved by linking azathioether macrocycles to urea groups. A series of receptors based on compound **55** were synthesised by Tasker and co-workers¹²⁸. The complexation of a transition metal, such as $\text{Cu}(\text{II})$ or $\text{Ni}(\text{II})$, to the salen-based recognition pocket results in the transference of the phenolic protons to the amine groups of the morpholine moieties, creating as a result a binding site for oxo-anions by bringing the two groups into proximity.



55

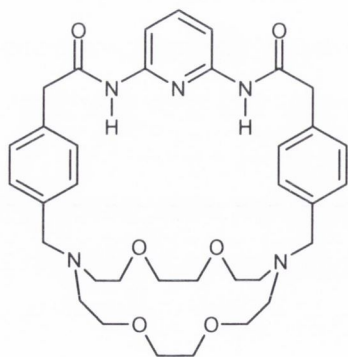


56

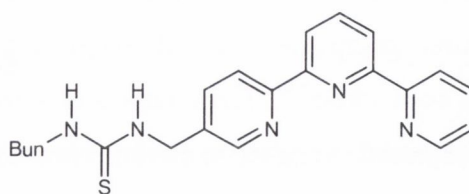
Analysis by X-ray diffraction of the complex **55**.NiSO₄ revealed the sulphate to be bound to the quaternary amines *via* hydrogen bonds. Electrostatic interactions with the salen-bound Ni²⁺ cation also contribute to binding. The researchers demonstrated the ability of this receptor to extract CuSO₄ into chloroform from an aqueous solution of CuSO₄ at pH 3.8.

Another important aspect of simultaneous anion and cation binding is the recognition of organic ion-pairs, since at physiological pH amino acids exist as zwitterions. Kilburn and co-workers synthesised receptor **57**, structurally related to receptor **53**, which was shown to take out mono-potassium salts of several dicarboxylic acids from water into CDCl₃.¹³⁰

The combination of pyridyl fragments and urea or thiourea residues enables the simultaneous binding of transition metal cations and dicarboxylic acidic anions. For example, upon formation of a Ru(II) complex between two terpyridyl fragments of compound **58**, the arrangement in space of the thiourea residues enables the system to selectively extract glutarate anions.¹³¹

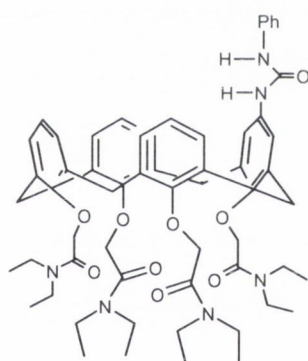


57

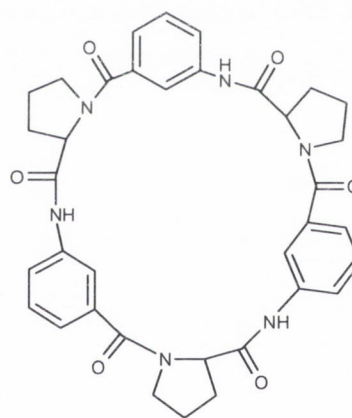


58

Schmidtchen covalently linked triaza-18-crown-6 with a positively charged polyammonium macrocycle to give a receptor able to efficiently bind zwitterionic compounds such as γ -amino butyric acid.¹³² Sessler and co-workers have also reported several ditopic receptors for the transport of aromatic α -amino acids making use of protonated sapphyrins.¹³³ These protonated sapphyrins have also been used as building blocks for the synthesis of receptors for polyanions.^{134,135} Yet another approach for carboxylate recognition was described by Ungaro and co-workers through the synthesis of a calix[4]arene based system, **59**.¹³⁶ The binding of Na^+ by four amide groups on the lower rim of the calix was found to increase the binding of carboxylate anions, such as benzoate, propionate and isobutyrate. The authors based their explanation for this effect on the fact that Na^+ complexation rigidifies the calixarene apolar cavity and induces an electron-withdrawing effect on the upper rim thiourea moiety. As a consequence, the hydrogen ability of the thiourea NH groups is enhanced, thus increasing carboxylate anion recognition.



59



60

An alternative method for the development of heteroditopic receptors employing cyclic peptides has been proposed by Kubik and Goddard.¹³⁷ These authors have shown that the cyclic peptide **60** can be used to bind ammonium iodide salts with positive cooperativity. The receptor was found to adopt a conformation similar to the conical conformation of the calixarenes and, similarly, bind cations through cation- π interactions, while complexing the iodide anion *via* hydrogen bonding to the peptide NH groups.

1.7. Conclusion

In the first part of this chapter, the purpose was to highlight the field of anion sensing, based on optical chemosensors. This involved a brief overview of fluorescence based sensors that have been developed. It has been described how one can take advantage of the photophysical properties of lanthanide based luminescent complexes, and hence employ these systems in the sensing of desirable analytes. Furthermore, advantages of such lanthanide complexes over conventional fluorescent systems have been highlighted.

In the second part, this chapter highlighted the recognition of both cations and anions by using heteroditopic receptors. This involved a review of the synthetic heteroditopic receptors reported in the literature. Their mode of function, as well their relevance on the detection and extraction of toxic ions from aqueous environments and use as artificial carriers and channels for the transport of inorganic and organic salts across membranes has been described.

The main focus of this thesis will be the synthesis and physical studies of chemosensors for anion recognition, as well as the synthesis and binding evaluation of a novel heteroditopic receptor. *Chapter 2* will detail the design and synthesis of a novel lanthanide luminescent system for the detection of anions. The synthesis of cyclen based Tb(III) and Eu(III) diaryl urea complexes and their photophysical properties are described. Furthermore, the ability of the Tb(III) complex to function as a sensor for anions is demonstrated. In order to further understand the binding processes involved in the recognition process between the lanthanide complex and anionic species, *Chapter 3* describes the synthesis of three simple amido urea receptors and evaluates their binding interactions with anions. *Chapter 4* deals with the design and synthesis of a novel heteroditopic receptor. Its ability to function as a fluorescent sensor for chloride will be demonstrated. The binding with transition metals such as Cu(II) and Fe(II) will also be discussed. The interaction of such transition metal complexes with anions will be analysed. Finally, *Chapter 5* examines the self-assembly between Eu(III) and the heteroditopic receptor, described in the previous chapter. In addition, evaluation of the lanthanide complex towards binding with anionic species will be reported.

Chapter 2

Cyclen based lanthanide luminescent devices for anion sensing

2.1 Introduction

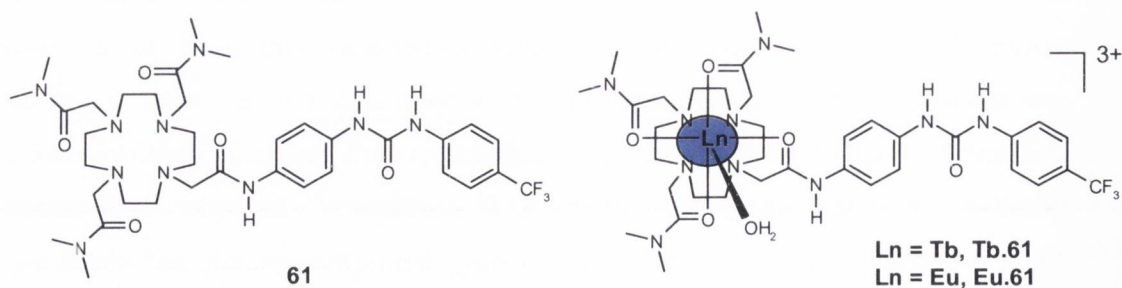
The development of luminescent devices for anion recognition and sensing is currently an area of extreme interest within the research community.^{14,15,20,21,27,29,138} The motivation behind such research is based on the fact that anions play an important role in biology, in medicine, and in the environment.^{9,10} In most cases, anion recognition has been accomplished by the use of either charge neutral or positively charged receptors. Charge neutral receptors are usually designed by using hydrogen bond donors groups such as amides,²⁴ urea and thioureas, among others.¹³⁹⁻¹⁴¹ In contrast, positively charged receptors often consist of guanidinium derivatives,³² ammonium centers,³⁴ or metal coordination complexes.^{142,143} Often these systems employ fluorescence as the mode of detection. Nevertheless, due to their short lifetimes (in the nanosecond range) fluorescence based systems can be affected by autofluorescence and light scattering, from surrounding biological environments, constituting a major drawback when working *in vivo*.¹⁴⁴ The need to overcome such problem has led to the development of metal based luminescent chemosensors that possess long-lived excited states.⁸⁶ Amongst such systems are various lanthanide luminescent complexes.^{52,60,145} The use of lanthanide luminescence for sensing purposes will be discussed below. This will be followed by the design and synthesis of novel urea based cyclen lanthanide complexes for anion recognition.

2.1.1 Lanthanide luminescent sensors

The large positive charge of the lanthanide ions, their strong electrostatic bonding nature and long-lived excited states, allied with the sensitivity of their emission spectra to the coordination environment, make lanthanide ions ideal sensors for the detection of anions. Nevertheless, there are also some drawbacks that need to be taken into consideration when using lanthanide ions. Free lanthanide ions are toxic due to their size similarity to Ca(II).⁷⁶ Furthermore, protic solvents quench lanthanide luminescence by non-radiative vibrational decay through the O-H oscillators.⁵⁷ In order to overcome such drawbacks and use these ions for *in vivo* sensing, thermodynamically and kinetically stable complexes of these ions are required.^{75,77,78} As extensively detailed in Chapter 1, this can be achieved by incorporating these ions into organic ligands. The idea behind the chelation with such ligands is to build a pre-organised system bearing several donor atoms,

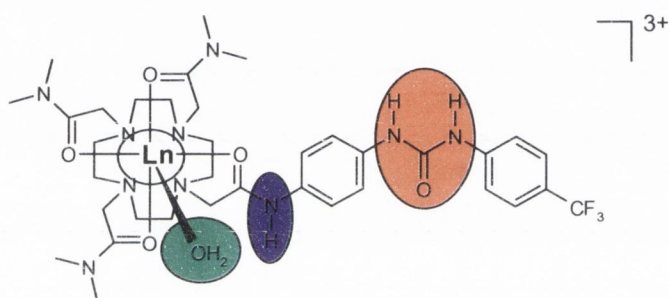
generating suitable interactions with the metal ion which increases their stability¹⁴⁶ as well as providing shielding from solvent molecules.¹⁴⁷ Cyclen (1,4,7,10-tetraazacyclododecane) derivatives are commonly used as they are known to form kinetically and thermodynamically stable complexes with lanthanide ions.^{67,148-151} Another drawback associated with lanthanide ions is their low absorption coefficients, resulting in inefficient direct excitation.^{55,81,152} This problem can be solved by means of indirect excitation.⁶⁷ The excited state of lanthanide ions can be populated by energy transfer from the triplet excited state of an organic antenna or a chromophore, resulting in sensitised lanthanide luminescence.⁸¹ This can be achieved either by direct coordination of the antenna to the lanthanide ion, or by the covalent attachment of the antenna to the aforementioned organic ligand framework. A very attractive aspect of luminescent lanthanide chemosensors is that by incorporating an appropriate recognition moiety into the antenna, it is possible to achieve sensing through selective modulation of the lanthanide luminescence. Such modulation is caused by the binding of the analyte to the receptor/antenna, which subsequently alters the efficiency of the sensitisation process.⁸⁶

Inspired by the above, the aim of this project was to design and develop novel chemosensors able to sense anionic species. In order to accomplish this, ligand **61** and the corresponding Tb(III) and Eu(III) complexes, **Tb.61** and **Eu.61**, were designed. As required, the cyclen derivative **61** is able to fulfil the high coordination requirements of these metal ions, by the four nitrogen donor atoms of the ring and four additional oxygen donor atoms on the pendant arms, and hence give rise to very stable lanthanide complexes. The remaining coordination site will be occupied by a solvent molecule.



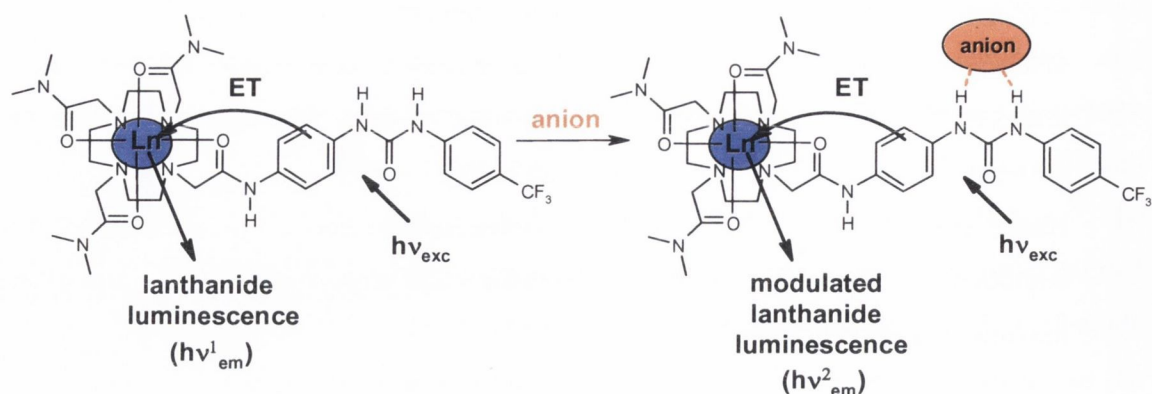
The design of **Ln.61** endowed these systems with three possible binding sites for anion recognition. As depicted in **Scheme 2.1.1**, the binding sites are circled in different colours

for easy visualisation. Urea (orange) and amide (purple) are recognised as being good hydrogen bond donors and hence good receptors for anions,^{21,24,26,140} while the displacement of labile solvent molecules (green) by anionic species has been successfully achieved.^{86,101,153-156} However, the combination of these binding sites within the same molecule, with the aim of achieving anion recognition has not been demonstrated to date. Hence, the objective of this project was to generate a luminescent anion sensor, using the combination of these multiple binding sites for anion recognition, with the aim of achieving maximum anion binding affinity.



Scheme 2.1.1: Proposed anion binding sites within **Ln.61**. Orange ellipse represents the hydrogen bonding between the urea moiety and the anion. The purple ellipse corresponds to the possible interaction with the amide moiety. Finally, the green circle symbolizes the direct interaction with the lanthanide ion, by replacement of the solvent molecule.

As previously stated lanthanide $f-f$ transitions are Laporte-forbidden, which make direct excitation of these metal ions difficult.⁶⁷ So, the design of **Ln.61** envisaged indirect excitation of the lanthanide ion by the covalently attached antenna (**Scheme 2.1.2**). The diaryl-urea in **Ln.61** plays a dual role, functioning both as an anion recognition moiety, and as the sensitising antenna. Hence, any perturbation on the antenna, such as anion recognition, shall lead to the modulation of the sensitisation process with concomitant changes in the lanthanide luminescence ($h\nu_{em}^2$), **Scheme 2.1.2**. In addition to the recognition through the urea moiety depicted in **Scheme 2.1.2**, binding through the amide or directly to the metal centre are expected to further modulate the lanthanide luminescence.

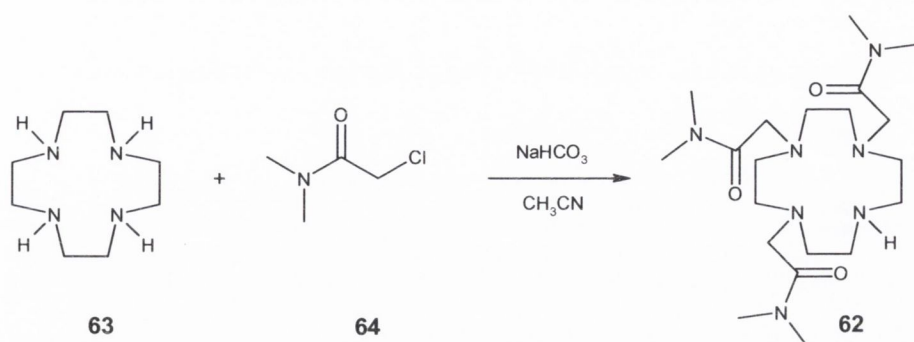


Scheme 2.1.2: Schematic representation of lanthanide luminescence modulation, upon anion recognition, through the urea moiety. The metal bound solvent molecule was removed in order to simplify the scheme.

The synthesis and characterisation of ligand **61** and the corresponding Tb(III) and Eu(III) complexes, **Tb.61** and **Eu.61**, will be presented in the following sections. Furthermore, the ability of these complexes to function as anion sensing devices will be investigated.

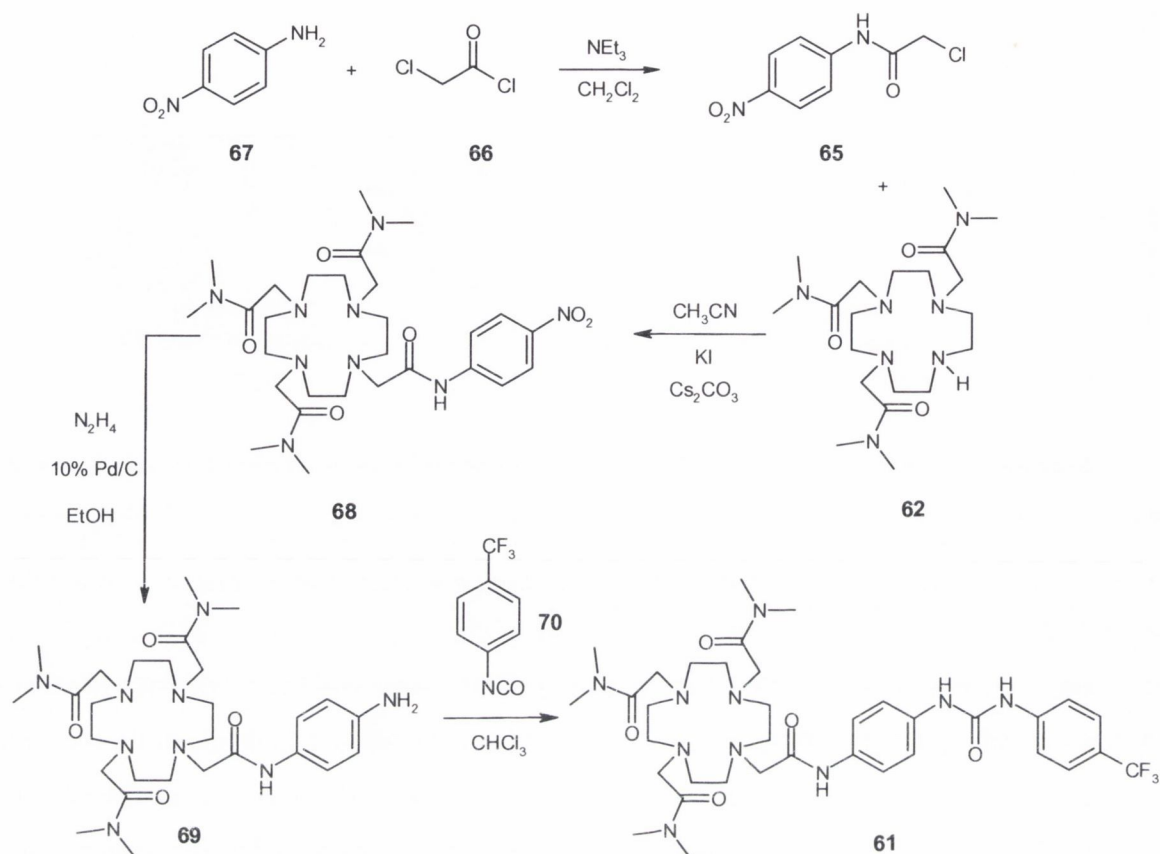
2.2 Synthesis and characterisation of ligand **61**

The first approach to the synthesis of host **61** was to synthesize the tri-arm acetamide cyclen based compound **62**, as depicted in **Scheme 2.2**. Synthesis of this compound involved the *N*-alkylation of cyclen, **63**, with three pendant amide arms. The synthesis was successfully achieved by reacting three equivalents of the α -chloroamide, 2-chloro-*N,N*-dimethyl acetamide, **64**, with cyclen in dry CH_3CN at 65°C for three days, in the presence of NaHCO_3 (**Scheme 2.2**).¹⁵⁷ The desired product was then purified by alumina column chromatography using a gradient elution (CH_2Cl_2 to 30% CH_3OH). Upon drying the resulting residue under vacuum, off white foam was obtained in 69% yield.



Scheme 2.2 Synthetic route of the acetamide tri-arm cyclen (**62**), by direct alkylation with three acetamide arms

The synthesis of host **61** is outlined in **Scheme 2.2.1**. The synthesis of the chloro *N*-(nitro-phenyl) acetamide, **65**, was achieved in one step by reacting chloroacetyl chloride, **66**, with *p*-nitroaniline, **67**, in the presence of triethylamine (NEt₃) at low temperature (-10°C) in dry CH₂Cl₂, followed by extraction using 0.1 M HCl. Compound **68** was obtained in a 74 % yield, by heating **65** and **62** under reflux in dry CH₃CN, in the presence of Cs₂CO₃ and KI. After filtration and solvent removal under reduced pressure, the nitro derivative, **68**, was then purified by column chromatography on alumina, using a gradient elution (CH₂Cl₂ to 20% CH₃OH). This was followed by reduction of the nitro group to the corresponding amine, **69**, using N₂H₄·H₂O, in the presence of 10% Pd/C catalyst in ethanol at 90°C. Finally, the amino derivative was reacted overnight with trifluoro-*p*-tolyl isocyanate, **70**, in chloroform at room temperature. The solvent was removed under reduced pressure to yield a pale brown solid, which was then purified by alumina column chromatography under gradient elution conditions (CH₂Cl₂ to 20% CH₃OH) to give the desired product as a yellow solid in 67 % yield.

Scheme 2.2.1 Synthetic route of ligand **61**

The product was characterised using conventional methods, such as NMR and IR spectroscopy, ESMS, accurate mass and elemental analysis. The ^1H -NMR spectrum of **61** (Figure 2.2.1) showed the presence of the three N-H broad singlets at 10.07, 9.94 and 9.48 ppm respectively, as well as the expected resonances for the aromatic protons. The CH_3 (18H) and CH_2 (8H) protons of the arms, as well as the cyclen CH_2 (16H) protons were associated with signals occurring in the broad area between 3.0 - 2.0 ppm with total integration of 42. The ^{13}C -NMR spectrum showed the presence of the four quaternary aromatic resonances at 153.08 ppm, 143.30 ppm, 135.16 ppm, and 133.13 ppm respectively, as well as the four aromatic CH peaks. The presence of the CF_3 group was also observed in the ^{19}F spectrum, showing the typical resonance for this group at -61.88 ppm. ESMS analysis showed the presence of a single peak at 763.42, corresponding to the $\text{M} + \text{H}$ species.

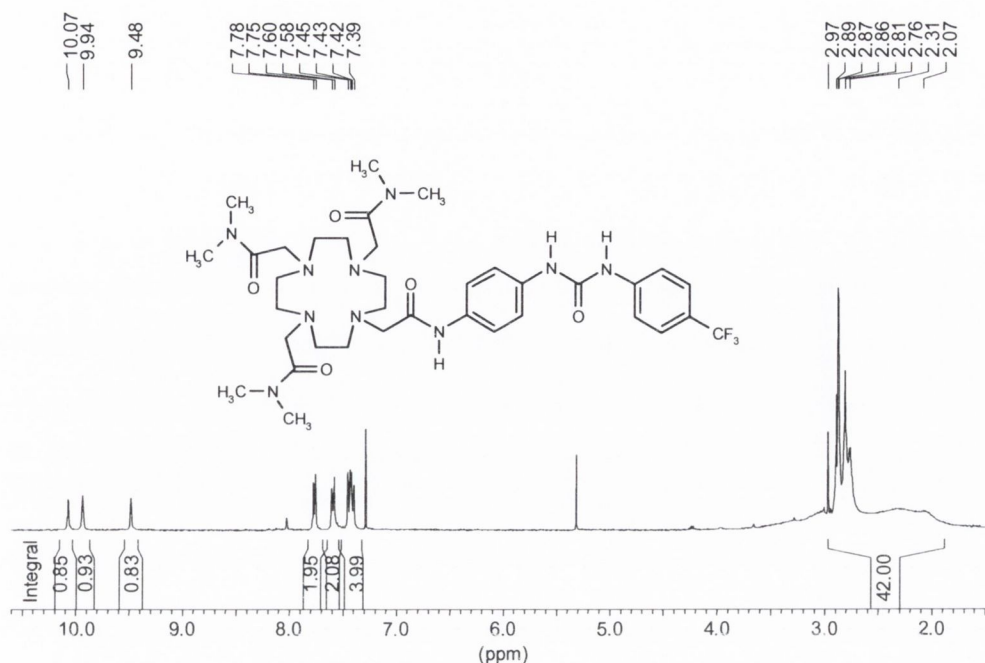
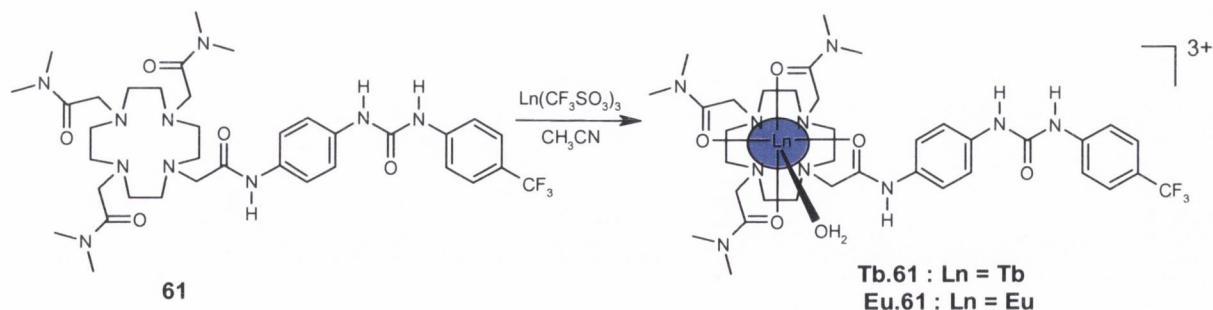


Figure 2.2.1 $^1\text{H-NMR}$ of the ligand **61** (400 MHz, CDCl_3)

2.3 Synthesis and characterisation of the lanthanide complexes of **61**, Ln.**61**

The synthesis of the metal complexes **Tb.61** and **Eu.61** was achieved by refluxing ligand **61** with equivalent amounts of Tb(III) and Eu(III) respectively, as their triflate salts ($(\text{CF}_3\text{SO}_3)_3$), in CH_3CN under an inert atmosphere (Scheme 2.3). After solvent reduction, these solutions were dropped into stirring dry diethyl ether which resulted in the precipitation of hygroscopic pale beige solids in a 74 % and 68 % yield for **Tb.61** and **Eu.61**, respectively. These compounds were characterised using the aforementioned methods.



Scheme 2.3: Synthesis of **Tb.61** and **Eu.61** complexes by reacting **61** with equivalent amounts of Ln(III) triflates, Tb(III)(CF_3SO_3)₃ and Eu(III)(CF_3SO_3)₃ respectively.

Lanthanides are known to be NMR shift reagents. Protons in close proximity to the paramagnetic metal centre will experience an extra magnetic field, resulting in the shift of their resonances in the NMR spectrum. Lanthanide complexes also give rise to fast relaxation times, which leads to peak broadening.^{81,158} These are characteristics that can be employed to indicate ion complexation.

The $^1\text{H-NMR}$ (400 MHz, CD_3OD) spectra of both complexes showed the presence of the paramagnetic lanthanide ions, as evident from the broad resonances appearing over a large ppm range, which are indicative of the shifted axial and equatorial protons of the cyclen ring due to the presence of the Ln(III) ion. This was clear evidence that complexation had occurred. In **Figure 2.3** is depicted the $^1\text{H-NMR}$ (400 MHz, CD_3OD) spectrum for **Tb.61**. The broad resonances appearing over a large ppm range (from 160 ppm to -130 ppm) are clearly shown in the the total $^1\text{H-NMR}$ spectrum obtained for **Tb.61**, as depicted in the insert in **Figure 2.3**.

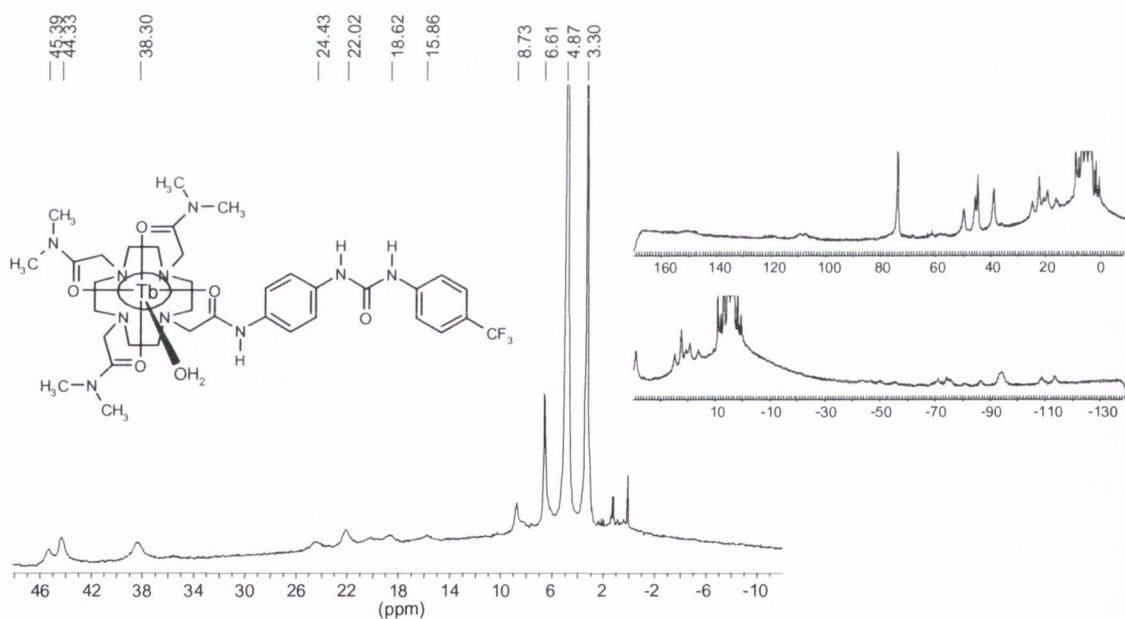


Figure 2.3: Partial $^1\text{H-NMR}$ (400 MHz, CD_3OD) of **Tb.61** complex, showing the broadening of the peaks and large shifts due to the presence of the paramagnetic metal centre. Insert: The total $^1\text{H-NMR}$ spectrum of **Tb.61**, showing broad peaks appearing over a large ppm range (160 ppm to -130 ppm).

The ESMS proved very useful in the characterisation of the complexes. The spectra, for both Tb(III) and Eu(III) complexes, revealed a number of peaks, corresponding to the m/z

of the complex with differing numbers of triflate counter ions. All of the peaks present were associated with the desired complexes, as both the Tb(III) and Eu(III) characteristic isotopic distribution patterns were observed for all of them. The peaks depicted in **Figure 2.3.1** and **Figure 2.3.2** correspond to the $M/2$ and $[M + \text{triflate}]/2$ species for the **Tb.61** and **Eu.61** complexes, respectively.

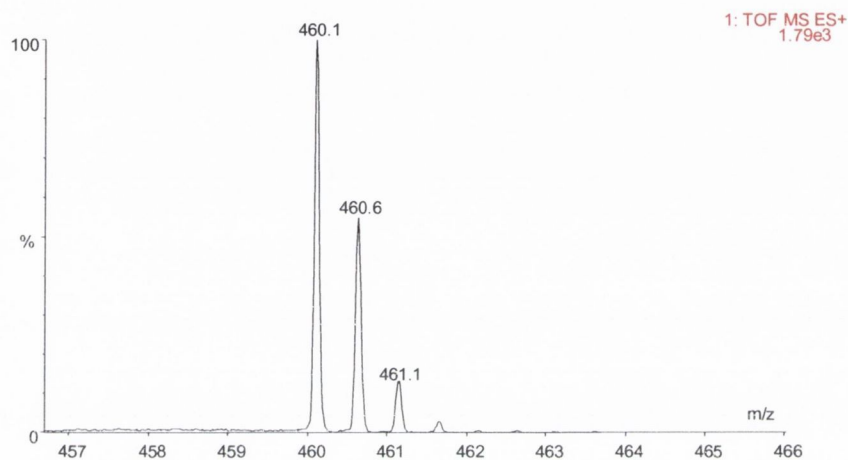


Figure 2.3.1 ES Mass Spectrum of **Tb.61** showing the terbium characteristic isotopic distribution pattern. The peak shown corresponds to the $M/2$ species.

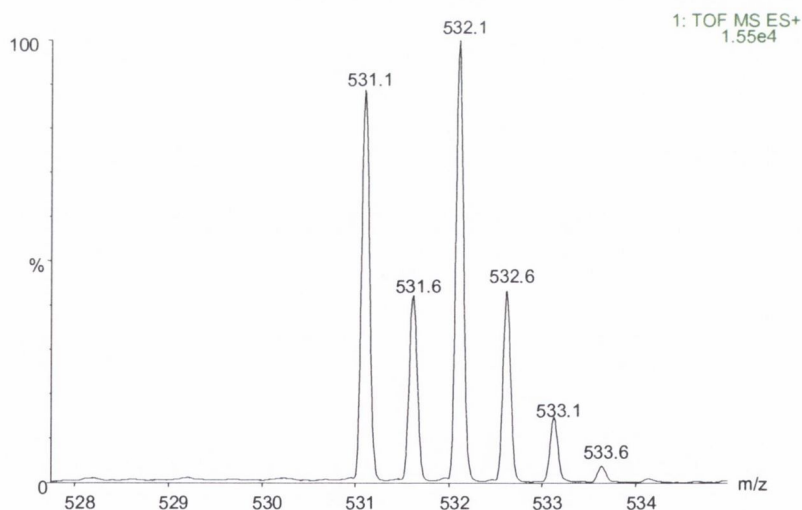


Figure 2.3.2 ES Mass Spectrum of **Eu.61** showing the europium characteristic isotopic distribution pattern. The peak shown corresponds to the $[M + \text{triflate}]/2$ species.

Infrared spectroscopy (IR) is another very useful tool in determining whether the successful complexation with the metal ion had occurred.^{159,160} In the present case, the

carbonyl bonds of ligand **2** are expected to be involved in the coordination process, by donating electron density to the metal centre, resulting in the change of the IR stretching frequency. This was indeed found to be the case, as upon Tb(III) and Eu(III) complexation the IR stretching frequency of the carbonyl band in **61** decrease from 1646 cm⁻¹ to 1619 cm⁻¹ and 1618 cm⁻¹ for **Tb.61** and **Eu.61**, respectively (Table 2.3).

Compound	Carbonyl stretching (cm ⁻¹)
Ligand 61	1646
Tb.61	1619
Eu.61	1618

Table 2.3.: IR carbonyl stretching frequencies observed for ligand **61** and corresponding Ln(III) complexes (**Tb.61** and **Eu.61**).

2.3.1 Determination of metal bound water molecules

As stated before, ligand **61** can provide eight coordination sites for the lanthanide ions. Tb(III) and Eu(III) generally possess a coordination number of nine in such tetrasubstituted cyclen complexes, with the ninth site being occupied by a solvent molecule.^{67,86} Hence, both complexes **Tb.61** and **Eu.61** were expected to possess one such metal bound water molecule. In order to determine the number of these bound water molecules, the hydration number (q) was determined by measuring the excited state lifetimes (τ) of the complexes in H₂O ($\tau_{\text{H}_2\text{O}}$) and D₂O ($\tau_{\text{D}_2\text{O}}$), respectively. This was achieved by direct excitation of the lanthanide ions at 366 and 395 nm for Tb(III) and Eu(III), respectively. From the measured values, q was determined by using **Equation 1** or **Equation 2**, introduced in Chapter 1, for **Tb.61** or **Eu.61**, respectively.

$$q^{\text{Tb(III)}} = 5 [(1/\tau_{\text{H}_2\text{O}} - 1/\tau_{\text{D}_2\text{O}}) - 0.06] \quad \text{Equation 1}$$

$$q^{\text{Eu(III)}} = 1.2 [(1/\tau_{\text{H}_2\text{O}} - 1/\tau_{\text{D}_2\text{O}}) - 0.25 - 0.075x] \quad \text{Equation 2}$$

In order to determine the number of these solvent molecules, the hydration state, q , was determined by measuring the excited state lifetimes (τ) of both complexes in H₂O ($\tau_{\text{H}_2\text{O}}$) and D₂O ($\tau_{\text{D}_2\text{O}}$), by direct excitation of Tb(III) and Eu(III) at 366 nm and 395 nm, respectively. The luminescence decays were found to be single exponential for both the Tb(III) and Eu(III) complexes. The measured lifetimes, as well as the determined q values

are summarized in **Table 2.3.1**. In the case of **Tb.61** the lifetime in H₂O ($\tau_{\text{H}_2\text{O}}$) and D₂O ($\tau_{\text{D}_2\text{O}}$) was measured to be 1.362 ms and 2.044 ms, respectively. Using **Equation 1** a q value of 0.93 was determined, indicating the presence of a single metal bound water molecule. **Eu.61**, gave rise to shorter lifetimes in both solvents. The lifetime in H₂O ($\tau_{\text{H}_2\text{O}}$) and D₂O ($\tau_{\text{D}_2\text{O}}$) was measured to be 0.253 ms and 0.399 ms, respectively. Using **Equation 2** a q value of 1.17 was determined, indicating that **Eu.61** also possess a single metal bound water molecule. As can be expected the complexes possess shorter lifetimes in H₂O than in D₂O (**Table 2.3.1**). This is attributed to quenching of the excited state of the lanthanide metal ion by the O-H oscillators.⁶⁸ The presence of such oscillators provides an efficient pathway for non-radiative deactivation *via* energy transfer to the vibrational states of the O-H oscillators. This deactivation pathway becomes much less efficient upon replacement of O-H by O-D oscillators, hence higher lifetimes are observed in D₂O.⁵⁷ The results of the lifetime analysis confirms, as predicted earlier, the presence of one bound water molecule in each one of the complexes, **Tb.61** and **Eu.61**.

Complex	$\tau_{\text{H}_2\text{O}}(\text{ms})$	$\tau_{\text{D}_2\text{O}}(\text{ms})$	$q (\pm 0.5)$
Tb.61	1.362	2.044	0.93
Eu.61	0.253	0.399	1.17

Table 2.3.1: Measured lifetimes and determined q values for **Tb.61** and **Eu.61** showing the presence of one metal bound water molecule in both complexes.

After detailed characterisation both complexes were considered to be successfully synthesised in high purity. The following sections will focus on the photophysical properties of these complexes. Detailed studies performed in order to evaluate the complexes ability to function as luminescent sensing devices for anionic species will also be presented and discussed within the following sections of this chapter.

2.4 Photophysical properties of Tb.61 and Eu.61 complexes

The design of the lanthanide based complexes, **Tb.61** and **Eu.61**, envisaged indirect excitation of the Tb(III) and Eu(III) ions by a covalently attached diaryl-urea antenna. This antenna is expected to be able to transfer its energy, *via* the triplet excited state, to the excited states of Tb(III) and Eu(III), ⁵D₄ and ⁵D₀ respectively. The spectra of both **Tb.61**

and **Eu.61** were recorded in CH_3CN by exciting the solutions at 280 nm (wavelength of maximum absorbance of the antenna, λ_{max}). The obtained spectra, **Figure 2.4**, shows the characteristic emission bands for the terbium (green) and europium (red) ions, demonstrating that such sensitisation is possible. Nevertheless, the Eu(III) complex, **Eu.61**, showed a much weaker emission intensity than **Tb.61**, implying that the antenna is not able to populate the Eu(III) excited state efficiently. This is most likely to occur due to quenching of the Eu(III) excited state through efficient non-radiative deactivation pathways *via* energy transfer. The fact that, **Eu.61** possesses such low lifetimes when compared to **Tb.61** (0.253 ms and 1.362 ms respectively) is a clear indication that the quenching processes are more efficient for the former metal complex.

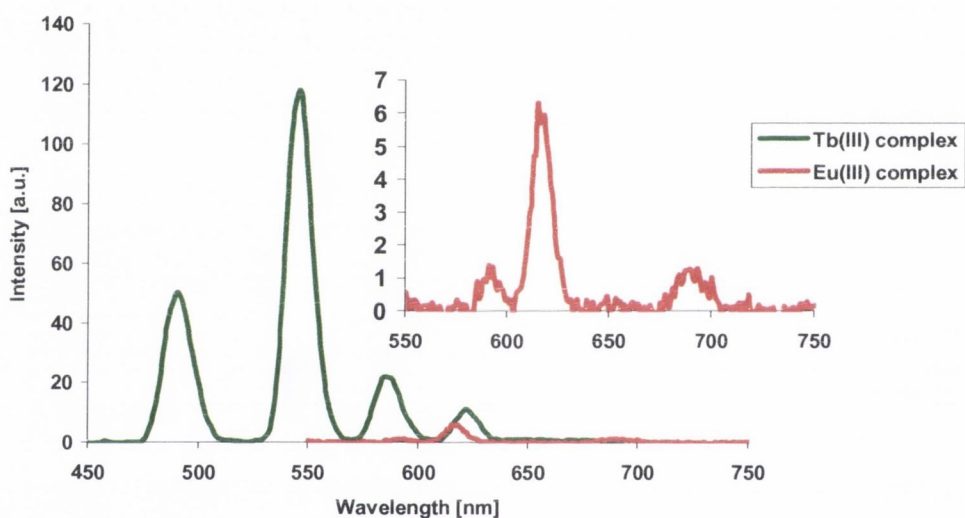


Figure 2.4: Lanthanide luminescence spectra of **Tb.61** (green) and **Eu.61** (red) in CH_3CN , when using an excitation wavelength of 280 nm. Insert shows the weaker sensitisation of the europium metal ion.

Due to the less efficient sensitisation of europium complex, **Eu.61**, by the covalently attached antenna, no further studies were performed on this complex. Therefore, the following sections will focus exclusively on the studies carried out on **Tb.61** in the presence of anions.

2.5 Photophysical studies of **Tb.61** towards the binding with anions

The formation and stability of the binding between anions (G) and **Tb.61** (L) was investigated by UV-Visible and luminescence spectroscopy. This was done by carrying out titrations on a stock solution of **Tb.61** (4 μM) with incremental small additions of known concentration of the different anion solutions, as their tetrabutylammonium salts (TBA^+), in CH_3CN . Protic solvents, such as H_2O , can strongly compete with anion binding sites, resulting in very weak association constants in these solvents. Therefore, after preliminary evaluation using various solvents, CH_3CN was selected as the solvent to use. The anions studied included acetate (CH_3COO^-), dihydrogenphosphate (H_2PO_4^-), dihydrogenpyrophosphate ($\text{H}_2\text{P}_2\text{O}_7^{2-}$), fluoride (F^-) and chloride (Cl^-).

The binding constants were determined by fitting the data, obtained from the changes in the UV-Visible and luminescence measurements, using the non-linear least-squares regression program, SPECFIT (Appendix A0).^{161,162} Using this method, different stoichiometries between anion and **Tb.61** as well as their binding constants ($\log K$) can be evaluated. The program also takes into account the ability of the theoretical data to fit well with the experimental data, in the form of the sum of the squared standard deviation (SSD). However, this program is unable to accurately fit the data whenever the binding constant $\geq 10^7 \text{ dm}^3 \text{ mol}^{-1}$, since, at equilibrium, the ratio of the anion-bound complex concentration to those of its precursors becomes very large, which can lead to a significant error. Moreover, for species to be accurately fitted with SPECFIT, they need to be present in concentrations between 10% and 90% of formation. Outside this range of concentrations, large errors are often associated with the calculated $\log K$ values.

The absorption spectrum of **Tb.61** exhibits one broad band centred at 280 nm ($\log \epsilon = 4.46$), assigned to the $\pi\text{-}\pi^*$ transitions of the ligand. When exciting the sample at 280 nm, a very weak fluorescence spectrum was observed showing a peak at 304 nm and a broad shoulder at 330 nm. Moreover, four transitions corresponding to the lanthanide emission could also be seen. Using the same excitation wavelength, the phosphorescence emission for the lanthanide ion was also obtained as expected. The spectrum shows four well defined bands at 490 nm, 546 nm, 586 nm, and 622 nm, corresponding to the deactivation of $^5\text{D}_4$, to the ground states, $^7\text{F}_J$ ($J = 6, J = 5, J = 4$ and $J = 3$, respectively).^{58,163,164} The three spectra for **Tb.61** are shown in **Figure 2.5**.

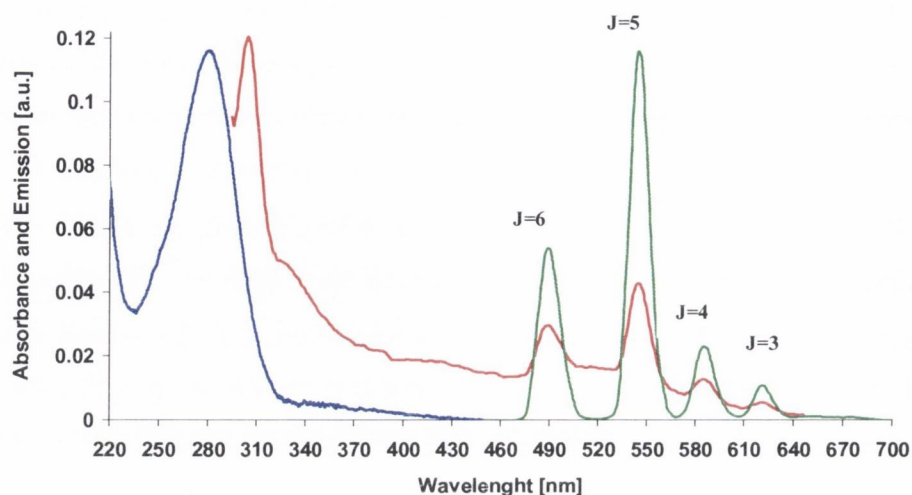


Figure 2.5: Absorption (blue), Fluorescence (red), and Phosphorescence (green) spectra of **Tb.61** in CH_3CN . The fluorescence emission intensity was divided by a factor of 3400 and the phosphorescence emission intensity was divided by a factor of 1400, in order to compare all three spectra in the same figure. The excitation wavelength used for obtaining both the emission spectra was 280 nm.

Upon titration of 10 mL solutions of **Tb.61** ($4 \mu\text{M}$) in CH_3CN with different solutions of the anions mentioned above, dramatic changes were observed on both the absorption and the emission spectra. The observed changes on the UV-Visible absorption, fluorescence, and phosphorescence emission will be discussed in detail in the following sections. With regards to the fluorescence emission the obtained results will also be presented. Nevertheless, the discussion will be somewhat limited once the emission spectra was ‘contaminated’ by the presence of the Tb(III) emission bands occurring at longer wavelength. This factor plays an important role, especially with regards to the determination of the binding constants.

2.5.1 Photophysical studies of Ln.61 towards binding with CH_3COO^-

The interaction between **Tb.61** and CH_3COO^- was investigated through spectrophotometric titration experiments. The changes on the UV-Visible, fluorescence, and lanthanide luminescence were followed. **Figure 2.5.1** shows the family of absorption spectra recorded during the course of the titration. The band centred at 278 nm experienced

an initial small increase in the absorbance, followed by a progressive decrease, while a new band centred at 288 nm followed the opposite behaviour. The lack of a clear isosbestic point suggests the presence of more than two species at equilibrium in solution.¹⁶⁵

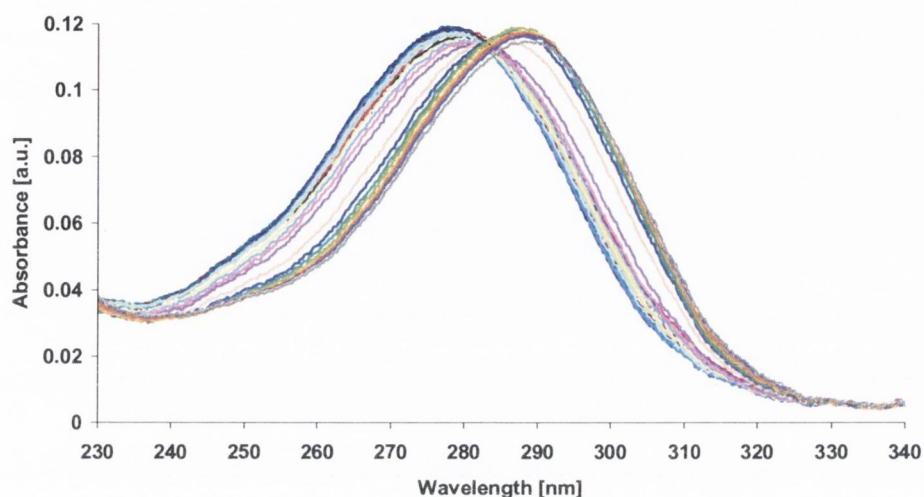


Figure 2.5.1: Absorption spectra showing the changes in absorbance of **Tb.61** ($4 \mu\text{M}$) upon gradual additions of CH_3COO^- ($0 \rightarrow 74.9 \mu\text{M}$) in CH_3CN .

The profile of the absorbance changes at 270 nm and 300 nm versus the number of equivalents of CH_3COO^- added, shown in **Figure 2.5.1.1**, indicates the presence of a possible two step binding process. As can be observed, the first binding occurs up to one equivalent of added anion, corresponding to an increase in absorbance for the band at 278 nm. These changes are ascribed to the formation of the 1:1 (G:H) complex between CH_3COO^- and **Tb.61**. This is then followed by a second CH_3COO^- binding, leading to a decrease in the absorbance for the band at 278 nm (**Figure 2.5.1.1**).

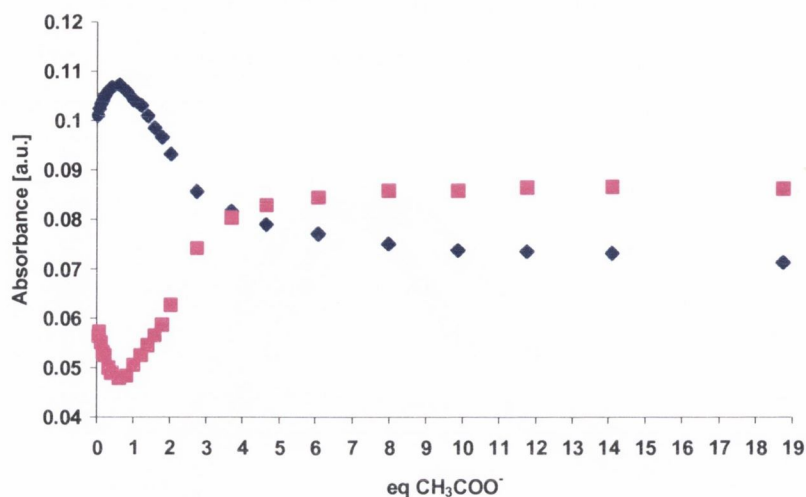


Figure 2.5.1.1: Profile of the absorbance changes at 270 nm (blue) and 300 nm (pink), upon gradual additions of CH_3COO^- ($0 \rightarrow 74.9 \mu\text{M}$) in CH_3CN , versus the number of equivalents of acetate added.

From the changes observed in **Figure 2.5.1**, binding constants for the formation of a 1:1 (G:H) complex, $\log K_{1:1} = 6.27 \pm 0.12$, and for the formation of a 2:1 (G_2 :H) complex, $\log K_{2:1} = 5.84 \pm 0.09$, were determined using the non-linear least squares regression program SPECFIT. The excellent fit to the experimental data, shown in **Figure 2.5.1.2**, is very good evidence that the correct binding model has been used.

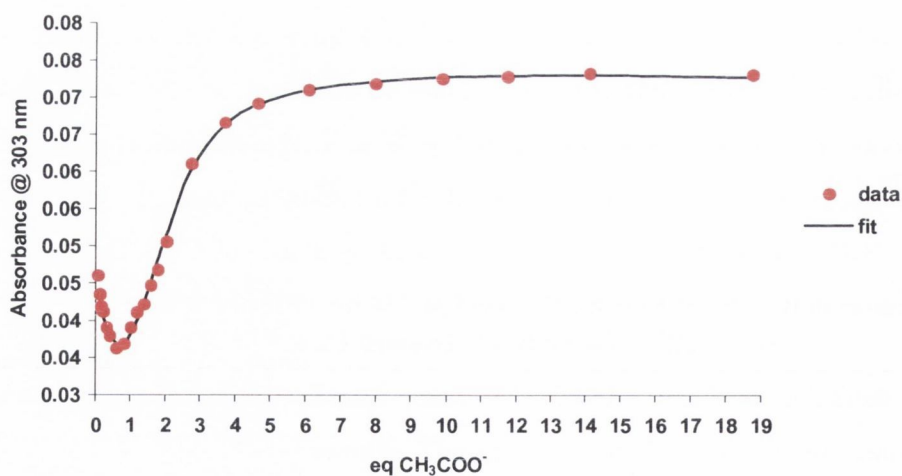


Figure 2.5.1.2: Experimental binding isotherm for the UV-Visible titration of **Tb.61** ($4 \mu\text{M}$) with CH_3COO^- in CH_3CN and corresponding fit using the SPECFIT program.

The diagram of the species present in solution for the titration of **Tb.61** with CH_3COO^- is shown in **Figure 2.5.1.3**. As can be observed, there are two dominant species present in solution upon titration with CH_3COO^- , these being the 1:1 (G:H) complex (green line), reaching a maximum of *ca.* 45% formation upon addition of 1 equivalent of CH_3COO^- , and the 2:1 (G_2 :H) complex (pink line) whose formation tends to *ca.* 100% upon an excess addition of CH_3COO^- .

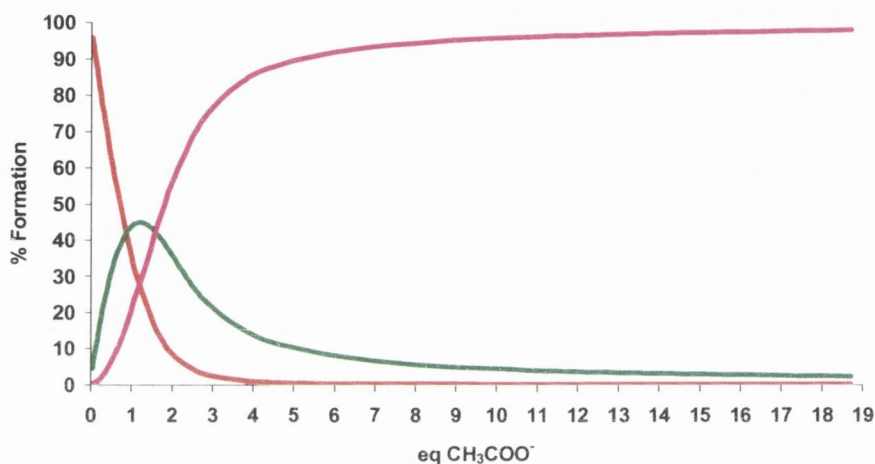


Figure 2.5.1.3: Speciation diagram for the UV-Visible titration of **Tb.61** ($4 \mu\text{M}$) with CH_3COO^- . Red line refers to the free receptor **Tb.61**, the green line to the 1:1 (G:H) complex and the pink line to the 2:1 (G_2 :H) complex.

The changes in fluorescence emission upon titration of **Tb.61** with CH_3COO^- were also recorded after excitation at 280 nm. As shown in **Figure 2.5.1.4** the observed changes correspond mainly to an increase in the emission intensity in the shoulder at 330 nm, due to the complex formation between CH_3COO^- and **Tb.61**. As a consequence of anion coordination, the energy levels of the receptor change, inducing enhancement of the fluorescence emission. Insert in **Figure 2.5.1.4** depicts the profile of the number of equivalents of CH_3COO^- added during the titration, versus the emission intensity at 330 nm.

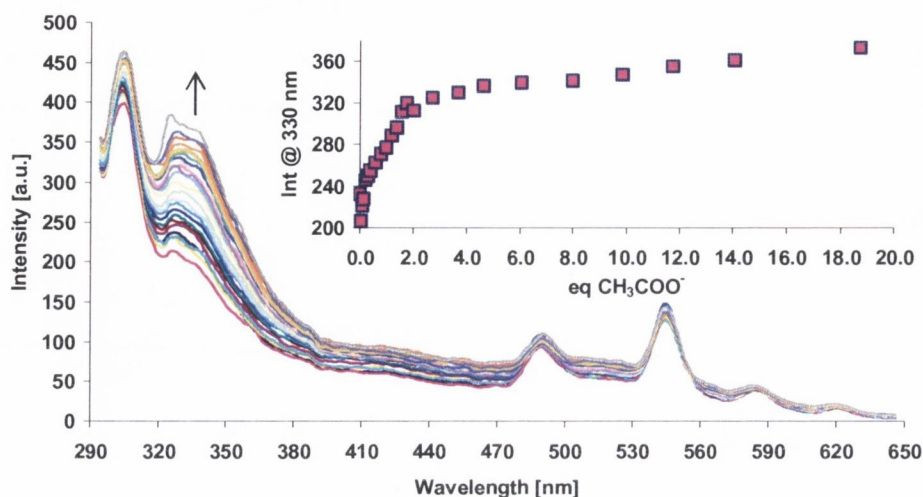


Figure 2.5.14: Fluorescence emission spectra showing the changes in emission intensity of **Tb.61** ($4 \mu\text{M}$) upon gradual additions of CH_3COO^- ($0 \rightarrow 74.9 \mu\text{M}$) in CH_3CN . The excitation wavelength used was 280 nm . Insert: The profile of the emission intensity at 330 nm versus the number of equivalents of CH_3COO^- .

Contrary to what happened in the absorbance, saturation was not reached in this case. This factor allied with the presence of the lanthanide emission bands proved to be problematic when attempting to determine the binding constants. Therefore, the data taken into account for the determination of the binding constants included only the first eight equivalents. By fitting these changes, binding constants for the formation of a 1:1 (G:H) complex, $\log K_{1:1} = 5.78 \pm 0.30$, and for the formation of a 2:1 (G_2 :H) complex, a $\log K_{2:1}$ of 5.11 ± 0.51 , were determined. The experimental binding isotherm and correspondent fit are shown in **Figure 2.5.15**. As can be observed, the fit is not as good as the one shown for the UV-Visible titration earlier. This is mainly due to the poor quality of the fluorescence data. Nevertheless, the binding constants were within acceptable agreement with those obtained for the ground state changes (**Table 2.5.1**). The speciation distribution diagram (insert on **Figure 2.5.15**) also followed the same behaviour as seen earlier, further supporting the formation of the 1:1 and 2:1 interaction between CH_3COO^- and **Tb.61**.

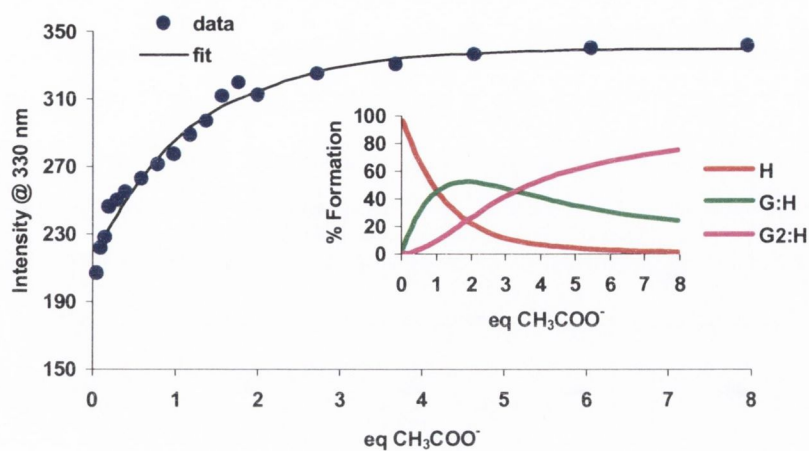


Figure 2.5.1.5: Experimental binding isotherm for the fluorescence titration of **Tb.61** ($4 \mu\text{M}$) with CH_3COO^- in CH_3CN and the corresponding fit using the SPECFIT program. Insert: The speciation distribution diagram.

When exciting the sample at 280 nm , the lanthanide luminescence emission for the titration of **Tb.61** with CH_3COO^- was also followed, as can be seen in **Figure 2.5.1.6**.

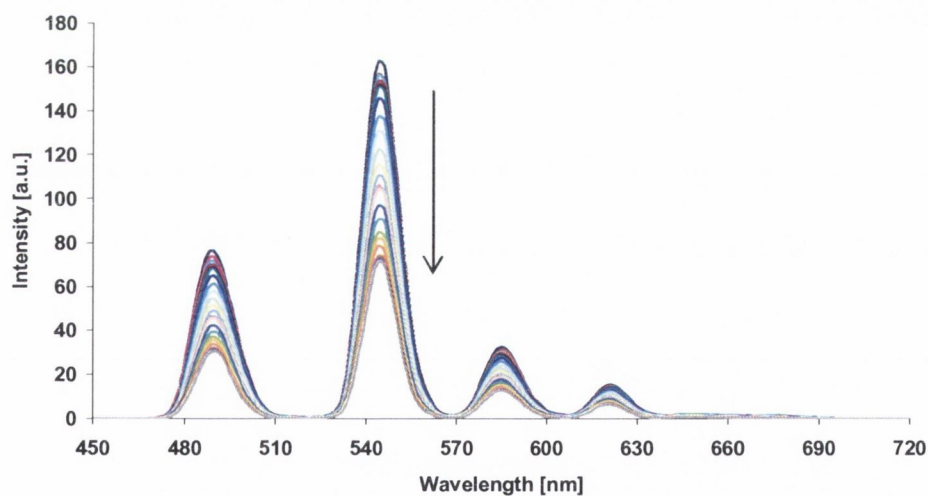


Figure 2.5.1.6: Phosphorescence emission spectra showing the changes in emission intensity of **Tb.61** ($4 \mu\text{M}$) upon gradual additions of CH_3COO^- ($0 - 74.9 \mu\text{M}$) in CH_3CN , when using an excitation wavelength of 280 nm .

Here, the emission intensity decreased by *ca.* 56% upon addition of CH_3COO^- . As explained before, the urea chromophore has a dual function, both as a receptor and an

antenna. In the absence of a guest there is an efficient energy transfer from the antenna to the lanthanide excited state. But, in the presence of CH_3COO^- , energy transfer from the anion-bound complex to the lanthanide excited state is less efficient. The binding of CH_3COO^- is most likely to lower the energy levels of the antenna excited state, hence making the transfer of energy from the antenna T_1 to 5D_4 unfavorable.

As observed for the changes in the absorbance, a two step binding process is observed, **Figure 2.5.1.7**, with the initial binding process occurring up to 1.8 equivalents of anion added, followed by the binding of a second CH_3COO^- to **Tb.61**. The binding of two CH_3COO^- molecules to **Tb.61** is further supported by the determination of binding constants, as $\log K_{1:1} = 6.87$ for the 1:1 (G:H) and $\log K_{2:1} = 5.12$ for the 2:1 ($G_2:H$).

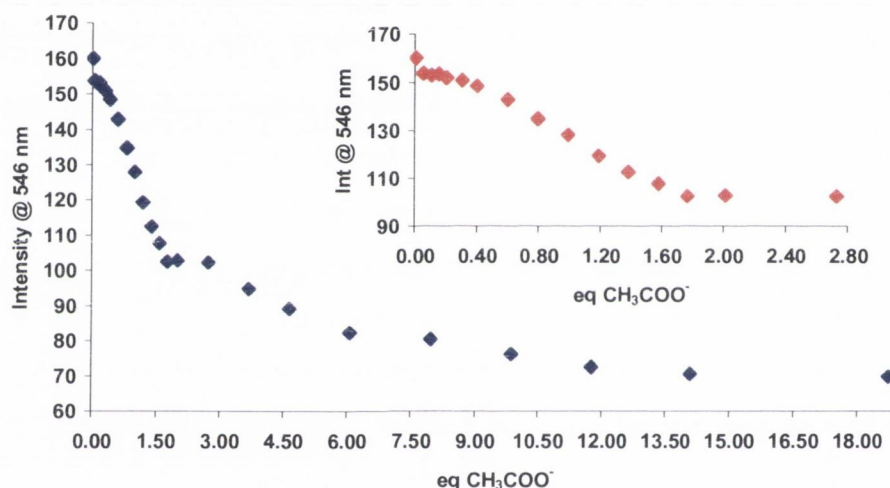


Figure 2.5.1.7: Profile of the emission intensity changes at 546 nm, upon gradual additions of CH_3COO^- (0 \rightarrow 74.9 μM) in CH_3CN , versus the number of equivalents of acetate added. Insert: Cut of the same profile up to two equivalents of acetate added.

The good fit to the experimental data, **Figure 2.5.1.8**, obtained when determining the binding constants further supports the formation of the two species discussed above.

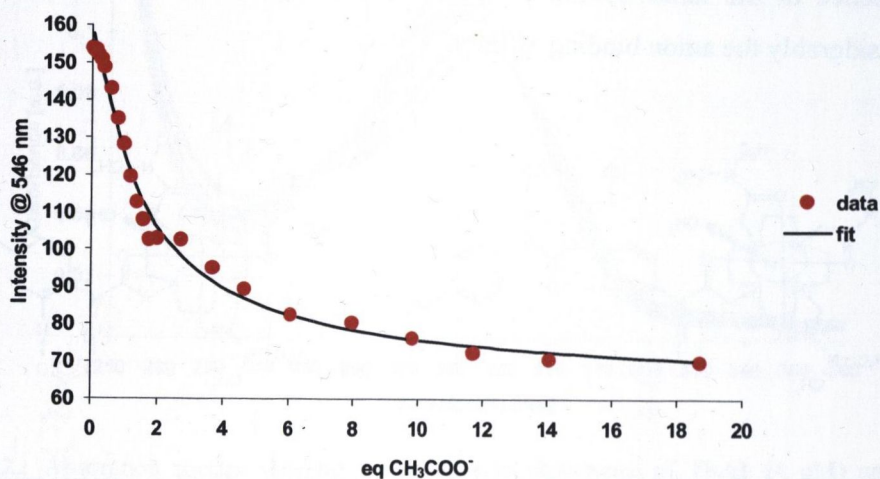


Figure 2.5.18: Experimental binding isotherm for the lanthanide luminescence titration of **Tb.61** (4 μ M) with CH_3COO^- in CH_3CN and corresponding fit using the SPECFIT program.

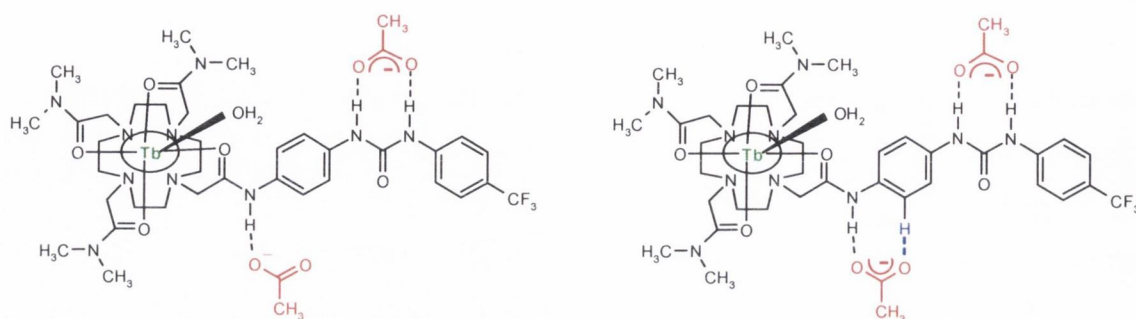
In **Table 2.5.1** are summarised all the determined values for $\log K_{n:m}$, during the titration of **Tb.61** with CH_3COO^- . These values reveal a good agreement between all the spectroscopic titrations, confirming the presence of two main species in solution, as G:L and G₂:L. Moreover, the results suggest higher stability constants for the formation of the 1:1 complex, in comparison to the 2:1 complex formation.

Anion (G)	Technique	Species (G _n :L _m)	$\log K_{n:m}$	Std. Deviation (\pm)
CH_3COO^-	Absorbance	G:L	6.27	0.12
		G ₂ :L	5.84	0.09
	Fluorescence	G:L	5.78	0.30
		G ₂ :L	5.11	0.51
	Phosphorescence	G:L	6.87	0.46
		G ₂ :L	5.12	0.49

Table 2.4.1: Binding constants and binding modes between CH_3COO^- (G) and sensor **Tb.61** (L)

Taking into consideration the discussion above, the proposed binding between **Tb.61** and CH_3COO^- is depicted in **Scheme 2.5.1.1**. We suggest that the strongest binding occurs through hydrogen bonding between the acetate and the urea moiety of receptor **Tb.61** and that a second interaction occurs between the acetate and the hydrogen of the amide, which

can possibly also interact with an aromatic CH (depicted in blue on the scheme below). The presence of the latter hydrogen in close proximity to the NH is proposed to enhance considerably the anion binding affinity.¹⁶⁶



Scheme 2.5.1.1: Proposed binding mode between the urea receptor **Tb.61** and acetate anion.

Although, most hydrogen bonding anion receptors rely on the use of NH or OH moieties, there is increasing evidence of hydrogen bond interactions between aromatic CH groups and anions. For instance, Jeong *et al.* have shown aromatic CH hydrogen bonding to the carboxylate ion,¹⁶⁷ while Steed *et al.* found that CH – anion interactions are both important and directional interactions in anion binding systems.¹⁶⁸ Furthermore, Hay *et al.* found that even in the absence of electron withdrawing substituents, simple arenes form hydrogen bonds with anions. Hence, when present in a receptor, even moderately acidic CH groups can considerably enhance anion binding affinity. Therefore, they should be considered as additional binding sites within the host cavity.¹⁶⁶

2.5.2 Photophysical studies of **Tb.61** towards binding with H_2PO_4^-

The interaction between **Tb.61** and H_2PO_4^- was investigated following the same procedure described above. **Figure 2.5.2** shows the changes recorded during the course of the UV-Visible titration of **Tb.61** upon gradual additions of H_2PO_4^- . It is clear from the changes that the band centred at 280 nm experienced a bathochromic shift to 288 nm, while the formation of a new band centred at 234 nm was also observed. The lack of well defined isosbestic points is an additional indication that more than two species are present in solution.¹⁶⁵

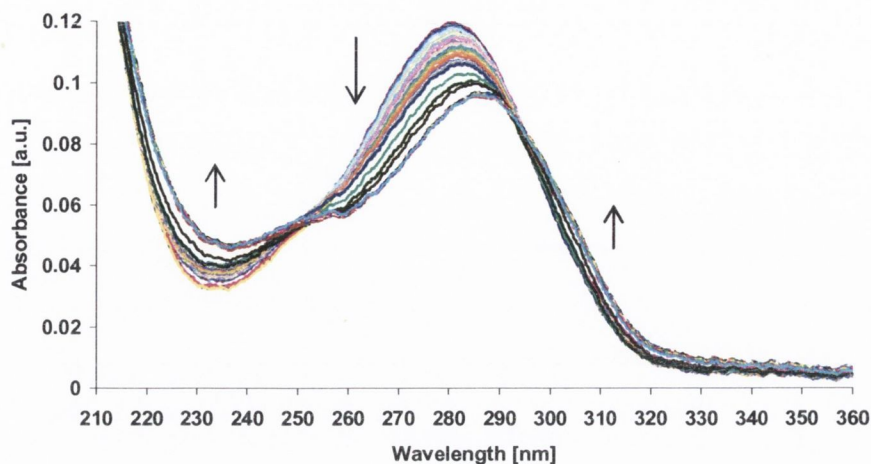


Figure 2.5.2.: Absorption spectra showing the changes in absorbance of **Tb.61** ($4 \mu\text{M}$) upon gradual additions of H_2PO_4^- ($0 \rightarrow 57.3 \mu\text{M}$) in CH_3CN .

The profile of the absorbance changes at 234 nm and 270 nm versus the number of equivalents of added H_2PO_4^- , as shown in **Figure 2.5.2.1**, suggests the occurrence of multi stepwise equilibria. As can be seen there is a noticeable flex point occurring up to one equivalent of anion added, corresponding to the formation of the 1:1 complex ($\text{G}:\text{H}$). This is then followed by a second binding to an equivalent of H_2PO_4^- to form a 2:1 complex ($\text{G}_2:\text{H}$), while a possible third binding is apparent between the addition of two and four equivalents of the anion, corresponding to the formation of 3:1 complex ($\text{G}_3:\text{H}$).

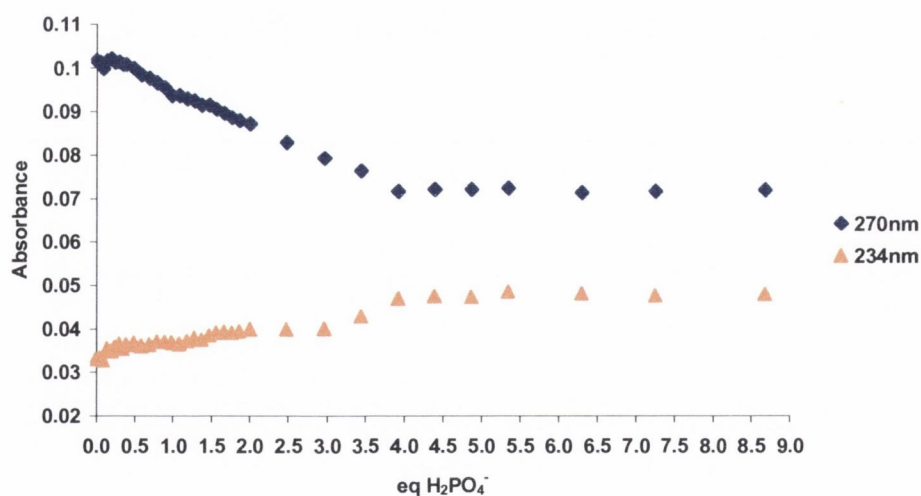


Figure 2.5.2.1: Profile of the absorbance changes at 270 nm and at 330 nm, upon gradual additions of H_2PO_4^- ($0 \rightarrow 57.3 \mu\text{M}$) in CH_3CN , versus the number of equivalents of H_2PO_4^- added.

From these, the data was thus fitted to the following binding model; 1:1 (G:L), 1:2 (G:L₂), 2:1 (G₂:L), 2:2 (G₂:L₂), and 3:1 (G₃:L), where G represents H₂PO₄⁻ and L **Tb.61**. From this fitting analysis, the respective binding constants were determined, and these are summarised in **Table 2.5.2**. Both the G:L and the G₃:L species were found to possess high binding constants of log *K* > 7 (log *K*_{1:1} = 7.06 ± 0.24 and log *K*_{3:1} = 7.95 ± 0.21, respectively).

Anion (G)	Species (G _n :L _m)	log <i>K</i> _{n:m}	Std. Deviation (±)
H ₂ PO ₄ ⁻	G:L	> 7 (7.06)	0.24
	G:L ₂	4.87	0.47*
	G ₂ :L	5.66	0.95*
	G ₂ :L ₂	6.79	0.37
	G ₃ :L	> 7 (7.95)	0.21

Table 2.5.2: Binding constants for the binding of H₂PO₄⁻ with **Tb.61** determined from the UV-Visible titration data, using SPECFIT.* Species present in solution in less than 10% formation.

The good fit to the experimental data, shown in **Figure 2.5.2.2**, further supports the multiple binding interactions between H₂PO₄⁻ and **Tb.61** discussed above.

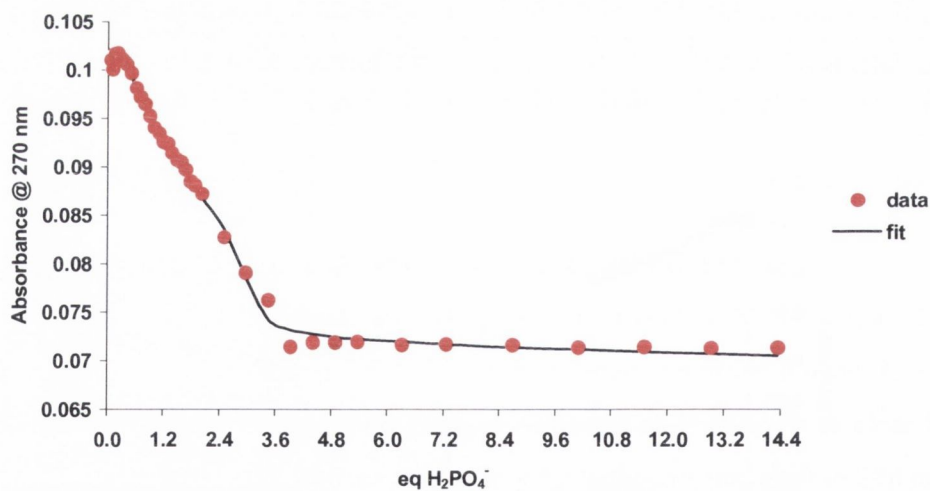


Figure 2.5.2.2: Experimental binding isotherm for the UV-Visible titration of **Tb.61** (4 μM) with H₂PO₄⁻ and corresponding fit using the SPECFIT program.

The speciation distribution diagram, depicted in **Figure 2.5.2.3**, shows that all the species accounted in the binding model were found to be present in solution. Nevertheless, the predominant species in solution correspond to the formation of the 1:1 (G:L) and the 3:1 (G₃:L) complexes. Initially, up to 1.5 equivalents of H₂PO₄⁻, the G:L is the dominant species, but upon further addition of the anion, the G₃:L begins to dominate in solution. The 2:2 (G₂:L₂) accounts for *ca.* 10% formation, while the 1:2 (G:L₂) and the 2:1 (G₂:L) species form in less than *ca.* 5% (**Figure 2.5.2.3**).

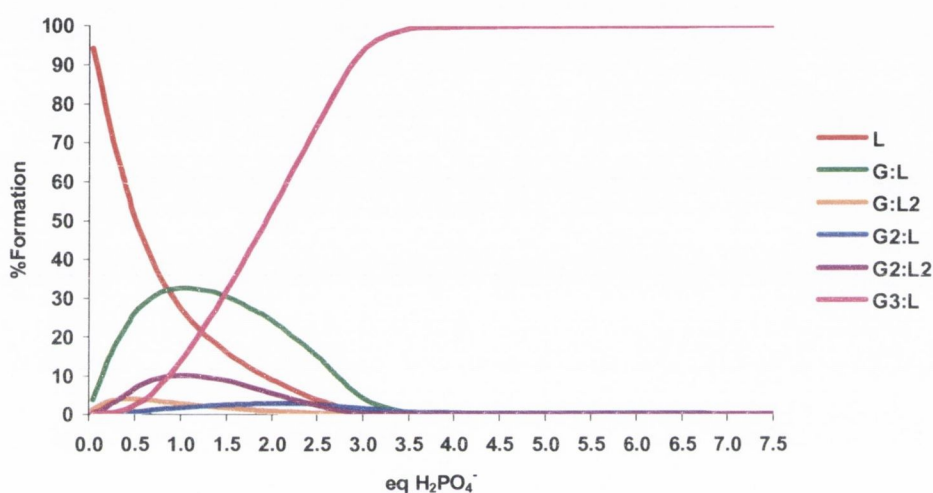


Figure 2.5.2.3: Speciation diagram for the UV-Visible titration of the ligand (L) **Tb.61** (4 μ M) with H₂PO₄⁻ in CH₃CN.

The fluorescence emission was also followed by exciting the sample at 280 nm, and was observed to increase dramatically, with the formation of a new band centred at 422 nm, as illustrated in **Figure 2.5.2.4**.

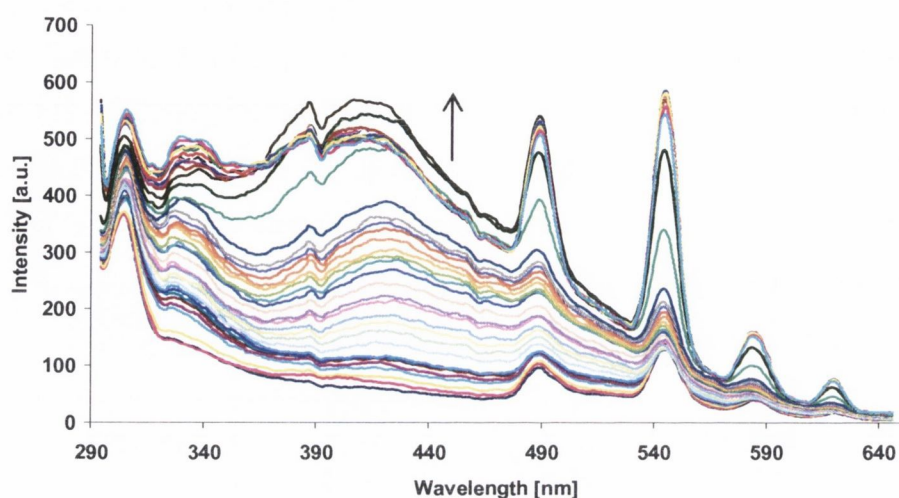


Figure 2.5.2.4: Fluorescence spectra showing the changes in emission intensity of **Tb.61** (4 μM) upon gradual additions of H_2PO_4^- (0 \rightarrow 57.3 μM), by exciting the sample at 280 nm.

The binding constants were determined using the same binding model used above. The binding constants and corresponding stoichiometries are shown in **Table 2.5.2.1**. These results are in agreement with those of the ground state.

Anion (G)	Species ($G_n:L_m$)	$\log K_{n:m}$	Std. Deviation (\pm)
H_2PO_4^-	G:L	6.86	0.21
	G:L ₂	5.15	0.25*
	G ₂ :L	5.34	0.94*
	G ₂ :L ₂	6.84	0.53*
	G ₃ :L	> 7 (7.95)	0.20

Table 2.5.2.1: Binding constants for the binding of H_2PO_4^- with **Tb.61** determined from the fluorescence titration data, using SPECFIT.* Species present in solution in less than 10% formation.

Although the binding constant for the formation of $G_2:L_2$ was observed to be quite high ($\log K_{2:2} = 6.84 \pm 0.53$), this species was found to be present in less than 5% in solution (**Figure 2.5.2.5**). As seen in **Figure 2.5.2.5**, the predominant species are G:L, and $G_3:L$, the latter being the dominant species present in solution after the addition of *ca.* 3.6 equivalents of H_2PO_4^- .

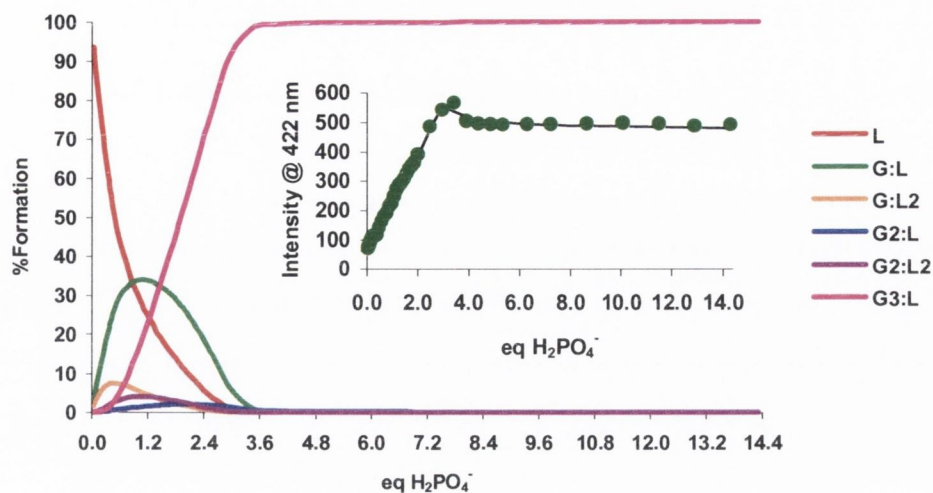


Figure 2.5.2.5: Speciation diagram for the fluorescence titration of **Tb.61** ($4 \mu\text{M}$) with H_2PO_4^- . Insert: The experimental binding isotherm (green dots) and corresponding fit (black line) using the SPECFIT program.

The changes in Tb(III) luminescence upon titration of **Tb.61** with H_2PO_4^- were also investigated, by exciting at 280 nm, as shown in **Figure 2.5.2.6**. Upon addition of H_2PO_4^- two different processes were observed. Firstly, the emission intensity was reduced by *ca.* 69% (insert in **Figure 2.5.2.6**), followed by a large enhancement for the Tb(III) emission intensity.

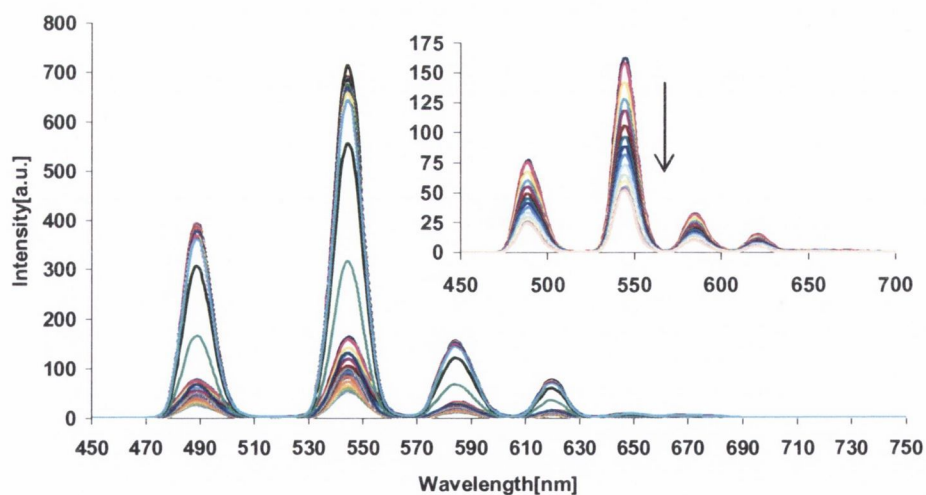


Figure 2.5.2.6: Lanthanide luminescence spectra showing the changes in the emission intensity of **Tb.61** ($4 \mu\text{M}$) upon gradual additions of H_2PO_4^- ($0 \rightarrow 57.3 \mu\text{M}$), by exciting the sample at 280 nm. Insert: The changes up to one equivalent of added anion.

The profile of the emission intensity changes at 546 nm versus the number of equivalents of H_2PO_4^- added is shown in **Figure 2.5.2.7**. As can be seen, the emission intensity of the Tb(III) was reduced up to one equivalent of added anion. This was immediately followed by a slow increase in the emission intensity up to two equivalents of anion. However, the major changes took place between *ca.* 2 \rightarrow 3.5 equivalents of H_2PO_4^- . The binding process was found to be in good agreement with those discussed above for both the UV-Visible and the fluorescence titrations. At this stage, at least a three stepwise equilibria can be expected, involving the formation of the 1:1 ($\text{G}_1:\text{L}$), 2:1 ($\text{G}_2:\text{L}$), and 3:1 ($\text{G}_3:\text{L}$) complexes.

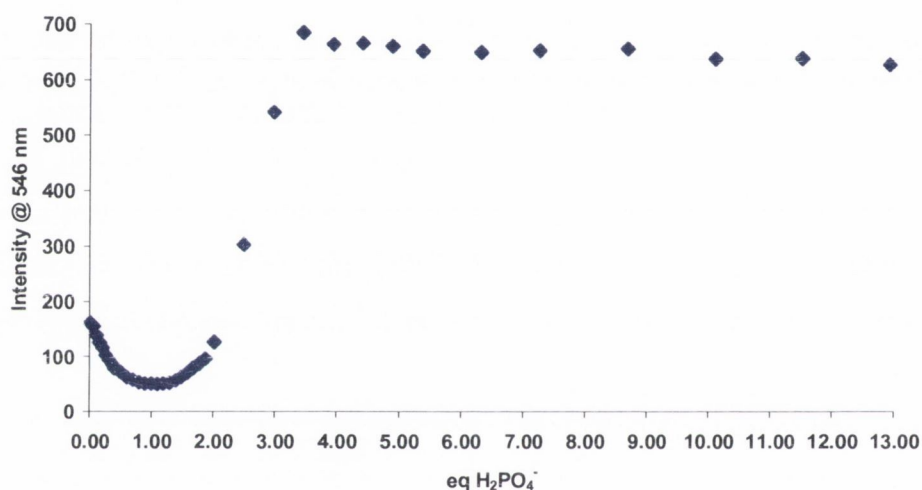
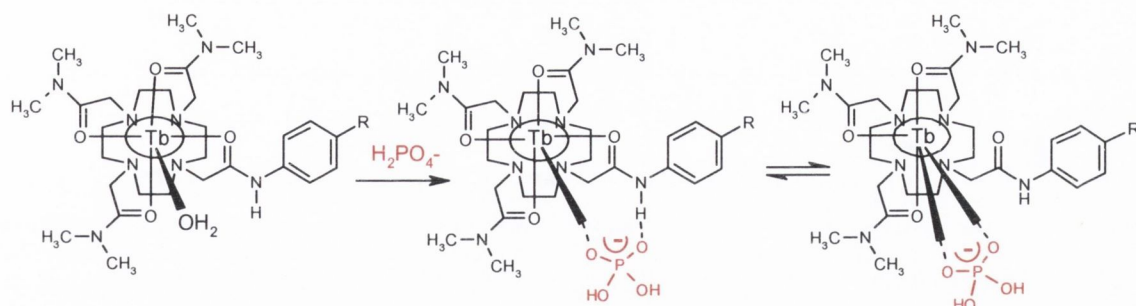


Figure 2.5.2.7: Changes in luminescent emission intensity at 546 nm versus the number of equivalents of H_2PO_4^- (0 \rightarrow 57.3 μM) in CH_3CN .

In the presence of H_2PO_4^- two distinct processes were initially taking place. First, the binding of H_2PO_4^- to the antenna is responsible for the lowering of the energy of the antenna triplet state, hence making the energy transfer to the lanthanide excited state less efficient. The result is the observed ‘switching off’ in the lanthanide emission. The second process, the ‘switching on’ of the lanthanide luminescence, is proposed to be due to the removal of the quenching effect from a metal bound water molecule, which could possibly occur in a stepwise manner as shown in **Scheme 2.5.2**.



Scheme 2.5.2: Schematic representation for the proposed binding mechanism leading to the luminescent enhancement or 'switching on' of the Tb(III) emission, due to the removal of a metal bound water molecule, upon binding with H_2PO_4^- . The urea binding moiety was removed for clarity.

The ability of anions to bind directly to lanthanide centres by displacement of bound water molecules has been well established in similar complexes possessing two bound water molecules, even in more competitive solvents.^{86,101,154,155} However, in structurally similar nine coordinate complexes possessing one axial bound water molecule, there are much fewer examples of such reports. Aime *et al.* have however observed the binding of F^- to such complexes by replacing the inner sphere water molecule.¹⁵³ By fitting the lanthanide luminescence changes to the binding model discussed above (G:L , G:L_2 , $\text{G}_2:\text{L}$, $\text{G}_2:\text{L}_2$, and $\text{G}_3:\text{L}$) the respective binding constants were determined (**Table 2.5.2.2**).

Anion (G)	Species ($\text{G}_n:\text{L}_m$)	$\log K_{n:m}$	Std. Deviation (\pm)
H_2PO_4^-	G:L	> 7 (7.04)	0.14
	G:L_2	4.59	0.24*
	$\text{G}_2:\text{L}$	4.90	0.82*
	$\text{G}_2:\text{L}_2$	7.20	0.18*
	$\text{G}_3:\text{L}$	> 7 (8.04)	0.12

Table 2.5.2.2: Binding constants for the binding of H_2PO_4^- with **Tb.61** determined from the lanthanide luminescence titration data, using SPECFIT.*Species present in solution in less than 10% formation.

The fit to the experimental data is shown in **Figure 2.5.2.8**, and further supports the multiple-step binding interactions between H_2PO_4^- and **Tb.61** involved in the sensing process.

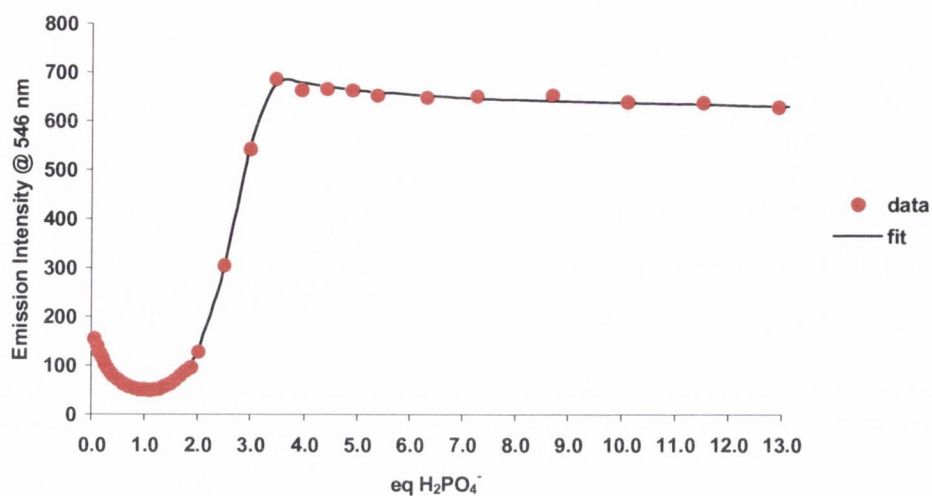


Figure 2.5.2.8: Experimental binding isotherm for the lanthanide luminescence titration of **Tb.61** ($4 \mu\text{M}$) with H_2PO_4^- in CH_3CN and corresponding fit using the SPECFIT program.

The speciation distribution diagram is shown in **Figure 2.5.2.9**. Once again, the predominant species were found to be the G:L and $\text{G}_3\text{:L}$ with high binding constants of $\log K > 7$ ($\log K_{1:1} = 7.04 \pm 0.14$ and $\log K_{3:1} = 8.04 \pm 0.12$, respectively), while G:L₂, G₂:L, and G₂:L₂ were only shown to be formed in less than *ca.* 10%.

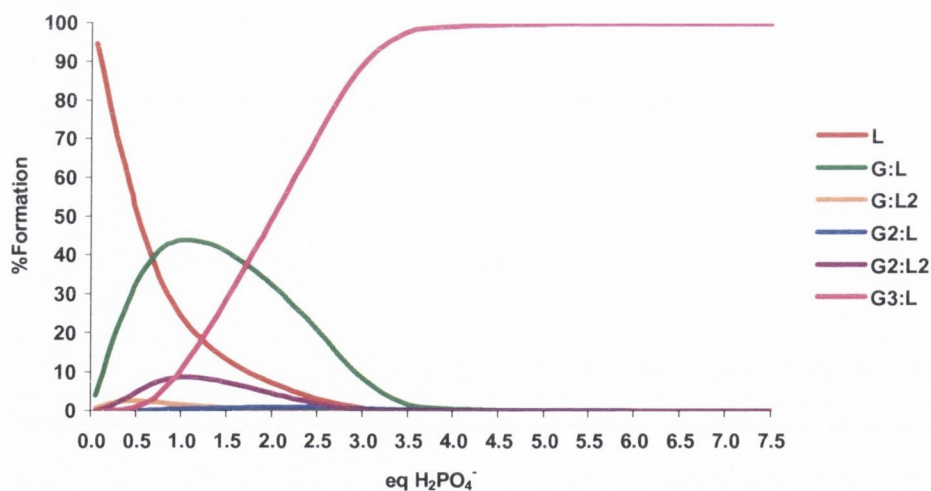
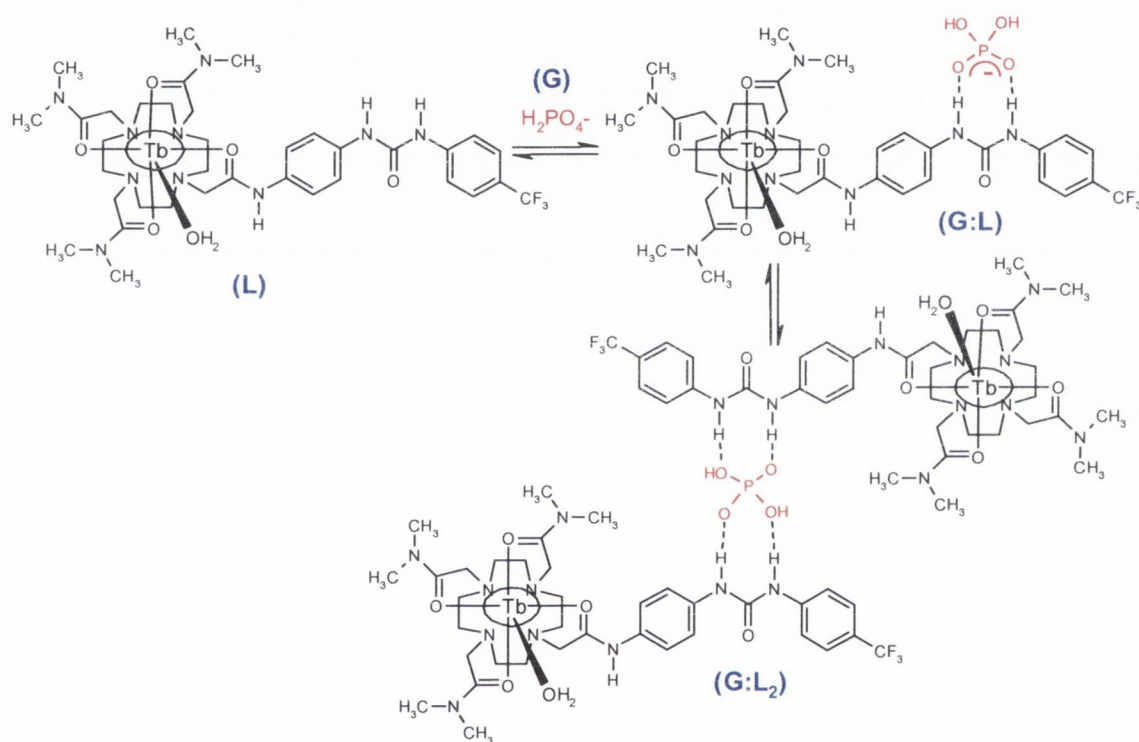


Figure 2.5.2.9: Speciation distribution diagram for the lanthanide luminescence titration of **Tb.61** ($4 \mu\text{M}$) with H_2PO_4^- in CH_3CN .

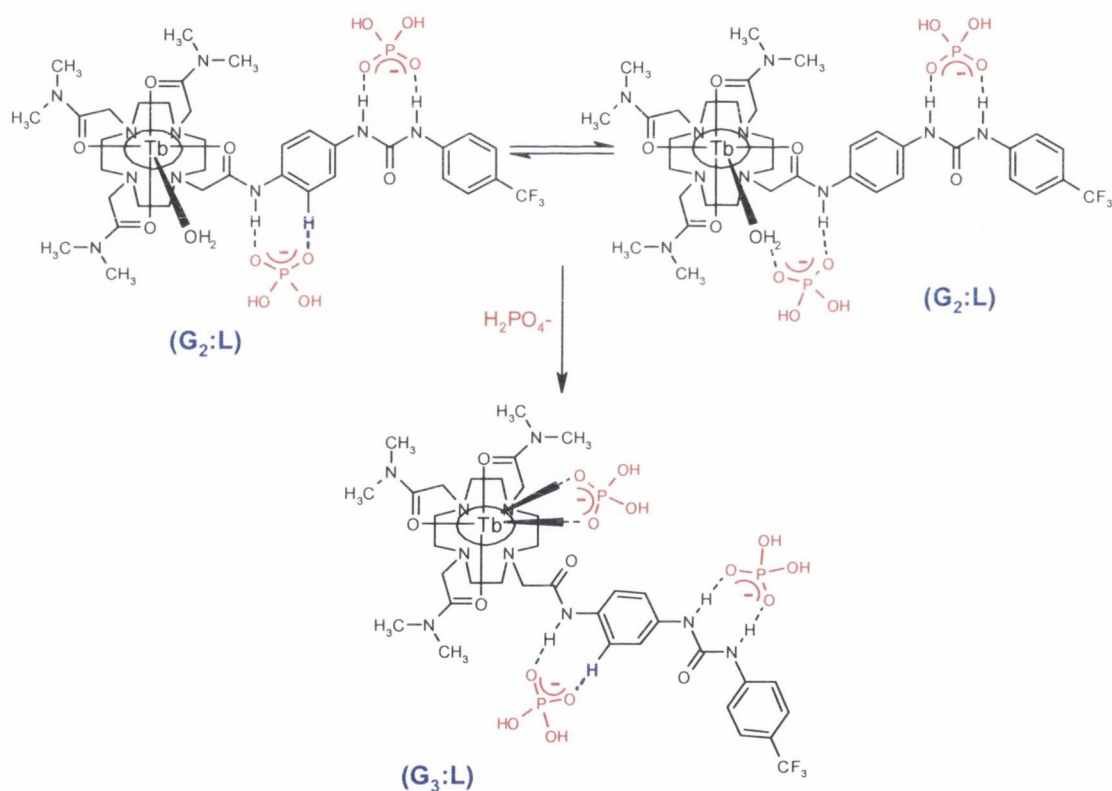
As discussed above, the fitting of the titration data indicated the occurrence of five possible stepwise equilibria. The formation of the 1:1 complex (G:L) between H_2PO_4^- and **Tb.61** was expected to take place at the urea moiety, as illustrated in **Scheme 2.5.2.1**. However, H_2PO_4^- should also be able to form a 1:2 complex (G:L_2), which was indeed observed. This binding is ascribed to the formation of four hydrogen bonds between H_2PO_4^- and the urea moieties of two **Tb.61** molecules to bind one H_2PO_4^- , giving rise to a self-assembly bridged complex as depicted in **Scheme 2.5.2.1**. Nevertheless, the latter was only observed in less than 10%.



Scheme 2.5.2.1: Proposed 1:1 (G:L) and 1:2 (G:L₂) binding modes between H_2PO_4^- and receptor **Tb.61**.

On further addition of H_2PO_4^- the 2:1 ($\text{G}_2\text{:L}$) and 2:2 ($\text{G}_2\text{:L}_2$) complexes are also formed. The presence of a second binding site within **Tb.61** was already discussed for CH_3COO^- (Section 2.5.1). Based on that discussion, the binding between the amide, combined with the possible interaction of a neighbor hydrogen of the aromatic ring can also be considered, as depicted in **Scheme 2.5.2.2**. Furthermore, taking into account the increase (*ca.* 48%) in the emission intensity between 1 → 2 equivalents of the anion, the

interaction of H_2PO_4^- with the metal bound water molecule is also possible, as described in **Scheme 2.5.2.2**. The binding of H_2PO_4^- to the hydrogen atom of the bound water molecule should reduce the quenching ability of the water molecule, by reducing the O-H vibrational pathway for non-radiative deactivation of the Tb(III) excited state. Nevertheless, upon further addition of H_2PO_4^- (up to *ca.* 3.5 equivalents) the formation of the 3:1 ($\text{G}_3:\text{L}$) species was associated with a remarkable increase in the Tb(III) emission intensity, which can possibly be attributed to the direct binding of H_2PO_4^- to the Tb(III) center, by replacement of the bound water molecule (**Scheme 2.5.2.2**). Hence, this would suppress completely the non-radiative pathway from the O-H oscillators. Although difficult to prove without evidence from X-ray crystallography analysis, the proposed structures for $\text{G}_2:\text{L}$ and $\text{G}_3:\text{L}$ are tentatively depicted in **Scheme 2.5.2.2**.



Scheme 2.5.2.2: Proposed 2:1 ($\text{G}_2:\text{L}$) and 3:1 ($\text{G}_3:\text{L}$) binding modes between H_2PO_4^- and receptor **Tb.61**.

In order to better visualise the correlations among the binding constants determined from the titrations, all the determined values and corresponding stoichiometries are summarized below in **Table 2.5.2.3**. These results demonstrate the multiple-step binding

process involved in the interaction between H_2PO_4^- and **Tb.61**. Analysis of the ground state, the emission from the singlet and the Tb(III) excited states clearly demonstrated the formation of the dominant 1:1 and 3:1 complexes with large binding constants ($\log K$) in CH_3CN .

Anion (G)	Method	Species ($G_n:L_m$)	$\log K_{n:m}$	Std. Deviation (\pm)
H_2PO_4^-	Absorbance	G:L	> 7 (7.07)	0.23
		G:L ₂	4.87	0.47*
		G ₂ :L	5.64	0.95*
		G ₂ :L ₂	6.79	0.37*
		G ₃ :L	> 7 (7.94)	0.21
	Fluorescence	G:L	6.86	0.21
		G:L ₂	5.15	0.25*
		G ₂ :L	5.34	0.94*
		G ₂ :L ₂	6.84	0.53*
		G ₃ :L	> 7 (7.95)	0.20
	Phosphorescence	G:L	> 7 (7.04)	0.14
		G:L ₂	4.59	0.24*
		G ₂ :L	4.90	0.82*
		G ₂ :L ₂	7.20	0.18*
		G ₃ :L	> 7 (8.04)	0.12

Table 2.5.2.3: Binding constants and binding modes between H_2PO_4^- and **Tb.61**. *Species present in solution in less than 10% formation.

2.5.3 Photophysical studies of **Tb.61** towards binding with $\text{H}_2\text{P}_2\text{O}_7^{2-}$

The interaction between host **Tb.61** and the $\text{H}_2\text{P}_2\text{O}_7^{2-}$ was next investigated following the same procedure already described above. **Figure 2.5.3** shows the family of absorption spectra recorded during the course of the titration of **Tb.61** with $\text{H}_2\text{P}_2\text{O}_7^{2-}$. The band centred at 280 nm was observed to decrease, and was accompanied by a bathochromic shift to *ca.* 286 nm. As before, no clear isosbestic point was observed, which suggests the presence of more than two species in equilibrium, since not all spectra pass through the same point.¹⁶⁵

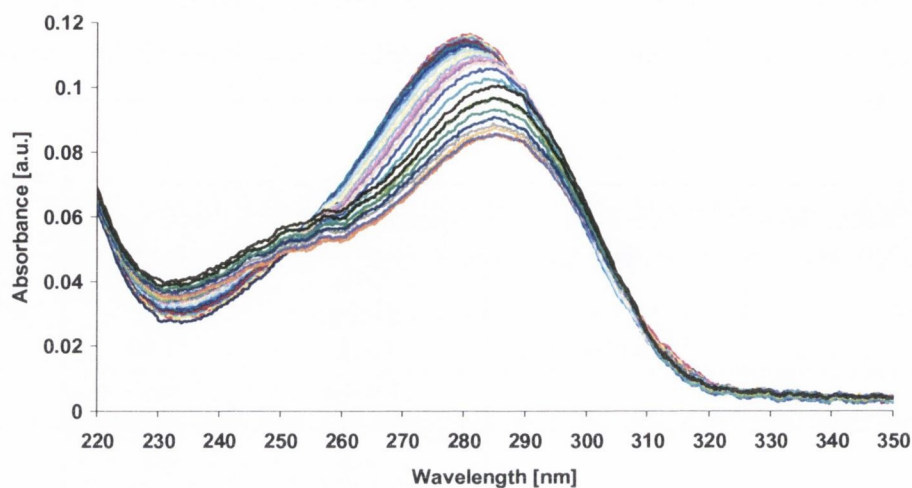


Figure 2.5.3: The absorption spectra of Tb.61 (4 μM) showing the changes upon gradual additions of $\text{H}_2\text{P}_2\text{O}_7^{2-}$ (0 \rightarrow 56.3 μM) in CH_3CN .

The profile of the absorbance changes at 280 nm versus the number of equivalents of $\text{H}_2\text{P}_2\text{O}_7^{2-}$ added is shown in **Figure 2.5.3.1**.

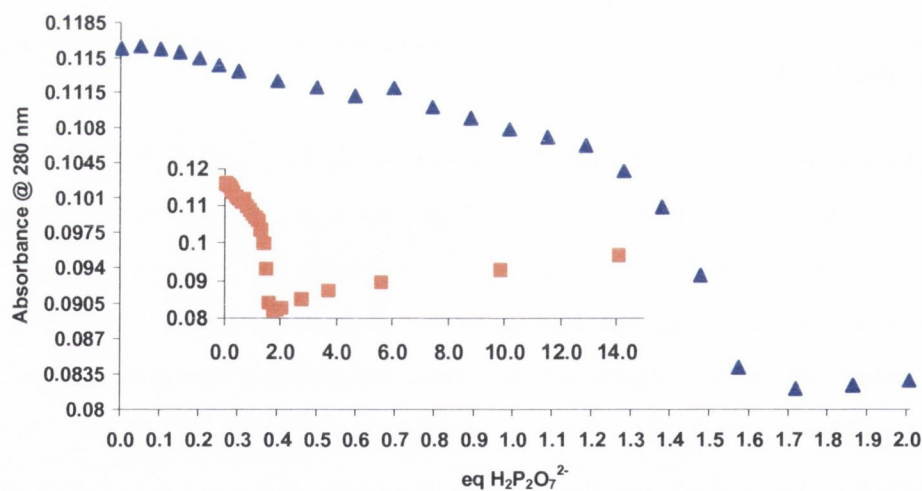


Figure 2.5.3.1: Profile of the absorbance changes at 280 nm versus the number of equivalents of $\text{H}_2\text{P}_2\text{O}_7^{2-}$ added. Here are shown the changes up to two equivalents of $\text{H}_2\text{P}_2\text{O}_7^{2-}$ added. Insert: The profile for all titration, up to ca. 14.1 equivalents of $\text{H}_2\text{P}_2\text{O}_7^{2-}$.

Once again, by looking at the titration profile two binding events can be seen. In the first section, corresponding to the addition of *ca.* 0.6 equivalents of $\text{H}_2\text{P}_2\text{O}_7^{2-}$, a small decrease in the band centred at *ca.* 280 nm takes place, accompanied by a small increase at *ca.* 234 nm (**Figure 2.5.3.2**). This can possibly be attributed to the formation of a 1:2 (G:L₂) complex between $\text{H}_2\text{P}_2\text{O}_7^{2-}$ and **Tb.61**. On further addition of $\text{H}_2\text{P}_2\text{O}_7^{2-}$ (0.6 - 1.2 equivalents), the absorption spectrum undergoes an additional decrease, as well as being shifted by 3 nm to 283 nm (**Figure 2.5.3.2**). Such changes are most likely associated with the formation of a 1:1 (G:L) complex. In contrast, only minimal changes were observed at 234 nm. However, the bigger changes were observed upon addition of *ca.* 2 equivalents of $\text{H}_2\text{P}_2\text{O}_7^{2-}$. This caused a big decrease in the 280 nm band, along with a red shift to *ca.* 286 nm (**Figure 2.5.3.2**). Once again, the changes at 234 nm were minor. The possible formation of a 2:1 (G₂:L) complex can be credited for these changes. However, upon further addition of $\text{H}_2\text{P}_2\text{O}_7^{2-}$, a plateau between *ca.* 1.7 and *ca.* 2.0 equivalents (**Figure 2.5.3.1**) was observed, followed by an increase at both the 280 nm and the 234 nm bands. This absorption enhancement continued, and even after the addition of *ca.* 14 equivalents of $\text{H}_2\text{P}_2\text{O}_7^{2-}$, no saturation has been reached (**Figure 2.5.3.2**).

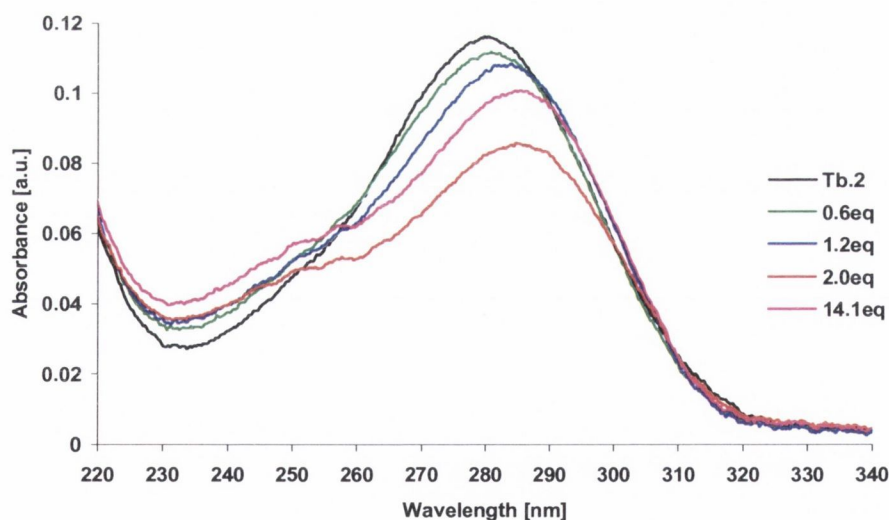


Figure 2.5.3.2: Absorption spectra recorded upon addition of different equivalents of $\text{H}_2\text{P}_2\text{O}_7^{2-}$ (0 → 56.3 μM) to a solution of **Tb.61** (4 μM).

The binding constants, $\log K$ for these changes, were determined by fitting the obtained data to a binding model including the 1:1 (G:L), 1:2 (G:L₂), 2:1 (G₂:L), and 2:2 (G₂:L₂) (**Table 2.5.3**). Values of $\log K_{1:1} = 7.47 \pm 0.19$, $\log K_{1:2} = 5.50 \pm 0.33$, $\log K_{2:1} = 6.02 \pm 0.30$, and $\log K_{2:2} = 5.70 \pm 0.94$ were determined. The high error associated with binding constant for G₂:L₂ can be overlooked, as this species, although contributing to the binding process, is present in solution in a very small concentration (**Figure 2.5.3.3**). The predominant species in solution correspond to the formation of the 1:1 (G:L) and the 2:1 (G₂:L) complexes respectively, as shown in **Figure 2.5.3.3**. In fact, after addition of *ca.* 1.2 equivalents of H₂P₂O₇²⁻, the G.L is the dominant species in solution (*ca.* 60%). However, in the presence of *ca.* 2 equivalents of H₂P₂O₇²⁻ the G₂:L becomes the predominant species in solution. The experimental binding isotherm and corresponding fit, obtained for the calculation of the binding constants, are shown as an insert on **Figure 2.5.3.3**.

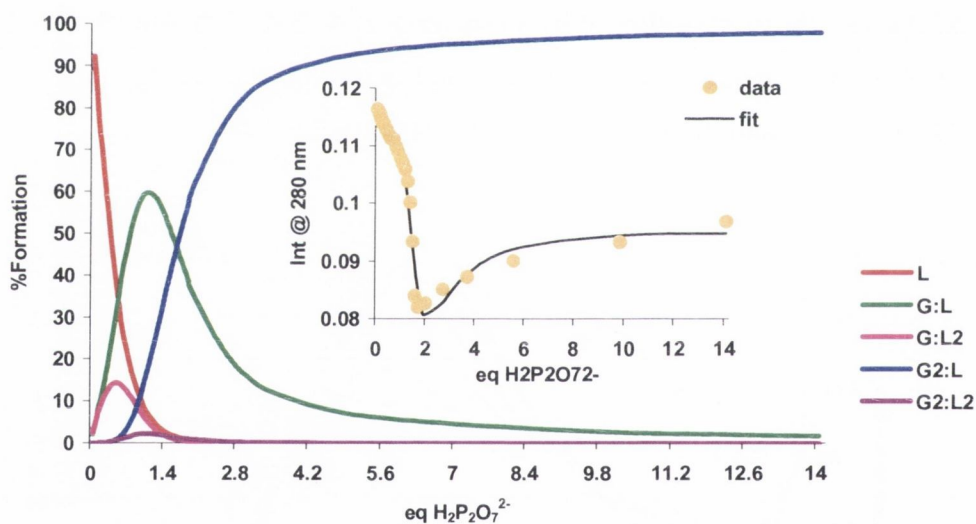


Figure 2.5.3.3: Speciation diagram for the UV-Visible titration of **Tb.61** (L) (4 μ M) with H₂P₂O₇²⁻ (G) (0 \rightarrow 56.3 μ M) in CH₃CN. Insert: The experimental binding isotherm and corresponding fit using the SPECFIT program.

The fluorescence emission was also affected upon titration with H₂P₂O₇²⁻, when exciting at 280 nm. Similarly to what was observed for the titration with H₂PO₄⁻, the emission intensity increased dramatically, with the evolution of a new band centred at 422 nm, **Figure 2.5.3.4** insert. Analysis of the emission intensity at 422 nm (**Figure 2.5.3.4**),

revealed that such changes occurred up to the addition of *ca.* 2 equivalents, after which only minor changes were observed. The observed emission enhancement can therefore be attributed to the binding of $\text{H}_2\text{P}_2\text{O}_7^{2-}$. The profile in **Figure 2.5.3.4** shows almost a linear behaviour up to one equivalent $\text{H}_2\text{P}_2\text{O}_7^{2-}$, from which high binding constants can be anticipated.

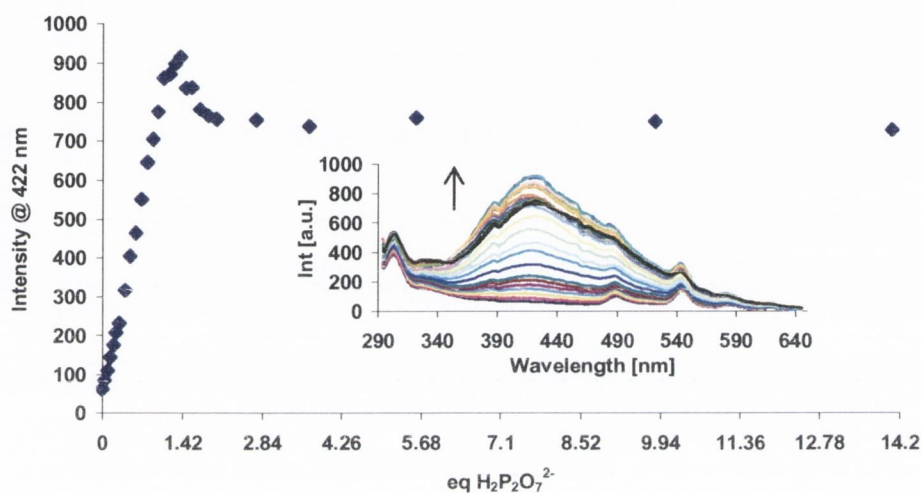


Figure 2.5.3.4.: Binding profile of the fluorescence emission intensity changes at 422 nm versus the number of equivalents of $\text{H}_2\text{P}_2\text{O}_7^{2-}$ added. Insert: The changes in the fluorescence spectra of **Tb.61** ($4 \mu\text{M}$) upon gradual additions of $\text{H}_2\text{P}_2\text{O}_7^{2-}$ ($0 \rightarrow 56.3 \mu\text{M}$) in CH_3CN .

The speciation distribution diagram for this titration showing the presence of the different species in solution is presented in **Figure 2.5.3.5**. The profile was obtained by fitting the emission changes following the same binding model used for the ground state. The results are in good agreement with those discussed above for the UV-Visible titration. Once again the predominant species in solution correspond to the formation of the G:L and the $\text{G}_2\text{:L}$ complexes. The good fit to the binding isotherm (insert in **Figure 2.5.3.5**) clearly supports the multiple step binding interactions involved in the sensing process. From this fitting, binding constants for the different interactions between $\text{H}_2\text{P}_2\text{O}_7^{2-}$ and **Tb.61** were determined, and these are listed in **Table 2.5.3**. As expected, the binding constant for G:L was found to be very high, with a $\log K_{1:1} = 7.68 \pm 0.13$, while the binding constants for G:L₂, G₂:L, and G₂:L₂ were determined as $\log K_{1:2} = 6.19 \pm 0.28$, $\log K_{2:1} = 6.48 \pm 0.25$, and $\log K_{2:2} = 5.83 \pm 0.71$, respectively.

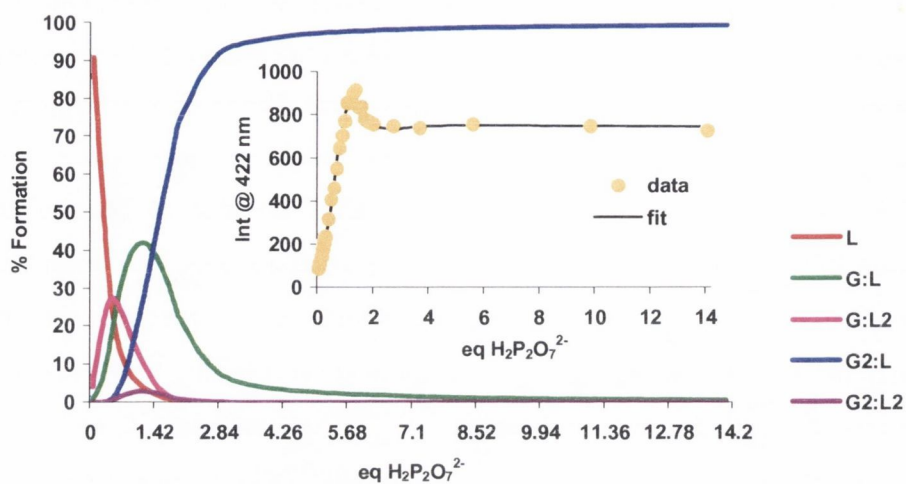


Figure 2.5.3.5: Speciation diagram for the changes in the fluorescence titration of **Tb.61** (L) with $\text{H}_2\text{P}_2\text{O}_7^{2-}$ (G) in CH_3CN . Insert: The experimental binding isotherm and corresponding fit obtained using the SPECFIT program.

The Tb(III) luminescence changes, upon titration of **Tb.61** with $\text{H}_2\text{P}_2\text{O}_7^{2-}$, were also investigated by exciting at 280 nm. The spectra obtained during the course of the titration are presented as an insert in **Figure 2.5.3.6**.

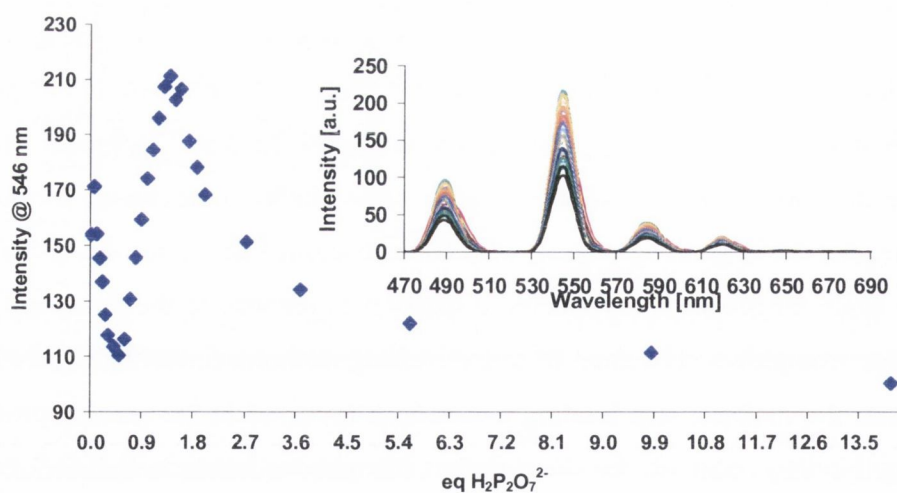


Figure 2.5.3.6: Profile of Tb(III) emission intensity at 546 nm versus the number of equivalents of $\text{H}_2\text{P}_2\text{O}_7^{2-}$ added. Insert: The family of spectra obtained upon titration of **Tb.61** (4 μM) with $\text{H}_2\text{P}_2\text{O}_7^{2-}$ (0 \rightarrow 56.3 μM) in CH_3CN .

The titration profile for the Tb(III) emission changes at 546 nm, shown in **Figure 2.5.3.6**, revealed that upon addition of 0.5 equivalents of $\text{H}_2\text{P}_2\text{O}_7^{2-}$ the emission intensity was observed to decrease by *ca.* 28%, but was then observed to increase by *ca.* 48% up to the addition of *ca.* 1.4 equivalents of anion. After this addition the intensity was quenched once again. This step-like profile, being very similar to the one observed for the ground state, was once again a clear indication of the presence of several different binding interactions occurring upon binding of $\text{H}_2\text{P}_2\text{O}_7^{2-}$ to **Tb.61**. In order to determine the binding constants, these changes were fitted using the SPECFIT program. The values obtained were in good agreement with those determined for the changes in the ground state and singlet excited state (**Table 2.5.3**) discussed above. Once again the 1:1 binding was determined to be the strongest, with $\log K_{1:1} = 7.40 \pm 0.12$. Binding constants of; $\log K_{1:2} = 5.94 \pm 0.26$, $\log K_{2:1} = 5.34 \pm 0.15$, and $\log K_{2:2} = 6.19 \pm 0.43$ were also determined for the 1:2, 2:1 and the 2:2 stoichiometries, respectively. The good fit to the binding isotherm further supports the used multiple-step binding model (insert in **Figure 2.5.3.6**). Also keeping in very good agreement with the other two techniques, the speciation distribution diagram, **Figure 2.5.3.6**, showed the presence of G:L and $\text{G}_2\text{:L}$ as the predominant species in solution.

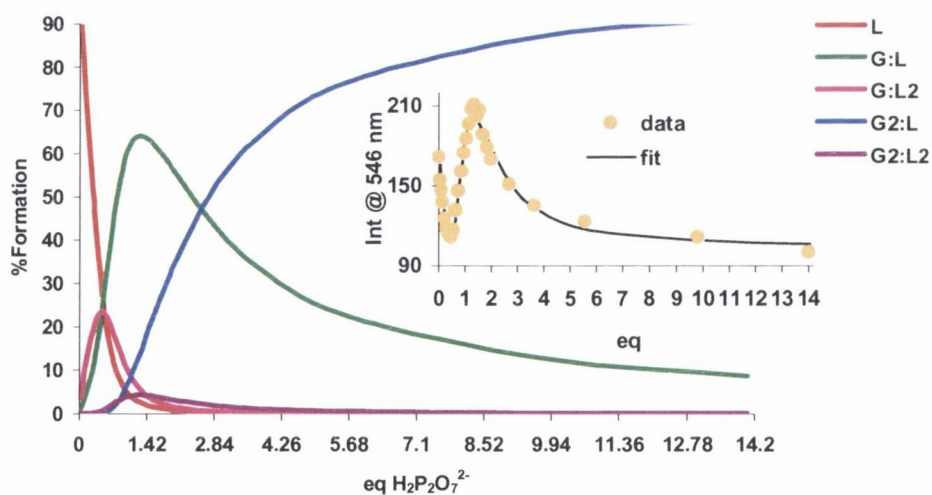
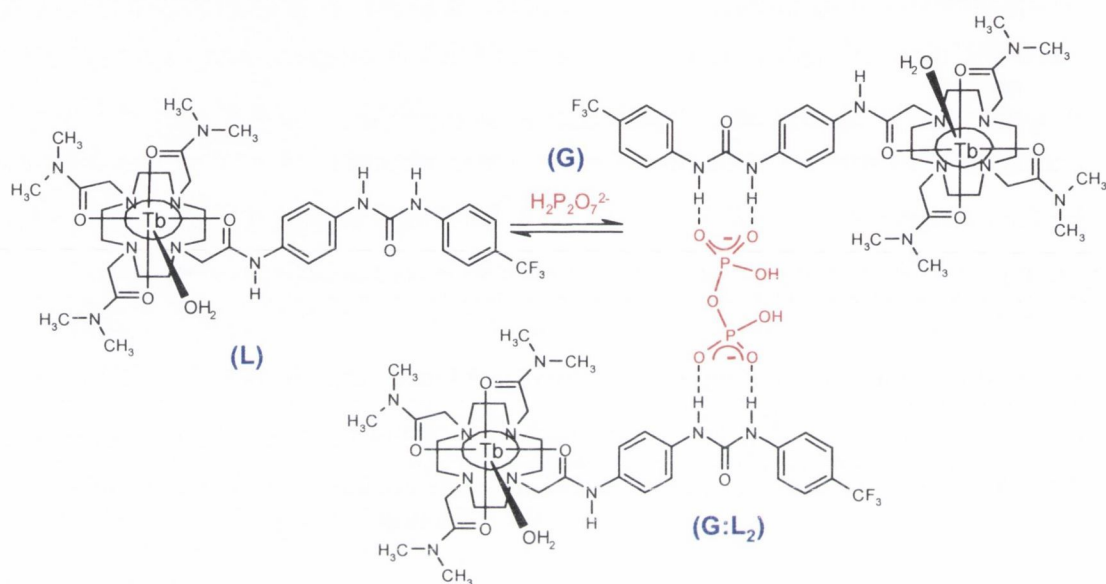


Figure 2.5.3.6: Speciation distribution diagram for the lanthanide luminescence titration of **Tb.61** (L) with $\text{H}_2\text{P}_2\text{O}_7^{2-}$ (G) in CH_3CN . Insert: The experimental binding isotherm and corresponding fit using the non-linear program SPECFIT.

As discussed above, the fitting of the binding data indicated the occurrence of four stepwise equilibria. Due to the divalent nature of $\text{H}_2\text{P}_2\text{O}_7^{2-}$, this anion should be able to bind two molecules of **Tb.61**, as tentatively depicted in **Scheme 2.5.3**. Since the quenching in the emission intensity was observed to occur over 0.5 equivalents of added anion, it is reasonable to believe that these changes are associated with the formation of the 1:2 (G:L₂) complex.



Scheme 2.5.3.: Proposed 1:2 (G:L₂) binding mode between divalent anion $\text{H}_2\text{P}_2\text{O}_7^{2-}$ and receptor **Tb.61**.

Nevertheless, upon further addition of anion the luminescence emission intensity was observed to be ‘switched on’ again. Since this occurs within the addition of a second 0.5 equivalents of $\text{H}_2\text{P}_2\text{O}_7^{2-}$, it is reasonable to attribute this change to the formation of the 1:1 complex (G:L). The possible binding between at least one of the multiple oxygen atoms of $\text{H}_2\text{P}_2\text{O}_7^{2-}$ to the hydrogen’s of the bound water molecule, would remove to some extent the O-H vibrations responsible for the quenching of the metal luminescence, leading to the observed enhancement of the emission intensity. However, upon further addition of $\text{H}_2\text{P}_2\text{O}_7^{2-}$ the intensity was quenched once more, which can possibly be associated with the formation of the 2:1 (G₂:L) and the 2:2 (G₂:L₂) complexes.

Table 2.5.3 summarises the determined binding constants for the titration of $\text{H}_2\text{P}_2\text{O}_7^{2-}$ with **Tb.61**. As can be observed, the UV-Visible, the fluorescence, and the Tb(III) luminescence all follow the same pattern, which further confirms the proposed multiple-

binding model. As can clearly be seen from these binding constants, **Tb.61** binds strongly $\text{H}_2\text{P}_2\text{O}_7^{2-}$. In particular, through the formation of the 1:1 complex ($\log K > 7$).

Anion	Technique	Species ($G_n:L_m$)	$\log K_{n:m}$	Std. Deviation (\pm)
$\text{H}_2\text{P}_2\text{O}_7^{2-}$	Absorbance	G:L	> 7 (7.47)	0.19
		G:L ₂	5.50	0.33
		G ₂ :L	6.02	0.30
		G ₂ :L ₂	5.70	0.94*
	Fluorescence	G:L	> 7 (7.68)	0.13
		G:L ₂	6.19	0.28
		G ₂ :L	6.48	0.25
		G ₂ :L ₂	5.83	0.71*
	Phosphorescence	G:L	> 7 (7.40)	0.12
		G:L ₂	5.94	0.26
		G ₂ :L	5.34	0.15
		G ₂ :L ₂	5.89	0.43*

Table 2.5.3: Binding constants and binding modes between $\text{H}_2\text{P}_2\text{O}_7^{2-}$ and **Tb.61**. *Species present in solution in less than 10%.

2.5.4 Photophysical studies of **Tb.61** towards binding with F^-

The studies involving F^- , were carried out following the same procedure discussed above. The changes in the absorbance spectra upon titration of **Tb.61** with F^- are shown in **Figure 2.5.4**.

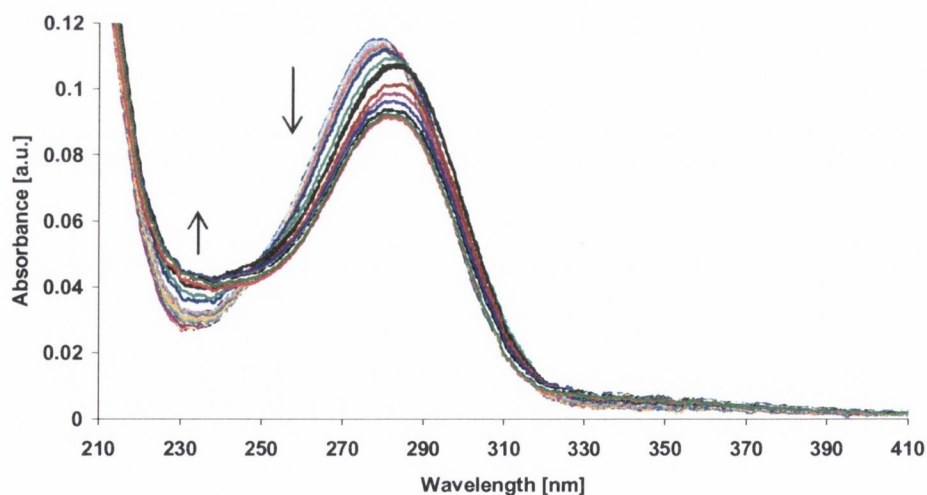


Figure 2.5.4: Absorption spectra showing the changes in the absorption spectra of **Tb.61** ($4 \mu\text{M}$) upon gradual additions of F^- ($0 \rightarrow 66.6 \mu\text{M}$) in CH_3CN .

The band centred at 280 nm decreased during the titration, while a small increase was observed at *ca.* 234 nm. As stated before, the lack of a well defined isosbestic point can indicate the presence of a binding process other than the simple 1:1.¹⁶⁵ Although, at first sight, these changes looked very similar to those studied above, in particular for the titration of H_2PO_4^- and $\text{H}_2\text{P}_2\text{O}_7^{2-}$, this was not the case. By looking closely, different changes could be seen during the course of the titration with F^- , and **Figure 2.5.4.1** clearly shows that at least two different processes are taking place. In case **a)** the changes up to the addition of seven equivalents of F^- are shown. Here, a bathchromic shift (280 nm to 283 nm) is observed, accompanied by the formation of two isosbestic points at *ca.* 249 nm and *ca.* 285 nm respectively. However, in case **b)**, the further addition of F^- (8 \rightarrow 17 equivalents) gives rise to a hypsochromic (or blue shift), resulting in total loss of the isosbestic point at *ca.* 285 nm, and contributing to some loss in definition of the isosbestic point at *ca.* 249 nm. This was an indication of new species being formed upon addition of large excess of F^- .

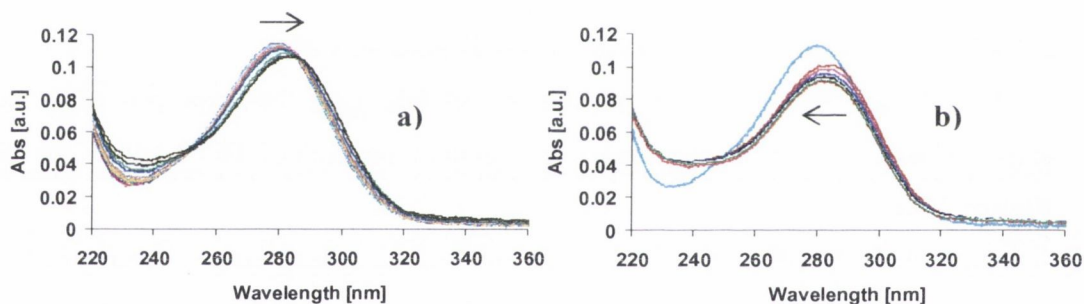


Figure 2.5.4.1: Absorption spectra showing the changes in the absorbance of **Tb.61** (4 μM) upon gradual additions of: **a)** 0 \rightarrow 7 equivalents of F^- ; **b)** 8 \rightarrow 17 equivalents of F^- , light blue line represent free **Tb.61**.

The observed changes in the absorption spectra are therefore assigned to multiple binding interactions between F^- and **Tb.61**, as well as possible deprotonation of the urea and amide moieties to form HF_2^- .^{21,169-171} Taking these complex binding interactions into consideration, the binding constants were determined using the SPECFIT program. This gave rise to an intricate binding model: 1:1 ($\text{G}:\text{L}$), 1:2 ($\text{G}:\text{L}_2$), 2:1 ($\text{G}_2:\text{L}$), 2:2 ($\text{G}_2:\text{L}_2$), 3:1 ($\text{G}_3:\text{L}$), 4:1 ($\text{G}_4:\text{L}$), and 5:1 ($\text{G}_5:\text{L}$), where G represents F^- and L represents **Tb.61**. The fit to the binding isotherm arising from this binding model is shown in **Figure 2.5.4.2**, and demonstrate that the model correlates well with the obtained results.

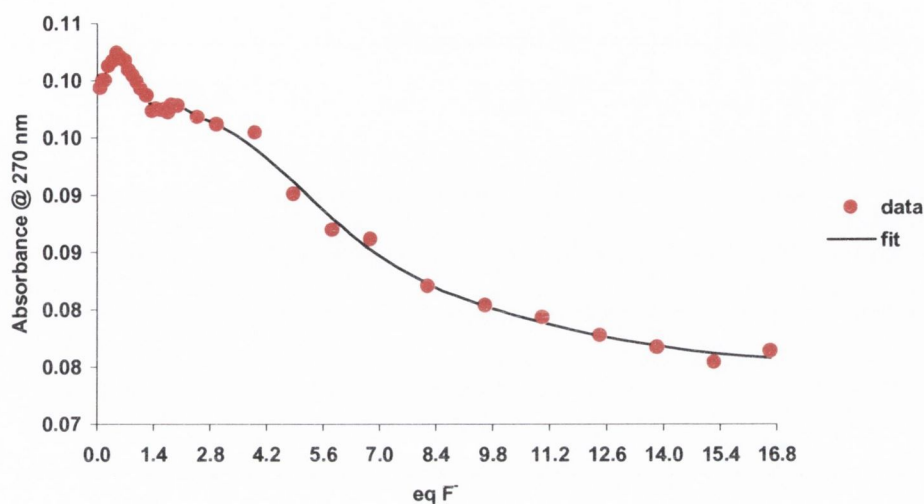


Figure 2.5.4.2: Experimental binding isotherm for the absorption titration of **Tb.61** (4 μM) with F^- in CH_3CN , and corresponding fit using the SPECFIT program.

The binding constants determined from this fit are listed in **Table 2.5.4**. These binding constants were found to be somewhat lower than those observed for the previous anions studied above. Nevertheless, the formation of the G:L complex, ascribed to the binding between F^- and the urea moiety on **Tb.61**, accounts for the higher value of $\log K_{1:1} = 5.97 \pm 0.18$.

Technique	Species ($\text{G}_n:\text{L}_m$)	$\log K_{n:m}$	Std. Deviation (\pm)
Absorbance	G:L	5.97	0.18
	G:L ₂	4.73	0.31*
	G ₂ :L	5.16	0.16
	G ₂ :L ₂	5.52	0.45*
	G ₃ :L	4.49	0.19
	G ₄ :L	4.82	0.31
	G ₅ :L	3.51	0.70*

Table 2.5.4: Binding constants for the UV-Visible titration of F^- with **Tb.61**. *Species present in solution in less than 10% formation.

The resulting speciation distribution diagram, **Figure 2.5.4.3**, shows the presence of the different species, expressed as a percentage relative to the number of equivalents of F^- present in solution. The predominant species in solution correspond to the formation of

G:L, G₂:L, G₃:L, and G₄:L complexes. All the other species were found to be formed in less than 10%. Analysis, using the SPECFIT program, revealed that for the first five equivalents of fluoride added (**Figure 2.5.4.1**, case **a**) the binding model includes the species G:L, G:L₂, G₂:L, G₂:L₂, and G₃:L. This strongly suggests that the binding interactions involved in case **b**) (**Figure 2.5.4.1**) are related to the formation of the remaining species, G₄:L, and G₅:L, which are believed to be related with either interaction with the metal ion or to deprotonation processes mentioned above.

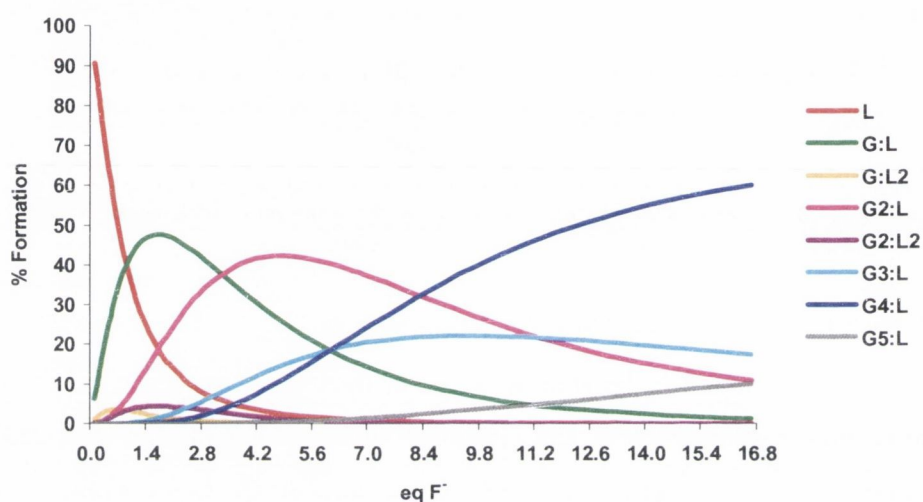


Figure 2.5.4.3: Speciation distribution diagram for the absorption titration of **Tb.61** (L) with F⁻ (G) in CH₃CN.

The same approach can be taken when analyzing the data obtained for the fluorescence, since two distinct processes can clearly be observed upon titration with F⁻ (**Figure 2.5.4.4**). Here, upon addition of zero to five equivalents of anion, the emission intensity experienced an enhancement for both the bands centred at *ca.* 305 nm and the shoulder at *ca.* 330 nm. Nonetheless, a new band centred at *ca.* 423 nm was only observed to form and increase upon excess addition of anion (5 → 17 equivalents), which can be compared with case **b**) for the ground state studies, as both spectra change around the same equivalents of F⁻.

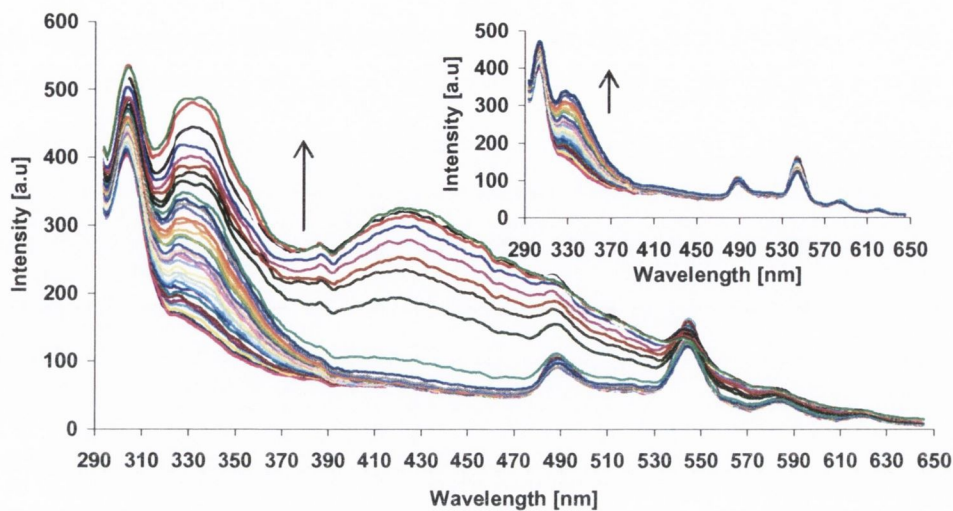


Figure 2.5.4.4: Fluorescence spectra showing the changes in emission intensity of **Tb.61** ($4 \mu\text{M}$) upon gradual additions of F^- ($0 - 66.6 \mu\text{M}$) in MeCN. Insert: The titration from 0 – 5 equivalents of F^- .

The distinct behaviour exhibited by the two bands at *ca.* 330 and *ca.* 423 nm, upon titration with F^- , can be clearly observed in **Figure 2.5.4.5**.

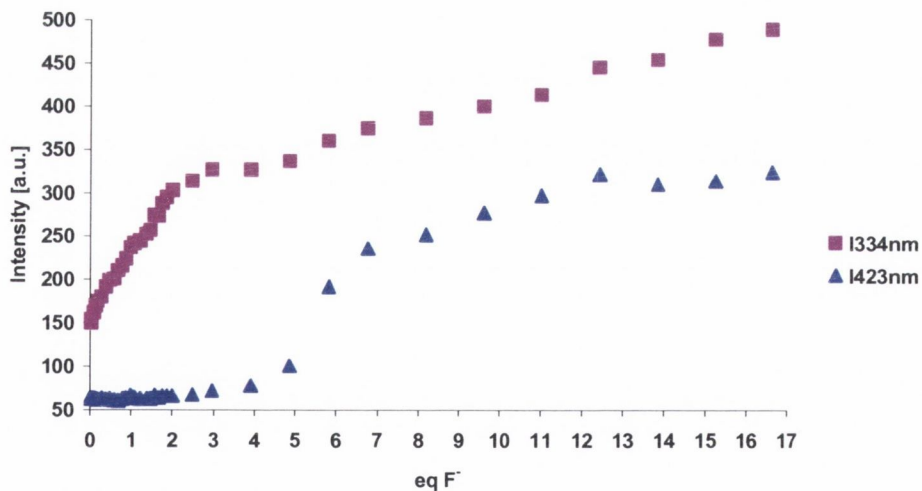


Figure 2.5.4.5.: Titration profile of the fluorescence emission intensity changes at 334 nm and 423 nm respectively, as a function of added equivalents of F^- .

The first three equivalents of anion added correspond to the bigger changes at *ca.* 330 nm, while there were no changes observed at *ca.* 423 nm. In comparison to the case **a)** for the ground state investigations, these changes are ascribed to the binding of the anion to the receptor of **Tb.61**. Indeed, the band at *ca.* 423 nm only started to form after the addition of five equivalents of F^- , which can be related to both the interaction of the anion with the metal center and deprotonation processes.

Taking into account the previously discussed binding model, several binding constants were determined by fitting the data to that model ($G:L$, $G:L_2$, $G_2:L$, $G_2:L_2$, $G_3:L$, $G_4:L$, and $G_5:L$). The resulting speciation distribution diagram and fit to the experimental binding isotherm are shown in **Figure 2.5.4.6**. In this case, the predominant species in solution, upon addition of six equivalents of F^- , is clearly the 5:1 complex, which was not observed previously for the ground state investigations. This is a clear indication of the complexity of the binding process.

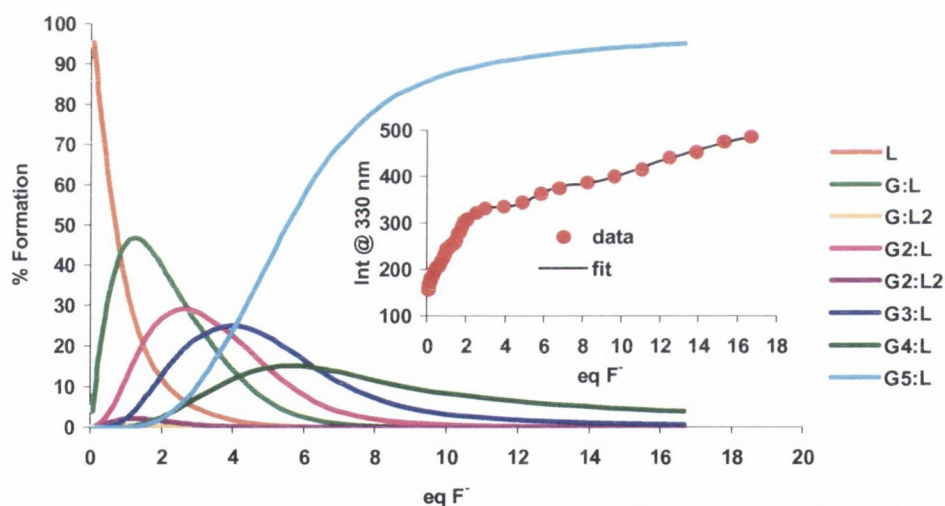


Figure 2.5.4.6: Speciation distribution diagram for the fluorescence titration of **Tb.61** (L) with F^- (G) in CH_3CN . Insert: The experimental binding isotherm and corresponding fit using the SPECFIT model.

The binding constants determined from this fit are listed in **Table 2.5.4**. Once again the formation of the $G:L$ species show the highest binding constant of $\log K_{1:1} = 6.29 \pm 0.11$, which is in good agreement with that determined for the ground state ($\log K_{1:1} = 5.97 \pm 0.18$). However, two noticeable differences can be seen for the formation of the 3:1 and 5:1

species, which show higher binding constants when determined from the singlet excited state changes. Also, while the formation of the $G_5:L$ was observed to be very low ($< 10\%$) for the ground state, this species showed a much higher percentage formation ($\sim 90\%$) for the excited state.

Technique	Species ($G_n:L_m$)	$\log K_{n:m}$	Std. Deviation (\pm)
Fluorescence	$G:L$	6.29	0.11
	$G:L_2$	3.92	0.87*
	$G_2:L$	5.58	0.25
	$G_2:L_2$	5.11	0.53*
	$G_3:L$	5.44	0.09
	$G_4:L$	5.07	0.23
	$G_5:L$	5.69	0.15

Table 2.5.4: Binding constants for the UV-Visible titration of F^- with **Tb.61**. *Species present in solution in less than 10% formation.

The lanthanide luminescence was also followed by excitation of **Tb.61** at 280 nm, **Figure 2.5.4.7**. As for the UV-Visible and the fluorescence discussed above, the occurrence of different binding processes was also observed during the course of the titration with F^- .

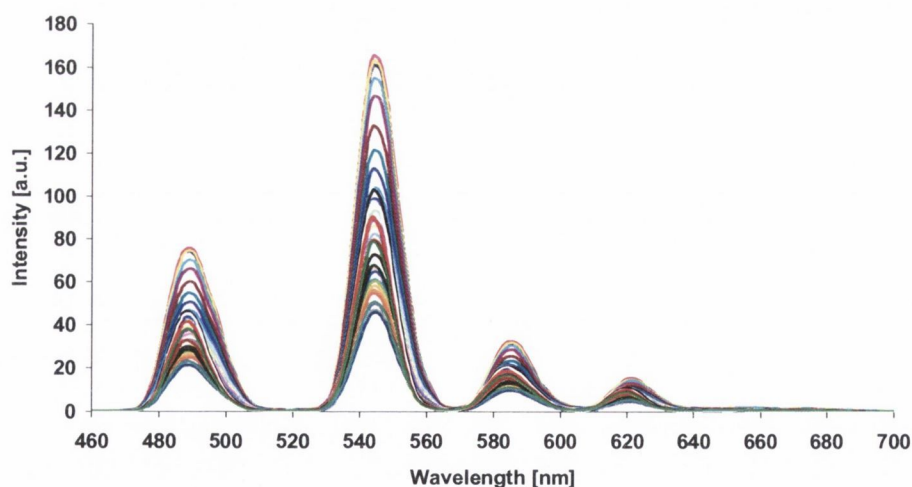


Figure 2.5.4.7: Tb(III) luminescence spectra showing the changes in the emission intensity of **Tb.61** ($4 \mu M$) upon gradual additions of F^- ($0 \rightarrow 66.6 \mu M$) in CH_3CN .

To better understand the possible interactions, the spectra corresponding to the changes associated with the various processes observed upon binding of F^- to **Tb.61** are shown in **Figure 2.5.4.8**. First, the Tb(III) emission intensity decreased by *ca.* 72% upon addition of 0 \rightarrow 4 equivalents of F^- . It is believed that the quenching is due to the binding of the anion at the antenna of **Tb.61**. Upon further addition of F^- , a luminescent enhancement of *ca.* 55% was observed. This was also accompanied by a hypsochromic shift of *ca.* 2 nm. This is ascribed to the possible binding of F^- to the metal ion, or that the binding has an effect on the coordination environment of Tb(III). This was then followed by a decrease in the luminescence. These changes are well illustrated in the profile of the lanthanide emission intensity changes at 546 nm versus the number of equivalents of F^- added, as shown in the insert of **Figure 2.5.4.8**.

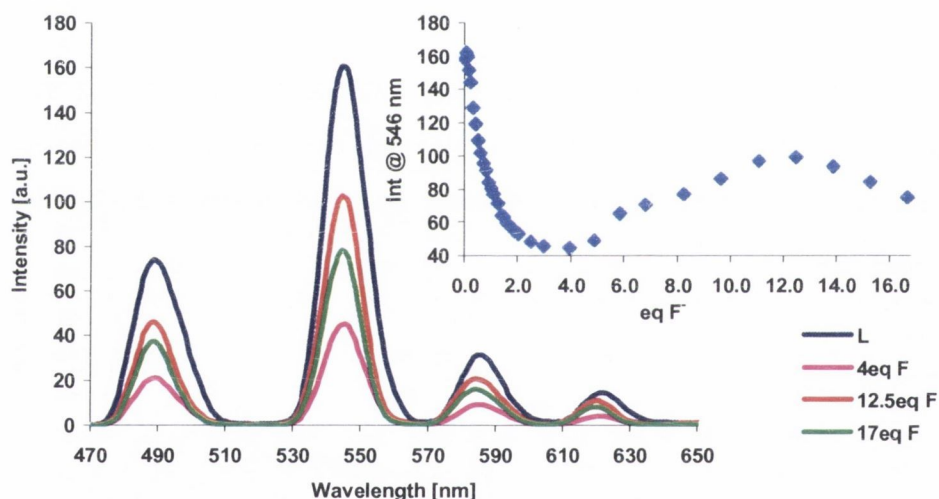


Figure 2.5.4.8: The Tb(III) luminescence spectra showing the changes in emission intensity of **Tb.61** (4 μ M) upon gradual additions of F^- in CH_3CN . L represents the free **Tb.61**. Insert: The profile for the Tb(III) emission intensity changes at 546 nm versus the number of equivalents of F^- .

The determination of the binding constants in such a complex system was not straightforward. One reason being the possible deprotonation of the receptor by F^- to form HF_2^- . In a first approach, the binding constants for the first portion of the profile (0 \rightarrow 7 equivalents F^-) were determined. The fit to the binding model including the species $G:L$, $G:L_2$, $G_2:L$, $G_2:L_2$, and $G_3:L$ is shown in **Figure 2.5.4.9**.

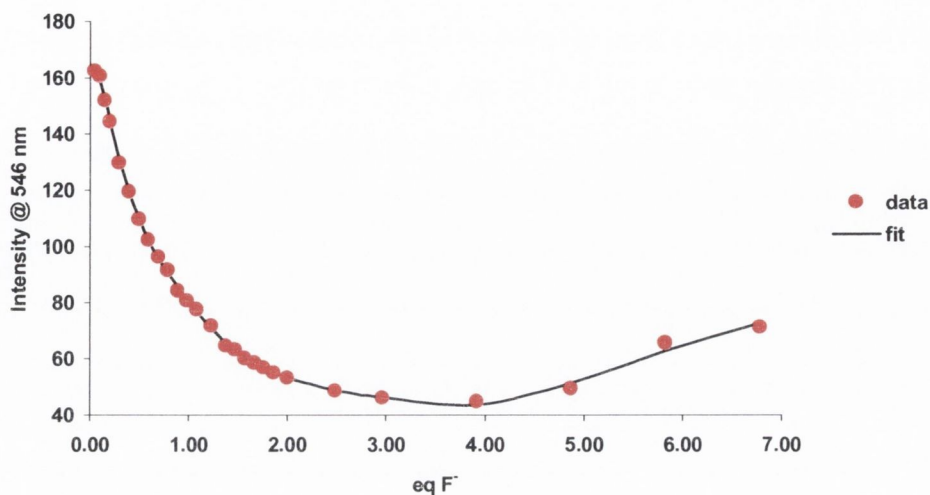


Figure 2.5.4.9: Experimental binding isotherm for the lanthanide luminescence titration of **Tb.61** ($4 \mu\text{M}$) with F^- and corresponding fit using the SPECFIT program.

The values of the binding constants determined from this fit were, in a second approach, used as fixed values on the final binding model for the complete titration ($0 \rightarrow 17$ equivalents of F^-). The speciation distribution diagram as well as the binding isotherm and corresponding fit are shown in **Figure 2.5.4.10**. All the binding constants are summarised in **Table 2.5.4**.

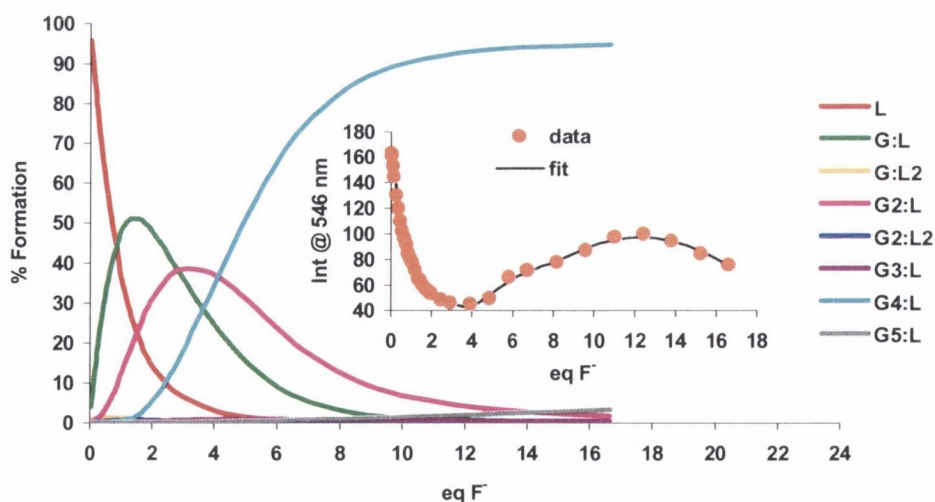


Figure 2.5.4.10: Speciation diagram for the lanthanide luminescence titration of the ligand (L) **Tb.61** ($4 \mu\text{M}$) with F^- (G) in CH_3CN . Inset: The experimental binding isotherm and corresponding fit using the SPECFIT program.

Table 2.5.4 summarises all the binding modes and determined values for corresponding binding constants, regarding the different techniques followed during the titration of ligand **Tb.61** with F^- . It can be seen that the Tb(III) excited state investigations, give rise to a very high binding constant for the formation of the 4:1 ($G_4:L$) complex ($\log K_{4:1} = 6.90 \pm 0.01$), contrasting with what was found for both the ground state and singlet excited stae . This can be possibly due to either the binding of F^- to the metal centre, or that the binding has an effect on the coordination environment of Tb(III). While these studies clearly indicate the presence of multiple binding interactions for the binding of F^- to **Tb.61**, the discrepancies found for the various techniques, does not allow us to draw decisive conclusions.

Anion	Technique	Species ($G_n:L_m$)	$\log K_{n:m}$	Std. Deviation (\pm)
F^-	Absorbance	G:L	5.97	0.18
		G:L ₂	4.73	0.31*
		G ₂ :L	5.16	0.16
		G ₂ :L ₂	5.52	0.45*
		G ₃ :L	4.49	0.19
		G ₄ :L	4.82	0.31
		G ₅ :L	3.51	0.70*
	Phosphorescence	G:L	6.07 [#]	0.02
		G:L ₂	4.13 [#]	0.04*
		G ₂ :L	5.36 [#]	0.01
		G ₂ :L ₂	4.47	0.16*
		G ₃ :L	3.42	0.62*
		G ₄ :L	6.90	0.01
		G ₅ :L	2.85	0.77*
	Fluorescence	G:L	6.29	0.11
		G:L ₂	3.92	0.87*
		G ₂ :L	5.58	0.25
		G ₂ :L ₂	5.11	0.53*
		G ₃ :L	5.44	0.09
		G ₄ :L	5.07	0.23
		G ₅ :L	5.69	0.15

Table 2.5.4: Binding constants and binding modes between F^- and sensor **Tb.61**. *Species present in solution in less than 10%. [#] represents the values previously found and so considered as fixed values.

2.5.5 Photophysical studies of Tb.61 towards binding with Cl⁻

The interaction between **Tb.61** and Cl⁻ was also investigated following the same procedure described above. The changes on the absorption spectra upon gradual additions of Cl⁻ are shown in **Figure 2.5.5**. These changes were much less prominent than those observed for the anions discussed so far. Here, the band centred at *ca.* 280 nm experienced a small decrease, as well as a small bathochromic shift to *ca.* 282 nm. Overall the changes were only minor as demonstrated in the insert on **Figure 2.5.5** for the changes in the absorbance at 264 nm and 310 nm versus the number of equivalents of Cl⁻ added. By fitting these changes a binding constant of $\log K_{1:1} = 5.49 \pm 0.07$ was determined for the 1:1 (G:L) binding interaction between Cl⁻ and **Tb.61**.

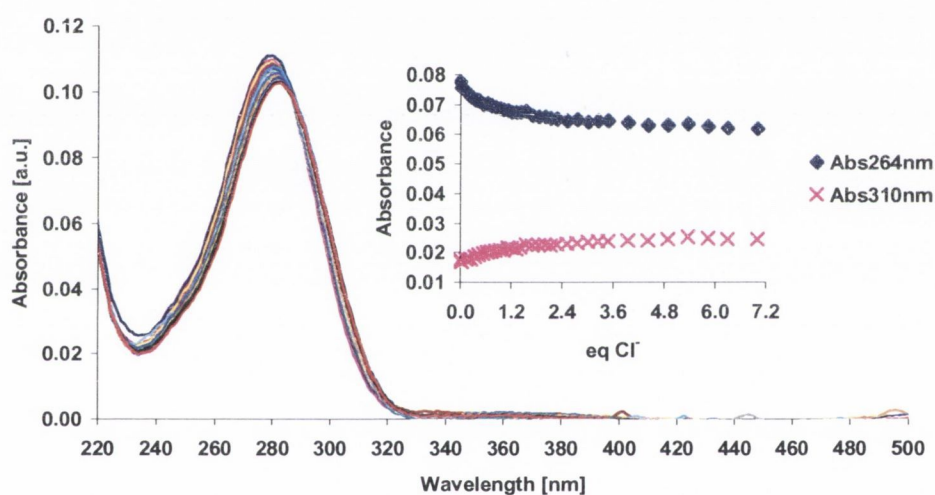


Figure 2.5.5: Absorption spectra showing the changes in absorbance of **Tb.61** (4 μM) upon gradual additions of Cl⁻ (0 \rightarrow 28.1 μM) in CH₃CN. Insert: The profile of the absorbance changes at 264 nm and 310 nm versus the number of equivalents of Cl⁻.

As observed for the ground state, the changes observed on the emission spectrum, upon excitation at 280 nm, were also minimal, **Figure 2.5.5.1**.

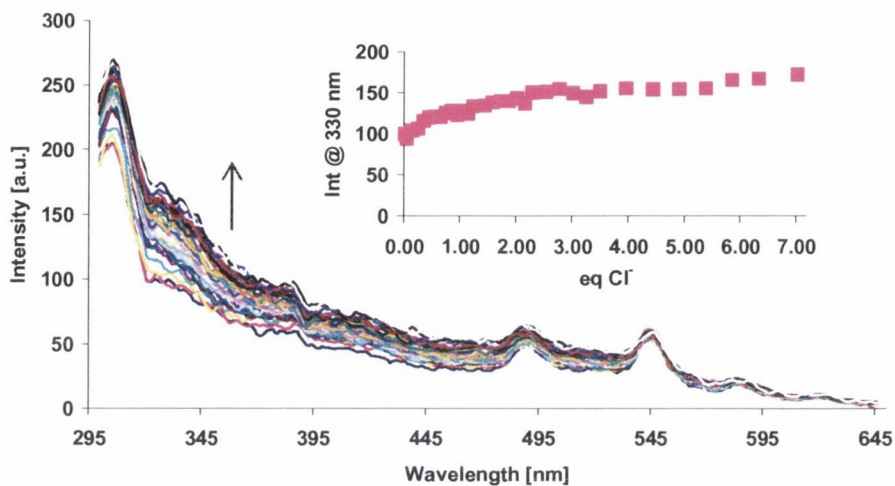


Figure 2.5.5.1: Fluorescence emission spectra showing the changes in emission intensity of **Tb.61** ($4 \mu\text{M}$) upon gradual additions of Cl^- ($0 \rightarrow 28.1 \mu\text{M}$) in CH_3CN . Insert: The changes at 330 nm as a function of Cl^- equivalents.

A binding constant of $\log K_{1:1} = 5.39 \pm 0.06$ was determined for the 1:1 (G:L) binding interaction between Cl^- and **Tb.61**, which is in a good agreement with that obtained for the UV-Visible titration.

In contrast, the most significant changes were observed for the lanthanide emission as shown in **Figure 2.5.5.2**. The intensity was observed to decrease by *ca.* 60% upon addition of Cl^- .

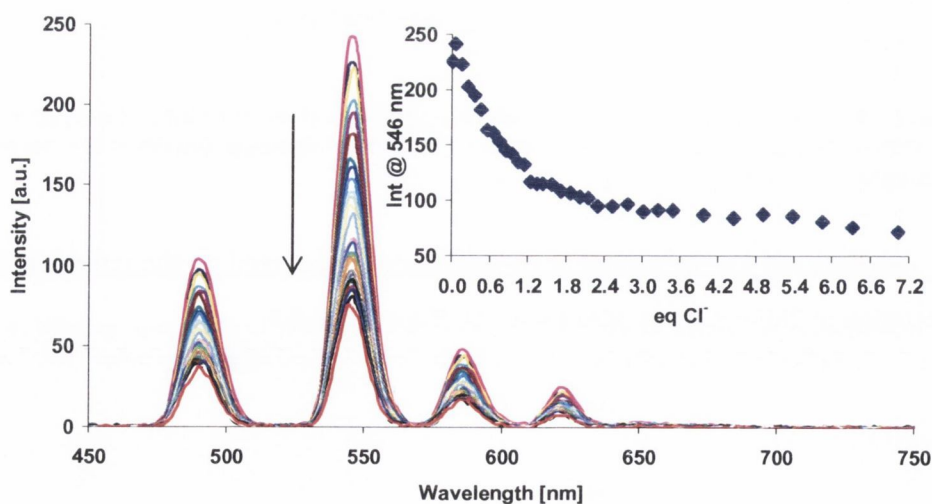


Figure 2.5.5.2: Changes in the lanthanide emission of **Tb.61** ($4 \mu\text{M}$) upon gradual additions of Cl^- ($0 - 28.1 \mu\text{M}$) in CH_3CN . Insert: The changes at 546 nm as a function of Cl^- equivalents.

From these changes, a binding constant of $\log K_{1:1} = 6.06 \pm 0.03$ was determined for the 1:1 (G:L) binding interaction between Cl^- and **Tb.61**. The resulting speciation distribution diagram and fit to the binding isotherm are shown in **Figure 2.5.5.3**.

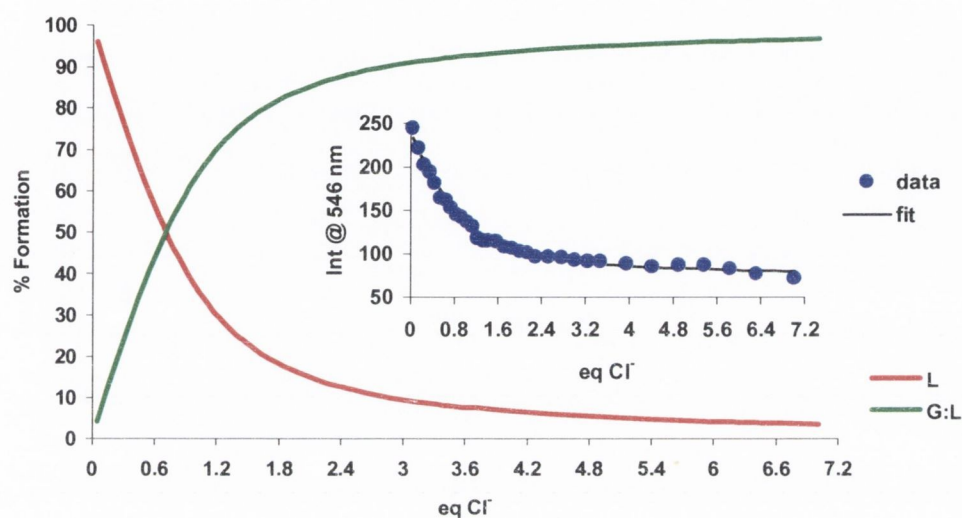


Figure 2.5.5.3: Speciation diagram for the lanthanide luminescence titration of **Tb.61** (L) with Cl^- (G) in CH_3CN . Insert: The experimental binding isotherm and corresponding fit using the SPECFIT program.

Table 2.5.5 summarises the binding constants determined for the titration of **Tb.61** with Cl^- . These values reveal a very good agreement between the ground state, the fluorescence, and the lanthanide luminescence, which further support the 1:1 binding interaction between Cl^- and **Tb.61**.

Anion	Technique	Species ($G_n:L_m$)	$\log K_{n:m}$	Std. Deviation (\pm)
Cl^-	Absorbance	1:1	5.49	0.07
	Fluorescence	1:1	5.39	0.06
	Phosphorescence	1:1	6.06	0.03

Table 2.5.5: Binding constants and binding modes between Cl^- and sensor **Tb.61**.

2.6 Selectivity of **Tb.61** towards H_2PO_4^- over CH_3COO^-

With the aim of demonstrating the selectivity of **Tb.61** towards H_2PO_4^- , the Tb(III) emission of this sensor was recorded in the presence of CH_3COO^- , which quenched the lanthanide emission. However, upon addition of H_2PO_4^- , the emission was increased,

giving rise to a large enhancement of the Tb(III) luminescence, **Figure 2.6**. These results demonstrate the ability of **Tb.61** to function as a selective luminescent sensor for H_2PO_4^- .

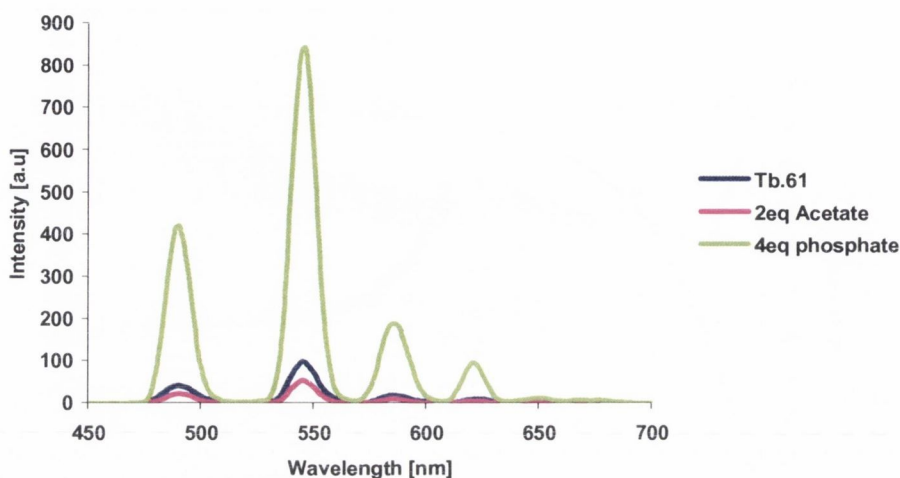


Figure 2.6: Changes in the **Tb.61** ($4 \mu\text{M}$) emission spectra showing selectivity towards H_2PO_4^- over CH_3COO^- .

2.7 Conclusions

In this chapter the synthesis and characterisation of the novel ligand **61** and corresponding Tb(III) and Eu(III) complexes **Tb.61** and **Eu.61** have been discussed. It has been shown through lifetime measurements that each complex possesses one metal bound water molecule.

These lanthanide complexes were designed to work as luminescent sensors for the detection of anions by incorporating hydrogen bonding receptor moieties into a covalently attached antenna. The urea based antenna was expected to efficiently transfer its excited state energy to the excited state of the lanthanide ion, resulting in Ln(III) emission. Although this was indeed observed to be the case for Tb(III), the sensitisation process was inefficient for Eu(III).

Photophysical studies were carried out on **Tb.61** upon addition of different anions. Analysis of the ground and the singlet excited state and the Tb(III) excited states have shown evidence of multiple binding interactions for anions such as CH_3COO^- , H_2PO_4^- , $\text{H}_2\text{P}_2\text{O}_7^{2-}$, and F^- . The bigger spherical Cl^- , on the other hand, was observed to form only 1:1 complexes with the sensor. Binding constants determined for the different binding

interactions were found to be high, which reflects the strong anion affinity of the sensor due to the presence of multiple binding sites as well as the positively charged Tb(III) metal centre. Amongst these anions, H_2PO_4^- was the one found to give rise to the most dramatic enhancements in the Tb(III) emission, which were attributed to the direct interaction with the metal centre. Furthermore, H_2PO_4^- was found to be selectively detected over CH_3COO^- .

In summary, a novel Tb(III) luminescent sensor, **Tb.61**, for anions has been developed by taking advantage of a combination of hydrogen bonding and metal ion coordination binding sites for anionic species.

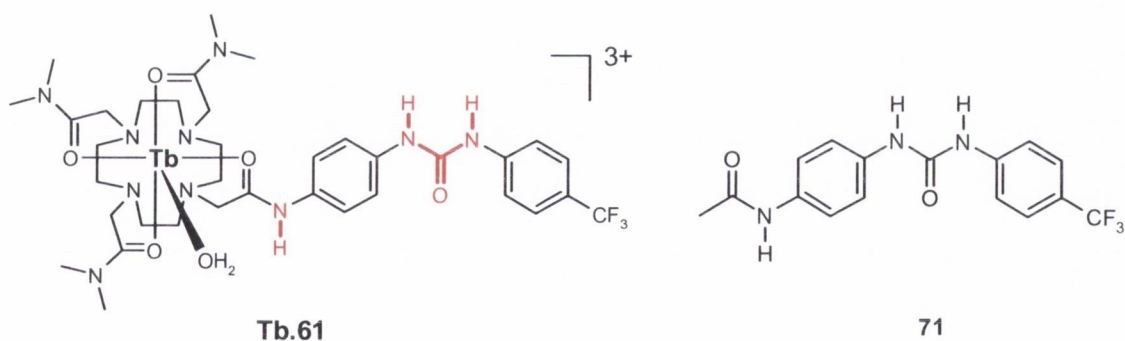
In order to gain further insight into the nature of the multiple binding interactions and to be able to prove the presence of a second binding site within the diaryl antenna, an investigation into the spectroscopic properties of a series of model compounds was set out. Titrations in the presence of several anions were therefore undertaken. The obtained results will be presented and discussed in the next chapter.

Chapter 3

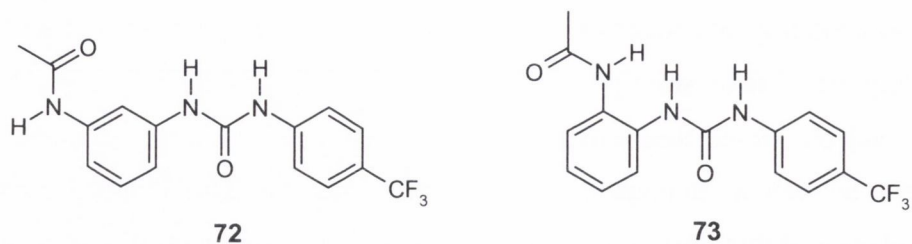
Simple urea-amide receptors for anion recognition

3.1 Introduction

As observed in Chapter 2, the lanthanide luminescent sensor **Tb.61** gave rise to multiple binding interactions for anions such as H_2PO_4^- , CH_3COO^- , $\text{H}_2\text{P}_2\text{O}_7^{2-}$, and F^- . These binding interactions were proposed to take place *via* hydrogen bonding through both the urea and the amide functionalities incorporated in the receptor component of the sensor **Tb.61**, as well as through direct interaction with the Tb(III) metal centre. Due to the complexity of this host architecture, it was proven somewhat difficult to fully understand the binding process. Hence, control experiments to compare the binding ability of simple receptor analogues to that of **Tb.61** would be of great value to corroborate the proposed binding interactions. Therefore, the aim of this project was to synthesize and evaluate the binding ability of a simple model receptor such as **71** in order to gain better understanding of the binding process, as well as to be able to further substantiate the proposed binding process for the interaction of **Tb.61** with the various anions. As can be observed below, receptor **71** is analogous to the anion recognition component of **Tb.61**. So, the model receptor **71** is expected to have similar binding behaviour to that observed for the recognition part of **Tb.61**, which would allow for comparative analysis to be drawn.



With the purpose of further investigate the role of the amide moiety on the binding process, receptors **72** and **73** were synthesised. By changing the relative position of the acetamide group to that of the urea moiety on the aromatic ring, different binding interactions and anion affinities are expected to be observed for these receptors.

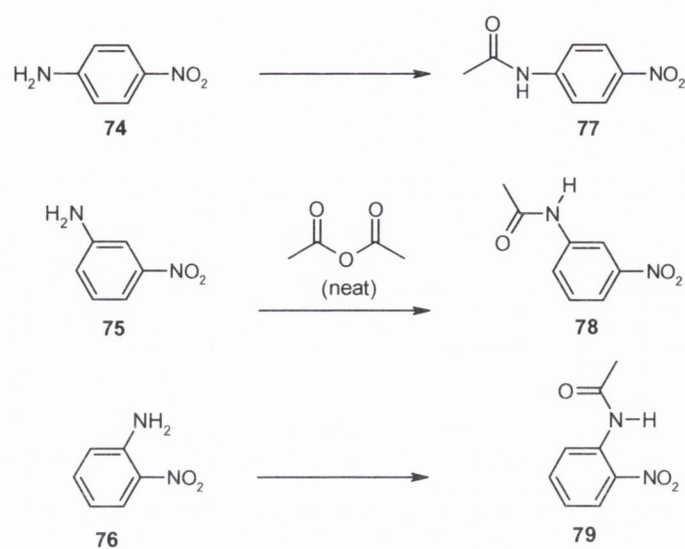


The simplicity of receptors **71** - **73** (allied with simple synthesis) makes them very attractive for anion binding studies. Anion receptors combining both urea and amide hydrogen bonding groups are usually structurally complex and have in the past been difficult to synthesise.¹⁷² Consequently, **71** - **73** are a new family of compounds that have not previously been studied, which would give a valuable insight on the binding process of simple amidourea receptors.

The synthesis and characterisation of **71**, **72**, and **73** will be presented in the following section. Also presented and discussed will be the three receptors X-ray crystal structures, as well as their packing in the solid state. Furthermore, the ability of these receptors to bind a variety of various anions will be investigated.

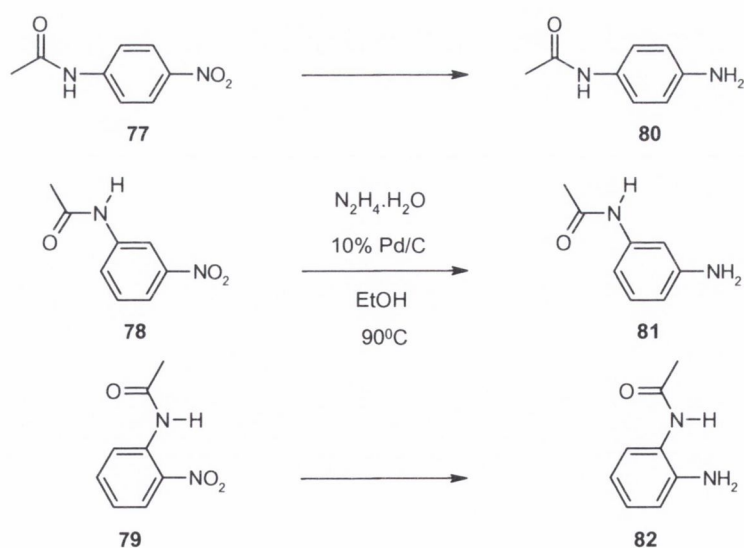
3.2 Synthesis of receptors **71**, **72** and **73**

Receptors **71**, **72**, and **73**, were synthesised in three easy and high yielding steps. The first step was achieved by reacting the commercially available nitroaniline derivatives **74**, **75**, and **76** with neat acetic anhydride to form the desired acetamide functionalities **77**, **78**, and **79**, respectively (**Scheme 3.2**). The precipitates obtained were filtered and washed twice with diethyl ether to yield **77** and **78** as pale beige solids in 83% and 57%, respectively, while **79** was obtained as a yellow crystalline solid in 57% yield.



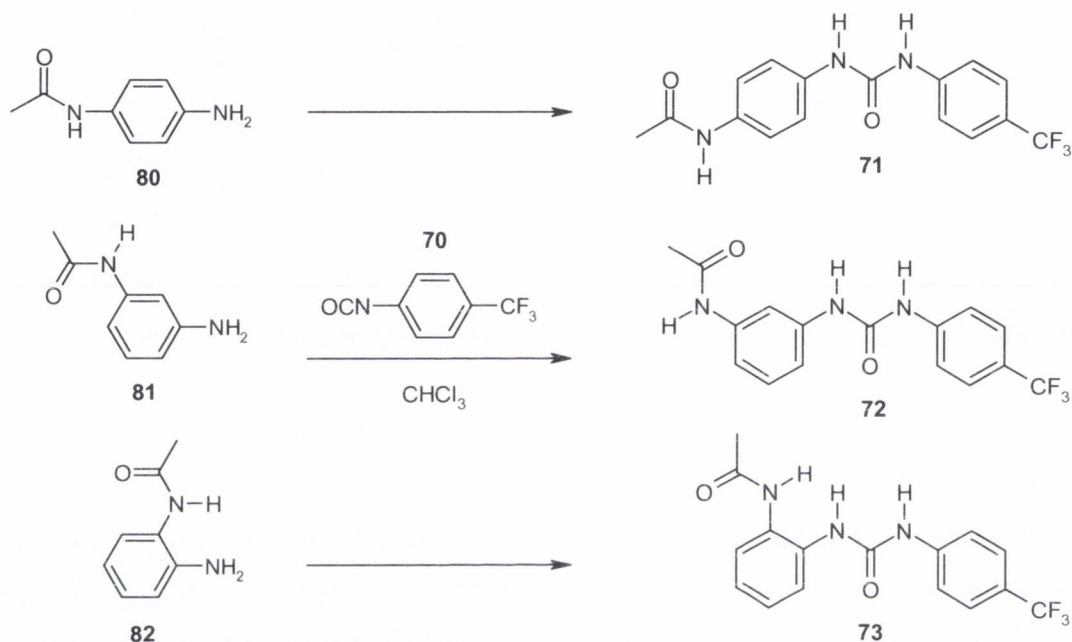
Scheme 3.2: Synthesis of the nitro acetamide precursors **77**, **78**, and **79**

This was followed by the reduction of the nitro group in **77**, **78**, and **79** to the corresponding aniline derivatives, **80**, **81**, and **82** respectively, by using hydrazine monohydrate ($\text{N}_2\text{H}_4 \cdot \text{H}_2\text{O}$) in the presence of 10% Pd/C catalyst. The reactions were carried out in ethanol at 90°C , as shown in **Scheme 3.2.1**. After solvent removal, **80** and **82** were obtained as off white solids in 99% yield, while **81** was isolated as a pale pink crystalline solid in 52% yield.



Scheme 3.2.1: Reduction of the nitro compounds to the corresponding amino derivatives **80**, **81**, and **82**

Finally, the aniline derivatives **80**, **81**, and **82** were reacted with trifluoro-*p*-tolyl isocyanate, **70**, in CHCl_3 at room temperature, **Scheme 3.2.2**. The solids were recrystallised from a mixture of hot $\text{CHCl}_3:\text{CH}_3\text{OH}$ (receptors **71** and **73**) or $\text{CH}_3\text{CN}:\text{H}_2\text{O}$ (receptor **72**) to give the pure receptors **71**, **72**, and **73** as white solids in 90%, 70%, and 88% yields respectively.



Scheme 3.2.2: Reaction with isocyanate to form the final receptors **71**, **72**, and **73**

3.3 Characterization of receptors **71**, **72**, and **73**

The three compounds were fully characterized by the use of conventional methods, such as NMR spectroscopy, ESMS, accurate mass and IR. The ^1H NMR spectrum of **71** in d_6 -DMSO showed the presence of three singlets at 9.88, 9.05, and 8.71 ppm, corresponding to the two urea NH protons and the amide NH proton (**Figure 3.3**). Another clear indication of the successful synthesis of this receptor was the presence of a singlet at 2.02 ppm, corresponding to the three CH_3 protons. The ^{13}C NMR showed the presence of two resonances for the quaternary carbonyl groups, at 167.98 and 152.32 ppm, as well as four quaternary aromatic resonances, and six aromatic peaks. The presence of the methyl group was observed at 23.83 ppm. The presence of the CF_3 group was also seen in the ^{19}F

spectrum, at -60.54 ppm. ESMS analysis showed the presence of a single peak at 360.09, corresponding to the M + Na species of **71**.

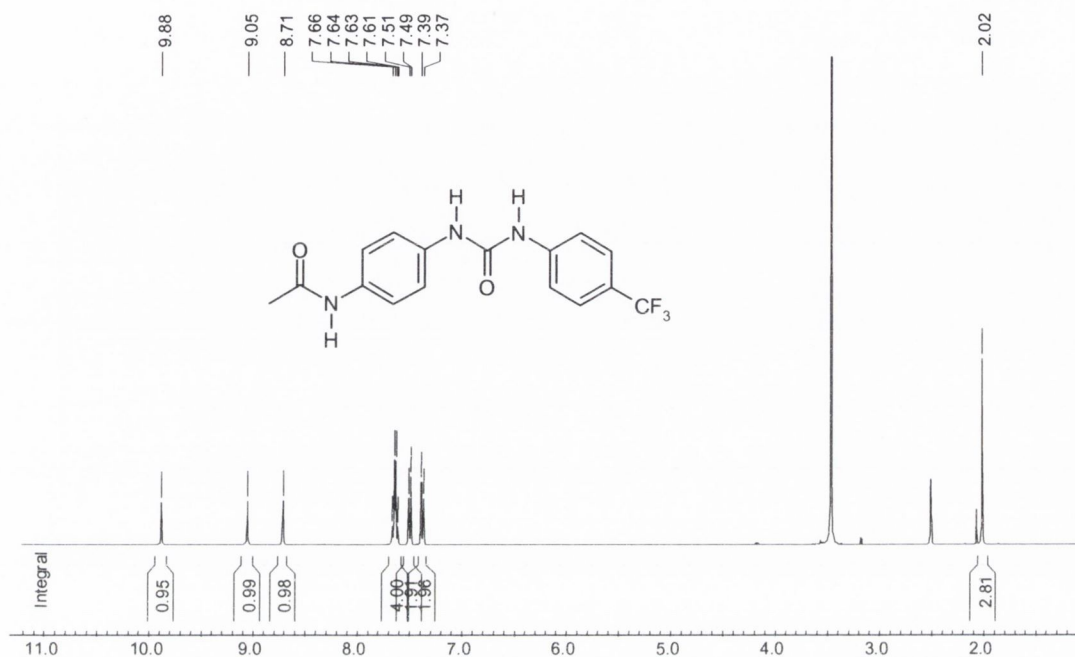


Figure 3.3: The ^1H NMR (d_6 -DMSO, 400 MHz) spectrum of receptor **71**.

The ^1H NMR spectrum of **72** in d_6 -DMSO showed similar results, **Figure 3.3.1**, with the three NH protons appearing as broad singlets at 9.95, 9.29, and 8.87 ppm respectively. A clear indication of the successful synthesis was obtained by the presence of the singlet at 7.79 ppm, assigned to the aromatic proton (H_1) between both the amide and the urea substituents. The ^{13}C NMR also gave a good indication that the desired compound had been synthesised due to the presence of two peaks for the quaternary carbonyl groups, at 168.36 and 152.16 ppm, respectively. Once again, the ^{19}F NMR spectrum revealed the presence of the CF_3 group at -60.56 ppm. ESMS analysis showed the presence of two peaks at 338.13 and 360.09, corresponding to the M + H and M + Na species respectively.

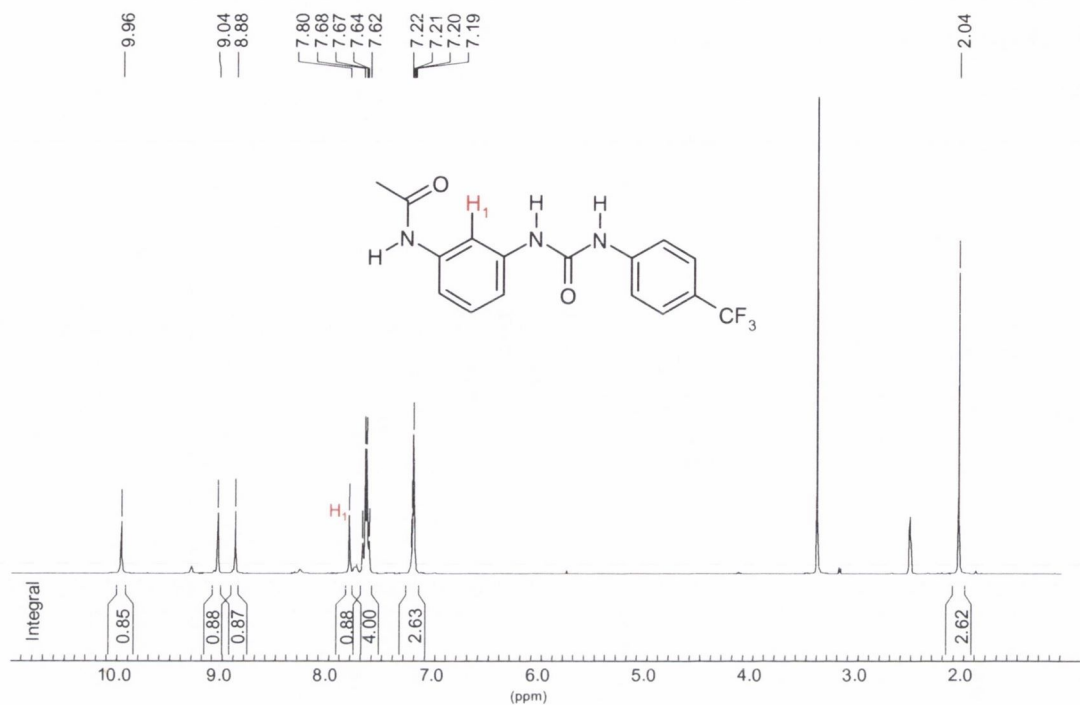


Figure 3.3.1: The ¹H NMR (d₆-DMSO, 400 MHz) spectrum of receptor **72**.

The ¹H NMR spectrum of **73** showed interesting features, **Figure 3.3.2**, as the previous well define separations between the broad peaks for the three NH protons (amide and the two urea protons) were no longer observed. Both N-H2A (urea proton) and N-H3 (amide proton) resonances appeared close together at 9.68 and 9.66 ppm, with N-H1 resonancing at 8.32 ppm. A possible explanation would be the presence of a hydrogen-bonding interaction between the oxygen of the acetamide moiety and the N-H2A proton, which was indeed observed in the crystal structure (**Figure 3.4.3** in Section 3.4). The ¹³C NMR showed the presence of the two peaks for the quaternary carbonyl groups, at 169.26 and 152.44 ppm, respectively. The ¹⁹F spectrum revealed the presence of the CF₃ group at -60.54 ppm. ESMS analysis showed the presence of a single peak at 360.09, corresponding to the M + Na species of **73**.

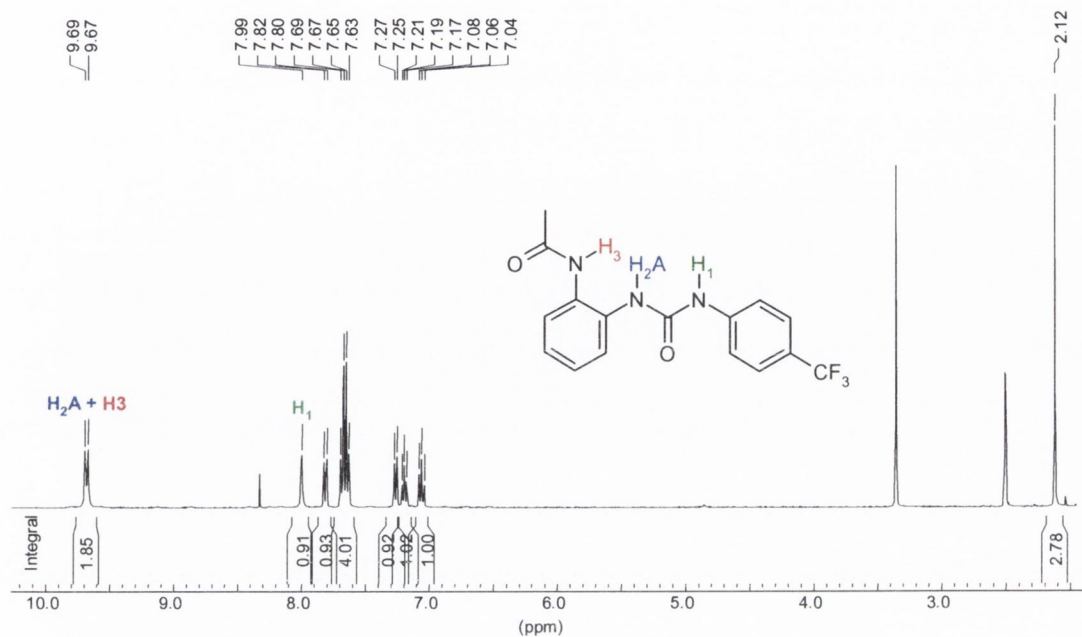


Figure 3.3.2: The ^1H NMR (d_6 -DMSO, 400 MHz) spectrum of compound **73**.

Upon recrystallisation from $\text{CHCl}_3:\text{MeOH}$, cold MeOH, or a mixture of $\text{CH}_3\text{CN}:\text{H}_2\text{O}$, single off-white crystals of receptors **71** – **73** suitable for X-ray diffraction studies were obtained. The crystal structure of these receptors, as obtained by Dr Thomas McCabe, will be analysed in the following section.

3.4 Crystal structure analysis of receptors **71**, **72**, and **73**

The crystal structures of receptors **71**, **72** and **73** are shown in **Figures 3.4**, **3.4.1** and **3.4.2** respectively, with selected bond lengths and angles detailed in **Tables 3.4**, **3.4.1** and **3.4.2** respectively. These crystal structures clearly show that the relative location of the amide moiety has a profound effect on the structure of the bi-aryl receptor. In all three receptors, the NH protons of the urea moiety were found to be in the *syn* conformation (*i.e.* NH protons are facing in the same direction), which makes the receptors suitable for directional hydrogen bonding.²⁸ In order to obtain optimal hydrogen bonding interactions between a urea receptor and an anion, the $\text{NH}\cdots\text{A}$ bonds must be linear.²⁸ The electronic structural calculations performed by Hay and coworkers showed that anion complexation may cause distortions to the urea geometry, which would optimise the linearity of the

NH...A bonds.²⁸ These researchers calculated the optimal O...O distance to be 2.27 Å for oxyanions, in order to achieve linear N-H...O angles for the *syn* conformation of the urea.

The crystal structure of receptor **71** (Figure 3.4) showed that the urea moiety is significantly shifted out of the plane of both the CF₃ substituted phenyl ring as well as the acetamide substituted phenyl ring, with torsion angles of -22.07° and -43.92° respectively.

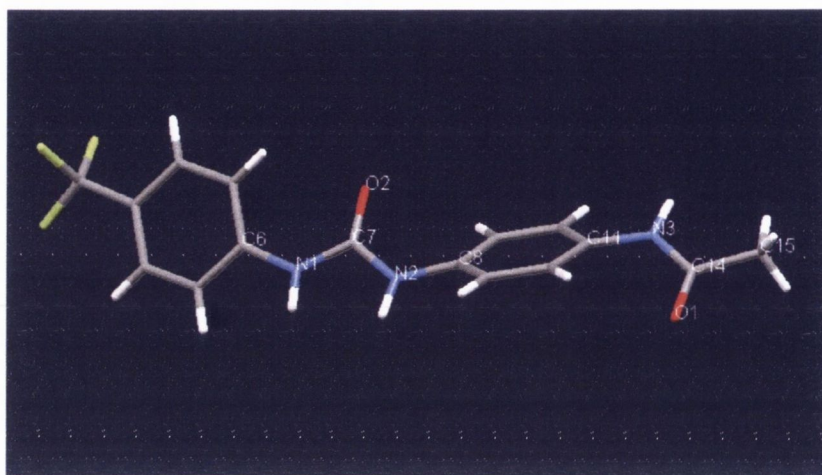


Figure 3.4: Molecular structure of receptor **71**, obtained by X-ray crystallography.

Bond	Length (Å)	Bond	Angle (°)
O(2)-C(7)	1.225(3)	O(2)-C(7)-N(1)	123.3(2)
O(1)-C(14)	1.227(3)	O(2)-C(7)-N(2)	123.6(2)
N(1)-C(7)	1.360(3)	O(1)-C(14)-N(3)	123.4(2)
N(1)-C(6)	1.398(3)	O(1)-C(14)-C(15)	120.9(2)
C(7)-N(2)	1.357(3)	C(14)-N(3)-C(11)	126.61(19)
C(8)-N(2)	1.408(3)	N(3)-C(14)-C(15)	115.7(2)
N(3)-C(14)	1.334(3)	C(7)-N(1)-C(6)	127.4(2)
N(3)-C(11)	1.416(3)	N(2)-C(7)-N(1)	113.2(2)
C(14)-C(15)	1.496(4)	C(7)-N(2)-C(8)	124.9(2)

Table 3.4: Selected bond lengths and bond angles observed in X-ray crystallographic study of **71**

As observed for **71**, the crystal structure of receptor **72** (Figure 3.4.1) showed that the urea moiety is significantly shifted out of the plane of both the CF₃ substituted phenyl ring

as well as the acetamide substituted phenyl ring, with torsion angles of -38.57° and 48.92° respectively.

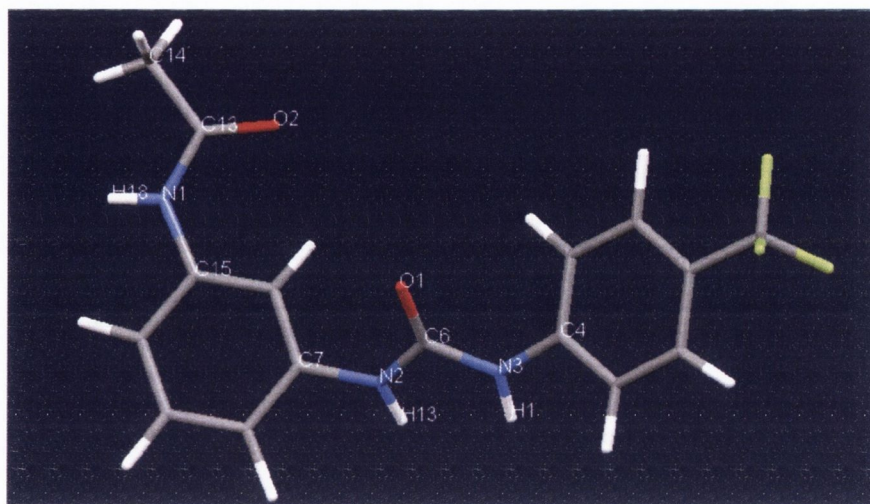


Figure 3.4.1: Molecular structure of receptor **72**, obtained by X-ray crystallography. The solvent molecule (CH_3OH) has been omitted for clarity.

Bond	Length (Å)	Bond	Angle (°)
O(1)-C(6)	1.240(3)	O(1)-C(6)-N(2)	123.6(2)
O(2)-C(13)	1.239(3)	O(1)-C(6)-N(3)	122.9(2)
N(1)-C(13)	1.352(3)	O(2)-C(13)-N(1)	123.7(3)
N(1)-C(15)	1.418(3)	O(2)-C(13)-C(14)	120.9(2)
N(2)-C(6)	1.365(3)	N(2)-C(6)-N(3)	113.5(2)
N(2)-C(7)	1.420(3)	C(6)-N(2)-C(7)	124.3(2)
N(3)-C(6)	1.371(3)	C(6)-N(3)-C(4)	124.7(2)
N(3)-C(4)	1.408(3)	C(13)-N(1)-C(15)	128.9(2)

Table 3.4.1: Selected bond lengths and bond angles for **72**.

Analysis of the crystal structure obtained for receptor **73**, showed the presence of hydrogen bond interactions between the oxygen atom of the acetamide and the hydrogen (**H2A**) of the urea moiety, **Figure 3.4.2**. These findings further supported the results observed on the ^1H NMR spectrum. Once again, the urea moiety was found to be significantly shifted out of the plane of both the substituted phenyl rings, with torsion

angles of -42.83° and 61.32° in relation to the CF_3 substituted phenyl ring and the acetamide substituted phenyl ring respectively.

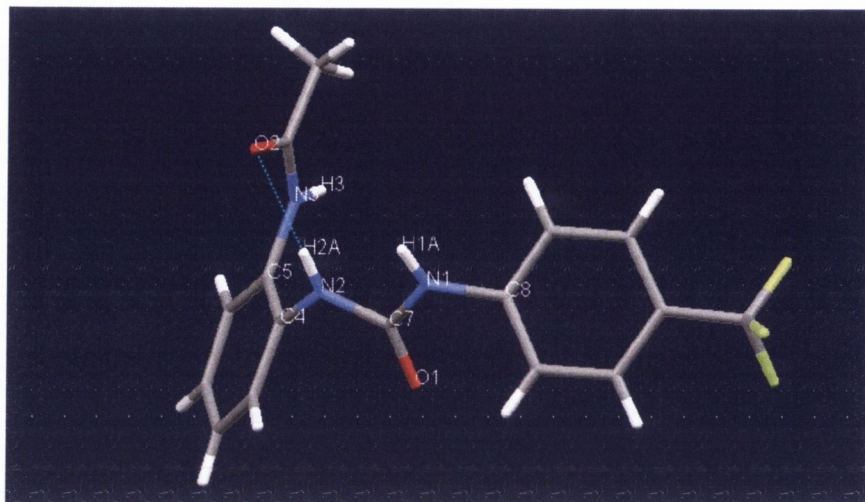


Figure 3.4.2: Molecular structure of receptor **73**, obtained by X-ray crystallography.

Bond	Length (Å)	Bond	Angle (°)
O(1)-C(7)	1.241(4)	O(1)-C(7)-N(2)	123.0(3)
O(2)-C(15)	1.247(5)	O(1)-C(7)-N(1)	123.2(3)
N(1)-C(8)	1.419(5)	O(2)-C(15)-N(3)	122.9(3)
N(1)-C(7)	1.371(5)	O(2)-C(15)-C(16)	121.9(4)
N(2)-C(4)	1.431(5)	N(1)-C(7)-N(2)	113.9(3)
N(2)-C(7)	1.362(5)	C(7)-N(1)-C(8)	123.0(3)
N(3)-C(15)	1.347(5)	C(4)-N(2)-C(7)	121.6(3)
N(3)-C(5)	1.431(5)	C(5)-N(3)-C(15)	127.3(3)
C(4)-C(5)	1.396(5)	N(2)-C(4)-C(5)	122.0(3)

Table 3.4.2: Selected bond lengths and angles for **73**.

The crystal structure packing of **71** – **73** are shown in **Figures 3.4.3**, **3.4.4** and **3.4.5**, respectively. The space group for **71** and **73** was found to be $P2(1)/c$, while it was found to be $P1$ for **72** (see appendix A1). All three structures gave rise to intermolecular hydrogen bonding networks. The view along the crystallographic b and c -axis of the packing diagram

of **71** (Figure 3.4.3) clearly shows the intermolecular hydrogen bonding network existent between the amide and the urea moieties of neighbouring molecules.

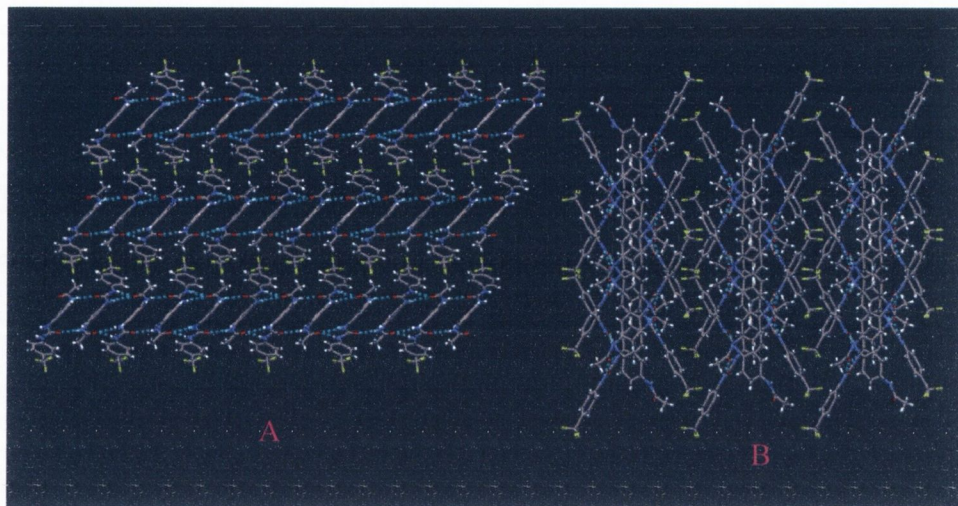


Figure 3.4.3: The packing diagram of **71**, when viewed along the A) crystallographic b-axis and B) crystallographic c-axis: O red, N dark blue, C dark grey, H white, F yellow.

In the case of receptor **72**, the packing diagram showed intermolecular hydrogen bonding between the urea protons and the oxygen atom of a neighbour urea moiety, while the amide moiety was found to be involved in intramolecular hydrogen bonding interactions with neighbour solvent (CH_3OH) molecules, as shown in **Figures 3.4.4**.

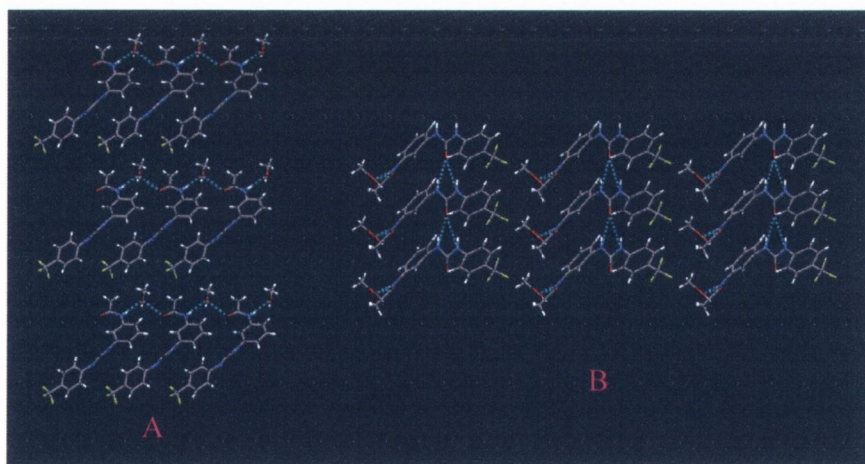


Figure 3.4.4: The packing diagram of **72**, when viewed along the A) crystallographic a-axis and B) crystallographic b-axis: O red, N dark blue, C dark grey, H white, F yellow.

In contrast to the receptors discussed above, receptor **73** gave rise to a more complex packing network, as shown in **Figures 3.4.5**. In this case, the packing was formed of both intramolecular and intermolecular hydrogen bonding interactions among the amide and urea moieties.

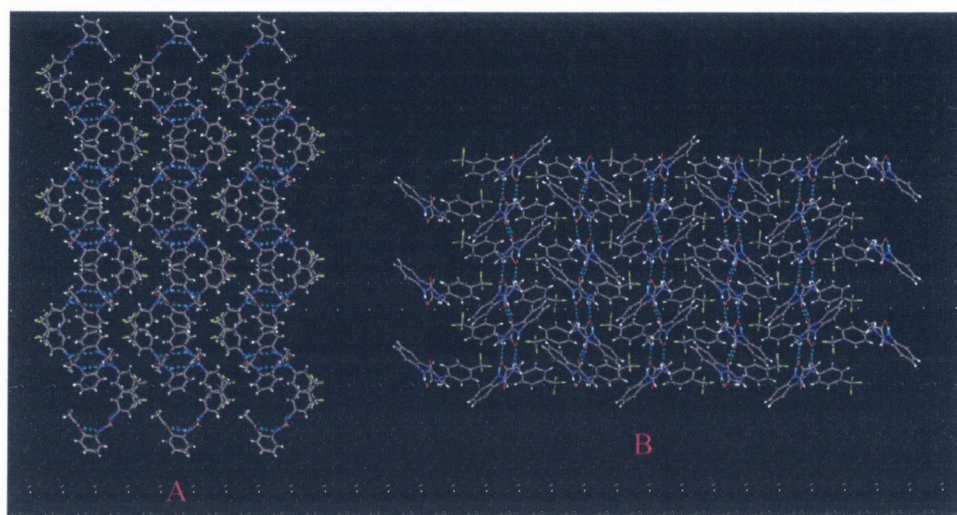


Figure 3.4.5: The packing diagram of **73** showing the complex intra- and intermolecular bonding network existent between the amide and urea moieties, when viewed along the **A)** crystallographic *c*-axis and **B)** crystallographic *a*-axis: O red, N dark blue, C dark grey, H white, F yellow.

It should be noted, that although these different structural properties for **71** – **73** are observed in the solid state, they may have an influence on the binding affinities of the active recognition sites in solution. With this in mind, the binding ability of these receptors towards various anions in solution was investigated. The results of these studies will be discussed in the following sections.

3.5 Absorption properties of receptors 71-73

The absorption spectra of **71**, **72**, and **73** are shown in **Figure 3.5**, when recorded at room temperature in CH_3CN . Receptors **71** and **73** both exhibited a broad band centred at *ca.* 274 nm ($\log \epsilon = 4.57$) and *ca.* 260 nm ($\log \epsilon = 4.46$) respectively, assigned to their π - π^* transitions. Receptor **72**, however, showed a broad band centred at *ca.* 257 nm ($\log \epsilon = 4.50$), assigned to the π - π^* transitions. In addition, a smaller band at *ca.* 224 nm ($\log \epsilon = 4.31$) was observed. The significant 17-14 nm difference in the λ_{max} of **71** and either **72** or **73** can be attributed to the relative location of the amide to that of the urea moiety, as well

as possible weak internal charge transfer (ICT) contributions. Upon excitation at the λ_{max} , the receptors gave rise to weak fluorescence emission.

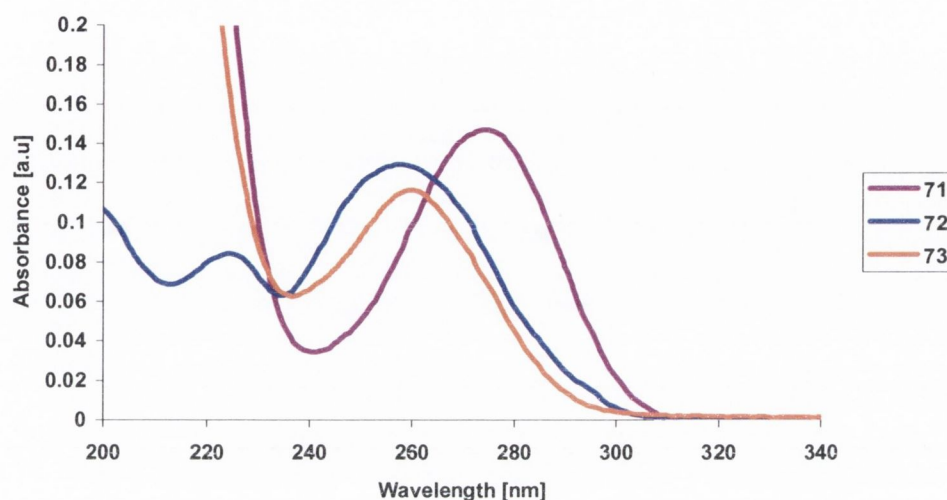


Figure 3.5: The absorption spectra of receptors **71** (purple), **72** (blue) and **73** (orange), when recorded in CH_3CN .

3.6 Absorption studies upon addition of anions

In order to evaluate the response of these receptors to the presence of anions, titrations were carried out at room temperature in CH_3CN , in a similar manner previously described for **Tb.61** (Chapter 2). The anion binding ability of receptors **71-73**, as well as the stoichiometries for the resulting binding interactions was investigated by carrying out titrations of a stock solution of these receptors ($4 \mu\text{M}$) with gradual additions of various anion solutions, as their tetrabutylammonium salts (TBA^+). However, a minimum amount of DMSO ($< 0.1\%$) was used for the preparation of the stock solution of **71** and **73** in order to maximize the solubility of these sensors in CH_3CN , while receptor **72** was found to be fully soluble in CH_3CN . The anions studied included acetate (CH_3COO^-), dihydrogenphosphate (H_2PO_4^-), dihydrogenpyrophosphate ($\text{H}_2\text{P}_2\text{O}_7^{2-}$), fluoride (F^-), and chloride (Cl^-).

The spectroscopic studies performed in order to evaluate the anion binding ability of such receptors will be presented in the following sections. For clarity, the results and subsequent discussion will be presented separately for each receptor.

3.6.1 Absorption studies performed on **71**

The changes in the absorption spectrum upon titration of **71** (model compound for **Tb.61**) with the various anions showed a bathochromic shift with formation of a clear isosbestic point. The family of spectra obtained for the titration of **71** with H_2PO_4^- are presented in **Figure 3.6.1**, which clearly shows that the absorption is significantly affected upon interaction with the anion. Similar results were obtained for the interaction of **71** with the remaining studied anions, which are presented in the Appendix section (Appendix 2).

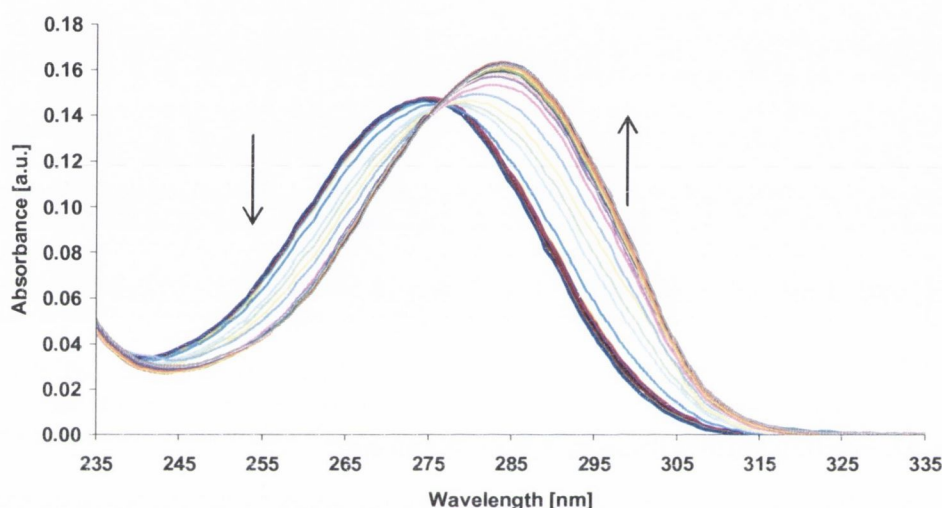


Figure 3.6.1.: Changes in the absorption spectra of model receptor **71** ($4 \mu\text{M}$) upon gradual additions of H_2PO_4^- ($0 \rightarrow 1.63 \text{ mM}$) in MeCN.

Here, the band centred at *ca.* 274 nm was shifted to *ca.* 284 nm with the formation of a clear isosbestic point at *ca.* 276 nm. The same behaviour was observed for $\text{H}_2\text{P}_2\text{O}_7^{2-}$, while both CH_3COO^- and F^- exhibited the bigger shifts, *ca.* 286 nm and *ca.* 287 nm respectively (see Appendix 2). These changes constitute a clear evidence of the binding interaction between **71** and the anions through hydrogen bonding. The spectral changes observed for Cl^- were less significant and occurred only at relatively higher concentration of the anion (see Appendix 2). From the changes observed upon titration with the different anions, binding constants ($\log K$) for complex formation between the anions (G) and **71** (L) were determined by fitting the data using the non-linear least squares regression program SPECFIT (Chapter 2). The obtained stoichiometries and corresponding $\log K$ values are

listed in **Table 3.6.1**. For anions such as CH_3COO^- , H_2PO_4^- , and F^- two distinct binding modes were clearly observed, which was supported by the good fit obtained from SPECFIT. The changes observed for the titration of **71** with H_2PO_4^- at 284 nm and corresponding fit obtained from SPECFIT are shown in **Figure 3.6.1.1**.

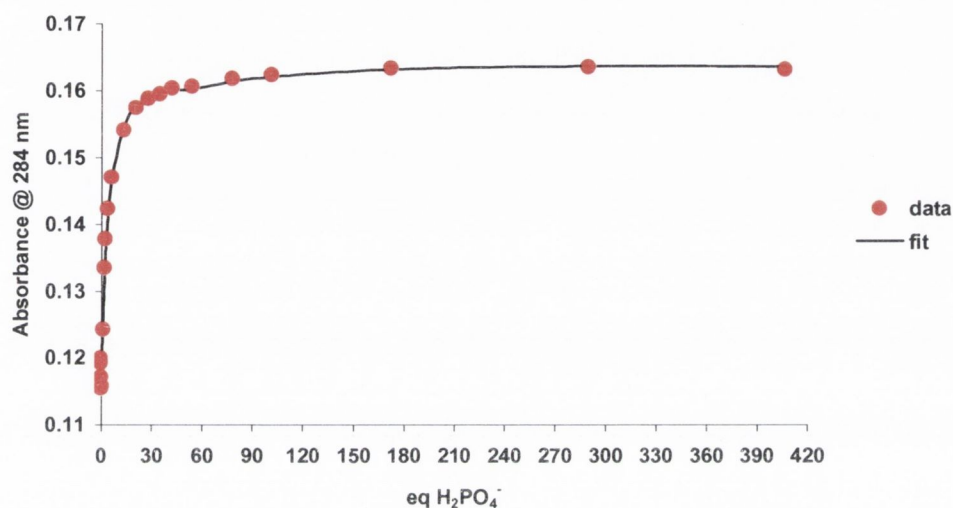


Figure 3.6.1.1.: Experimental binding isotherm for the titration of **71** ($4 \mu\text{M}$) with H_2PO_4^- and corresponding fit from SPECFIT.

The first binding mode was ascribed to the interaction between the anions and the urea moiety of **71** through hydrogen bonding. Both CH_3COO^- and F^- gave rise to similar binding constants of $\log K_{1:1} = 5.29 \pm 0.03$ and $\log K_{1:1} = 5.25 \pm 0.05$, respectively. These constants were found to be marginally higher than the one determined for H_2PO_4^- , $\log K_{1:1} = 4.93 \pm 0.05$. This higher affinity between simple urea based receptors and F^- or CH_3COO^- over H_2PO_4^- has been well documented for related urea or thiourea motives.^{21,29,173} Moreover, upon further addition of anion, a second binding interaction was observed. This interaction was ascribed to the binding of two anion ions to one molecule of **71**, giving rise to the $\text{G}_2:\text{L}$ complexes, as shown in the speciation distribution diagram depicted in **Figure 3.6.1.2**, for the interaction of **71** with H_2PO_4^- . This diagram shows that the $\text{G}:\text{L}$ complex is present in a very high percentage (*ca.* 80%), being the predominant species in solution after an initial addition of 20 equivalents of H_2PO_4^- . Furthermore, a second binding interaction between two of these anions and one molecule of **71** takes place giving rise to the formation of a 2:1

(G₂:L) complex, which becomes the dominant species in solution at higher concentrations (> 20 equivalents H₂PO₄⁻). Similar results were obtained for CH₃COO⁻ and F⁻ (see Appendix 2).

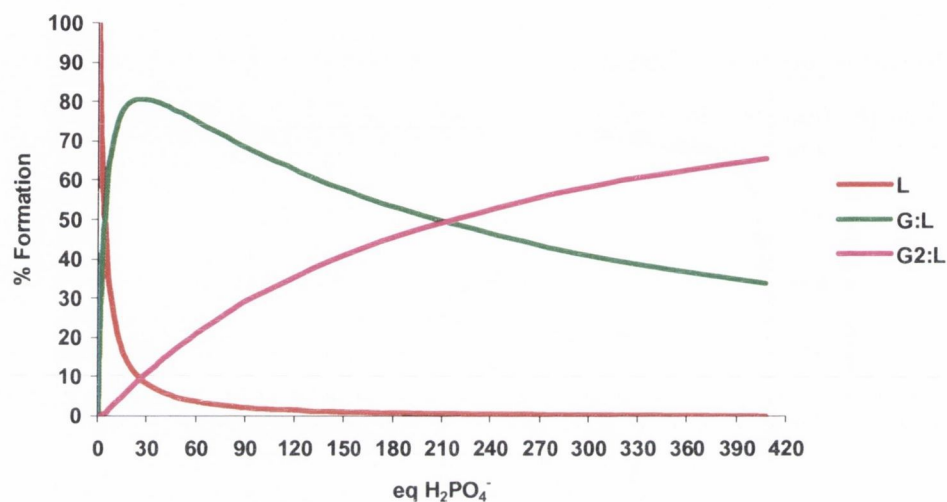
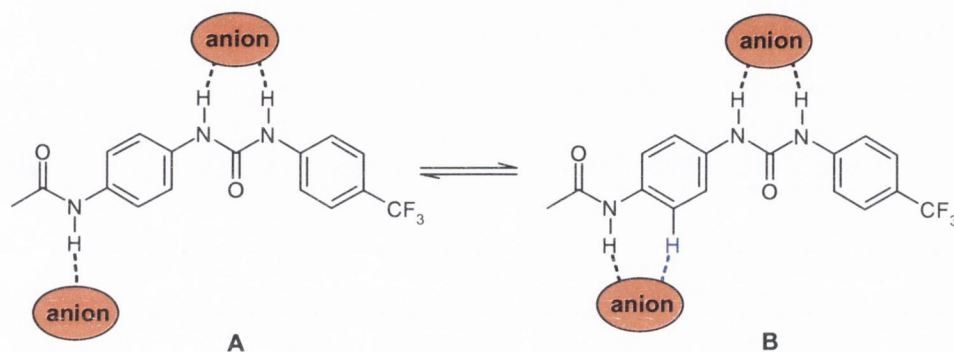


Figure 3.6.1.2: Speciation diagram for the titration of **71** (L) with H₂PO₄⁻ (G) in MeCN. Speciation is shown relative to the number of equivalents of H₂PO₄⁻.

The determined binding constants, $\log K_{2:1} \sim 3-4$, were found to be weaker than those obtained for the 1:1 interaction ($\log K_{1:1} \sim 5-6$), but nevertheless reasonably strong (**Table 3.6.1**). These binding constants, although weaker than those determined for **Tb.61** ($\log K_{1:1} \sim 6-7$, $\log K_{2:1} \sim 5-6$) follow the same pattern, as the 1:1 binding interaction was found to be stronger than the 2:1 for both **Tb.61** and **71**. Such higher binding constants exhibited by **Tb.61**, when comparing to those obtained for the simple model receptor **71**, are most likely due to possible electrostatic interactions between the anions and the metal centre. These results further substantiate the proposed multiple binding interactions between such anions and the lanthanide luminescent sensor **Tb.61** (Chapter 2). So, in agreement with the proposed binding modes for **Tb.61**, the 2:1 binding interactions for **71** are anticipated to take place through the hydrogen of the amide moiety (which is *para* to the urea moiety in **71**) as shown in **Scheme 3.6.1**. The interaction depicted as **A** in **Scheme 3.6.1** shows the possible single hydrogen bonding interaction between the amide and the anion, which was not expected to give rise to such relatively strong 2:1 (anion:receptor) binding constants. However, as discussed in Chapter 2, Hay *et al.* have shown that aryl protons can participate

in hydrogen bonding to anions.¹⁶⁶ Therefore, the interaction depicted as **B** in **Scheme 3.6.1** should also be taken into consideration. The possible interaction of the aromatic proton to the anion (shown in blue in **Scheme 3.6.1**) would increase the binding affinity of the amide moiety towards anions, which would explain the relatively high binding constants obtained for these 2:1 interactions.



Scheme 3.6.1: Proposed binding interactions between anions (CH_3COO^- , H_2PO_4^- , and F^-) and **71** to form the $\text{G}_2\text{:L}$ species.

Conversely, $\text{H}_2\text{P}_2\text{O}_7^{2-}$ and Cl^- were observed to only form 1:1 complexes with **71**. **Figure 3.6.1.3** clearly shows G:L as the only species present in solution, upon addition of the divalent $\text{H}_2\text{P}_2\text{O}_7^{2-}$ anion (*ca.* 5 equivalents). This was further supported by the excellent fit to the experimental binding isotherm, as shown in **Figure 3.6.1.3** insert.

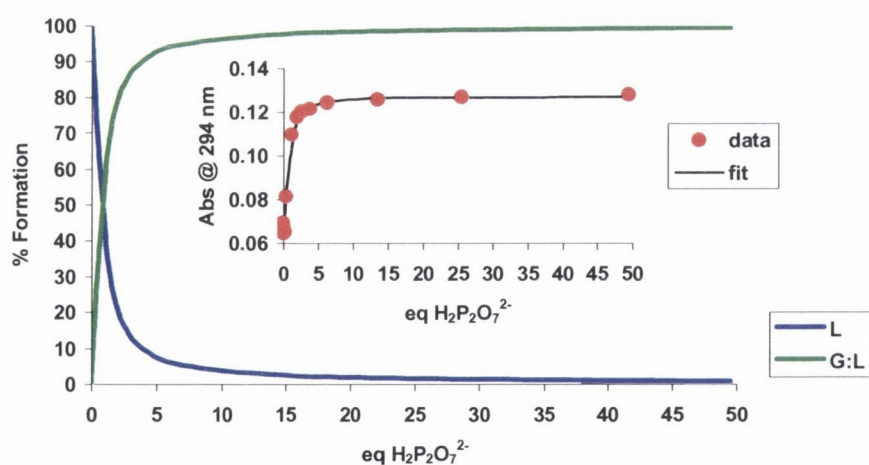


Figure 3.6.1.3: Speciation diagram for the titration of **71** (L) with $\text{H}_2\text{P}_2\text{O}_7^{2-}$ (G) in MeCN. Speciation is shown relative to the number of equivalents of $\text{H}_2\text{P}_2\text{O}_7^{2-}$. Insert: The fit to the experimental binding isotherm.

Among the titrated anions, Cl^- showed the weakest interaction with receptor **71**, with $\log K_{1:1} = 3.45 \pm 0.06$, while $\text{H}_2\text{P}_2\text{O}_7^{2-}$ was observed to possess a much higher binding constant of $\log K_{1:1} = 5.88 \pm 0.09$. In fact, among the anions studied, $\text{H}_2\text{P}_2\text{O}_7^{2-}$ showed the higher binding constant for the formation of the G:L complex, **Table 3.6.1**. The higher binding affinity to $\text{H}_2\text{P}_2\text{O}_7^{2-}$ can be explained by taking into account the possibility of simultaneous binding interactions through the oxygen atoms of each phosphate to both the urea and amide functionalities in **71**.

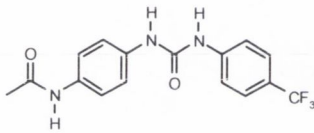
Receptor (L)	Anion (G)	Binding mode ($G_n:L_m$)	Log $K_{n:m}$	Std. Deviation (\pm)
 <p style="text-align: center;">71</p>	CH_3COO^-	G:L	5.29	0.03
		$G_2:L$	3.50	0.19
	F^-	G:L	5.25	0.05
		$G_2:L$	2.72	0.23
	H_2PO_4^-	G:L	4.93	0.05
		$G_2:L$	3.08	0.43
$\text{H}_2\text{P}_2\text{O}_7^{2-}$	G:L	5.88	0.09	
Cl^-	G:L	3.45	0.06	

Table 3.6.1: Binding constants and binding modes between anions and model receptor **71**

As mentioned before, by changing the position of the acetamide moiety on the aromatic ring different spectral properties for the final compound were expected. This structural change was also expected to have an influence on the binding affinity of the different receptors. The following section will focus on the results obtained for receptor **72**, upon addition of the various anions.

3.6.2 Absorption studies performed on **72**

Upon addition of the various anions, the absorption spectrum of **72** experienced bathochromic shifts for both the bands centred at *ca.* 224 nm and *ca.* 257 nm, with the concomitant formation of two isosbestic points. Similar results were observed for all the anions studied, see Appendix 2. The family of spectra obtained for the titration with H_2PO_4^- are presented in **Figure 3.6.2**.

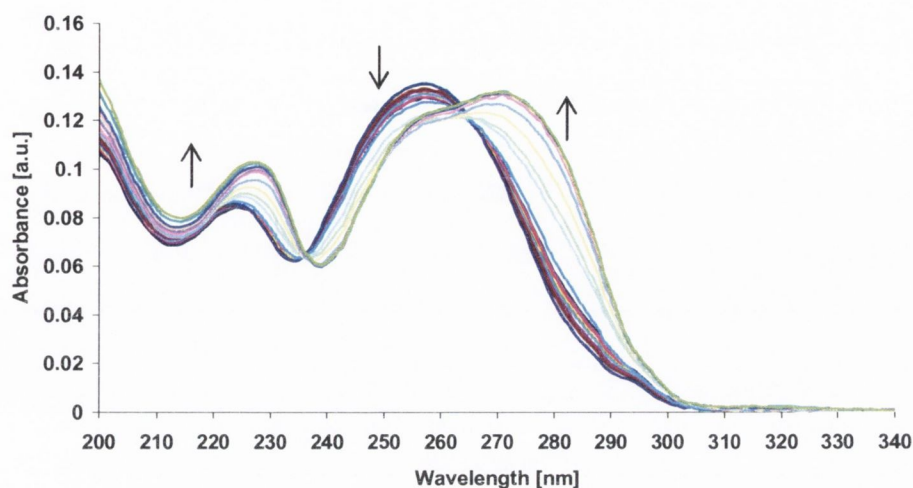


Figure 3.6.2: Absorption spectra showing the changes in absorbance of receptor **72** ($4 \mu\text{M}$) upon gradual additions of H_2PO_4^- ($0 \rightarrow 0.235 \text{ mM}$) in MeCN.

The band centred at *ca.* 224 nm was shifted to *ca.* 227 nm with the formation of a clear isosbestic point at *ca.* 236 nm, while the band centred at *ca.* 257 nm experienced a larger shift to *ca.* 272 nm. This shift was also accompanied with the formation of an isosbestic point at *ca.* 263 nm, as shown in **Figure 3.6.2**. Once again the same behaviour was observed for $\text{H}_2\text{P}_2\text{O}_7^{2-}$ (see Appendix 2). As previously observed (Section 3.6.1), CH_3COO^- and F^- exhibited larger shifts, *ca.* 274 nm with an isosbestic point at *ca.* 266 nm. The observed changes strongly indicate the binding between **72** and the anion through hydrogen bonds. The spectral changes observed for Cl^- occurred only at higher concentration, and the bathochromic shift caused by the interaction with Cl^- was the smallest among the anions studied. Nevertheless, this shift (*ca.* 12 nm) was considerable when compared with the one observed for **71** (*ca.* 6 nm).

By fitting the changes for each titration, the binding constants for these anions and **72** were determined using SPECFIT. In comparison with **71**, receptor **72** displayed a more intricate behavior. In fact, best fittings of the overall titration data were obtained by assuming the existence of multiple stepwise equilibria. For H_2PO_4^- , F^- , and $\text{H}_2\text{P}_2\text{O}_7^{2-}$, the changes observed were best fitted to 1:1, 1:2 and 2:1 (anion:receptor) stoichiometries, as

shown in **Figure 3.6.2.1** for the titration of **72** with H_2PO_4^- . Insert in **Figure 3.6.2.1** shows the good fit to the experimental data at lower concentrations of H_2PO_4^- .

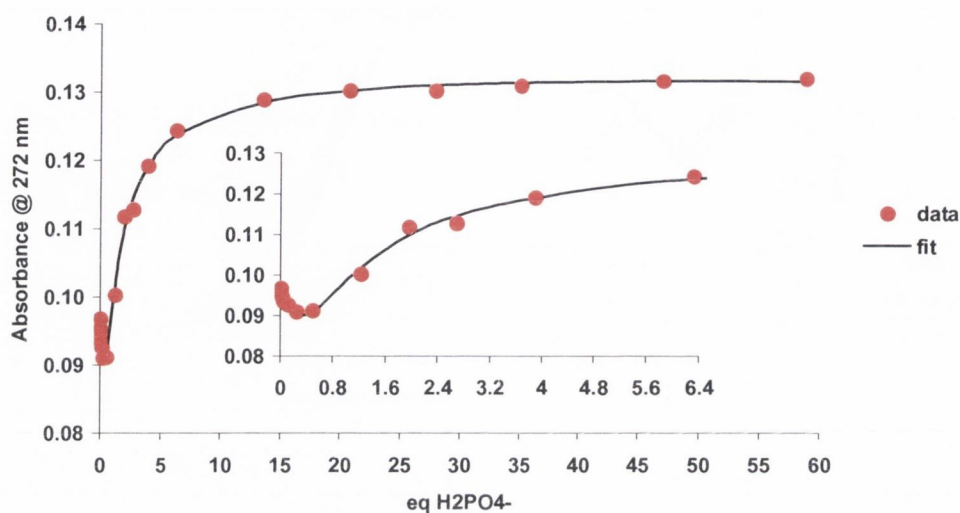


Figure 3.6.2.1.: Experimental binding isotherm for the titration of **72** ($4 \mu\text{M}$) with H_2PO_4^- and corresponding fit from SPECFIT. Insert: Fraction of the binding isotherm for the same titration, showing the good fit at lower concentrations of H_2PO_4^- .

Hence, for such anions, three steps were found to be involved, in which (i) the anion (G) interact with two molecules of **72** to give the self-assembly complex G:L_2 ($\text{G} + 2\text{L} \rightarrow \text{G:L}_2$) (ii) the G:L complex is formed upon further addition of anion ($\text{G:L}_2 + \text{G} \rightarrow 2\text{G:L}$), and (iii) the G:L complex interacts with another anion to form $\text{G}_2\text{:L}$ ($\text{G:L} + \text{G} \rightarrow \text{G}_2\text{:L}$). This is clearly observed in the distribution diagram of the species present at the equilibrium in the course of the titration with H_2PO_4^- , determined by SPECFIT from the $\log K$ values for a $4 \mu\text{M}$ solution of **72**, **Figure 3.6.2.2**. Analysis of this diagram clearly shows that upon an initial addition of H_2PO_4^- a self-assembly complex between two molecules of **72** and H_2PO_4^- (G:L_2), corresponding to *ca.* 11% in solution is formed. Nevertheless, on further addition of H_2PO_4^- the G:L complex becomes the predominant species in solution, reaching its maximum concentration (*ca.* 75%) with addition of *ca.* 4 equivalents of H_2PO_4^- . Furthermore, the $\text{G}_2\text{:L}$ complex forms on addition of a bigger excess of H_2PO_4^- , and becomes the predominant species in solution upon *ca.* 20 equivalents of anion.

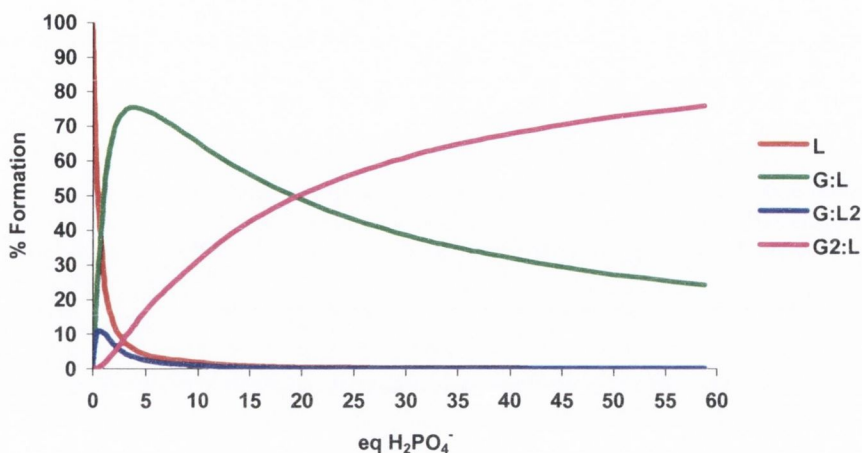


Figure 3.6.2.2: Speciation diagram for the absorption titration of **72** (L) with H_2PO_4^- (G) in MeCN. Speciation is shown relative to the number of equivalents of H_2PO_4^- .

The binding constants for the three stepwise equilibria, as determined through nonlinear least-squares treatment of the titration data, associated errors, and corresponding binding modes are reported in **Table 3.6.2**. Both F^- and H_2PO_4^- exhibited the largest binding constants for the 1:1 interaction with $\log K_{1:1} = 6.13 \pm 0.09$ and $\log K_{1:1} = 6.05 \pm 0.07$, respectively. A much weaker binding constant of $\log K_{1:1} = 3.54 \pm 0.21$ was found for the 1:1 interaction with $\text{H}_2\text{P}_2\text{O}_7^{2-}$. This shows that by varying the acetamide moiety from the *para* position (**71**) to the *meta* position, we were able to induce changes on the 1:1 binding affinity of receptor **72**. In addition, the interaction of **72** with anions such as F^- , H_2PO_4^- , and $\text{H}_2\text{P}_2\text{O}_7^{2-}$ lead to the formation of the G:L₂ species, which was not observed for **71**. In contrast to the 1:1 interaction, $\text{H}_2\text{P}_2\text{O}_7^{2-}$ was found to possess the higher binding constant for the formation of the self-assembly G:L₂ complex, with $\log K_{1:2} = 6.06 \pm 0.19$. F^- and H_2PO_4^- exhibited, once again, very similar constants for the 1:2 interaction with $\log K_{1:2} = 5.48 \pm 0.29$ and $\log K_{1:2} = 5.30 \pm 0.26$, respectively. Binding constants for the 2:1 interactions ($\log K_{2:1} \sim 3 - 4$) were once again found to be weaker (**Table 3.6.2**). With a constant of $\log K_{2:1} = 3.29 \pm 0.26$, F^- exhibited the weakest interaction among them.

Regarding CH_3COO^- and Cl^- , two stepwise equilibria were found to better fit the titration data, as shown for the titration of **72** with CH_3COO^- in **Figure 3.6.2.3**. However, CH_3COO^- gave rise to the formation of the G:L and G₂:L complexes in solution, **Figure**

3.6.2.3 insert, while interaction with Cl^- gave rise to the G:L and the self-assembly G:L₂ species (see Appendix 2).

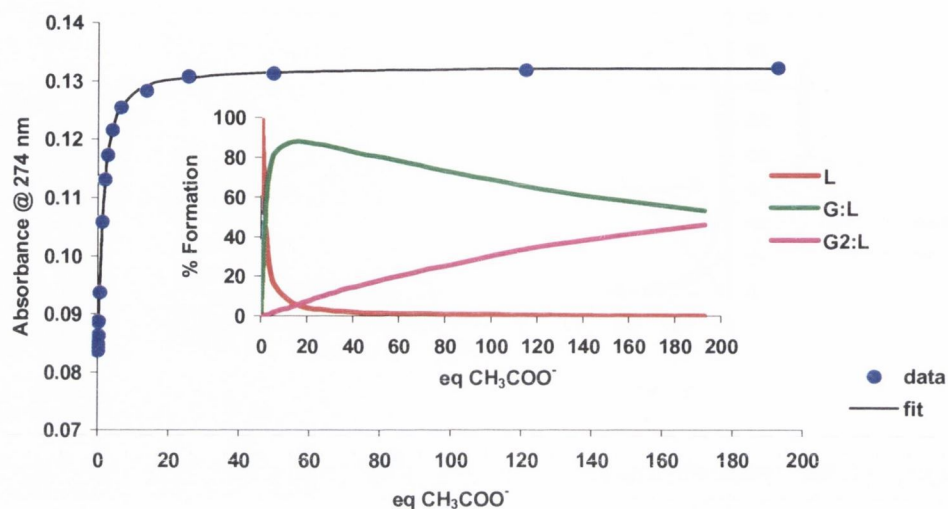


Figure 3.6.2.3.: Experimental binding isotherm for the titration of **72** (4 μM) with CH_3COO^- and corresponding fit from SPECFIT. *Insert:* The speciation distribution diagram for the titration of **72** (L) with CH_3COO^- (G). Speciation is shown relative to the number of equivalents of CH_3COO^- .

The binding constants determined from the fitting of the CH_3COO^- titration data were found to be $\log K_{1:1} = 5.41 \pm 0.02$ and $\log K_{2:1} = 3.06 \pm 0.38$ for the 1:1 and 2:1 interactions of CH_3COO^- with **72**, respectively. These constants were found to be quite similar to those obtained for the interaction of acetate with **71** (Table 3.6.1). In contrast, the binding interaction of **72** with Cl^- was found to be very different to that of **71**, as only a weak 1:1 interaction ($\log K_{1:1} = 3.45 \pm 0.06$) was observed for **71**, while Cl^- was found to form stronger complexes with **72**. Binding constants of $\log K_{1:1} = 4.86 \pm 0.09$ and $\log K_{1:2} = 6.42 \pm 0.21$ were determined by fitting the titration data for 1:1 and 1:2 (anion:receptor) stoichiometries, respectively. The speciation distribution diagram, shown in Figure 3.6.2.4, clearly illustrate that the initial addition of Cl^- (ca. 5 equivalents) gives rise to the interaction with two molecules of **72**, forming the self-assembly G:L₂ species in ca. 32% in solution. However, the 1:1 complex begins to dominate after the addition of ca. 12 equivalents of Cl^- , becoming eventually the predominant species in solution.

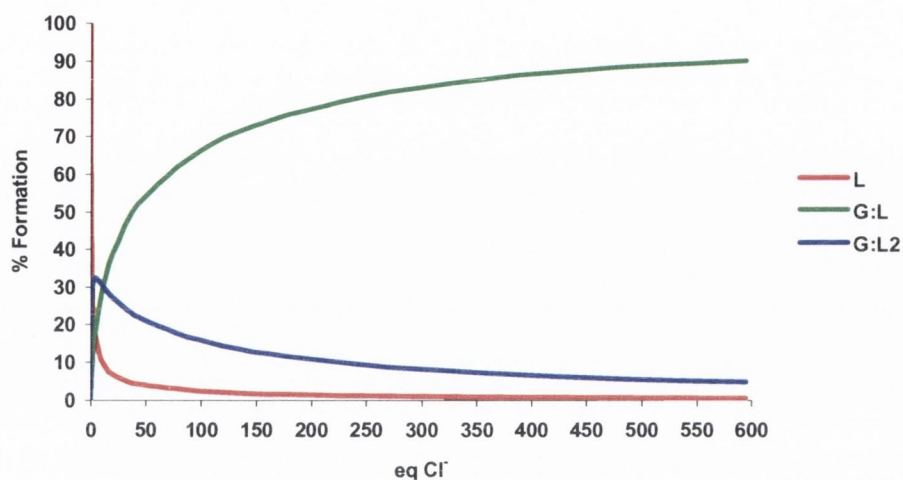
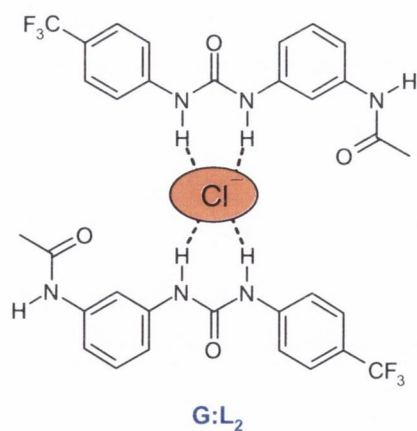


Figure 3.6.2.4: Speciation distribution diagram for the titration of **72** (L) with Cl⁻ (G) in MeCN. Speciation is shown relative to the number of equivalents of Cl⁻.

These results show that **72** has significantly higher binding affinity for Cl⁻. It has previously been demonstrated that simple urea receptors do not bind strongly to the big spherical anions, but rather through multiple binding interactions.¹⁷⁴⁻¹⁷⁸ These results indicate that a simple modification of the receptor structure can lead to astonishing results on the anion binding affinity. While receptor **71** binds very weakly to Cl⁻, receptor **72** was found to bind this anion strongly in a 1:2 (G:L₂) fashion, as tentatively depicted in **Scheme 3.6.3**.



Scheme 3.6.3: Proposed binding interactions between Cl⁻ and **72**.

The above discussed binding constants and associated stoichiometries are summarised below in **Table 3.6.2**.

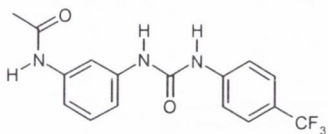
Receptor (L)	Anion (G)	Binding mode (G _n :L _m)	Log K _{n:m}	Std. Deviation (±)
 <p style="text-align: center;">72</p>	CH ₃ COO ⁻	G:L	5.41	0.02
		G ₂ :L	3.06	0.38
	F ⁻	G:L	6.13	0.09
		G:L ₂	5.48	0.29
		G ₂ :L	3.29	0.26
	H ₂ PO ₄ ⁻	G:L	6.05	0.07
		G:L ₂	5.30	0.26
		G ₂ :L	4.15	0.12
	H ₂ P ₂ O ₇ ²⁻	G:L	3.54	0.21
		G:L ₂	6.06	0.19
		G ₂ :L	4.04	0.14
	Cl ⁻	G:L	4.86	0.09
		G:L ₂	6.42	0.21

Table 3.6.2: Binding constants and binding modes between anions and receptor **72**, using the SPECFIT program.

In summary, the observed 1:2 binding interaction demonstrates the ability of **72** to participate in anion induced self-assembly complex formation, which was clearly absent in the binding interactions of **71**. It is also worth noting that, with exception of the divalent anion H₂P₂O₇²⁻, the 1:1 binding interaction resulted in higher binding constants for **72** than **71**. This can possibly be due to an increase of the inductive effect between the electron withdrawing amide and urea moieties, which would be stronger for **72** over **71** (*meta* versus *para* substitution), rendering the urea protons more acidic and hence better hydrogen donors. Another interesting feature observed for the binding of both **71** and **72** is the presence of reasonable strong binding constants (log K_{2:1} ~ 3 - 4) for the 2:1 interactions (G₂:L). This is possibly due to the existence of a positive allosteric effect upon formation of the anion complex through the binding of the urea hydrogen atoms. So, while the amide initially enhances the binding properties of the urea moiety through inductive effect, the subsequent anion binding, with the formation of the G:L complex, would make the amide more electron deficient and hence a better anion acceptor.

Contrasting to either **71** or **72**, receptor **73** offers the possibility of cooperative binding between the amide and the urea functionalities due to the close proximity of these hydrogen bonding donors. This was clearly observed in the X-ray crystal structure presented in **Figure 3.4.2** (Section 3.4). The following section will focus on the evaluation of the binding affinity of receptor **73** to the various anions.

3.6.3 Absorption studies performed on **73**

Upon addition of various anions to a solution of **73**, the band centred at *ca.* 260 nm experienced a bathochromic shift, with the concomitant formation of an isosbestic point. Similar behaviour was observed for all of the anions studied (see Appendix 2). The family of spectra obtained for the titration of **73** with CH_3COO^- are presented in **Figure 3.6.3**, where it can be seen that the band centred at *ca.* 260 nm experienced a 10 nm bathochromic shift to *ca.* 270 nm, with the concomitant formation of a clear isosbestic point at *ca.* 263 nm. Similar changes were also observed for F^- , H_2PO_4^- , and $\text{H}_2\text{P}_2\text{O}_7^{2-}$ (see Appendix 2). Smaller spectral changes were once again observed for Cl^- , where the band centred at *ca.* 260 nm experienced a small red shift to *ca.* 264 nm, with the appearance of an isosbestic point at *ca.* 262 nm (see Appendix 2). It is also worth noting that these changes were only observed at high concentrations of Cl^- , suggesting a weaker binding interaction between Cl^- and **73**.

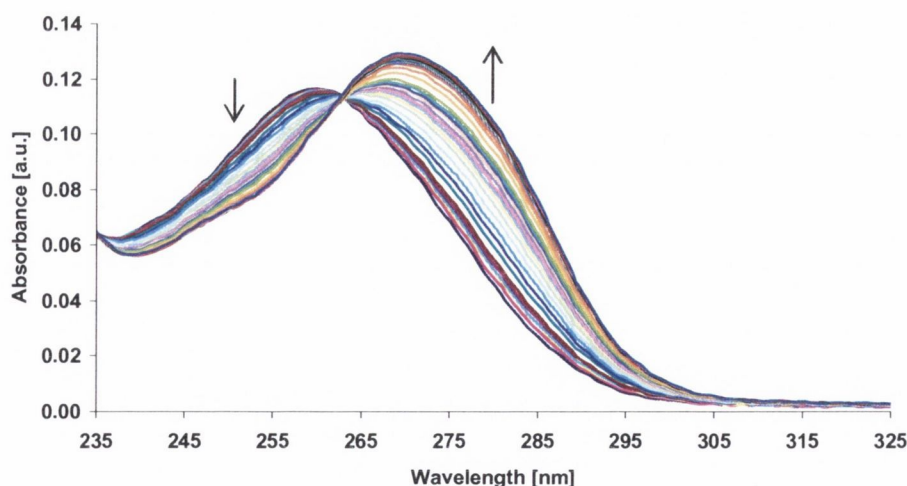


Figure 3.6.3.: Absorption spectra showing the changes in absorbance of receptor **73** ($4 \mu\text{M}$) upon gradual additions of CH_3COO^- ($0 \rightarrow 32 \mu\text{M}$) in MeCN.

The changes in absorbance both at 260 nm and 270 nm, for the titration of **73** with CH_3COO^- , were plotted as a function of the number of equivalents of CH_3COO^- , **Figure 3.6.3.1**. The titration profile clearly shows the decrease in absorbance at *ca.* 260 nm and simultaneous increase at the new band centred at *ca.* 270 nm.

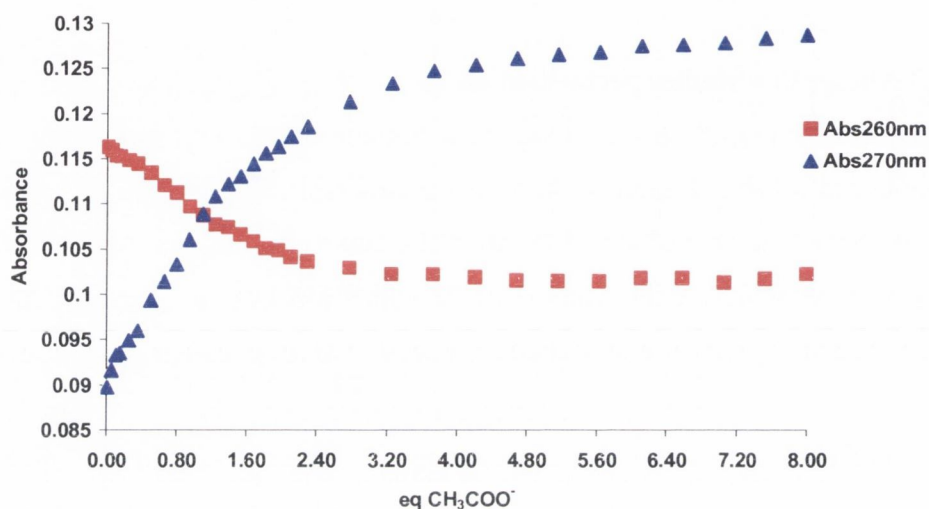


Figure 3.6.3.1.: Changes in the absorbance of receptor **73** ($4 \mu\text{M}$) at 260 nm and 270 nm with respect to the number of equivalents of CH_3COO^- .

In order to evaluate the strength of the binding interactions between the anions and **73**, the observed changes were fitted using the SPECFIT program. An excellent fit to the experimental binding isotherm was observed for the 1:1 interaction taking place between the various anions and receptor **73** (see Appendix), which is a good indication of the simple 1:1 binding interaction between the receptor (**73**) and the anions. **Figure 3.6.3.2** shows the fit to the titration with CH_3COO^- . From this, the binding constants and corresponding binding modes were determined, which are summarised in **Table 3.6.3**.

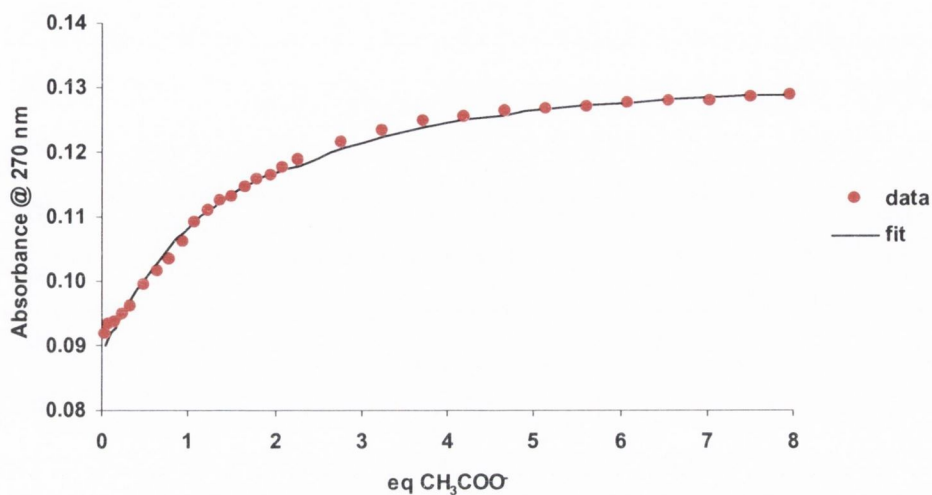


Figure 3.6.3.2.: Experimental binding isotherm for the titration of **73** (4 μM) with CH_3COO^- and corresponding fit from SPECFIT.

The speciation distribution diagrams were also obtained (see Appendix 2). **Figure 3.6.3.3** shows such a diagram for the titration of **73** with CH_3COO^- , which demonstrates that the G:L complex was the only species formed in solution upon addition of CH_3COO^- (0 \rightarrow 8 equivalents).

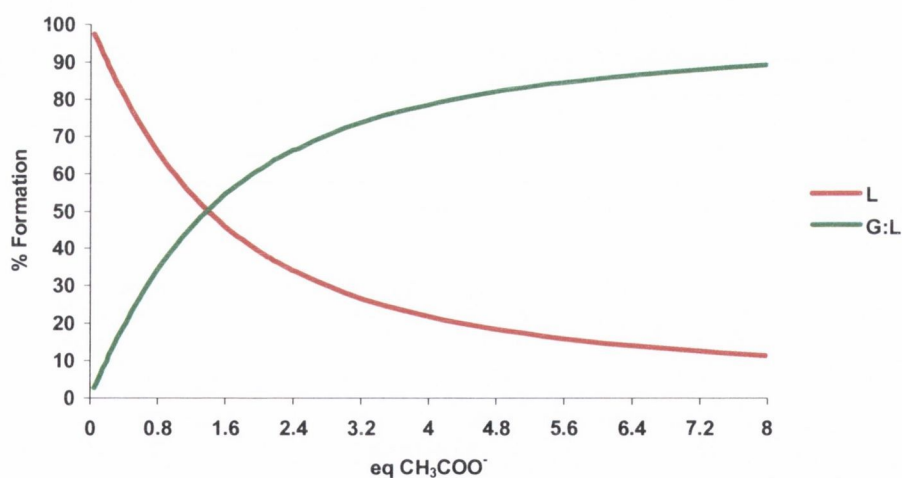


Figure 3.6.3.3: Speciation diagram for the titration of **73** (L) with CH_3COO^- (G) in MeCN. Speciation is shown relative to the number of equivalents of CH_3COO^- .

In contrast to receptors **71** and **72**, only the 1:1 binding mode was observed for the interaction of **73** with the anions studied, suggesting that the amide was not free to participate in a second anion binding interaction as observed for both **71** and **72**.

As predicted, Cl^- was found to interact weakly with **73**, with a binding constant of $\log K_{1:1} = 3.60 \pm 0.05$. The stronger interaction was observed for $\text{H}_2\text{P}_2\text{O}_7^{2-}$ with a binding constant of $\log K_{1:1} = 6.46 \pm 0.06$. For H_2PO_4^- , F^- , and CH_3COO^- the binding constants for the 1:1 interaction with **73**, were determined as being $\log K_{1:1} = 5.72 \pm 0.05$, $\log K_{1:1} = 5.63 \pm 0.05$, and $\log K_{1:1} = 5.45 \pm 0.02$, respectively. Taking this into account, the binding affinity of **73** to anions is proposed to be; $\text{H}_2\text{P}_2\text{O}_7^{2-} > \text{H}_2\text{PO}_4^- > \text{F}^- > \text{CH}_3\text{COO}^- > \text{Cl}^-$.

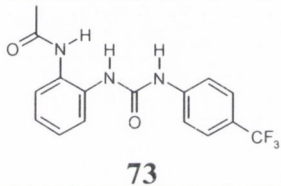
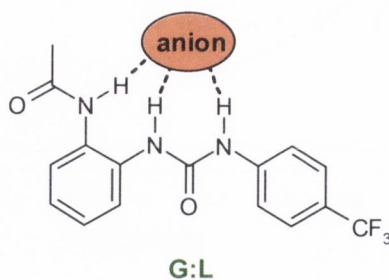
Receptor (L)	Anion (G)	Binding mode ($G_n:L_m$)	Log $K_{n:m}$	Std. Deviation (\pm)
 73	CH_3COO^-	G:L	5.45	0.02
	F^-	G:L	5.63	0.05
	H_2PO_4^-	G:L	5.72	0.05
	$\text{H}_2\text{P}_2\text{O}_7^{2-}$	G:L	6.46	0.06
	Cl^-	G:L	3.60	0.05

Table 3.6.3: Binding constants and binding modes between various anions and model receptor **73**

By comparing these binding constants with those obtained for **71** (Table 3.6.1), the $\log K_{1:1}$ values associated with **73** were found to be higher. The presence of the amide hydrogen in closer proximity to the urea hydrogen atoms can be held responsible for such higher binding affinity. As depicted in Scheme 3.6.3, the binding between the three hydrogen atoms and the anions is viable. Therefore, this cooperation between the urea and amide moieties can lead to the formation of stronger bound complexes.



Scheme 3.6.3: Proposed binding interactions between anions ($\text{H}_2\text{P}_2\text{O}_7^{2-}$, H_2PO_4^- , CH_3COO^- , F^- , and Cl^-) and **73** to form the G:L complexes.

3.7 Conclusions

In conclusion, three novel anion receptors **71**, **72**, and **73** possessing both amide and urea binding sites have been successfully synthesized and characterized. Crystals suitable for X-ray crystal structure analysis were obtained for all three receptors. These showed that the relative location of the amide and urea functional groups plays a major role in the ability of such receptors to form large solid state networks through the formation of either intra (**73**) or intermolecular hydrogen bonding interactions. Their anion recognition ability, through the incorporation of both urea and amide hydrogen bonding groups, was tested by spectroscopic methods. The simple and high yielding synthetic route renders these compounds greater advantage over more synthetically challenging receptors containing similar binding moieties.

All the three receptors revealed different binding interactions with the various anions, such as CH_3COO^- , H_2PO_4^- , $\text{H}_2\text{P}_2\text{O}_7^{2-}$, F^- and Cl^- . This shows that by changing the position of the amide moiety on the aromatic ring, and hence by introducing small changes on the structure of the receptor, different binding interactions and binding affinities can be induced.

Receptor **71** showed to interact with F^- , CH_3COO^- , and H_2PO_4^- through the urea as well as the amide moieties, forming the 1:1 and 2:1 complexes, respectively. The binding interaction through the amide moiety, although reasonably high ($\log K_{2:1} \sim 3-4$), was found to be significantly weaker than the binding interaction taking place through the urea moiety ($\log K_{1:1} \sim 5$). In addition, only one binding mode was observed for the interaction of $\text{H}_2\text{P}_2\text{O}_7^{2-}$ and Cl^- with **71**, corresponding to the formation of the 1:1 complexes. These results further support those obtained for the lanthanide luminescent sensor **Tb.61**, discussed in Chapter 2, where the binding interactions were proposed to take place both through the urea and amide moieties. In a similar manner to that observed for **71**, higher binding constants were also determined for the 1:1 binding interaction. The binding affinity for the interaction of **71** with the various anions was observed to follow the trend; $\text{H}_2\text{P}_2\text{O}_7^{2-} > \text{CH}_3\text{COO}^- \geq \text{F}^- > \text{H}_2\text{PO}_4^- > \text{Cl}^-$.

Only one binding interaction was observed between **73** and the anions studied. The binding constants were found to be higher than those observed for **71**. The anion binding affinity was also observed to change considerably. This was ascribed to the possible mutual

hydrogen bonding cooperation between the urea and amide moieties upon anion recognition. The binding affinity of **73** to the various anions was observed to be; $\text{H}_2\text{P}_2\text{O}_7^{2-} > \text{H}_2\text{PO}_4^- > \text{F}^- > \text{CH}_3\text{COO}^- > \text{Cl}^-$.

Among the three compounds, receptor **72** exhibited the most intricate binding process. Multiple binding interactions were observed with the various anions. The formation of 1:1, 1:2, and 2:1 complexes were observed between $\text{H}_2\text{P}_2\text{O}_7^{2-}$, F^- , H_2PO_4^- , and this receptor. Similar affinities were shown for F^- and H_2PO_4^- , with high 1:1 binding constants. On the other hand, $\text{H}_2\text{P}_2\text{O}_7^{2-}$ showed to interact strongly with two molecules of **72**, giving rise to the self-assembly 1:2 complex. Nevertheless, the most interesting results were obtained for the interaction with Cl^- , which gave rise to a very strong binding constant for the interaction with two molecules of **72** to form the self-assembly G:L₂ complex. So, **72** show higher affinity to Cl^- over **71** and **73**.

In summary, the three new structurally simple anion receptors, **71-73**, only differ in the relative position of the amide moiety to that of the urea site. This simple modification was shown to play a major role in the binding interactions of the various anions to these receptors. Receptor **73** was found to strongly bind anions such as CH_3COO^- , H_2PO_4^- , $\text{H}_2\text{P}_2\text{O}_7^{2-}$, F^- and Cl^- only in a 1:1 fashion. In comparison, both **71** and **72** gave rise to stepwise binding interactions. In both cases, the formation of 2:1 (anion:receptor) strong anion bound complexes was proposed to take place through the amide moiety. The high values determined for the binding constants of such simple receptors, were ascribed to the existence of both inductive and positive allosteric effects. So, while the amide initially enhances the binding properties of the urea moiety, the subsequent anion binding, with the formation of the anion:receptor complex, makes the amide a better anion acceptor.

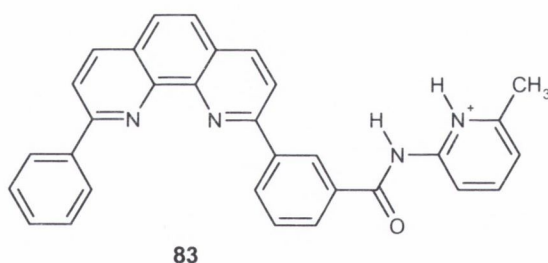
Chapter 4

*Sensing based on a fluorescent heteroditopic
receptor*

4.1 Introduction

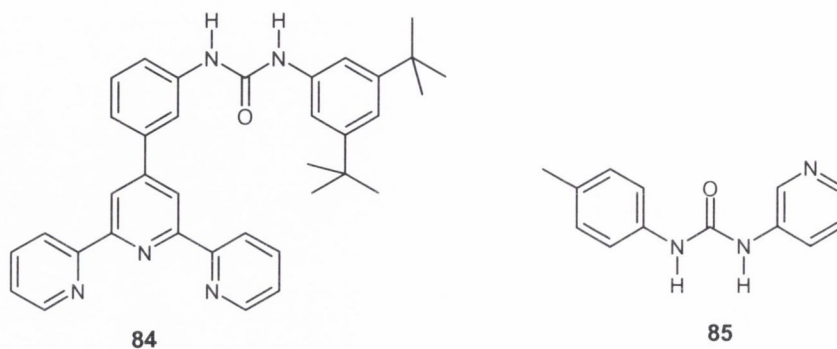
The development of new heteroditopic receptors able to coordinate both anionic and cationic species is a growing area of interest.^{13,179} In general, heteroditopic receptors have been designed by combining functionalities such as cation binding crown ethers and modified calixarenes, with anion binding Lewis-acidic metal centres such as pyrroles, amido, and urea groups.^{104,105} Such receptors may exhibit interesting cooperative and allosteric binding behaviours. Hence, the binding affinity of one ion (cation/anion) can be facilitated by the coordination of the other ion (cation/anion) due to electrostatic interactions and conformational effects.¹⁰⁶

While several such receptors incorporating moieties for alkali metal recognition have been reported, there are still few examples of such systems including transition metal recognition units.¹²⁸ Pyridyl fragments, such as bipyridine (*bipy*), terpyridine (*terpy*), and phenanthroline (*phen*), are known to bind strongly transition metal cations.^{131,180} One of the first examples employing the *phen* moiety was provided by Hamilton and collaborators, who reported compound **83**.¹⁸¹ In the presence of Cu(I) ions, two **83** molecules were observed to self-assemble giving rise to the formation of the complex **Cu(I):83₂**, which was found to strongly bind dicarboxylic acids in CHCl₃ through the acylaminopyridine moieties.

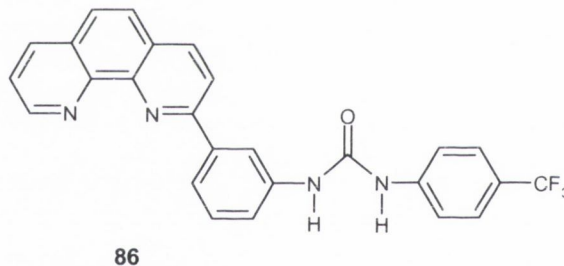


By combining a terpyridine moiety with an urea unit, within the same molecule, Branda *et al.* achieved a similar result with receptor **84**.¹⁸² Upon formation of a Fe(II) complex between two *terpy* fragments of **84**, the arrangement of the two urea units enables the complex to bind a porphyrinic bis-carboxylate dianion. In DMSO, the fluorescence emission intensity of the porphyrin was quenched upon titration with the **Fe(II):84₂**

complex. Similar photophysical behaviour was observed in a more competitive solvent mixture, 10% H₂O/MeCN.



More recently, Steed and co-workers showed that the **Ag(I):85**₂ complex forms a stable adduct with NO₃⁻ through hydrogen bonding to both of the self-assembled urea fragments. The studies were carried out both in solid state and acetone solution by NMR titrations.^{183,184}



During the course of this research, Fabbrizzi *et al.* reported receptor **86**.¹⁴² In comparison to receptor **83**, receptor **86** forms a stable 1:2 complex with Cu(I) ions in solution, **Cu(I):86**₂. This complex was indeed found to act as an anion receptor in an aprotic solvent mixture, THF:MeCN (4:1 v/v). In the presence of anions such as Cl⁻ and H₂PO₄⁻, the complex adopts a geometrical arrangement in which the two urea units interact with a single anion, giving rise to the 1:1 adduct, **(Cu(I):86₂):anion**. In contrast, upon addition of CH₃COO⁻, the complex rearranges to interact with two acetate anions.

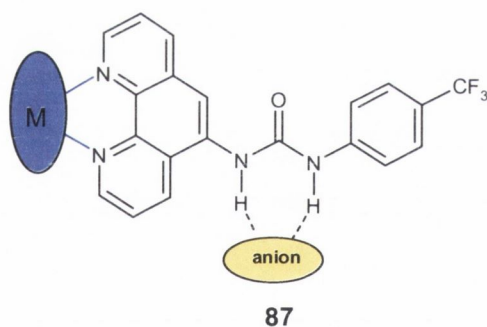
These studies were used to highlight the fact that metals, in the present case transition metals, can be used to suitably assemble hydrogen bond donor units, such as urea moieties,

in order to create suitable binding sites for anion recognition.³¹ In addition, these studies constitute an important step towards the design of heteroditopic receptors for transition metal salts. As mentioned in Chapter 1, research in the field of ion-pair recognition is relevant to the detection and extraction of toxic ions from aqueous environments, as well as to the design of artificial carriers and channels for the transport of inorganic and organic salts across membranes.¹⁰⁴

With this in mind we set out to develop a novel heteroditopic receptor. The following sections detail the synthesis, characterisation, and photophysical studies of such a receptor.

4.2 Design and synthesis of heteroditopic receptor 87

The heteroditopic receptor **87** was designed for the recognition of both anions and transition metal ions. The design principle of **87** relied upon the use of a phenanthroline (*phen*) moiety, as the metal binding site, and the incorporation of a urea moiety for anion recognition. Hence, receptor **87** was expected to bind transition metal ions through the nitrogen atoms of the *phen* moiety, while the interaction with anions would take place *via* hydrogen bonding between the NH's of the urea and the anions, as depicted in **Scheme 4.2**.

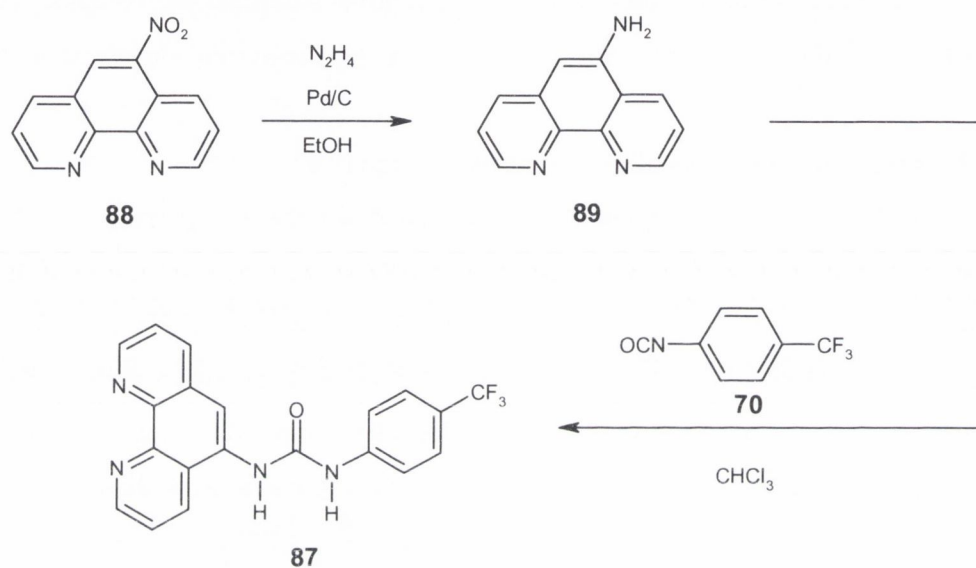


Scheme 4.2: Proposed binding sites for transition metal ions (M) and anions, within receptor **87**.

4.2.1 Synthesis and characterisation of **87**

The synthesis of receptor **87** was carried out as outlined in **Scheme 4.2.1**. The first step involved the reduction of the available 5-nitro-1,10-phenanthroline, **88**, using hydrazine monohydrate (N₂H₄·H₂O), in the presence of 10% Pd/C catalyst in ethanol at 95°C, under an inert atmosphere. A yellow solid was obtained after removal of the solvent under

reduced pressure. This solid was washed twice with diethyl ether to produce a pale yellow solid in 92% yield. Finally, this amino derivative, **89**, was reacted with trifluoro-*p*-tolyl isocyanate, **70**, in chloroform at room temperature, under an inert atmosphere to yield an off white precipitate, which was filtered and washed with cold CHCl_3 . This solid was finally recrystallised from a hot mixture of CHCl_3 :MeOH to yield the desired receptor as a white crystalline solid in 88% yield.



Scheme 4.2.1: Synthesis of the phenanthroline based heteroditopic receptor **87**.

The compounds were characterized by the conventional methods, such as ^1H , and ^{13}C NMR spectroscopy, ESMS, and IR. The ^1H -NMR (d_6 -DMSO) spectrum of **87**, **Figure 4.2.1**, showed the presence of the two N-H singlets at 9.55 and 9.12 ppm, as well as the expected set of doublets for the phenyl aromatic protons. The ^{13}C NMR (d_6 -DMSO) showed all the expected 18 signals. These consisted of one quaternary resonance at 152.87 ppm for the carbon of the urea carbonyl group. The seven CH resonances at 149.87, 148.74, 135.61, 132.08, 123.68, 122.95, and 116.07 ppm were assigned to the *phen* moiety, while the signals at 126.25 and 118.00 ppm were assigned to the CH resonances of the aromatic phenyl group. The remainder signals correspond to the quaternary resonances of the *phen* as well as the aromatic phenyl moiety. The presence of the CF_3 group was revealed by analysis of the ^{19}F NMR spectrum, showing the typical resonance at -60.58

ppm, for this group. Electrospray mass spectrometry (ES-MS) showed one peak at $m/z = 383.11$ corresponding to $[M + H]$, confirming the presence of the desired compound.

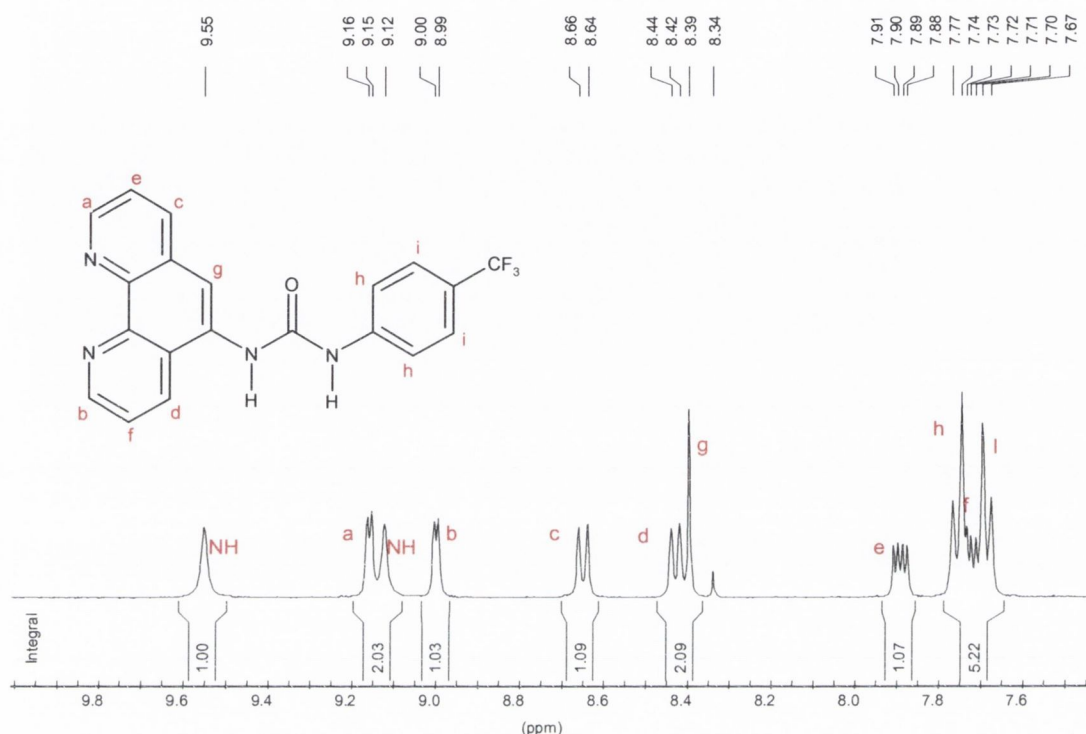


Figure 4.2.1: ¹H NMR of the heteroditopic receptor **87** (400 MHz, d₆ – DMSO)

Single crystals suitable for X-ray crystallographic diffraction studies were isolated from a solution mixture of CHCl₃ and ethanol. The crystal structure as resolved by Dr. Thomas McCabe is presented in **Figure 4.2.2**, and shows that the urea moiety is coplanar with the phenyl group (torsion angle of -0.26°), while being significantly shifted out of the plane of the *phen* moiety (torsion angle of -34.37°). Another feature is that the NH protons of the urea were found to be in the *syn* conformation (*i.e.* NH protons are facing in the same direction). Electronic structural calculations carried out by Hay and co-workers on urea complexes of Cl⁻, NO₃⁻, and ClO₄⁻ showed that the *syn* conformation provides a more stable hydrogen bonding interaction with these anions than the *anti* conformation (*i.e.* NH protons are pointing in opposite directions).²⁸

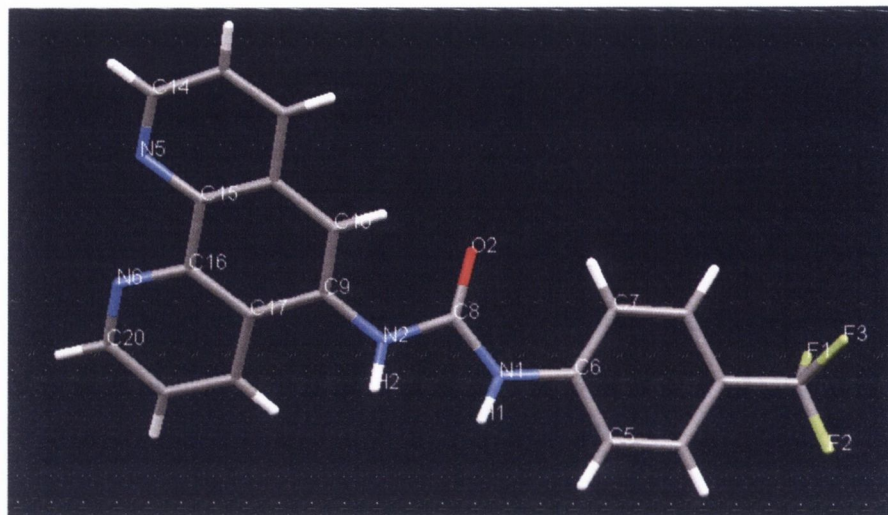


Figure 4.2.2: Molecular structure of receptor **87**, obtained by X-ray crystallography.

Table 4.2.1 details some selected bond angles and bond lengths obtained from the X-ray diffraction data. Bond angles of $125.4(2)^\circ$ and $122.7(2)^\circ$ were found for $N1-C8-O$ and $N2-C8-O$ respectively, while a bond angle of $111.9(2)^\circ$ was measured for $N1-C8-N2$. These bond angles indicate an approximate trigonal planar geometry of receptor **87** at the carbon atom (C8) between the urea atoms. As is clear from looking at the crystal structure, the two urea NH protons are ideally situated for directional hydrogen bonding interactions with anions that can participate in more linear processes, such as CH_3COO^- .²⁸

Bond	Length (Å)	Bond	Angle (°)
C(5)-C(6)	1.387(4)	C(5)-C(6)-N(1)	116.2(2)
C(6)-C(7)	1.386(4)	C(7)-C(6)-N(1)	124.4(2)
N(1)-C(6)	1.405(3)	C(8)-N(1)-C(6)	127.7(2)
N(1)-C(8)	1.359(3)	O(2)-C(8)-N(1)	125.4(2)
O(2)-C(8)	1.216(3)	O(2)-C(8)-N(2)	122.7(2)
N(2)-C(8)	1.383(3)	N(1)-C(8)-N(2)	111.9(2)
N(2)-C(9)	1.405(3)	C(8)-N(2)-C(9)	125.1(2)
C(9)-C(10)	1.355(4)	C(10)-C(9)-N(2)	122.4(2)
C(9)-C(17)	1.451(4)	N(2)-C(9)-C(17)	117.5(2)

N(5)-C(14)	1.322(4)	C(14)-N(5)-C(15)	117.4(2)
N(5)-C(15)	1.357(3)	N(5)-C(15)-C(16)	118.0(2)
C(15)-C(16)	1.447(4)	N(6)-C(16)-C(15)	117.3(2)
N(6)-C(16)	1.359(3)	C(20)-N(6)-C(16)	117.7(2)
N(6)-C(20)	1.319(4)	N(6)-C(20)-C(19)	123.7(3)

Table 4.2.1: Selected bond lengths and angles for **87**.

The crystal structure packing of **87** was also examined and the view along the crystallographic a-axis is shown in **Figure 4.2.3**. A P2(1)/c space group was found for this system. The obtained network showed a complex packing, with the formation of zig-zag chains (**Figure 4.2.3**). This kind of network has been previously observed, within the Gunnlaugsson group, for simple diaryl ureas.¹⁷³

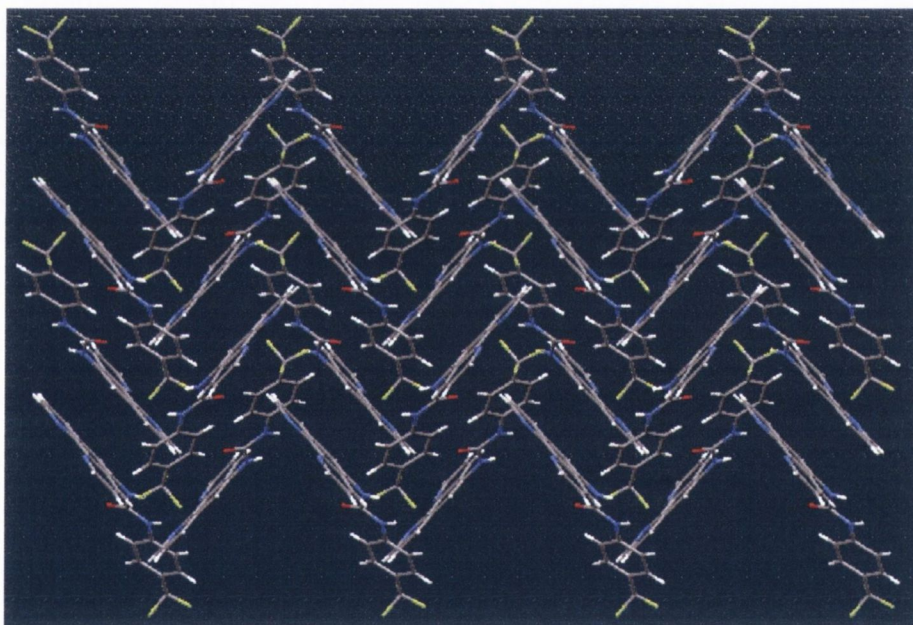


Figure 4.2.3: Packing diagram as viewed along the crystallographic a-axis of the structure of **87**: O red, N dark blue, C dark grey, H white, F yellow.

The structural properties observed in the solid state may affect the binding affinities of the active recognition sites in solution. This will be evaluated in the following sections of this chapter, where the binding ability of **87** towards various anions as well as transition metal ions in solution will be addressed.

4.3 Photophysical properties of receptor **87**

The photophysical properties of **87** were investigated in CH₃CN (a minimum amount of DMSO (< 0.1%) had to be used in order to ensure total solubility of **87** in CH₃CN). The absorption spectrum of the free receptor **87** exhibited two bands; a band centred at 266 nm ($\log \epsilon = 4.50$), assigned to the $\pi\text{-}\pi^*$ transition of the *phen* moiety (in accordance with the reported absorption peak at 265 nm for the 1,10-phenanthroline unit¹⁶⁰), and a low absorbing broad shoulder centred at around 320 nm ($\log \epsilon = 3.85$) due to the $n\text{-}\pi^*$ transitions. The fluorescence emission spectrum of **87** was also recorded in CH₃CN, when exciting the sample at both 265 and 320 nm. In both occasions, a broad emission band centred at 422 nm was observed, as shown in **Figure 4.3** for the excitation at 265 nm, which was once again assigned to the *phen* chromophore.

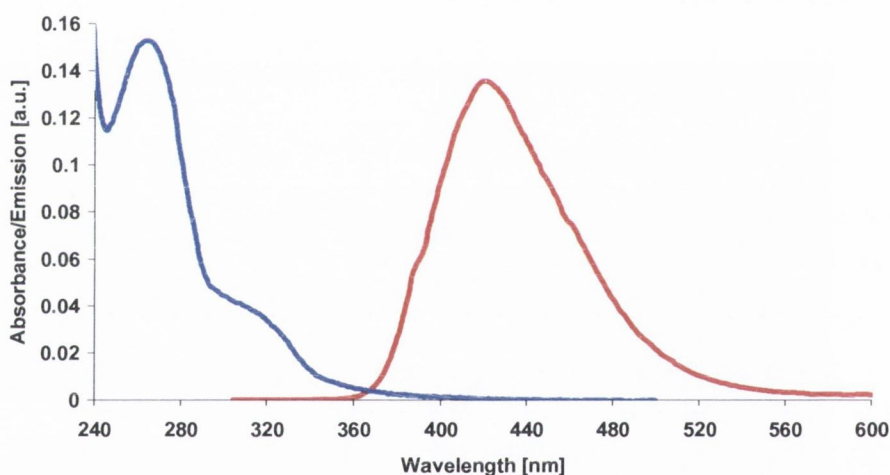


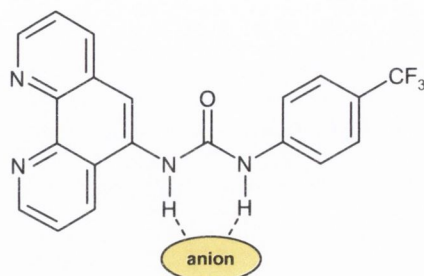
Figure 4.3: Absorption (blue) and Fluorescence (red) spectra of **87** in CH₃CN. The fluorescence emission intensity was divided by a factor of 1000, in order to compare both spectra on the same graph.

The photophysical studies performed on **87** to determine its binding affinity toward several anions, such as CH₃COO⁻, H₂PO₄⁻, F⁻, and Cl⁻, will be discussed in the following section.

4.4 Photophysical studies of **87** with anions

As previously mentioned, it is widely recognised that ureas are particularly good hydrogen bond donors and hence excellent receptors for anions.^{21,26,140} Accordingly, **87**

was expected to be able to bind anions, with the binding process most likely taking place *via* hydrogen bonding between the hydrogen protons of the urea moiety in **87** and the negatively charged species, as shown in **Scheme 4.4**.



Scheme 4.4: Proposed binding mode between the urea based receptor **87** and anions.

The anion binding affinity of receptor **87** ($4.8 \mu\text{M}$) was studied in CH_3CN , by using spectrophotometric methods such as UV-Visible and fluorescence. In the preparation of the stock solution of **87** a minimum amount of DMSO ($< 0.1\%$) had to be used in order to maximize the solubility of the sensor in CH_3CN . The anion guest solutions were also prepared in CH_3CN , as their tetrabutylammonium salts (TBA^+).

The changes in the absorption spectra during the titrations of **87** with the various anions showed an increase in the absorbance at both the 266 nm and the 320 nm bands upon increasing concentrations of the anions, such as acetate (CH_3COO^-), dihydrogenphosphate (H_2PO_4^-), fluoride (F^-), and chloride (Cl^-). Such response was an indication of the changes occurring in the ground state of the sensor upon hydrogen bonding to these anions. For CH_3COO^- , H_2PO_4^- , Cl^- no shifts or isosbestic points were observed, as shown in **Figure 4.4** for the titration of **87** with CH_3COO^- . In contrast to these results, only minor changes were observed for Br^- and ClO_4^- , which occurred only at high anion concentrations.

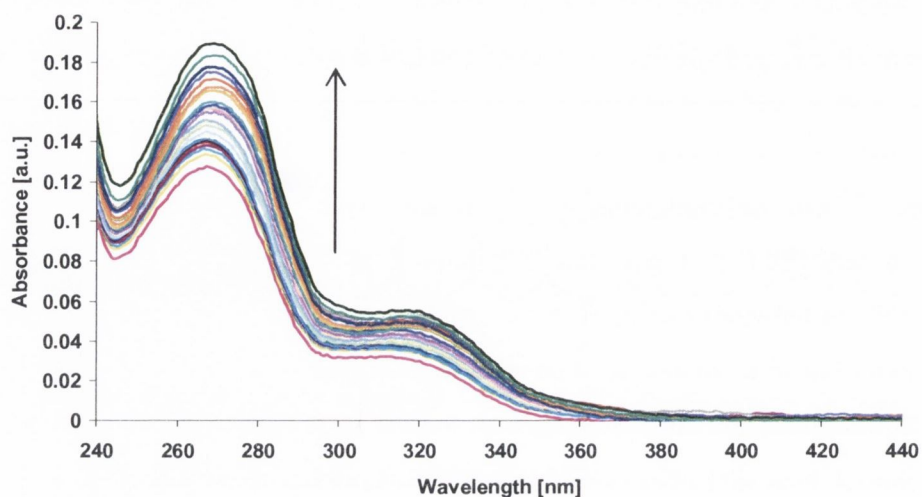


Figure 4.4: Absorption spectra showing the changes in absorbance of **87** ($4.8 \mu\text{M}$) upon gradual additions of CH_3COO^- ($0 \rightarrow 1.53 \text{ mM}$) in CH_3CN .

In the case of F^- , a bathochromic shift (red shift) was observed for both bands over the course of the titration, with the band at 266 nm being shifted to 270 nm and the band at 320 nm shifted to 325 nm . Although a shift was observed, the system lacks the formation of a clear isosbestic point as shown in **Figure 4.4.1**, indicating the possibility of an equilibrium more complex than the 1:1 host-guest relationship.¹⁶⁵ These changes were assigned to the initial formation of a 1:1 hydrogen bonding complex between the urea recognition moiety of **87** and F^- , $\text{F}^-:\mathbf{87}$, followed by binding and subsequent deprotonation of the urea unit induced by a second fluoride ion.⁵⁰ Hence, after a first equilibrium step in which F^- binds the urea moiety of **87** to give the $\text{F}^-:\mathbf{87}$ complex, a second equilibrium step involving the interaction of this complex with another fluoride ion emerges, giving rise to the bifluoride species (HF_2^-). This deprotonation process has been observed and well documented throughout the literature.^{21,50,169-171,185,186}

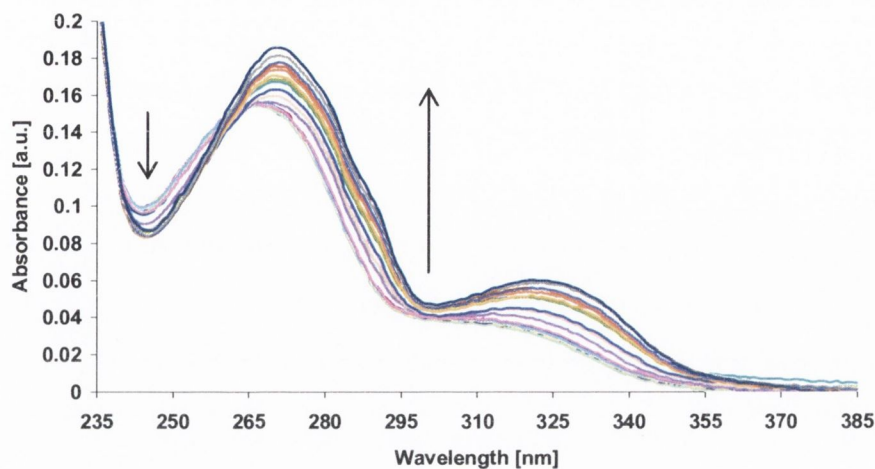


Figure 4.4.1: Changes in the absorption spectra of **87** ($4.8 \mu\text{M}$) upon gradual additions of F^- ($0 \rightarrow 1.09 \text{ mM}$) in CH_3CN .

The fluorescence emission of **87** was also monitored upon addition of the various anions, following excitation at both the 265 nm and the 320 nm transitions. Similar results were obtained on both occasions. Upon addition of CH_3COO^- , H_2PO_4^- , and F^- the fluorescence emission intensity was considerably quenched, or ‘switched off’ (by *ca.* 98%, 94%, and 93% for these anions, respectively), as shown in **Figure 4.4.2** for the changes obtained for CH_3COO^- . These changes are once again assigned to the formation of a complex between the urea receptor and the anion, through hydrogen bonding.

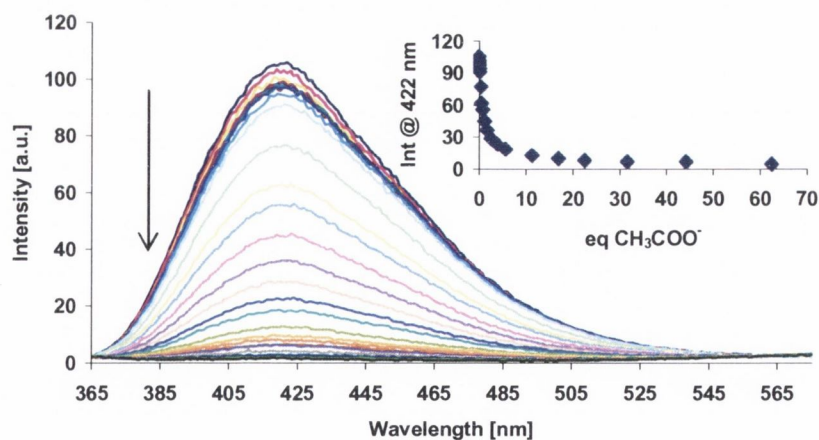


Figure 4.4.2: Changes in the fluorescence emission intensity of **87** ($4.8 \mu\text{M}$) upon gradual additions of CH_3COO^- ($0 \rightarrow 1.53 \text{ mM}$), in CH_3CN upon excitation at 265 nm. Insert: The changes in the fluorescence emission intensity at 422 nm as a function of equivalents of CH_3COO^- .

The titration profile for the number of equivalents of CH_3COO^- vs. the emission intensity at 422 nm is shown as an insert in **Figure 4.4.2**. It clearly shows that around twenty five equivalents of acetate were needed to “fully” quench the emission intensity. The above clearly demonstrates the ability of **87** to function as a luminescent ‘on-off’ switch for these anions. It is also worth pointing out that no other spectral changes were observed in the fluorescence emission spectra, such as shifts in the λ_{max} or the formation of any other long wavelength emitting species. Hence, it is proposed that upon anion recognition, photoinduced electron transfer (PET) from the electron rich anion:receptor to the *phen* excited state is activated, thus causing the fluorescence emission to ‘switch off’. Therefore, this can be considered as being an anion modulated PET quenching, even though no formal covalent spacer separates the fluorophore from the urea receptor.^{42,43} As for the excited state investigation discussed above, addition of Br^- did not give rise to any significant quenching in the emission except at very high concentrations.

Analysis of the changes in the emission intensity against $-\log [\text{anion}]$ can allow for a prediction of the binding stoichiometry for the interactions.¹⁶⁵ By looking at the profile of $-\log [\text{CH}_3\text{COO}^-]$ and $-\log [\text{H}_2\text{PO}_4^-]$ versus the relative emission intensity at 422 nm, as shown in **Figure 4.4.3**, it can be seen that the changes occur over two log units, which is indicative of a 1:1 binding interaction.

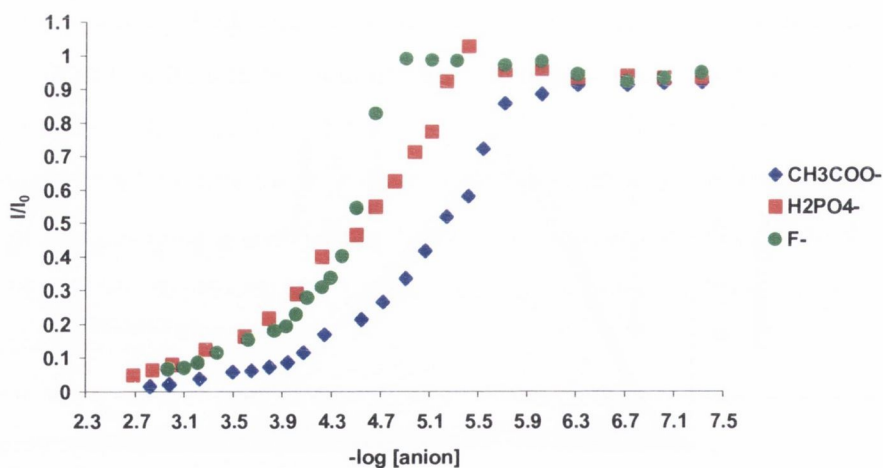


Figure 4.4.3: Changes in the relative emission intensity of **87** ($4.8 \mu\text{M}$) at 422 nm upon gradual additions of CH_3COO^- ($0 \rightarrow 1.53 \text{ mM}$), H_2PO_4^- ($0 \rightarrow 3.49 \text{ mM}$), and F^- ($0 \rightarrow 1.09 \text{ mM}$), versus $-\log [\text{anion}]$.

The changes in the emission intensity for the titration with F^- occur over less than two log units, suggesting more than just a simple 1:1 binding process. This is in agreement with the absorption data above, suggesting the presence of two stepwise equilibria possibly involving the interaction of the formed $F^-:87$ complex with a second F^- to give HF_2^- .^{21,50,171}

Once the stoichiometry has been assessed, the titration data was then fitted to an equilibrium model, using the nonlinear least-squares program SPECFIT. From the fluorescence changes observed during the titrations with CH_3COO^- and $H_2PO_4^-$, the best fit was observed for the 1:1 binding stoichiometry. From these fits, binding constants of $\log K_{1:1} = 5.19 \pm 0.03$ and $\log K_{1:1} = 4.35 \pm 0.06$ were obtained for $CH_3COO^-:87$ and $H_2PO_4^-:87$ respectively. These values indicate a strong binding interaction between **87** and these anions in CH_3CN . The fact that CH_3COO^- is bound more strongly than $H_2PO_4^-$, reflects the ability of the former 'Y' shaped anion to interact with the receptor in a more linear hydrogen bonding manner. For the titration with F^- , the data was better fitted to a 1:1 and 2:1 (anion:host) two step equilibrium model. From the changes observed for the titration with F^- , binding constants of $\log K_{1:1} = 4.75 \pm 0.26$ and $\log K_{2:1} = 4.73 \pm 0.21$ were obtained for $F^-:87$ and $F_2^-:87$ respectively. The good agreement between the experimental data and the obtained fit for the titration with F^- is shown in **Figure 4.4.4**, which further supports the binding model used when determining the binding constants.

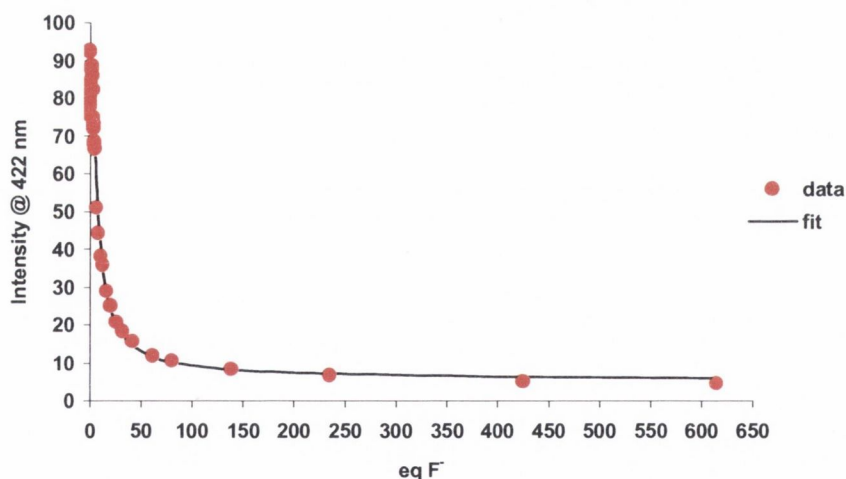


Figure 4.4.4: Fitting of the fluorescence emission data for the titration of **87** (4.8 μM) with F^- at 422 nm.

Further information about the binding equilibrium process can be extracted from analysis of the speciation distribution diagram. Such diagrams usually show the percentage of a species present at equilibrium as a function of concentration or number of equivalents of added guest. The diagram of the species present at equilibrium during the course of the titration of **87** with F^- is shown in **Figure 4.4.5**, and demonstrates that there are three species present in solution; the free receptor **87** (red line), the $F^-:$ **87** complex (green line), and the product of the interaction between $F^-:$ **87** and another F^- ion (pink line). This can be represented using the two step equilibrium shown below.



It is clear, that an initial addition of F^- leads to the formation of the 1:1 ($F^-:$ **87**) complex in approximately 50%, corresponding to step (i). However, a further addition of F^- leads to the formation of the 2:1 ($F^-_2:$ **87**) species, step (ii). This species is seen to clearly dominate after the addition of four equivalents of anion, comprising *ca.* 90% of the total composition once equilibrium has been reached.

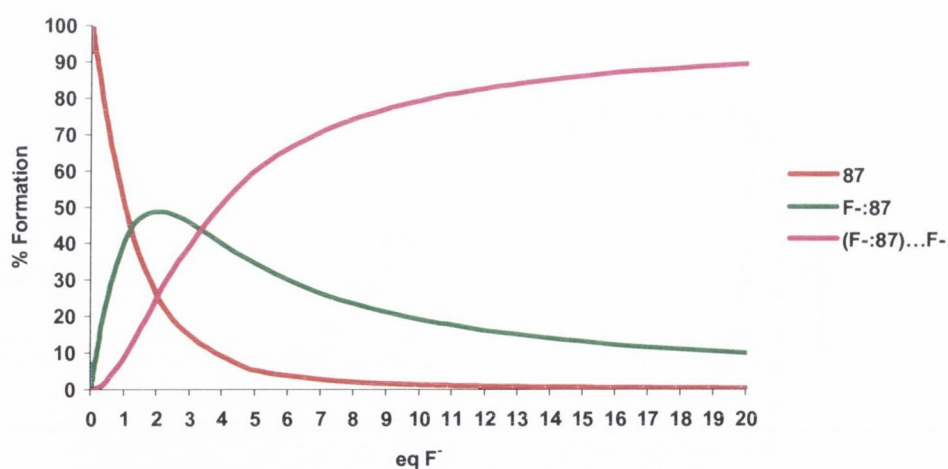


Figure 4.4.5: Speciation distribution diagram for the titration of **87** (4.8 μM) with F^- .

The results discussed so far show the ability of **87** to function as a luminescent ‘on-off’ sensor for CH_3COO^- , H_2PO_4^- , and F^- . However, the most interesting results were observed for the fluorescence titration of **87** with Cl^- . Here, the fluorescence studies for Cl^- revealed a *ca.* 45% enhancement of the emission intensity, as shown in **Figure 4.4.6**, and not the quenching as observed for the anions studied so far. The ‘switching on’ of the emission intensity was accompanied by a shift towards longer wavelengths (422 nm \rightarrow 428 nm), with the formation of an isoemissive point at 399 nm, **Figure 4.4.6**.

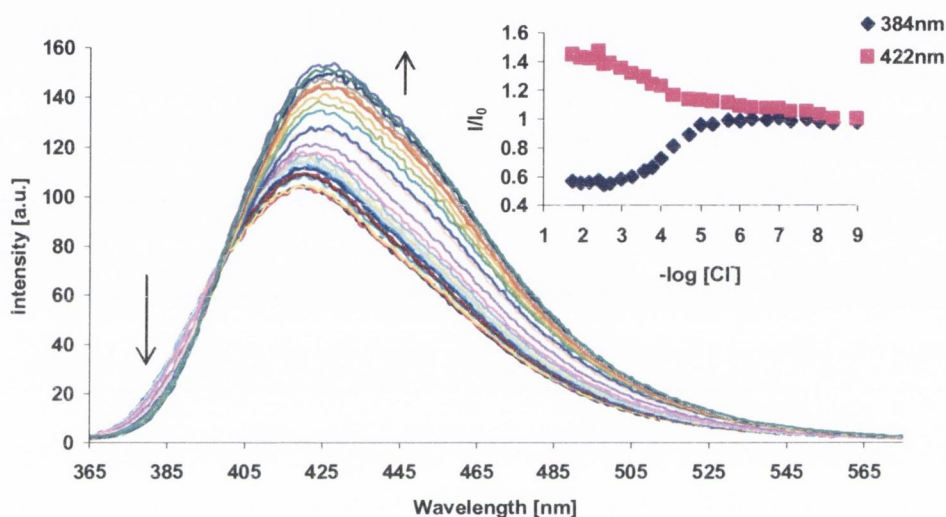
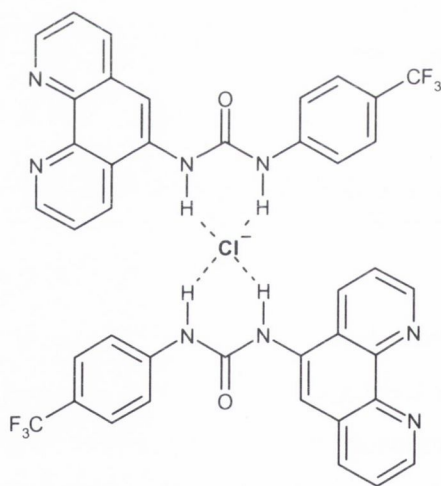


Figure 4.4.6: Fluorescence spectra showing the changes in the emission intensity of **87** (4.8 μM) upon gradual additions of Cl^- (0 \rightarrow 17.50 mM). Insert: The relative intensity at both 384 nm and 422 nm as a function of $-\log[\text{Cl}^-]$.

As can be noted from these results, the PET quenching mechanism operating on the recognition process of CH_3COO^- , H_2PO_4^- , and F^- is not operating for the binding of Cl^- . Therefore, it was proposed that the enhancement of the emission intensity, upon recognition of Cl^- , is due to a reduction in the PET quenching effect from the receptor to the excited state of the *phen* fluorophore, as a result of the bound spherical anion ‘blocking’ the pathway of the electron transfer.

As mentioned previously, analysis of the changes in the emission intensity at a given wavelength against $-\log[\text{anion}]$ can allow a prediction of the binding stoichiometry.¹⁶⁵ By looking at the profile of $-\log[\text{Cl}^-]$ versus the relative emission intensity at 422 nm, shown as the insert in **Figure 4.4.6**, it can be observed that the changes occur over three log units,

indicating a recognition process more complex than a simple 1:1 binding interaction. This was further supported by fitting the titration data, using SPECFIT, which indicated the occurrence of two binding interactions between **87** and Cl^- , giving rise to the 1:1 ($\text{Cl}^-:\mathbf{87}$) and 1:2 ($\text{Cl}^-:\mathbf{87}_2$) species in solution. Binding constant of $\log K_{1:1} = 3.84 \pm 0.14$ and $\log K_{1:2} = 5.94 \pm 0.16$ were determined for the 1:1 and 1:2 binding interactions, respectively. While these results imply that **87** binds Cl^- strongly, through the formation of a 1:2 ($\text{Cl}^-:\mathbf{87}_2$) stoichiometry, it has been demonstrated throughout the literature, that such simple urea based receptors do not bind, or only interact very weakly, with large spherical anions such as Cl^- .²⁹ On the other hand, it has also been demonstrated that such spherical anions interact with receptors through multiple binding interactions.^{175-177,187,188} In the present case, interaction of Cl^- with two molecules of **87** was observed through the formation of the $\text{Cl}^-:\mathbf{87}_2$ species in CH_3CN . Without X-ray crystallographic data it is difficult to predict the structure of the $\text{Cl}^-:\mathbf{87}_2$ complex. Nevertheless, the binding interaction is proposed to take place through hydrogen bonding between the four urea NH protons of two self-assembled molecules of **87** and Cl^- , as tentatively depicted in **Scheme 4.4.1**.



Scheme 4.4.1: Proposed 1:2 binding mode between Cl^- and the urea receptor **87** ($\text{Cl}^-:\mathbf{87}_2$).

Analysis of the speciation distribution diagram, presented in **Figure 4.4.7**, clearly shows that the initial addition of Cl^- gives rise to the formation of the 1:2 ($\text{Cl}^-:\mathbf{87}_2$) complex (blue line) in *ca.* 27%, resulting from the self-assembly of two molecules of **87** in order to

bind Cl^- . However, upon further addition of Cl^- , the 1:1 ($\text{Cl}^-:\mathbf{87}$) species (green line) begins to dominate.

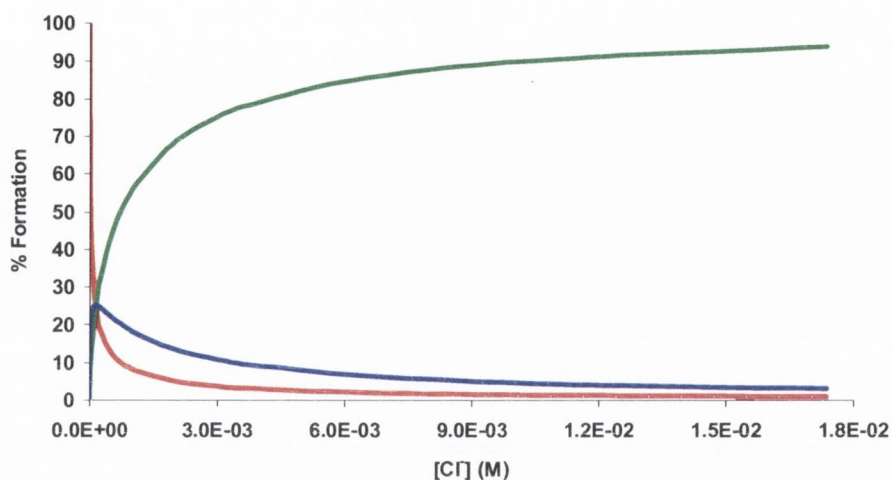


Figure 4.4.7: Speciation distribution diagram for the titration of **87** ($4.8 \mu\text{M}$) with Cl^- . The species present were found to be; free receptor **87** (red), $\text{Cl}^-:\mathbf{87}$ complex (green), and the $\text{Cl}^-:\mathbf{87}_2$ complex (blue).

By plotting the changes in the emission intensities induced by all of the anions studied, a direct comparison of the sensor sensitivity towards these anions can be assessed. The profile of the relative emission intensities, **Figure 4.4.8**, shows the preference of sensor **87** towards CH_3COO^- . This sensitivity can be further supported by the binding constants ($\text{Log } K$) obtained for the 1:1 association between the sensor and the different anions studied, **Table 4.4**. Nevertheless, the different behaviour of the Cl^- ion works as an impediment towards this direct comparison of sensor sensitivity towards the various anions. Consequently, these results provide us with a powerful tool to determine the nature of the bound anion, that is, the ‘switching on’ versus the ‘switching off’ of the fluorescence emission intensity.

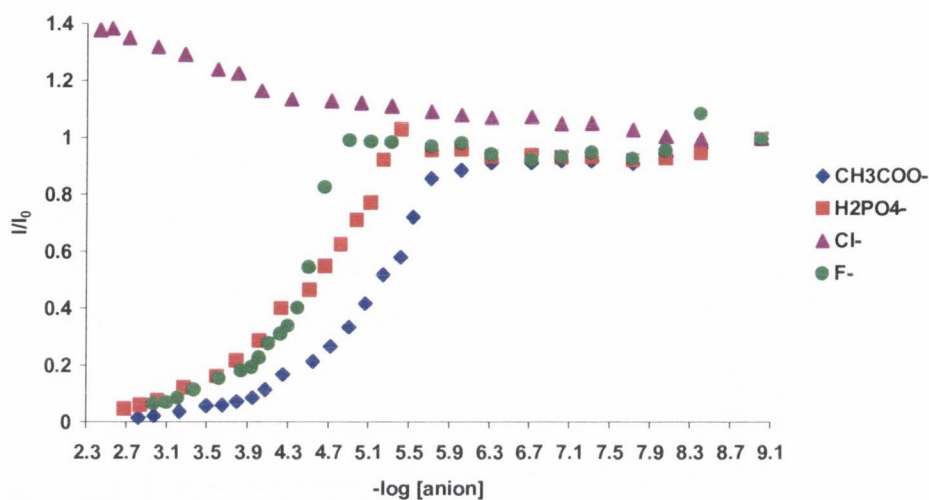


Figure 4.4.8: Comparison of the changes occurring in the relative fluorescence emission intensity at 422 nm of **87** upon addition of several anions.

The binding constants ($\log K$) and binding modes obtained for the fluorescence titrations of the urea receptor **87** with the various anions are summarised in **Table 4.4**. Full titration data including absorption spectra, fluorescence spectra, binding isotherms with corresponding fits, and speciation distribution diagrams are presented in the Appendix section (A3.1).

Anion	Binding mode (anion: 87)	$\log K$	Std. Deviation (\pm)
CH_3COO^-	1:1	5.19	0.03
F^-	1:1	4.75	0.26
	2:1	4.73	0.21
H_2PO_4^-	1:1	4.35	0.06
Cl^-	1:1	3.84	0.14
	1:2	5.94	0.16

Table 4.4 Binding constants ($\log K$) and binding modes obtained for the fluorescence titrations of **87** with the various anions in CH_3CN , using the SPECFIT program.

With the aim of demonstrating the selectivity of **87** towards Cl^- , the luminescence of this receptor was recorded in the presence of CH_3COO^- , which quenched the fluorescence emission. Here the selectivity for Cl^- was clearly demonstrated, as upon addition of

increasing concentrations of Cl^- , the emission was restored, giving rise to the red shift as discussed above, **Figure 4.4.9**. Hence, these results clearly demonstrate that **87** is able to work as a selective fluorescent sensor for Cl^- .

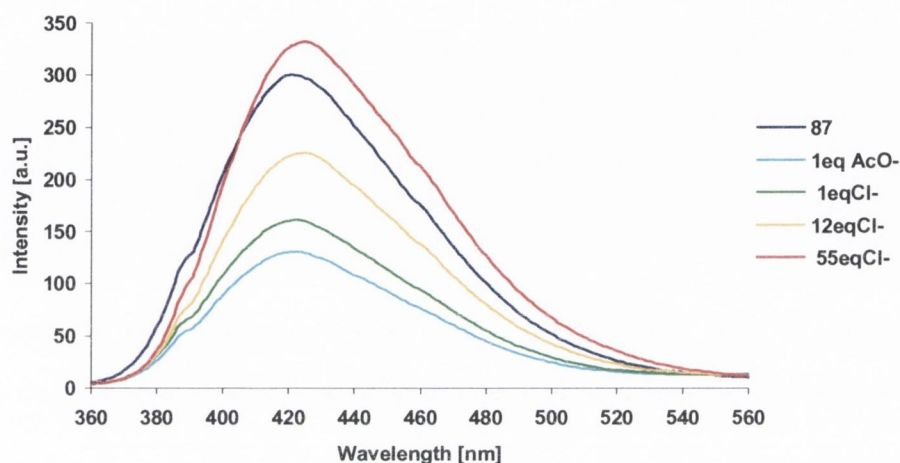


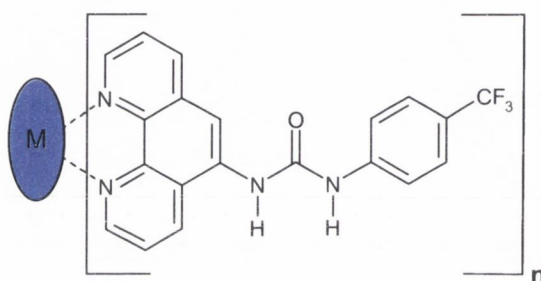
Figure 4.4.9: Selective binding of **87** ($4.8 \mu\text{M}$) to Cl^- over CH_3COO^- , in CH_3CN upon excitation at 265 nm.

These are very encouraging results, when considering the biological importance of Cl^- , which is known to fulfil or regulate a series of important cellular functions, including pH control, ion transport, regulation of cell volume and intermediary metabolism.⁶¹ Chloride ion channels are involved in the facilitated exchange of Cl^- for HCO_3^- in erythrocytes and the failure of this system has been demonstrated in cystic fibrosis patients.^{189,190} As a result there is considerable interest in devising effective ways of measuring extracellular (110 mM) and intracellular (5-15 mM) chloride concentrations.¹⁸⁷ However, Cl^- recognition is not trivial and often require the use of structurally complex hosts, such as those developed by Davis and Smith.^{139,191}

Through the nitrogen atoms of the *phen* moiety, receptor **87** is also expected to be able to bind cationic species. Therefore, **87** is an ideal “candidate” for the development of stable complexes with cations, such as transition metals. With this in mind, the next step was to investigate the formation of these complexes. The results from this investigation will be presented in the following section.

4.5 Photophysical studies of **87** with Cu(II) and Fe(II)

It is well known that 1,10-phenanthroline and its substituted derivatives are able to bind strongly with different metal ions.^{192,193} Intrinsic properties, such as structural rigidity and luminescence make *phen* ligands very attractive towards the sensing of metal cations.¹⁹⁴⁻¹⁹⁹ As previously mentioned, the binding process is expected to take place through the unshared electron pairs of the two aromatic nitrogens of the *phen* moiety in **87** and the positively charged species (M), as depicted in **Scheme 4.5**.



Scheme 4.5: Proposed binding mode between the *phen* moiety of receptor **87** and metal ions (M), where *n* represents the number of receptors coordinated to the metal.

Transition metals such as Cu(II) and Fe(II) are of extreme biological importance.²⁰⁰ Due to its presence in organs and tissues of the human body, as well as being a fundamental component of many enzymes, copper is one of the most relevant metal ions in biological systems.²⁰¹ In blood, copper is bound, in its most important oxidised state Cu(II), to albumin as well as other chelating peptides and amino acids.²⁰¹ Iron is essential in many biological processes²⁰⁰ and is of critical importance in the proliferation of cancer cells.²⁰² Fe(II) complexes are used on the treatment of hypochromic anaemia caused by iron deficiency.^{203,204} Consequently, there has been an increasing interest in metal ion therapeutics for both diagnosis and treatment.²⁰⁵ Hence, any advances on the sensing and coordination of these metals are particularly desirable.

The formation and stability of the complexes established between the metals and the sensor, **metal:87**, were investigated in a similar manner already described for the anions in Section 4.4. Titrations were carried out by addition of aliquots of the guest metal ion to a solution of known concentration of host **87** (4 μ M) in CH₃CN. Once again, due to the fact that **87** is poorly soluble in most organic solvents, a minimum amount of DMSO (< 0.1%)

had to be used on the preparation of the stock solution of **87** in order to maximize its solubility in CH_3CN . The metals studied [Cu(II) and Fe(II)] were used as their perchlorate salts ($[\text{Cu}^{\text{II}}(\text{ClO}_4)_2] \cdot 6\text{H}_2\text{O}$ and $[\text{Fe}^{\text{II}}(\text{ClO}_4)_2] \cdot \text{H}_2\text{O}$, respectively), which is a non-coordinating anion for the urea receptor. In order to account for the binding ability and selectivity of **87** towards the mentioned metal ions, both the changes in the absorbance and in the fluorescence were followed during the course of the titrations. The results obtained will be presented and discussed on the following sections.

4.5.1 Binding studies carried out on Cu(II)

Upon gradual additions of $[\text{Cu}(\text{ClO}_4)_2] \cdot 6\text{H}_2\text{O}$ to a solution of **87** ($4 \mu\text{M}$) significant changes were observed in the absorption spectra, with formation of three isosbestic points, as shown in **Figure 4.5.1**. The band at *ca.* 265 nm was also observed to experience a blue shift to *ca.* 260 nm, which can be attributed to the coordination of the metal ion to the lone pair of the nitrogen atoms of the *phen* moiety.²⁰⁶

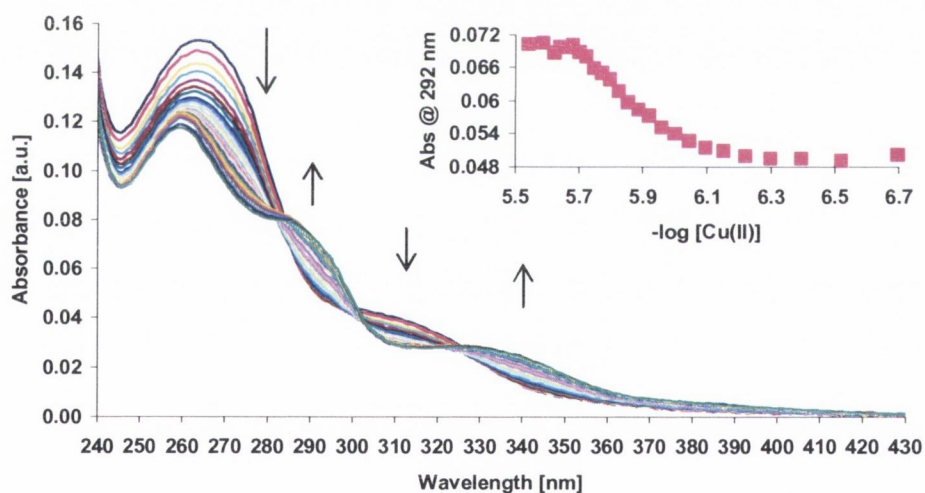


Figure 4.5.1: Changes in the absorption spectra of **87** ($4 \mu\text{M}$) upon addition of $\text{Cu}(\text{ClO}_4)_2$ ($0 \rightarrow 2.86 \mu\text{M}$). Insert: The changes in the absorbance at 292 nm as a function of $-\log [\text{Cu}(\text{II})]$.

By following the changes in the absorbance as a function of $-\log [\text{Cu}(\text{II})]$ for the 262 nm, 292 nm, 312 nm, and 340 nm bands, similar results were obtained. These changes occur over one log unit, as shown for the band at 292 nm on the insert in **Figure 4.5.1**,

which can be indicative of a stoichiometry other than 1:1 (between the metal ion and **87**).¹⁶⁵ In fact, plotting the number of equivalents of Cu(II) added versus the changes in the absorbance, as shown in **Figure 4.5.1.1** for the band at 292 nm, it can be observed that the changes occur up to 0.5 equivalents of Cu(II), after which the changes are only minimal. This is a clear indication of the binding of one Cu(II) ion to **87** in a 1:2 (**Cu:87₂**) stoichiometry.

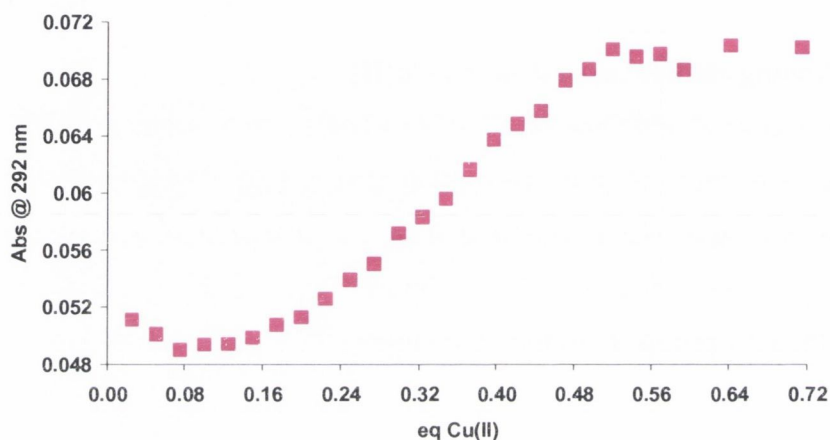


Figure 4.5.1.1: Profile of the changes in the absorbance at 292 nm vs. the number of equivalents of Cu(II).

Taking into account the discussion above, the UV-Visible titration data was fitted, using the nonlinear least-squares regression program SPECFIT, to the two step equilibrium model shown below. Here, the interaction of the Cu(II) ion with **87** gives rise to the formation of **Cu:87**, (i). However, due to the coordination requirements of the metal, interaction of **Cu:87** with a second molecule of **87** leads to the formation of the 1:2 (**Cu:87₂**) stoichiometry,(ii).



From this, binding constants of $\log K_{1:1} = 5.53 \pm 0.39$ and $\log K_{1:2} = 6.93 \pm 0.11$ were obtained for the formation of **Cu:87** and **Cu:87₂** respectively. The binding constant for the formation of the 1:1 complex carries a significant error (± 0.39), which can be associated to

the low percentage formation (< 10%) of this complex in solution (see Appendix A3.2). The excellent fit to the experimental data is shown in **Figure 4.5.1.2**.

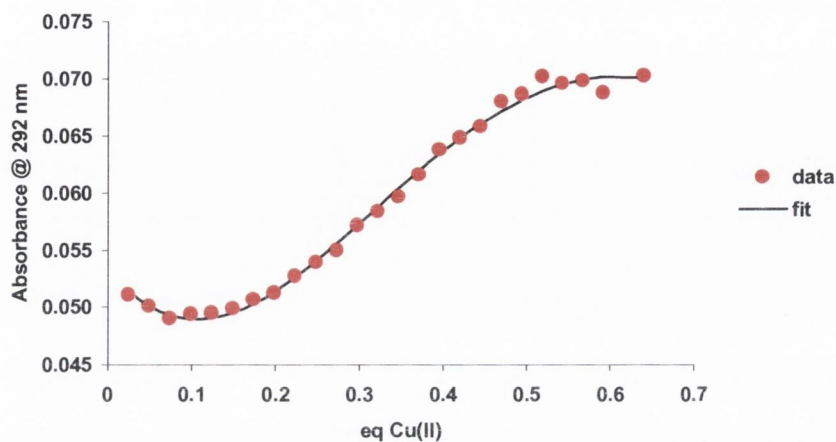


Figure 4.5.1.2: Experimental binding isotherm for the UV-Visible titration of **87** (4 μM) with Cu(II) in CH_3CN , and corresponding fit from SPECFIT.

The changes in the fluorescence emission intensity were followed by excitation at 266 nm or 320 nm. On all occasions, the emission intensity of the band centred at 422 nm was quenched by *ca.* 93% upon gradual additions of $\text{Cu}(\text{ClO}_4)_2$, as seen in **Figure 4.5.1.3** for the changes observed upon excitation at 266 nm.

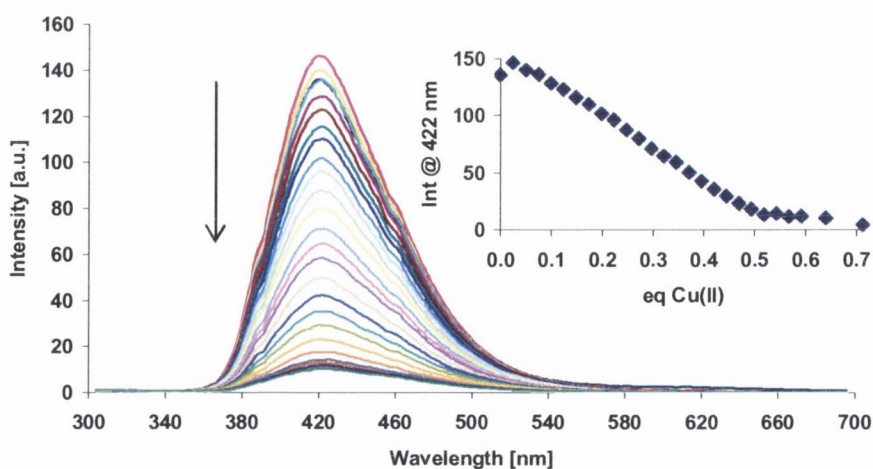
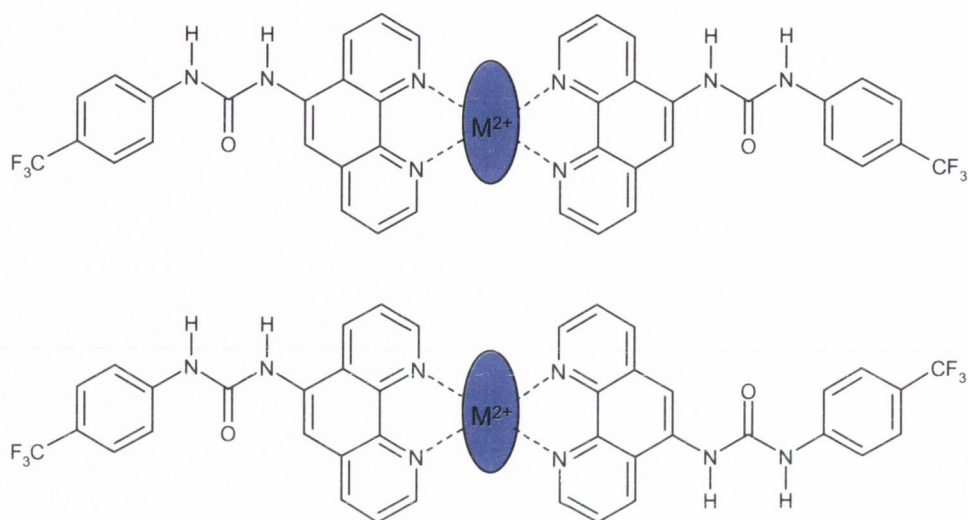


Figure 4.5.1.3: Changes in the fluorescence emission intensity of **87** (4 μM) upon addition of $\text{Cu}(\text{ClO}_4)_2$ (0 \rightarrow 2.86 μM), in CH_3CN . Insert: The decrease in the emission intensity up to 0.7 equivalents of Cu(II).

The fluorescence was almost fully quenched after the addition of *ca.* 0.5 equivalents of Cu(II), as shown on the insert in **Figure 4.5.1.3**, suggesting a 1:2 binding interaction between the guest metal ion and the host **87**, as tentatively depicted in **Scheme 4.5.1** for the two possible structural isomers, the *cis* and the *trans* isomer.



Scheme 4.5.1: Proposed structure for the 1:2 complex between Cu(II) and **87**, showing the two possible structural isomers, the *cis* and the *trans* isomers.

The observed changes were assigned to the coordination of Cu(II) to the *phen* moiety. Coordination to the metal can lead to quenching of the emission intensity through the formation of non-radiative charge-transfer states. The metal ion can also participate in the quenching by energy or electron transfer.²⁰⁶

The fitting of these changes using the nonlinear least-squares regression program SPECFIT indicated the formation of the expected 1:2 complex. The determined binding constants, $\log K_{1:1} = 5.95 \pm 0.18$ and $\log K_{1:2} = 6.90 \pm 0.08$, were found to be in good agreement with those obtained for the absorption changes discussed above. As observed for the ground state studies, an excellent fit to the experimental data was obtained, **Figure 4.5.1.4**.

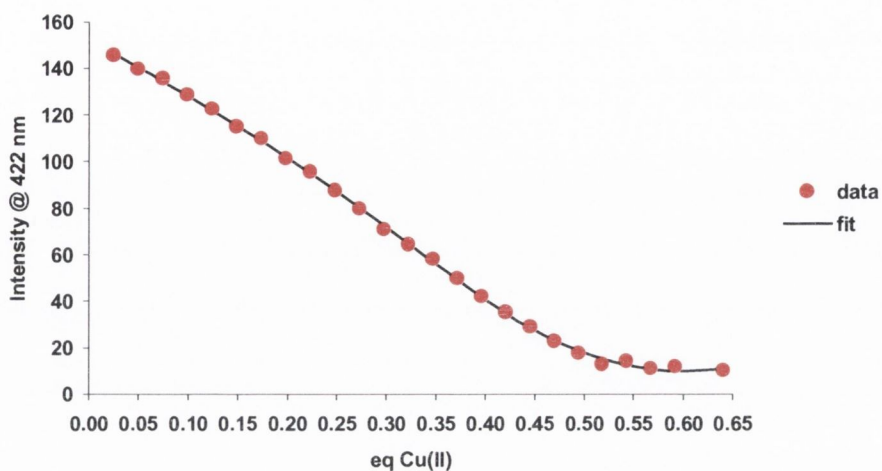


Figure 4.5.1.4: Fitting of the fluorescence emission data for the titration of **87** (4 μ M) with Cu(II) at 422 nm.

The binding constants ($\log K$) and binding modes obtained for the UV-Visible and fluorescence titrations of the *phen* receptor **87** with Cu(II) are summarised in Table 4.5.1.

Metal	Method	Binding mode ($\text{Cu}_n:\mathbf{87}_m$)	$\log K (\pm)$
Cu(II)	Absorbance	Cu: 87	$5.53 \pm 0.39^*$
		Cu: 87 ₂	6.93 ± 0.11
	Fluorescence	Cu: 87	$5.95 \pm 0.18^*$
		Cu: 87 ₂	6.90 ± 0.08

Table 4.5.1: Binding constants and binding modes between Cu(II) and sensor **87**. * Species present in solution in less than 10% formation.

In addition to the absorption and the luminescence titration measurements, complexation studies using electrospray mass spectrometry (ESMS) were also undertaken. ESMS has been devised as an useful method for establishing supramolecular interactions by means of the changes observed in the molecular mass.²⁰⁷ By adding an excess of $\text{Cu}(\text{ClO}_4)_2$ to a suspension of **87** in CH_3CN a green solid was immediately formed, which was indicative of the desired complex formation. The mass spectrum showed the presence of two peaks at $m/z = 382$ and $m/z = 827$, corresponding to the free host **87** and to the **Cu:87**₂ complex, respectively. The isotopic distribution pattern generated for **Cu:87**₂

compared well with the theoretical isotopic model for $C_{40}H_{26}N_8O_2F_9Cu$, shown in **Figure 4.5.1.5**.

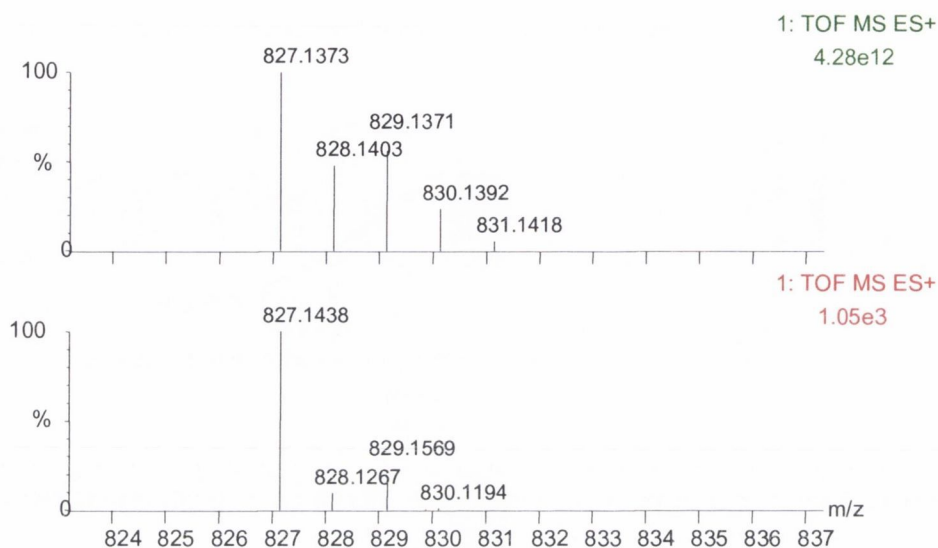


Figure 4.5.1.5: ESMS of $Cu.87_2$ ($C_{40}H_{26}N_8O_2FCu$) in comparison with its theoretical isotopic distribution model.

These results are in good agreement with those found for the absorption and the luminescence titration measurements, indicating the expected coordination of Cu(II) to two molecules of **87**. These results were expected as Cu(II) is well known for its distorted square planar geometry.²⁰⁸ However, a distorted octahedral geometry has been reported for the coordination of Cu(II) with *phen*.²⁰⁹ More recently, Gunnlaugsson *et al.* observed the 1:3 binding between Cu(II) and a Eu(III)-cyclen-*phen* conjugate.¹⁹⁹ In order to gain a better understanding of the stoichiometry and the geometry of the complex, attempts were made to grow crystals suitable for X-ray crystallographic structure determination.

Small crystals, which were grown by slow evaporation from a CH_3CN solution, were used for X-ray crystallographic diffraction studies. The obtained crystal structure, $(Cu_2:87_4).(ClO_4)_4.(CH_3CN)_2$, as solved by Dr. Thomas McCabe, is shown in **Figure 4.5.1.6**, while selected bond lengths and bond angles for the complex are given in **Table 4.5.1.1**. Due to the relatively small size of the crystals grown, the quality of the obtained data was somewhat poor (see Appendix A1.5). Nevertheless, analysis of the obtained structure can provide useful information about the coordination and geometry adopted by

the Cu(II) ion in the solid state. The remarkable structure was found to involve the formation of a dinuclear complex, through interaction of two copper ions with four molecules of **87**.

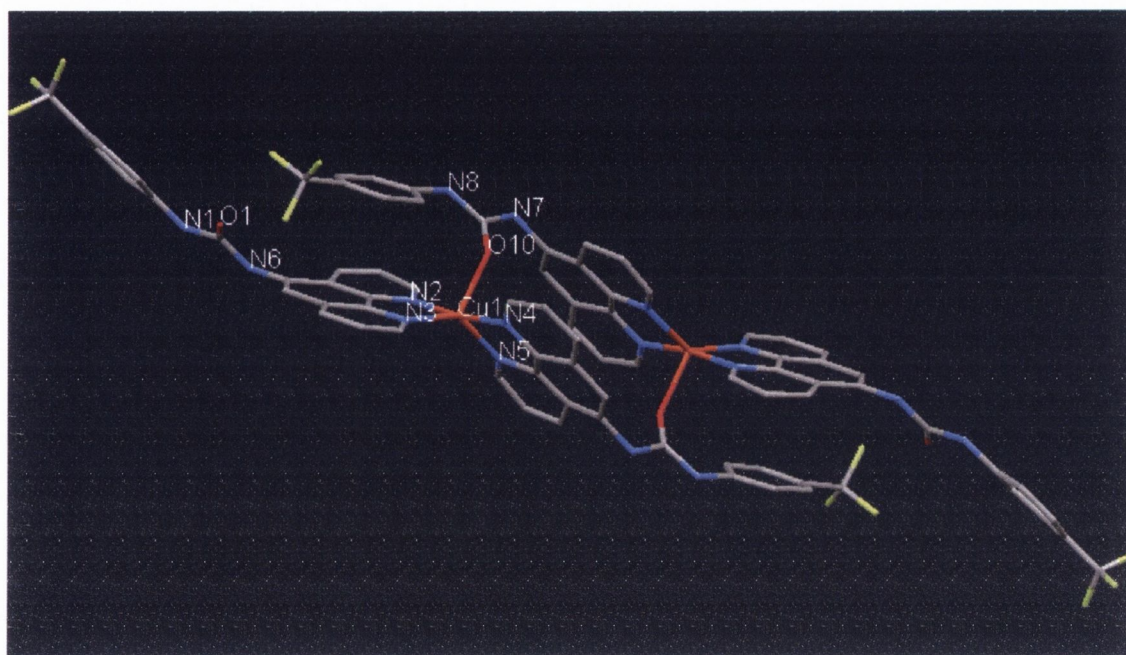


Figure 4.5.1.6: Molecular structure of $(\text{Cu}_2:87_4) \cdot (\text{ClO}_4)_4 \cdot (\text{CH}_3\text{CN})_2$, obtained by X-ray crystallography, showing the bonding interactions between Cu(II) and **87**. Hydrogen atoms as well as solvent molecules and perchlorate counter ions were omitted for clarity.

Each Cu(II) ion is in a similar distorted square-pyramidal geometry, coordinated by four nitrogen atoms from the two *phen* ligands and one oxygen atom from the urea moiety of a neighbour molecule of **87**. The Cu1-O10 distance was found to be 2.105(10) Å, which is indicative of a relatively strong bond between the Cu(II) ion and the oxygen atom. As expected for such geometry, the bond distances Cu1-N2 and Cu1-N4 were found to be shorter (1.968(11) Å and 1.995(14) Å, respectively) than the bond distances Cu1-N3 and Cu1-N5 (2.004(13) Å and 2.071(13) Å, respectively).²¹⁰ The N2, Cu and N4 atoms are almost co-linear, since the N2-Cu1-N4 angle is 169.3(5). The angles N2-Cu1-O10, N2-Cu1-N3, N2-Cu1-N5, N4-Cu1-O10, N4-Cu1-N3 and N4-Cu1-N5 were found to be in the range of $90 \pm 10^\circ$, being 84.4(4), 82.4(5), 103.7(5), 82.7(4), 94.7(5) and 85.2(4), respectively. Once again, the NH protons of each urea moiety were found to be in the *syn* conformation (*i.e.* NH protons are facing in the same direction).

Bond	Length (Å)	Bond	Angle (°)
Cu(1)-N(2)	1.968(11)	N(2)-Cu(1)-N(3)	82.4(5)
Cu(1)-N(3)	2.004(13)	N(4)-Cu(1)-N(5)	85.2(4)
Cu(1)-N(4)	1.995(14)	N(2)-Cu(1)-N(5)	103.7(5)
Cu(1)-N(5)	2.071(13)	N(4)-Cu(1)-N(3)	94.7(5)
Cu(1)-O(10)	2.105(10)	N(2)-Cu(1)-N(4)	169.3(5)
O(1)-C(8)	1.205(16)	N(3)-Cu(1)-N(5)	139.9(5)
O(10)-C(43)	1.29(2)	N(2)-Cu(1)-O(10)	89.4(4)
N(1)-C(8)	1.399(18)	N(3)-Cu(1)-O(10)	116.3(4)
N(6)-C(8)	1.457(18)	N(5)-Cu(1)-O(10)	103.5(4)
N(8)-C(43)	1.41(2)	N(4)-Cu(1)-O(10)	82.7(4)
N(7)-C(43)	1.386(19)	C(43)-O(10)-Cu(1)	135.5(9)
N(1)-C(5)	1.373(17)	N(1)-C(8)-N(6)	110.0(12)
N(6)-C(9)	1.387(15)	C(8)-N(1)-C(5)	123.2(13)
N(8)-C(36)	1.421(17)	C(9)-N(6)-C(8)	121.4(12)
N(7)-C(30)	1.490(18)	O(1)-C(8)-N(1)	126.1(15)
		O(1)-C(8)-N(6)	123.5(15)
		O(10)-C(43)-N(7)	123.7(15)
		O(10)-C(43)-N(8)	119.7(15)
		N(7)-C(43)-N(8)	116.6(16)

Table 4.5.1.1: Selected bond lengths and bond angles for $\text{Cu}_2\cdot 87_4$.

The structure of five coordinated dinuclear Cu(II) complexes with 1,10-phenanthroline, exhibiting a distorted square-pyramidal geometry have been reported. For instance, Ciu and collaborators reported a mononuclear complex of this type, where the Cu(II) ion is coordinated by four nitrogen atoms from two chelating *phen* ligands and one oxygen atom from a formate ligand.²¹¹ Devereux *et al.* reported a series of dinuclear complexes, showing the two Cu(II) centres linked by a dicarboxylate ligand.²¹² Each Cu(II) is coordinated by four nitrogen atoms of the two *phen* ligands and one oxygen from a single chelating carboxylate function of the dicarboxylate ligand, with the second carboxylate group of the diacid uncoordinated.²¹²

A view of the packing in the solid state, along the crystallographic b-axis, as determined from this study is shown in **Figure 4.5.1.7**. Intramolecular hydrogen bonding networks were observed between the dinuclear complex (NH proton of the urea) and perchlorate anions. Stacking among the *phen* moieties of the dinuclear complex, as well as the phenyl rings and the *phen* moiety is observed. The stacking distance was found to be

3.66(3) and 3.66(6), respectively, which is in the range of average values in π - π stacking interactions.²¹³

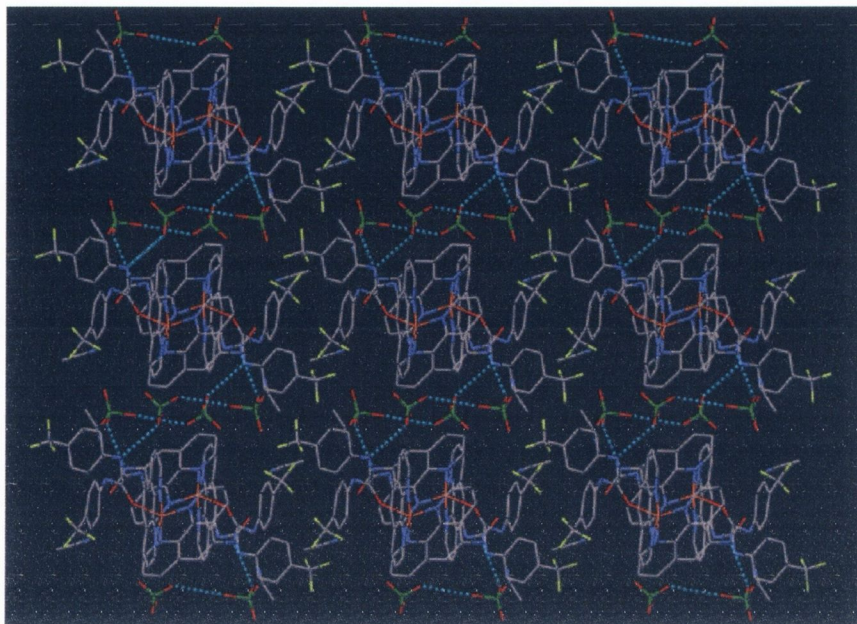


Figure 4.5.1.7: Packing diagram as viewed along the crystallographic b-axis of the structure of $\text{Cu}_2\text{:874}$. Hydrogen atoms were omitted for clarity. O red, N dark blue, C dark grey, F yellow, Cl green.

Even though this geometry is observed in the solid state, it is possible that such coordination environment may also be present in solution, which would have reasonable influence on the binding ability of the urea active sites in solution. Hence, this may have a significant impact in the binding interactions of the metal complex with the various anions.

4.5.2 Binding studies carried out on Fe(II)

The spectrophotometric binding studies of **87** with Fe(II) were carried out following the same procedure as described above for the copper ion. The changes in the absorption and the fluorescence spectra, were followed upon titration of $[\text{Fe}(\text{ClO}_4)_2]\cdot\text{H}_2\text{O}$ to a solution of **87** (4 μM). Significant changes were observed in the absorption spectra, with the concomitant formation of three isosbestic points, as shown in **Figure 4.5.2**. This is assigned to the changes in the $\pi \rightarrow \pi^*$ transitions upon coordination of the metal ion to the *phen* moiety. Charge-transfer processes indicating significant interactions between the molecular orbitals of the ligand and those of the Fe(II) metal center were also observed by

the presence of a MLCT band at long wavelength (520 nm), as discussed later in Section 4.6.

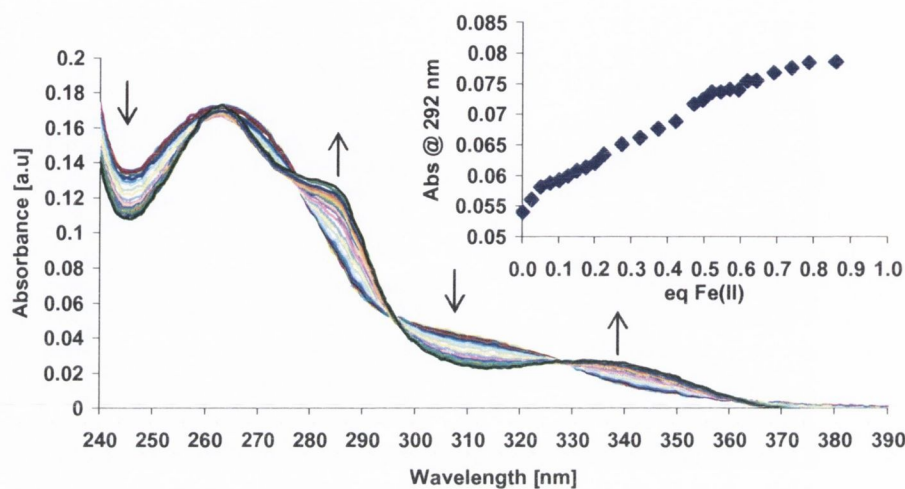


Figure 4.5.2: Changes in the absorption spectra of **87** upon addition of $\text{Fe}(\text{ClO}_4)_2$ (0 \rightarrow 4.01 μM). Insert: The changes in the absorbance at 292 nm as a function of the number equivalents of $\text{Fe}(\text{II})$.

As can be observed, from the insert in **Figure 4.5.2** these changes occur over *ca.* 0.6 equivalents of $\text{Fe}(\text{II})$, after which the changes are minimal. The fact that the changes are occurring over 0.6 equivalents of $\text{Fe}(\text{II})$ added is a strong indication of the formation of a 1:2 complex, **Fe:1₂**, as observed previously for $\text{Cu}(\text{II})$. Fitting the spectral changes, using the SPECFIT program, further supported the formation of the 1:2 (**Fe:87₂**) complex with determined binding constants of $\log K_{1:1} = 5.67 \pm 0.32$ and $\log K_{1:2} = 6.04 \pm 0.37$. Although the binding constant for the 1:1 (**Fe:87**) interaction was found to be similar to the one determined for the $\text{Cu}(\text{II})$ complex ($\log K_{1:1} = 5.53 \pm 0.39$), the binding constant for the 1:2 (**Fe:87₂**) was found to be lower when compared to the formation of **Cu:87₂** ($\log K_{1:2} = 6.93 \pm 0.11$).

The changes in the fluorescence emission intensity were followed by excitation at 266 nm or 320 nm. In both cases, the emission intensity of the band centred at 422 nm was quenched by *ca.* 91% upon gradual additions of $\text{Fe}(\text{ClO}_4)_2$, as shown in **Figure 4.5.2.1** upon excitation at 266 nm. These changes occur over one log unit, as revealed in **Figure**

4.5.2.1 insert, indicating, as expected, that the binding process is more complex than just a simple 1:1 interaction.

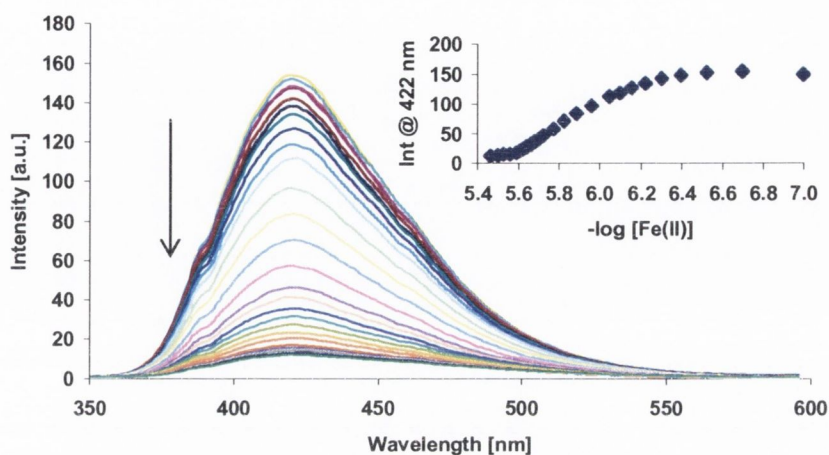


Figure 4.5.2.1: Changes in the fluorescence emission spectra of **87** ($4 \mu\text{M}$) upon addition of $\text{Fe}(\text{ClO}_4)_2$ ($0 \rightarrow 4.01 \mu\text{M}$), in CH_3CN . Insert: The changes in the fluorescence emission intensity at 422 nm as a function of $-\log[\text{Fe}(\text{II})]$.

In agreement with the ground state, the changes were observed to occur up to *ca.* 0.6 equivalents of $\text{Fe}(\text{II})$, after which the changes were only minimal. Once again, this indicated the formation of the 1:2 (**Fe:87**₂) complex, as previously observed for $\text{Cu}(\text{II})$. So, these changes were fitted to a two consecutive stepwise equilibrium model, which gave rise to binding constants of $\log K_{1:1} = 5.57 \pm 0.18$ and $\log K_{1:2} = 5.97 \pm 0.18$ for the formation of **Fe:87** and **Fe:87**₂ respectively. These values are indicative of the strong interaction between metal and ligand leading to the formation of the 1:2 complex, which is in good agreement with the binding constant determined for the ground state ($\log K_{1:2} = 6.04 \pm 0.32$). As discussed above for the absorption titration, the binding constant for the formation of **Fe:87**₂ was found to be lower than the one determined for the formation of **Cu:87**₂ ($\log K_{1:2} = 6.90 \pm 0.08$). The excellent fit to the experimental data, as shown in **Figure 4.5.2.2**, is a good evidence of the correct binding model used when determining these binding constants.

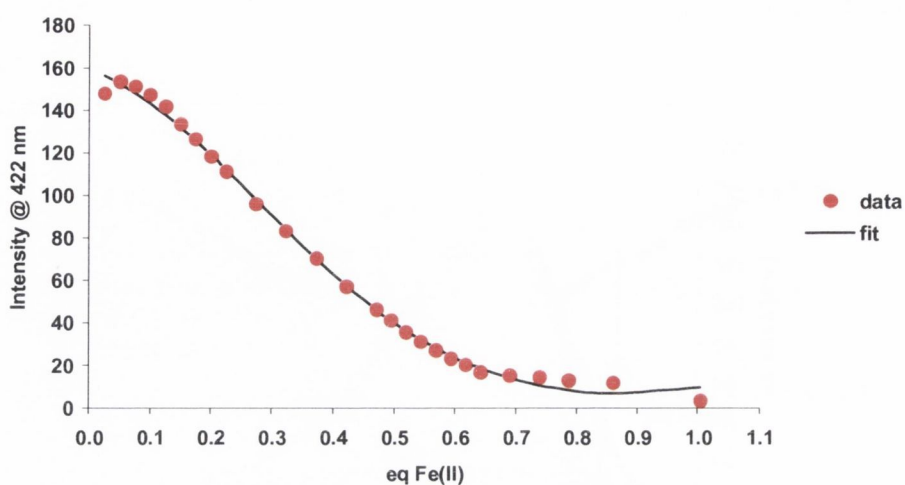


Figure 4.5.2.2: Binding isotherm and corresponding fit of the fluorescence emission data for the titration of **87** (4 μ M) with Fe(II) at 422 nm.

The binding constants ($\log K$) and binding modes determined from the absorption and the fluorescence titrations of **87** with Fe(II) are summarised in **Table 4.5.2**. As can be observed, the binding constants determined from both the absorption and the fluorescence studies were found to be in good agreement. When comparing the binding interactions of both Cu(II) and Fe(II) with **87**, it was found that these metals interact strongly with the *phen* ligand to form **Cu:87** and **Fe:87**, respectively, with similar binding constants (**Table 4.5.1** and **Table 4.5.2**). In contrast, the binding constant for the formation of **Cu:87₂** was found to be higher ($\log K_{1:2} \sim 7$) than that determined for the formation of **Fe:87₂** ($\log K_{1:2} \sim 6$).

Metal	Method	Binding mode (Cu _n :87 _m)	$\log K (\pm)$
Fe(II)	Absorbance	Fe:87	5.67 ± 0.32
		Fe:87 ₂	6.04 ± 0.37
	Fluorescence	Fe:87	5.57 ± 0.18
		Fe:87 ₂	5.97 ± 0.18

Table 4.5.2: Binding constants and binding modes between Fe(II) and sensor **87**.

As for Cu(II), attempts to provide further insight into the binding process taking place between Fe(II) and **87**, either by complexation studies using electrospray mass

spectrometry (ESMS) or X-ray crystallography were made. However, all the attempts failed to produce successful results.

These studies illustrated the fact that Cu(II) and Fe(II) form strong 1:2 (**M:87**₂) complexes in solution, by coordinating to the *phen* moiety of two molecules of **87**. As a consequence of this self-assembly, two urea moieties are introduced within the complex. This is a desirable property, as more binding sites are created for anion recognition. In addition, the metal may orientate these urea moieties creating suitable binding sites for selective anion recognition. Therefore, the presence of the metal ion is expected to cooperatively affect the binding behavior towards the anionic species.

With this in mind, studies on the binding affinity of these metal complexes (**Cu:87**₂ and **Fe:87**₂) with various anions were undertaken and the results will be presented in the following sections.

4.6 Photophysical studies on the metal complexes towards binding with anions

The binding affinity of the metal complexes, **Cu:87**₂ and **Fe:87**₂, towards various anions was studied using spectrophotometric methods such as UV-Visible and fluorescence. In order to assess the interaction between the guest anions (G) and the host metal complexes (H), titrations were carried out in a manner previously described. 1 mM metal complex stock solutions were prepared by adding 0.5 equivalents of Cu(ClO₄)₂ or Fe(ClO₄)₂ to a suspension of **87** in CH₃CN. Complex formation was signalled by naked eye visualisation of green and red coloured clear solutions for Cu(II) and Fe(II), respectively. However, after dilution to 4 μM (host metal complexes concentration used in the studies performed in this section), these solutions changed to colourless and faint red for Cu(II) and Fe(II) respectively. The absorption spectra of such solutions were recorded, and the obtained results presented in **Figure 4.6**. As can be observed, both spectra are relatively similar in shape except for the appearance of the band centred at *ca.* 520 nm for the Fe(II) complex, which can be attributed to the metal-to-ligand charge-transfer (MLCT) transition upon coordination of this metal to the *phen* ligand. Such MLCT bands are characteristic of this kind of Fe(II) complexes.^{142,214} The fluorescence emission spectra of the Cu(II) complex and Fe(II) complex, when excited at 260 nm or 335 nm, gave rise to an emission band centred at 422 nm. In addition, the fluorescence emission spectra of the Fe(II)

complex when exciting at the MLCT band, 520 nm, gave rise to a weak emission band centred at *ca.* 616 nm.

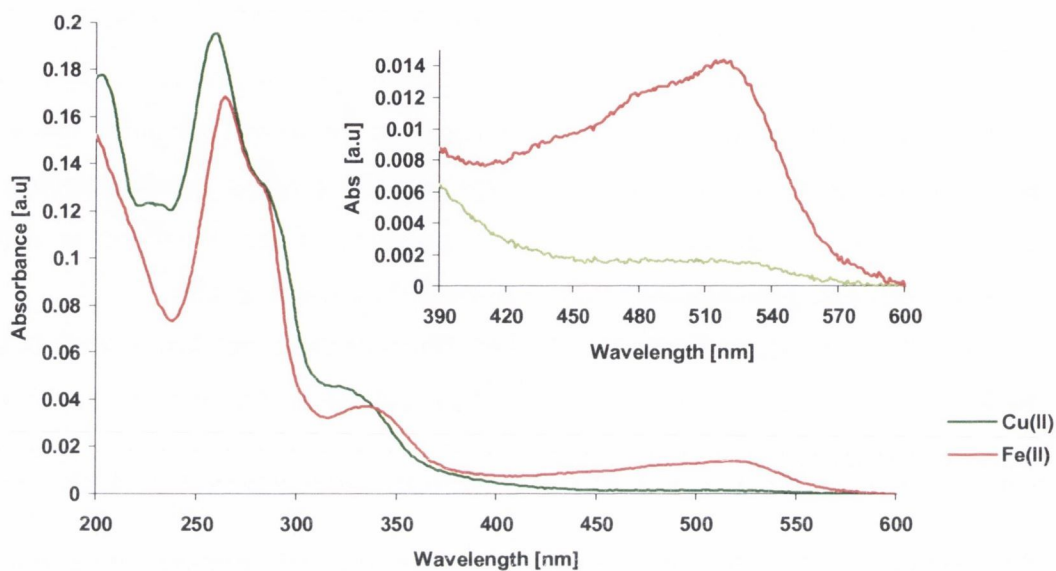


Figure 4.6: Absorption spectra of the free host Cu(II) and Fe(II) metal complexes (4 μ M) in CH_3CN . Insert: Fraction of the absorption spectra, showing the presence of the MLCT band (λ_{max} at 520 nm) for the Fe(II) complex.

4.6.1 Ground state investigations

4.6.1.1 Interaction of Fe:87₂ with anions

The changes in the absorption spectra during the titrations of **Fe:87₂** with the various anions showed a decrease in the absorbance for all the bands (including the MLCT band, insert in **Figure 4.6.1.1**), upon increasing concentration of the anions such as CH_3COO^- , F^- , and Cl^- . For these anions no significant shifts or isosbestic points were observed, as shown in **Figure 4.6.1.1** for the titration of **Fe:87₂** with CH_3COO^- .

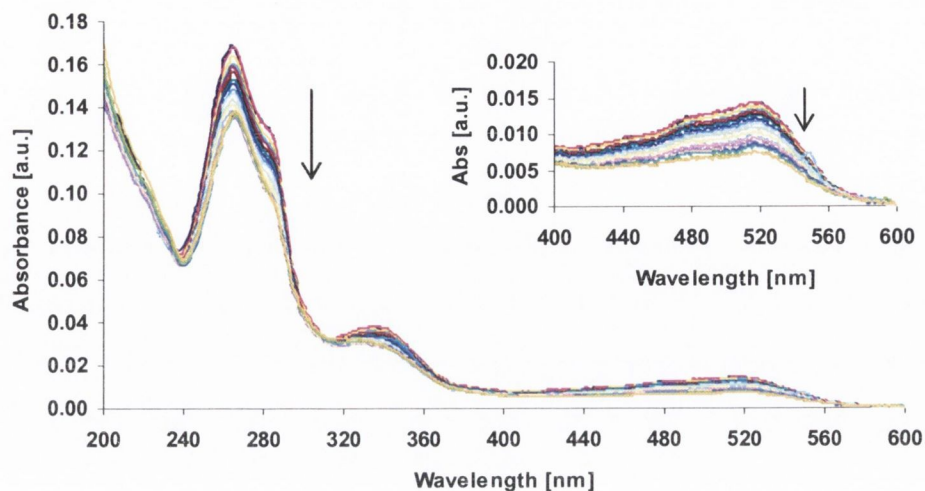


Figure 4.6.1.1: Changes in the absorption spectra of Fe:87_2 upon addition of CH_3COO^- ($0 \rightarrow 14.50 \mu\text{M}$). Insert: Fraction of the absorption spectra, showing the changes at the MLCT band (λ_{max} at 520 nm).

The titration profile shown in **Figure 4.6.1.1.1** for the band at 264 nm clearly indicate that such changes are occurring over the addition of one equivalent of CH_3COO^- , indicating the formation of a 1:1 (**G:H**) adduct. Furthermore, the titration profile does not show any curvature suggesting a strong interaction between the guest and the host species, which prevents the determination of a reliable binding constant ($\log K$). In fact, a $\log K_{1:1} > 7$ was found using the nonlinear least-squares regression program SPECFIT.

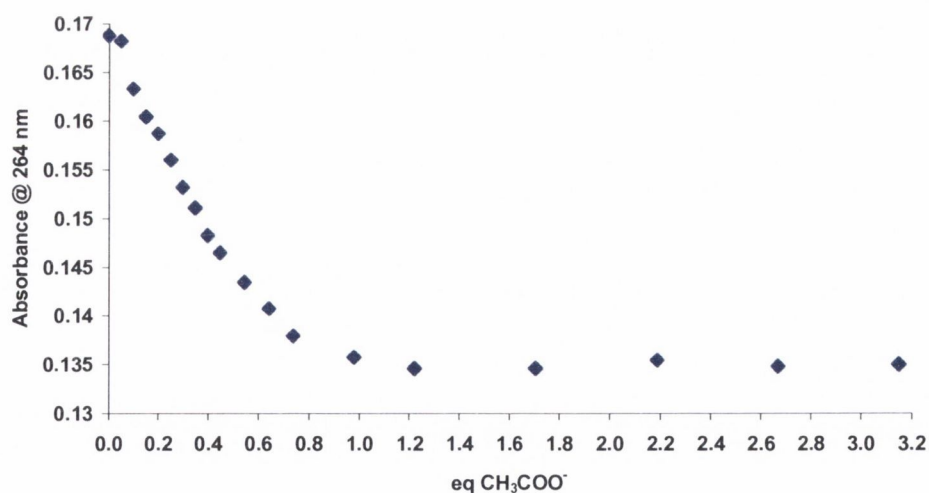


Figure 4.6.1.1.1: Changes in the absorbance at 264 nm of Fe:87_2 as a function of the number equivalents of CH_3COO^- ($0 \rightarrow 14.50 \mu\text{M}$).

Similar results were obtained for the titrations of **Fe:87₂** with F^- and Cl^- , showing 1:1 interactions with the host metal complex. The absorbance spectra and titration profiles are shown in the Appendix A3.3.1. Fitting the obtained titration data to a 1:1 equilibrium model, using the SPECFIT program, gave rise to binding constants of $\log K_{1:1} = 5.88 \pm 0.12$ and $\log K_{1:1} = 5.76 \pm 0.25$ for the interaction of **Fe:87₂** with F^- and Cl^- respectively.

In the case of $H_2PO_4^-$, a different behaviour was observed, **Figure 4.6.1.1.2**. An initial addition of 0.5 equivalents of $H_2PO_4^-$ led to a significant decrease in the absorbance, followed by an immediate increase up to the addition of two equivalents of added anion. By looking at the titration graph depicted on the insert in **Figure 4.6.1.1.2**, it can be seen that the first part of the profile ($0 \rightarrow 0.5$ equivalents $H_2PO_4^-$) does not show any curvature, which is an indication of a strong interaction between one $H_2PO_4^-$ and two **Fe:87₂**, to form the 1:2 (G:H₂) stoichiometry. However, this also prevented the determination of reliable binding constants for the interaction of $H_2PO_4^-$ to **Fe:87₂**. The second component of the profile, insert in **Figure 4.6.1.1.2**, shows a gradual increase in the absorbance, which indicates the formation of the possible 1:1 (G:H) and 2:1 (G₂:H) species in solution. A similar behaviour was observed for the titration with $H_2P_2O_7^{2-}$ (see Appendix A.3.3.1).

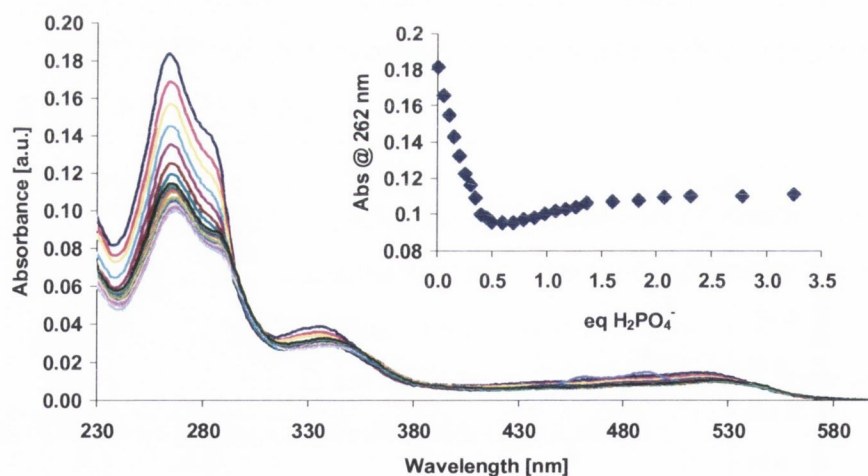


Figure 4.6.1.1.2: Changes in the absorption spectra of **Fe:87₂** upon addition of $H_2PO_4^-$ ($0 \rightarrow 13 \mu M$). Insert: The changes in the absorbance at 262 nm as a function of the number of equivalents of $H_2PO_4^-$.

4.6.1.2 Interaction of Cu:87₂ with anions

The changes observed for the titration of Cu:87₂ with CH₃COO⁻ gave similar results to those discussed above for the Fe(II) complex. A decrease in absorbance accompanied by a 4 nm red shift for the band centred at *ca.* 260 nm was observed upon addition of CH₃COO⁻, as shown in **Figure 4.6.1.2**. As previously mentioned, it can clearly be observed that the MLCT band is not present in the absorption spectra of the Cu(II) complex. The titration profile shown on the insert in **Figure 4.6.1.2** clearly indicates the formation of a 1:1 adduct, as the changes are occurring over *ca.* 1.2 equivalents of CH₃COO⁻. Fitting these changes using the SPECFIT program gave rise to a binding constant of $\log K_{1:1} = 6.78 \pm 0.25$, which although high was found to be not as strong as the binding constant for the interaction with the Fe(II) complex ($\log K_{1:1} > 7$). For the interactions of Cu:87₂ with Cl⁻ and F⁻ it was not possible to determine reliable binding constants, as addition of Cl⁻ gave rise to only minor changes in the absorbance spectra, while addition of F⁻ gave rise to more complex spectra. The absorbance spectra and titration profiles are presented in the Appendix A.3.3.2.

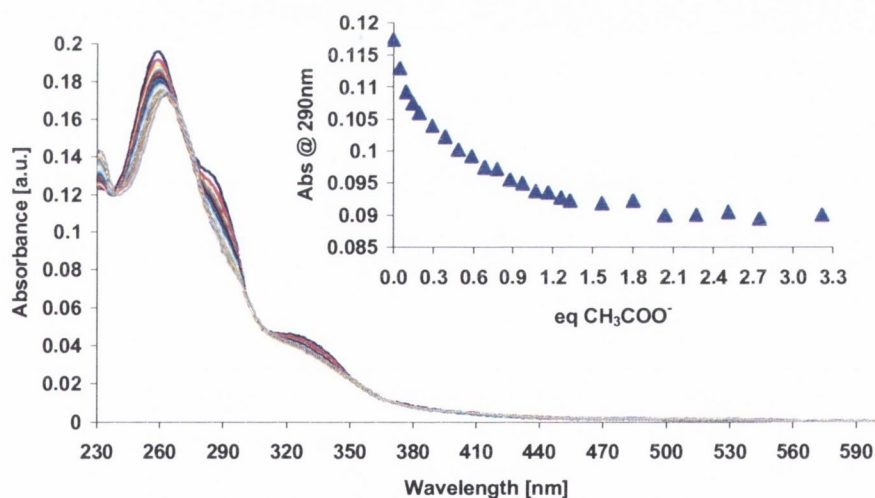


Figure 4.6.1.2: Changes in the absorption spectra of Cu:87₂ upon addition of CH₃COO⁻ (0 → 12.90 μM). Insert: The changes in the absorbance at 290 nm as a function of the number equivalents of CH₃COO⁻.

Upon addition of H₂PO₄⁻, a different behaviour was observed, similar to that seen for the interaction of H₂PO₄⁻ with Fe:87₂. An initial addition of 0.5 equivalents of H₂PO₄⁻ led to the decrease in absorbance, which was followed by an immediate increase up to the

addition of two equivalents of added anion. As discussed for the titration with **Fe:87₂**, the decrease in absorbance can be attributed to the possible formation of the 1:2 (G:H₂) stoichiometry between H₂PO₄⁻ and **Cu:87₂**. Once again it was not possible to determine reliable binding constants for the interaction between these anions and the metal complex, as the binding process showed too complex (Appendix A3.4.1, Figure A3.4.1.2).

4.6.2 Excited state investigations

The fluorescence emission spectra of the hosts (H), **Fe:87₂** and **Cu:87₂**, when excited at 260 nm, gave rise to a band centred at 422 nm. Upon titration of **Cu:87₂** with CH₃COO⁻ and F⁻ the emission intensity was enhanced by *ca.* 74% and 50% respectively, as is evident from **Figure 4.6.2** for the titration of **Cu:87₂** with CH₃COO⁻. For the titration of **Cu:87₂** with CH₃COO⁻, the changes in emission intensity were observed to occur over two log units (insert in **Figure 4.6.2**), which are indicative of 1:1 binding interaction between the host and the guest anion.

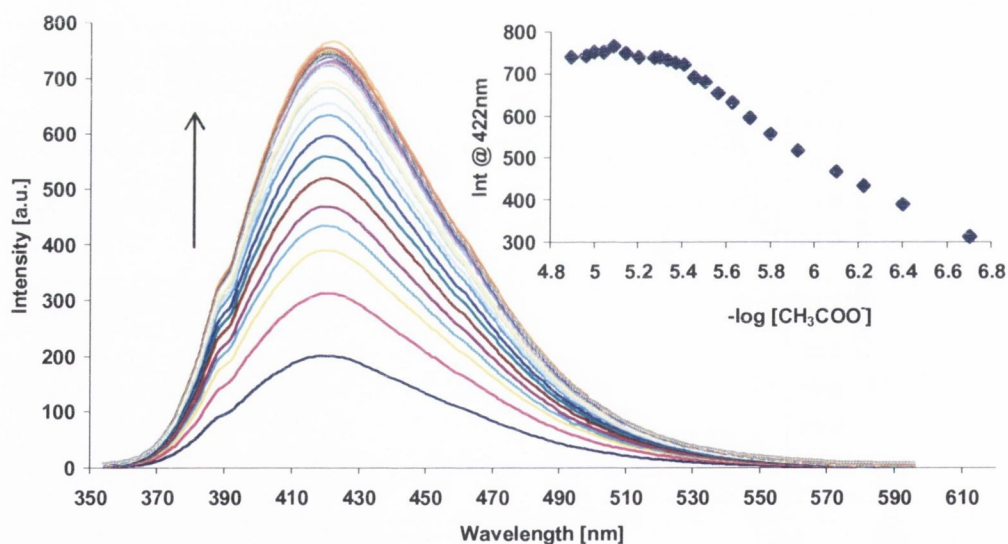


Figure 4.6.2: Changes in the fluorescence emission spectra of **Cu:87₂** upon addition of CH₃COO⁻ (0 → 12.90 μM), in CH₃CN when exciting the sample at 260 nm. Insert: The changes in emission intensity at 422 nm as a function of -log [CH₃COO⁻].

The titration profile shown in **Figure 4.6.2.1** clearly indicates that such changes are occurring over the addition of one equivalent of CH₃COO⁻, further supporting the

formation of a 1:1 (H:G) adduct between the host (H) and the guest anion (G). The fitting of these changes using SPECFIT also indicated the formation of the 1:1 complex, with a $\log K_{1:1} = 6.95 (\pm 0.17)$, which was in good agreement with the ground state studies ($\log K_{1:1} = 6.78 \pm 0.25$). This binding constant, reflecting a strong interaction between CH_3COO^- and **Cu:87**₂, is at least 60-fold higher than that observed for the interaction with the simple receptor **87** (5.19 ± 0.03). Such results show a positive effect on the binding of CH_3COO^- , due to the presence of the metal ion. Similarly to that observed for the ground state studies, no reliable binding constants were determined for the titrations with both F^- and Cl^- . The fluorescence emission spectra and titration profiles are presented in the Appendix A3.4.2.

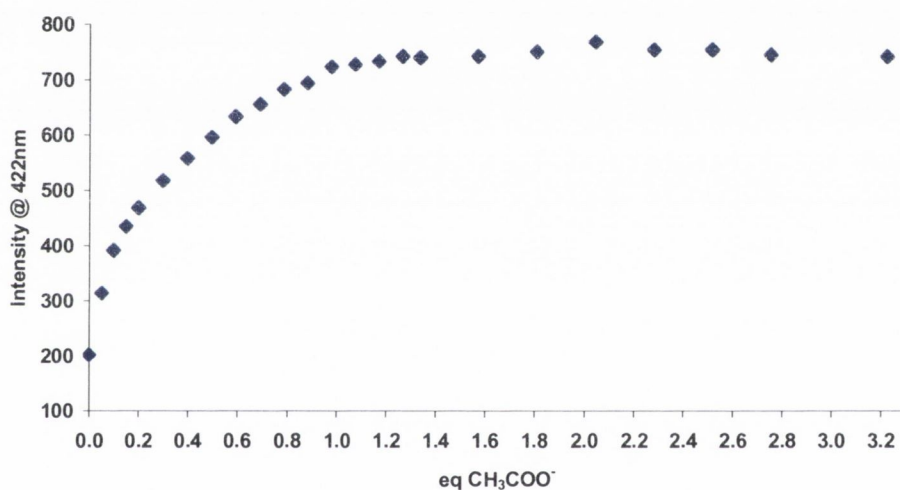


Figure 4.6.2.1: Changes in the emission intensity at 422 nm of **Cu:87**₂ as a function of the number of equivalents of CH_3COO^- .

Titration of **Fe:87**₂ with CH_3COO^- , F^- , and Cl^- gave rise to emission intensity enhancements of *ca.* 70%, 69%, and 56%, respectively. **Figure 4.6.2.2** illustrates the changes in the fluorescence emission spectra for the titration of **Fe:87**₂ with CH_3COO^- , when exciting at 260 nm. Similar results were observed when exciting at 335 nm. However, excitation at 520 nm gave rise to a weak emission band centred at 616 nm, which did not change upon addition of F^- (see Appendix A.3.3.2, Figure A.3.3.2). The fluorescence emission spectra and titration profiles, for the remaining anions, are presented in Appendix A3.3.2.

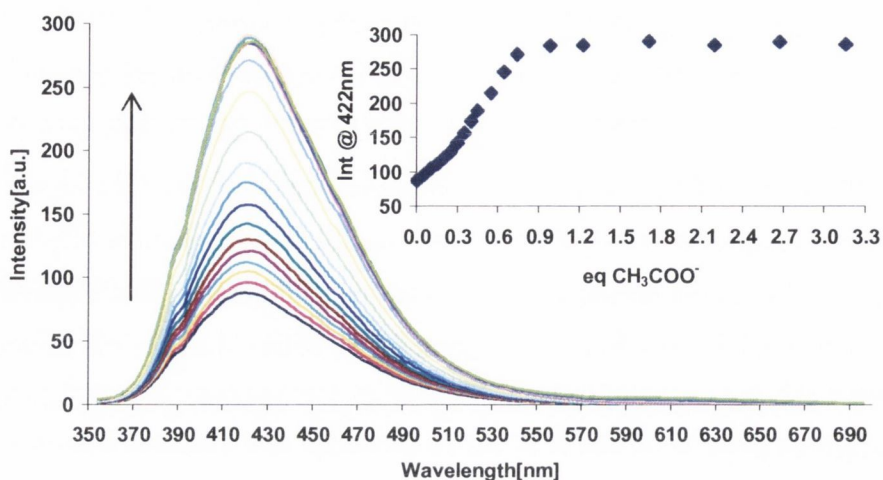


Figure 4.6.2.2: Changes in the fluorescence emission spectra of **Fe:87₂** upon addition of CH_3COO^- (0 \rightarrow 12.60 μM), in CH_3CN when exciting the sample at 260 nm. Inset: The changes in emission intensity at 422 nm as a function of the number of equivalents of CH_3COO^- .

The changes in emission intensity, for the titrations of **Fe:87₂** with the mentioned anions, were observed to occur over one equivalent of added anion, as shown on the profile inserted in **Figure 4.6.2.2** for the titration with CH_3COO^- . The steep slope on this profile is an indication of a very strong binding interaction. In fact, by fitting these changes to a 1:1 equilibrium model, a $\log K_{1:1} > 7$ was found. Following the same procedure, $\log K_{1:1}$ of 5.96 ± 0.06 and 6.08 ± 0.04 were determined for the binding interactions with F^- and Cl^- respectively. The determined values are in total agreement with those obtained for the ground state studies (> 7 , 5.88 ± 0.12 and 5.76 ± 0.25 for the interactions with CH_3COO^- , F^- and Cl^- , respectively). The high values obtained for the binding constants show an enhancement on the binding interactions with the anions, when compared to the values determined for the interactions with the simple receptor **87** (Section 4.4). In particular, the binding constant of Cl^- to **Fe:87₂** is at least 173-fold higher than that observed for the 1:1 interaction of this anion to **87** (3.84 ± 0.14).

Interestingly, as found for the absorption, the fluorescence titration of either metal complex with H_2PO_4^- gave rise to a different binding process. The emission intensity was quenched by *ca.* 90% and 46% upon addition of H_2PO_4^- to CH_3CN solutions of **Fe:87₂** and **Cu:87₂** respectively, as shown in **Figure 4.6.2.3** for the titration of **Fe:87₂** with H_2PO_4^- .

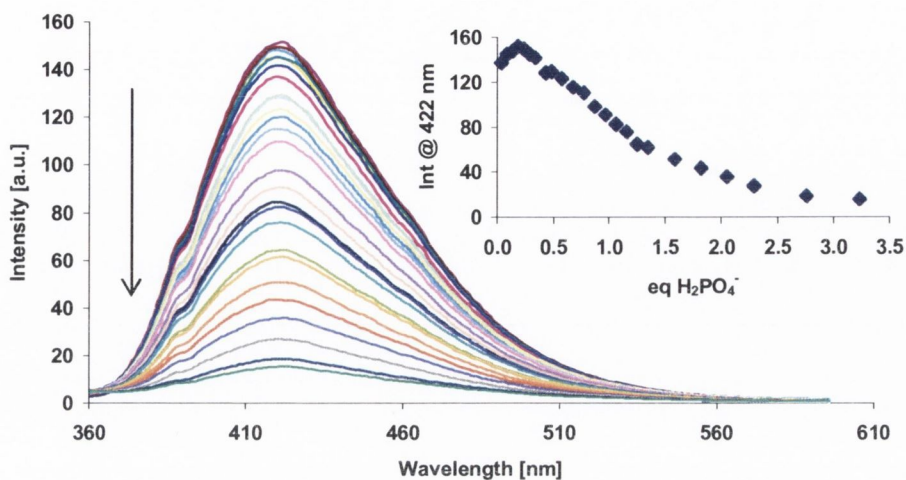


Figure 4.6.2.3: Changes on the fluorescence emission spectra of **Fe:87₂** upon addition of H₂PO₄⁻ (0 → 13 μM), in CH₃CN when exciting the sample at 260 nm. Insert: The changes in emission intensity at 422 nm as a function of the number of equivalents of H₂PO₄⁻.

The titration profile inserted in **Figure 4.6.2.3** indicates a complex binding interaction, as the changes are taking place over more than three equivalents of added H₂PO₄⁻. In addition, at least three different binding processes are taking place between 0 → 0.5 equivalents, 0.5 → 1 equivalents, and 1 → 3.5 equivalents of added anion. The profile is also very steep, which indicates strong interactions between the host and the anion. Similar behaviour was observed for the titration with **Cu:87₂**. Due to these factors, it was not possible to determine reliable binding constants for the interaction of either **Fe:87₂** or **Cu:87₂** with H₂PO₄⁻.

The fact that dihydrogenphosphate quenched the emission intensity, as opposed to the enhancement observed for the other anions studied, lead us to investigate the interaction with dihydrogenpyrophosphate (H₂P₂O₇²⁻). Upon addition of this anion to either **Fe:87₂** or **Cu:87₂**, the emission intensity was quenched by *ca.* 71% for both titrations. Titration with **Cu:87₂** resulted in a profile similar to that obtained for the interaction with H₂PO₄⁻. On the other hand, titration with **Fe:87₂** gave rise to a simpler profile, with changes occurring over the addition of one equivalent of added anion, as shown on the insert in **Figure 4.6.2.4**.

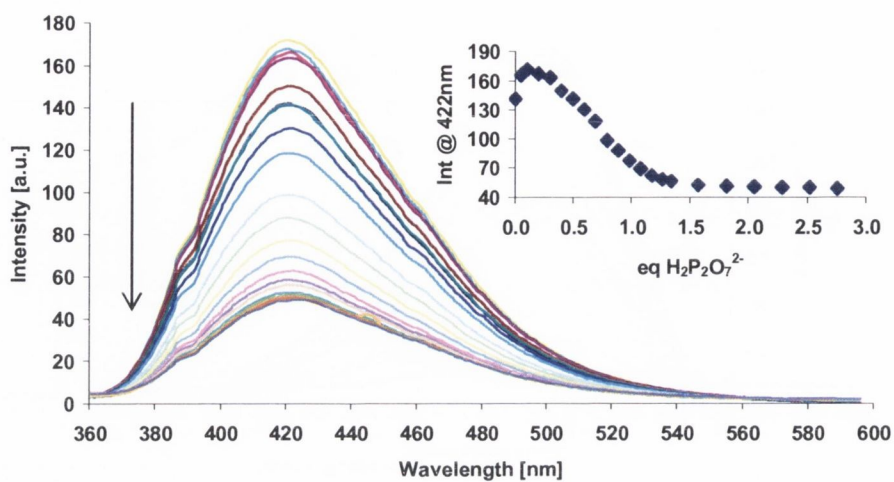


Figure 4.6.2.4: Changes on the fluorescence emission spectra of **Fe:87₂** upon addition of $\text{H}_2\text{P}_2\text{O}_7^{2-}$ ($0 \rightarrow 11 \mu\text{M}$), in CH_3CN when exciting the sample at 260 nm. Insert: The changes in emission intensity at 422 nm as a function of the number of equivalents of $\text{H}_2\text{P}_2\text{O}_7^{2-}$.

As discussed above, the fluorescence emission intensity of either **Fe:87₂** or **Cu:87₂** was only quenched upon addition of H_2PO_4^- and $\text{H}_2\text{P}_2\text{O}_7^{2-}$, while it has been enhanced upon the addition of the remainder anions discussed in this section, as shown in **Figure 4.6.2.5** for the titrations of **Fe:87₂**.

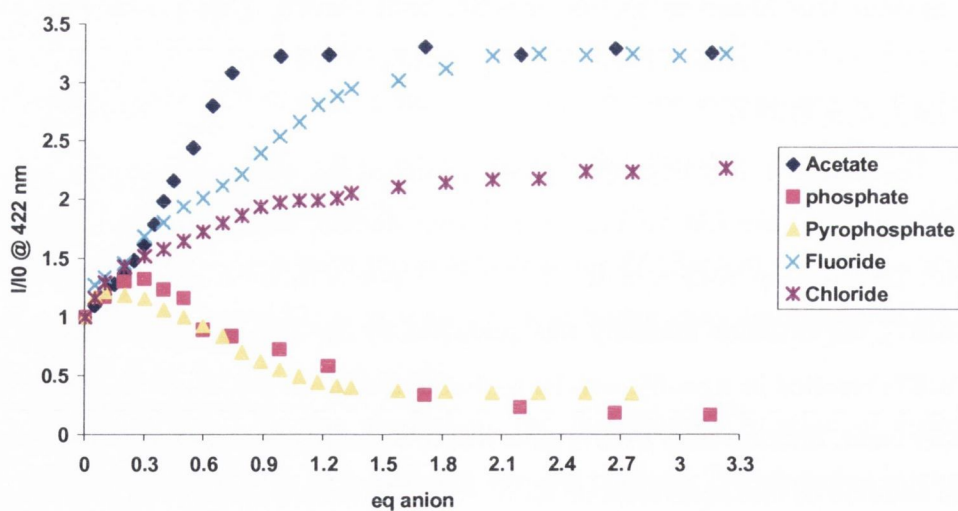


Figure 4.6.2.5: Changes on the relative emission intensity of **Fe:87₂** upon addition of the various anions, in CH_3CN when exciting the sample at 260 nm.

These results are very interesting, as they provide us with a powerful tool to determine the nature of the bound anion, that is, the 'switching off' versus the 'switching on' of the fluorescence emission intensity. Since phosphate anions play critical roles in a range of biological processes, as well as in the environment, the above results are promising regarding the use of either Fe(II) or Cu(II) *phen* coordinated complexes of **87** as new devices for the emission-based discrimination of phosphate ions at a μM level.

4.7 Conclusions

In this chapter the successful synthesis and characterisation of a novel heteroditopic receptor **87** has been discussed. A crystal structure was obtained, which shows ideal *syn* conformation of the NH protons of the urea moiety for directional binding with anions.

Spectrophotometric studies (UV-Visible and fluorescence) were carried out for **87** upon addition of various anions, in order to evaluate its binding affinity. While only minor changes were observed in the ground state upon anion recognition, the fluorescence emission was significantly affected. While anions such as CH_3COO^- , H_2PO_4^- , and F^- quenched the emission intensity of **87**, recognition of Cl^- gave rise to an enhancement of such emission intensity. Selectivity of **87** for Cl^- was demonstrated by competitive measurements. Consequently, these results demonstrate the development of **87** as a novel selective fluorescent sensor for Cl^- .

The ability of **87** to bind transition metals such as Cu(II) and Fe(II) was also evaluated. Binding studies in solution revealed strong interaction between the metal ions and the *phen* moiety of two molecules of **87**, giving rise to the formation of the **Cu:87₂** and **Fe:87₂** complexes. Preliminary studies on small crystals of the Cu(II) complex showed the formation of a dinuclear complex in the solid state, through interaction of two copper ions with four molecules of **87**. Each Cu(II) ion was found to be in a distorted square-pyramidal geometry, coordinated by four nitrogen atoms from the two *phen* ligands and one oxygen atom from the urea moiety of a neighbour molecule of **87**.

Finally, the influence of the metal ion on the binding affinity towards anions was investigated, by using spectrophotometric methods such as UV-Visible and fluorescence. Analysis of the titrations of the various anions with either **Cu:87₂** or **Fe:87₂**, showed the formation of 1:1 adducts between the metal complexes and CH_3COO^- , F^- , and Cl^- , with

concomitant enhancement in the emission intensity. The metal induced enhancement on the binding affinity, resulting in higher binding constants than those observed for the simple receptor **87**. In addition, a new method for discriminating the nature of the bound anion was devised, as only the addition of phosphates, H_2PO_4^- and $\text{H}_2\text{P}_2\text{O}_7^{2-}$, quenched the emission intensity.

By increasing the number of anion binding sites, through self-assembly to higher coordination metals, the construction of improved anion receptor is expected to be achieved. The formation of self-assembly complexes between **87** and the Eu(II) metal center, and its binding affinity towards anions will be presented and discussed in the next chapter.

Chapter 5

*Anion sensing using a Eu(III) induced
supramolecular self-assembly architecture*

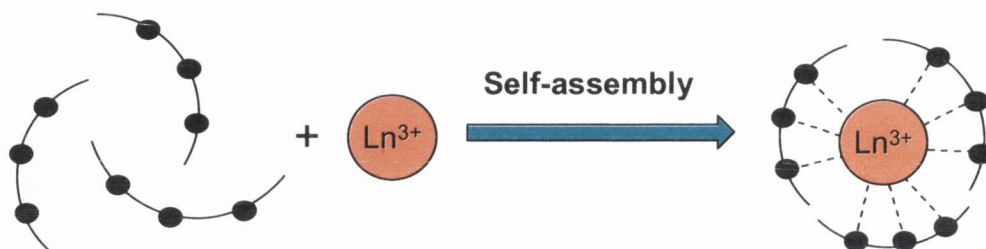
5.1 Introduction

Self-assembly has emerged as a new approach in chemical synthesis, nanotechnology, polymer science, materials science, and engineering.²¹⁵ Novel architectures based on self-assembly from structurally defined building blocks are at the centre of supramolecular chemistry.^{154,216,217} Molecular self-assembly, by definition, is the spontaneous association of molecules under thermodynamic equilibrium conditions into stable, structurally well defined architectures. These are held together by relatively weak, noncovalent interactions, such as hydrogen bonding, Van der Waals and hydrophobic-hydrophilic interactions, ionic bonds (electrostatic interactions), and metal-ligand coordination interactions.^{57,218-223} Metal-ligand interactions are often labile and are mainly of electrostatic nature, where the structures formed are usually the thermodynamically most stable products. In particular, metal-directed self-assembly is emerging as one of the most promising approaches to the generation of complex supramolecular architectures.^{224,225} Self-assembly has been employed in a wide variety of novel supramolecular architectures including boxes, cages, catenanes, dendrimers, grids, helicates and rotaxanes among others.²²⁶⁻²²⁹

5.2 Design of a Eu(III) self-assembly system

The previous chapter dealt with the sensing of transition metal ions through the self-assembly between these metal ions and the *phen* based ligand **87**. However, our interest was drawn to the rather fascinating spectroscopic properties exhibited by some lanthanide ions (Chapters 1 and 2). Amongst them, lanthanide luminescent systems possess large Stokes shifts (relative to biological substances) and long excited state lifetimes, enabling the separation of the luminescent signal from the background biological autofluorescence. As such, lanthanide ion complexes render greater advantages over fluorescence systems which can be affected by autofluorescence and light scattering. Due to these properties, lanthanide luminescent systems are of special interest with regards to *in vivo* applications.^{52,55-58}

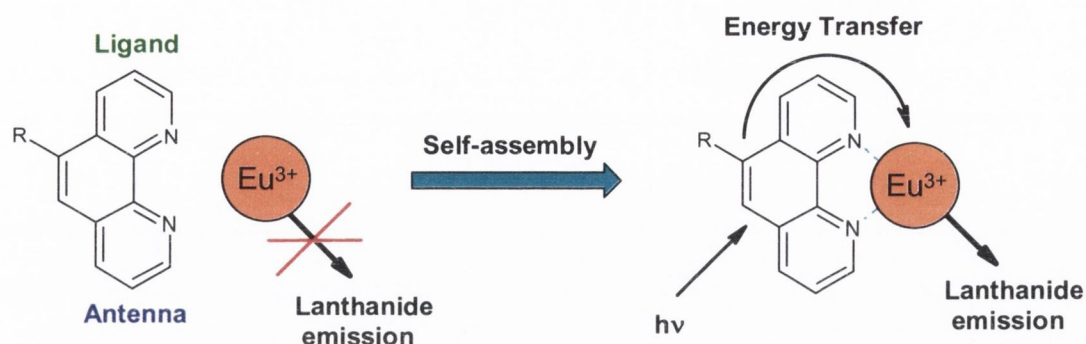
Moreover, trivalent lanthanide ions possess relatively high charge densities and have strong electrostatic nature in their bonding as well as high coordination numbers, most frequently between eight and ten. This offers the opportunity to self-assemble sizeable coordinating units around the metal center as tentatively depicted in **Scheme 5.2**.^{55,58,230}



Scheme 5.2: Schematic representation of the self-assembly process between a lanthanide ion, Ln^{3+} , and a random group of ligands

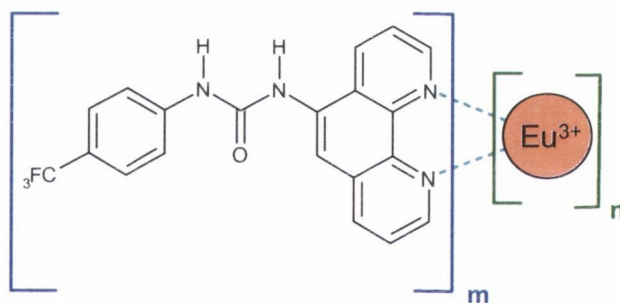
Although possessing all the mentioned advantages, there is a slight drawback when using the trivalent lanthanide ions. In order for a lanthanide ion to emit, an excited state must first be produced by light excitation. As explained in Chapter 1, due to their low extinction coefficients associated with Laporte-forbidden $f-f$ transitions, direct excitation of a lanthanide ion is very difficult. One way to overcome this disadvantage is by means of indirect excitation, using a sensitising chromophore or antenna, which can transfer its own excited state energy onto the lanthanide ion, resulting in the production of the desired lanthanide emission.⁵⁹⁻⁶¹

Bearing all this in mind, in order to develop a supramolecular Eu(III) self-assembly system the choice of both a suitable ligand, or receptor, able to bind the lanthanide ion, as well as a suitable antenna is of extreme importance. Herein, the 1,10-phenanthroline (*phen*) was selected as it can function simultaneously as both the antenna and the receptor unit for the lanthanide ions, **Scheme 5.2.1**. *Phen* and its derivatives are known to be able to populate the Eu(III) excited state ($^5\text{D}_0$) and hence promote the lanthanide emission.²³¹⁻²³⁴ Regarding the function as a receptor, or ligand unit, the bidentate *phen* moiety, and its derivatives, are known to play an important role as molecular scaffolds for supramolecular assemblies.^{220,235} Since the hard Lewis acidity of the Ln(III) favours bonding to atoms which can act as hard Lewis bases, such as nitrogen and oxygen atoms, the presence of two nitrogen atoms on these bidentate ligands renders them suitable for the bonding of lanthanide ions in an aprotic solvent (**Scheme 5.2.1**).



Scheme 5.2.1: Schematic representation of the sensitisation of the Eu(III) self-assembly complex with *phen* derivatives.

As discussed above, lanthanide ions offer the opportunity to self-assemble sizeable coordinating units around the metal centre (**Scheme 5.2**). So, by increasing the number of anion binding sites, such as urea moieties, through self-assembly to the high coordinating Eu(III), the development of improved anion receptors would be expected. With this in mind, we set out to develop a novel anion sensing self-assembly system based upon coordination of Eu(III) to the urea based ligand **87**, **Scheme 5.2.2**.

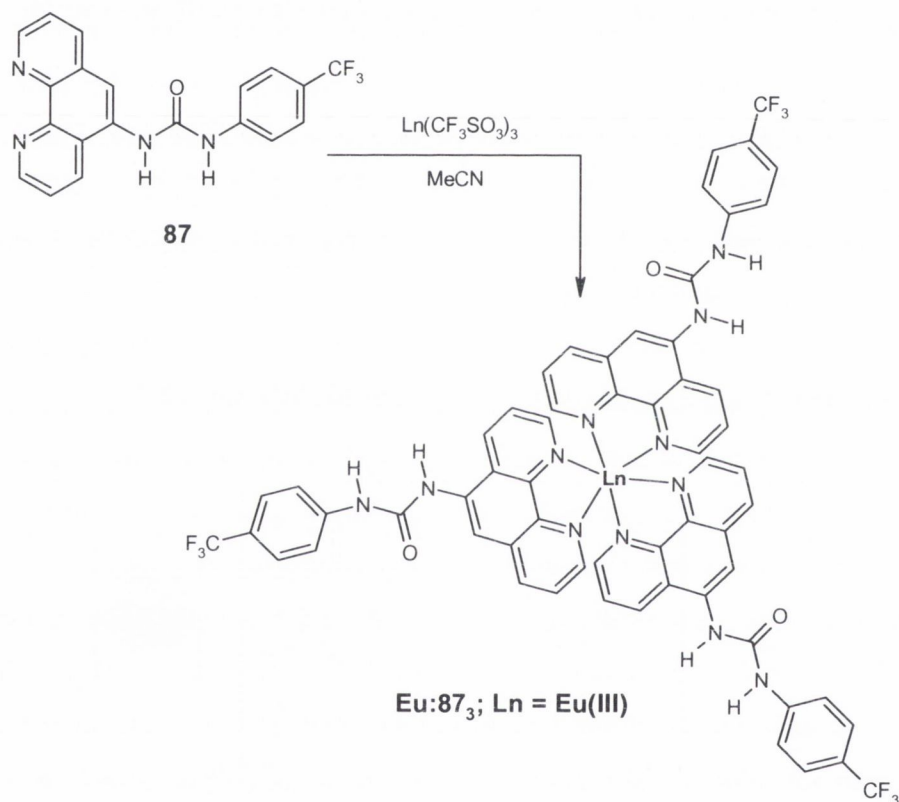


Scheme 5.2.2: Schematic representation of the self-assembly between Eu(III) and ligand **87** in the formation of the $\text{Eu}_n:\mathbf{87}_m$ complex.

The following sections detail the synthesis, characterisation and photophysical studies of the self-assembly system. The binding interactions between such a system and various anions will also be discussed.

5.3 Synthesis and characterisation of the europium complex, Eu:87₃

The synthesis of complex **Eu:87₃** was accomplished by reacting **87** with 0.5 equivalents of Eu(III) triflate ((CF₃SO₃)₃), in CH₃CN. In **Scheme 5.3** is shown the synthetic approach for the mentioned complex. Being insoluble in CH₃CN, receptor **87** forms a suspension in this solvent. Nevertheless, upon addition of Eu(CF₃SO₃)₃ a clear solution was observed within minutes. The reaction mixture was stirred at room temperature overnight. The observed off white precipitate was isolated by filtration, and dried under vacuum to produce a bright yellow solid in a modest 28% yield.



Scheme 5.3: Synthesis of **Eu:87₃** complex by reaction of **87** with Eu(III)(CF₃SO₃)₃.

The successful synthesis of **Eu:87₃** was supported by ¹H NMR spectroscopy. It is well known that protons in close proximity to the paramagnetic lanthanide ion are influenced by the presence of the unpaired *f* electrons, leading to more efficient relaxation of the nuclear spins and hence broadening of resonances, as well as shifts in the ¹H NMR frequency.²³⁶

Although Eu(III) did not give rise to large chemical shifts for the formation of **Eu:87₃**, complex formation can be pointed out by signal broadening of the *phen* moiety protons more closely related with the binding, such as **a**, **b**, **e** and **f**, due to the presence of the paramagnetic metal center, **Figure 5.3**.

Another strong confirmation of successful complex formation was given by its photophysical properties. Although **Eu:87₃** is a yellow solid to the naked eye, it shows an intense red colour under the UV lamp, which confirms that the lanthanide ion is being strongly sensitized by the ligands.

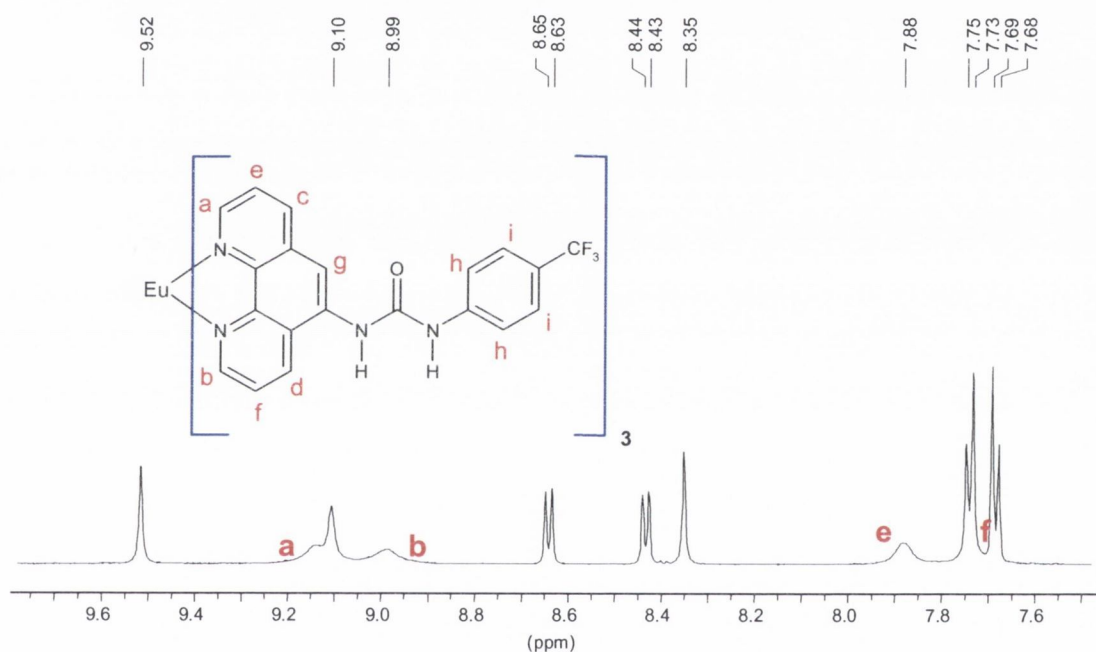


Figure 5.3: ¹H NMR of the lanthanide complex, **Eu:87₃** (600 MHz, *d*₆ – DMSO)

The ¹⁹F spectrum, revealed the presence of the CF₃ group at -60.56 ppm as well as a resonance at -78.29 ppm assigned to the triflate [(CF₃SO₃)₃] counter ions. The ESMS also showed that complexation had occurred as a typical europium isotopic distribution pattern was observed, as shown in **Figure 5.3.1** for the *m/z* = [M/2] peak.

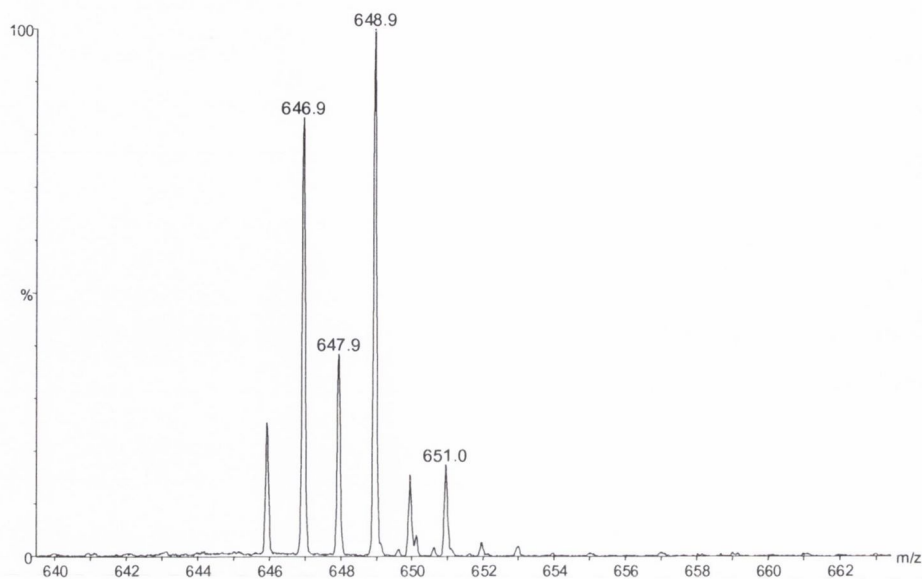


Figure 5.3.1: Mass spectrum of **Eu:87₃** showing the characteristic europium isotopic distribution pattern for the $m/z = [M/2]$ peak

Successful coordination of Eu(III) to the *phen* moiety of **87** was further supported by the changes observed in the IR spectrum of **Eu:87₃**, when compared to that of the free ligand **87**. The bonds in closer proximity to the metal coordination site are expected to be the most influenced by the complexation process.²³⁷ The out-of-plane bending vibrations of the hydrogen atoms on the *phen* decreased from 848 cm^{-1} and 738 cm^{-1} to 844 cm^{-1} and 734 cm^{-1} , respectively.¹⁶⁰ The bands due to the interactions between ring C=C and C=N stretching vibrations of the *phen* moiety at 1613 , 1563 , 1505 and 1473 cm^{-1} increased to 1657 , 1605 , 1543 and 1485 cm^{-1} , respectively, indicating the coordination of the Eu(III) metal ion through the nitrogens of the *phen* moiety.^{159,237}

5.4. Determination of bound water molecules of the lanthanide complex, **Eu:87₃**

As discussed in the previous chapters, trivalent lanthanide ions have a high coordination number requirement, usually nine for Eu(III). Whenever this requirement is not fulfilled, any vacant coordination sites are occupied by solvent molecules such as water or coordinating anions.^{52,57,81} The phenanthroline framework, through its nitrogen atoms, provides two coordination sites for the lanthanide ion. Therefore, the three ligands of **87** in **Eu:87₃** will provide in total six coordination sites, which leaves the lanthanide ion

coordinatively unsaturated. Hence, the remaining binding sites are most likely to be occupied by three solvent molecules. In order to determine the number of these solvent molecules, the hydration state, q , was determined by measuring the excited state lifetimes (τ) of the complex in H₂O ($\tau_{\text{H}_2\text{O}}$) and D₂O ($\tau_{\text{D}_2\text{O}}$), by direct excitation of the Eu(III) at 395 nm. Values of 0.33 and 1.83 ms were obtained for the lifetimes in H₂O ($\tau_{\text{H}_2\text{O}}$) and D₂O ($\tau_{\text{D}_2\text{O}}$), respectively. From these values, and using the modified Horrocks equation developed by Parker *et al.*⁶⁸, **Equation 2** (Chapter 1) q was determined as 2.6. This indicates the presence of *ca.* three bound water molecules (**Table 5.4**). This further supports the presence of the 1:3 (**Eu:87**₃) desired supramolecular assembly.

Complex	$\tau_{\text{H}_2\text{O}}(\text{ms})$	$\tau_{\text{D}_2\text{O}}(\text{ms})$	$q (\pm 0.5)$
Eu:87 ₃	0.333	1.825	2.64

Table 5.4.: Measured lifetimes and q value found for the lanthanide complex, **Eu:87**₃.

Having established the above, the next step was to establish the stoichiometry between the lanthanide ion and ligand **87** in solution. The following sections will focus on the use of different methods to determine the stoichiometric ratio between Eu(III) and ligand **87**, **Eu_n:87_m**, in solution.

5.5 Job's Method for stoichiometry determination

One of the methods used to determine the stoichiometry involved in the G_nH_m complex formation, is the Job's method, or method of continuous variation. In this method, a series of solutions of Eu(III) (G) and ligand **87** (H) in CH₃CN, were prepared by maintaining the total concentration of [G] + [H] constant at 5 μM .²³⁸ By excitation at 265 nm, the luminescence emission intensity of these solutions was measured. The intensity recorded at 616 nm (J = 2 band) was then plotted as a function of the mole fraction, $f = [\text{G}]/([\text{G}]+[\text{H}])$, **Figure 5.5**. The value at the extreme, a maximum in the present case, f_{max} , is related to the complexation stoichiometry according to the **Equation 5.5**.²³⁸

$$m/n = f_{\text{max}} / (1 - f_{\text{max}}) \quad \text{Equation 5.5}$$

So, the presence of a maximum at $f_{\max} = 0.25$ is indicative of the formation of a complex with composition $G_1:H_3$ (**Eu**₁:**87**₃) as $m/n = 0.25/(1 - 0.25) = 1/3$ implying that $n = 1$ and $m = 3$.

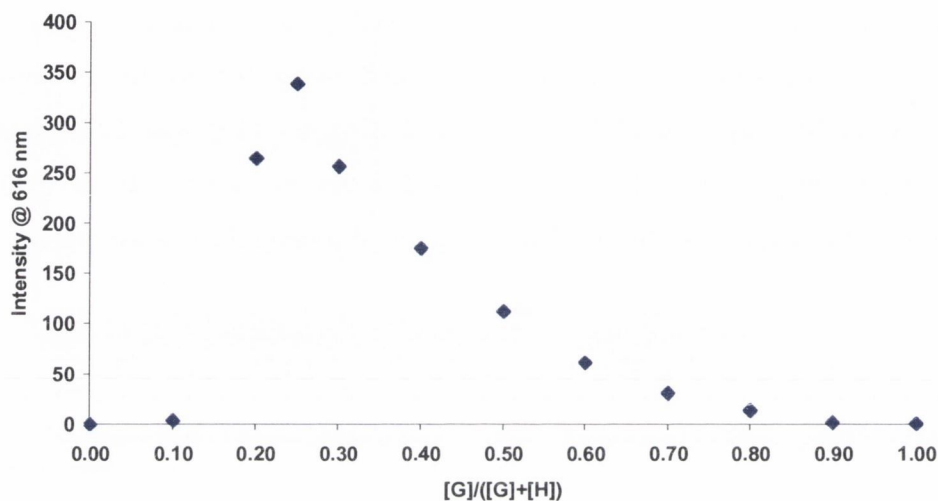


Figure 5.5: Job's plot for the determination of the complex $G_n:H_m$ stoichiometry between Eu(III) (G) and **87** (L). Changes in the luminescence emission intensity at 616 nm as a function of the guest mole fraction, $[G]/([G]+[H])$ in CH_3CN , upon excitation at 265 nm. Total concentration $[G] + [H]$ maintained constant at $5\mu M$.

5.6 Photophysical studies of receptor **87** with Eu(III)

The formation and stability of the self-assembly complexes formed between Eu(III) and ligand **87**, $Eu_n:\mathbf{87}_m$, was investigated, through photophysical measurements, by titrating a stock solution of **87** ($10\mu M$) with a solution of $Eu(CF_3SO_3)_3$ in CH_3CN under ambient conditions. However, a minimum amount of DMSO ($< 0.1\%$) had to be used in the preparation of the stock solution of receptor **87**, in order to maximize the solubility of this receptor in CH_3CN . The same solutions were used for both the UV-visible and luminescence (fluorescence and lanthanide luminescence) measurements.

5.6.1 UV-Visible absorption studies

As discussed in the previous chapter, the spectrum of the free ligand **87** shows the presence of a band centred at 265 nm, assigned to the $\pi-\pi^*$ transition of the *phen* moiety,

and a broad shoulder centred at around 320 nm. The changes in the absorption spectra obtained during the course of the titration of **87** with Eu(III) are presented in **Figure 5.6.1**.

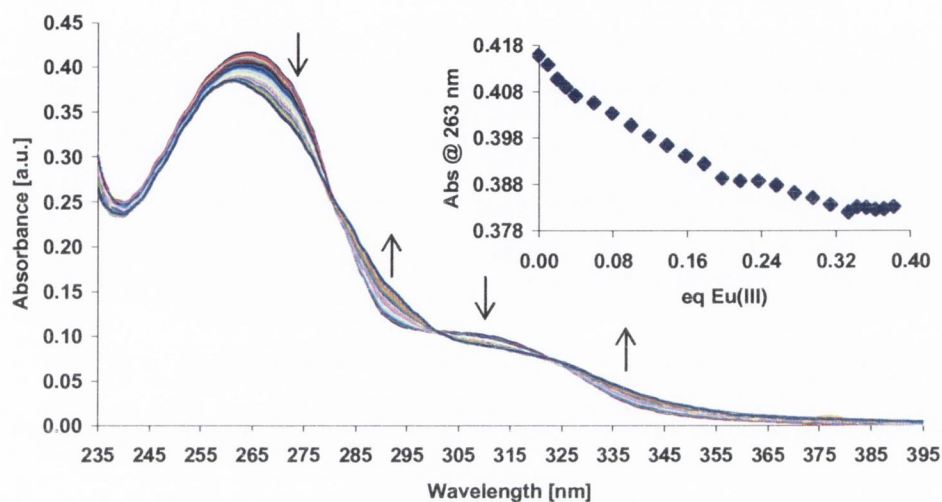


Figure 5.6.1: Changes on the absorption spectra of **87** (10 μM) upon addition of Eu(CF₃SO₃)₃. Insert: The changes in absorbance at 263 nm as a function of equivalents of Eu(III).

As can be observed, upon addition of Eu(III), three distinct isosbestic points at 280 nm, 300 nm, and 323 nm were formed. The band centred at 265 nm also experienced a hypsochromic shift to 260 nm, while the shoulder centred at 320 nm experienced essentially the same 5 nm shift towards the red to 325 nm. Similar 5 nm hypsochromic shift has been previously observed for the interaction of Cu(II) with **87** (Chapter 4). Also, comparable hypsochromic shifts have previously been reported for the interactions of cations with *N*-monoaza-15-crown-5 derivatives, and have been ascribed to the interaction of the lone pair of the nitrogen atoms with the cations.²³⁹ The profile of the number of equivalents of Eu(III) added as a function of the changes in the absorbance, clearly indicated the formation of a complex with 1:3 (**Eu:87**₃) stoichiometry, as no changes were observed beyond the addition of 0.33 equivalents of the trivalent lanthanide ion, **Figure 5.6.1** insert.

5.6.2 Fluorescence studies

The fluorescence changes observed upon addition of Eu(III) were followed by exciting the sample at both 265 nm and 320 nm. A fluorescent band centred at 422 nm was observed upon excitation at both these wavelengths. The emission intensity was “switched off” by 33% in the presence of the lanthanide, as can be observed in **Figure 5.6.2**. The insert in **Figure 5.6.2** shows the changes in emission intensity at 422 nm versus the number of equivalents of Eu(III) added. This supports the 1:3 (**Eu:87**₃) stoichiometry, observed above for the absorption titration.

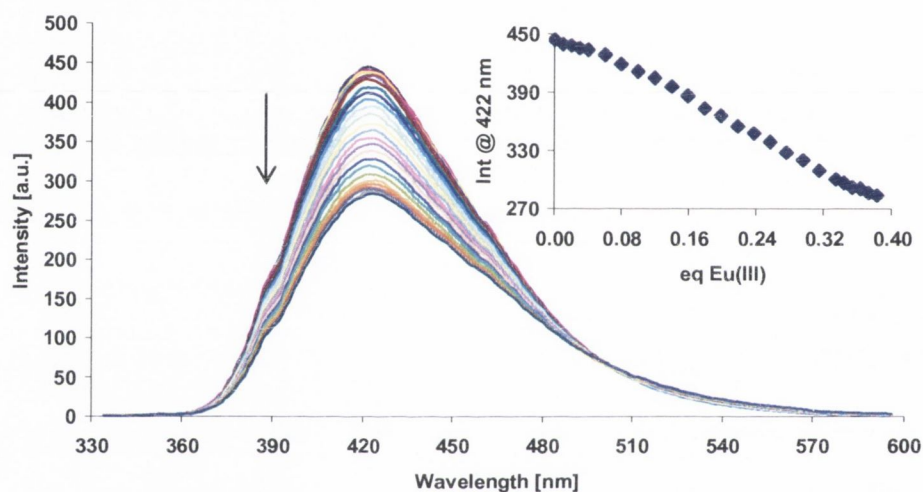


Figure 5.6.2: Changes in the fluorescence emission spectra of **87** (10 μ M) upon addition of $\text{Eu}(\text{CF}_3\text{SO}_3)_3$, in CH_3CN when exciting at 320 nm. Insert: The changes in emission intensity at 422 nm as a function of equivalents of Eu(III).

The quenching of the fluorescence is a direct consequence of the complexation of the metal ion at the *phen* moiety. It is likely that this coordination provides an additional pathway for the quenching of **87** based luminescence, for instance by providing additional vibrational pathways for deactivation of the excited state.²⁴⁰ Due to the presence of the Eu(III) ion, the quenching of the fluorescence can indicate energy transfer from the antenna, *via* the triplet excited state, to the Eu(III) excited state giving rise to the characteristic Eu(III) emission, which will be discussed in the next section.

5.6.3 Lanthanide luminescence studies

The lanthanide luminescence changes were also investigated during the course of the titration by exciting at both 265 nm and 320 nm, which gave rise to similar results. The family of spectra obtained upon gradual additions of Eu(III) to a solution of **87**, when exciting at 265 nm, are presented in **Figure 5.6.3**. As expected, in the absence of the lanthanide metal centre, Ln(III), **87** does not exhibit long wavelength emission. However, upon addition of Eu(III) the lanthanide emission was clearly observed, proving the sensitisation process occurring from the antenna.

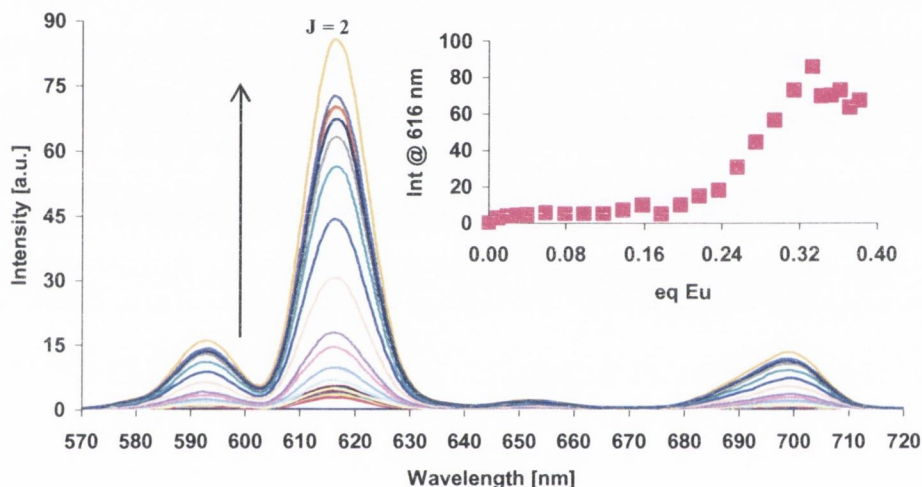


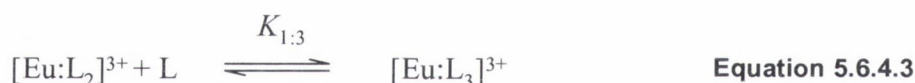
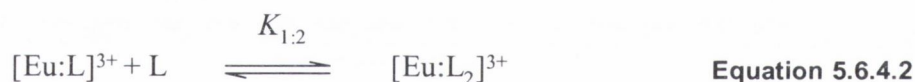
Figure 5.6.3: Changes in the lanthanide luminescence emission spectra of **87** (10 μM) upon addition of $\text{Eu}(\text{CF}_3\text{SO}_3)_3$ when exciting at 265 nm. Insert: The changes in the lanthanide emission intensity at 616 nm as a function of equivalents of Eu(III).

The emission spectrum showed the characteristic Eu(III) bands at 594, 616, 652, and 700 nm, **Figure 5.6.3**. These bands correspond to the deactivation of the $^5\text{D}_0$ excited state to the lower lying $^7\text{F}_J$ ground state levels ($^5\text{D}_0 \rightarrow ^7\text{F}_1$, $^5\text{D}_0 \rightarrow ^7\text{F}_2$, $^5\text{D}_0 \rightarrow ^7\text{F}_3$, and $^5\text{D}_0 \rightarrow ^7\text{F}_4$ transitions, respectively), giving rise to the red luminescence of Eu(III).²⁴¹ The fact that such emission is being observed shows that the *phen* ligand, **87**, is able to work as a sensitizer for Eu(III), which clearly indicates the formation of a complex between Eu(III) and **87**. Although any of the bands can be used to analyse the data, the band at 616 nm ($J = 2$ band) was used as it gave rise to the largest emission intensity. This was expected, since the $J = 2$ band is known to be very sensitive to changes in the coordination environment of

the metal ion.^{163,164,242} The insert in **Figure 5.6.3** shows the changes in the emission intensity at 616 nm ($J = 2$ band) up to the addition of 0.33 equivalents of Eu(III), after which only minor changes were observed in the emission spectra. Furthermore, since the lanthanide emission intensity reached its maximum at 0.33 equivalents of Eu(III) added, it also demonstrates the formation of the self-assembly complex with a stoichiometry of 1:3 (**Eu:87₃**) between Eu(III) and the *phen* ligand.

5.6.4 Stability constants, log K , for the formation of **Eu:87₃**

From the changes observed from the UV-Visible, fluorescence, and lanthanide luminescence titrations, stability constants for the formation of the self-assembly complex **Eu:87₃** were obtained using the nonlinear least-squares regression analysis program SPECFIT. The complexation mechanism for the formation of **Eu:87₃** can be expressed by the three equilibrium steps described in **Equations 5.6.4.1**, **5.6.4.2** and **5.6.4.3**, corresponding to the formation of **Eu:87**, **Eu:87₂**, and **Eu:87₃**, respectively.



The binding constants for each of these steps were determined by fitting the experimental data to the **Eu:87**, **Eu:87₂** and **Eu:87₃** complexation model. The model used fitted well to the experimental data, as shown in **Figure 5.6.4** for the UV-visible titration. From the fits, relatively weak binding constants of $\log K \sim 4$ were determined for the 1:1 (**Eu:87**) and the 1:2 (**Eu:87₂**) stoichiometries, while stronger binding constants of $\log K \sim 6$ were found for the 1:3 (**Eu:87₃**) stoichiometry, **Table 5.6.4**. As can be observed, the values found are in good agreement between those determined from the UV-visible data and those obtained from the emission studies (**Table 5.6.4**). As expected, the **Eu:87₃** complex shows the higher binding constant implying that **Eu:87₃** is the most stable species in solution.

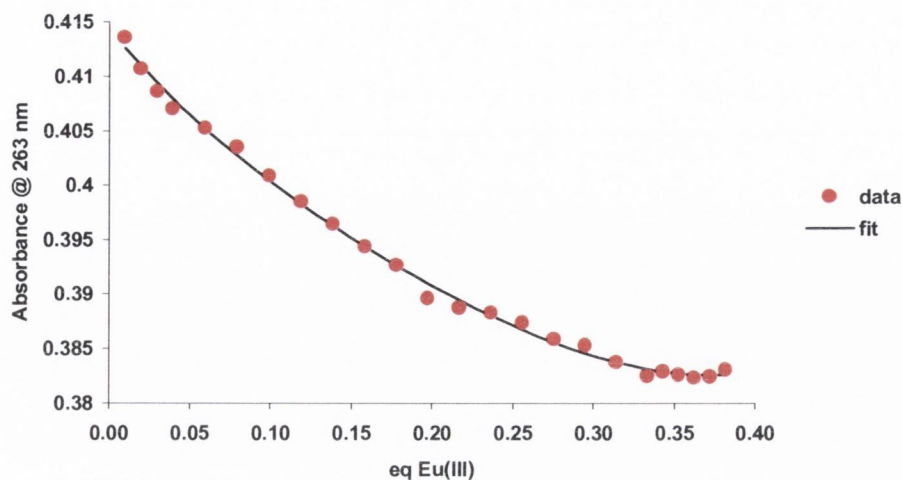


Figure 5.6.4: Experimental binding isotherm for the UV-Visible titration of **Eu:87₃** (4 μ M) with Eu(III) (0 \rightarrow 3.82 μ M) in CH_3CN , and the corresponding fit at 263 nm obtained using SPECIFIT.

Metal:87	Technique	Species (Eu:87_m)	$\log K_{n:m}$	Std. Deviation (\pm)
Eu(III):87	Absorbance	Eu:87	3.86	0.012
		Eu:87₂	3.68	0.016
		Eu:87₃	5.92	0.031
	Fluorescence	Eu:87	3.88	0.008
		Eu:87₂	3.60	0.016
		Eu:87₃	5.90	0.024
	Phosphorescence	Eu:87	3.61	0.011
		Eu:87₂	3.67	0.016
		Eu:87₃	6.02	0.017

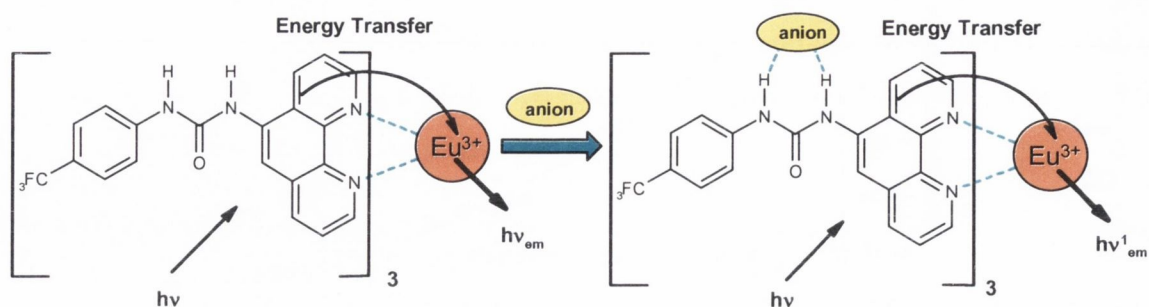
Table 5.6.4: Binding constants and binding modes between Eu(III) and **87**.

Once the stoichiometry of the complex in solution had been established, the binding ability of **Eu:87₃** system towards anions was investigated. The binding modes and binding constants determined for the titrations with the various anions will be discussed in the following sections.

5.7 Anion sensing by **Eu:87₃**

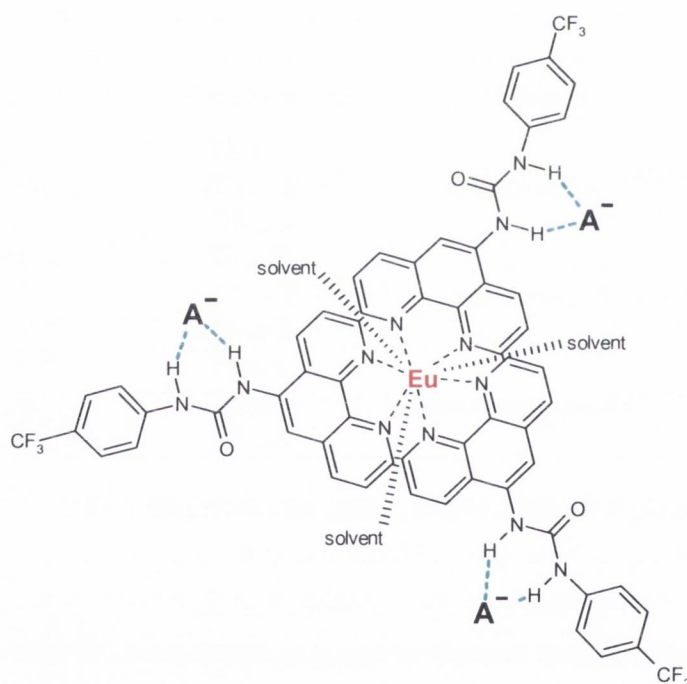
The sensitised lanthanide emission ($h\nu_{em}$) is achieved when the antenna **87** transfers its energy through the triplet excited state to the 5D_0 excited state of the Eu(III) ion. Hence,

any perturbation on the system, such as anion recognition, would lead to the modulation of the lanthanide emission ($h\nu_{em}^1$), as shown in **Scheme 5.7**.



Scheme 5.7: Modulation of the Eu(III) emission upon anion recognition.

The supramolecular complex **Eu:87₃** possesses three urea moieties, which makes it a promising sensor for anionic species, as tentatively depicted in **Scheme 5.7.1**.

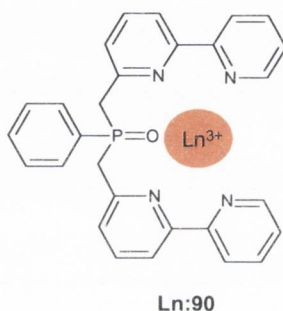


Scheme 5.7.1: Schematic illustration of the proposed anion binding sites within sensor **Eu:87₃**.

Each one of these urea moieties can bind individually to a particular anion, or depending on the orientation of the three molecules of **87** around the metal centre, there is also the possibility of cooperation between these urea moieties.¹⁴² In addition, the anion

can interact directly with the lanthanide ion through displacement of the solvent molecules. Also possible would be the displacement of the *phen* based antenna by competitive anions. Lanthanide based sensing devices, triggered by displacement assays, have received considerable attention in the past few years.^{86,101,154,243,244}

Studies carried out in CH₃CN on Eu(III) and Tb(III) complexes of the pentadentate ligand, **Ln:88**, revealed that the introduction of several anions (such as Cl⁻, F⁻, and NO₃⁻) led to an increase of the luminescence intensity of the metal complex, which was ascribed to the displacement of solvent molecules from the Ln(III) coordination by competing anions, and changes in the coordination of the *bipy* moieties.^{156,245,246}



The presence of two distinct binding sites (urea moieties and Eu(III) solvent coordinated molecules) in **Eu:87₃** provides this system with a great versatility for anion recognition.

5.7.1 Photophysical studies of **Eu:87₃** complex towards binding with anions

The formation and stability of the complexes formed between the anions (G) and the sensor (H), **Eu:87₃**, were investigated by carrying out titrations on a stock solution of **Eu:87₃** (4 μM) with gradual additions of different anion solutions, as their tetrabutylammonium salts (TBA⁺), in CH₃CN. However, a minimum amount of DMSO (< 0.1%) had to be used in the preparation of the stock solution of **Eu:87₃**, in order to maximize the solubility of the sensor in CH₃CN. This Eu(III) complex was found to be very stable in solution over a long period of time.

In **Figure 5.7.1** are shown the observed spectra for absorption (black line), fluorescence (blue line), and lanthanide luminescence (red line). Both the fluorescence and phosphorescence shown were obtained upon excitation at 260 nm. The absorption spectrum

of **Eu:87₃** (4 μM) in CH_3CN , exhibited a main band centred at 260 nm, and two broad shoulders centred at 292 and 325 nm. When exciting at these wavelengths, a broad emission band centred at 420 nm was observed for the fluorescence. Regarding the lanthanide luminescence, the emission spectrum of **Eu:87₃** showed the characteristic Eu(III) bands at 580 ($J = 0$), 591 ($J = 1$), 612 ($J = 2$), 652 ($J = 3$), and 700 ($J = 4$) nm, **Figure 5.7**.

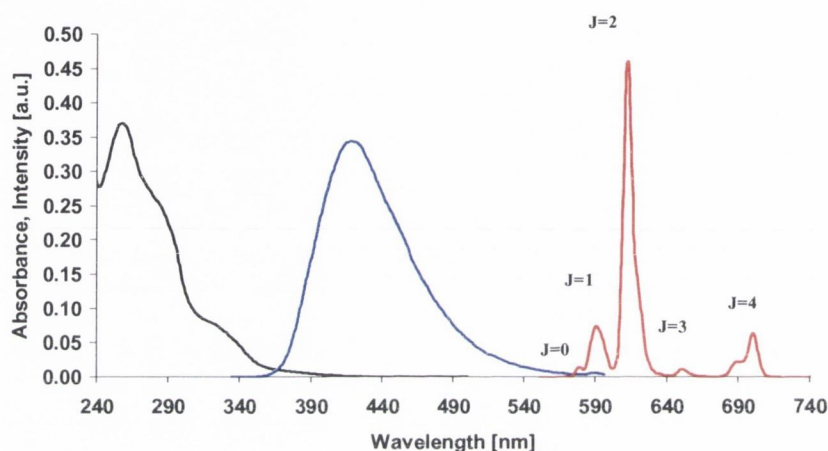


Figure 5.7.1: Absorption (black), Fluorescence (blue), and Phosphorescence (red) spectra of **Eu:87₃** in CH_3CN . The fluorescence emission intensity was divided by a factor of 800 and the phosphorescence by a factor of 1300, in order to compare all the three spectra in the same graph.

The changes in the UV-Visible spectra, fluorescence emission, and lanthanide luminescence of **Eu:87₃** upon addition of various anions, such as acetate (CH_3COO^-), dihydrogenphosphate (H_2PO_4^-), fluoride (F^-), chloride (Cl^-), bromide (Br^-) and iodide (I^-), were examined. The results from these investigations will be discussed in the following sections.

5.7.2 Changes in the absorption spectra of **Eu:87₃** upon anion recognition

The family of spectra showing the changes in absorption of **Eu:87₃** upon addition of CH_3COO^- are shown in **Figure 5.7.2**. The band centred at 260 nm experienced an increase in the absorbance, accompanied by a bathochromic shift to 265 nm, while both the shoulders at 292 nm and 325 nm experienced a decrease in the absorbance. These changes were accompanied by the formation of a clear isosbestic point at 280 nm. The insert in

Figure 5.7.2 shows the changes occurring at 292 nm versus the number of equivalents of CH_3COO^- , which clearly demonstrates that the major changes are taking place upon addition of two equivalents of CH_3COO^- . Following further addition of anion, the changes are less noticeable and occur up to the addition of three equivalents of CH_3COO^- , after which no more changes were observed. Such results are indicative of a 3:1 ($\text{G}_3:\text{H}$) binding interaction between the guest CH_3COO^- (G) and the host **Eu:87₃** (H), which was expected due to the presence of the three urea moieties within the host self-assembly complex.

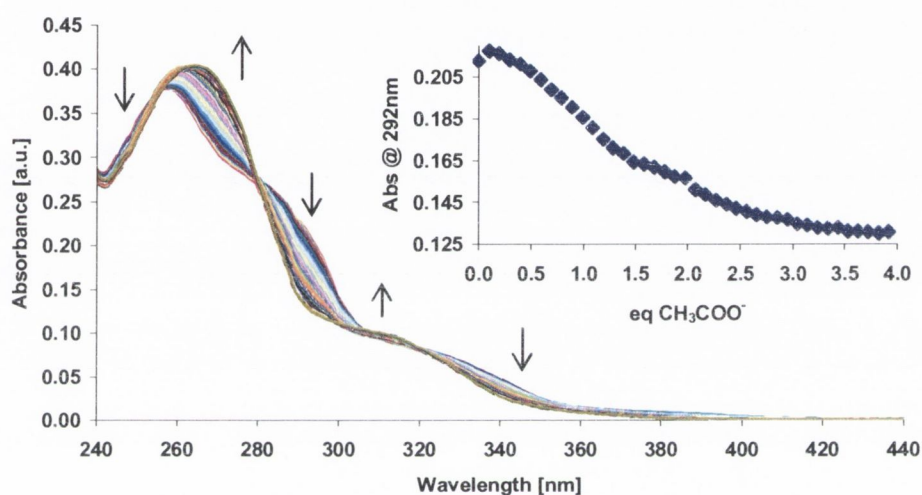


Figure 5.7.2: Changes in the absorption spectra of **Eu:87₃** (4 μM) upon addition of CH_3COO^- (0 → 16.10 μM). Inset: The changes in absorbance at 292 nm as a function of equivalents of CH_3COO^- .

However, nonlinear least-squares fitting of the titration data, using the SPECFIT program, indicated the occurrence of only two binding interactions. The best fit to the experimental data was obtained when taking into account the 1:1 ($\text{G}:\text{H}$) and 2:1 ($\text{G}_2:\text{H}$) binding interactions between CH_3COO^- (G) and **Eu:87₃** (H), **Figure 5.7.2.1**. From this, binding constants of $\log K_{1:1} = 6.23 \pm 0.26$ and $\log K_{2:1} = 6.17 \pm 0.17$ were determined, **Table 5.7.2**. As can be observed in the speciation diagram, insert in **Figure 5.7.2.1**, the $\text{G}:\text{H}$ complex forms in *ca.* 35% upon addition of one equivalent of CH_3COO^- , after which the $\text{G}_2:\text{H}$ becomes the predominant species in solution. The absence of the 3:1 ($\text{G}_3:\text{H}$) binding interaction could possibly be attributed to the fact that such interaction is weak, as

expected by the small changes observed in the titration profile between 2 → 3 equivalents of CH_3COO^- , hence not perceived by the fitting program.

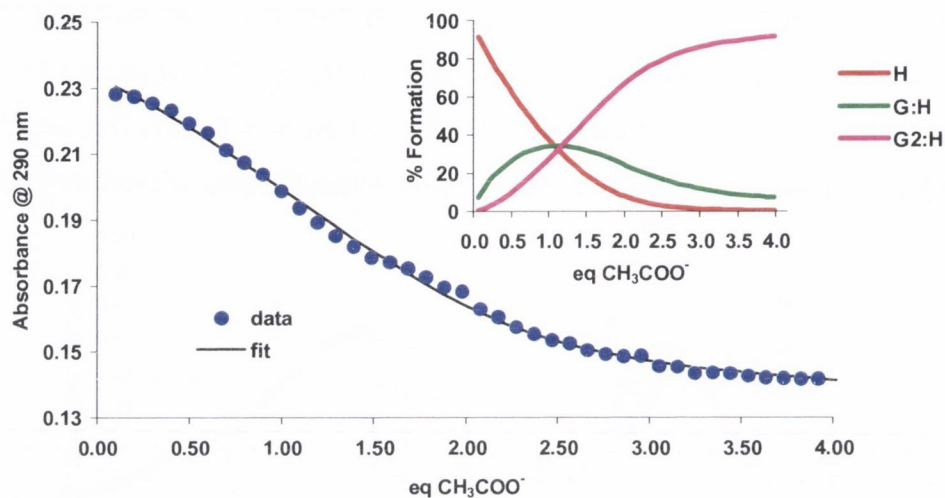


Figure 5.7.2.1: Experimental binding isotherm for the UV-Visible titration of **Eu:87₃** (4 μM) with CH_3COO^- (0 → 16.10 μM) in CH_3CN and the corresponding fit at 290 nm obtained using SPECFIT. Insert: The speciation distribution diagram; H refers to the host **Eu:87₃**, and G to the guest anion, CH_3COO^- .

Another anion following a similar binding model to that described above was F^- . The family of spectra showing the changes in absorption of **Eu:87₃** upon addition of F^- are shown in **Figure 5.7.2.2**. In comparison with CH_3COO^- , the band at *ca.* 260 nm also experienced a shift to *ca.* 265 nm. However, the isosbestic point observed at *ca.* 280 nm was not as clear as previously observed for CH_3COO^- . The insert in **Figure 5.7.2.2** shows the changes occurring at 292 nm versus the number of equivalents of F^- , which once again clearly demonstrate that the major changes are taking place up to the addition of two equivalents of F^- , after which the changes are only minimal. However, in this case, the changes occurring over the addition of two equivalents of F^- are much more abrupt, showing no curvature in the titration profile shown in the insert of **Figure 5.7.2.2**, from which stronger binding constants can be anticipated. Hence, similarly to the previous anion, this can possibly indicate the formation of strong 1:1 (G:H) and 2:1 (G₂:H) binding interactions between F^- and **Eu:87₃**.

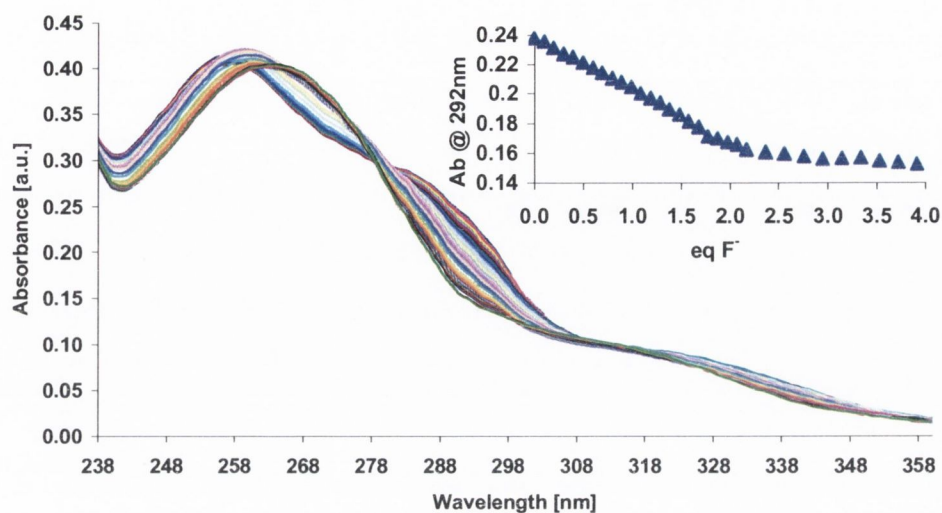


Figure 5.7.2.2: Changes in the absorption spectra of **Eu:87₃** (4 μM) upon addition of F⁻ (0 → 18.00 μM). Insert: The changes in absorbance at 292 nm as a function of equivalents of F⁻.

Once again, only the formation of the G:H and G₂:H species were observed when fitting the absorption data, using the SPECFIT program. The obtained fit to the experimental data and corresponding speciation distribution diagram are presented in **Figure 5.7.2.3**.

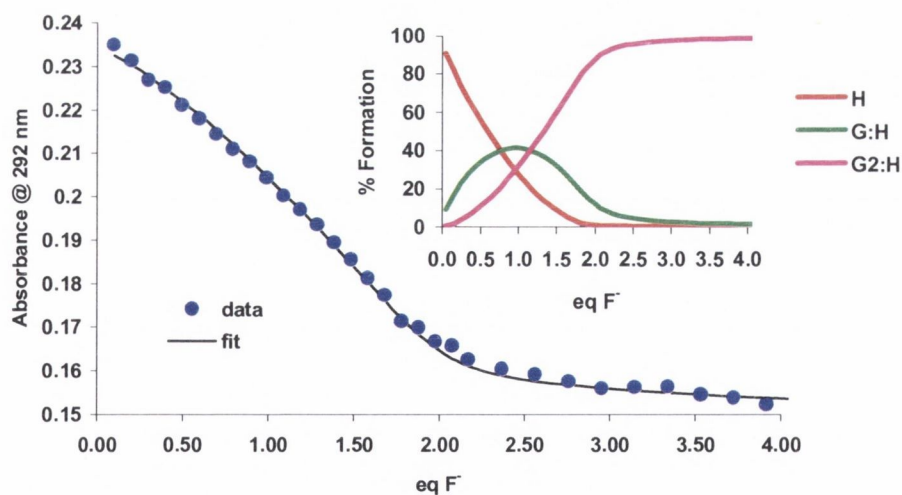


Figure 5.7.2.3: Experimental binding isotherm for the UV-Visible titration of **Eu:87₃** (4 μM) with F⁻ (0 → 18.00 μM) in CH₃CN and the corresponding fit obtained using SPECFIT. Insert: The speciation distribution diagram; H refers to the host **Eu.87₃**, while G refers to the guest anion, F⁻.

In this particular case, the G:H complex forms in *ca.* 40% upon addition of one equivalent of F^- , after which, the $G_2:H$ complex becomes the predominant species in solution. As mentioned above, by the very steep shape of the binding profile, high binding constants were anticipated. In fact, binding constants of $\log K_{1:1} > 7$ and $\log K_{2:1} = 6.97 \pm 0.27$ were determined for the binding interaction of F^- with the Eu(III) complex, **Table 5.7.2**.

By looking at the binding towards bigger spherical anions, such as Cl^- , a similar behavior to that of CH_3COO^- and F^- was observed. Yet again the major changes in absorbance were found to occur upon addition of two equivalents of anion. The changes in the absorption spectra of **Eu:87₃** upon addition of Cl^- are shown in **Figure 5.7.2.4**. As can be observed, upon anion recognition, the band at *ca.* 260 nm was shifted to *ca.* 263 nm with the concomitant formation of an isosbestic point at 259 nm. The insert in **Figure 5.7.2.4** shows the changes at 250 nm versus the number of equivalents of Cl^- . As observed for CH_3COO^- and F^- , the main changes also occurred upon addition of two equivalents of Cl^- . Binding constants of $\log K_{1:1} = 5.67 \pm 0.28$ and $\log K_{2:1} = 5.46 \pm 0.16$ were determined, when fitting the titration data using the program SPECFIT. These values were found to be smaller than those previously determined for CH_3COO^- and F^- (**Table 5.7.2**).

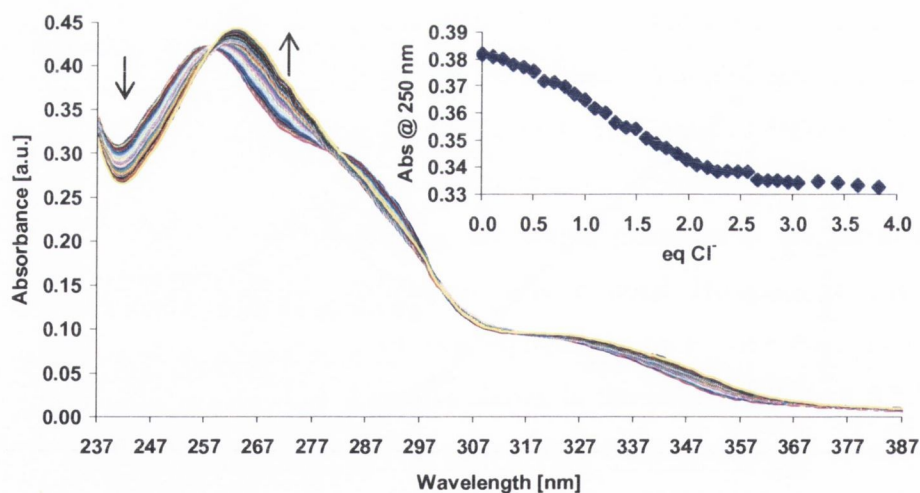


Figure 5.7.2.4: Changes in the absorption spectra of **Eu:87₃** (4 μ M) upon addition of Cl^- (0 \rightarrow 16.10 μ M). Insert: The changes in absorbance at 250 nm as a function of equivalents of Cl^- .

The changes in the absorption spectra of **Eu:87₃** upon addition of both Br⁻ and I⁻ were found to be the smallest among the anions studied, as can be observed in **Figure 5.7.2.5** and **Figure 5.7.2.6** for the titration of **Eu:87₃** with Br⁻ and I⁻, respectively. These results were expected, as such anions are known to be non-coordinating with urea based receptors.²⁹ The bigger changes observed at *ca.* 250 nm for the titration with I⁻, **Figure 5.7.2.6**, are related to the absorbance of this anion in this region of the spectrum. For these reasons we were unable to determine the binding constants involved in the interaction of Br⁻ and I⁻ with **Eu:87₃**.

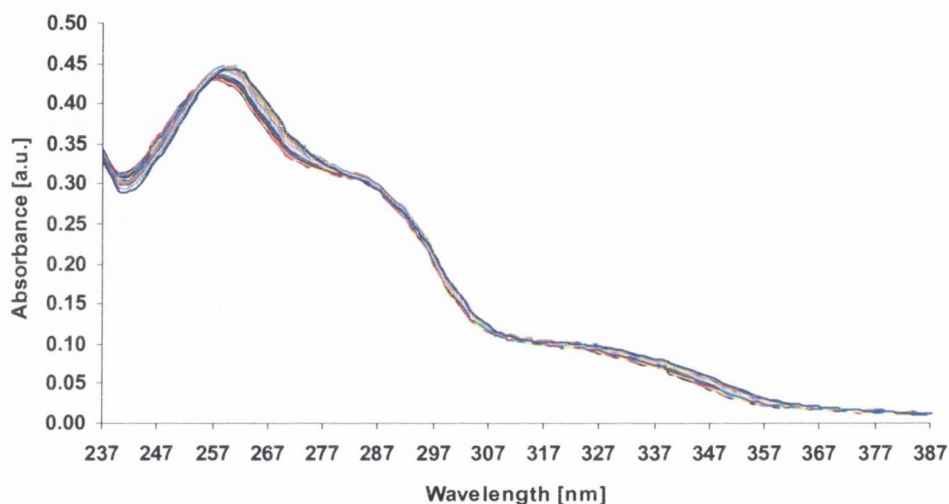


Figure 5.7.2.5: Changes in the absorption spectra of **Eu:87₃** (4 μM) upon addition of Br⁻ (0 → 16.00 μM).

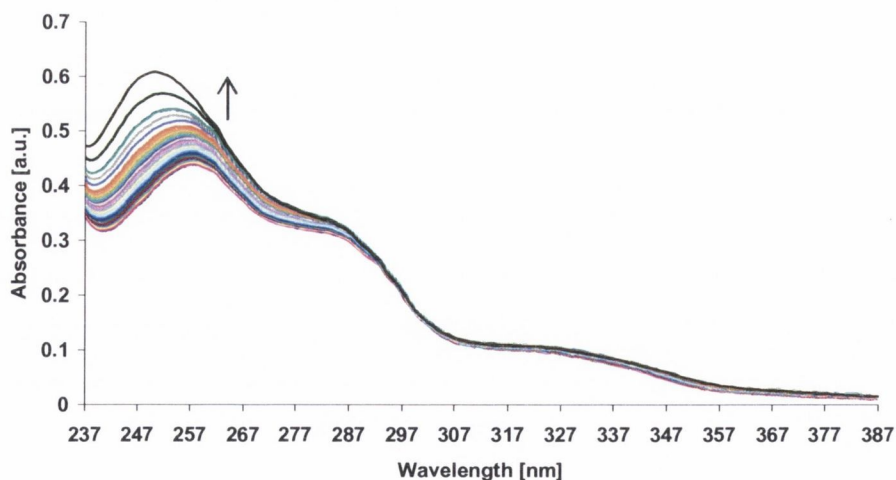


Figure 5.7.2.6: Changes in the absorption spectra of **Eu:87₃** (4 μM) upon addition of I⁻ (0 → 19.90 μM).

The titration of **Eu:87₃** with H_2PO_4^- showed interesting and somewhat unexpected results. The changes in the absorption spectra of **Eu:87₃** upon addition of H_2PO_4^- are shown in **Figure 5.7.2.7**. As can be observed, the major changes occurred at the *ca.* 260 nm and *ca.* 292 nm bands, while only minor changes were observed at longer wavelengths.

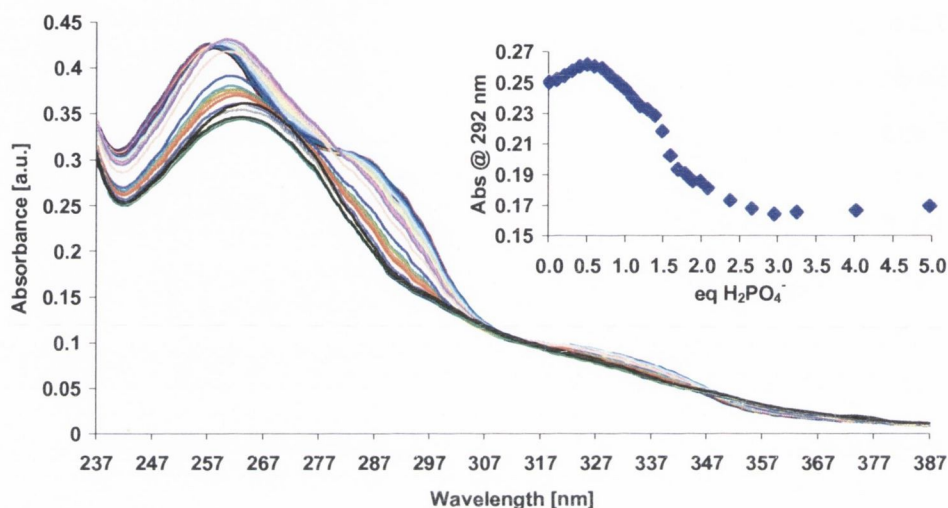


Figure 5.7.2.7: Changes in the absorption spectra of **Eu:87₃** (4 μM) upon addition of H_2PO_4^- (0 → 19.90 μM). Insert: The changes in absorbance at 292 nm as a function of equivalents of H_2PO_4^- .

The insert in **Figure 5.7.2.7** shows the changes taking place at 292 nm as a function of the equivalents of H_2PO_4^- . Although, in this case, the major changes also occur upon addition of two equivalents of H_2PO_4^- , there is a striking difference between these changes and those seen for the anions discussed above. In the present case, the results obtained indicate the formation of a 1:2 complex between the anion and the host, G:H₂. As can be seen in **Figure 5.7.2.8**, the band at *ca.* 260 nm was observed to decrease upon addition of H_2PO_4^- accompanied by a bathochromic shift. However, the band at *ca.* 292 nm experienced an initial increase upon addition of 0.5 equivalents of anion, which can possibly be attributed to the formation of a 1:2 (G:H₂) complex between H_2PO_4^- and **Eu:87₃**. This was followed by a decrease in the absorbance upon further addition of H_2PO_4^- (0.5 → 1.2 equivalents), which is most likely associated with the formation of the 1:1 (G:H) complex. The bigger changes were nevertheless experienced between the addition of *ca.* 1.4 → 2.4 equivalents of H_2PO_4^- (**Figure 5.7.2.8**) indicating the possible formation of a

2:1 ($G_2:H$). However, additional changes were observed upon further addition of $H_2PO_4^-$ ($2 \rightarrow 5$ equivalents), which once again are indicative of the 3:1 ($G_3:H$) binding interactions in solution (**Figure 5.7.2.7** and **Figure 5.7.2.8**).

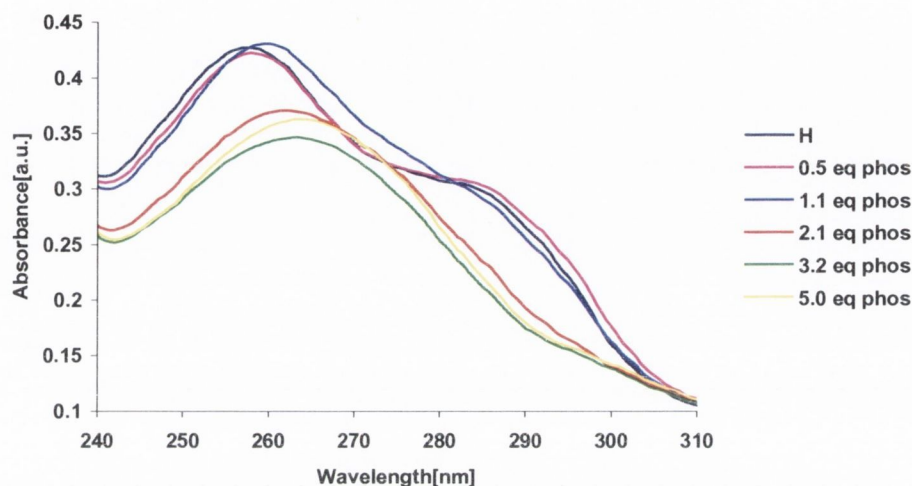


Figure 5.7.2.8.: Fraction of the absorption spectra recorded upon addition of different equivalents of $H_2PO_4^-$ ($0 \rightarrow 19.90 \mu M$) to a solution of **Eu:87₃**.

The binding constants, $\log K$ for these changes, were determined by fitting the titration data using the SPECFIT program. The best fit was obtained taking into account the 1:1 ($G:H$), 1:2 ($G:H_2$), 2:1 ($G_2:H$) and 2:2 ($G_2:H_2$) binding interactions between **Eu:87₃** and $H_2PO_4^-$, **Figure 5.7.2.9**. Once again we were unable to fit for the possible 3:1 ($G_3:H$) binding interaction. From this fit, values of $\log K_{1:1} > 7$, $\log K_{1:2} = 5.44 \pm 0.39$, $\log K_{2:1} = 5.55 \pm 0.32$, and $\log K_{2:2} = 5.74 \pm 0.89$ were determined (**Table 5.7.2**). The high error associated with binding constant for $G_2:H_2$ can be overlooked, as this species, although contributing for the binding process is present in solution in a very small concentration (insert in **Figure 5.7.2.9**). The predominant species in solution correspond to the formation of the 1:1 ($G:H$) and the 2:1 ($G_2:H$) binding interactions respectively, as shown in the speciation distribution diagram inserted in **Figure 5.7.2.9**.

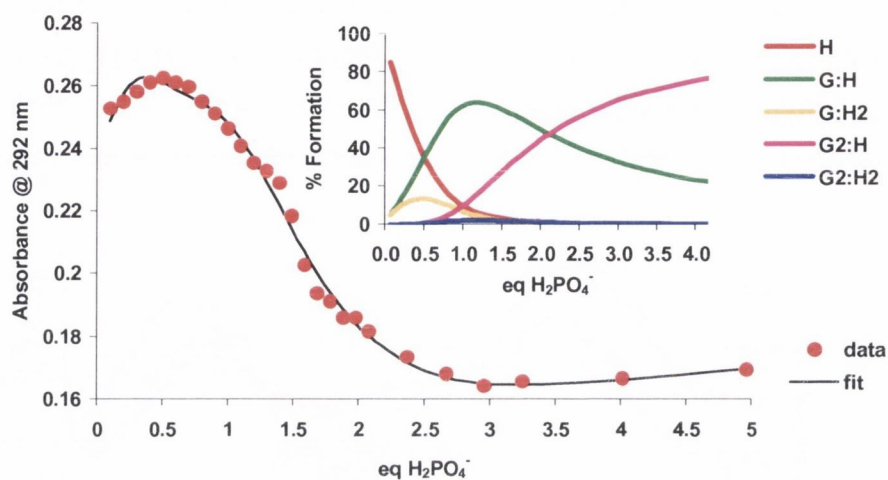


Figure 5.7.29: Experimental binding isotherm for the UV-Visible titration of **Eu:87₃** (4 μ M) with H_2PO_4^- in CH_3CN and corresponding fit from SPECFIT. Insert shows the Speciation diagram. H refers to the host **Eu:87₃**, while G refers to the guest anion, H_2PO_4^- .

In **Table 5.7.2** are summarised the obtained binding constants, using the SPECFIT program, for all the absorption titrations of **Eu:87₃** with the various anions.

Technique	Anion (G)	Species ($\text{G}_n:\text{H}_m$)	$\log K_{n:m}$	Std. Deviation (\pm)
Absorbance	CH_3COO^-	G:H	6.23	0.26
		G ₂ :H	6.17	0.17
	F^-	G:H	> 7 (7.25)	0.24
		G ₂ :H	6.97	0.20
	Cl^-	G:H	5.67	0.28
		G ₂ :H	5.46	0.16
	Br^-	-	-	-
	I^-	-	-	-
	H_2PO_4^-	G:H	> 7 (7.17)	0.15
		G:H ₂	5.44	0.39
		G ₂ :H	5.55	0.32
		G ₂ :H ₂	5.75	0.89*

Table 5.7.2: Binding constants and binding modes between the different anions (G) and **Eu:87₃** (H) for the UV-Visible titration. * Species present in solution in less than 10% formation.

In summary, the absorption studies gave rise to interesting results for the binding interactions of the various anions to **Eu:87₃**. Here, high binding constants were determined for the 1:1 and 2:1 interactions with anions such as CH_3COO^- , H_2PO_4^- , F^- and Cl^- . Although

changes were observed for the addition of *ca.* three equivalents of anion, we were unable to fit for the possible 3:1 (G₃:H) interaction. This can possibly be attributed to either the small changes induced by this species or a weak interaction between a third anion and **Eu:87₃**. For Br⁻ and I⁻ the changes observed were too small to allow for an accurate determination of the binding constants using the SPECFIT program. To better understand these binding interactions, the fluorescence emission was also followed, and the obtained results will be discussed in the following section.

5.7.3 Changes in the fluorescence emission spectra of **Eu:87₃** upon anion recognition

The fluorescence emission of **Eu:87₃** was also monitored upon addition of the various anions, following excitation at both the 260 nm and the 330 nm transitions. Similar results were obtained on both occasions. Upon addition of CH₃COO⁻, F⁻, Cl⁻, Br⁻, and I⁻ the fluorescence emission intensity was enhanced (by *ca.* 62%, 58%, 34%, 10%, and 16%, respectively). Although H₂PO₄⁻ was also observed to enhance the fluorescence emission, its behaviour was somewhat different from the anions mentioned, and therefore will be discussed later within this section.

The changes in the fluorescence emission spectra of **Eu:87₃** upon addition of CH₃COO⁻ are presented in **Figure 5.7.3**.

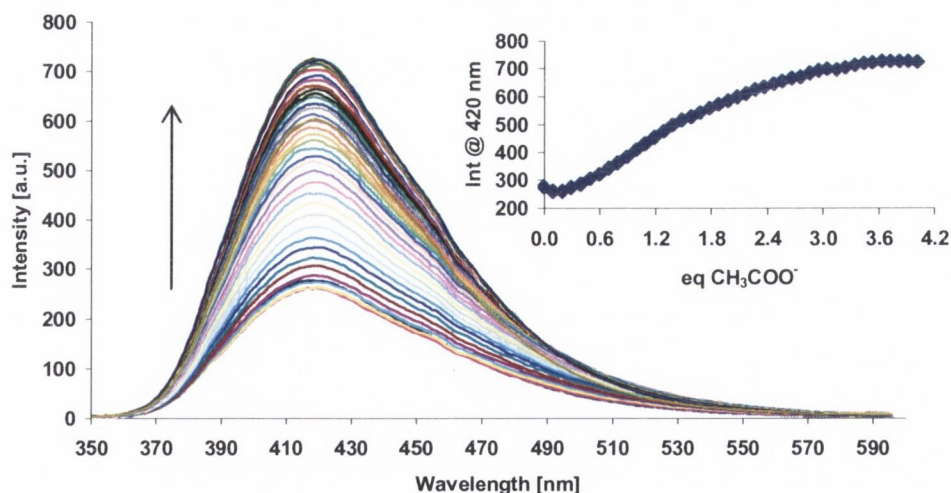


Figure 5.7.3: Changes in the fluorescence emission spectra of **Eu:87₃** (4 μM) upon addition of CH₃COO⁻ (0 → 16.10 μM), in CH₃CN when exciting at 266 nm. Insert: The changes in emission intensity at 420 nm as a function of equivalents of CH₃COO⁻.

In comparison to the ground state studies, the insert in **Figure 5.7.3** clearly shows that the changes in the emission intensity at 420 nm occur upon addition of three equivalents of CH_3COO^- , which, once again, is indicative of the 3:1 ($\text{G}_3:\text{H}$) binding stoichiometry between CH_3COO^- (G) and **Eu:87₃** (H). As previously mentioned, due to the presence of the three urea moieties, interaction of various anions with **Eu:87₃** was expected to give rise to the formation of the 1:1 (G:H), 2:1 ($\text{G}_2:\text{H}$) and 3:1 ($\text{G}_3:\text{H}$) complexes, and hence give rise to three binding constants ($K_{1:1}$, $K_{2:1}$ and $K_{3:1}$, respectively). However, fitting the changes in the fluorescence emission, observed upon titration with CH_3COO^- , indicated the occurrence of only two binding interactions. The best fit to the experimental data was obtained by taking into account the 1:1 (G:H) and 2:1 ($\text{G}_2:\text{H}$) binding interactions between CH_3COO^- (G) and **Eu:87₃** (H), **Figure 5.7.3.1**. From this, binding constants of $\log K_{1:1} = 6.29 \pm 0.16$ and $\log K_{2:1} = 5.71 \pm 0.12$ were determined, **Table 5.7.3**. The $\log K_{1:1}$ was found to be higher than that determined for the metal free sensor **87**, $\log K_{1:1} = 5.19$, (Chapter 4, **Table 4.4**). The obtained speciation distribution diagram is shown in insert **Figure 5.7.3.1**. These results were found to be in good agreement with those from the ground state investigations (**Table 5.7.2**). Once again, the reason associated with the impossibility to fit for the 3:1 ($\text{G}_3:\text{H}$) stoichiometry is not clear at this stage. However, as previously mentioned for the ground state studies, this can possibly be attributed to the weak formation of such species, and hence not in the detection range of the fitting program used.

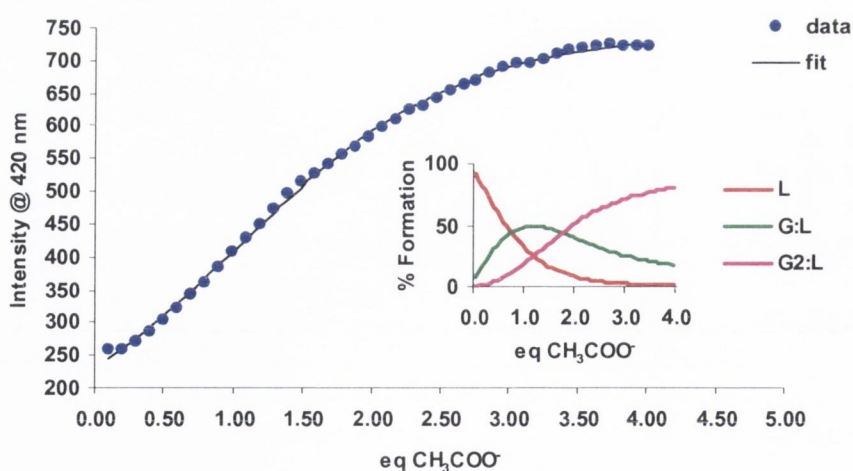


Figure 5.7.3.1: Experimental binding isotherm for the fluorescence titration of **Eu:87₃** (4 μM) with CH_3COO^- in CH_3CN and corresponding fit using SPECFIT. Insert: Speciation distribution diagram; H refers to **Eu:87₃**, and G to CH_3COO^- .

The fluorescence emission spectra of **Eu:87₃** upon addition of F⁻ showed similar changes to those discussed above for CH₃COO⁻, **Figure 5.7.3.2**.

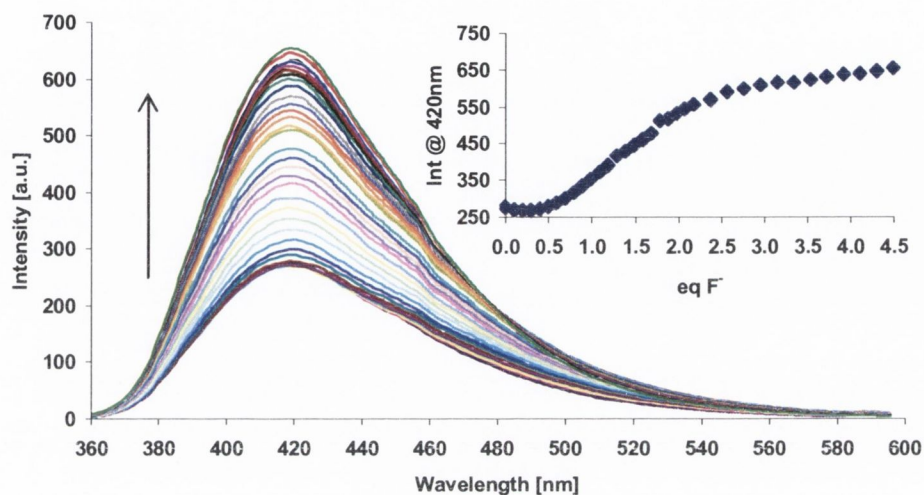


Figure 5.7.3.2: Changes in the fluorescence emission spectra of **Eu:87₃** (4 μM) upon addition of F⁻ (0 → 18.00 μM), in CH₃CN when exciting at 266 nm. Insert: The changes in emission intensity at 420 nm as a function of equivalents of F⁻.

Once again, the changes in the emission intensity at 420 nm indicated the possible 3:1 (G₃:H) stoichiometry, insert **Figure 5.7.3.2**. In this case, and in contrast to what has been observed so far, the best fit to the fluorescence titration data was obtained by taking into account the 3:1 (G₃:H) stoichiometry, **Figure 5.7.3.3**. From this, binding constants of $\log K_{1:1} > 7$, $\log K_{2:1} = 6.46 \pm 0.23$ and $\log K_{3:1} = 3.76 \pm 0.83$ were determined, **Table 5.7.3**. The large error associated with the formation of the 3:1 stoichiometry can be attributed to the low percentage formation (< 5%) of this species in solution (insert in **Figure 5.7.3.3**), which is consistent with the explanation given above for the absence of such stoichiometry in the previous fittings. From the speciation distribution diagram, insert in **Figure 5.7.3.3**, it is also clear that an initial addition of F⁻ leads to the formation of the 1:1 (G:H) complex, after which the 2:1 (G₂:H) species begins to dominate and eventually becomes the predominant species in solution.

The values for the binding constants were found to be in good agreement with those determined from the ground state investigations (1:1 and 2:1 binding interactions), **Table**

5.7.2. In addition, these values were found to be much higher than those obtained for the interaction of F^- with **87** (Chapter 4, Table 4.4).

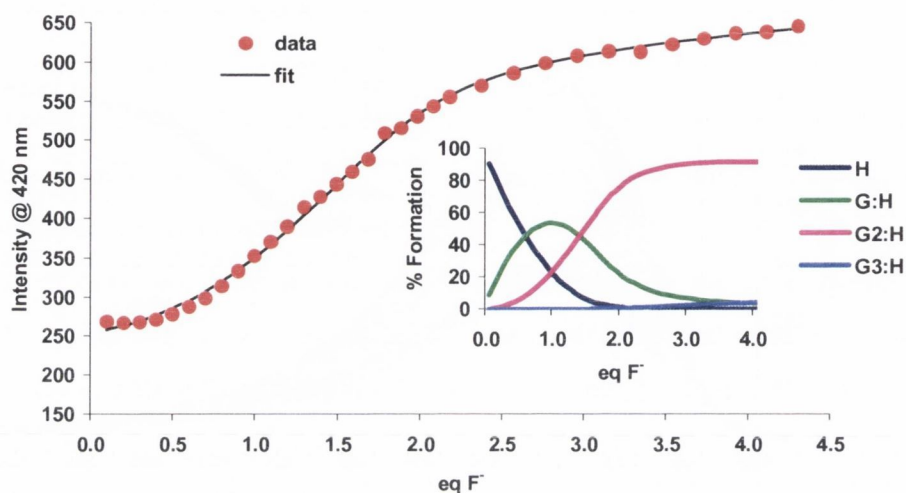


Figure 5.7.3.3: Experimental binding isotherm for the fluorescence titration of **Eu:87₃** (4 μ M) with F^- in CH_3CN , and corresponding fit using SPECFIT. Insert: Speciation distribution diagram; H refers to **Eu:87₃**, and G refers to F^- .

For Cl^- , the emission intensity enhancement (34%) was observed to be less significant than those discussed above for both CH_3COO^- and F^- . The changes in the fluorescence emission spectra of **Eu:87₃** upon addition of Cl^- are shown in **Figure 5.7.3.4**.

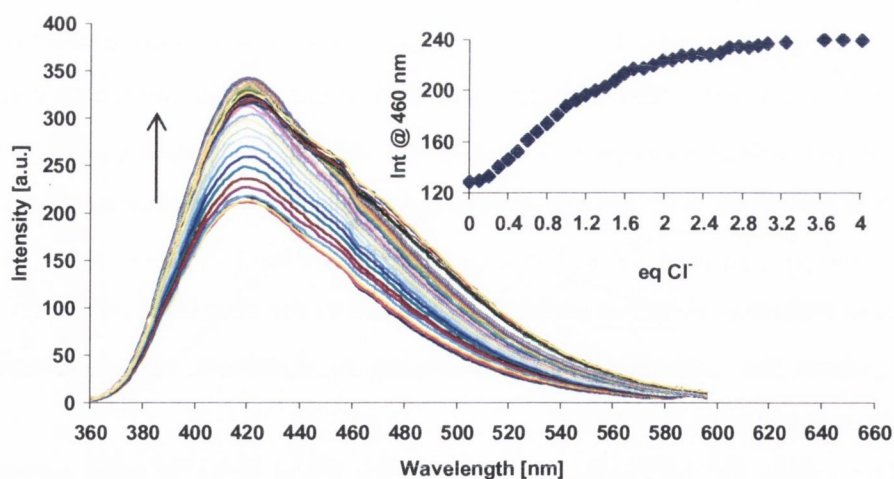


Figure 5.7.3.4: Changes in the fluorescence emission spectra of **Eu:87₃** (4 μ M) upon addition of Cl^- (0 \rightarrow 16.10 μ M), in CH_3CN when exciting at 266 nm. Insert: The changes in emission intensity at 460 nm as a function of equivalents of Cl^- .

Once again, while the titration profile shows changes occurring up to the addition of three equivalents of Cl^- , insert in **Figure 5.7.3.4**, the fitting of the fluorescence emission changes indicated the occurrence of only two binding interactions. The best fit to the experimental data was obtained by taking into account the 1:1 (G:H) and 2:1 (G_2 :H) binding interactions between Cl^- (G) and **Eu:87**₃ (H), **Figure 5.7.3.5**. From this, binding constants of $\log K_{1:1} = 5.90 \pm 0.17$ and $\log K_{2:1} = 5.45 \pm 0.22$ were determined, **Table 5.7.3**. These results were found to be in good agreement with those from the ground state investigations (**Table 5.7.2**). The $\log K_{1:1}$ was found to be much higher than that determined for the metal free sensor **87**, $\log K_{1:1} = 3.84$, (Chapter 4, **Table 4.4**). The obtained speciation distribution diagram is shown in the insert in **Figure 5.7.3.5**, and shows the 2:1 (G_2 :H) as the predominant stoichiometry in solution after the addition of *ca.* 2 equivalents of Cl^- .

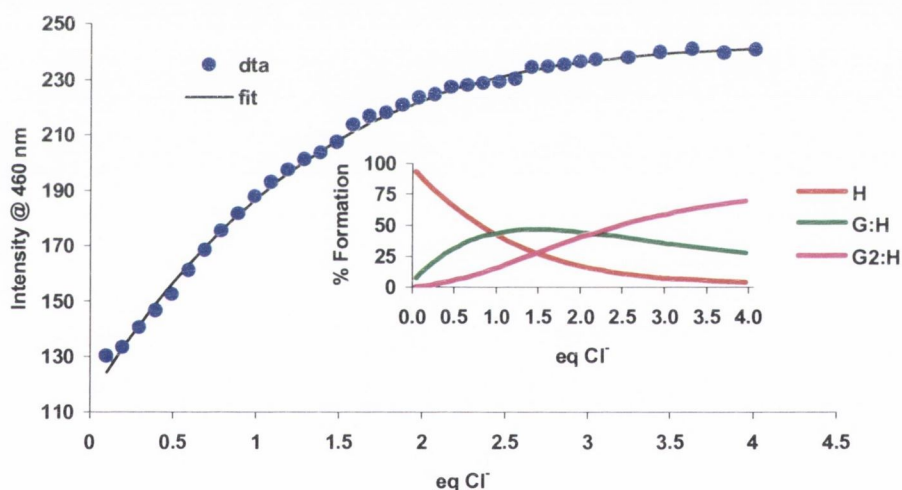


Figure 5.7.3.5: Experimental binding isotherm for the fluorescence titration of **Eu:87**₃ (4 μM) with Cl^- in CH_3CN and corresponding fit using SPECFIT. Insert: The speciation distribution diagram; H refers to the host **Eu:87**₃, while G refers to the guest anion, Cl^- .

The changes in the emission intensity of **Eu:87**₃ upon addition of either Br^- or I^- were found to be the smallest among the anions studied (enhancements of 10% and 16%, respectively), as shown in **Figure 5.7.3.6** for the titration with Br^- .²⁹ For this reason, and similarly to the absorption studies, it was not possible to determine reliable binding constants for the interaction of these anions with **Eu:87**₃.

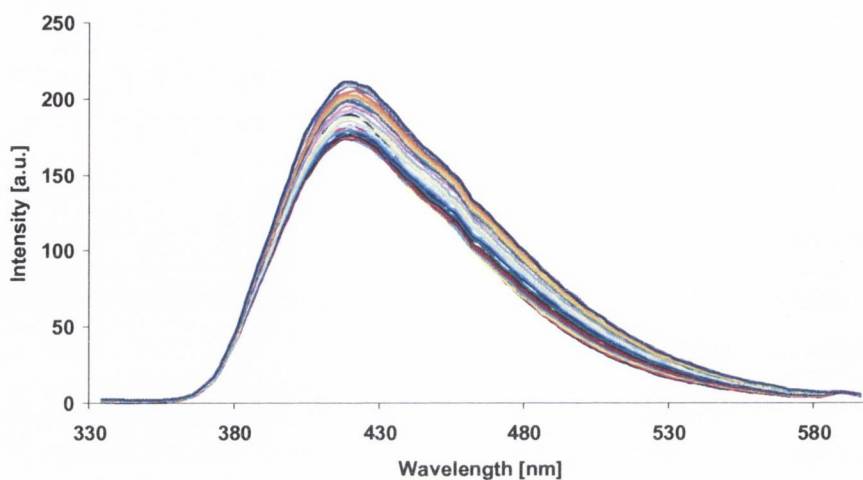


Figure 5.7.3.6: Changes in the fluorescence emission spectra of **Eu:87₃** (4 μM) upon addition of Br^- (0 \rightarrow 16.00 μM), in CH_3CN when exciting at 266 nm.

The changes in the fluorescence emission spectra of **Eu:87₃** upon addition of H_2PO_4^- are depicted in **Figure 5.7.3.7**. Similarly to the results obtained from the absorption investigations, the fluorescence titration with H_2PO_4^- also showed distinct binding interactions. Analysing the titration profile of the changes in the emission intensity as a function of equivalents of H_2PO_4^- , insert in **Figure 5.7.3.7**, it can clearly be seen that initially, from 0 \rightarrow 0.5 equivalents of H_2PO_4^- , the emission intensity was reduced by *ca.* 20%, which suggests the 1:2 (G:H₂) interaction between H_2PO_4^- (G) and **Eu:87₃** (H). Subsequently, upon further addition of anion (0.5 \rightarrow *ca.* 3 equivalents of H_2PO_4^-), the emission intensity was considerably enhanced. These changes are indicative of the expected formation of the 1:1 (G:H), 2:1 (G₂:H) and 3:1 (G₃:H) stoichiometries in solution for the binding interactions of H_2PO_4^- to **Eu:87₃**, giving rise to the corresponding $\log K_{1:1}$, $\log K_{2:1}$ and $\log K_{3:1}$ binding constants, representing the stepwise binding of a single H_2PO_4^- to each one of the three urea moieties present in **Eu:87₃**.

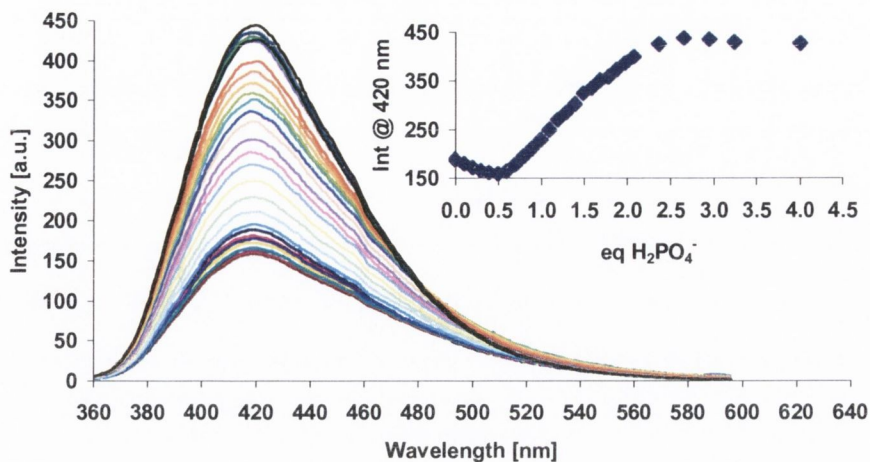


Figure 5.7.3.7: Changes in the fluorescence emission spectra of **Eu:87₃** (4 μM) upon addition of H_2PO_4^- (0 \rightarrow 19.90 μM). Insert: The changes in emission intensity at 420 nm as a function of equivalents of H_2PO_4^- .

In agreement with the absorption studies, when fitting the data using the SPECFIT program the 3:1 ($\text{G}_3:\text{H}$) was not observed, which as previously discussed can be attributed to the very small percentage formation of this species in solution. The titration data was fitted according to the model involving the 1:1 ($\text{G}:\text{H}$), 1:2 ($\text{G}:\text{H}_2$), 2:1 ($\text{G}_2:\text{H}$), and 2:2 ($\text{G}_2:\text{H}_2$) binding interactions. As can be observed in **Figure 5.7.3.8**, the model fitted well with the experimental data.

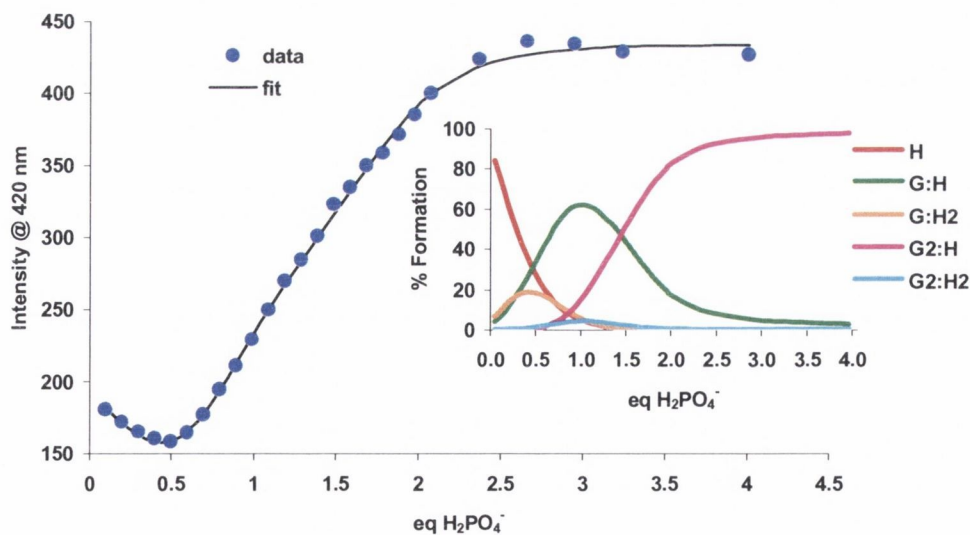


Figure 5.7.3.8: Experimental binding isotherm for the fluorescence titration of **Eu:87₃** (4 μM) with H_2PO_4^- in CH_3CN , and corresponding fit using SPECFIT. Insert: Speciation distribution diagram; H refers to **Eu:87₃**, and G to H_2PO_4^- .

From this fit, binding constants of $\log K_{1:2} = 5.71 \pm 0.36$, $\log K_{2:1} = 6.70 \pm 0.31$ and $\log K_{2:2} = 5.87 \pm 0.90$ were determined, **Table 5.7.3**. These binding constants carry a significant error as the 1:1 binding stoichiometry, from which $\log K_{1:2}$ and $\log K_{2:1}$ are derived, was found to be higher than seven ($\log K_{1:1} > 7$) and hence too high to be determined accurately using the SPECFIT program. As can be observed in the speciation distribution diagram, insert in **Figure 5.7.3.8**, the 2:2 binding stoichiometry forms in less than 10% (*ca.* 4%), which accounts for the high error associated with this binding constant. The insert in **Figure 5.7.3.8** clearly shows that after the addition of *ca.* 2 equivalents of H_2PO_4^- the $\text{G}_2\text{:H}$ complex becomes the dominant species in solution. In comparison to the binding interaction of the free sensor **87** with H_2PO_4^- ($\log K_{1:1} = 4.35$, Chapter 4, **Table 4.4**) the $\log K_{1:1}$ for the interaction of **Eu:87**₃ with H_2PO_4^- was found to be much higher (**Table 5.7.3**).

Summarised in **Table 5.7.3** are the results of all the binding constants, $\log K$, and associated binding modes, obtained for the fluorescence titrations carried out on **Eu:87**₃ with the various anions.

Technique	Anion (G)	Species ($\text{G}_n\text{:H}_m$)	$\log K_{n:m}$	Std. Deviation (\pm)
Fluorescence	CH_3COO^-	G:H	6.29	0.16
		$\text{G}_2\text{:H}$	5.71	0.12
	F^-	G:H	> 7 (7.18)	0.17
		$\text{G}_2\text{:H}$	6.46	0.23
		$\text{G}_3\text{:H}$	3.76	0.83*
	Cl^-	G:H	5.90	0.17
		$\text{G}_2\text{:H}$	5.45	0.22
	Br^-	-	-	-
	I^-	-	-	-
	H_2PO_4^-	G:H	> 7 (8.35)	0.30
		G:H_2	5.71	0.36
		$\text{G}_2\text{:H}$	6.70	0.31
$\text{G}_2\text{:H}_2$		5.87	0.90*	

Table 5.7.3: Binding constants and binding modes between the different anions (G) and **Eu:87**₃ (H) for the fluorescence titration. * Species present in solution in less than 10% formation.

The results obtained from the fluorescence studies for the binding interactions of the various anions to **Eu:87**₃ were found to be in agreement with those of the ground state investigations (Section 5.7.2). In comparison to the binding interaction of the free sensor **87**

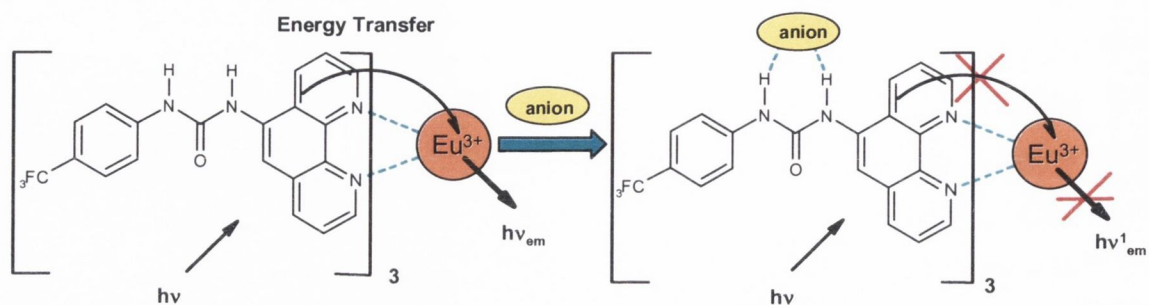
with the various anions ($\log K_{1:1}$, Chapter 4, **Table 4.4**) the $\log K_{1:1}$ for the interaction of **Eu:87₃** with these anions was found to be higher on all occasions (**Table 5.7.3**), which was expected due to the presence of the metal ion, and hence due to possible additional electrostatic interactions with the anions. Once again, although changes were observed for the addition of *ca.* 3 equivalents of anion, we were only able to fit for the possible 3:1 (G₃:H) stoichiometry for the interaction with F⁻. From this fit, a binding constant of $\log K_{3:1} = 3.76 \pm 0.83$ was found, which reflects a weak interaction between 3 molecules of F⁻ and **Eu:87₃**. In addition, the speciation distribution diagram revealed that this species is present in solution in less than 5%, which accounts for the high error associated with the binding constant. So, although present, it can be in general difficult for the fitting program SPECFIT to account for the 3:1 species in solution.

In summary, the fluorescence emission intensity was significantly enhanced upon addition of the various anions such as CH₃COO⁻, F⁻, H₂PO₄⁻ and Cl⁻. In contrast, Br⁻ and I⁻ gave only rise to small changes. The increase in the emission intensity can be explained by considering possible conformational changes within **Eu:87₃**, induced by the presence of the various anions. These changes can lead to the removal of existing vibrational pathways, as well as the removal of present PET quenching mechanism able to deactivate the excited state, and hence the increase in fluorescence emission intensity. Another explanation would be the possibility of complex dissociation. As previously mentioned, direct coordination of competitive anions to the metal centre, by displacement of the *phen* based antenna, can lead to the possible gradual dissociation of the Eu(III) complex. Consequently, the energy transfer from the excited state of the antenna to the excited state of the Eu(III) would no longer take place, hence the increase in the fluorescence emission intensity. As the mechanism through which the anions are binding to the **Eu:87₃** is not yet clear at this stage, the lanthanide luminescence was also followed as an attempt to clarify the results.

5.7.4 Changes in the lanthanide luminescence of **Eu:87₃** upon anion recognition

Although significant changes were observed for both the UV-Visible and the fluorescence emission upon anion titrations, the most striking changes were observed for the lanthanide emission. The lanthanide luminescence was followed after excitation at both 260 nm and 330 nm. In general, the emission intensity for the ⁵D₀ → ⁷F_J transitions was

gradually reduced, or ‘switched off’, in the presence of anions such as CH_3COO^- , H_2PO_4^- , Cl^- , Br^- and I^- , indicating that upon recognition of these anions, the antenna is unable to participate in the energy transfer process to the lanthanide excited state, **Scheme 5.7.4**.



Scheme 5.7.4: Schematic representation of the lanthanide luminescence quenching upon anion recognition at the urea receptors within **Eu:87₃**.

One possible explanation for the quenching of the emission intensity is attributed to an energy mismatch between the lowest triplet state (T_1) of the antenna and the 5D_0 excited state of Eu(III), making the energy transfer from the triplet state of the antenna, T_1 , to the excited state of the Eu(III), 5D_0 , less favorable.

Another explanation for the gradual quenching of the emission intensity would be the possible dissociation of the Eu(III) self-assembly complex upon addition of the various anions. In this case, the Eu(III) emission would be expected to be reduced, as energy transfer from the antenna would be prevented. If this is the case, the direct coordination of competitive anions to Eu(III) by gradual displacement of the coordinating antenna, would give rise to lanthanide based displacement assays.^{154,247}

The changes in the lanthanide luminescence emission spectra observed for the titration of **Eu:87₃** with CH_3COO^- are shown in **Figure 5.7.4**. Here, the emission intensity was gradually quenched upon addition of *ca.* 3 equivalents of CH_3COO^- , though the major changes were observed between $0 \rightarrow ca. 2$ equivalents. Once again, although any of the bands can be used to analyse the data, as each one gives rise to similar results, the insert in **Figure 5.7.4** shows the profile of the changes in the luminescence intensity at 612 nm ($J = 2$ band) as a function of the number of equivalents of CH_3COO^- . This illustrates that the major changes occur for *ca.* 2.5 equivalents of CH_3COO^- , implying the binding between three CH_3COO^- and one molecule of **Eu:87₃**, as previously found for the absorption and

fluorescence studies. As previously discussed, the fitting of the data using SPECFIT does not take into account the possible 3:1 binding stoichiometry.

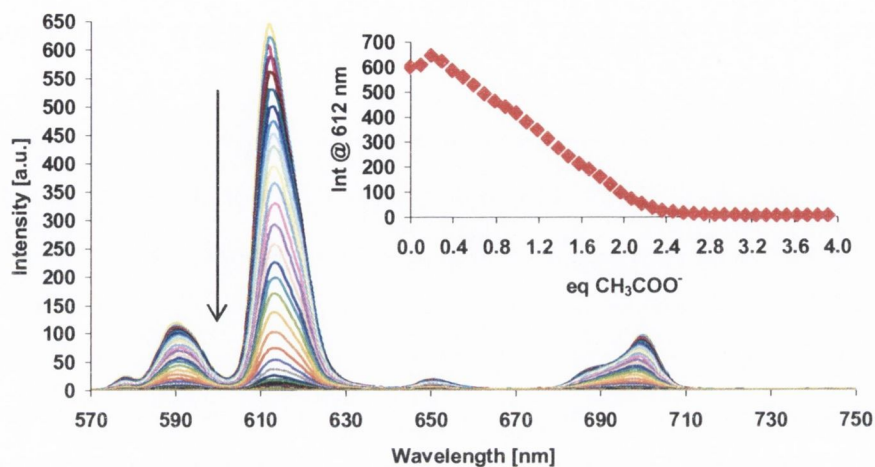


Figure 5.7.4: Changes in the lanthanide emission spectra of **Eu:87₃** (4 μM) upon addition of CH_3COO^- (0 → 16.10 μM). Insert: The changes in the intensity at 612 nm as a function of equivalents of CH_3COO^- .

Figure 5.7.4.1 shows the good fit to the experimental data from the titration with CH_3COO^- , obtained by using the 1:1 (G:H) and 2:1 (G_2 :H) binding stoichiometries. From this, strong binding constants of $\log K_{1:1} = 6.56 \pm 0.12$ and $\log K_{2:1} = 7.11 \pm 0.06$ were determined, **Table 5.7.4**.

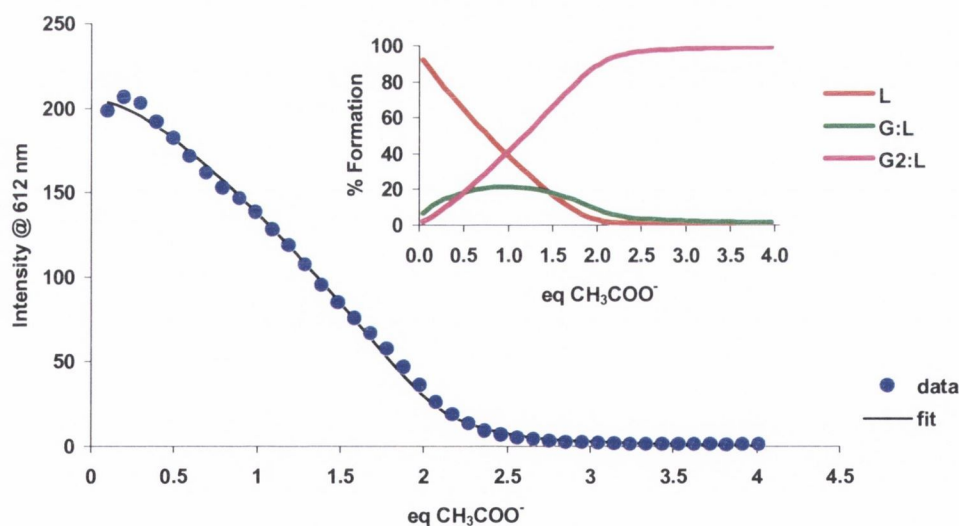


Figure 5.7.4.1: Experimental binding isotherm for the lanthanide luminescence titration of **Eu:87₃** (4 μM) with CH_3COO^- in CH_3CN , and corresponding fit using SPECFIT. Insert: The speciation distribution diagram; H refers to **Eu:87₃**, while G refers to CH_3COO^- .

The speciation distribution diagram, insert in **Figure 5.7.4.1**, shows that the G₂:H complex is the dominant species in solution after the addition of *ca.* 2 equivalent of CH₃COO⁻.

The distinct binding interaction previously discussed for **Eu:87₃** upon titration with H₂PO₄⁻, both in the absorption and the fluorescence studies, was once again observed in the lanthanide luminescence. The changes in the lanthanide emission spectra of **Eu:87₃** upon gradual addition of H₂PO₄⁻ are presented in **Figure 5.7.4.2**. The emission intensity experienced an initial small decrease in intensity (*ca.* 11%) upon addition of *ca.* 0.5 equivalents of H₂PO₄⁻ (insert in **Figure 5.7.4.2**), which can be associated with the formation of the 1:2 (G:H₂) binding stoichiometry, between one H₂PO₄⁻ and two molecules of **Eu:87₃**, as previously found for both the absorption and the fluorescence. This can be attributed to the possible formation of four hydrogen bonds by this anion. However, the major changes were observed upon further addition of H₂PO₄⁻ (0.5 → *ca.* 1.2 equivalents of H₂PO₄⁻), where the emission intensity was dramatically quenched by 98%, insert in **Figure 5.7.4.2**, after which no more changes were observed.

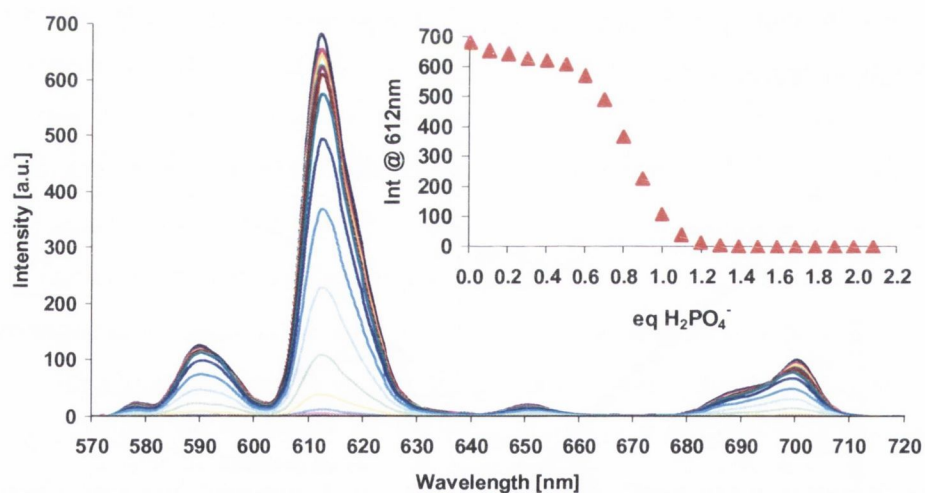


Figure 5.7.4.2: Changes in the lanthanide emission spectra of **Eu:87₃** (4 μM) upon addition of H₂PO₄⁻ (0 → 19.90 μM), in CH₃CN when exciting at 260 nm. Insert: The changes in intensity at 614 nm as a function of equivalents of H₂PO₄⁻.

Although the changes were observed to occur upon addition of *ca.* 1.2 equivalents of H_2PO_4^- , the best fit to the experimental data was obtained by taking into account the 1:1 (G:H), 1:2 (G:H₂), 2:1 (G₂:H), and 2:2 (G₂:H₂) stoichiometries, **Figure 5.7.4.3**.

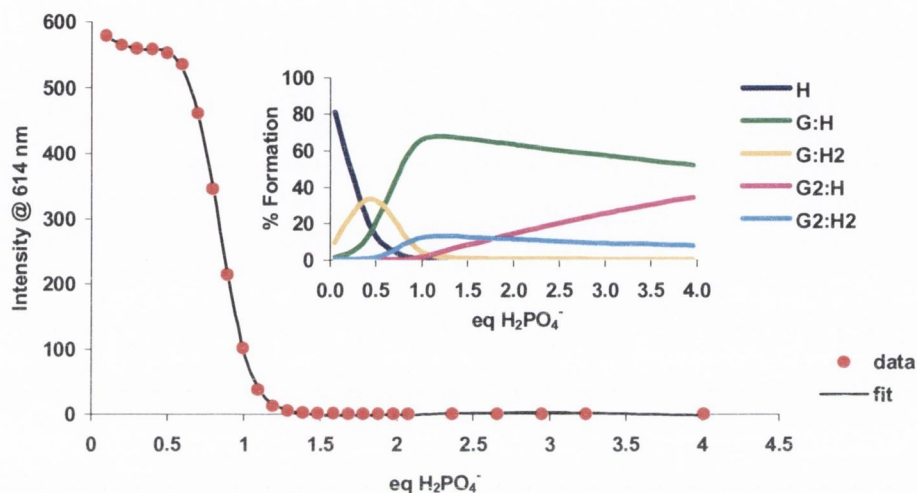


Figure 5.7.4.3: Experimental binding isotherm for the lanthanide luminescence titration of **Eu:87₃** (4 μM) with H_2PO_4^- in CH_3CN , and corresponding fit using SPECFIT. Insert: The speciation distribution diagram; H refers to **Eu:87₃**, while G refers to the H_2PO_4^- .

From this fit, binding constants of $\log K_{1:2} = 6.51 \pm 0.15$, $\log K_{2:1} = 4.80 \pm 0.09$ and $\log K_{2:2} = 6.96 \pm 0.12$ were determined for the 1:2, 2:1 and 2:2 respectively, while $\log K_{1:1}$ was found to be much higher than seven, **Table 5.7.4**. The speciation diagram (insert in **Figure 5.7.4.3**) confirms the presence of the G:H₂ species in solution. It further supports the previous suggestion of the G:H complex being the dominant, and hence more stable species present in solution.

The binding with the spherical anions such as Cl^- , Br^- and I^- , also lead to a significant quenching of the lanthanide emission (*ca.* 95%, 76% and 72%, respectively). The changes in the lanthanide emission spectra of **Eu:87₃** upon addition of Cl^- are shown in **Figure 5.7.4.4**. Once again, as observed for both the absorption and the fluorescence, while the titration profile shows changes occurring up to the addition of three equivalents of Cl^- , insert in **Figure 5.7.4.4**, fitting the changes in the lanthanide emission intensity indicated the occurrence of only two binding interactions.

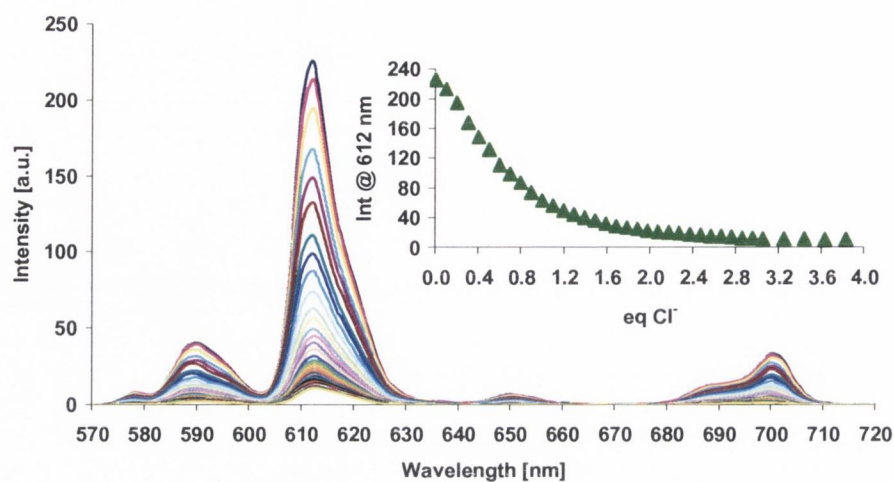


Figure 5.7.4.4: Changes in the lanthanide emission spectra of **Eu:87₃** (4 μM) upon addition of Cl^- (0 \rightarrow 16.10 μM), in CH_3CN when exciting at 260 nm. Insert: The changes in intensity at 612 nm as a function of equivalents of Cl^- .

The best fit to the experimental data was obtained by taking into account the 1:1 (G:H) and 2:1 (G_2 :H) binding interactions between Cl^- (G) and **Eu:87₃** (H), **Figure 5.7.4.5**. From this, binding constants of $\log K_{1:1} = 6.48 \pm 0.12$ and $\log K_{2:1} = 4.88 \pm 0.37$ were determined, **Table 5.7.4**, which were found to be somewhat different from those obtained for the absorption (**Table 5.7.2**) and fluorescence (**Table 5.7.3**) investigations.

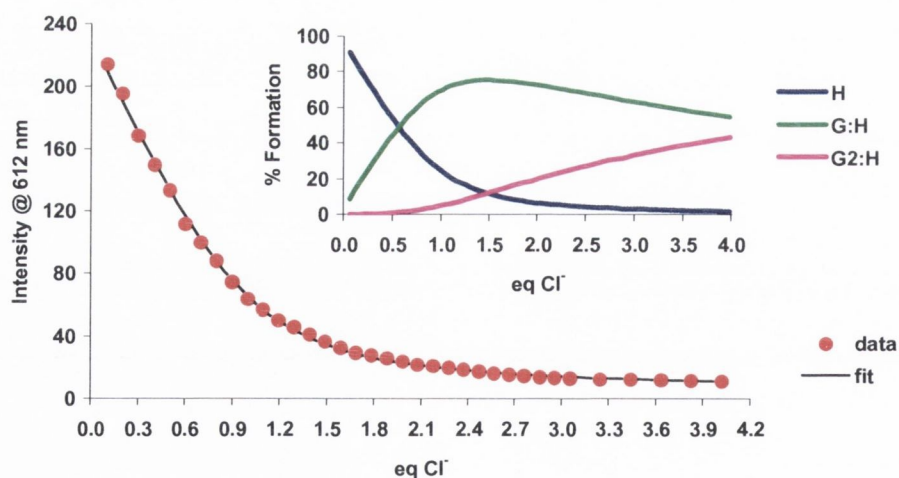


Figure 5.7.4.5: Experimental binding isotherm for the lanthanide luminescence titration of **Eu:87₃** (4 μM) with Cl^- in CH_3CN , and corresponding fit using SPECFIT. Insert: The speciation distribution diagram; H refers to **Eu:87₃**, while G refers to Cl^- .

As mentioned above, Br^- and I^- showed a very similar behaviour. This is clearly shown in the profile of the changes in the emission intensity at 612 nm as a function of number of equivalents of added anion, **Figure 5.7.4.6**. From this profile, it becomes evident that the major changes occur between $0 \rightarrow \text{ca. } 1.2$ equivalents of anion, after which the changes become much smaller, suggesting a stronger binding interaction for the 1:1 (G:H) stoichiometry, between the mentioned anions and **Eu:87**₃. Similarly to the titration with Cl^- , the experimental data was fitted to the 1:1 (G:H) and 2:1 (G_2 :H) binding stoichiometries for both Br^- and I^- . The fits gave rise to similar binding constants of $\log K_{1:1} = 6.29 \pm 0.17$ and $\log K_{2:1} = 4.91 \pm 0.42$ for the titration with Br^- , $\log K_{1:1} = 6.41 \pm 0.18$ and $\log K_{2:1} = 5.19 \pm 0.40$ for the titration with I^- , **Table 5.7.4**. In contrast to the expected small changes observed in both the absorption and the fluorescence emission spectra (as these anions are non-coordinating to urea moieties), such halide anions (Br^- and I^-) gave rise significant changes in the lanthanide luminescence emission. This fact indicates that a different binding interaction, other than the hydrogen bonding to the urea moieties of **Eu:87**₃, must be present in solution. A possible explanation would be the dissociation of the self-assembly complex, **Eu:87**₃, upon addition of such anions. The possible binding of the anions directly to the Eu(III) would probably lead to the displacement of the antenna, **87**, hence gradually quenching the emission intensity. Such displacement of the antenna by coordinating anions has been previously reported for lanthanide complexes.^{86,89,154,156,244,248}

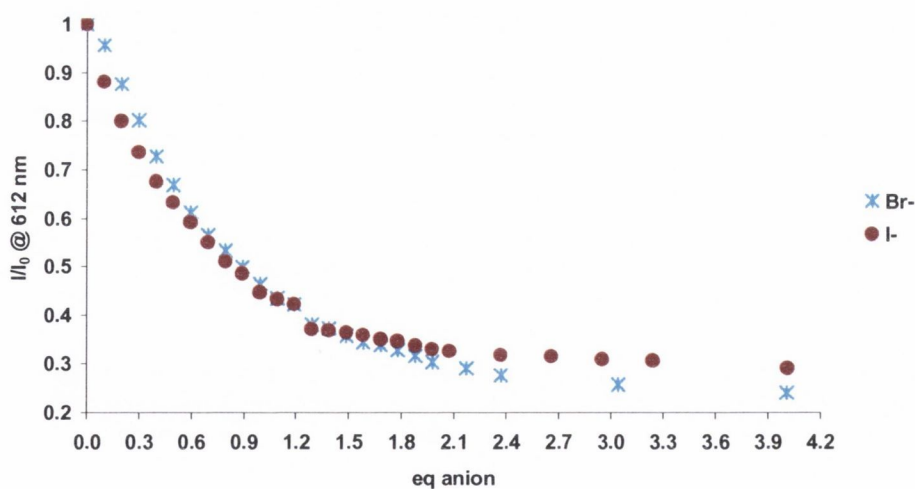


Figure 5.7.4.6: Changes on the relative lanthanide emission intensity (I/I_0 , where I_0 represents the intensity of the free host) of **Eu:87**₃ (4 μM) at 612 nm as a function of number of equivalents of Br^- and I^- .

The changes in the lanthanide emission spectra of **Eu:87₃** upon addition of F⁻ are shown in **Figure 5.7.4.7**. In contrast to the changes discussed above for CH₃COO⁻, H₂PO₄⁻, Cl⁻, Br⁻ and I⁻, the Eu(III) emission intensity was enhanced (*ca.* 63%) upon an initial addition of F⁻, after which the emission was fully quenched. These changes can clearly be observed by analysis of the titration profile shown in the insert in **Figure 5.7.4.7**. The initial increase in intensity, observed between 0 → 1 equivalents of F⁻, can be ascribed to the possible direct interaction of F⁻ to the Eu(III) ion in **Eu:87₃** by displacement of solvent molecules, leading to the formation of the 1:1 (G:H) complex. This hypothesis was further supported by analysing the evolution of the emission spectrum during the titration, in particular the changes in the structure of the more symmetry-sensitive transitions (⁵D₀ → ⁷F₂ and ⁵D₀ → ⁷F₄), **Figure 5.7.4.8**, indicating that F⁻ coordinates directly to Eu(III).²⁴⁸ Fluoride anions are known to coordinate efficiently to lanthanide ions, and were already reported to replace metal bound water molecules.^{57,153} A similar behaviour can also be observed in the present case, particularly when considering that CH₃CN molecules form much weaker coordinative bonds with the lanthanide metal centre.¹⁵⁶

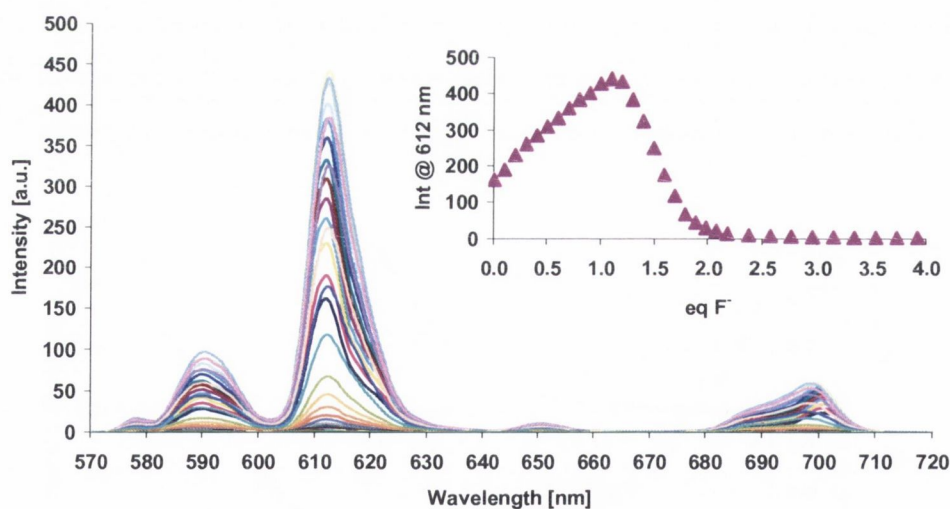


Figure 5.7.4.7: Changes in the lanthanide emission intensity of **Eu:87₃** (4 μM) upon addition of F⁻ (0 → 18.00 μM). Insert: The changes in intensity at 612 nm as a function of equivalents of F⁻.

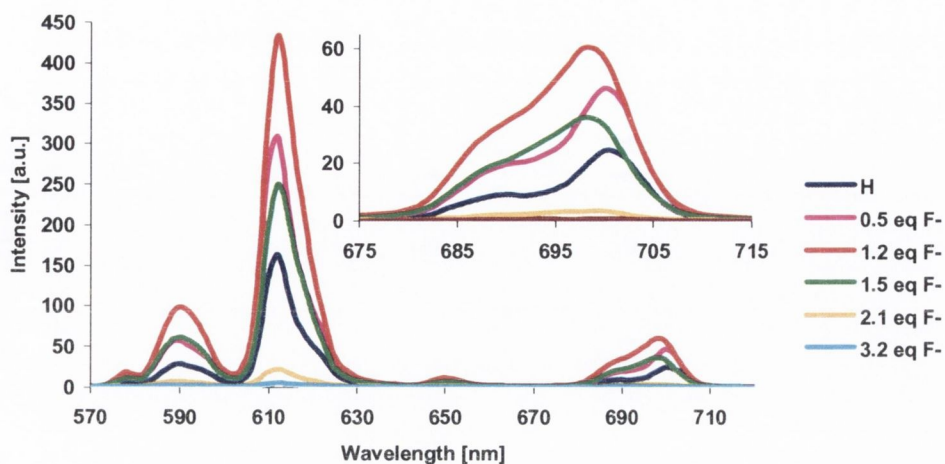


Figure 5.7.4.8.: Changes in the lanthanide emission intensity of **Eu:87₃** ($4 \mu\text{M}$) upon addition of different equivalents of F^- . Insert: Fraction of the lanthanide emission spectra for the ${}^5\text{D}_0 \rightarrow {}^7\text{F}_4$ transition ($J = 4$ band).

However, upon further addition of F^- ($1 \rightarrow \text{ca. } 2$ equivalents of F^-), the emission intensity was dramatically quenched (**Figure 5.7.4.8**), indicating the possible formation of the 2:1 ($\text{G}_2:\text{H}$) binding stoichiometry. This quenching can be associated to either the possible binding of the anion to the urea moieties, or to the metal ion by displacement of the *phen* coordinating antenna¹⁵⁶, hence the decrease in emission intensity. Once again, the changes between the addition of *ca.* 2 equivalents of F^- (formation of $\text{G}_2:\text{H}$) and *ca.* 3 equivalents of F^- (formation of $\text{G}_3:\text{H}$) were only minor. The steep profile between both $0 \rightarrow 1$ equivalents, and $1 \rightarrow 2$ equivalents of F^- are indicative of strong binding constants for the formation of the 1:1 ($\text{G}:\text{H}$) and the 2:1 ($\text{G}_2:\text{H}$) complexes. This was completely supported by the results obtained from the fitting of the titration data by using the SPECFIT program, **Figure 5.7.4.9**, as the binding constants determined from this fit, $\log K_{1:1}$ and $\log K_{2:1}$, were found to be very high with values above seven (10.35 and 8.20, respectively), **Table 5.7.4**. As can be observed in the speciation distribution diagram in the insert in **Figure 5.7.4.9**, the $\text{G}:\text{H}$ is present in 90% after the addition of one equivalent of F^- , after which the $\text{G}_2:\text{H}$ species becomes the dominant species in solution after *ca.* 2 equivalents of F^- .

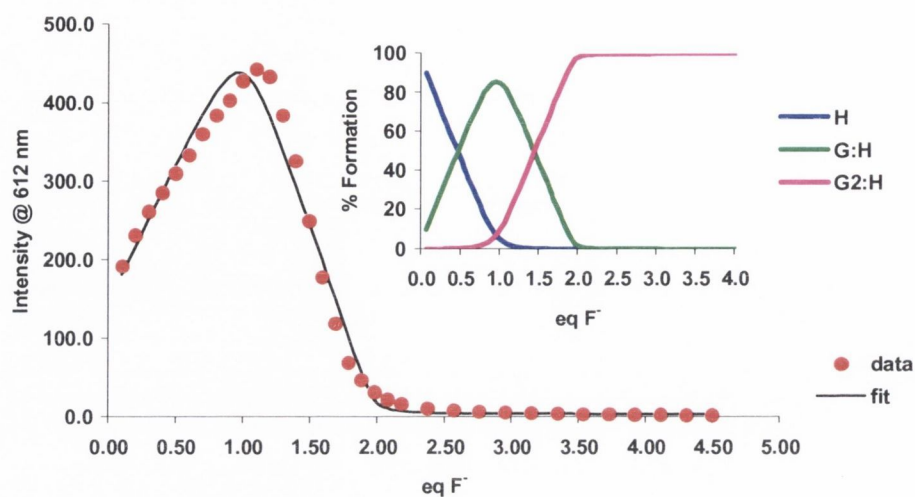


Figure 5.7.4.9: Experimental binding isotherm for the lanthanide luminescence titration of **Eu:87₃** (4 μM) with F⁻ in CH₃CN, and corresponding fit using SPECFIT. Insert: The speciation distribution diagram; H refers to **Eu:87₃**, while G refers to F⁻.

The values determined by fitting the data obtained from the lanthanide luminescence titration of the various anions with **Eu:87₃**, using the nonlinear program SPECFIT, are summarised in **Table 5.7.4**.

Technique	Anion (G)	Species (G _n :H _m)	log K _{n:m}	Std. Deviation (±)
Phosphorescence	CH ₃ COO ⁻	G:H	6.56	0.12
		G ₂ :H	> 7 (7.11)	0.06
	H ₂ PO ₄ ⁻	G:H	> 7 (8.61)	0.09
		G:H ₂	6.51	0.15
		G ₂ :H	4.80	0.09
	Cl ⁻	G ₂ :H ₂	6.96	0.12*
		G:H	6.48	0.12
		G ₂ :H	4.88	0.37
	Br ⁻	G:H	6.29	0.17
		G ₂ :H	4.91	0.42
	I ⁻	G:H	6.41	0.18
		G ₂ :H	5.19	0.40
	F ⁻	G:H	> 7 (10.35)	0.36
		G ₂ :H	> 7 (8.20)	0.53

Table 5.7.4: Binding constants and binding modes between the different anions (G) and **Eu:87₃** (H) for the lanthanide luminescence titration. * Species present in solution in less than 10% formation.

This table clearly shows the strong nature of the interactions taking place between the various anions and **Eu:87₃**, as the binding constants, $\log K$, were found to be relatively high. Among the anions studied, fluoride noticeably showed the strongest interactions. In general, these values were found to be higher than those determined from the absorption (**Table 5.7.2**) and the fluorescence (**Table 5.7.3**) titrations.

In summary, the lanthanide luminescence emission intensity was significantly modulated upon addition of the various anions such as CH_3COO^- , F^- , H_2PO_4^- , Cl^- , Br^- and I^- . The emission intensity was gradually 'switched off' in the presence of CH_3COO^- , H_2PO_4^- , Cl^- , Br^- and I^- . However, H_2PO_4^- was the only anion observed to give rise to the 1:2 (G:H₂) stoichiometry, which can be attributed to the possible formation of four hydrogen bonds by this anion. Br^- and I^- gave rise to significant quenching of the emission intensity, in contrast to the small changes observed for both the absorption and the fluorescence. Hence, this was attributed to the possible dissociation of the self-assembly complex (**Eu:87₃**), as opposed to the binding to the urea moieties. The most interesting changes were, however, observed for the titration with F^- . Upon an initial addition of this anion (1 equivalent), the emission intensity was significantly enhanced, which was ascribed to the direct binding of F^- to the Eu(III) by displacement of solvent molecule. This was then followed by a decrease of the emission intensity upon further addition of F^- , which can possibly be related to the binding of this anion to the urea moieties of **Eu:87₃**, or to the gradual dissociation of the self-assembly complex by displacement of the coordinating *phen* based antenna. By comparing the binding constants obtained upon addition of the various anions, and in particular for F^- , it can be observed that they are higher than those obtained for the Eu(III) complex formation (**Table 5.6.4**), which can also be indicative of complex dissociation.

5.8 Conclusions

In this chapter the formation, characterisation, and photophysical studies of the novel supramolecular assembly **Eu:87₃**, between the *phen* based ligand **87** and Eu(III) in CH_3CN , have been presented and discussed.

Despite the insolubility of ligand **87** in CH_3CN , it became fully soluble in the presence of europium triflate ($\text{Eu}(\text{CF}_3\text{SO}_3)_3$). The obtained yellow solid (**Eu:87₃**) showed an intense red colour under the UV lamp, indicative of the lanthanide sensitization by receptor **87**.

The use of $^1\text{H-NMR}$ spectroscopy further supported the presence of an Eu(III) coordinated complex, as signal broadening of the *phen* moiety protons most closely located to the paramagnetic metal center was observed. Further indication of the interaction between **87** and the lanthanide was provided by the determination of the number of metal bound water molecules, $q = 2.64$, which is consistent with the expected 1:3 (**Eu:87₃**) supramolecular assembly. Successful coordination of Eu(III) to the *phen* moiety of **87** was also confirmed by the changes observed in the IR spectrum of **Eu:87₃**, when compared to that of the free ligand **87**. Moreover, the stoichiometry of the complex in solution was assessed by using Job's method, or method of continuous variation, which was shown to be 1:3, **Eu:87₃**, in CH_3CN .

In order to gain some insight into the metal complex species present in solution, an investigation into the ground state and the excited state (fluorescence and lanthanide luminescence) properties of the complex was undertaken. The lanthanide luminescence of the Eu(III) was 'switched on' in the presence of ligand **87**, establishing the sensitization of the metal ion through the antenna (ligand **87**). From the changes observed in the UV-Visible, fluorescence, and lanthanide luminescence titrations, binding constants ($\log K$) for the self-assembly complex formation, between **87** and the lanthanide metal centre, were determined for the 1:1 (**Eu:87**), 1:2 (**Eu:87₂**), and 1:3 (**Eu:87₃**) complexes, by using the nonlinear least-squares fitting model SPECFIT. The determined values were found to be in agreement for the different techniques used. As expected, the **Eu:87₃** species showed the highest binding constant, suggesting that **Eu:87₃** was the most stable complex formed in solution. Based on these results, it is possible to conclude that the presence of the Eu(III) metal ion, in CH_3CN solution, induces the formation of a self-assembly supramolecular system between Eu(III) and **87** in a 1:3 (**Eu:87₃**) stoichiometry.

The ability of the self-assembly architecture **Eu:87₃**, (H), to sense anionic species (G), such as CH_3COO^- , H_2PO_4^- , F^- , Cl^- , Br^- and I^- was investigated. Both the UV-Visible and the luminescence studies were carried out by titrating a solution of **Eu:87₃** in CH_3CN with the various anions. From the changes observed during these titrations, binding constants ($\log K$), for the interaction between **Eu:87₃** and the various anions were determined by using the nonlinear least-squares fitting program SPECFIT. Although the titration profiles showed evidence of the formation of the 3:1 ($\text{G}_3:\text{H}$) stoichiometry in solution, we were unable to fit

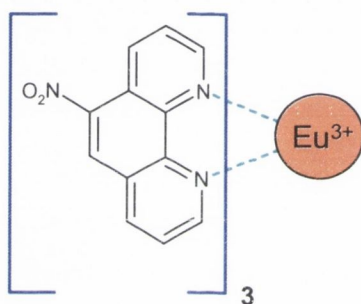
for this species in the majority of the cases, suggesting that either the recognition of the third anion is very weak or that the spectral changes are too small to be fitted. This was supported by the only $\log K_{3:1}$ determined for the fluorescence titration with F^- , which was found to be both weak and form in very low percentage in solution (< 5%). The binding constants determined from both the absorption (**Table 5.7.2**) and the fluorescence (**Table 5.7.3**) were found to be in good agreement for anions such as CH_3COO^- , $H_2PO_4^-$, F^- and Cl^- , while for Br^- and I^- the changes were too small to be fitted.

The lanthanide luminescence was observed to be gradually ‘switched off’ for anions such as CH_3COO^- , $H_2PO_4^-$, Cl^- , Br^- and I^- , indicating that upon anion recognition the antenna is unable to participate in the energy transfer process to the lanthanide excited state. Two possible mechanism can be associated with the quenching of the lanthanide emission intensity; (i) anion binding at the urea moiety can lead to an energy mismatch between the lowest triplet state (T_1) of the antenna and the 5D_0 excited state of Eu(III), making the energy transfer from the triplet state of the antenna to the excited state of the Eu(III) less favorable, or (ii) anion coordination to Eu(III) by displacement of the *phen* antenna, leading to the dissociation of the Eu(III) self-assembly complex (**Eu:873**) and hence gradual quenching of the emission, as energy transfer from the antenna would be prevented.

In contrast to the absorption and the fluorescence studies, both Br^- and I^- induced significant changes in the lanthanide luminescence spectra. This indicated that a binding interaction other than hydrogen bonding to the urea moieties of **Eu:873** must be present in solution, and hence was attributed to the possible dissociation of the self-assembly complex.

The most interesting results were observed for the titration with the fluoride ion, as only for this anion was the emission intensity ‘switched on’ (63%) upon an initial addition of F^- (0 \rightarrow 1 equivalents of F^-). Such emission intensity enhancement was ascribed to the direct coordination of F^- to Eu(III), by displacement of solvent molecules. However, upon further addition of F^- (1 \rightarrow 2 equivalents of F^-) the emission intensity was ‘switched off’ due to probable dissociation of the self-assembly complex **Eu:873**, by displacement of the *phen* based antenna.

In this work, we have therefore demonstrated that the luminescence intensity of the novel self-assembly system **Eu:87**₃ changes dramatically in the presence of anions, which provides the possibility to employ this complex as a luminescent sensor for anions. However, the mechanism through which the anions are interacting with **Eu:87**₃ is not clear. In order to further investigate the possibility of the dissociation of the Eu(III) complex upon addition of anions, titration of the complex shown below with the various anions will be carried out in the near future. The lack of the urea binding sites in this ligand implies that the only site available for anion recognition is at the Eu(III) centre directly, by displacement of either solvent molecules or coordinating ligands. Therefore, the changes observed upon addition of anions would have to be attributed to the direct interaction with the metal ions.



Chapter 6

Experimental procedures

6.1 General Experimental Details

All chemicals were obtained from Sigma-Aldrich Ireland Ltd. (Aldrich, Sigma and Fluka/Riedel de Haën), Lancaster or Acros Organics and unless specified, were used without further purification. Deuterated solvents for NMR use were purchased from Apollo Scientific. Dry solvents were prepared using standard procedures, according to Vogel, with distillation under dry argon prior to each use.²⁴⁹ Chromatographic columns were run using Aluminum Oxide (activated, Neutral, Brockmann I STD grade 150 mesh) or Silica gel 60 (230-400 mesh ASTM). Analytical TLC was performed using Merck Kieselgel 60 F₂₅₄ silica gel plates or Polygram Alox N/UV₂₅₄ aluminium oxide plates. Visualisation was by UV light (254 nm), by exposure to iodine vapour or with 2% ninhydrin in ethanol spray reagent. NMR spectra were recorded using a Brüker DPX-400 Avance spectrometer, operating at 400.13 MHz for ¹H-NMR, 100.6 MHz for ¹³C-NMR, and 376.46 MHz for ¹⁹F-NMR, or a Brüker AV-600 spectrometer, operating at 600.1 MHz for ¹H-NMR and 150.2 MHz for ¹³C-NMR. Shifts are referenced relative to the internal solvent signals. NMR data were processed using Brüker Win-NMR 5.0 software. Electrospray mass spectra were recorded on a Micromass LCT spectrometer, running Mass Lynx NT V 3.4 on a Waters 600 controller connected to a 996 photodiode array detector with HPLC-grade methanol, water or acetonitrile as carrier solvents. Detection was in positive (ES+) mode only. Accurate molecular masses were determined by a peak-matching method, using leucine enkephaline (H-Tyr-Gly-Gly-Phe-Leu-OH) as the standard internal reference (*m/z* = 556.2771); and reported within 5 ppm of the expected mass. Samples were prepared in non-chlorinated HPLC-grade solvents. Elemental analysis was carried out, by Ms Ann Connolly, at the Microanalytical Laboratory, School of Chemistry and Chemical Biology, University College Dublin. Melting points were determined using an Electrothermal IA9000 digital melting point apparatus. Infrared spectra were recorded either on a Mattson Genesis II FTIR spectrometer equipped with a Gateway 2000 4DX2-66 workstation or a Perkin Elmer Spectrum One FT-IR Spectrometer fitted with a universal ATR sampling accessory. When using the former, solid samples were dispersed in KBr and recorded as clear pressed discs. X-ray diffraction studies were carried out by Dr Thomas McCabe (School of Chemistry, Trinity College Dublin) using a Bruker SMART APEX single crystal CD diffractometer.

6.2 Ultraviolet-Visible and Luminescence spectroscopy

UV-Visible and luminescence titration measurements were performed on a Varian Cary-50 and Varian Cary Eclipse spectrophotometers respectively. The solvents used were of HPLC grade. All the stock solutions (10^{-3} M) were prepared in CH_3CN . However, in Chapters 4 and 5, the compounds under study (87 and $\text{Eu}:87_3$, respectively) were firstly dissolved in DMSO (10 μL) and then diluted in a 10 mL volumetric flask with CH_3CN . Solutions with the molar concentrations used in the measurements (4 μM in Chapters 2 and 4, 10 μM and 4 μM in Chapter 5) were prepared by dilution of the corresponding 10^{-3} M stock solutions. The concentration of the ligands and complexes investigated were the same for both the UV-visible and luminescence measurements. All the anions and metals solutions were prepared in CH_3CN . The titration experiments performed in this work were carried out as described in the corresponding Chapters. The settings of the fluorimeter for the fluorescence and lanthanide luminescence measurements, carried out in Chapters 2, 4, and 5 are reported in **Tables 6.2.1-6.2.8**.

Table 6.2.1 Fluorescence settings for titrations in Chapter 2 ($[\text{Tb}.61] = 4 \mu\text{M}$ in CH_3CN)

<u>Fluorescence Settings</u>	
Mode: Fluorescence	Excitation: 280 nm
Scan Control: medium	PMT Voltage: Medium
Excitation slit width: 10 nm	Emission slit width: 10 nm

Table 6.2.2 Lanthanide luminescence settings for titrations in Chapter 2 ($[\text{Tb}.61] = 4 \mu\text{M}$ in CH_3CN)

<u>Luminescence Settings</u>	
Mode: Phosphorescence	Excitation: 280 nm
Total Decay: 0.02 ms	Scan: 450-720 nm
Flash: 1	Delay: 0.1 ms
Gate: 10 ms	PMT Voltage: High
Excitation slit width: 10 nm	Emission slit width: 10 nm

Table 6.2.3 Fluorescence settings for titrations in Chapter 4 of 87 with transition metals ($[87.Cu] = 4 \mu M$ in CH_3CN)

<u>Fluorescence Settings</u>	
Mode: Fluorescence	Excitation: 266 nm
Scan Control: medium	PMT Voltage: Medium
Excitation slit width: 5 nm	Emission slit width: 5 nm

Table 6.2.4 Fluorescence settings for titrations in Chapter 4 of the transition metals Cu(II) and Fe(II) complexes with anions ($[87.Cu] = 4 \mu M$ in CH_3CN)

<u>Fluorescence Settings</u>	
Mode: Fluorescence	Excitation: 260 nm
Scan Control: medium	PMT Voltage: Medium
Excitation slit width: 10 nm	Emission slit width: 10 nm

Table 6.2.5 Fluorescence settings for titrations in Chapter 5 of 87 with Eu(III) ($[87] = 10 \mu M$ in CH_3CN)

<u>Fluorescence Settings</u>	
Mode: Fluorescence	Excitation: 265 nm
Scan Control: medium	PMT Voltage: Medium
Excitation slit width: 10 nm	Emission slit width: 5 nm

Table 6.2.6 Lanthanide luminescence settings for titrations in Chapter 5 of 87 with Eu(III) ([87] = 10 μM in CH_3CN)

<u>Luminescence Settings</u>	
Mode: Phosphorescence	Excitation: 265 nm
Total Decay: 0.02 ms	Scan: 550-720 nm
Flash: 1	Delay: 0.1 ms
Gate: 10 ms	PMT Voltage: Medium
Excitation slit width: 10 nm	Emission slit width: 10 nm

Table 6.2.7 Fluorescence settings for titrations in Chapter 5 of the Eu(III) complex with anions ([Eu:87₃] = 4 μM in CH_3CN)

<u>Fluorescence Settings</u>	
Mode: Fluorescence	Excitation: 260 nm
Scan Control: medium	PMT Voltage: Medium
Excitation slit width: 5 nm	Emission slit width: 5 nm

Table 6.2.8 Lanthanide luminescence settings for titrations in Chapter 5 of the Eu(III) complex with anions ([Eu:87₃] = 4 μM in CH_3CN)

<u>Luminescence Settings</u>	
Mode: Phosphorescence	Excitation: 260 nm
Total Decay: 0.02 ms	Scan: 550-720 nm
Flash: 1	Delay: 0.1 ms
Gate: 10 ms	PMT Voltage: Medium
Excitation slit width: 5 nm	Emission slit width: 5 nm

6.3 Lifetime measurements for Tb(III) and Eu(III) complexes

Luminescence lifetime measurements were carried out in H₂O and D₂O, on a Varian Carey Eclipse Fluorimeter. The settings for the Tb(III) and Eu(III) complexes are displayed below in **Table 6.3.1** and **Table 6.3.2** respectively.

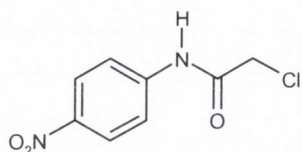
Table 6.3.1 Luminescence lifetime settings for Tb(III) complex in Chapter 2

<u>Lifetime Settings</u>	
Direct excitation: Tb(III) – 366 nm	
Emission: Tb(III) – 545 nm	
No. Cycles: 100	Total Decay: 10 ms
Flash: 1	Delay: 0.1 ms
Gate: 0.1 ms	PMT Voltage: High
Excitation slit width: 20	Emission slit width: 20

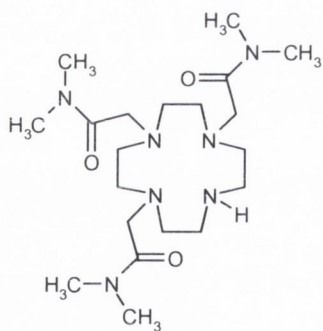
Table 6.3.2 Luminescence lifetime settings for Eu(III) complex in Chapter 2 and Chapter 5

<u>Lifetime Settings</u>	
Direct excitation: Eu(III) – 395 nm	
Emission: Eu(III) – 615 nm	
No. Cycles: 100	Total Decay: 10 ms
Flash: 1	Delay: 0.1 ms
Gate: 0.1 ms	PMT Voltage: High
Excitation slit width: 20	Emission slit width: 20

6.4 Experimental details for Chapter 2

2-Chloro-*N*-(4-nitro-phenyl)-acetamide (**65**)

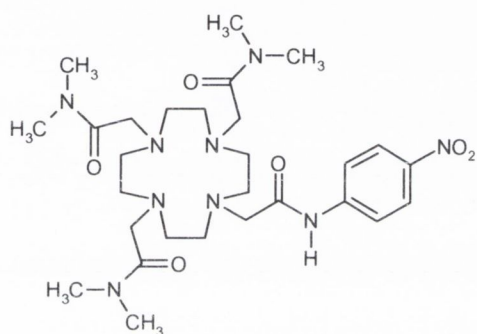
A solution of 4-nitro-phenylamine (**67**) (0.30 g, 2.17 mmol) and triethylamine (0.66 g, 6.51 mmol) in CH_2Cl_2 (30 mL) was cooled below 0°C in an ice/acetone bath. A solution of chloroacetyl chloride (0.25 g, 2.17 mmol) in CH_2Cl_2 (10 mL) was then added dropwise over a 30 min period. The reaction mixture was then allowed to warm up to room temperature and stirred for 48 hours. The brown solution was washed with 0.1 M HCl (4 x 25 mL). The organic layer was dried over K_2CO_3 , filtered and the solvent was removed under reduced pressure to yield a brown solid (0.62 g, 79% yield). Recrystallisation from hot EtOH yielded brown crystals (0.37 g, 48% yield). m.p. $178\text{--}179^\circ\text{C}$; ^1H NMR (400 MHz, $d_6\text{-(CD}_3)_2\text{CO}$, δ_{H}) 10.01 (s, 1H, NH), 8.25 (d, 2H, Ar-H, $J = 8.0$ Hz), 7.94 (d, 2H, Ar-H, $J = 8.5$ Hz), 4.33 (s, 2H, CH_2); ^{13}C NMR (100 MHz, $d_6\text{-(CD}_3)_2\text{CO}$, δ_{C}) 165.85, 145.01, 143.97, 125.27, 119.79, 43.75; MS (ES $^-$) m/z : 213.1 [M – H].

2-(4,7-Bis-dimethylcarbamoylmethyl-1,4,7,10-tetraaza-cyclododec-1-yl)-*N,N*-dimethyl-acetamide (**62**)¹⁵⁷

1,4,7,10 tetraazacyclododecane (**63**) (1.00 g, 5.80 mmol) was placed in a 50 mL single neck RBF. To this was added NaHCO_3 (1.46 g, 17.40 mmol) and dry CH_3CN (20 mL). The RBF was placed in an ice/acetone bath and allowed to cool. A solution of 2-Chloro-*N,N*-dimethyl-acetamide, **64**, (2.12 g, 17.40 mmol) in CH_3CN (5 mL) was added quickly and the solution was stirred at 0°C for ten minutes. The solution was then stirred at 85°C under an argon atmosphere for 72 hours. The resulting yellow solution was filtered through celite and the solvent removed under reduced pressure. The obtained dark yellow viscous oil was dissolved in CH_2Cl_2 and purified by alumina column chromatography using a gradient elution 100 to 90:10 CH_2Cl_2 : CH_3OH . The desired product was collected as an off-white foam after drying under vacuum (1.70 g, 69% yield). Calculated for $\text{C}_{20}\text{H}_{42}\text{N}_7\text{O}_3$: $m/z = 428.3349$ [M + H], Found: 428.3352; ^1H NMR (400 MHz, CDCl_3 , δ_{H}) 10.01 (br s, 1H, NH), 3.52 (s, 2H, CH_2), 3.56 (s, 4H, CH_2), 3.07 (s, 8H,

Cyclen CH₂), 3.02 (s, 3H, CH₃), 2.95 (s, 6H, CH₃), 2.88 (s, 9H, CH₃), 2.84 (br m, 8H, Cyclen CH₂); ¹³C NMR (100 MHz, CDCl₃, δ_C), 169.87, 169.74, 55.17, 54.54, 53.10, 53.02, 51.24, 49.73, 49.24, 45.80, 36.39, 36.03, 35.63, 35.03, 34.87; MS (ES⁺) *m/z*: 428.33 [M + H]

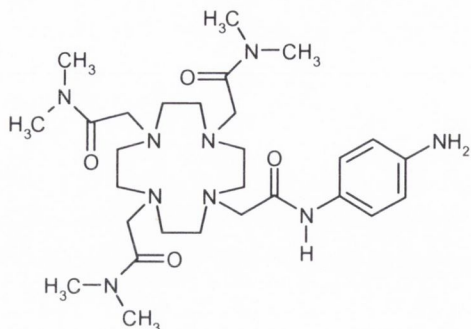
2-{4,7-bis-dimethylcarbamoylmethyl-10-[(4-nitro-phenylcarbamoyl)-methyl]-1,4,7,10-tetraaza-cyclododec-1-yl}-*N,N*-dimethyl-acetamide (68)



To a solution of **62** (0.28 g, 0.66 mmol) and **65** (0.16 g, 0.73 mmol) in CH₃CN (20 mL) was added KI (0.12 g, 0.73 mmol) and caesium carbonate (0.24 g, 0.73 mmol). The reaction mixture was stirred at 82°C under an argon atmosphere for 72 hours. The brown solution was filtered through celite and the solvent was removed under reduced

pressure. The brown residue was purified by alumina column chromatography under gradient elution conditions (CH₂Cl₂ to 20% CH₃OH). The desired product was collected as a brown solid after drying under vacuum (0.30 g, 74% yield). m.p. 79-80°C; Calculated for C₂₈H₄₈N₉O₆ *m/z* = 606.3734 [M + H]. Found *m/z* = 606.3728; ¹H NMR (400 MHz, CDCl₃, δ_H) 11.26 (s, 1H, NH), 8.17 (d, 2H, Ar-CH, *J* = 9.4 Hz), 8.05 (d, 2H, Ar-CH, *J* = 9.4 Hz), 2.93 – 2.85 (26H, CH₂CONCH₃), 2.70 – 2.00 (16H, Cyclen CH₂); ¹³C NMR (100 MHz, CDCl₃, δ_C) 171.81, 170.41, 170.21, 145.21, 142.11, 123.87, 119.04, 57.15, 54.64, 54.50, 53.04, 49.72, 35.75, 35.63, 35.22, 35.13; MS (ES⁺) *m/z*: 606.37 [M + H], 628.35 [M + Na]; IR (KBr) ν_{max} (cm⁻¹) 3434, 2966, 2821, 1648, 1554, 1504, 1174, 1104.

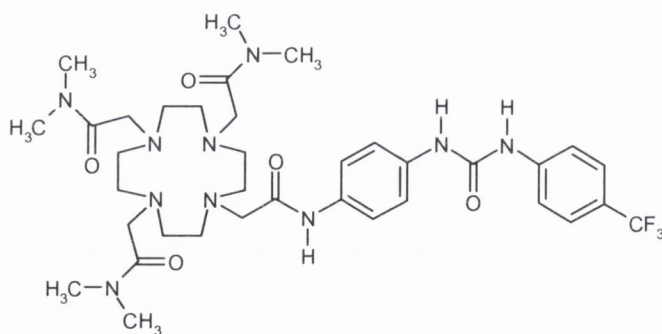
2-{4[(4-amino-phenylcarbamoyl)-methyl]-7,10-bis-dimethylcarbamoylmethyl-1,4,7,10-tetraaza-cyclododec-1-yl}-*N,N*-dimethyl-acetamide (69)



To a stirring solution of **68** (0.08 g, 0.13 mmol) and 10 % Pd/C catalyst in EtOH (3 mL), a solution of hydrazine monohydrate (0.05 g, 1.03 mmol) in EtOH (5 mL) was added dropwise. The reaction mixture was then heated under reflux overnight, under an argon atmosphere. The brown solution was filtered through celite and the solvent was

removed under reduced pressure to yield the product as a brown resin. The brown residue was purified by alumina column chromatography under gradient elution conditions (CH₂Cl₂ to 20% CH₃OH). The desired product was collected as a brown foam after drying under vacuum, which returned to a resin state over time (0.06 g, 88% yield). Calculated for C₂₈H₄₉N₉O₄Na *m/z* = 598.3805 [M + Na]. Found *m/z* = 598.3830; ¹H NMR (400 MHz, CDCl₃, δ_H) 10.07 (s, 1H, NH), 7.57 (d, 2H, Ar-H, *J* = 8.0 Hz), 6.54 (d, 2H, Ar-H, *J* = 8.5 Hz), 3.4 – 2.4 (m, 42H, CH₂CONCH₃ + CH₂ cyclen); ¹³C NMR (100 MHz, CDCl₃, δ_C) 170.97, 170.72, 169.80, 142.55, 130.74, 121.15, 114.93, 57.99, 54.95, 53.46, 52.42, 50.90, 36.25, 36.09, 35.65, 35.53; MS (ES⁺) *m/z*: 598.38 [M + Na]

2-(4,7-Bis-dimethylcarbamoylmethyl-10-{4-(3-*p*-tolyl-ureido)-phenylcarbamoyl}-methyl)-1,4,7,10-tetraaza-cyclododec-1-yl)-*N,N*-dimethyl-acetamide (61)

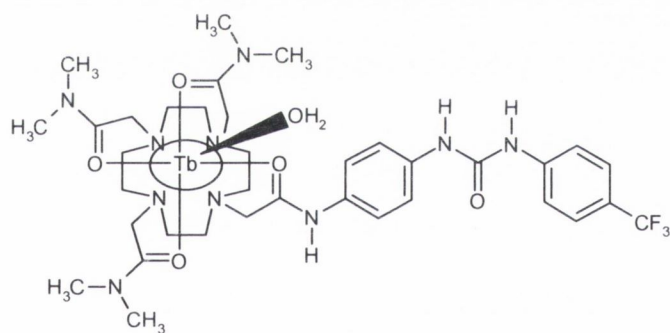


To a solution of **69** (0.15 g, 0.26 mmol) in CHCl₃ (7 mL) was added trifluoro-*p*-tolyl isocyanate (**70**) (0.05 g, 0.26 mmol). The reaction mixture was left stirring under an argon atmosphere at room temperature overnight. The solvent

was removed under reduced pressure to yield a pale brown residue. The residue was purified by alumina column chromatography under gradient elution conditions (CH₂Cl₂ to

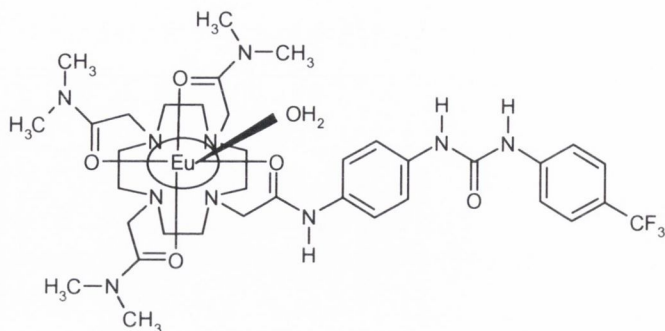
10% CH₃OH) to yield the desired product as a yellow solid (0.13 g, 67% yield). m.p. 187-189°C; Required for C₃₆H₅₄N₁₀O₅F₃·CH₂Cl₂·2H₂O: C, 50.28; H, 6.73; N, 15.85%; Found: C, 49.96; H, 6.32; N, 15.62 %; Calculated for C₃₆H₅₄N₁₀O₅F₃ $m/z = 763.4231$ [M + H]. Found $m/z = 763.4248$; ¹H NMR (400 MHz, CDCl₃, δ_H) 10.07 (br s, 1H, NH), 9.94 (br s, 1H, NH), 9.48 (br s, 1H, NH), 7.76 (d, 2H, Ar-CH, $J = 8.5$ Hz), 7.59 (d, 2H, Ar-CH, $J = 8.5$ Hz), 7.42 (m, 4H, Ar-CH), 7.35 (d, 2H Ar-CH, $J = 8.2$ Hz), 3 – 2 (m, 42H, CH₂CONCH₃, CH₂CONH, and CH₂ cyclen); ¹³C NMR (100 MHz, CDCl₃, δ_C) 170.47, 170.16, 169.48, 153.08, 143.30, 135.16, 133.13, 125.54, 125.27, 119.67, 118.40, 117.42, 57.50, 54.51, 54.31, 51.52, 50.36, 49.61, 36.04, 35.63, 35.49, 35.19, 35.02; ¹⁹F NMR (376 MHz, CDCl₃, δ_F) -61.88 (CF₃); MS (ES⁺) m/z : 763.42 [M + H]; IR ν_{max} (cm⁻¹) 3243, 2967, 2819, 1646, 1512, 1406, 1309, 1231, 1201, 1181, 1159, 1102, 1066, 1005, 951, 901, 842, 732.

Tb(III) complex of **61**, Tb.61



A solution of **61** (0.05 g, 0.07 mmol) and Tb(CF₃SO₃)₃ (0.04 g, 0.07 mmol) in CH₃CN (5 mL) was heated under reflux, under an argon atmosphere for 48 hours. The complex was isolated by precipitation from dry diethyl ether

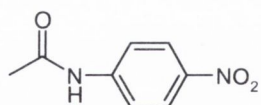
(200 mL) as a pale beige solid (0.07 g, 74% yield); Required for C₃₆H₅₄N₁₀O₅F₃·Tb·(CF₃SO₃)₃·H₂O·3CH₂Cl₂: C, 30.73; H, 3.74; N, 8.53%; Found: C, 30.17; H, 3.55; N, 8.91 %; Calculated for C₃₆H₅₂N₁₀O₅F₃Tb $m/z = 920.3228$ [M]. Found $m/z = 920.3286$; ¹H NMR (400 MHz, CD₃OD, δ_H) 75.92, 51.76, 47.91, 46.87, 40.93, 26.92, 24.70, 21.16, 11.17, 9.03, 7.29, 5.72; ¹⁹F NMR (376 MHz, CD₃OD, δ_F) -64.20 (CF₃), -79.85 (CF₃SO₃); MS (ES⁺) m/z : 460.16 [(M + H)/2], 920.32 [M]; IR ν_{max} (cm⁻¹) 3488, 3354, 2940, 1619, 1538, 1514, 1411, 1316, 1242, 1224, 1158, 1114, 1081, 1068, 1027, 957, 910, 842, 824, 758.

Eu(III) complex of 61, Eu.61

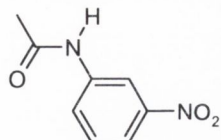
A solution of **16** (0.02 g, 0.02 mmol) and $\text{Eu}(\text{CF}_3\text{SO}_3)_3$ (0.01 g, 0.02 mmol) in CH_3CN (5 mL) was freeze thawed twice and left stirring at 82°C under an argon atmosphere for 48 hours. The complex was isolated by precipitation from dry diethyl ether (100 mL) as a hygroscopic solid (0.02 g, 68% yield); ^1H NMR (400 MHz, CD_3OD , δ_{H}) 31.32, 10.86, 7.73, 7.66, 6.93, 4.90, 3.32, 3.03, 1.40, 1.30, 0.93, -8.11; ^{19}F NMR (376 MHz, CD_3OD , δ_{F}) -63.81 (CF_3), -80.60 (CF_3SO_3); MS (ES^+) m/z : 457.03 [(M + H)/2], 531.99 [(M+trif)/2]; IR ν_{max} (cm^{-1}) 3293, 2928, 1617, 1538, 1513, 1410, 1317, 1242, 1224, 1157, 1112, 1081, 1067, 1027, 956, 909, 838, 822, 757.

6.5 Experimental details for Chapter 3**6.5.1 Procedure 1: General experimental procedure for compounds 77, 78, and 79**

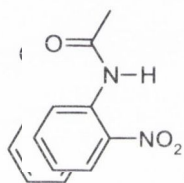
The relevant nitroaniline was placed into a small beaker and acetic anhydride was added. The solution was then stirred at room temperature overnight. The resulting precipitate was then filtered and washed twice with diethyl ether. The solid was collected and dried under vacuum.

N-(4-Nitro-phenyl)-acetamide (77)

77 was synthesised according to Procedure 1, using 4-nitroaniline (0.70 g, 5.07 mmol). The product was isolated as a pale beige solid (0.76 g, 83% yield). m.p. $208\text{--}210^\circ\text{C}$; ^1H NMR (400 MHz, $(\text{CD}_3)_2\text{CO}$, δ_{H}) 9.75 (br s, 1H, NH), 8.22 (d, 2H, CH, $J = 9.5$ Hz), 7.90 (d, 2H, CH, $J = 9.0$ Hz), 2.17 (s, 3H, CH_3); ^{13}C NMR (100 MHz, $(\text{CD}_3)_2\text{CO}$, δ_{C}) 168.43, 145.03, 142.28, 124.27, 118.06, 117.98, 23.11; IR ν_{max} (cm^{-1}) 3272, 3093, 1680, 1618, 1597, 1565, 1502, 1493, 1403, 1346, 1331, 1302, 1268, 1179, 1113, 1005, 966, 865, 848, 831, 749, 697, 687.

N-(3-Nitro-phenyl)-acetamide (78)

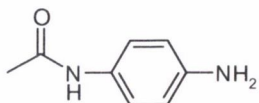
78 was synthesised according to Procedure 1, using 3-nitroaniline (0.68 g, 4.92 mmol). The product was isolated as a pale beige solid (0.50 g, 57% yield). m.p. 148-150 °C; ^1H NMR (400 MHz, CD_3OD , δ_{H}) 8.61 (s, 1H, CH), 7.94 (d, 1H, CH, $J = 8.0$ Hz), 7.85 (d, 1H, CH, $J = 7.4$ Hz), 7.54 (t, 1H, CH, $J = 8.5$ Hz, 8.0 Hz), 2.18 (s, 3H, CH_3); ^{13}C NMR (100 MHz, CD_3OD , δ_{C}) 170.13, 147.99, 139.45, 128.95, 124.39, 117.40, 113.33, 22.04; IR ν_{max} (cm^{-1}) 3289, 3260, 3192, 3129, 3096, 2861, 2809, 1671, 1598, 1547, 1525, 1476, 1424, 1368, 1348, 1324, 1293, 1276, 1260, 1162, 1077, 1016, 983, 885, 822, 804, 759, 737, 690, 669.

N,N-(2-Nitro-phenyl)-acetamide (79)

79 was synthesised according to Procedure 1, using 2-nitroaniline (0.51 g, 3.69 mmol). The product was isolated as a bright yellow solid (0.38 g, 57% yield). m.p. 89-91 °C; ^1H NMR (400 MHz, CDCl_3 , δ_{H}) 10.35 (br s, 1H, NH), 8.78 (d, 1H, CH, $J = 8.5$ Hz), 8.22 (d, 1H, CH, $J = 8.5$ Hz), 7.66 (t, 1H, CH, $J = 7.3$ Hz, 8.5 Hz), 7.20 (t, 1H, CH, $J = 7.3$ Hz, 8.3 Hz), 2.31 (s, 3H, CH_3); ^{13}C NMR (100 MHz, CDCl_3 , δ_{C}) 168.62, 135.82, 134.40, 135.54, 125.27, 122.77, 121.71, 25.20; IR ν_{max} (cm^{-1}) 3369, 3090, 1698, 1607, 1583, 1497, 1413, 1367, 1340, 1272, 1225, 1161, 1145, 1083, 1038, 999, 858, 834, 793, 788, 748, 705, 688.

6.5.2 Procedure 2: General experimental procedure for compounds 80, 81, and 82

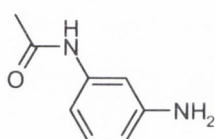
The relevant nitro acetamide was placed in a 25 mL RBF with the catalyst, 10% Pd/C and $\text{CH}_3\text{CH}_2\text{OH}$ was added. Hydrazine monohydrate was subsequently added and the reaction mixture was stirred at 95 °C overnight under an argon atmosphere. The mixture was filtered while hot, through celite, and the solvent removed under reduced pressure. The obtained solid was washed with diethyl ether. Once collected the solid was dried under vacuum.

N-(4-Amino-phenyl)-acetamide (80)

80 was synthesised according to Procedure 2, using N-(4-Nitro-phenyl)-acetamide (**77**) (0.60 g, 3.33 mmol), and hydrazine

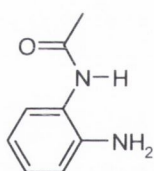
monohydrate (0.85 g, 26.6 mmol). The product was isolated as an off white solid (0.49 g, 98% yield). m.p. 155-157 °C; ^1H NMR (400 MHz, $(\text{CD}_3)_2\text{CO}$, δ_{H}) 8.80 (br s, 1H, NH), 7.33 (d, 2H, CH, $J = 8.5$ Hz), 6.61 (d, 2H, CH, $J = 9.04$ Hz), 4.43 (broad s, 2H, NH_2), 2.00 (s, 3H, CH_3); ^{13}C NMR (100 MHz, $(\text{CD}_3)_2\text{CO}$, δ_{C}) 166.58, 143.98, 129.27, 120.26, 113.73, 22.66

N-(3-Amino-phenyl)-acetamide (81)



81 was synthesised according to Procedure 2, using N-(3-Nitro-phenyl)-acetamide (**78**) (0.38 g, 2.11 mmol), and hydrazine monohydrate (0.54 g, 17.0 mmol). The product was isolated as a pale pink crystalline solid (0.16 g, 52% yield). m.p. 86-89 °C; ^1H NMR (400 MHz, CD_3OD , δ_{H}) 7.04 (d, 1H, CH, $J = 8.5$ Hz), 7.00 (s, 1H, CH), 6.80 (d, 1H, CH, $J = 8.0$ Hz), 6.48 (d, 1H, CH, $J = 8.0$ Hz), 2.09 (s, 3H, CH_3); ^{13}C NMR (100 MHz, CD_3OD , δ_{C}) 169.69, 147.42, 138.67, 128.44, 110.77, 109.32, 106.58, 22.00; IR ν_{max} (cm^{-1}) 3376, 3297, 3082, 1671, 1606, 1546, 1491, 1437, 1366, 1323, 1310, 1259, 1188, 1163, 1072, 1014, 966, 988, 847, 773, 687.

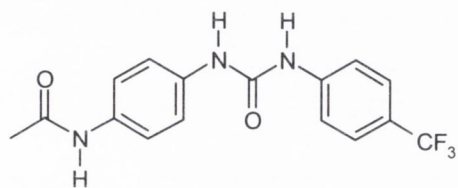
N-(2-Amino-phenyl)-acetamide (82)



82 was synthesised according to Procedure 2, using N-(2-Nitro-phenyl)-acetamide (**79**) (0.25 g, 1.39 mmol), and hydrazine monohydrate (0.36 g, 11.0 mmol). The product was isolated as an off white crystalline solid (0.21 g, 99% yield). m.p. 126-128 °C; ^1H NMR (400 MHz, CDCl_3 , δ_{H}) 7.09 (d, 1H, CH, $J = 7.5$ Hz), 7.03 (t, 1H, CH, $J = 7.5$ Hz), 6.85 (d, 1H, CH, $J = 7.5$ Hz), 6.72 (t, 1H, CH, $J = 7.5$ Hz), 2.16 (s, 3H, CH_3); ^{13}C NMR (100 MHz, CDCl_3 , δ_{C}) 170.39, 141.50, 126.45, 125.34, 123.16, 117.56, 116.58, 21.12; IR ν_{max} (cm^{-1}) 3455, 3363, 3271, 3046, 2927, 1638, 1586, 1533, 1496, 1456, 1369, 1299, 1255, 1219, 1156, 1138, 1042, 1012, 963, 924, 858, 847, 742.

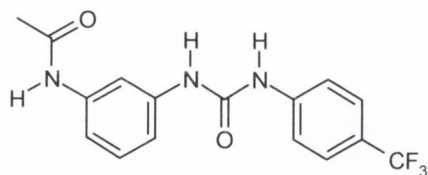
6.5.3 Procedure 3: General experimental procedure for compounds 71, 72, and 73

The relevant amino acetamide was placed in a 10 mL RBF and dissolved with CHCl_3 . Trifluoro-*p*-tolyl isocyanate (1.1 equivalents) was added and the solution was then stirred at room temperature overnight under an argon atmosphere. The resulting precipitate was filtered and washed with cold CHCl_3 . The obtained solid was then dried under vacuum.

N-{4-[3-(4-Trifluoromethyl-phenyl)-ureido]-phenyl}-acetamide (71)

71 was synthesised according to Procedure 3, using N-(4-Amino-phenyl)-acetamide (**80**) (0.20 g, 1.33 mmol), and trifluoro-*p*-tolyl isocyanate (0.27 g, 14.6 mmol). The product was isolated and recrystallised

from a mixture of $\text{CHCl}_3:\text{CH}_3\text{OH}$ to yield the pure compound as an off white solid (0.41 g, 90% yield). m.p. decomposes above 300 °C; Required for $\text{C}_{16}\text{H}_{14}\text{F}_3\text{N}_3\text{O}_2$: C, 56.97; H, 4.18; N, 12.46%; Found: C, 56.63; H, 4.12; N, 12.26 %; Calculated for $\text{C}_{16}\text{H}_{14}\text{N}_3\text{O}_2\text{F}_3\text{Na}$ $m/z = 360.0936$ [M + Na]. Found $m/z = 360.0939$; ^1H NMR (400 MHz, d_6 - $(\text{CD}_3)_2\text{SO}$, δ_{H}) 9.87 (br s, 1H, NH), 9.05 (br s, 1H, NH), 8.71 (s, 1H, NH), 7.64 (d, 4H, CH, $J = 9.0$ Hz), 7.50 (d, 2H, CH, $J = 9.0$ Hz), 7.38 (d, 2H, CH, = 9.0 Hz), 2.02 (s, 3H, CH_3); ^{13}C NMR (100 MHz, d_6 - $(\text{CD}_3)_2\text{SO}$, δ_{C}) 167.98, 152.31, 143.52, 134.45, 134.08, 126.08, 125.90, 119.64, 118.95, 117.75, 23.83; ^{19}F NMR (376 MHz, d_6 - $(\text{CD}_3)_2\text{SO}$, δ_{F}) -60.54 (CF_3); MS (ES^+) m/z : 360.09 [M + Na]; IR ν_{max} (cm^{-1}) 3330, 3275, 3144, 3089, 1693, 1647, 1605, 1546, 1512, 1403, 1318, 1303, 1242, 1214, 1185, 1162, 1102, 1066, 1015, 969, 839, 824, 788, 757, 670.

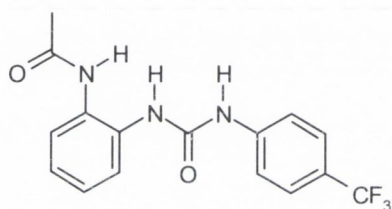
N-{3-[3-(4-Trifluoromethyl-phenyl)-ureido]-phenyl}-acetamide (72)

72 was synthesised according to Procedure 3, using N-(3-Amino-phenyl)-acetamide (**81**) (0.09 g, 0.57 mmol), and trifluoro-*p*-tolyl isocyanate (0.12 g, 0.62 mmol).

The product was isolated and recrystallised from a mixture of $\text{CH}_3\text{CN}:\text{H}_2\text{O}$ to yield the pure compound as an off white solid (0.13 g, 70% yield). m.p. 202-205 °C; Required for $\text{C}_{16}\text{H}_{14}\text{F}_3\text{N}_3\text{O}_2 \cdot \text{H}_2\text{O}$: C, 54.09; H, 4.54; N, 11.83%;

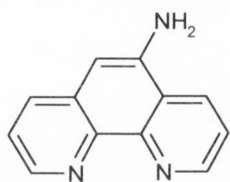
Found: C, 53.66; H, 4.40; N, 11.76%; Calculated for $C_{16}H_{14}N_3O_2F_3Na$ $m/z = 360.0936$ [M + Na]. Found $m/z = 360.0947$; 1H NMR (400 MHz, d_6 -(CD_3) $_2$ SO, δ_H) 9.95 (br s, 1H, NH), 9.04 (broad s, 1H, NH), 8.87 (br s, 1H, NH), 7.79 (s, 1H, CH), 7.65 (d, 4H, CH, $J = 9.0$ Hz), 7.20 (m, 3H, CH), 2.04 (s, 3H, CH_3); ^{13}C NMR (100 MHz, d_6 -(CD_3) $_2$ SO, δ_C) 168.36, 152.16, 143.45, 139.80, 139.57, 128.99, 126.11, 126.07, 125.90, 123.22, 121.86, 121.55, 117.75, 113.01, 112.94, 108.95, 24.04; ^{19}F NMR (376 MHz, d_6 -(CD_3) $_2$ SO, δ_F) -60.56 (CF_3); MS (ES^+) m/z : 338.13 [M + H], 360.09 [M + Na]; IR ν_{max} (cm^{-1}) 3299, 1640, 1599, 1545, 1441, 1408, 1327, 1292, 1222, 1165, 1128, 1107, 1067, 1016, 964, 880, 841, 779, 750, 690.

N-{2-[3-(4-Trifluoromethyl-phenyl)-ureido]-phenyl}-acetamide (73)

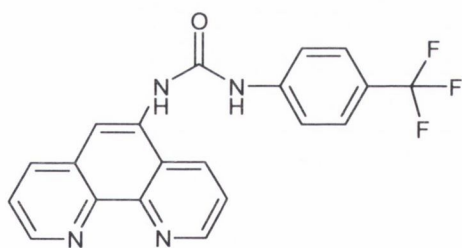


73 was synthesised according to Procedure 3, using N-(2-Amino-phenyl)-acetamide (**82**) (0.08 g, 0.53 mmol), and trifluoro-*p*-tolyl isocyanate (0.10 g, 0.54 mmol). The product was isolated and recrystallised from a mixture of $CHCl_3:CH_3OH$ to yield the pure compound as a white solid (0.16 g, 88% yield). m.p. 204-206 °C; Required for $C_{16}H_{14}F_3N_3O_2 \cdot 1/4CHCl_3$: C, 53.16; H, 3.91; N, 11.44%; Found: C, 53.50; H, 3.88; N, 11.54%; Calculated for $C_{16}H_{14}N_3O_2F_3Na$ $m/z = 360.0936$ [M + Na]. Found $m/z = 360.0940$; 1H NMR (400 MHz, d_6 -(CD_3) $_2$ SO, δ_H) 9.68 (s, 1H, NH), 9.66 (s, 1H, NH), 7.99 (s, 1H, NH), 7.81 (d, 1H, CH, $J = 8.5$ Hz), 7.66 (d, 4H, CH, $J = 8.5$ Hz), 7.26 (d, 1H, CH, $J = 8.0$ Hz), 7.19 (t, 1H, CH, $J = 7.5$ Hz, 8.0 Hz), 7.06 (t, 1H, CH, $J = 8.0$ Hz, 7.5 Hz), 2.11 (s, 3H, CH_3); ^{13}C NMR (100 MHz, d_6 -(CD_3) $_2$ SO, δ_C) 169.26, 152.44, 143.64, 133.18, 128.70, 121.79, 121.47, 126.09, 125.92, 125.82, 123.23, 122.85, 117.72, 23.29; ^{19}F NMR (376 MHz, d_6 -(CD_3) $_2$ SO, δ_F) -60.54 (CF_3); MS (ES^+) m/z : 360.09 [M + Na]; IR ν_{max} (cm^{-1}) 3253, 3188, 3123, 3053, 1678, 1649, 1605, 1542, 1503, 1475, 1440, 1408, 1316, 1248, 1165, 1108, 1067, 1042, 1015, 969, 951, 849, 821, 746, 673.

6.6 Synthetic procedures for Chapter 4 and Chapter 5

[1,10]Phenanthrolin-5-ylamine (89)

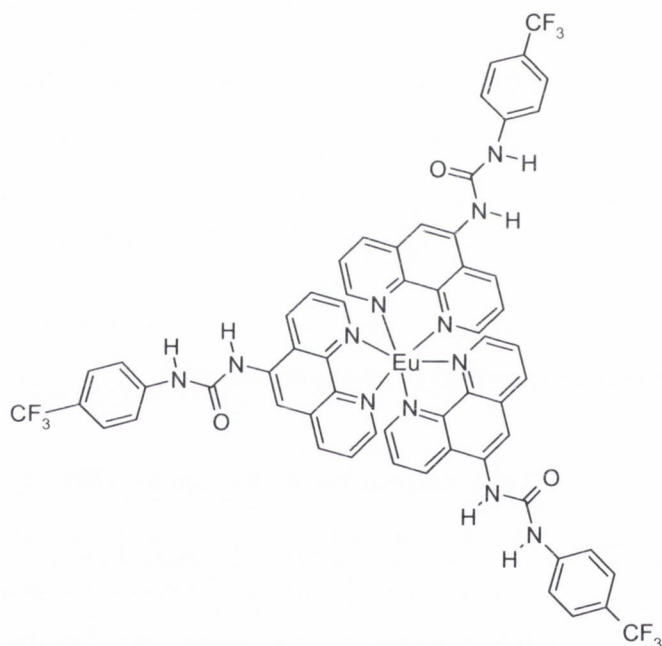
To a solution of 5-nitro-1,10-phenanthroline (2.0 g, 8.88 mmol) in EtOH (50mL) was added Pd/C. To this, a solution of hydrazine monohydrate (1.38 mL, 0.04 mol) in EtOH (10 mL) was added dropwise. The reaction mixture was stirred at 95°C overnight under an argon atmosphere. The mixture was filtered, while hot, through celite to yield a yellow solution. The solvent was then removed under reduced pressure to yield a yellow solid. This solid was washed twice with diethyl ether to yield a pale yellow solid (1.60 g, 92% yield). m.p. 248-250°C (lit. m.p. 245-246°C)²⁵⁰ Calculated for C₁₂H₁₀N₃ $m/z = 196.0875$ [M + H]. Found $m/z = 196.0880$. ¹H NMR (400 MHz, *d*₆-(CD₃)₂SO, δ_{H}): 9.06 (d, 1H, CH, $J = 4.0$ Hz), 8.69 (m, 2H, CH), 8.04 (d, 1H, CH, $J = 8.0$ Hz), 7.74 (dd, 1H, CH, $J = 4.0$ Hz), 7.50 (dd, 1H, CH, $J = 4.5$ Hz), 6.89 (s, 1H, CH), 6.19 (s, 2H, NH₂); ¹³C NMR (100 MHz, *d*₆-(CD₃)₂SO, δ_{C}): 149.37, 146.16, 144.83, 142.71, 140.47, 132.74, 130.88, 130.59, 123.23, 122.09, 121.83, 101.76; MS (ES⁺) $m/z = 196.09$ [M + H]; IR ν_{max} (cm⁻¹) 3415, 3319, 3217, 1635, 1610, 1593, 1562, 1505, 1488, 1455, 1427, 1406, 1303, 1127, 1107, 1034, 884, 841, 825, 812, 739, 710, 661.

1-[1,10]Phenanthrolin-5-yl-3-(4-trifluoromethyl-phenyl)-urea (87)

To a suspension of the amine (89) (1.0 g, 5.12 mmol) in CHCl₃ (40 mL) trifluoro-*p*-tolyl isocyanate (0.79 mL, 5.63 mmol) was added. After five minutes all the amine was dissolved, and a dark yellow solution was observed. The reaction mixture was stirred overnight at room temperature, under an argon atmosphere. An off white precipitate was observed on the reaction vessel. This precipitate was filtered and washed with cold CHCl₃. The obtained solid was recrystallised from MeOH to yield a pale solid (1.38 g, 88% yield). m.p. decomposes above 290°C; Calculated for C₂₀H₁₄N₄OF₃ $m/z = 383.1120$ [M + H]. Found $m/z = 383.1107$. ¹H NMR (400 MHz, *d*₆-(CD₃)₂SO, δ_{H}): 9.55 (br s, 1H, NH), 9.16 (d, 1H, *phen*-CH, $J = 4.0$ Hz), 9.12 (br s, 1H, NH), 9.00 (d, 1H, *phen*-

CH, $J = 4.0$ Hz), 8.65 (d, 1H, *phen*-CH, $J = 8.5$ Hz), 8.43 (d, 1H, *phen*-CH, $J = 8.0$ Hz), 8.39 (s, 1H, *phen*-CH), 7.89 (dd, 1H, *phen*-CH, $J = 4.0$ Hz, $J = 4.0$ Hz), 7.72 (m, 5H, *phen*-CH + Ar-CH); ^{13}C NMR (100 MHz, d_6 -(CD_3) $_2\text{SO}$, δ_{C}): 152.87, 149.87, 148.74, 145.89, 143.34, 143.13, 135.61, 132.08, 130.44, 128.50, 126.25, 126.22, 123.77, 123.68, 122.95, 122.21, 118.01, 116.07; ^{19}F NMR (376 MHz, d_6 -(CD_3) $_2\text{SO}$, δ_{F}): -60.58 (CF_3); MS (ES^+) $m/z = 383.11$ (M + H). IR ν_{max} (cm^{-1}) 3394, 3284, 3211, 3089, 1711, 1613, 1563, 1505, 1472, 1411, 1377, 1329, 1310, 1270, 1202, 1162, 1153, 1108, 1097, 1066, 1017, 988, 945, 878, 848, 826, 803, 737, 711, 691.

Europium complex of **87**, Eu:87₃



To a suspension of the urea (**87**) (0.10 g, 0.26 mmol) in CH_3CN (20 mL) was added $\text{Eu}(\text{CF}_3\text{SO}_3)_3$ (0.06 g, 0.11 mmol). Within few minutes a clear yellow solution was observed. The reaction mixture was stirred overnight, at room temperature under an argon atmosphere. The precipitate was isolated by filtration, and dried under vacuum to produce a bright yellow solid in (0.13 g, 28% yield). ^1H NMR (600 MHz,

d_6 -(CD_3) $_2\text{SO}$, δ_{H}): 9.52 (s, 1H, NH), 9.15 (br s, 1H, *phen*-CH), 9.10 (s, 1H, NH), 8.98 (br s, 1H, *phen*-CH), 8.64 (d, 1H, *phen*-CH, $J = 8.6$ Hz), 8.43 (d, 1H, *phen*-CH, $J = 7.6$ Hz), 8.35 (s, 1H, *phen*-CH), 7.88 (br s, 1H, *phen*-CH), 7.74 (d, 2H, Ar-CH, $J = 8.6$ Hz), 7.70 (br s, 1H, *phen*-CH), 7.69 (d, 2H, Ar-CH, $J = 8.6$ Hz); ^{19}F NMR (376 MHz, d_6 -(CD_3) $_2\text{SO}$, δ_{F}): -60.56 (CF_3), -78.29 (CF_3SO_3); MS (ES^+) $m/z = 558.00$ [(M-2*phen* ligands) + Na] 648.95 [M/2], 684.91 [(M/2) + 2 H_2O].; IR ν_{max} (cm^{-1}) 3334, 1656, 1605, 1542, 1412, 1314, 1223, 1160, 1107, 1066, 1026, 844, 808, 733, 719, 695.

General Conclusion

General Conclusion

The work described in this Thesis accounts for the synthesis, characterisation and photophysical evaluation of novel sensors for anions. Detailed analysis of the binding interactions between such sensors and various anions were carried out through spectrophotometric measurements. Furthermore, binding constants for such binding interactions were determined using the non-linear least-squares regression program SPECFIT. In order to further corroborate the obtained results, other techniques will be pursued in the future. Techniques such as $^1\text{H-NMR}$, $^{31}\text{P-NMR}$, detailed lifetime measurements and computational studies would definitely contribute to further substantiate as well as to better understand the results presented and discussed herein.

In Chapter 2, a novel cyclen based lanthanide luminescent sensor (**Tb.61**) has been developed by taking advantage of a combination of hydrogen bonding and *f*-metal ion coordination binding sites for anionic species. This sensor was found to display good selectivity for H_2PO_4^- over other competitive anions such as CH_3COO^- . Analysis of the data gathered from the experimental procedures clearly showed the ability of the Tb(III) complex to signal the presence of anions in CH_3CN , through multiple binding interactions. Amongst the techniques mentioned above, although at much higher concentrations, $^{31}\text{P-NMR}$ titrations would potentially help to clarify the binding interactions between **Tb.61** and H_2PO_4^- . However for the remaining anions, analysis using NMR ($^1\text{H-NMR}$ titrations) are expected to be difficult due to the presence of the paramagnetic metal ion. Lanthanide lifetime measurements would be one of the best methods to corroborate the hypothesis presented for the direct binding of the anions to the Tb(III) centre, by displacement of solvent molecules. Nevertheless, the experimental procedure would have to be carried out in water or protic solvents in order to be able to calculate the number of bound water molecules (q), in the absence and presence of the anions. It should, however, be taken in consideration that the use of another solvent would potentially lead to different results, due to possible hydrogen bonding interactions between the sensor and the protic solvents.

Chapter 3 describes the synthesis of three new structurally simple anion receptors, **71-73**, based on the use of combined aryl amide and urea moieties as hydrogen bonding sites. These receptors differ only in the relative position of the amide moiety to that of the urea

functionality. This simple modification was shown to play a major role in the binding interactions of the various anions to these receptors. For these structurally simple receptors, $^1\text{H-NMR}$ titrations upon addition of anions are expected to further elucidate the binding mechanisms. An additional method for acquiring further information would be to take advantage of computational studies, such as DFT calculations, which are being carried out at present.

The development of a *phen* based heteroditopic receptor (**87**) has been reported in Chapter 4. The ability of such urea functionalised receptor to work as a selective fluorescent sensor for chloride in CH_3CN was demonstrated. Such receptor was also shown to bind strongly with transition metals such as Cu(II) and Fe(II) , giving rise to the formation of the 1:2 (metal:receptor) stoichiometry. The metal was found to induce enhancements in the anion binding affinity, resulting in higher binding constants than those observed for the simple urea based receptor. As already mentioned above, $^1\text{H-NMR}$ titrations would give valuable additional information regarding the binding process between the sensor and the anions studied.

Chapter 5 discusses the formation, characterisation, and photophysical studies of a novel supramolecular self-assembly complex (**Eu:87₃**), between Eu(III) and the *phen* based heteroditopic receptor. The lanthanide luminescence of the Eu(III) was 'switched on' in the presence of **87**, establishing the sensitization of the metal ion by this receptor. Furthermore, it was demonstrated that the luminescence intensity of the novel self-assembly system **Eu:87₃** changes dramatically in the presence of anions, which provides the possibility to employ this complex as a luminescent sensor for anions. Although, the mechanism through which the anions are interacting with **Eu:87₃** is yet not clear, the most probable path is likely to be the dissociation of the complex due to the displacement of the ligand molecules by the anions. To further enlighten the mechanism through which the anions bind to this system, lanthanide lifetime measurements (as described above for Chapter 2) would be expected to provide very useful information.

References

References

- (1) Steed, J. W.; Atwood, J. L. *Supramolecular Chemistry*; John Wiley & Sons Ltd: Chichester, England, 2000.
- (2) Lehn, J.-M. *Angew. Chem. Int. Ed.* **1988**, *27*, 89-112.
- (3) Czarnik, A. W. *Acc. Chem. Res.* **1994**, *27*, 302-308.
- (4) de Silva, A. P.; Gunaratne, H. Q. N.; Gunnlaugsson, T.; Huxley, A. J. M.; McCoy, C. P.; Rademacher, J. T.; Rice, T. E. *Coord. Chem. Rev.* **1997**, *97*, 1515-1566.
- (5) de Silva, A. P.; Fox, D. B.; Huxley, A. J. M.; Moody, T. S. *Coord. Chem. Rev.* **2000**, *205*, 41-57.
- (6) Fabbrizzi, L. In *Encyclopedia of Supramolecular Chemistry*; Atwood, J. L., Steed, J. W., Eds.; Marcel Dekker, Inc.: New York, 2004; Vol. 2, pp 1053-1059.
- (7) Bissel, R. A.; de Silva, A. P.; Gunaratne, H. Q. N.; Lynch, P. L. M.; Maguire, G. E. M.; McCoy, C. P.; Sandanayake, K. R. A. S. *Top. Curr. Chem.* **1993**, *168*, 223-264.
- (8) de Silva, A. P.; Gunaratne, H. Q. N.; Gunnlaugsson, T. *Tetrahedron Lett.* **1998**, *39*, 5077-5080.
- (9) Bianchi, A.; Bowman-James, K.; Garcia-Espana, E. *Supramolecular Chemistry of Anions*; Wiley-VCH: New York, 1997.
- (10) Mason, C. F. *Biology of Freshwater Pollution*; 2nd ed.; Longman: New York, 1991.
- (11) Gale, P. A. *Chem. Rev.* **2000**, *199*, 181-233.
- (12) Gale, P. A. *Coord. Chem. Rev.* **2001**, *213*, 79-128.
- (13) Beer, P. D.; Gale, P. A. *Angew. Chem. Int. Ed.* **2001**, *40*, 486-516.
- (14) Martinez-Manez, R.; Sancenon, F. *Chem. Rev.* **2003**, *103*, 4419-4476.
- (15) Martinez-Manez, R.; Sancenon, F. *Journal of Fluorescence* **2005**, *15*, 267-285.
- (16) Pedersen, C. J. *J. Am. Chem. Soc.* **1967**, *89*, 7017-7036.
- (17) Park, C. H.; Simmons, H. E. *J. Am. Chem. Soc.* **1968**, *90*, 2431-2432.
- (18) Graf, E.; Lehn, J.-M. *J. Am. Chem. Soc.* **1976**, *98*, 6403-6405.
- (19) Graf, E.; Lehn, J.-M. *J. Am. Chem. Soc.* **1975**, *97*, 5022-5024.
- (20) Sessler, J. L.; Gale, P. A.; Cho, W.-S. *Anion receptor chemistry*; Royal Society of Chemistry: Cambridge, UK, 2006.
- (21) Gunnlaugsson, T.; Ali, H. D. P.; Glynn, M.; Kruger, P. E.; Hussey, G. M.; Pfeffer, F. M.; dos Santos, C. M. G.; Tierney, J. *Journal of Fluorescence* **2005**, *15*, 287-299.
- (22) Schmidtchen, F. P.; Berger, M. *Chem. Rev.* **1997**, *97*, 1609-1646.
- (23) Gale, P. A.; Quesada, R. *Coord. Chem. Rev.* **2006**, *250*, 3219-3244.
- (24) Bondy, C. R.; Loeb, S. J. *Coord. Chem. Rev.* **2003**, *240*, 77-97.
- (25) Choi, K.; Hamilton, A. D. *Coord. Chem. Rev.* **2003**, *240*, 101-110.
- (26) Gale, P. A. In *Encyclopedia of supramolecular chemistry*; Atwood, J. L., Steed, J. W., Eds.; M. Dekker: New York, 2004, pp 31-40.
- (27) Gale, P. A. *Acc. Chem. Res.* **2006**, *39*, 465-475.
- (28) Hay, B. P.; Firman, T. K.; Moyer, B. A. *J. Am. Chem. Soc.* **2005**, *127*, 1810-1819.
- (29) Gunnlaugsson, T.; Glynn, M.; Tocci (nee Hussey), G. M.; Kruger, P. E.; Pfeffer, F. M. *Coord. Chem. Rev.* **2006**, *250*, 3094-3117.
- (30) Sessler, J. L.; Camiolo, S.; Gale, P. A. *Coord. Chem. Rev.* **2003**, *240*, 17-55.
- (31) Beer, P. D.; Hayes, E. J. *Coord. Chem. Rev.* **2003**, *240*, 167-189.
- (32) Best, M. D.; Tobey, S. L.; Anslyn, E. V. *Coord. Chem. Rev.* **2003**, *240*, 3-15.
- (33) Blondeau, P.; Segura, M.; Pérez-Fernández, R.; de Mendoza, J. *Chem. Soc. Rev.* **2007**, *36*, 198-210.

- (34) Llinares, J. M.; Powell, D. H.; Bowman-James, K. *Coord. Chem. Rev.* **2003**, *240*, 57-75.
- (35) Gilbert, A.; Baggot, J. *Essentials of Molecular Photochemistry*; CRC. Press: London, 1991.
- (36) Turro, N. J. *Modern Molecular Photochemistry*; Universal Science Books: Sausalito California, 1991.
- (37) Kavarnos, G. J.; Turro, N. J. *Chem. Rev.* **1986**, *86*, 401-449.
- (38) Czarnik, A. W. *Fluorescent Chemosensors for Ion and Molecular Recognition*; ACS Books: Washington, DC, 1993.
- (39) Desvergne, J. P.; Czarnik, A. W. *Chemosensors of Ion and Molecular Recognition*; Kluwer Academic: Dordrecht, 1997.
- (40) Huston, M. E.; Akkaya, E. U.; Czarnik, A. W. *J. Am. Chem. Soc.* **1989**, *111*, 8735-8737.
- (41) Vance, D. H.; Czarnik, A. W. *J. Am. Chem. Soc.* **1994**, *116*, 9397-9398.
- (42) Gunnlaugsson, T.; Davis, A. P.; Glynn, M. *Chem. Commun.* **2001**, 2556-2557.
- (43) Gunnlaugsson, T.; Davis, A. P.; Hussey, G. M.; Tierney, J.; Glynn, M. *Org. Biomol. Chem.* **2004**, *2*, 1856 - 1863.
- (44) Gunnlaugsson, T.; Davis, A. P.; O'Brien, J. E.; Glynn, M. *Org. Lett.* **2002**, *4*, 2449-2452.
- (45) Kim, S. K.; Yoon, J. *Chem. Commun.* **2002**, 770-771.
- (46) Kwon, J. Y.; Jang, Y. J.; Kim, S. K.; Lee, K.-H.; Kim, J. S.; Yoon, J. *J. Org. Chem.* **2004**, *69*, 5155-5157.
- (47) Xu, G.; Tarr, M. A. *Chem. Commun.* **2004**, 1050 - 1051.
- (48) Cho, E. J.; Moon, J. W.; Ko, S. W.; Lee, J. Y.; Kim, S. K.; Yoon, J.; Nam, K. C. *J. Am. Chem. Soc.* **2003**, *125*, 12376-12377.
- (49) Lee, J. Y.; Cho, E. J.; Mukamel, S.; Nam, K. C. *J. Org. Chem.* **2004**, *69*, 943-950.
- (50) Gunnlaugsson, T.; Kruger, P. E.; Lee, T. C.; Parkesh, R.; Pfeffer, F. M.; Hussey, G. M. *Tetrahedron Lett.* **2003**, *44*, 6575-6578.
- (51) Parker, D.; Williams, J. A. G. *J. Chem. Soc., Dalton Trans.* **1996**, 3613 - 3628.
- (52) Parker, D. *Coord. Chem. Rev.* **2000**, *205*, 109-130.
- (53) *Frontiers in Lanthanide Chemistry Chem. Rev.* **2002**, *102*, 1807-2476.
- (54) Piguet, C.; Bunzli, J.-C. G. *Chem. Soc. Rev.* **1999**, *28*, 347-358.
- (55) Faulkner, S.; Pope, S. J. A.; Burton-Pye, B. P. *Appl. Spectr. Rev.* **2005**, *40*, 1-31.
- (56) Bunzli, J.-C. G. *Acc. Chem. Res.* **2006**, *39*, 53-61.
- (57) Sabbatini, N.; Guardigli, M. *Coord. Chem. Rev.* **1993**, *123*, 201-228.
- (58) Bunzli, J.-C. G.; Piguet, C. *Chem. Soc. Rev.* **2005**, *34*, 1048-1077.
- (59) Parker, D.; Williams, J. A. G. *J. Chem. Soc., Perkin Trans. 2* **1996**, 1581-1586.
- (60) Parker, D.; Senanayake, P. K.; Williams, J. A. G. *J. Chem. Soc., Perkin Trans. 2* **1998**, 2129 - 2140.
- (61) Parker, D.; Williams, J. A. G. In *Metal Ions in Biological Systems: the lanthanides and their interrelations with biosystems*; Sigel, A., Siegel, H., Eds.; Marcel Dekker Inc.: New York, 2003; Vol. 40, pp 233-280.
- (62) Bunzli, J.-C. G.; Puiguet, C. *Chem. Rev.* **2002**, *102*, 1897-1928.
- (63) Bunzli, J.-C. G. *J. Alloys and Compounds* **2006**, *408-412*, 934-944.
- (64) Forster, T. H. *Discuss. Faraday Soc.* **1959**, *27*, 7-17.
- (65) Dexter, D. L. *J. Chem. Phys.* **1953**, *215*, 836-850.

- (66) Faulkner, S.; Matthews, J. L. In *Comprehensive Coordination Chemistry*; 2 ed.; Ward, M. D., Ed.; Elsevier: Oxford, 2004; Vol. 9, pp 1-32.
- (67) Gunnlaugsson, T.; Leonard, J. P. *Chem. Commun.* **2005**, 3114-3131.
- (68) Beeby, A.; Clarkson, I. M.; Dickins, R. S.; Faulkner, S.; Parker, D.; Royle, L.; de Sousa, A. S.; Williams, J. A. G.; Woods, M. J. *Chem. Soc., Perkin Trans. 2* **1999**, 493-503.
- (69) Parker, D. *Chem. Soc. Rev.* **2004**, *33*, 156-165.
- (70) Kropp, J. L.; Windsor, M. W. *J. Chem. Phys.* **1965**, *42*, 1599-1609.
- (71) Horrocks, W. D.; Sudnick, D. R. *J. Am. Chem. Soc.* **1979**, *101*, 334.
- (72) Horrocks, W. D.; Sudnick, D. R. *Acc. Chem. Res.* **1981**, *14*, 384-392.
- (73) Supkowski, R. M.; Horrocks, W. D. *Inorg. Chim. Acta* **2002**, *340*, 44-48.
- (74) Beeby, A.; Dickins, R. S.; Faulkner, S.; Parker, D.; Williams, J. A. G. *Chem. Commun.* **1997**, 1401-1402.
- (75) Caravan, P.; Ellison, J. J.; McMurry, T. J.; Lauffer, R. B. *Chem. Rev.* **1999**, *99*, 2293-2352.
- (76) Franklin, S. J. *Curr. Opin. Chem. Biol.* **2001**, *5*, 201-208.
- (77) Lauffer, R. B. *Chem. Rev.* **1987**, *87*, 901-927.
- (78) Toth, E.; Burai, L.; Merbach, A. E. *Coord. Chem. Rev.* **2001**, *216-217*, 363-382.
- (79) Balzani, V.; Berghmans, E.; Lehn, J.-M.; Sabbatini, N.; Terörde, R.; Ziessel, R. *Helv. Chim. Acta* **1990**, *73*, 2083-2089.
- (80) Pietraszkiewicz, M. *Comprehensive Supramolecular Chemistry* **1996**, *10*, 225-266.
- (81) Parker, D.; Dickins, R. S.; Puschmann, H.; Crossland, C.; Howard, J. A. *Chem. Rev.* **2002**, *102*, 1977-2010.
- (82) Zucchi, G.; Ferrand, A.-C.; Scopelliti, R.; Bunzli, J.-C. G. *Inorg. Chem.* **2002**, *41*, 2459-2465.
- (83) Beeby, A.; Bushby, L. M.; Maffeo, D.; Williams, J. A. G. *J. Chem. Soc., Perkin Trans. 2* **2000**, 1281 - 1283.
- (84) Dadabhoy, A.; Faulkner, S.; Sammes, P. G. *J. Chem. Soc., Perkin Trans. 2* **2002**, 348-357.
- (85) Quici, S.; Marzanni, G.; Cavazzini, M.; Anelli, P. L.; Botta, M.; Gianolio, E.; Accorsi, G.; Armaroli, N.; Barigelletti, F. *Inorg. Chem.* **2002**, *41*, 2777-2784.
- (86) Gunnlaugsson, T.; Harte, A. J.; Leonard, J. P.; Nieuwenhuyzen, M. *Supramolecular Chemistry* **2003**, *15*, 505-519.
- (87) Gunnlaugsson, T.; Harte, A. J.; Leonard, J. P.; Nieuwenhuyzen, M. *Chem. Commun.* **2002**, 2134 - 2135.
- (88) Shinoda, S.; Miyake, H.; Tsukube, H. In *Handbook on the physics and chemistry of rare earths*; Elsevier, 2005; Vol. 35, pp 273-335.
- (89) Dickins, R. S.; Gunnlaugsson, T.; Parker, D.; Peacock, R. D. *Chem. Commun.* **1998**, 1643 - 1644.
- (90) Wang, E.; Meyerhoff, M. E. *Anal. Chim. Acta* **1993**, *283*, 673-682.
- (91) Vasseur, M.; Frangne, R.; Alvarado, F. *Am. J. Physiol.* **1993**, *264*, C27-C31.
- (92) Bretonnière, Y.; Cann, M. J.; Parker, D.; Slater, R. *Chem. Commun.* **2002**, 1930 - 1931.
- (93) Bretonnière, Y.; Cann, M. J.; Parker, D.; Slater, R. *Org. Biomol. Chem.* **2004**, *2*, 1624 - 1632.
- (94) Atkinson, P.; Bretonnière, Y.; Parker, D. *Chem. Commun.* **2004**, 438 - 439.

- (95) Bruce, J. I.; Dickins, R. S.; Govenlock, L. J.; Gunnlaugsson, T.; Lopinski, S.; Lowe, M. P.; Parker, D.; Peacock, R. D.; Perry, J. J. B.; Aime, S.; Botta, M. *J. Am. Chem. Soc.* **2000**, *122*, 9674-9684.
- (96) Faulkner, S.; Burton-Pye, B. P.; Khan, T.; Martin, L. R.; Wray, S. D.; Skabara, P. J. *Chem. Commun.* **2002**, 1668 - 1669.
- (97) Faulkner, S.; Carrie, M.-C.; Pope, S. J. A.; Squire, J.; Beeby, A.; Sammes, P. G. *Dalton Trans.* **2004**, 1405-1409.
- (98) Pope, S. J. A.; Coe, B. J.; Faulkner, S.; Bichenkova, E. V.; Yu, X.; Douglas, K. T. *J. Am. Chem. Soc.* **2004**, *126*, 9490-9491.
- (99) Li, C.; Wong, W.-T. *Tetrahedron Letters* **2004**, *45*, 6055-6058.
- (100) Pope, S. J. A.; Kenwright, A. M.; Boote, V. A.; Faulkner, S. *Dalton Trans.* **2003**, 3780 - 3784.
- (101) Harte, A. J.; Jensen, P.; Plush, S. E.; Kruger, P. E.; Gunnlaugsson, T. *Inorg. Chem.* **2006**, *45*, 9465-9474.
- (102) Plush, S. E.; Gunnlaugsson, T. *Org. Lett.* **2007**, *9*, 1919-1922.
- (103) Mateos-Timoneda, M. A.; Kerckhoffs, J. M. C. A.; Crego-Calama, M.; Reinhoudt, D. N. *Angew. Chem. Int. Ed.* **2005**, *44*, 3248-3253.
- (104) Kirkovits, G. J.; Shriver, J. A.; Gale, P. A.; Sessler, J. L. *Journal of Inclusion Phenomena and Macrocyclic Chemistry* **2001**, *41*, 69-75.
- (105) Reetz, M. T. In *Comprehensive Supramolecular Chemistry*; Atwood, L., Davies, J. E. D., MacNicol, D. D., Vogtle, F., Eds.; Pergamon: Oxford, 1996; Vol. 2, pp 553-562.
- (106) Beer, P. D.; Stokes, S. E. *Polyhedron* **1995**, *14*, 2631-2635.
- (107) Kovbasyuk, L.; Kramer, R. *Chem. Rev.* **2004**, *104*, 3161-3187.
- (108) Reetz, M. T.; Niemeyer, C. M.; Harms, K. *Angew. Chem., Int. Ed. Engl.* **1991**, *30*, 1472-1474.
- (109) Reetz, M. T.; Johnson, B. M.; Harms, K. *Tetrahedron Lett.* **1994**, *35*, 2525-2528.
- (110) Rudkevich, D. M.; Brzozka, Z.; Palys, M.; Visser, H. C.; Verboom, W.; Reinhoudt, D. N. *Angew. Chem., Int. Ed. Engl.* **1994**, *33*, 467-468.
- (111) Rudkevich, D. M.; Mercer-Chalmers, J. D.; Verboom, W.; Ungarro, R.; de Jong, F.; Reinhoudt, D. N. *J. Am. Chem. Soc.* **1995**, *117*, 6124-6125.
- (112) Rudkevich, D. M.; Stauthamer, W. P. R. V.; Verboom, W.; Engbersen, J. F. J.; Harkema, S.; Reinhoudt, D. N. *J. Am. Chem. Soc.* **1992**, *114*, 9671-9673.
- (113) Schreeder, J.; van Duynhoven, J. P. M.; Engbersen, J. F. J.; Reinhoudt, D. N. *Angew. Chem. Int. Ed.* **1996**, *35*, 1090-1093.
- (114) Beer, P. D.; Drew, M. G. B.; Knubley, R. J.; Ogden, M. I. *J. Chem. Soc., Dalton Trans.* **1995**, 3117 - 3123.
- (115) Evans, A. J.; Beer, P. D. *Dalton Trans.* **2003**, 4451-4456.
- (116) Beer, P. D.; Graydon, A. R. *J. Organomet. Chem.* **1994**, *466*, 241-247.
- (117) Beer, P. D.; Dent, S. W. *Chem. Commun.* **1998**, 825 - 826.
- (118) Cooper, J. B.; Drew, M. G. B.; Beer, P. D. *J. Chem. Soc., Dalton Trans.* **2001**, 392 - 401.
- (119) Nishizawa, S.; Shigemori, K.; Teramae, N. *Chem. Lett.* **1999**, 1185-1186.
- (120) Beer, P. D.; Hopkins, P. K.; McKinney, J. D. *Chem. Commun.* **1999**, 1253 - 1254.
- (121) Gunning, P. T. *Org. Biomol. Chem.* **2005**, *3*, 3877-3879.

- (122) Cooper, J. B.; Drew, M. G. B.; Beer, P. D. *J. Chem. Soc., Dalton Trans.* **2000**, 2721-2728.
- (123) Oton, F.; Tarraga, A.; Velasco, M. D.; Molina, P. *Dalton Trans.* **2005**, 1159-1161.
- (124) Suksai, C.; Leeladee, P.; Jainuknan, D.; Tuntulani, T.; Muangsin, N.; Chailapakul, O.; Kongsaree, P.; Pakavatchai, C. *Tetrahedron Lett.* **2005**, *46*, 2765-2769.
- (125) Mahoney, J. M.; Beatty, A. M.; Smith, B. D. *J. Am. Chem. Soc.* **2001**, *123*, 5847-5848.
- (126) koulov, A. V.; Mahoney, J. M.; Smith, B. D. *Org. Biomol. Chem.* **2003**, *1*, 27-29.
- (127) Tozawa, T.; Misawa, Y.; Tokita, S.; Kubo, Y. *Tetrahedron Lett.* **2000**, *41*, 5219-5223.
- (128) White, D. J.; Laing, N.; Miller, H.; Parsons, S.; Coles, S.; Tasker, P. A. *Chem. Commun.* **1999**, 2077 - 2078.
- (129) Love, J. B.; Vere, J. M.; Glenny, M. W.; Blake, A. J.; Schröder, M. *Chem. Commun.* **2001**, 2678 - 2679.
- (130) Flack, S. S.; Chaumette, J.-L.; Kilburn, J. D.; Langley, G. J.; Webster, M. J. *Chem. Soc. Chem. Commun.* **1993**, 399-401.
- (131) Goodman, M. S.; Jubian, V.; Linton, B.; Hamilton, A. D. *J. Am. Chem. Soc.* **1995**, *117*, 11610-11611.
- (132) Schmidtchen, F. P. *J. Org. Chem.* **1986**, *51*, 5161-5168.
- (133) Sessler, J. L.; Andrievsky, A. *Chem. Commun.* **1996**, 1119-1120.
- (134) Kral, V.; Andrievsky, A.; Sessler, J. L. *J. Am. Chem. Soc.* **1995**, *117*, 2953-2954.
- (135) Kral, V.; Andrievsky, A.; Sessler, J. L. *J. Chem. Soc. Chem. Commun.* **1995**, 2349-2351.
- (136) Pelizzi, N.; Casanati, A.; Friggeri, A.; Ungaro, R. *J. Chem. Soc., Perkin Trans. 2* **1998**, 1307-1312.
- (137) Kubik, S.; Goddard, R. *J. Org. Chem.* **1999**, *64*, 9475-9486.
- (138) Garcia-Garrido, S. E.; Caltagirone, C.; Light, M. E.; Gale, P. A. *Chem. Commun.* **2007**, 1450-1452.
- (139) Davis, A. P.; Joos, J.-B. *Coord. Chem. Rev.* **2003**, *240*, 143-156.
- (140) Bowman-James, K. *Acc. Chem. Res.* **2005**, *38*, 671-678.
- (141) Brooks, S. J.; Gale, P. A.; Light, M. E. *Chem. Commun.* **2005**, 4696 - 4698.
- (142) Amendola, V.; Boiocchi, M.; Colasson, B.; Fabbrizzi, L. *Inorg. Chem.* **2006**, *45*, 6138-6147.
- (143) Goetz, S.; Kruger, P. E. *Dalton Trans.* **2006**, 1277-1284.
- (144) Lakowicz, J. R. *Principles of fluorescence spectroscopy*; 2nd ed.; Kluwer Academic/Plenum, 1999.
- (145) Bunzli, J.-C. G.; Andre, N.; Elhabiri, M.; Muller, G.; Piguet, C. *Journal of Alloys and Compounds* **2000**, *303-304*, 66-74.
- (146) Morrow, J. R.; Chin, K. O. A. *Inorg. Chem.* **1994**, *33*, 5036-5041.
- (147) Georges, J. *Analyst* **1993**, *118*, 1481 - 1486.
- (148) Wainwright, K. P. *Coord. Chem. Rev.* **1997**, *166*, 35-90.
- (149) Lincoln, S. F. *Coord. Chem. Rev.* **1997**, *166*, 255-289.
- (150) Meyer, M.; Dahaoui-Gindrey, V.; Lecomte, C.; Guillard, R. *Coord. Chem. Rev.* **1998**, *178-180*, 1313-1405.
- (151) Lukeš, I.; Kotek, J.; Vojtišek, P.; Hermann, P. *Coord. Chem. Rev.* **2001**, *216-217*, 287-312.

- (152) Klink, S. I.; Hebbink, G. A.; Grave, L.; Oude Alink, P. G. B.; van Veggel, F. C. J. M.; Werts, M. H. V. *J. Phys. Chem. A* **2002**, *106*, 3681-3689.
- (153) Aime, S.; Botta, M.; Fasano, M.; Marques, M. P. M.; Geraldes, C. F. G. C.; Pubanz, D.; Merbach, A. E. *Inorg. Chem.* **1997**, *36*, 2059-2068.
- (154) Leonard, J. P.; dos Santos, C. M. G.; Plush, S. E.; McCabe, T.; Gunnlaugsson, T. *Chem. Commun.* **2007**, 129-131.
- (155) Faulkner, S.; Burton-Pye, B. P. *Chem. Commun.* **2005**, 259-261.
- (156) Charbonniere, L. J.; Ziessel, R.; Montalti, M.; Prodi, L.; Zaccheroni, N.; Boehme, C.; Wipff, G. *J. Am. Chem. Soc.* **2002**, *124*, 7779-7788.
- (157) Gunnlaugsson, T.; Leonard, J. P.; Mulready, S.; Nieuwenhuyzen, M. *Tetrahedron* **2004**, *60*, 105-113.
- (158) Ren, J.; Zhang, S.; Sherry, A. D.; Geraldes, C. F. G. C. *Inorg. Chim. Acta* **2002**, *339*, 273-282.
- (159) Socrates, G. *Infrared Characteristic Group Frequencies*; John Wiley & Sons, 1980.
- (160) Yan, B.; Zhang, H.; Wang, S.; Ni, J. *Monatshfte fur chemie, chemical monthly* **1998**, *129*, 567-575.
- (161) Gampp, H.; Maeder, M.; Meyer, C. J.; Zuberbuhler, A. D. *Talanta* **1985**, *32*, 95-101.
- (162) Maeder, M.; Zuberbuhler, A. D. *Anal. Chem.* **1990**, *62*, 2220-2224.
- (163) Richardson, F. S. *Chem. Rev.* **1982**, *82*, 541-552.
- (164) Woods, M.; Sherry, A. D. *Inorg. Chem.* **2003**, *42*, 4401-4408.
- (165) Connors, K. A. *Binding constants: the measurement of molecular complex stability*; 1st ed.; John Wiley & Sons: New York, 1987.
- (166) Bryantsev, V. S.; Hay, B. P. *J. Am. Chem. Soc.* **2005**, *127*, 8282-8283.
- (167) Jeong, K.-S.; Cho, Y. L. *Tetrahedron Lett.* **1997**, *38*, 3279-3282.
- (168) Belcher, W. J.; Fabre, M.; Farhan, T.; Steed, J. W. *Org. Biomol. Chem.* **2006**, *4*, 781-786.
- (169) Shenderovich, I. G.; Tolstoy, P. M.; Golubev, N. S.; Smirnov, S. N.; Denisov, G. S.; Limbach, H.-H. *J. Am. Chem. Soc.* **2003**, *125*, 11710-11720.
- (170) Boiocchi, M.; Del Boca, L.; Gomez, D. E.; Fabbriizzi, L.; Licchelli, M.; Monzani, E. *J. Am. Chem. Soc.* **2004**, *126*, 16507-16514.
- (171) Gunnlaugsson, T.; Kruger, P. E.; Jensen, P.; Tierney, J.; Ali, H. D. P.; Hussey, G. M. *J. Org. Chem.* **2005**, *70*, 10875-10878.
- (172) Brooks, S. J.; Gale, P. A.; Light, M. E. *Chem. Commun.* **2006**, 4344 - 4346.
- (173) Ali, H. D. P.; PhD Thesis, Trinity College Dublin, 2007.
- (174) Bondy, C. R.; Gale, P. A.; Loeb, S. J. *J. Am. Chem. Soc.* **2004**, *126*, 5030-5031.
- (175) Bai, Y.; Zhang, B.-G.; Xu, J.; Duan, C.-Y.; Dang, D.-B.; Liu, D.-J.; Meng, Q.-J. *New J. Chem.* **2005**, *29*, 777-779.
- (176) Schazmann, B.; Alhashimy, N.; Diamond, D. *J. Am. Chem. Soc.* **2006**, *128*, 8607-8614.
- (177) Blázquez, M. T.; Muñoz, F. M.; Sáez, S.; Simón, L. M.; Alonso, Á.; Raposo, C.; Lithgow, A.; Alcázar, V.; Morán, J. R. *Heterocycles* **2006**, *69*, 73-81.
- (178) dos Santos, C. M. G.; McCabe, T.; Gunnlaugsson, T. *Tetrahedron Lett.* **2007**, *48*, 3135-3139.
- (179) Lankshear, M. D.; Cowley, A. R.; Beer, P. D. *Chem. Commun.* **2006**, 612 - 614.

- (180) Itsikson, N. A.; Zyryanov, G. V.; Chupakhin, O. N.; Matern, A. I. *Russian Chem. Rev.* **2005**, *74*, 747-755.
- (181) Goodman, M. S.; Weiss, J.; Hamilton, A. D. *Tetrahedron Lett.* **1994**, *35*, 8943-8946.
- (182) Norsten, T. B.; Chichak, K.; Branda, N. R. *Chem. Commun.* **2001**, 1794 - 1795.
- (183) Turner, D. R.; Spencer, E. C.; Howard, J. A. K.; Tocher, D. A.; Steed, J. W. *Chem. Commun.* **2004**, 1352 - 1353.
- (184) Turner, D. R.; Smith, B.; Spencer, E. C.; Goeta, A. E.; Evans, I. R.; Tocher, D. A.; Howard, J. A.; Steed, J. W. *New J. Chem.* **2005**, *29*, 90-98.
- (185) Camiolo, S.; Gale, P. A.; Hursthouse, M. B.; Light, M. E. *Org. Biomol. Chem.* **2003**, *1*, 741 - 744.
- (186) Evans, L. S.; Gale, P. A.; Light, M. E.; Quesada, R. *New J. Chem.* **2006**, *30*, 1019 - 1025.
- (187) Davis, A. P.; Sheppard, D. N.; Smith, B. D. *Chem. Soc. Rev.* **2007**, *36*, 348-357.
- (188) Davis, A. P. *Coord. Chem. Rev.* **2006**, *250*, 2939-2951.
- (189) Hanrahan, J. W.; Tabchami, J. A.; Becq, F.; Matthews, C. J.; Augustinas, O.; Jensen, T. J.; Chang, X.-B.; Riordan, J. R. *Ion channels and genetic diseases edited by*; Rockefeller University Press: New York, 1995.
- (190) Boon, J. M.; Smith, B. D. *Curr. Opin. Chem. Biol.* **2002**, *6*, 749-756.
- (191) McNally, B. A.; Koulov, A. V.; Smith, B. D.; Joos, J.-B.; Davies, A. P. *Chem. Commun.* **2005**, 1087-1089.
- (192) Hancock, R. D.; Martell, A. E. *Chem. Rev.* **1989**, *89*, 1875-1914.
- (193) Sammes, P. G.; Yahioğlu, G. *Chem. Soc. Rev.* **1994**, *23*, 327-334.
- (194) Armaroli, N.; De Cola, L.; Balzani, V.; Sauvage, J.-P.; Dietrich-Buchecker, C. O.; Kern, J.-M. *J. Chem. Soc., Faraday Trans.* **1992**, *88*, 553-556.
- (195) Bencini, A.; Bernardo, M. A.; Bianchi, A.; Fusi, V.; Giorgi, C.; Pina, F.; Valtancoli, B. *Eur. J. Inorg. Chem.* **1999**, 1911-1918.
- (196) Aragoni, M. C.; Arca, M.; Demartin, F.; Devillanova, F. A.; Isaia, F.; Garau, A.; Lippolis, V.; Jalali, F.; Papke, U.; Shamsipur, M.; Tei, L.; Yari, A.; Verani, G. *Inorg. Chem.* **2002**, *41*, 6623-6632.
- (197) Armaroli, N. *Photochem. Photobiol. Sci.* **2003**, *2*, 73-87.
- (198) Bazzicalupi, C.; Bencini, A.; Berni, E.; Bianchi, A.; Borsari, L.; Giorgi, C.; Valtancoli, B.; Lodeiro, C.; Lima, J. C.; Parola, J.; Pina, F. *Dalton Trans.* **2004**, 591-597.
- (199) Gunnlaugsson, T.; Leonard, J. P.; Senechal, K.; Harte, A. J. *Chem. Commun.* **2004**, 782-783.
- (200) Lippard, S. J.; Berg, J. M. *Principles of bioinorganic chemistry*; University Science Books: Mill Valley, CA, 1994.
- (201) Sarkar, B. *Chem. Rev.* **1999**, *99*, 2535-2544.
- (202) Kicic, A.; Chua, A. C. G.; Baker, E. *Anti-Cancer Drug Design* **2001**, *16*, 195-207.
- (203) Schwietert, C. W.; McCue, J. P. *Coord. Chem. Rev.* **1999**, *184*, 67-89.
- (204) Reichert, D. E.; Lewis, J. S.; Anderson, C. J. *Coord. Chem. Rev.* **1999**, *184*, 3-66.
- (205) Zvimba, J. N.; Jackson, G. E. *Polyhedron* **2007**, *26*, 2395-2404.
- (206) Pina, F.; Bernardo, M. A.; García-España, E. *Eur. J. Inorg. Chem.* **2000**, 2143-2157.
- (207) Ng, K.-Y.; Cowley, A. R. b.; Beer, P. D. *Chem. Commun.* **2006**, 3676-3678.

- (208) Cooton, F. A.; Wilkinson, G. *Advanced Inorganic chemistry*; 5 ed.; John Wiley & Sons: New York, 1988.
- (209) Potocnak, I.; Pohlova, M.; Wagner, C.; Jager, L. *Acta Cryst.* **2002**, *E58*, m595-m596.
- (210) Masood, M. A.; Hodgson, D. J. *Inorg. Chem.* **1993**, *32*, 4839-4844.
- (211) Cui, J.-Z.; Yi, Y.-J.; Zhang, H.; Gao, H.-L.; Wang, H.-T. *Acta Cryst.* **2007**, *E63*, m587-m588.
- (212) Devereux, M.; McCann, M.; Cronin, J. F.; Ferguson, G.; McKee, V. *Polyhedron* **1999**, *18*, 2141-2148.
- (213) Janiak, C. *J. Chem. Soc., Dalton Trans.* **2000**, 3885-3896.
- (214) Senechal-David, K.; Leonard, J. P.; Plush, S. E.; Gunnlaugsson, T. *Org. Lett.* **2006**, *8*, 2727-2730.
- (215) Zhang, S. *Materials Today* **2003**, 20-27.
- (216) Badjic', J. D.; Balzani, V.; Credi, A.; Silvi, S.; Stoddart, J. F. *Science* **2004**, *303*, 1845-1849.
- (217) Chichak, K. S.; Cantrill, S. J.; Pease, A. R.; Chiu, S.-H.; Cave, G. W. V.; Atwood, J. L.; Stoddart, J. F. *Science* **2004**, *304*, 1308-1312.
- (218) Whitesides, G. M.; Mathias, J. P.; Seto, C. T. *Science* **1991**, *254*, 1312-1319.
- (219) Lehn, J.-M. *Science* **1993**, *260*, 1762-1763.
- (220) Lehn, J.-M. *Supramolecular Chemistry, Concepts and Perspectives*; VCH: Weinheim, Germany, 1995.
- (221) Lehn, J.-M. *Science* **2002**, *295*, 2400-2403.
- (222) Zhang, S. *Nature Biotechnology* **2003**, 1171-1178.
- (223) Elemans, J. A. A. W.; Rowan, A. E.; Nolte, R. J. M. *J. Mater. Chem.* **2003**, *13*, 2661-2670.
- (224) Lessmann, J. J.; Horrocks, W. D. *Inorg. Chem.* **2000**, *39*, 3114-3124.
- (225) Fochi, F.; Jacopozzi, P.; Wegelius, E.; Rissanen, K.; Cozzini, P.; Marastoni, E.; Fiscaro, E.; Manini, P.; Fokkens, R.; Dalcanale, E. *J. Am. Chem. Soc.* **2001**, *123*, 7539-7552.
- (226) Sauvage, J.-P.; Dietrich-Buchecker, C. *Molecular Catenanes, Rotaxanes and Knots*; Wiley-VCH: Weinheim, Germany, 1999.
- (227) Elhabiri, M.; Scopelliti, R.; Bunzli, J.-C. G.; Piguet, C. *J. Am. Chem. Soc.* **1999**, *121*, 10747-10762.
- (228) Leininger, S.; Olenyuk, B.; Stang, P. J. *Chem. Rev.* **2000**, *100*, 853-908.
- (229) Dichtel, W. R.; Miljanic', O. S.; Spruell, J. M.; Heath, J. R.; Stoddart, J. F. *J. Am. Chem. Soc.* **2006**, *128*, 10388-10390.
- (230) Leonard, J. P.; Jensen, P.; McCabe, T.; O'Brien, J. E.; Peacock, R. D.; Kruger, P. E.; Gunnlaugsson, T. *J. Am. Chem. Soc.* **2007**, *129*, 10986-10987.
- (231) Yajima, S.; Hasegawa, Y. *Bull. Chem. Soc. of Japan* **1998**, *71*, 2825-2829.
- (232) You, B.; Kim, H. J.; Park, N. G.; Kim, Y. S. *Bull. Korean Chem. Soc.* **2001**, *22*, 1005-1008.
- (233) Shavaleev, N. M.; Moorcraft, L. P.; Pope, S. J. A.; Bell, Z. R.; Faulkner, S.; Ward, M. D. *Chem. Commun.* **2003**, 1134-1135.
- (234) Gunnlaugsson, T.; Leonard, J. P.; Senechal, K.; Harte, A. J. *J. Am. Chem. Soc.* **2003**, *125*, 12062-12063.
- (235) Balzani, V.; Juris, A.; Venturi, M. *Chem. Rev.* **1996**, *96*, 759-833.

- (236) Akitt, J. W. *NMR and chemistry : an introduction to modern NMR spectroscopy*; 4th ed ed.; Stanley Thornes, 2000.
- (237) Campos-Vallette, M. M.; Clavijo, R. E.; Mendizabal, F.; Zamudio, W.; Baraona, R.; Diaz, G. *Vibrational Spectroscopy* **1996**, *12*, 37-44.
- (238) Schneider, H. J.; Yatsimirsky, A. K. *Principles and Methods in Supramolecular Chemistry*; Wiley & Sons: England, 2000.
- (239) Letard, J.-F.; Lapouyade, R.; Rettig, W. *Pure & Appl. Chem.* **1993**, *65*, 1705-1712.
- (240) Shavaleev, N. M.; Accorsi, G.; Virgili, D.; Bell, Z. R.; Lazarides, T.; Calogero, G.; Armaroli, N.; Ward, M. D. *Inorg. Chem.* **2005**, *44*, 61-72.
- (241) Werts, M. H. V.; Jukes, R. T. F.; Verhoeven, J. W. *Phys. Chem. Chem. Phys.* **2002**, *4*, 1542-1548.
- (242) Jørgensen, C. K.; Judd, B. R. *Molecular Physics* **1964**, *8*, 281 - 290.
- (243) Mahajan, R. K.; Kaur, I.; Kaur, R.; Uchida, S.; Onimaru, A.; Shinoda, S.; Tsukube, H. *Chem. Commun.* **2003**, 2238-2239.
- (244) Pope, S. J. A.; Burton-Pye, B. P.; Berridge, R.; Khan, T.; Skabara, P. J.; Faulkner, S. *Dalton Trans.* **2006**, 2907 - 2912.
- (245) Ziessel, R.; Charbonniere, L. J. *J. Alloys and Compounds* **2004**, *374*, 283-288.
- (246) Prodi, L. *New J. Chem.* **2005**, *29*, 20-31.
- (247) Wright, A. T.; Anslyn, E. V. *Chem. Soc. Rev.* **2006**, *35*, 14-28.
- (248) Montalti, M.; Prodi, L.; Zaccheroni, N.; Charbonniere, L.; Douce, L.; Ziessel, R. *J. Am. Chem. Soc.* **2001**, *123*, 12694-12695.
- (249) Vogel, A. I.; Furniss, B. S.; Tatchell, A. R.; Hannaford, A. J.; Smith, P. W. G. *Vogel's Textbook of Practical Organic Chemistry*; 5th ed.; Longman, 1989.
- (250) Garcia-Fresnadillo, D.; Orellana, G. *Helv. Chim. Acta* **2001**, *84*, 2708-2730.

Appendix

Appendix A0 – Binding Constants (log *K*) determination

Within this body of work, the binding constants have been determined by using the nonlinear least-squares program SPECFIT/32TM, which is a multivariate data analysis program for modeling and fitting experimental data sets (such as chemical kinetics and equilibrium titrations) obtained from multivariate spectrophotometric measurements. The fitting methodology, which relies on the use of various mathematical parameters¹⁶¹, uses the Levenberg-Marquardt procedure to minimise the least-squares residuals between the data set and the model system.¹⁶² In order to solve the number of species (speciation) present at equilibrium, SPECFIT takes advantage of the Newton-Raphson method. The model used specifies various states of interaction, for instance complexation between two species, in terms of the overall stability constants (β). Considering the two stepwise equilibrium process involved in the binding interaction between a host (M) and a guest (L) to form the 1:2 (ML₂) complex, the equilibrium constants K_1 and K_2 implicated in the interaction can be expressed using Equation A0.1 and Equation A0.2.



The stepwise binding constants K_1 and K_2 can be determined using Equations A0.3 and A0.4.

$$K_1 = \frac{[ML]}{[M][L]} \quad \text{Equation A0.3}$$

$$K_2 = \frac{[ML_2]}{[ML][L]} \quad \text{Equation A0.4}$$

The overall equilibrium constant for this process, $\beta_{1:2}$, is the product of the two stepwise constants K_1 and K_2 ($\beta = K_1.K_2$). SPECFIT yields binding constants as cumulative log β

values. So, for the 1:2 (M:L₂) equilibrium process this is translated by the $\log \beta_{1:2}$, which represents the sum of the individual constants ($\log \beta_{1:2} = \log K_1 + \log K_2$). Therefore, for any multi-step equilibrium, by subtraction of successive $\log \beta$ values, the $\log K$ for each equilibrium step can then be determined.

Appendix 1 – Crystallographic data

A1.1: Crystallographic data for 71

Identification code	cs030m	
Empirical formula	C ₁₆ H ₁₄ F ₃ N ₃ O ₂	
Formula weight	337.30	
Temperature	150 K	
Wavelength	0.71073 Å	
Crystal system	Monoclinic	
Space group	P2(1)/c	
Unit cell dimensions	a = 11.9903(12) Å	α = 90°.
	b = 7.6035(8) Å	β = 105.585(2)°.
	c = 17.4995(18) Å	γ = 90°.
Volume	1536.7(3) Å ³	
Z	4	
Density (calculated)	1.458 Mg/m ³	
Absorption coefficient	0.123 mm ⁻¹	
F(000)	696	
Crystal size	0.31 x 0.11 x 0.05 mm ³	
Theta range for data collection	1.76 to 25.00°.	
Index ranges	-13 ≤ h ≤ 14, -9 ≤ k ≤ 9, -20 ≤ l ≤ 20	
Reflections collected	11791	
Independent reflections	2701 [R(int) = 0.0560]	
Completeness to theta = 25.00°	100.0 %	
Absorption correction	Sadabs	
Refinement method	Full-matrix least-squares on F ²	
Data / restraints / parameters	2701 / 0 / 218	
Goodness-of-fit on F ²	1.007	
Final R indices [I > 2σ(I)]	R1 = 0.0477, wR2 = 0.1048	
R indices (all data)	R1 = 0.0910, wR2 = 0.1224	
Largest diff. peak and hole	0.231 and -0.152 e.Å ⁻³	

A1.1.1: CIF file for 71

```

data_cs030m

_audit_creation_method          SHELXL-97
_chemical_name_systematic
;
?
;
_chemical_name_common           ?
_chemical_melting_point         ?
_chemical_formula_moiety        ?
_chemical_formula_sum           'C16 H14 F3 N3 O2'
_chemical_formula_weight        337.30

loop_
_atom_type_symbol
_atom_type_description
_atom_type_scatter_dispersion_real
_atom_type_scatter_dispersion_imag
_atom_type_scatter_source
'C' 'C' 0.0033 0.0016
'International Tables Vol C Tables 4.2.6.8 and 6.1.1.4'
'H' 'H' 0.0000 0.0000
'International Tables Vol C Tables 4.2.6.8 and 6.1.1.4'
'N' 'N' 0.0061 0.0033
'International Tables Vol C Tables 4.2.6.8 and 6.1.1.4'
'O' 'O' 0.0106 0.0060
'International Tables Vol C Tables 4.2.6.8 and 6.1.1.4'
'F' 'F' 0.0171 0.0103
'International Tables Vol C Tables 4.2.6.8 and 6.1.1.4'

_symmetry_cell_setting          Monoclinic
_symmetry_space_group_name_H-M P2(1)/c

loop_
_symmetry_equiv_pos_as_xyz
'x, y, z'
'-x, y+1/2, -z+1/2'
'-x, -y, -z'
'x, -y-1/2, z-1/2'

_cell_length_a                  11.9903(12)
_cell_length_b                  7.6035(8)
_cell_length_c                  17.4995(18)
_cell_angle_alpha               90.00
_cell_angle_beta                105.585(2)
_cell_angle_gamma               90.00
_cell_volume                    1536.7(3)
_cell_formula_units_Z           4
_cell_measurement_temperature   571(2)
_cell_measurement_reflns_used   1644
_cell_measurement_theta_min     2.42
_cell_measurement_theta_max     19.71

```

```

_exptl_crystal_description      plate
_exptl_crystal_colour          colourless
_exptl_crystal_size_max        0.31
_exptl_crystal_size_mid        0.11
_exptl_crystal_size_min        0.05
_exptl_crystal_density_meas    ?
_exptl_crystal_density_diffn   1.458
_exptl_crystal_density_method  'not measured'
_exptl_crystal_F_000           696
_exptl_absorpt_coefficient_mu  0.123
_exptl_absorpt_correction_type 'multi-scan'
_exptl_absorpt_correction_T_min 0.880285
_exptl_absorpt_correction_T_max 1.0000
_exptl_absorpt_process_details 'Blessing, Acta Cryst. (1995) A51 33-38.'
```

```

_exptl_special_details
;
?
;
```

```

_diffn_ambient_temperature     571(2)
_diffn_radiation_wavelength    0.71073
_diffn_radiation_type          MoK\alpha
_diffn_radiation_source        'fine-focus sealed tube'
_diffn_radiation_monochromator  graphite
_diffn_measurement_device_type  'CCD area detector'
_diffn_measurement_method      'phi and omega scans'
_diffn_detector_area_resol_mean ?
_diffn_standards_number        ?
_diffn_standards_interval_count ?
_diffn_standards_interval_time ?
_diffn_standards_decay_%       ?
_diffn_reflns_number           11791
_diffn_reflns_av_R_equivalents 0.0560
_diffn_reflns_av_sigmaI/netI   0.0463
_diffn_reflns_limit_h_min      -13
_diffn_reflns_limit_h_max      14
_diffn_reflns_limit_k_min      -9
_diffn_reflns_limit_k_max      9
_diffn_reflns_limit_l_min      -20
_diffn_reflns_limit_l_max      20
_diffn_reflns_theta_min        1.76
_diffn_reflns_theta_max        25.00
_reflns_number_total           2701
_reflns_number_gt              1702
_reflns_threshold_expression    >2sigma(I)
```

```

_computing_data_collection      'Bruker SMART'
_computing_cell_refinement      'Bruker SMART'
_computing_data_reduction       'Bruker SAINT'
_computing_structure_solution   'SHELXS-97 (Sheldrick, 1990)'
_computing_structure_refinement 'SHELXL-97 (Sheldrick, 1997)'
_computing_molecular_graphics   'Bruker SHELXTL'
_computing_publication_material 'Bruker SHELXTL'
```

```
_refine_special_details
```

```

;
Refinement of F2 against ALL reflections. The weighted R-factor wR
and
goodness of fit S are based on F2, conventional R-factors R are based
on F, with F set to zero for negative F2. The threshold expression of
F2 > 2sigma(F2) is used only for calculating R-factors(gt) etc. and
is
not relevant to the choice of reflections for refinement. R-factors
based
on F2 are statistically about twice as large as those based on F, and
R-
factors based on ALL data will be even larger.
;

```

```

_refine_ls_structure_factor_coef Fsqd
_refine_ls_matrix_type full
_refine_ls_weighting_scheme calc
_refine_ls_weighting_details
'calc w=1/[\s^2^(Fo^2^)+(0.0584P)^2^+0.0788P] where P=(Fo^2^+2Fc^2^)/3'
_atom_sites_solution_primary direct
_atom_sites_solution_secondary difmap
_atom_sites_solution_hydrogens geom
_refine_ls_hydrogen_treatment constr
_refine_ls_extinction_method none
_refine_ls_extinction_coef ?
_refine_ls_number_reflns 2701
_refine_ls_number_parameters 218
_refine_ls_number_restraints 0
_refine_ls_R_factor_all 0.0910
_refine_ls_R_factor_gt 0.0477
_refine_ls_wR_factor_ref 0.1224
_refine_ls_wR_factor_gt 0.1048
_refine_ls_goodness_of_fit_ref 1.007
_refine_ls_restrained_S_all 1.007
_refine_ls_shift/su_max 0.001
_refine_ls_shift/su_mean 0.000

```

```

loop_
_atom_site_label
_atom_site_type_symbol
_atom_site_fract_x
_atom_site_fract_y
_atom_site_fract_z
_atom_site_U_iso_or_equiv
_atom_site_adp_type
_atom_site_occupancy
_atom_site_symmetry_multiplicity
_atom_site_calc_flag
_atom_site_refinement_flags
_atom_site_disorder_assembly
_atom_site_disorder_group
O2 O 0.68790(16) -0.0091(2) 0.17175(9) 0.0582(5) Uani 1 1 d . . .
O1 O 0.31619(17) 0.8452(2) 0.08726(10) 0.0651(6) Uani 1 1 d . . .
N3 N 0.34717(18) 0.6401(3) 0.18377(11) 0.0491(6) Uani 1 1 d . . .
H3 H 0.3297 0.6099 0.2265 0.059 Uiso 1 1 calc R . .
N1 N 0.73440(19) -0.0585(3) 0.05578(11) 0.0533(6) Uani 1 1 d . . .
H1 H 0.7272 -0.0162 0.0091 0.064 Uiso 1 1 calc R . .

```

C14 C 0.2990(2) 0.7876(4) 0.14860(14) 0.0511(7) Uani 1 1 d . . .
 F2 F 1.08767(16) -0.6864(2) 0.14716(10) 0.0833(6) Uani 1 1 d . . .
 C6 C 0.7961(2) -0.2161(3) 0.07345(13) 0.0445(6) Uani 1 1 d . . .
 C8 C 0.5640(2) 0.2965(3) 0.10307(13) 0.0451(6) Uani 1 1 d . . .
 F3 F 0.93659(17) -0.8053(2) 0.16524(11) 0.0914(6) Uani 1 1 d . . .
 C5 C 0.8047(2) -0.3193(3) 0.01028(14) 0.0530(7) Uani 1 1 d . . .
 H5 H 0.7718 -0.2805 -0.0413 0.064 Uiso 1 1 calc R . . .
 C7 C 0.6845(2) 0.0356(4) 0.10394(14) 0.0476(7) Uani 1 1 d . . .
 C10 C 0.4176(2) 0.3505(3) 0.16986(14) 0.0482(7) Uani 1 1 d . . .
 H10 H 0.3664 0.3081 0.1971 0.058 Uiso 1 1 calc R . . .
 C12 C 0.5046(2) 0.5913(3) 0.12113(15) 0.0528(7) Uani 1 1 d . . .
 H12 H 0.5122 0.7117 0.1147 0.063 Uiso 1 1 calc R . . .
 F1 F 0.96369(17) -0.8030(2) 0.04953(11) 0.0862(6) Uani 1 1 d . . .
 N2 N 0.6298(2) 0.1827(3) 0.06891(12) 0.0584(6) Uani 1 1 d . . .
 H2 H 0.6358 0.2083 0.0223 0.070 Uiso 1 1 calc R . . .
 C9 C 0.4857(2) 0.2341(4) 0.14227(13) 0.0486(7) Uani 1 1 d . . .
 H9 H 0.4791 0.1139 0.1499 0.058 Uiso 1 1 calc R . . .
 C11 C 0.4241(2) 0.5281(3) 0.15788(13) 0.0428(6) Uani 1 1 d . . .
 C1 C 0.9122(2) -0.5358(3) 0.09810(14) 0.0497(7) Uani 1 1 d . . .
 C13 C 0.5733(2) 0.4756(4) 0.09425(15) 0.0556(7) Uani 1 1 d . . .
 H13 H 0.6273 0.5190 0.0696 0.067 Uiso 1 1 calc R . . .
 C4 C 0.8612(2) -0.4783(4) 0.02238(15) 0.0559(7) Uani 1 1 d . . .
 H4 H 0.8649 -0.5471 -0.0208 0.067 Uiso 1 1 calc R . . .
 C3 C 0.8483(2) -0.2722(4) 0.14955(14) 0.0568(7) Uani 1 1 d . . .
 H3A H 0.8451 -0.2031 0.1927 0.068 Uiso 1 1 calc R . . .
 C15 C 0.2190(3) 0.8798(4) 0.18786(18) 0.0794(10) Uani 1 1 d . . .
 H15A H 0.2538 0.9880 0.2108 0.119 Uiso 1 1 calc R . . .
 H15B H 0.2048 0.8060 0.2288 0.119 Uiso 1 1 calc R . . .
 H15C H 0.1471 0.9045 0.1492 0.119 Uiso 1 1 calc R . . .
 C2 C 0.9053(2) -0.4309(4) 0.16124(15) 0.0571(7) Uani 1 1 d . . .
 H2A H 0.9399 -0.4686 0.2127 0.069 Uiso 1 1 calc R . . .
 C16 C 0.9733(3) -0.7048(4) 0.11376(17) 0.0633(8) Uani 1 1 d . . .

loop_

_atom_site_aniso_label
 _atom_site_aniso_U_11
 _atom_site_aniso_U_22
 _atom_site_aniso_U_33
 _atom_site_aniso_U_23
 _atom_site_aniso_U_13
 _atom_site_aniso_U_12
 O2 0.0832(14) 0.0617(12) 0.0370(9) 0.0044(9) 0.0290(9) 0.0149(10)
 O1 0.0942(15) 0.0634(12) 0.0470(11) 0.0173(9) 0.0350(10) 0.0182(11)
 N3 0.0671(15) 0.0532(14) 0.0332(11) 0.0065(10) 0.0242(11) 0.0092(12)
 N1 0.0740(15) 0.0584(14) 0.0327(11) 0.0080(10) 0.0235(11) 0.0172(13)
 C14 0.0670(19) 0.0533(17) 0.0372(14) 0.0002(13) 0.0214(13) 0.0039(14)
 F2 0.0666(12) 0.0943(14) 0.0854(13) 0.0082(10) 0.0140(10) 0.0243(10)
 C6 0.0516(16) 0.0487(16) 0.0366(13) 0.0072(12) 0.0178(12) 0.0017(13)
 C8 0.0552(16) 0.0477(16) 0.0359(13) 0.0010(12) 0.0184(12) 0.0065(13)
 F3 0.1127(15) 0.0752(13) 0.0953(14) 0.0368(11) 0.0432(12) 0.0211(11)
 C5 0.0624(18) 0.0662(19) 0.0310(13) 0.0011(12) 0.0137(12) 0.0115(15)
 C7 0.0586(17) 0.0527(17) 0.0357(13) -0.0018(12) 0.0197(12) -0.0014(14)
 C10 0.0535(16) 0.0542(17) 0.0422(14) 0.0083(12) 0.0220(13) 0.0015(14)
 C12 0.0667(18) 0.0437(16) 0.0569(16) -0.0001(13) 0.0321(15) -0.0035(14)
 F1 0.1163(15) 0.0662(11) 0.0753(12) -0.0074(10) 0.0242(11) 0.0208(10)
 N2 0.0835(17) 0.0590(15) 0.0429(12) 0.0107(11) 0.0345(12) 0.0182(13)
 C9 0.0586(17) 0.0434(15) 0.0468(15) 0.0071(12) 0.0197(13) -0.0013(13)

```

C11 0.0517(16) 0.0482(16) 0.0305(12) 0.0004(11) 0.0143(12) -0.0003(13)
C1 0.0551(17) 0.0513(16) 0.0442(15) 0.0039(13) 0.0156(13) 0.0019(14)
C13 0.0631(18) 0.0562(18) 0.0568(16) 0.0060(14) 0.0320(14) -0.0024(15)
C4 0.0648(18) 0.0643(19) 0.0404(14) -0.0049(13) 0.0170(13) 0.0110(15)
C3 0.076(2) 0.0606(18) 0.0337(13) -0.0013(13) 0.0141(13) 0.0108(16)
C15 0.104(3) 0.078(2) 0.070(2) 0.0117(17) 0.048(2) 0.029(2)
C2 0.0667(19) 0.0660(19) 0.0366(14) 0.0085(13) 0.0105(13) 0.0078(16)
C16 0.073(2) 0.065(2) 0.0522(17) 0.0100(16) 0.0173(16) 0.0111(17)

```

```
_geom_special_details
```

```
;
```

All esds (except the esd in the dihedral angle between two l.s. planes) are estimated using the full covariance matrix. The cell esds are taken into account individually in the estimation of esds in distances, angles and torsion angles; correlations between esds in cell parameters are only used when they are defined by crystal symmetry. An approximate (isotropic) treatment of cell esds is used for estimating esds involving l.s. planes.

```
;
```

```
loop_
```

```

  _geom_bond_atom_site_label_1
  _geom_bond_atom_site_label_2
  _geom_bond_distance
  _geom_bond_site_symmetry_2
  _geom_bond_publ_flag
O2 C7 1.225(3) . ?
O1 C14 1.227(3) . ?
N3 C14 1.334(3) . ?
N3 C11 1.416(3) . ?
N1 C7 1.360(3) . ?
N1 C6 1.398(3) . ?
C14 C15 1.496(4) . ?
F2 C16 1.346(3) . ?
C6 C3 1.378(3) . ?
C6 C5 1.382(3) . ?
C8 C13 1.379(3) . ?
C8 C9 1.387(3) . ?
C8 N2 1.408(3) . ?
F3 C16 1.342(3) . ?
C5 C4 1.374(3) . ?
C7 N2 1.357(3) . ?
C10 C11 1.372(3) . ?
C10 C9 1.376(3) . ?
C12 C13 1.372(3) . ?
C12 C11 1.383(3) . ?
F1 C16 1.328(3) . ?
C1 C4 1.373(3) . ?
C1 C2 1.383(3) . ?
C1 C16 1.468(4) . ?
C3 C2 1.374(4) . ?

```

```
loop_
```

```

  _geom_angle_atom_site_label_1
  _geom_angle_atom_site_label_2

```


_geom_angle_atom_site_label_3
 _geom_angle
 _geom_angle_site_symmetry_1
 _geom_angle_site_symmetry_3
 _geom_angle_publ_flag

C14 N3 C11 126.61(19) . . ?
 C7 N1 C6 127.4(2) . . ?
 O1 C14 N3 123.4(2) . . ?
 O1 C14 C15 120.9(2) . . ?
 N3 C14 C15 115.7(2) . . ?
 C3 C6 C5 119.0(2) . . ?
 C3 C6 N1 123.7(2) . . ?
 C5 C6 N1 117.3(2) . . ?
 C13 C8 C9 118.6(2) . . ?
 C13 C8 N2 119.2(2) . . ?
 C9 C8 N2 122.1(2) . . ?
 C4 C5 C6 121.1(2) . . ?
 O2 C7 N2 123.6(2) . . ?
 O2 C7 N1 123.3(2) . . ?
 N2 C7 N1 113.2(2) . . ?
 C11 C10 C9 121.1(2) . . ?
 C13 C12 C11 119.7(2) . . ?
 C7 N2 C8 124.9(2) . . ?
 C10 C9 C8 119.9(2) . . ?
 C10 C11 C12 119.2(2) . . ?
 C10 C11 N3 118.3(2) . . ?
 C12 C11 N3 122.4(2) . . ?
 C4 C1 C2 118.7(2) . . ?
 C4 C1 C16 122.0(2) . . ?
 C2 C1 C16 119.3(2) . . ?
 C12 C13 C8 121.4(2) . . ?
 C1 C4 C5 120.1(2) . . ?
 C2 C3 C6 119.6(2) . . ?
 C3 C2 C1 121.4(2) . . ?
 F1 C16 F3 106.2(3) . . ?
 F1 C16 F2 105.8(2) . . ?
 F3 C16 F2 104.3(2) . . ?
 F1 C16 C1 114.1(2) . . ?
 F3 C16 C1 112.7(2) . . ?
 F2 C16 C1 112.9(3) . . ?

_diffraction_measured_fraction_theta_max	1.000
_diffraction_refl_theta_full	25.00
_diffraction_measured_fraction_theta_full	1.000
_refine_diff_density_max	0.231
_refine_diff_density_min	-0.152
_refine_diff_density_rms	0.038

A1.2: Crystallographic data for 72.CH₃OH

Identification code	cs082	
Empirical formula	C8.50 H9 Cl0 F1.50 N1.50 O1.50	
Formula weight	184.67	
Temperature	150 K	
Wavelength	0.71070 Å	
Crystal system	triclinic	
Space group	P1	
Unit cell dimensions	a = 4.649(3) Å	α = 87.993(13)°.
	b = 6.738(5) Å	β = 89.247(17)°.
	c = 13.324(10) Å	γ = 88.20(2)°.
Volume	416.9(5) Å ³	
Z	2	
Density (calculated)	1.471 Mg/m ³	
Absorption coefficient	0.124 mm ⁻¹	
F(000)	192	
Crystal size	0.20 x 0.20 x 0.08 mm ³	
Theta range for data collection	3.03 to 31.24°.	
Index ranges	-6 ≤ h ≤ 6, -9 ≤ k ≤ 9, -19 ≤ l ≤ 18	
Reflections collected	8994	
Independent reflections	4404 [R(int) = 0.0316]	
Completeness to theta = 31.24°	90.6 %	
Max. and min. transmission	0.9901 and 0.9756	
Refinement method	Full-matrix least-squares on F ²	
Data / restraints / parameters	4404 / 3 / 242	
Goodness-of-fit on F ²	0.980	
Final R indices [I > 2σ(I)]	R1 = 0.0520, wR2 = 0.1331	
R indices (all data)	R1 = 0.0643, wR2 = 0.1445	
Absolute structure parameter	0.7(8)	
Extinction coefficient	0.070(11)	
Largest diff. peak and hole	0.309 and -0.487 e.Å ⁻³	

A1.2.1: CIF file for 72.CH₃OH

```

data_cs082

_audit_creation_method          SHELXL-97
_chemical_name_systematic
;
?
;
_chemical_name_common           ?
_chemical_melting_point         ?
_chemical_formula_moiety        ?
_chemical_formula_sum           'C17 H18 C20 F3 N3 O3'
_chemical_formula_weight        368.34

loop_
_atom_type_symbol
_atom_type_description
_atom_type_scatter_dispersion_real
_atom_type_scatter_dispersion_imag
_atom_type_scatter_source
'C' 'C' 0.0033 0.0016
'International Tables Vol C Tables 4.2.6.8 and 6.1.1.4'
'H' 'H' 0.0000 0.0000
'International Tables Vol C Tables 4.2.6.8 and 6.1.1.4'
'Cl' 'Cl' 0.1484 0.1585
'International Tables Vol C Tables 4.2.6.8 and 6.1.1.4'
'F' 'F' 0.0171 0.0103
'International Tables Vol C Tables 4.2.6.8 and 6.1.1.4'
'N' 'N' 0.0061 0.0033
'International Tables Vol C Tables 4.2.6.8 and 6.1.1.4'
'O' 'O' 0.0106 0.0060
'International Tables Vol C Tables 4.2.6.8 and 6.1.1.4'

_symmetry_cell_setting          Triclinic
_symmetry_space_group_name_H-M  P1

loop_
_symmetry_equiv_pos_as_xyz
'x, y, z'

_cell_length_a                  4.649(3)
_cell_length_b                  6.738(5)
_cell_length_c                  13.324(10)
_cell_angle_alpha                87.993(13)
_cell_angle_beta                89.247(17)
_cell_angle_gamma                88.20(2)
_cell_volume                     416.9(5)
_cell_formula_units_Z            1
_cell_measurement_temperature    108(2)
_cell_measurement_reflns_used    ?
_cell_measurement_theta_min      ?
_cell_measurement_theta_max      ?

_exptl_crystal_description      prism

```

```

_exptl_crystal_colour          colourless
_exptl_crystal_size_max       0.20
_exptl_crystal_size_mid       0.20
_exptl_crystal_size_min       0.08
_exptl_crystal_density_meas    ?
_exptl_crystal_density_diffn   1.467
_exptl_crystal_density_method  'not measured'
_exptl_crystal_F_000          191
_exptl_absorpt_coefficient_mu  0.124
_exptl_absorpt_correction_type 'multi-scan'
_exptl_absorpt_correction_T_min 0.8090
_exptl_absorpt_correction_T_max 1.0000
_exptl_absorpt_process_details 'Blessing, Acta Cryst. (1995) A51 33-
38.'

_exptl_special_details
;
?
;

_diffn_ambient_temperature     108(2)
_diffn_radiation_wavelength    0.71070
_diffn_radiation_type          MoK\alpha
_diffn_radiation_source        'fine-focus sealed tube'
_diffn_radiation_monochromator  graphite
_diffn_measurement_device_type  'Rigaku Saturn 724'
_diffn_measurement_method      'omega and phi scans'
_diffn_detector_area_resol_mean ?
_diffn_standards_number        ?
_diffn_standards_interval_count ?
_diffn_standards_interval_time ?
_diffn_standards_decay_%       ?
_diffn_reflns_number           6314
_diffn_reflns_av_R_equivalents 0.0281
_diffn_reflns_av_sigmaI/netI   0.0491
_diffn_reflns_limit_h_min      -5
_diffn_reflns_limit_h_max      5
_diffn_reflns_limit_k_min      -8
_diffn_reflns_limit_k_max      8
_diffn_reflns_limit_l_min      -15
_diffn_reflns_limit_l_max      15
_diffn_reflns_theta_min        3.03
_diffn_reflns_theta_max        24.99
_reflns_number_total           2777
_reflns_number_gt              2441
_reflns_threshold_expression    >2sigma(I)

_computing_data_collection     'Rigaku Crystalclear'
_computing_cell_refinement     'Rigaku Crystalclear'
_computing_data_reduction      'Rigaku Crystalclear'
_computing_structure_solution  'SHELXS-97 (Sheldrick, 1990)'
_computing_structure_refinement 'SHELXL-97 (Sheldrick, 1997)'
_computing_molecular_graphics  'Shelxtl'
_computing_publication_material 'Shelxtl'

_refine_special_details
;

```

Refinement of F^2 against ALL reflections. The weighted R-factor wR and goodness of fit S are based on F^2 , conventional R-factors R are based on F , with F set to zero for negative F^2 . The threshold expression of $F^2 > 2\sigma(F^2)$ is used only for calculating R-factors(gt) etc. and is not relevant to the choice of reflections for refinement. R-factors based on F^2 are statistically about twice as large as those based on F , and R-factors based on ALL data will be even larger.

```

_refine_ls_structure_factor_coef  Fsqd
_refine_ls_matrix_type            full
_refine_ls_weighting_scheme       calc
_refine_ls_weighting_details
'calc w=1/[\s^2^(Fo^2)+(0.0606P)^2+0.0000P] where P=(Fo^2+2Fc^2)/3'
_atom_sites_solution_primary      direct
_atom_sites_solution_secondary    difmap
_atom_sites_solution_hydrogens    geom
_refine_ls_hydrogen_treatment     constr
_refine_ls_extinction_method      SHELXL
_refine_ls_extinction_coef        0.031(8)
_refine_ls_extinction_expression
'Fc^*=kFc[1+0.001xFc^2\l^3/sin(2\q)]^-1/4^'
_refine_ls_abs_structure_details
'Flack H D (1983), Acta Cryst. A39, 876-881'
_refine_ls_abs_structure_Flack    0.0(8)
_refine_ls_number_reflns          2777
_refine_ls_number_parameters      239
_refine_ls_number_restraints      3
_refine_ls_R_factor_all           0.0440
_refine_ls_R_factor_gt            0.0398
_refine_ls_wR_factor_ref          0.1010
_refine_ls_wR_factor_gt          0.0983
_refine_ls_goodness_of_fit_ref    1.019
_refine_ls_restrained_S_all       1.018
_refine_ls_shift/su_max           0.200
_refine_ls_shift/su_mean          0.004

```

```

loop_
  _atom_site_label
  _atom_site_type_symbol
  _atom_site_fract_x
  _atom_site_fract_y
  _atom_site_fract_z
  _atom_site_U_iso_or_equiv
  _atom_site_adp_type
  _atom_site_occupancy
  _atom_site_symmetry_multiplicity
  _atom_site_calc_flag
  _atom_site_refinement_flags
  _atom_site_disorder_assembly
  _atom_site_disorder_group
F1 F 0.7956(4) 1.8397(3) -0.30639(15) 0.0389(5) Uani 1 1 d . . .
F2 F 0.3838(4) 1.8390(3) -0.23144(15) 0.0434(5) Uani 1 1 d . . .

```

```

F3 F 0.4545(4) 1.6799(2) -0.36715(14) 0.0376(5) Uani 1 1 d . . .
O1 O 0.5487(4) 0.9239(3) 0.01091(15) 0.0231(4) Uani 1 1 d . . .
O2 O 0.2782(4) 0.9040(3) 0.33477(16) 0.0276(5) Uani 1 1 d . . .
N1 N 0.3292(4) 0.5658(3) 0.33760(16) 0.0192(5) Uani 1 1 d . . .
H18 H 0.2722 0.4587 0.3667 0.023 Uiso 1 1 d R . .
N2 N 0.9827(4) 0.7890(3) 0.06583(16) 0.0199(5) Uani 1 1 d . . .
H13 H 1.1707 0.7989 0.0615 0.024 Uiso 1 1 d R . .
N3 N 0.9735(5) 1.0416(3) -0.05326(17) 0.0201(5) Uani 1 1 d . . .
H1 H 1.1681 1.0189 -0.0572 0.024 Uiso 1 1 d R . .
C1 C 0.5444(6) 1.4968(4) -0.1275(2) 0.0233(6) Uani 1 1 d . . .
H2 H 0.3934 1.5796 -0.1020 0.028 Uiso 1 1 calc R . .
C2 C 0.8846(6) 1.4198(4) -0.2589(2) 0.0252(6) Uani 1 1 d . . .
H3 H 0.9661 1.4500 -0.3231 0.030 Uiso 1 1 calc R . .
C3 C 0.9809(6) 1.2514(4) -0.2039(2) 0.0234(6) Uani 1 1 d . . .
H4 H 1.1302 1.1679 -0.2300 0.028 Uiso 1 1 calc R . .
C4 C 0.8567(5) 1.2058(4) -0.11011(19) 0.0206(6) Uani 1 1 d . . .
C5 C 0.6394(5) 1.3286(4) -0.0721(2) 0.0226(6) Uani 1 1 d . . .
H5 H 0.5552 1.2980 -0.0083 0.027 Uiso 1 1 calc R . .
C6 C 0.8162(6) 0.9181(4) 0.0082(2) 0.0198(6) Uani 1 1 d . . .
C7 C 0.8712(5) 0.6386(4) 0.13164(19) 0.0190(6) Uani 1 1 d . . .
C8 C 0.9938(5) 0.4471(4) 0.1276(2) 0.0207(6) Uani 1 1 d . . .
C9 C 0.8926(6) 0.2995(4) 0.1943(2) 0.0215(6) Uani 1 1 d . . .
H7 H 0.9763 0.1691 0.1932 0.026 Uiso 1 1 calc R . .
C10 C 0.6727(5) 0.3409(4) 0.2616(2) 0.0214(6) Uani 1 1 d . . .
H8 H 0.6024 0.2385 0.3054 0.026 Uiso 1 1 calc R . .
C11 C 0.6503(5) 0.6840(4) 0.20019(19) 0.0184(6) Uani 1 1 d . . .
H9 H 0.5684 0.8147 0.2021 0.022 Uiso 1 1 calc R . .
C12 C 0.5789(6) 1.7243(4) -0.2794(2) 0.0259(7) Uani 1 1 d . . .
C13 C 0.2066(6) 0.7383(4) 0.3678(2) 0.0221(6) Uani 1 1 d . . .
C14 C -0.0261(6) 0.7187(4) 0.4472(2) 0.0238(6) Uani 1 1 d . . .
H10 H -0.2038 0.7850 0.4230 0.036 Uiso 1 1 calc R . .
H11 H 0.0347 0.7806 0.5086 0.036 Uiso 1 1 calc R . .
H12 H -0.0604 0.5777 0.4616 0.036 Uiso 1 1 calc R . .
C15 C 0.5527(5) 0.5343(4) 0.2655(2) 0.0198(6) Uani 1 1 d . . .
C16 C 0.6703(6) 1.5431(4) -0.2199(2) 0.0209(6) Uani 1 1 d . . .
O3 O 0.1728(4) 0.2187(3) 0.45301(15) 0.0289(5) Uani 1 1 d . . .
H17 H 0.0366 0.2400 0.4009 0.035 Uiso 1 1 d R . .
C17 C 0.3765(8) 0.1878(5) 0.5314(3) 0.0403(8) Uani 1 1 d . . .
H14 H 0.3157 0.0784 0.5765 0.060 Uiso 1 1 calc R . .
H15 H 0.3880 0.3092 0.5694 0.060 Uiso 1 1 calc R . .
H16 H 0.5659 0.1544 0.5023 0.060 Uiso 1 1 calc R . .

```

```
loop_
```

```

_atom_site_aniso_label
_atom_site_aniso_U_11
_atom_site_aniso_U_22
_atom_site_aniso_U_33
_atom_site_aniso_U_23
_atom_site_aniso_U_13
_atom_site_aniso_U_12
F1 0.0367(11) 0.0245(10) 0.0549(12) 0.0121(8) -0.0075(9) -0.0041(8)
F2 0.0504(11) 0.0311(10) 0.0459(11) 0.0085(8) 0.0110(9) 0.0261(8)
F3 0.0482(11) 0.0291(10) 0.0353(10) 0.0052(8) -0.0170(8) 0.0020(8)
O1 0.0148(10) 0.0238(11) 0.0299(10) 0.0061(8) 0.0012(8) 0.0025(8)
O2 0.0322(11) 0.0165(11) 0.0336(11) 0.0015(8) 0.0071(8) 0.0020(8)
N1 0.0187(12) 0.0151(11) 0.0234(12) 0.0008(9) 0.0031(9) 0.0013(9)
N2 0.0123(11) 0.0216(13) 0.0252(12) 0.0064(9) -0.0012(9) 0.0006(9)

```

N3 0.0123(11) 0.0179(12) 0.0293(13) 0.0069(9) 0.0009(9) 0.0038(9)
 C1 0.0220(15) 0.0202(15) 0.0275(15) -0.0022(12) 0.0015(12) 0.0051(11)
 C2 0.0290(16) 0.0201(15) 0.0255(15) 0.0060(11) 0.0027(12) 0.0057(12)
 C3 0.0204(15) 0.0187(14) 0.0303(16) 0.0016(12) 0.0025(12) 0.0056(11)
 C4 0.0202(15) 0.0175(14) 0.0235(15) 0.0035(11) -0.0047(12) 0.0041(11)
 C5 0.0189(15) 0.0233(15) 0.0252(14) -0.0003(12) 0.0017(11) 0.0046(12)
 C6 0.0208(16) 0.0167(14) 0.0217(14) 0.0016(11) 0.0014(11) 0.0011(11)
 C7 0.0194(14) 0.0182(14) 0.0190(13) 0.0038(10) -0.0014(11) -0.0018(11)
 C8 0.0163(14) 0.0203(14) 0.0253(14) -0.0008(11) -0.0033(11) 0.0023(11)
 C9 0.0229(14) 0.0148(14) 0.0267(14) -0.0003(11) -0.0006(11) 0.0027(11)
 C10 0.0209(15) 0.0159(14) 0.0273(15) 0.0014(11) 0.0007(11) -0.0011(11)
 C11 0.0187(14) 0.0143(13) 0.0217(13) 0.0025(10) 0.0000(11) 0.0036(10)
 C12 0.0278(16) 0.0187(15) 0.0310(16) 0.0000(12) -0.0036(13) 0.0040(13)
 C13 0.0217(15) 0.0187(14) 0.0258(15) -0.0006(12) -0.0018(12) 0.0017(12)
 C14 0.0210(15) 0.0245(15) 0.0257(14) -0.0003(12) 0.0024(11) 0.0027(12)
 C15 0.0175(14) 0.0199(14) 0.0223(14) -0.0023(11) -0.0028(11) -0.0025(11)
 C16 0.0196(14) 0.0168(14) 0.0261(14) 0.0020(11) -0.0049(11) 0.0012(11)
 O3 0.0347(12) 0.0204(11) 0.0310(11) 0.0045(8) 0.0024(9) 0.0023(9)
 C17 0.052(2) 0.0330(18) 0.0354(18) -0.0003(14) 0.0010(16) 0.0107(16)

_geom_special_details

;

All esds (except the esd in the dihedral angle between two l.s. planes)
 are estimated using the full covariance matrix. The cell esds are taken
 into account individually in the estimation of esds in distances, angles
 and torsion angles; correlations between esds in cell parameters are
 only
 used when they are defined by crystal symmetry. An approximate
 (isotropic)
 treatment of cell esds is used for estimating esds involving l.s.
 planes.

;

loop_

_geom_bond_atom_site_label_1
 _geom_bond_atom_site_label_2
 _geom_bond_distance
 _geom_bond_site_symmetry_2
 _geom_bond_publ_flag
 F1 C12 1.330(3) . ?
 F2 C12 1.343(3) . ?
 F3 C12 1.357(3) . ?
 O1 C6 1.243(3) . ?
 O2 C13 1.240(3) . ?
 N1 C13 1.350(4) . ?
 N1 C15 1.422(3) . ?
 N1 H18 0.8548 . ?
 N2 C6 1.368(3) . ?
 N2 C7 1.422(3) . ?
 N2 H13 0.8800 . ?
 N3 C6 1.368(3) . ?
 N3 C4 1.417(3) . ?
 N3 H1 0.9140 . ?
 C1 C16 1.385(4) . ?
 C1 C5 1.394(4) . ?
 C1 H2 0.9500 . ?
 C2 C16 1.385(4) . ?

C2 C3 1.394(4) . ?
 C2 H3 0.9500 . ?
 C3 C4 1.398(4) . ?
 C3 H4 0.9500 . ?
 C4 C5 1.388(4) . ?
 C5 H5 0.9500 . ?
 C7 C8 1.397(4) . ?
 C7 C11 1.399(4) . ?
 C8 C9 1.399(4) . ?
 C9 C10 1.380(4) . ?
 C9 H7 0.9500 . ?
 C10 C15 1.404(4) . ?
 C10 H8 0.9500 . ?
 C11 C15 1.392(4) . ?
 C11 H9 0.9500 . ?
 C12 C16 1.487(4) . ?
 C13 C14 1.509(4) . ?
 C14 H10 0.9800 . ?
 C14 H11 0.9800 . ?
 C14 H12 0.9800 . ?
 O3 C17 1.425(4) . ?
 O3H17 0.9500 . ?
 C17 H14 0.9800 . ?
 C17 H15 0.9800 . ?
 C17 H16 0.9800 . ?

loop_

_geom_angle_atom_site_label_1
 _geom_angle_atom_site_label_2
 _geom_angle_atom_site_label_3
 _geom_angle
 _geom_angle_site_symmetry_1
 _geom_angle_site_symmetry_3
 _geom_angle_publ_flag
 C13 N1 C15 129.2(2) . . ?
 C13 N1 H18 117.2 . . ?
 C15 N1 H18 113.6 . . ?
 C6 N2 C7 124.2(2) . . ?
 C6 N2 H13 117.9 . . ?
 C7 N2 H13 117.9 . . ?
 C6 N3 C4 124.6(2) . . ?
 C6 N3 H1 118.1 . . ?
 C4 N3 H1 117.3 . . ?
 C16 C1 C5 120.0(3) . . ?
 C16 C1 H2 120.0 . . ?
 C5 C1 H2 120.0 . . ?
 C16 C2 C3 120.1(3) . . ?
 C16 C2 H3 120.0 . . ?
 C3 C2 H3 120.0 . . ?
 C2 C3 C4 119.7(3) . . ?
 C2 C3 H4 120.1 . . ?
 C4 C3 H4 120.1 . . ?
 C5 C4 C3 119.9(2) . . ?
 C5 C4 N3 121.8(2) . . ?
 C3 C4 N3 118.2(2) . . ?
 C4 C5 C1 120.0(3) . . ?
 C4 C5 H5 120.0 . . ?

C1 C5 H5 120.0 . . ?
 O1 C6 N3 122.9(2) . . ?
 O1 C6 N2 123.8(2) . . ?
 N3 C6 N2 113.3(2) . . ?
 C8 C7 C11 121.3(2) . . ?
 C8 C7 N2 118.1(2) . . ?
 C11 C7 N2 120.5(2) . . ?
 C7 C8 C9 118.7(3) . . ?
 C10 C9 C8 120.8(3) . . ?
 C10 C9 H7 119.6 . . ?
 C8 C9 H7 119.6 . . ?
 C9 C10 C15 120.0(2) . . ?
 C9 C10 H8 120.0 . . ?
 C15 C10 H8 120.0 . . ?
 C15 C11 C7 118.9(2) . . ?
 C15 C11 H9 120.6 . . ?
 C7 C11 H9 120.6 . . ?
 F1 C12 F2 106.9(2) . . ?
 F1 C12 F3 104.8(2) . . ?
 F2 C12 F3 105.6(2) . . ?
 F1 C12 C16 113.5(2) . . ?
 F2 C12 C16 113.2(2) . . ?
 F3 C12 C16 112.2(2) . . ?
 O2 C13 N1 123.6(3) . . ?
 O2 C13 C14 120.8(3) . . ?
 N1 C13 C14 115.6(2) . . ?
 C13 C14 H10 109.5 . . ?
 C13 C14 H11 109.5 . . ?
 H10 C14 H11 109.5 . . ?
 C13 C14 H12 109.5 . . ?
 H10 C14 H12 109.5 . . ?
 H11 C14 H12 109.5 . . ?
 C11 C15 C10 120.3(2) . . ?
 C11 C15 N1 123.0(2) . . ?
 C10 C15 N1 116.7(2) . . ?
 C2 C16 C1 120.3(2) . . ?
 C2 C16 C12 118.5(2) . . ?
 C1 C16 C12 121.2(2) . . ?
 C17 O3 H17 179.7 . . ?
 O3 C17 H14 109.5 . . ?
 O3 C17 H15 109.5 . . ?
 H14 C17 H15 109.5 . . ?
 O3 C17 H16 109.5 . . ?
 H14 C17 H16 109.5 . . ?
 H15 C17 H16 109.5 . . ?

_diffraction_measured_fraction_theta_max	0.997
_diffraction_refl_theta_full	24.99
_diffraction_measured_fraction_theta_full	0.997
_refine_diff_density_max	0.376
_refine_diff_density_min	-0.379
_refine_diff_density_rms	0.047

A1.3: Crystallographic data for 73

Identification code	cs085	
Empirical formula	C16 H14 F3 N3 O2	
Formula weight	337.30	
Temperature	150 K	
Wavelength	0.71070 Å	
Crystal system	monoclinic	
Space group	P21/c	
Unit cell dimensions	a = 11.322(17) Å	$\alpha = 90^\circ$.
	b = 15.80(2) Å	$\beta = 96.43(3)^\circ$.
	c = 8.821(12) Å	$\gamma = 90^\circ$.
Volume	1568(4) Å ³	
Z	1	
Density (calculated)	0.357 Mg/m ³	
Absorption coefficient	0.030 mm ⁻¹	
F(000)	174	
Crystal size	0.20 x 0.15 x 0.05 mm ³	
Theta range for data collection	2.66 to 24.99°.	
Index ranges	-11 ≤ h ≤ 13, -18 ≤ k ≤ 18, -10 ≤ l ≤ 10	
Reflections collected	7829	
Independent reflections	2756 [R(int) = 0.1018]	
Completeness to theta = 24.99°	99.7 %	
Refinement method	Full-matrix least-squares on F ²	
Data / restraints / parameters	2756 / 0 / 229	
Goodness-of-fit on F ²	1.040	
Final R indices [I > 2sigma(I)]	R1 = 0.0826, wR2 = 0.2227	
R indices (all data)	R1 = 0.1067, wR2 = 0.2512	
Largest diff. peak and hole	0.755 and -0.636 e.Å ⁻³	

A1.3.1: CIF file for 73

```

data_cs085

_audit_creation_method          SHELXL-97
_chemical_name_systematic
;
?
;
_chemical_name_common          ?
_chemical_melting_point        ?
_chemical_formula_moiety       ?
_chemical_formula_sum
'C64 H56 F12 N12 O8'
_chemical_formula_weight       1349.21

loop_
_atom_type_symbol
_atom_type_description
_atom_type_scatter_dispersion_real
_atom_type_scatter_dispersion_imag
_atom_type_scatter_source
'C' 'C' 0.0033 0.0016
'International Tables Vol C Tables 4.2.6.8 and 6.1.1.4'
'H' 'H' 0.0000 0.0000
'International Tables Vol C Tables 4.2.6.8 and 6.1.1.4'
'F' 'F' 0.0171 0.0103
'International Tables Vol C Tables 4.2.6.8 and 6.1.1.4'
'N' 'N' 0.0061 0.0033
'International Tables Vol C Tables 4.2.6.8 and 6.1.1.4'
'O' 'O' 0.0106 0.0060
'International Tables Vol C Tables 4.2.6.8 and 6.1.1.4'

_symmetry_cell_setting         Monoclinic
_symmetry_space_group_name_H-M P2(1)/c

loop_
_symmetry_equiv_pos_as_xyz
'x, y, z'
'-x, y+1/2, -z+1/2'
'-x, -y, -z'
'x, -y-1/2, z-1/2'

_cell_length_a                 11.322(17)
_cell_length_b                 15.80(2)
_cell_length_c                 8.821(12)
_cell_angle_alpha              90.00
_cell_angle_beta               96.43(3)
_cell_angle_gamma              90.00
_cell_volume                   1568(4)
_cell_formula_units_Z          1
_cell_measurement_temperature   108(2)
_cell_measurement_reflns_used  ?
_cell_measurement_theta_min    ?
_cell_measurement_theta_max    ?

```

```

_exptl_crystal_description      prism
_exptl_crystal_colour          colourless
_exptl_crystal_size_max        0.40
_exptl_crystal_size_mid        0.13
_exptl_crystal_size_min        0.08
_exptl_crystal_density_meas    ?
_exptl_crystal_density_diffn   1.429
_exptl_crystal_density_method  'not measured'
_exptl_crystal_F_000           696
_exptl_absorpt_coefficient_mu  0.120
_exptl_absorpt_correction_type 'Multi-scan'
_exptl_absorpt_correction_T_min 0.81540
_exptl_absorpt_correction_T_max 1.00000
_exptl_absorpt_process_details 'Blessing, Acta Cryst. (1995) A51 33-38.'

_exptl_special_details
;
?
;

_diffn_ambient_temperature     108(2)
_diffn_radiation_wavelength    0.71070
_diffn_radiation_type          MoK\alpha
_diffn_radiation_source        'fine-focus sealed tube'
_diffn_radiation_monochromator graphite
_diffn_measurement_device_type 'Rigaku Saturn 724'
_diffn_measurement_method      'omega and phi scans'
_diffn_detector_area_resol_mean ?
_diffn_standards_number        ?
_diffn_standards_interval_count ?
_diffn_standards_interval_time ?
_diffn_standards_decay_%       ?
_diffn_reflns_number           7829
_diffn_reflns_av_R_equivalents 0.1018
_diffn_reflns_av_sigmaI/netI   0.0891
_diffn_reflns_limit_h_min      -11
_diffn_reflns_limit_h_max      13
_diffn_reflns_limit_k_min      -18
_diffn_reflns_limit_k_max      18
_diffn_reflns_limit_l_min      -10
_diffn_reflns_limit_l_max      10
_diffn_reflns_theta_min        2.66
_diffn_reflns_theta_max        24.99
_reflns_number_total           2756
_reflns_number_gt              2063
_reflns_threshold_expression    >2sigma(I)

_computing_data_collection     'Rigaku Crystalclear'
_computing_cell_refinement     'Rigaku Crystalclear'
_computing_data_reduction      'Rigaku Crystalclear'
_computing_structure_solution  'SHELXS-97 (Sheldrick, 1990)'
_computing_structure_refinement 'SHELXL-97 (Sheldrick, 1997)'
_computing_molecular_graphics  'Shelxtl'
_computing_publication_material 'Shelxtl'

_refine_special_details

```

```

;
Refinement of F^2^ against ALL reflections. The weighted R-factor wR
and
goodness of fit S are based on F^2^, conventional R-factors R are based
on F, with F set to zero for negative F^2^. The threshold expression of
F^2^ > 2sigma(F^2^) is used only for calculating R-factors(gt) etc. and
is
not relevant to the choice of reflections for refinement. R-factors
based
on F^2^ are statistically about twice as large as those based on F, and
R-
factors based on ALL data will be even larger.
;

```

```

_refine_ls_structure_factor_coef  Fsqd
_refine_ls_matrix_type            full
_refine_ls_weighting_scheme       calc
_refine_ls_weighting_details
'calc w=1/[\s^2^(Fo^2^)+(0.1440P)^2+1.1423P] where P=(Fo^2^+2Fc^2^)/3'
_atom_sites_solution_primary      direct
_atom_sites_solution_secondary    difmap
_atom_sites_solution_hydrogens    geom
_refine_ls_hydrogen_treatment     mixed
_refine_ls_extinction_method      none
_refine_ls_extinction_coef        ?
_refine_ls_number_reflns          2756
_refine_ls_number_parameters       229
_refine_ls_number_restraints      0
_refine_ls_R_factor_all            0.1067
_refine_ls_R_factor_gt             0.0826
_refine_ls_wR_factor_ref           0.2512
_refine_ls_wR_factor_gt            0.2227
_refine_ls_goodness_of_fit_ref     1.040
_refine_ls_restrained_S_all        1.040
_refine_ls_shift/su_max            0.028
_refine_ls_shift/su_mean           0.001

```

```

loop_
  _atom_site_label
  _atom_site_type_symbol
  _atom_site_fract_x
  _atom_site_fract_y
  _atom_site_fract_z
  _atom_site_U_iso_or_equiv
  _atom_site_adp_type
  _atom_site_occupancy
  _atom_site_symmetry_multiplicity
  _atom_site_calc_flag
  _atom_site_refinement_flags
  _atom_site_disorder_assembly
  _atom_site_disorder_group
F1 F 1.1009(4) 0.3099(3) 0.4977(4) 0.1029(17) Uani 1 1 d . . .
F2 F 0.9976(3) 0.3853(2) 0.3448(7) 0.134(2) Uani 1 1 d . . .
F3 F 1.1416(4) 0.3210(3) 0.2771(5) 0.1007(16) Uani 1 1 d . . .
O1 O 0.7680(2) -0.02806(16) 0.4393(3) 0.0234(6) Uani 1 1 d . . .
O2 O 0.3961(2) -0.04941(17) 0.0865(3) 0.0274(7) Uani 1 1 d . . .
N2 N 0.6131(3) -0.06606(19) 0.2634(3) 0.0224(7) Uani 1 1 d . . .

```

H6 H 0.5822 -0.0628 0.1675 0.027 Uiso 1 1 calc R . .
 N1 N 0.7460(3) 0.03423(19) 0.2024(3) 0.0240(7) Uani 1 1 d . . .
 H5 H 0.7154 0.0274 0.1071 0.029 Uiso 1 1 calc R . .
 N3 N 0.3728(3) -0.03454(19) 0.3385(3) 0.0234(7) Uani 1 1 d . . .
 H11 H 0.3406 -0.0024 0.4043 0.028 Uiso 1 1 calc R . .
 C16 C 0.2647(4) 0.0595(3) 0.1584(6) 0.0382(11) Uani 1 1 d . . .
 C6 C 0.7985(3) 0.1799(3) 0.1737(4) 0.0289(9) Uani 1 1 d . . .
 H3 H 0.7280 0.1863 0.1054 0.035 Uiso 1 1 calc R . .
 C3 C 1.0045(3) 0.1608(3) 0.3715(4) 0.0271(9) Uani 1 1 d . . .
 H1 H 1.0758 0.1542 0.4383 0.032 Uiso 1 1 calc R . .
 C2 C 0.9738(3) 0.2399(3) 0.3120(4) 0.0290(9) Uani 1 1 d . . .
 C1 C 1.0503(4) 0.3143(3) 0.3554(5) 0.0342(10) Uani 1 1 d . . .
 C8 C 0.7127(3) -0.0206(2) 0.3104(4) 0.0208(8) Uani 1 1 d . . .
 C11 C 0.5749(4) -0.2363(3) 0.5452(4) 0.0308(9) Uani 1 1 d . . .
 H8 H 0.6200 -0.2813 0.5942 0.037 Uiso 1 1 calc R . .
 C10 C 0.6230(3) -0.1862(2) 0.4369(4) 0.0256(8) Uani 1 1 d . . .
 H7 H 0.7006 -0.1977 0.4111 0.031 Uiso 1 1 calc R . .
 C9 C 0.5574(3) -0.1190(2) 0.3662(4) 0.0206(8) Uani 1 1 d . . .
 C14 C 0.4433(3) -0.1040(2) 0.4008(4) 0.0221(8) Uani 1 1 d . . .
 C12 C 0.4604(4) -0.2197(3) 0.5808(4) 0.0297(9) Uani 1 1 d . . .
 H9 H 0.4273 -0.2531 0.6550 0.036 Uiso 1 1 calc R . .
 C15 C 0.3500(3) -0.0128(2) 0.1904(4) 0.0261(9) Uani 1 1 d . . .
 C13 C 0.3950(3) -0.1549(2) 0.5083(4) 0.0259(8) Uani 1 1 d . . .
 H10 H 0.3164 -0.1446 0.5315 0.031 Uiso 1 1 calc R . .
 C5 C 0.8276(3) 0.1015(2) 0.2373(4) 0.0230(8) Uani 1 1 d . . .
 C4 C 0.9324(3) 0.0911(3) 0.3350(4) 0.0275(9) Uani 1 1 d . . .
 H2 H 0.9541 0.0370 0.3758 0.033 Uiso 1 1 calc R . .
 C7 C 0.8716(4) 0.2493(3) 0.2094(5) 0.0317(9) Uani 1 1 d . . .
 H4 H 0.8522 0.3028 0.1641 0.038 Uiso 1 1 calc R . .
 H20 H 0.247(4) 0.085(3) 0.238(6) 0.047(14) Uiso 1 1 d . . .
 H22 H 0.291(7) 0.091(5) 0.080(9) 0.10(2) Uiso 1 1 d . . .
 H21 H 0.198(6) 0.037(4) 0.088(7) 0.074(19) Uiso 1 1 d . . .

loop_

_atom_site_aniso_label
 _atom_site_aniso_U_11
 _atom_site_aniso_U_22
 _atom_site_aniso_U_33
 _atom_site_aniso_U_23
 _atom_site_aniso_U_13
 _atom_site_aniso_U_12
 F1 0.154(4) 0.103(3) 0.0461(18) -0.004(2) -0.012(2) -0.089(3)
 F2 0.058(2) 0.0351(18) 0.293(7) -0.033(3) -0.043(3) -0.0047(16)
 F3 0.094(3) 0.111(3) 0.109(3) -0.049(2) 0.065(2) -0.074(2)
 O1 0.0275(14) 0.0285(14) 0.0145(12) 0.0020(11) 0.0028(10) 0.0002(10)
 O2 0.0302(15) 0.0356(15) 0.0159(12) -0.0023(11) 0.0007(10) 0.0047(12)
 N2 0.0276(17) 0.0262(17) 0.0130(14) 0.0022(13) 0.0002(11) -0.0011(12)
 N1 0.0298(18) 0.0284(17) 0.0135(14) 0.0009(13) 0.0015(12) -0.0055(13)
 N3 0.0290(18) 0.0246(16) 0.0166(15) -0.0034(13) 0.0028(12) 0.0049(12)
 C16 0.046(3) 0.041(3) 0.028(2) 0.002(2) 0.005(2) 0.016(2)
 C6 0.030(2) 0.033(2) 0.0224(19) 0.0042(17) -0.0005(15) 0.0006(17)
 C3 0.023(2) 0.036(2) 0.0220(18) 0.0018(17) 0.0001(14) -0.0038(16)
 C2 0.027(2) 0.033(2) 0.029(2) -0.0055(17) 0.0091(16) -0.0038(16)
 C1 0.037(2) 0.032(2) 0.034(2) 0.0002(19) 0.0071(17) -0.0093(18)
 C8 0.0227(19) 0.0220(18) 0.0180(17) -0.0021(15) 0.0040(14) 0.0030(14)
 C11 0.039(2) 0.028(2) 0.0241(19) 0.0038(17) -0.0018(16) -0.0006(17)
 C10 0.030(2) 0.0239(19) 0.0221(18) -0.0002(16) 0.0008(15) 0.0008(15)

C9 0.0249(19) 0.0222(18) 0.0143(16) -0.0008(14) 0.0008(13) -0.0035(14)
 C14 0.033(2) 0.0181(18) 0.0144(16) -0.0049(14) 0.0000(13) 0.0004(14)
 C12 0.041(2) 0.027(2) 0.0212(18) 0.0060(16) 0.0052(16) -0.0066(17)
 C15 0.028(2) 0.028(2) 0.0222(19) 0.0002(16) 0.0003(15) 0.0030(15)
 C13 0.030(2) 0.026(2) 0.0219(18) -0.0016(16) 0.0037(15) -0.0020(15)
 C5 0.0268(19) 0.029(2) 0.0145(16) -0.0005(15) 0.0058(14) -0.0023(15)
 C4 0.029(2) 0.032(2) 0.0213(18) 0.0004(16) 0.0039(15) -0.0004(16)
 C7 0.033(2) 0.028(2) 0.033(2) 0.0078(17) 0.0006(16) -0.0027(17)

_geom_special_details

;
 All esds (except the esd in the dihedral angle between two l.s. planes)
 are estimated using the full covariance matrix. The cell esds are taken
 into account individually in the estimation of esds in distances, angles
 and torsion angles; correlations between esds in cell parameters are
 only

used when they are defined by crystal symmetry. An approximate
 (isotropic)
 treatment of cell esds is used for estimating esds involving l.s.
 planes.

;

loop_

_geom_bond_atom_site_label_1
 _geom_bond_atom_site_label_2
 _geom_bond_distance
 _geom_bond_site_symmetry_2
 _geom_bond_publ_flag

F1 C1 1.323(6) . ?
 F2 C1 1.269(6) . ?
 F3 C1 1.310(5) . ?
 O1 C8 1.241(4) . ?
 O2 C15 1.247(5) . ?
 N2 C8 1.362(5) . ?
 N2 C9 1.431(5) . ?
 N2 H6 0.8800 . ?
 N1 C8 1.371(5) . ?
 N1 C5 1.419(5) . ?
 N1 H5 0.8800 . ?
 N3 C15 1.347(5) . ?
 N3 C14 1.431(5) . ?
 N3 H11 0.8800 . ?
 C16 C15 1.502(6) . ?
 C16 H20 0.86(6) . ?
 C16 H22 0.93(8) . ?
 C16 H21 0.99(6) . ?
 C6 C5 1.385(6) . ?
 C6 C7 1.389(6) . ?
 C6 H3 0.9500 . ?
 C3 C2 1.385(6) . ?
 C3 C4 1.387(5) . ?
 C3 H1 0.9500 . ?
 C2 C7 1.395(6) . ?
 C2 C1 1.485(6) . ?
 C11 C12 1.392(6) . ?
 C11 C10 1.398(5) . ?
 C11 H8 0.9500 . ?

C10 C9 1.401(5) . ?
 C10 H7 0.9500 . ?
 C9 C14 1.380(5) . ?
 C14 C13 1.399(5) . ?
 C12 C13 1.379(6) . ?
 C12 H9 0.9500 . ?
 C13 H10 0.9500 . ?
 C5 C4 1.396(5) . ?
 C4 H2 0.9500 . ?
 C7 H4 0.9500 . ?

 loop_
 _geom_angle_atom_site_label_1
 _geom_angle_atom_site_label_2
 _geom_angle_atom_site_label_3
 _geom_angle
 _geom_angle_site_symmetry_1
 _geom_angle_site_symmetry_3
 _geom_angle_publ_flag
 C8 N2 C9 121.6(3) . . ?
 C8 N2 H6 119.2 . . ?
 C9 N2 H6 119.2 . . ?
 C8 N1 C5 123.0(3) . . ?
 C8 N1 H5 118.5 . . ?
 C5 N1 H5 118.5 . . ?
 C15 N3 C14 127.3(3) . . ?
 C15 N3 H11 116.3 . . ?
 C14 N3 H11 116.3 . . ?
 C15 C16 H20 115(3) . . ?
 C15 C16 H22 107(5) . . ?
 H20 C16 H22 118(6) . . ?
 C15 C16 H21 106(4) . . ?
 H20 C16 H21 117(5) . . ?
 H22 C16 H21 91(5) . . ?
 C5 C6 C7 120.4(4) . . ?
 C5 C6 H3 119.8 . . ?
 C7 C6 H3 119.8 . . ?
 C2 C3 C4 120.8(4) . . ?
 C2 C3 H1 119.6 . . ?
 C4 C3 H1 119.6 . . ?
 C3 C2 C7 119.8(4) . . ?
 C3 C2 C1 120.2(4) . . ?
 C7 C2 C1 120.1(4) . . ?
 F2 C1 F3 106.4(5) . . ?
 F2 C1 F1 105.5(4) . . ?
 F3 C1 F1 102.8(4) . . ?
 F2 C1 C2 115.2(4) . . ?
 F3 C1 C2 113.6(4) . . ?
 F1 C1 C2 112.4(4) . . ?
 O1 C8 N2 123.0(3) . . ?
 O1 C8 N1 123.2(3) . . ?
 N2 C8 N1 113.9(3) . . ?
 C12 C11 C10 119.4(4) . . ?
 C12 C11 H8 120.3 . . ?
 C10 C11 H8 120.3 . . ?
 C11 C10 C9 120.4(4) . . ?
 C11 C10 H7 119.8 . . ?

C9 C10 H7 119.8 . . ?
 C14 C9 C10 119.6(3) . . ?
 C14 C9 N2 122.0(3) . . ?
 C10 C9 N2 118.4(3) . . ?
 C9 C14 C13 119.8(3) . . ?
 C9 C14 N3 122.9(3) . . ?
 C13 C14 N3 117.2(3) . . ?
 C13 C12 C11 120.1(3) . . ?
 C13 C12 H9 120.0 . . ?
 C11 C12 H9 120.0 . . ?
 O2 C15 N3 122.9(3) . . ?
 O2 C15 C16 121.9(4) . . ?
 N3 C15 C16 115.2(3) . . ?
 C12 C13 C14 120.7(4) . . ?
 C12 C13 H10 119.7 . . ?
 C14 C13 H10 119.7 . . ?
 C6 C5 C4 120.2(4) . . ?
 C6 C5 N1 117.6(3) . . ?
 C4 C5 N1 122.2(3) . . ?
 C3 C4 C5 119.2(4) . . ?
 C3 C4 H2 120.4 . . ?
 C5 C4 H2 120.4 . . ?
 C6 C7 C2 119.6(4) . . ?
 C6 C7 H4 120.2 . . ?
 C2 C7 H4 120.2 . . ?

_diffirn_measured_fraction_theta_max	0.997
_diffirn_reflms_theta_full	24.99
_diffirn_measured_fraction_theta_full	0.997
_refine_diff_density_max	0.756
_refine_diff_density_min	-0.637
_refine_diff_density_rms	0.084

A1.4: Crystallographic data for 87

Identification code	cs053m	
Empirical formula	C80 H52 F12 N16 O4	
Formula weight	1529.38	
Temperature	150 K	
Wavelength	0.71073 Å	
Crystal system	Monoclinic	
Space group	P21/c	
Unit cell dimensions	a = 13.1965(14) Å	$\alpha = 90^\circ$.
	b = 11.8685(12) Å	$\beta = 91.320(2)^\circ$.
	c = 11.0189(11) Å	$\gamma = 90^\circ$.
Volume	1725.4(3) Å ³	
Z	1	
Density (calculated)	1.472 Mg/m ³	
Absorption coefficient	0.117 mm ⁻¹	
F(000)	784	
Crystal size	0.60 x 0.31 x 0.16 mm ³	
Theta range for data collection	2.31 to 25.00°.	
Index ranges	-15 ≤ h ≤ 15, -14 ≤ k ≤ 14, -13 ≤ l ≤ 12	
Reflections collected	13251	
Independent reflections	3031 [R(int) = 0.0288]	
Completeness to theta = 25.00°	100.0 %	
Absorption correction	Semi-empirical from equivalents	
Max. and min. transmission	1.00000 and 0.857466	
Refinement method	Full-matrix least-squares on F ²	
Data / restraints / parameters	3031 / 0 / 253	
Goodness-of-fit on F ²	1.085	
Final R indices [I > 2σ(I)]	R1 = 0.0648, wR2 = 0.1693	
R indices (all data)	R1 = 0.0738, wR2 = 0.1760	
Largest diff. peak and hole	0.822 and -0.408 e.Å ⁻³	

A1.4.1: CIF file for 87

```

data_cs053m

_audit_creation_method          SHELXL-97
_chemical_name_systematic
;
?
;
_chemical_name_common          ?
_chemical_melting_point        ?
_chemical_formula_moiety       ?
_chemical_formula_sum
'C80 H52 F12 N16 O4'
_chemical_formula_weight       1529.38

loop_
_atom_type_symbol
_atom_type_description
_atom_type_scatter_dispersion_real
_atom_type_scatter_dispersion_imag
_atom_type_scatter_source
'C' 'C' 0.0033 0.0016
'International Tables Vol C Tables 4.2.6.8 and 6.1.1.4'
'H' 'H' 0.0000 0.0000
'International Tables Vol C Tables 4.2.6.8 and 6.1.1.4'
'F' 'F' 0.0171 0.0103
'International Tables Vol C Tables 4.2.6.8 and 6.1.1.4'
'N' 'N' 0.0061 0.0033
'International Tables Vol C Tables 4.2.6.8 and 6.1.1.4'
'O' 'O' 0.0106 0.0060
'International Tables Vol C Tables 4.2.6.8 and 6.1.1.4'

_symmetry_cell_setting         monoclinic
_symmetry_space_group_name_H-M P21/c

loop_
_symmetry_equiv_pos_as_xyz
'x, y, z'
'-x, y+1/2, -z+1/2'
'-x, -y, -z'
'x, -y-1/2, z-1/2'

_cell_length_a                 13.1965(14)
_cell_length_b                 11.8685(12)
_cell_length_c                 11.0189(11)
_cell_angle_alpha              90.00
_cell_angle_beta               91.320(2)
_cell_angle_gamma              90.00
_cell_volume                   1725.4(3)
_cell_formula_units_Z          1
_cell_measurement_temperature  396(2)
_cell_measurement_reflns_used  ?
_cell_measurement_theta_min    ?
_cell_measurement_theta_max    ?

```

```

_exptl_crystal_description      plate
_exptl_crystal_colour          colourless
_exptl_crystal_size_max        0.60
_exptl_crystal_size_mid        0.30
_exptl_crystal_size_min        0.16
_exptl_crystal_density_meas    ?
_exptl_crystal_density_diffn   1.472
_exptl_crystal_density_method  'not measured'
_exptl_crystal_F_000           784
_exptl_absorpt_coefficient_mu  0.117
_exptl_absorpt_correction_type multi-scan
_exptl_absorpt_correction_T_min 0.857466
_exptl_absorpt_correction_T_max 1.00000
_exptl_absorpt_process_details 'Blessing, Acta Cryst. (1995) A51 33-
38.'

_exptl_special_details
;
?
;

_diffn_ambient_temperature     396(2)
_diffn_radiation_wavelength    0.71073
_diffn_radiation_type          MoK\alpha
_diffn_radiation_source        'fine-focus sealed tube'
_diffn_radiation_monochromator graphite
_diffn_measurement_device_type 'Bruker Smart Apex'
_diffn_measurement_method      'omega scans'
_diffn_detector_area_resol_mean ?
_diffn_standards_number        ?
_diffn_standards_interval_count ?
_diffn_standards_interval_time ?
_diffn_standards_decay_%       ?
_diffn_reflns_number           13251
_diffn_reflns_av_R_equivalents 0.0288
_diffn_reflns_av_sigmaI/netI   0.0226
_diffn_reflns_limit_h_min      -15
_diffn_reflns_limit_h_max      15
_diffn_reflns_limit_k_min      -14
_diffn_reflns_limit_k_max      14
_diffn_reflns_limit_l_min      -13
_diffn_reflns_limit_l_max      12
_diffn_reflns_theta_min        2.31
_diffn_reflns_theta_max        25.00
_reflns_number_total            3031
_reflns_number_gt               2634
_reflns_threshold_expression    >2sigma(I)

_computing_data_collection      'Bruker Smart'
_computing_cell_refinement      'Bruker Smart'
_computing_data_reduction       'Bruker Saint'
_computing_structure_solution   'SHELXS-97 (Sheldrick, 1990)'
_computing_structure_refinement 'SHELXL-97 (Sheldrick, 1997)'
_computing_molecular_graphics   'Bruker Shelxtl'
_computing_publication_material 'Bruker Shelxtl'

_refine_special_details

```

```

;
Refinement of F^2^ against ALL reflections. The weighted R-factor wR
and
goodness of fit S are based on F^2^, conventional R-factors R are based
on F, with F set to zero for negative F^2^. The threshold expression of
F^2^ > 2sigma(F^2^) is used only for calculating R-factors(gt) etc. and
is
not relevant to the choice of reflections for refinement. R-factors
based
on F^2^ are statistically about twice as large as those based on F, and
R-
factors based on ALL data will be even larger.
;

```

```

_refine_ls_structure_factor_coef Fsqd
_refine_ls_matrix_type full
_refine_ls_weighting_scheme calc
_refine_ls_weighting_details
'calc w=1/[\s^2^(Fo^2^)+(0.0948P)^2+2.1675P] where P=(Fo^2^+2Fc^2^)/3'
_atom_sites_solution_primary direct
_atom_sites_solution_secondary difmap
_atom_sites_solution_hydrogens geom
_refine_ls_hydrogen_treatment constr
_refine_ls_extinction_method none
_refine_ls_extinction_coef ?
_refine_ls_number_reflns 3031
_refine_ls_number_parameters 253
_refine_ls_number_restraints 0
_refine_ls_R_factor_all 0.0739
_refine_ls_R_factor_gt 0.0650
_refine_ls_wR_factor_ref 0.1824
_refine_ls_wR_factor_gt 0.1753
_refine_ls_goodness_of_fit_ref 1.092
_refine_ls_restrained_S_all 1.092
_refine_ls_shift/su_max 0.009
_refine_ls_shift/su_mean 0.002

```

```

loop_
_atom_site_label
_atom_site_type_symbol
_atom_site_fract_x
_atom_site_fract_y
_atom_site_fract_z
_atom_site_U_iso_or_equiv
_atom_site_adp_type
_atom_site_occupancy
_atom_site_symmetry_multiplicity
_atom_site_calc_flag
_atom_site_refinement_flags
_atom_site_disorder_assembly
_atom_site_disorder_group
F1 F 0.5771(3) 0.1852(3) 0.8814(3) 0.1086(12) Uani 1 1 d . . .
F2 F 0.57455(15) 0.3580(2) 0.8397(2) 0.0665(8) Uani 1 1 d . . .
F3 F 0.66461(15) 0.2446(3) 0.7392(3) 0.0913(11) Uani 1 1 d . . .
O2 O 0.28041(14) 0.00664(16) 0.37463(17) 0.0263(5) Uani 1 1 d . . .
N1 N 0.24668(17) 0.17843(19) 0.4591(2) 0.0264(6) Uani 1 1 d . . .
H1 H 0.2030 0.2322 0.4568 0.032 Uiso 1 1 d R . .

```

N2 N 0.13386(17) 0.09976(19) 0.3255(2) 0.0254(5) Uani 1 1 d . . .
 H2 H 0.0983 0.1586 0.3409 0.031 Uiso 1 1 d R . .
 N5 N -0.03852(18) -0.20915(19) -0.0039(2) 0.0247(5) Uani 1 1 d . . .
 N6 N -0.15926(17) -0.0967(2) 0.1502(2) 0.0264(6) Uani 1 1 d . . .
 C1 C 0.5764(3) 0.2595(3) 0.7865(4) 0.0515(10) Uani 1 1 d . . .
 C2 C 0.4897(2) 0.2384(3) 0.7000(3) 0.0329(7) Uani 1 1 d . . .
 C3 C 0.4878(2) 0.1405(3) 0.6339(3) 0.0294(7) Uani 1 1 d . . .
 H3A H 0.5407 0.0893 0.6432 0.035 Uiso 1 1 calc R . .
 C4 C 0.4110(3) 0.3152(3) 0.6849(4) 0.0480(10) Uani 1 1 d . . .
 H4A H 0.4116 0.3820 0.7291 0.058 Uiso 1 1 calc R . .
 C5 C 0.3324(2) 0.2926(3) 0.6051(3) 0.0397(8) Uani 1 1 d . . .
 H5 H 0.2795 0.3440 0.5960 0.048 Uiso 1 1 calc R . .
 C6 C 0.3310(2) 0.1940(2) 0.5376(2) 0.0226(6) Uani 1 1 d . . .
 C7 C 0.4088(2) 0.1166(2) 0.5537(3) 0.0258(6) Uani 1 1 d . . .
 H7 H 0.4078 0.0491 0.5108 0.031 Uiso 1 1 calc R . .
 C8 C 0.22608(19) 0.0885(2) 0.3863(2) 0.0203(6) Uani 1 1 d . . .
 C9 C 0.09371(19) 0.0227(2) 0.2403(2) 0.0195(6) Uani 1 1 d . . .
 C10 C 0.1529(2) -0.0360(2) 0.1638(2) 0.0208(6) Uani 1 1 d . . .
 H10 H 0.2226 -0.0246 0.1668 0.025 Uiso 1 1 calc R . .
 C11 C 0.1109(2) -0.1147(2) 0.0788(2) 0.0200(6) Uani 1 1 d . . .
 C12 C 0.1715(2) -0.1764(2) -0.0014(2) 0.0256(6) Uani 1 1 d . . .
 H12 H 0.2414 -0.1668 -0.0003 0.031 Uiso 1 1 calc R . .
 C13 C 0.1264(2) -0.2505(2) -0.0808(2) 0.0280(7) Uani 1 1 d . . .
 H13 H 0.1649 -0.2911 -0.1353 0.034 Uiso 1 1 calc R . .
 C14 C 0.0210(2) -0.2641(2) -0.0784(2) 0.0282(7) Uani 1 1 d . . .
 H14 H -0.0089 -0.3149 -0.1326 0.034 Uiso 1 1 calc R . .
 C15 C 0.0058(2) -0.1336(2) 0.0729(2) 0.0197(6) Uani 1 1 d . . .
 C16 C -0.0586(2) -0.0725(2) 0.1547(2) 0.0205(6) Uani 1 1 d . . .
 C17 C -0.01518(19) 0.0053(2) 0.2381(2) 0.0199(6) Uani 1 1 d . . .
 C18 C -0.0814(2) 0.0567(2) 0.3201(2) 0.0250(6) Uani 1 1 d . . .
 H18 H -0.0564 0.1082 0.3770 0.030 Uiso 1 1 calc R . .
 C19 C -0.1817(2) 0.0310(3) 0.3159(3) 0.0299(7) Uani 1 1 d . . .
 H19 H -0.2258 0.0637 0.3703 0.036 Uiso 1 1 calc R . .
 C20 C -0.2178(2) -0.0454(3) 0.2285(3) 0.0310(7) Uani 1 1 d . . .
 H20 H -0.2869 -0.0609 0.2253 0.037 Uiso 1 1 calc R . .

 loop_
 _atom_site_aniso_label
 _atom_site_aniso_U_11
 _atom_site_aniso_U_22
 _atom_site_aniso_U_33
 _atom_site_aniso_U_23
 _atom_site_aniso_U_13
 _atom_site_aniso_U_12
 F1 0.108(3) 0.120(3) 0.095(2) 0.019(2) -0.070(2) -0.020(2)
 F2 0.0379(12) 0.0823(17) 0.0784(16) -0.0565(14) -0.0193(11) 0.0084(11)
 F3 0.0211(11) 0.145(3) 0.107(2) -0.086(2) -0.0118(12) 0.0091(13)
 O2 0.0251(10) 0.0222(10) 0.0312(11) -0.0073(8) -0.0078(8) 0.0068(8)
 N1 0.0234(12) 0.0207(12) 0.0345(13) -0.0094(10) -0.0105(10) 0.0092(9)
 N2 0.0233(12) 0.0199(11) 0.0328(13) -0.0094(10) -0.0077(10) 0.0059(9)
 N5 0.0319(13) 0.0221(12) 0.0200(11) -0.0001(9) -0.0027(9) -0.0061(10)
 N6 0.0233(12) 0.0294(13) 0.0264(12) 0.0020(10) 0.0004(10) -0.0073(10)
 C1 0.0312(19) 0.061(2) 0.061(2) -0.032(2) -0.0119(17) 0.0100(17)
 C2 0.0196(14) 0.0437(18) 0.0353(16) -0.0155(14) -0.0031(12) 0.0007(13)
 C3 0.0221(14) 0.0349(16) 0.0310(15) -0.0089(13) -0.0040(12) 0.0090(12)
 C4 0.0315(17) 0.042(2) 0.070(2) -0.0363(18) -0.0134(16) 0.0100(15)
 C5 0.0277(16) 0.0310(17) 0.060(2) -0.0195(16) -0.0148(15) 0.0111(13)

```

C6 0.0194(13) 0.0237(14) 0.0246(14) -0.0039(11) -0.0022(10) 0.0007(11)
C7 0.0248(14) 0.0244(14) 0.0281(15) -0.0100(12) -0.0052(11) 0.0048(11)
C8 0.0199(13) 0.0201(13) 0.0208(13) -0.0011(10) -0.0020(10) 0.0027(11)
C9 0.0232(13) 0.0160(13) 0.0191(12) 0.0011(10) -0.0042(10) 0.0001(10)
C10 0.0203(13) 0.0214(13) 0.0207(13) 0.0027(10) -0.0025(10) -0.0019(10)
C11 0.0263(14) 0.0153(13) 0.0182(13) 0.0056(10) -0.0019(10) 0.0005(10)
C12 0.0298(15) 0.0275(15) 0.0197(13) 0.0020(11) 0.0029(11) 0.0008(12)
C13 0.0381(17) 0.0260(15) 0.0201(13) -0.0030(11) 0.0051(12) 0.0008(12)
C14 0.0447(18) 0.0228(14) 0.0171(13) -0.0038(11) -0.0022(12) -0.0080(13)
C15 0.0282(14) 0.0159(13) 0.0148(12) 0.0053(10) -0.0021(10) -0.0031(11)
C16 0.0226(13) 0.0199(13) 0.0190(13) 0.0063(10) -0.0026(10) -0.0029(10)
C17 0.0228(14) 0.0172(13) 0.0196(13) 0.0046(10) -0.0020(10) 0.0021(10)
C18 0.0274(15) 0.0238(14) 0.0236(14) -0.0025(11) -0.0012(11) 0.0016(11)
C19 0.0285(15) 0.0335(16) 0.0280(15) -0.0006(12) 0.0063(12) 0.0042(12)
C20 0.0213(14) 0.0364(17) 0.0354(16) 0.0036(13) 0.0039(12) -0.0052(12)

```

```
_geom_special_details
```

```

;
All esds (except the esd in the dihedral angle between two l.s. planes)
are estimated using the full covariance matrix. The cell esds are taken
into account individually in the estimation of esds in distances, angles
and torsion angles; correlations between esds in cell parameters are
only
used when they are defined by crystal symmetry. An approximate
(isotropic)
treatment of cell esds is used for estimating esds involving l.s.
planes.

```

```
;
```

```
loop_
```

```

_geom_bond_atom_site_label_1
_geom_bond_atom_site_label_2
_geom_bond_distance
_geom_bond_site_symmetry_2
_geom_bond_publ_flag
F1 C1 1.368(5) . ?
F2 C1 1.309(4) . ?
F3 C1 1.298(4) . ?
O2 C8 1.216(3) . ?
N1 C8 1.359(3) . ?
N1 C6 1.405(3) . ?
N2 C8 1.383(3) . ?
N2 C9 1.405(3) . ?
N5 C14 1.321(4) . ?
N5 C15 1.357(3) . ?
N6 C20 1.320(4) . ?
N6 C16 1.359(3) . ?
C1 C2 1.493(4) . ?
C2 C3 1.371(4) . ?
C2 C4 1.390(4) . ?
C3 C7 1.380(4) . ?
C4 C5 1.371(4) . ?
C5 C6 1.387(4) . ?
C6 C7 1.386(4) . ?
C9 C10 1.355(4) . ?
C9 C17 1.451(4) . ?
C10 C11 1.426(4) . ?

```

C11 C15 1.405(4) . ?
 C11 C12 1.410(4) . ?
 C12 C13 1.367(4) . ?
 C13 C14 1.401(4) . ?
 C15 C16 1.447(4) . ?
 C16 C17 1.414(4) . ?
 C17 C18 1.410(4) . ?
 C18 C19 1.359(4) . ?
 C19 C20 1.398(4) . ?

loop_

_geom_angle_atom_site_label_1
 _geom_angle_atom_site_label_2
 _geom_angle_atom_site_label_3
 _geom_angle
 _geom_angle_site_symmetry_1
 _geom_angle_site_symmetry_3
 _geom_angle_publ_flag
 C8 N1 C6 127.7(2) . . ?
 C8 N2 C9 125.1(2) . . ?
 C14 N5 C15 117.4(2) . . ?
 C20 N6 C16 117.7(2) . . ?
 F3 C1 F2 109.1(3) . . ?
 F3 C1 F1 103.2(3) . . ?
 F2 C1 F1 103.5(3) . . ?
 F3 C1 C2 113.7(3) . . ?
 F2 C1 C2 114.4(3) . . ?
 F1 C1 C2 111.8(3) . . ?
 C3 C2 C4 119.2(3) . . ?
 C3 C2 C1 119.1(3) . . ?
 C4 C2 C1 121.8(3) . . ?
 C2 C3 C7 121.3(3) . . ?
 C5 C4 C2 120.1(3) . . ?
 C4 C5 C6 120.6(3) . . ?
 C5 C6 C7 119.3(3) . . ?
 C5 C6 N1 116.2(2) . . ?
 C7 C6 N1 124.5(2) . . ?
 C3 C7 C6 119.5(3) . . ?
 O2 C8 N1 125.4(2) . . ?
 O2 C8 N2 122.7(2) . . ?
 N1 C8 N2 111.9(2) . . ?
 C10 C9 N2 122.4(2) . . ?
 C10 C9 C17 120.1(2) . . ?
 N2 C9 C17 117.5(2) . . ?
 C9 C10 C11 121.6(2) . . ?
 C15 C11 C12 117.5(2) . . ?
 C15 C11 C10 120.2(2) . . ?
 C12 C11 C10 122.3(2) . . ?
 C13 C12 C11 119.4(3) . . ?
 C12 C13 C14 118.6(3) . . ?
 N5 C14 C13 124.0(3) . . ?
 N5 C15 C11 123.0(2) . . ?
 N5 C15 C16 118.0(2) . . ?
 C11 C15 C16 119.0(2) . . ?
 N6 C16 C17 122.9(2) . . ?
 N6 C16 C15 117.3(2) . . ?
 C17 C16 C15 119.8(2) . . ?

C18 C17 C16 116.8(2) . . ?
C18 C17 C9 123.7(2) . . ?
C16 C17 C9 119.3(2) . . ?
C19 C18 C17 119.9(3) . . ?
C18 C19 C20 119.0(3) . . ?
N6 C20 C19 123.7(3) . . ?

_diffn_measured_fraction_theta_max	1.000
_diffn_reflns_theta_full	25.00
_diffn_measured_fraction_theta_full	1.000
_refine_diff_density_max	0.824
_refine_diff_density_min	-0.413
_refine_diff_density_rms	0.072

A1.5: Crystallographic data for $(\text{Cu}_2:87_4) \cdot (\text{ClO}_4)_4 \cdot (\text{CH}_3\text{CN})_2$

Identification code	cs053Cu	
Empirical formula	C84 H58 Cl4 Cu2 F12 N18 O22	
Formula weight	2168.38	
Temperature	150 K	
Wavelength	0.71070 Å	
Crystal system	triclinic	
Space group	P-1	
Unit cell dimensions	a = 10.941(7) Å	$\alpha = 97.902(8)^\circ$.
	b = 14.307(9) Å	$\beta = 91.04(2)^\circ$.
	c = 14.411(9) Å	$\gamma = 93.759(15)^\circ$.
Volume	2229(2) Å ³	
Z	1	
Density (calculated)	1.616 Mg/m ³	
Absorption coefficient	0.707 mm ⁻¹	
F(000)	1098	
Crystal size	0.10 x 0.03 x 0.01 mm ³	
Theta range for data collection	2.38 to 31.37°.	
Index ranges	-15 ≤ h ≤ 15, -20 ≤ k ≤ 20, -20 ≤ l ≤ 20	
Reflections collected	61977	
Independent reflections	13575 [R(int) = 0.2061]	
Completeness to theta = 31.37°	92.6 %	
Refinement method	Full-matrix least-squares on F ²	
Data / restraints / parameters	13575 / 0 / 636	
Goodness-of-fit on F ²	2.098	
Final R indices [I > 2σ(I)]	R1 = 0.3400, wR2 = 0.5175	
R indices (all data)	R1 = 0.3968, wR2 = 0.5465	
Largest diff. peak and hole	1.880 and -1.352 e.Å ⁻³	

A1.5.1: CIF file for (Cu₂:87₄).(ClO₄)₄.(CH₃CN)₂

```

data_cs053Cu

_audit_creation_method          SHELXL-97
_chemical_name_systematic
;
?
;
_chemical_name_common           ?
_chemical_melting_point         ?
_chemical_formula_moiety        ?
_chemical_formula_sum
'C88 H64 Cl4 Cu2 F12 N20 O20'
_chemical_formula_weight        2218.49

loop_
_atom_type_symbol
_atom_type_description
_atom_type_scatter_dispersion_real
_atom_type_scatter_dispersion_imag
_atom_type_scatter_source
'C' 'C' 0.0033 0.0016
'International Tables Vol C Tables 4.2.6.8 and 6.1.1.4'
'H' 'H' 0.0000 0.0000
'International Tables Vol C Tables 4.2.6.8 and 6.1.1.4'
'Cl' 'Cl' 0.1484 0.1585
'International Tables Vol C Tables 4.2.6.8 and 6.1.1.4'
'Cu' 'Cu' 0.3201 1.2651
'International Tables Vol C Tables 4.2.6.8 and 6.1.1.4'
'F' 'F' 0.0171 0.0103
'International Tables Vol C Tables 4.2.6.8 and 6.1.1.4'
'N' 'N' 0.0061 0.0033
'International Tables Vol C Tables 4.2.6.8 and 6.1.1.4'
'O' 'O' 0.0106 0.0060
'International Tables Vol C Tables 4.2.6.8 and 6.1.1.4'

_symmetry_cell_setting          ?
_symmetry_space_group_name_H-M ?

loop_
_symmetry_equiv_pos_as_xyz
'x, y, z'
'-x, -y, -z'

_cell_length_a                  10.941(7)
_cell_length_b                  14.307(9)
_cell_length_c                  14.411(9)
_cell_angle_alpha               97.902(8)
_cell_angle_beta               91.04(2)
_cell_angle_gamma              93.759(15)
_cell_volume                    2229(2)
_cell_formula_units_Z           1
_cell_measurement_temperature   98(2)
_cell_measurement_reflns_used   ?
_cell_measurement_theta_min     ?

```

```

_cell_measurement_theta_max      ?

_exptl_crystal_description      ?
_exptl_crystal_colour           ?
_exptl_crystal_size_max         ?
_exptl_crystal_size_mid         ?
_exptl_crystal_size_min         ?
_exptl_crystal_density_meas     ?
_exptl_crystal_density_diffn    1.653
_exptl_crystal_density_method   'not measured'
_exptl_crystal_F_000            1126
_exptl_absorpt_coefficient_mu   0.708
_exptl_absorpt_correction_type  ?
_exptl_absorpt_correction_T_min ?
_exptl_absorpt_correction_T_max ?
_exptl_absorpt_process_details  ?

_exptl_special_details
;
?
;

_diffn_ambient_temperature      98(2)
_diffn_radiation_wavelength     0.71070
_diffn_radiation_type           MoK\alpha
_diffn_radiation_source         'fine-focus sealed tube'
_diffn_radiation_monochromator  graphite
_diffn_measurement_device_type  ?
_diffn_measurement_method       ?
_diffn_detector_area_resol_mean ?
_diffn_standards_number         ?
_diffn_standards_interval_count ?
_diffn_standards_interval_time  ?
_diffn_standards_decay_%       ?
_diffn_reflns_number            43665
_diffn_reflns_av_R_equivalents  0.1787
_diffn_reflns_av_sigmaI/netI    0.1374
_diffn_reflns_limit_h_min       -13
_diffn_reflns_limit_h_max       13
_diffn_reflns_limit_k_min       -17
_diffn_reflns_limit_k_max       17
_diffn_reflns_limit_l_min       -17
_diffn_reflns_limit_l_max       17
_diffn_reflns_theta_min         2.38
_diffn_reflns_theta_max         25.00
_reflns_number_total            7829
_reflns_number_gt               5858
_reflns_threshold_expression     >2sigma(I)

_computing_data_collection      ?
_computing_cell_refinement      ?
_computing_data_reduction       ?
_computing_structure_solution   'SHELXS-97 (Sheldrick, 1990)'
_computing_structure_refinement 'SHELXL-97 (Sheldrick, 1997)'
_computing_molecular_graphics  ?
_computing_publication_material ?

```

```
_refine_special_details
;
Refinement of F2 against ALL reflections. The weighted R-factor wR
and
goodness of fit S are based on F2, conventional R-factors R are based
on F, with F set to zero for negative F2. The threshold expression of
F2 > 2sigma(F2) is used only for calculating R-factors(gt) etc. and
is
not relevant to the choice of reflections for refinement. R-factors
based
on F2 are statistically about twice as large as those based on F, and
R-
factors based on ALL data will be even larger.
;
```

```
_refine_ls_structure_factor_coef Fsqd
_refine_ls_matrix_type full
_refine_ls_weighting_scheme calc
_refine_ls_weighting_details
'calc w=1/[\s2(Fo2)+(0.2000P)2+0.0000P] where P=(Fo2+2Fc2)/3'
_atom_sites_solution_primary direct
_atom_sites_solution_secondary difmap
_atom_sites_solution_hydrogens geom
_refine_ls_hydrogen_treatment mixed
_refine_ls_extinction_method none
_refine_ls_extinction_coef ?
_refine_ls_number_reflns 7829
_refine_ls_number_parameters 660
_refine_ls_number_restraints 0
_refine_ls_R_factor_all 0.2896
_refine_ls_R_factor_gt 0.2529
_refine_ls_wR_factor_ref 0.5505
_refine_ls_wR_factor_gt 0.5266
_refine_ls_goodness_of_fit_ref 1.854
_refine_ls_restrained_S_all 1.854
_refine_ls_shift/su_max 0.347
_refine_ls_shift/su_mean 0.015
```

```
loop_
_atom_site_label
_atom_site_type_symbol
_atom_site_fract_x
_atom_site_fract_y
_atom_site_fract_z
_atom_site_U_iso_or_equiv
_atom_site_adp_type
_atom_site_occupancy
_atom_site_symmetry_multiplicity
_atom_site_calc_flag
_atom_site_refinement_flags
_atom_site_disorder_assembly
_atom_site_disorder_group
Cu1 Cu 0.55575(18) 0.74954(13) 0.43062(14) 0.0445(7) Uani 1 1 d . . .
F1 F 0.5653(11) 0.3233(9) 0.0441(9) 0.082(4) Uani 1 1 d . . .
F2 F 0.7260(10) 0.4179(9) 0.0377(8) 0.082(4) Uani 1 1 d . . .
F3 F 0.6809(12) 0.3599(8) 0.1642(7) 0.088(4) Uani 1 1 d . . .
F4 F 0.194(3) -0.1214(17) -0.1121(11) 0.270(18) Uani 1 1 d . . .
```

F5 F 0.0431(14) -0.1744(9) -0.0428(10) 0.110(5) Uani 1 1 d . . .
 F6 F 0.2152(11) -0.2204(11) -0.0126(12) 0.129(7) Uani 1 1 d . . .
 O1 O 0.4378(12) 0.2323(8) 0.2167(9) 0.069(4) Uani 1 1 d . . .
 O10 O 0.4922(11) 0.8027(8) 0.3117(8) 0.053(3) Uani 1 1 d . . .
 N1 N 0.2481(13) 0.1648(10) 0.2580(11) 0.061(4) Uani 1 1 d . . .
 H5 H 0.1945 0.1700 0.3029 0.073 Uiso 1 1 d R . . .
 N2 N 0.4168(13) 0.6539(9) 0.4184(10) 0.052(4) Uani 1 1 d . . .
 N3 N 0.6571(12) 0.6365(10) 0.4091(11) 0.056(4) Uani 1 1 d . . .
 N4 N 0.3077(12) 1.1551(10) 0.5751(11) 0.053(4) Uani 1 1 d . . .
 N5 N 0.4919(13) 1.1517(10) 0.4593(9) 0.052(4) Uani 1 1 d . . .
 N6 N 0.3287(12) 0.3096(10) 0.3404(9) 0.057(4) Uani 1 1 d . . .
 H6 H 0.2651 0.3027 0.3760 0.068 Uiso 1 1 d R . . .
 N7 N 0.3046(13) 0.8584(10) 0.2743(11) 0.060(4) Uani 1 1 d . . .
 H12 H 0.2480 0.8561 0.2298 0.072 Uiso 1 1 d R . . .
 N8 N 0.3598(13) 0.7135(10) 0.1972(9) 0.050(4) Uani 1 1 d . . .
 H11 H 0.2912 0.7136 0.1644 0.061 Uiso 1 1 d R . . .
 C1 C 0.161(2) -0.1434(14) -0.0337(17) 0.083(8) Uani 1 1 d . . .
 C2 C 0.184(2) -0.0637(16) 0.0431(16) 0.077(6) Uani 1 1 d . . .
 C3 C 0.3022(18) -0.0227(10) 0.0600(12) 0.057(5) Uani 1 1 d . . .
 H1 H 0.3671 -0.0484 0.0242 0.068 Uiso 1 1 calc R . . .
 C4 C 0.3271(19) 0.0541(14) 0.1271(12) 0.067(5) Uani 1 1 d . . .
 H2 H 0.4080 0.0832 0.1345 0.080 Uiso 1 1 calc R . . .
 C5 C 0.2351(14) 0.0903(10) 0.1850(12) 0.050(5) Uani 1 1 d . . .
 C6 C 0.1138(16) 0.0412(12) 0.1713(13) 0.059(5) Uani 1 1 d . . .
 H4 H 0.0493 0.0600 0.2115 0.071 Uiso 1 1 calc R . . .
 C7 C 0.0936(19) -0.0323(11) 0.1000(14) 0.069(6) Uani 1 1 d . . .
 H3 H 0.0134 -0.0623 0.0899 0.083 Uiso 1 1 calc R . . .
 C8 C 0.3472(16) 0.2377(13) 0.2655(14) 0.060(5) Uani 1 1 d . . .
 C9 C 0.4123(15) 0.3885(11) 0.3565(11) 0.048(4) Uani 1 1 d . . .
 C10 C 0.5281(15) 0.3804(11) 0.3528(11) 0.052(5) Uani 1 1 d . . .
 H27 H 0.5560 0.3187 0.3388 0.063 Uiso 1 1 calc R . . .
 C11 C 0.6238(17) 0.4636(14) 0.3694(12) 0.059(5) Uani 1 1 d . . .
 C12 C 0.7524(16) 0.4516(13) 0.3602(11) 0.054(5) Uani 1 1 d . . .
 H26 H 0.7842 0.3919 0.3419 0.065 Uiso 1 1 calc R . . .
 C13 C 0.8272(17) 0.5359(12) 0.3805(13) 0.059(5) Uani 1 1 d . . .
 H25 H 0.9137 0.5344 0.3764 0.071 Uiso 1 1 calc R . . .
 C14 C 0.7761(15) 0.6201(15) 0.4063(11) 0.058(5) Uani 1 1 d . . .
 H24 H 0.8320 0.6734 0.4245 0.069 Uiso 1 1 calc R . . .
 C15 C 0.3669(13) 0.4783(11) 0.3789(11) 0.041(4) Uani 1 1 d . . .
 C16 C 0.2422(18) 0.5010(13) 0.3817(12) 0.067(6) Uani 1 1 d . . .
 H28 H 0.1809 0.4502 0.3716 0.080 Uiso 1 1 calc R . . .
 C17 C 0.2040(16) 0.5919(11) 0.3980(10) 0.049(4) Uani 1 1 d . . .
 H30 H 0.1200 0.6045 0.3946 0.059 Uiso 1 1 calc R . . .
 C18 C 0.5771(17) 0.5538(12) 0.3943(10) 0.050(4) Uani 1 1 d . . .
 C19 C 0.4511(13) 0.5638(12) 0.3971(11) 0.048(4) Uani 1 1 d . . .
 C20 C 0.1253(11) 1.0085(13) 0.5666(12) 0.053(5) Uani 1 1 d . . .
 H17 H 0.0611 0.9600 0.5628 0.064 Uiso 1 1 calc R . . .
 C21 C 0.5867(19) 1.1488(16) 0.4031(14) 0.077(6) Uani 1 1 d . . .
 H22 H 0.6525 1.1954 0.4185 0.092 Uiso 1 1 calc R . . .
 C22 C 0.5972(19) 1.0848(13) 0.3254(10) 0.067(6) Uani 1 1 d . . .
 H21 H 0.6632 1.0923 0.2845 0.081 Uiso 1 1 calc R . . .
 C23 C 0.5112(18) 1.0080(16) 0.3057(13) 0.072(6) Uani 1 1 d . . .
 H18 H 0.5196 0.9612 0.2531 0.086 Uiso 1 1 calc R . . .
 C24 C 0.4065(14) 1.0011(10) 0.3685(11) 0.043(4) Uani 1 1 d . . .
 C25 C 0.4017(14) 1.0748(11) 0.4424(13) 0.047(4) Uani 1 1 d . . .
 C26 C 0.3076(13) 1.0817(9) 0.4985(11) 0.041(4) Uani 1 1 d . . .
 C27 C 0.2310(15) 1.1535(11) 0.6360(14) 0.054(5) Uani 1 1 d . . .

H16 H 0.2367 1.2048 0.6856 0.065 Uiso 1 1 calc R . .
 C28 C 0.1323(13) 1.0812(11) 0.6400(13) 0.047(4) Uani 1 1 d . . .
 H23 H 0.0764 1.0840 0.6898 0.056 Uiso 1 1 calc R . .
 C29 C 0.2155(14) 1.0065(11) 0.4961(13) 0.051(5) Uani 1 1 d . . .
 C30 C 0.3037(16) 0.9363(11) 0.3566(13) 0.056(5) Uani 1 1 d . . .
 C31 C 0.2133(14) 0.9327(12) 0.4174(13) 0.056(5) Uani 1 1 d . . .
 H19 H 0.1500 0.8834 0.4089 0.067 Uiso 1 1 calc R . .
 C32 C 0.631(2) 0.395(2) 0.0911(14) 0.086(8) Uani 1 1 d . . .
 C33 C 0.5584(19) 0.4834(13) 0.1228(11) 0.058(5) Uani 1 1 d . . .
 C34 C 0.4350(16) 0.4713(12) 0.1328(14) 0.058(5) Uani 1 1 d . . .
 H7 H 0.3949 0.4097 0.1232 0.070 Uiso 1 1 calc R . .
 C35 C 0.3682(16) 0.5504(10) 0.1571(11) 0.049(4) Uani 1 1 d . . .
 H8 H 0.2815 0.5443 0.1602 0.059 Uiso 1 1 calc R . .
 C36 C 0.4301(14) 0.6354(13) 0.1762(12) 0.053(4) Uani 1 1 d . . .
 C37 C 0.5600(17) 0.6495(14) 0.1746(10) 0.059(5) Uani 1 1 d . . .
 H9 H 0.6003 0.7104 0.1921 0.070 Uiso 1 1 calc R . .
 C38 C 0.3001(17) 0.6670(12) 0.4205(11) 0.057(5) Uani 1 1 d . . .
 H29 H 0.2764 0.7296 0.4380 0.068 Uiso 1 1 calc R . .
 C39 C 0.6274(18) 0.5691(14) 0.1459(12) 0.065(5) Uani 1 1 d . . .
 H10 H 0.7142 0.5737 0.1427 0.078 Uiso 1 1 calc R . .
 C43 C 0.3926(19) 0.7912(11) 0.2644(13) 0.059(5) Uani 1 1 d . . .
 N9 N 0.681(4) 0.9028(16) 0.1413(15) 0.178(15) Uani 1 1 d . . .
 C41 C 0.707(4) 0.853(2) 0.0845(19) 0.147(14) Uani 1 1 d . . .
 C42 C 0.736(2) 0.7839(15) 0.0063(14) 0.095(8) Uani 1 1 d . . .
 H13 H 0.6981 0.7991 -0.0513 0.142 Uiso 1 1 calc R . .
 H14 H 0.7057 0.7207 0.0174 0.142 Uiso 1 1 calc R . .
 H15 H 0.8255 0.7855 -0.0003 0.142 Uiso 1 1 calc R . .
 C11 Cl 0.9822(5) 0.2519(4) 0.4095(5) 0.0851(19) Uani 1 1 d . . .
 O2 O 1.0760(16) 0.1935(19) 0.4035(15) 0.166(10) Uani 1 1 d . . .
 O3 O 1.029(2) 0.3465(13) 0.4171(14) 0.144(8) Uani 1 1 d . . .
 O4 O 0.904(4) 0.2287(18) 0.345(4) 0.42(5) Uani 1 1 d . . .
 O5 O 0.926(5) 0.2333(14) 0.481(3) 0.42(4) Uani 1 1 d . . .
 C12 Cl 0.0083(5) 0.6987(4) 0.2071(6) 0.100(2) Uani 1 1 d . . .
 O6 O 0.070(3) 0.7849(17) 0.197(3) 0.237(17) Uani 1 1 d . . .
 O7 O -0.1099(14) 0.6986(19) 0.181(2) 0.225(16) Uani 1 1 d . . .
 O8 O 0.075(3) 0.639(2) 0.175(3) 0.37(4) Uani 1 1 d . . .
 O31 O 0.0257(19) 0.731(2) 0.312(3) 0.27(2) Uani 1 1 d . . .
 C50 C 0.0854(16) 0.3730(14) 0.155(3) 0.148(18) Uani 1 1 d . . .
 C51 C -0.005(4) 0.3956(18) 0.107(5) 0.42(5) Uani 1 1 d . . .
 H51A H 0.0251 0.4194 0.0501 0.625 Uiso 1 1 calc R . .
 H51B H -0.0480 0.4449 0.1444 0.625 Uiso 1 1 calc R . .
 H51C H -0.0617 0.3398 0.0887 0.625 Uiso 1 1 calc R . .
 N20 N 0.166(3) 0.3566(17) 0.1734(15) 0.118(8) Uani 1 1 d . . .

loop_

_atom_site_aniso_label
 _atom_site_aniso_U_11
 _atom_site_aniso_U_22
 _atom_site_aniso_U_33
 _atom_site_aniso_U_23
 _atom_site_aniso_U_13
 _atom_site_aniso_U_12
 Cu1 0.0542(13) 0.0323(11) 0.0460(12) 0.0082(8) -0.0082(9) -0.0069(9)
 F1 0.079(8) 0.078(8) 0.083(9) -0.017(7) -0.005(7) 0.034(7)
 F2 0.069(7) 0.117(10) 0.056(7) -0.011(6) 0.014(6) 0.031(7)
 F3 0.128(10) 0.083(8) 0.053(7) -0.007(6) -0.001(7) 0.055(8)
 F4 0.43(4) 0.26(2) 0.061(10) -0.084(13) 0.089(16) -0.27(3)

F5 0.122(12) 0.079(9) 0.121(12) -0.014(8) -0.045(9) 0.010(8)
 F6 0.079(9) 0.100(11) 0.180(16) -0.090(11) -0.030(9) 0.028(8)
 O1 0.075(9) 0.052(7) 0.067(9) -0.035(6) 0.006(7) -0.003(6)
 O10 0.058(7) 0.048(7) 0.050(7) 0.006(5) -0.023(6) -0.005(6)
 N1 0.057(9) 0.058(9) 0.069(10) 0.021(8) 0.023(8) -0.012(7)
 N2 0.053(9) 0.038(8) 0.060(10) -0.007(7) -0.003(7) 0.002(7)
 N3 0.043(8) 0.047(8) 0.074(10) 0.004(7) -0.015(7) -0.004(7)
 N4 0.040(8) 0.057(9) 0.065(10) 0.020(8) 0.019(7) 0.001(7)
 N5 0.059(9) 0.056(9) 0.043(8) 0.023(7) 0.013(7) -0.012(7)
 N6 0.050(8) 0.067(9) 0.045(8) -0.013(7) 0.031(7) -0.022(7)
 N7 0.062(9) 0.052(9) 0.064(10) 0.006(7) 0.003(8) -0.011(7)
 N8 0.059(9) 0.060(9) 0.036(8) 0.009(7) 0.010(7) 0.026(7)
 C1 0.091(16) 0.050(12) 0.088(17) -0.049(11) 0.047(14) -0.025(11)
 C2 0.078(15) 0.078(15) 0.077(15) 0.012(12) -0.026(12) 0.015(13)
 C3 0.086(14) 0.015(7) 0.066(12) -0.020(7) -0.006(10) 0.033(8)
 C4 0.076(13) 0.077(14) 0.045(11) 0.001(9) -0.005(10) 0.019(11)
 C5 0.046(9) 0.021(7) 0.070(12) -0.041(7) -0.005(8) 0.008(7)
 C6 0.047(10) 0.058(11) 0.068(12) -0.001(9) -0.011(9) 0.000(9)
 C7 0.069(13) 0.033(9) 0.092(15) -0.030(9) -0.050(12) -0.007(9)
 C8 0.045(10) 0.056(11) 0.083(14) 0.013(10) 0.028(10) 0.014(9)
 C9 0.045(10) 0.050(10) 0.043(9) -0.001(7) 0.004(8) -0.028(8)
 C10 0.056(11) 0.042(9) 0.052(11) -0.007(8) 0.028(9) -0.022(8)
 C11 0.061(12) 0.077(14) 0.040(10) 0.013(9) -0.007(9) 0.003(10)
 C12 0.070(12) 0.056(11) 0.037(9) 0.024(8) -0.001(8) -0.018(9)
 C13 0.060(11) 0.041(10) 0.077(13) 0.001(9) 0.018(10) 0.015(9)
 C14 0.039(10) 0.102(15) 0.035(9) 0.024(9) -0.007(7) 0.003(9)
 C15 0.025(8) 0.051(9) 0.052(10) 0.017(8) 0.027(7) 0.002(7)
 C16 0.082(14) 0.066(13) 0.047(11) 0.003(9) 0.012(10) -0.036(11)
 C17 0.073(11) 0.044(9) 0.026(8) -0.013(7) 0.042(8) -0.007(8)
 C18 0.075(12) 0.057(11) 0.021(8) 0.021(7) -0.016(8) -0.003(9)
 C19 0.026(8) 0.073(12) 0.035(9) -0.011(8) 0.005(7) -0.032(8)
 C20 0.000(6) 0.087(13) 0.071(12) 0.019(10) -0.006(7) -0.017(7)
 C21 0.071(14) 0.099(17) 0.060(13) 0.031(12) -0.010(11) -0.032(12)
 C22 0.097(15) 0.082(13) 0.012(8) -0.012(8) 0.007(8) -0.040(11)
 C23 0.079(14) 0.097(16) 0.040(11) 0.023(10) -0.006(10) -0.014(12)
 C24 0.048(9) 0.026(7) 0.053(10) -0.009(7) 0.020(8) 0.025(7)
 C25 0.033(9) 0.038(9) 0.068(12) -0.001(8) 0.012(8) 0.007(7)
 C26 0.035(8) 0.015(7) 0.066(11) -0.014(7) -0.024(8) 0.001(6)
 C27 0.047(10) 0.033(9) 0.079(13) 0.007(8) -0.019(10) -0.020(7)
 C28 0.029(8) 0.044(9) 0.068(12) 0.013(8) -0.008(8) -0.001(7)
 C29 0.034(9) 0.041(9) 0.073(12) 0.000(8) -0.034(9) -0.002(7)
 C30 0.056(11) 0.036(9) 0.068(12) -0.004(8) -0.034(10) -0.019(8)
 C31 0.025(8) 0.059(11) 0.083(14) 0.010(10) 0.030(9) -0.003(7)
 C32 0.076(14) 0.16(2) 0.037(11) 0.063(14) 0.024(11) 0.010(15)
 C33 0.081(14) 0.063(12) 0.033(9) 0.003(8) 0.009(9) 0.032(11)
 C34 0.049(11) 0.038(9) 0.090(14) 0.021(9) 0.001(10) 0.003(8)
 C35 0.068(11) 0.031(8) 0.051(10) 0.025(7) 0.007(8) -0.013(8)
 C36 0.039(10) 0.069(12) 0.054(11) 0.018(9) 0.005(8) -0.006(9)
 C37 0.078(13) 0.082(13) 0.013(7) -0.010(8) 0.025(8) 0.010(10)
 C38 0.073(13) 0.050(10) 0.042(10) 0.012(8) 0.008(9) -0.040(9)
 C39 0.069(12) 0.078(13) 0.045(11) 0.012(9) 0.027(9) -0.028(11)
 C43 0.089(15) 0.027(8) 0.069(12) 0.016(8) 0.034(11) 0.034(9)
 N9 0.39(5) 0.088(16) 0.065(14) 0.009(12) 0.11(2) 0.07(2)
 C41 0.28(4) 0.10(2) 0.067(17) 0.009(15) 0.08(2) 0.06(2)
 C42 0.16(2) 0.069(14) 0.051(13) 0.014(11) 0.023(14) -0.003(15)
 C11 0.057(3) 0.080(4) 0.101(5) -0.043(3) 0.022(3) -0.012(3)
 O2 0.092(13) 0.28(3) 0.17(2) 0.118(19) 0.075(13) 0.107(16)

O3 0.19(2) 0.103(14) 0.125(16) 0.024(12) -0.012(14) -0.089(14)
 O4 0.31(4) 0.077(18) 0.84(11) -0.06(4) -0.40(6) 0.05(2)
 O5 0.60(7) 0.038(11) 0.61(7) -0.03(2) 0.53(7) -0.02(2)
 C12 0.056(3) 0.057(3) 0.181(7) -0.008(4) 0.002(4) 0.017(3)
 O6 0.22(3) 0.122(19) 0.37(4) 0.10(2) 0.00(3) -0.13(2)
 O7 0.045(10) 0.26(3) 0.30(3) -0.19(2) -0.074(14) 0.057(13)
 O8 0.22(3) 0.27(3) 0.54(6) -0.31(4) -0.26(4) 0.18(3)
 O31 0.073(15) 0.23(3) 0.46(6) -0.16(4) -0.06(2) 0.085(18)
 C50 0.012(9) 0.031(10) 0.37(5) -0.083(18) 0.078(17) 0.008(8)
 C51 0.23(4) 0.047(16) 0.92(15) -0.18(4) -0.09(6) 0.13(2)
 N20 0.15(2) 0.110(18) 0.088(16) -0.015(13) 0.037(16) 0.018(17)

_geom_special_details

;

All esds (except the esd in the dihedral angle between two l.s. planes)
 are estimated using the full covariance matrix. The cell esds are taken
 into account individually in the estimation of esds in distances, angles
 and torsion angles; correlations between esds in cell parameters are
 only
 used when they are defined by crystal symmetry. An approximate
 (isotropic)
 treatment of cell esds is used for estimating esds involving l.s.
 planes.

;

loop_

_geom_bond_atom_site_label_1
_geom_bond_atom_site_label_2
_geom_bond_distance
_geom_bond_site_symmetry_2
_geom_bond_publ_flag
 Cu1 N2 1.966(14) . ?
 Cu1 N4 1.967(14) 2_676 ?
 Cu1 N3 2.012(14) . ?
 Cu1 N5 2.072(14) 2_676 ?
 Cu1 O10 2.093(11) . ?
 F1 C32 1.31(3) . ?
 F2 C32 1.36(2) . ?
 F3 C32 1.35(2) . ?
 F4 C1 1.27(3) . ?
 F5 C1 1.33(2) . ?
 F6 C1 1.35(3) . ?
 O1 C8 1.226(19) . ?
 O10 C43 1.26(2) . ?
 N1 C5 1.389(19) . ?
 N1 C8 1.45(2) . ?
 N1 H5 0.8800 . ?
 N2 C38 1.30(2) . ?
 N2 C19 1.36(2) . ?
 N3 C14 1.34(2) . ?
 N3 C18 1.41(2) . ?
 N4 C27 1.23(2) . ?
 N4 C26 1.415(19) . ?
 N4 Cu1 1.967(14) 2_676 ?
 N5 C21 1.33(2) . ?
 N5 C25 1.42(2) . ?
 N5 Cu1 2.072(14) 2_676 ?

N6 C9 1.396(18) . ?
N6 C8 1.41(2) . ?
N6 H6 0.8800 . ?
N7 C43 1.40(2) . ?
N7 C30 1.51(2) . ?
N7 H12 0.8800 . ?
N8 C43 1.39(2) . ?
N8 C36 1.40(2) . ?
N8 H11 0.8799 . ?
C1 C2 1.48(3) . ?
C2 C7 1.36(3) . ?
C2 C3 1.39(3) . ?
C3 C4 1.37(2) . ?
C3 H1 0.9500 . ?
C4 C5 1.40(2) . ?
C4 H2 0.9500 . ?
C5 C6 1.46(2) . ?
C6 C7 1.37(2) . ?
C6 H4 0.9500 . ?
C7 H3 0.9500 . ?
C9 C10 1.28(2) . ?
C9 C15 1.41(2) . ?
C10 C11 1.52(2) . ?
C10 H27 0.9500 . ?
C11 C18 1.42(2) . ?
C11 C12 1.43(2) . ?
C12 C13 1.41(2) . ?
C12 H26 0.9500 . ?
C13 C14 1.37(2) . ?
C13 H25 0.9500 . ?
C14 H24 0.9500 . ?
C15 C16 1.42(2) . ?
C15 C19 1.47(2) . ?
C16 C17 1.38(2) . ?
C16 H28 0.9500 . ?
C17 C38 1.45(2) . ?
C17 H30 0.9500 . ?
C18 C19 1.40(2) . ?
C20 C28 1.37(2) . ?
C20 C29 1.43(2) . ?
C20 H17 0.9500 . ?
C21 C22 1.36(3) . ?
C21 H22 0.9500 . ?
C22 C23 1.39(2) . ?
C22 H21 0.9500 . ?
C23 C24 1.48(2) . ?
C23 H18 0.9500 . ?
C24 C25 1.40(2) . ?
C24 C30 1.40(2) . ?
C25 C26 1.32(2) . ?
C26 C29 1.42(2) . ?
C27 C28 1.45(2) . ?
C27 H16 0.9500 . ?
C28 H23 0.9500 . ?
C29 C31 1.44(2) . ?
C30 C31 1.34(2) . ?
C31 H19 0.9500 . ?

C32 C33 1.56(3) . ?
 C33 C34 1.36(2) . ?
 C33 C39 1.39(3) . ?
 C34 C35 1.39(2) . ?
 C34 H7 0.9500 . ?
 C35 C36 1.34(2) . ?
 C35 H8 0.9500 . ?
 C36 C37 1.42(2) . ?
 C37 C39 1.42(3) . ?
 C37 H9 0.9500 . ?
 C38 H29 0.9500 . ?
 C39 H10 0.9500 . ?
 N9 C41 1.07(3) . ?
 C41 C42 1.45(3) . ?
 C42 H13 0.9800 . ?
 C42 H14 0.9800 . ?
 C42 H15 0.9800 . ?
 C11 O4 1.24(3) . ?
 C11 O5 1.27(3) . ?
 C11 O2 1.362(18) . ?
 C11 O3 1.404(16) . ?
 C12 O8 1.21(2) . ?
 C12 O7 1.340(15) . ?
 C12 O6 1.390(17) . ?
 C12 O31 1.52(4) . ?
 C50 N20 0.98(3) . ?
 C50 C51 1.28(6) . ?
 C51 H51A 0.9816 . ?
 C51 H51B 0.9818 . ?
 C51 H51C 0.9817 . ?

loop_

_geom_angle_atom_site_label_1
 _geom_angle_atom_site_label_2
 _geom_angle_atom_site_label_3
 _geom_angle
 _geom_angle_site_symmetry_1
 _geom_angle_site_symmetry_3
 _geom_angle_publ_flag
 N2 Cu1 N4 172.4(6) . 2_676 ?
 N2 Cu1 N3 83.9(6) . . ?
 N4 Cu1 N3 96.0(6) 2_676 . ?
 N2 Cu1 N5 103.5(5) . 2_676 ?
 N4 Cu1 N5 81.5(6) 2_676 2_676 ?
 N3 Cu1 N5 138.7(6) . 2_676 ?
 N2 Cu1 O10 90.3(5) . . ?
 N4 Cu1 O10 83.0(5) 2_676 . ?
 N3 Cu1 O10 117.0(5) . . ?
 N5 Cu1 O10 103.6(5) 2_676 . ?
 C43 O10 Cu1 134.0(11) . . ?
 C5 N1 C8 123.4(14) . . ?
 C5 N1 H5 120.5 . . ?
 C8 N1 H5 116.1 . . ?
 C38 N2 C19 118.1(14) . . ?
 C38 N2 Cu1 128.4(11) . . ?
 C19 N2 Cu1 113.2(10) . . ?
 C14 N3 C18 114.1(15) . . ?

C14 N3 Cu1 137.3(13) . . ?
 C18 N3 Cu1 108.5(11) . . ?
 C27 N4 C26 121.0(15) . . ?
 C27 N4 Cu1 127.6(13) . 2_676 ?
 C26 N4 Cu1 111.4(10) . 2_676 ?
 C21 N5 C25 116.5(16) . . ?
 C21 N5 Cu1 132.4(13) . 2_676 ?
 C25 N5 Cu1 111.1(10) . 2_676 ?
 C9 N6 C8 119.2(13) . . ?
 C9 N6 H6 122.2 . . ?
 C8 N6 H6 118.6 . . ?
 C43 N7 C30 123.4(15) . . ?
 C43 N7 H12 118.4 . . ?
 C30 N7 H12 118.2 . . ?
 C43 N8 C36 124.5(15) . . ?
 C43 N8 H11 118.3 . . ?
 C36 N8 H11 117.1 . . ?
 F4 C1 F5 108(3) . . ?
 F4 C1 F6 112(2) . . ?
 F5 C1 F6 102.3(17) . . ?
 F4 C1 C2 112.1(19) . . ?
 F5 C1 C2 112.6(17) . . ?
 F6 C1 C2 110(2) . . ?
 C7 C2 C3 119.0(19) . . ?
 C7 C2 C1 122(2) . . ?
 C3 C2 C1 119(2) . . ?
 C4 C3 C2 121.4(18) . . ?
 C4 C3 H1 119.3 . . ?
 C2 C3 H1 119.3 . . ?
 C3 C4 C5 120.8(18) . . ?
 C3 C4 H2 119.6 . . ?
 C5 C4 H2 119.6 . . ?
 N1 C5 C4 127.1(15) . . ?
 N1 C5 C6 116.0(14) . . ?
 C4 C5 C6 116.8(14) . . ?
 C7 C6 C5 119.4(17) . . ?
 C7 C6 H4 120.3 . . ?
 C5 C6 H4 120.3 . . ?
 C2 C7 C6 122.2(18) . . ?
 C2 C7 H3 118.9 . . ?
 C6 C7 H3 118.9 . . ?
 O1 C8 N6 126.1(16) . . ?
 O1 C8 N1 123.1(17) . . ?
 N6 C8 N1 110.6(14) . . ?
 C10 C9 N6 121.6(16) . . ?
 C10 C9 C15 120.0(14) . . ?
 N6 C9 C15 118.5(15) . . ?
 C9 C10 C11 124.0(16) . . ?
 C9 C10 H27 118.0 . . ?
 C11 C10 H27 118.0 . . ?
 C18 C11 C12 122.3(17) . . ?
 C18 C11 C10 115.5(16) . . ?
 C12 C11 C10 122.2(17) . . ?
 C13 C12 C11 114.2(17) . . ?
 C13 C12 H26 122.9 . . ?
 C11 C12 H26 122.9 . . ?
 C14 C13 C12 120.3(18) . . ?

C14 C13 H25 119.8 . . ?
 C12 C13 H25 119.9 . . ?
 N3 C14 C13 128.0(19) . . ?
 N3 C14 H24 116.0 . . ?
 C13 C14 H24 116.0 . . ?
 C9 C15 C16 127.6(15) . . ?
 C9 C15 C19 120.7(13) . . ?
 C16 C15 C19 111.6(14) . . ?
 C17 C16 C15 124.5(16) . . ?
 C17 C16 H28 117.7 . . ?
 C15 C16 H28 117.7 . . ?
 C16 C17 C38 116.0(17) . . ?
 C16 C17 H30 122.0 . . ?
 C38 C17 H30 122.0 . . ?
 C19 C18 N3 118.3(16) . . ?
 C19 C18 C11 121.0(16) . . ?
 N3 C18 C11 120.6(16) . . ?
 N2 C19 C18 115.9(14) . . ?
 N2 C19 C15 125.4(14) . . ?
 C18 C19 C15 118.7(16) . . ?
 C28 C20 C29 119.4(14) . . ?
 C28 C20 H17 120.3 . . ?
 C29 C20 H17 120.3 . . ?
 N5 C21 C22 125.3(19) . . ?
 N5 C21 H22 117.3 . . ?
 C22 C21 H22 117.3 . . ?
 C21 C22 C23 119.9(18) . . ?
 C21 C22 H21 120.0 . . ?
 C23 C22 H21 120.0 . . ?
 C22 C23 C24 118.5(18) . . ?
 C22 C23 H18 120.7 . . ?
 C24 C23 H18 120.8 . . ?
 C25 C24 C30 115.5(14) . . ?
 C25 C24 C23 116.0(16) . . ?
 C30 C24 C23 128.0(16) . . ?
 C26 C25 C24 122.0(14) . . ?
 C26 C25 N5 114.5(14) . . ?
 C24 C25 N5 123.3(14) . . ?
 C25 C26 N4 120.7(13) . . ?
 C25 C26 C29 121.2(14) . . ?
 N4 C26 C29 116.9(15) . . ?
 N4 C27 C28 126.7(17) . . ?
 N4 C27 H16 116.6 . . ?
 C28 C27 H16 116.6 . . ?
 C20 C28 C27 115.3(16) . . ?
 C20 C28 H23 122.3 . . ?
 C27 C28 H23 122.3 . . ?
 C26 C29 C20 120.4(15) . . ?
 C26 C29 C31 117.2(16) . . ?
 C20 C29 C31 122.3(14) . . ?
 C31 C30 C24 124.9(16) . . ?
 C31 C30 N7 118.3(14) . . ?
 C24 C30 N7 116.4(16) . . ?
 C30 C31 C29 117.4(15) . . ?
 C30 C31 H19 121.3 . . ?
 C29 C31 H19 121.3 . . ?
 F1 C32 F3 105.0(19) . . ?

F1 C32 F2 108.1(18) . . ?
 F3 C32 F2 105.6(17) . . ?
 F1 C32 C33 114.9(17) . . ?
 F3 C32 C33 112.4(17) . . ?
 F2 C32 C33 110.4(19) . . ?
 C34 C33 C39 124.5(17) . . ?
 C34 C33 C32 118.7(18) . . ?
 C39 C33 C32 116.6(19) . . ?
 C33 C34 C35 119.3(16) . . ?
 C33 C34 H7 120.4 . . ?
 C35 C34 H7 120.3 . . ?
 C36 C35 C34 118.1(17) . . ?
 C36 C35 H8 120.9 . . ?
 C34 C35 H8 121.0 . . ?
 C35 C36 N8 116.6(15) . . ?
 C35 C36 C37 123.9(17) . . ?
 N8 C36 C37 119.5(16) . . ?
 C36 C37 C39 117.7(17) . . ?
 C36 C37 H9 121.1 . . ?
 C39 C37 H9 121.2 . . ?
 N2 C38 C17 124.1(17) . . ?
 N2 C38 H29 117.9 . . ?
 C17 C38 H29 118.0 . . ?
 C33 C39 C37 116.0(18) . . ?
 C33 C39 H10 122.0 . . ?
 C37 C39 H10 122.0 . . ?
 O10 C43 N8 124.6(14) . . ?
 O10 C43 N7 122.0(17) . . ?
 N8 C43 N7 113.4(18) . . ?
 N9 C41 C42 177(5) . . ?
 C41 C42 H13 109.5 . . ?
 C41 C42 H14 109.5 . . ?
 H13 C42 H14 109.5 . . ?
 C41 C42 H15 109.5 . . ?
 H13 C42 H15 109.5 . . ?
 H14 C42 H15 109.5 . . ?
 O4 C11 O5 103(3) . . ?
 O4 C11 O2 112(2) . . ?
 O5 C11 O2 104(2) . . ?
 O4 C11 O3 114(2) . . ?
 O5 C11 O3 113.0(15) . . ?
 O2 C11 O3 110.0(15) . . ?
 O8 C12 O7 123.4(14) . . ?
 O8 C12 O6 106(3) . . ?
 O7 C12 O6 110(2) . . ?
 O8 C12 O31 115(2) . . ?
 O7 C12 O31 110.6(14) . . ?
 O6 C12 O31 85(2) . . ?
 N20 C50 C51 163(5) . . ?
 C50 C51 H51A 109.3 . . ?
 C50 C51 H51B 110.0 . . ?
 H51A C51 H51B 109.2 . . ?
 C50 C51 H51C 109.7 . . ?
 H51A C51 H51C 109.3 . . ?
 H51B C51 H51C 109.3 . . ?

_diffn_measured_fraction_theta_max 0.999

_diffrn_reflns_theta_full	25.00
_diffrn_measured_fraction_theta_full	0.999
_refine_diff_density_max	1.681
_refine_diff_density_min	-1.028
_refine_diff_density_rms	0.182

Appendix 2-UV-Vis titration and speciation data for Chapter 3

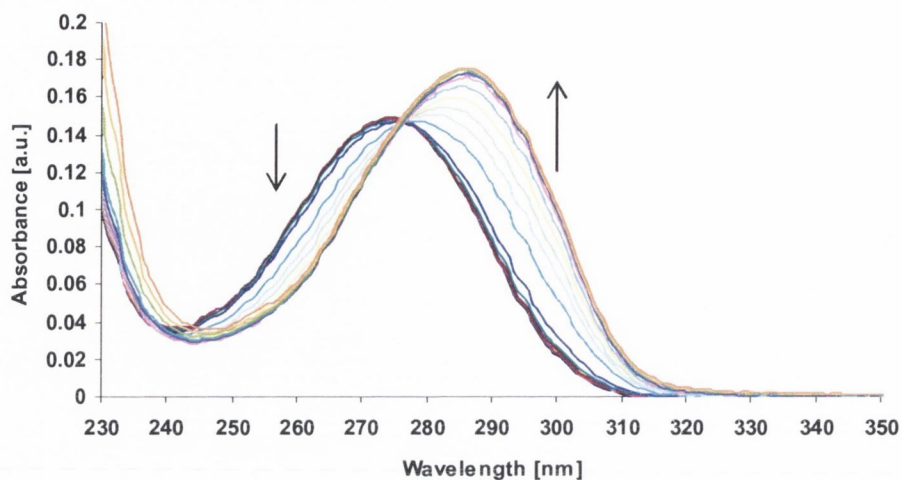


Figure 1: UV-Visible spectra showing the changes in absorbance of receptor **71** ($4 \mu\text{M}$) upon gradual additions of CH_3COO^- ($0 \rightarrow 1.48 \text{ mM}$) in CH_3CN .

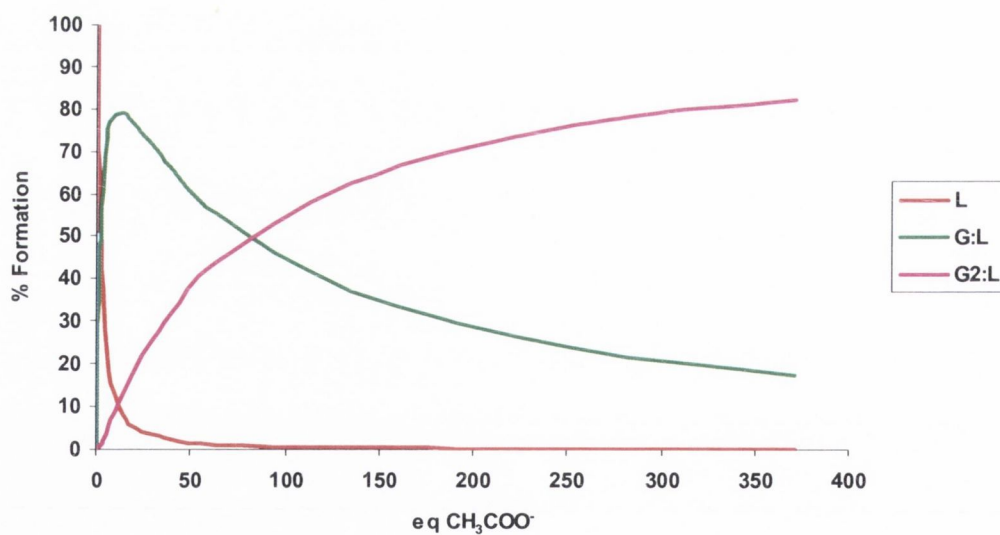


Figure 2: Speciation diagram for the UV-Visible titration of **71** (L) with CH_3COO^- (G) in MeCN. Speciation is shown relative to the number of equivalents of CH_3COO^- .

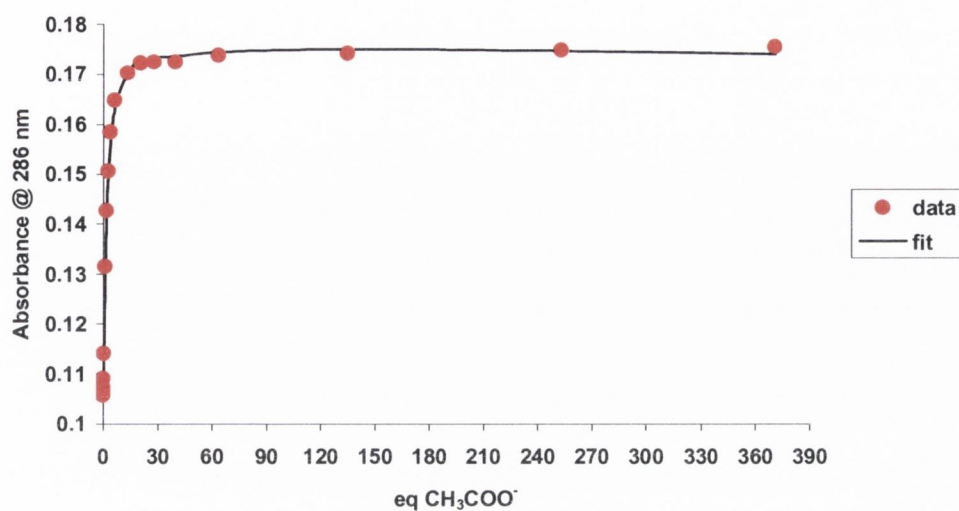


Figure 3: Experimental binding isotherm for the UV-Visible titration of **71** ($4 \mu\text{M}$) with CH_3COO^- and corresponding fit from SPECFIT. Data represented by the red circles, while the fit is represented by the solid black line.

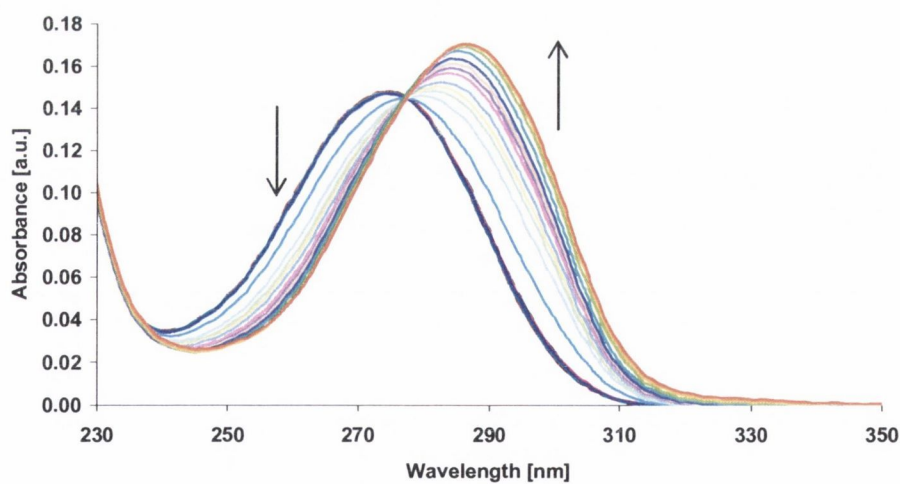


Figure 4: UV-Visible spectra showing the changes in absorbance of receptor **71** ($4 \mu\text{M}$) upon gradual additions of F^- ($0 \rightarrow 1.65 \text{ mM}$) in CH_3CN .

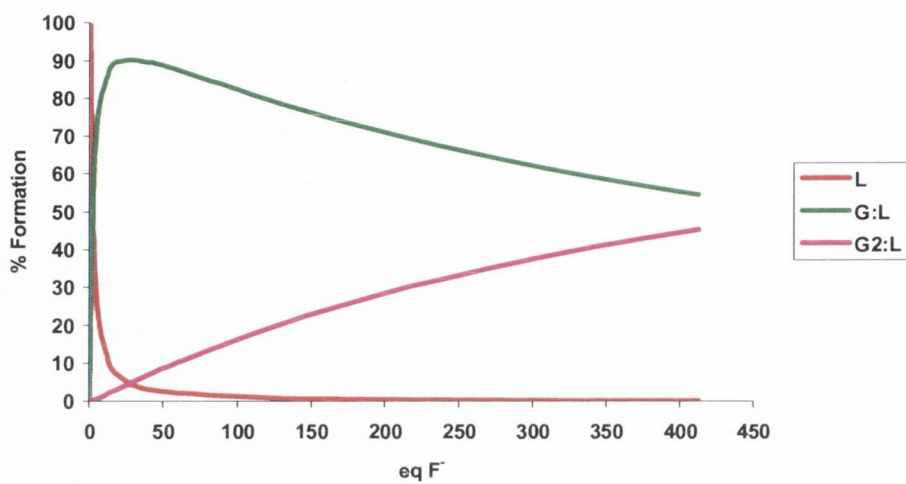


Figure 5: Speciation diagram for the UV-Visible titration of **71** (L) with F^- (G) in CH_3CN . Speciation is shown relative to the number of equivalents of F^- .

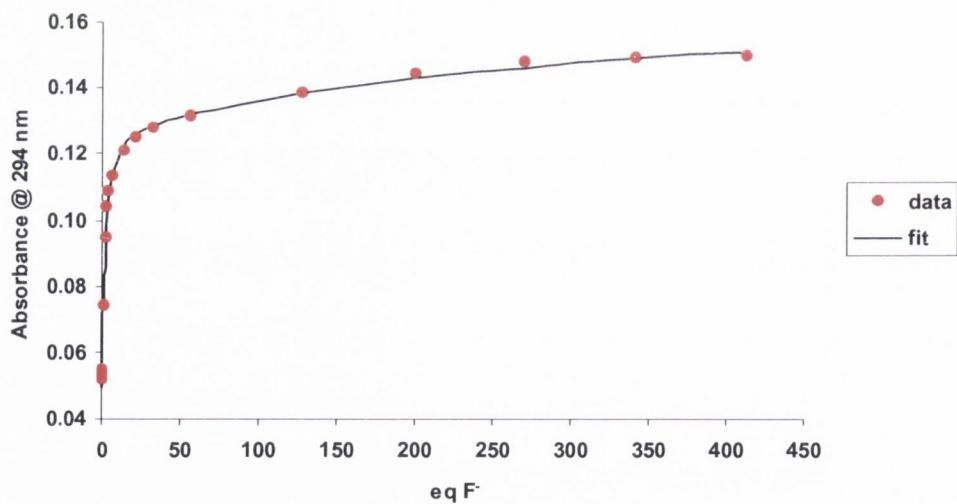


Figure 6: Experimental binding isotherm for the UV-Visible titration of **71** ($4 \mu M$) with F^- and corresponding fit from SPECFIT. Data represented by the red circles, while the fit is represented by the solid black line.

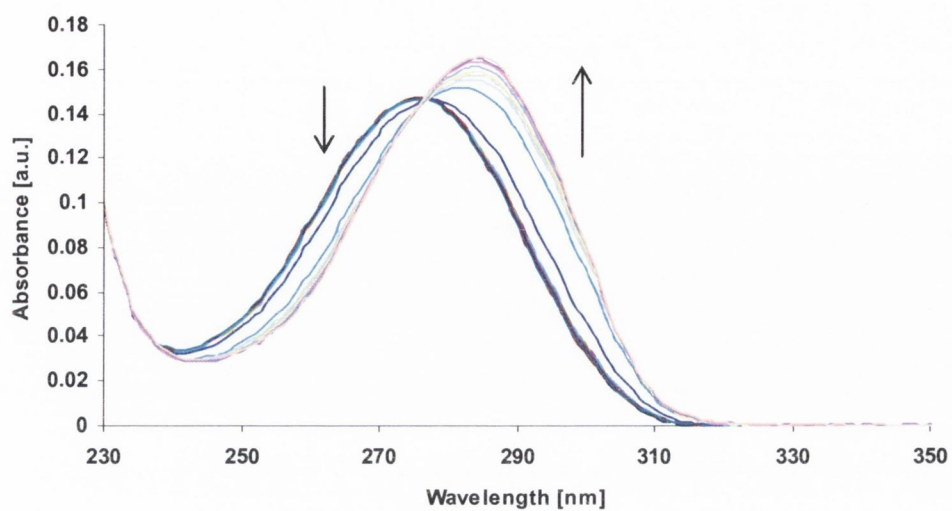


Figure 7: UV-Visible spectra showing the changes in absorbance of receptor **71** ($4 \mu\text{M}$) upon gradual additions of $\text{H}_2\text{P}_2\text{O}_7^{2-}$ ($0 \rightarrow 1.72 \text{ mM}$) in CH_3CN .

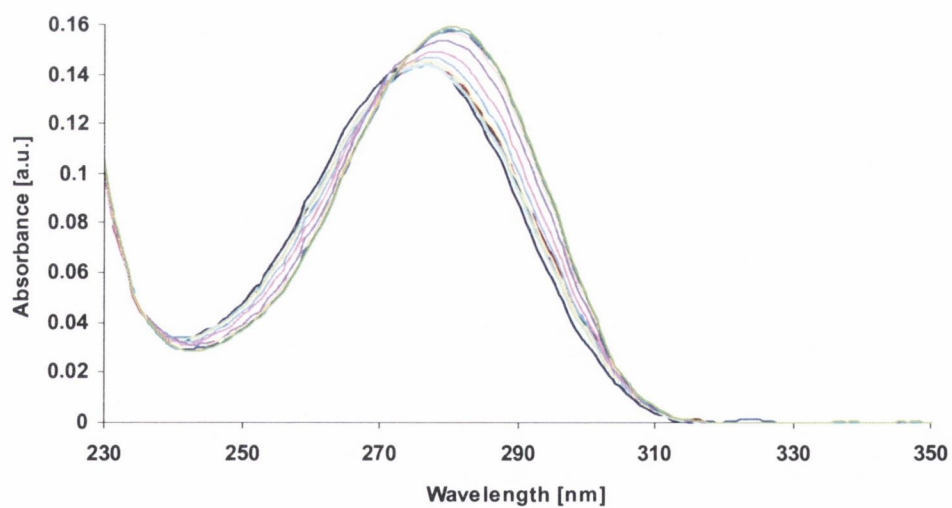


Figure 8: UV-Visible spectra showing the changes in absorbance of receptor **71** ($4 \mu\text{M}$) upon gradual additions of Cl^- ($0 \rightarrow 2.38 \text{ mM}$) in CH_3CN .

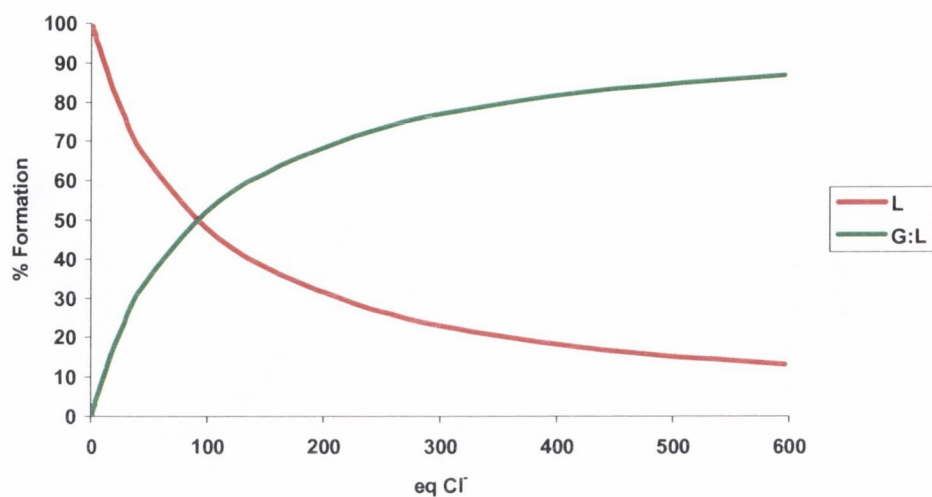


Figure 9: Speciation diagram for the UV-Visible titration of **71** (L) with Cl⁻ (G) in CH₃CN. Speciation is shown relative to the number of equivalents of Cl⁻.

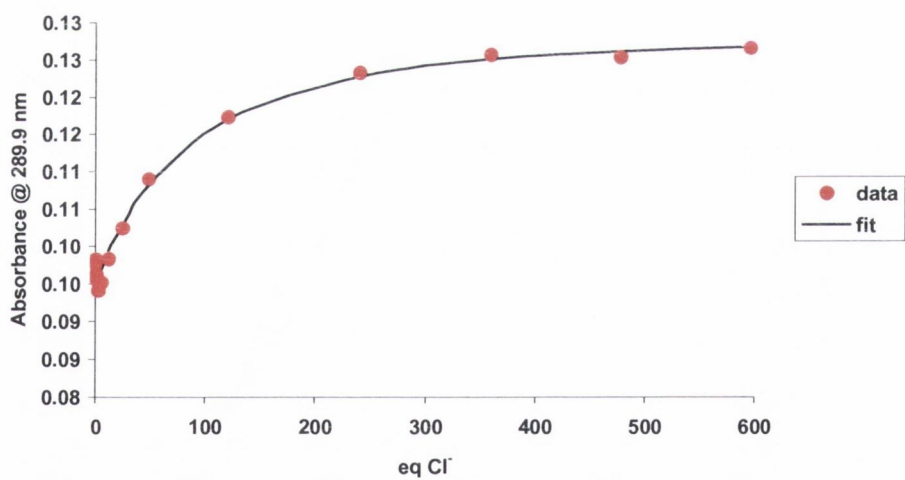


Figure 10: Experimental binding isotherm for the UV-Visible titration of **71** (4 μ M) with Cl⁻ and corresponding fit from SPECFIT. Data represented by the red circles, while the fit is represented by the solid black line.

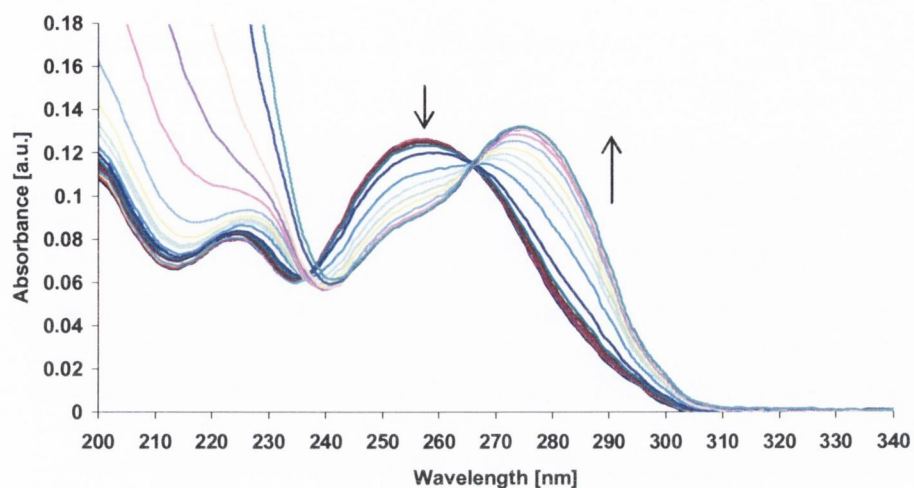


Figure 11: UV-Visible spectra showing the changes in absorbance of receptor **72** ($4 \mu\text{M}$) upon gradual additions of CH_3COO^- ($0 \rightarrow 0.77 \text{ mM}$) in CH_3CN .

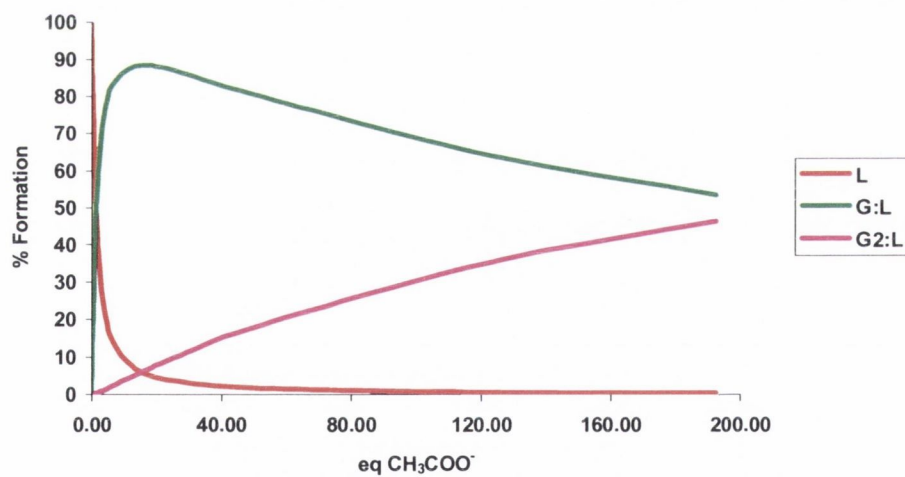


Figure 12: Speciation diagram for the UV-Visible titration of **72** (L) with CH_3COO^- (G) in CH_3CN . Speciation is shown relative to the number of equivalents of CH_3COO^- .

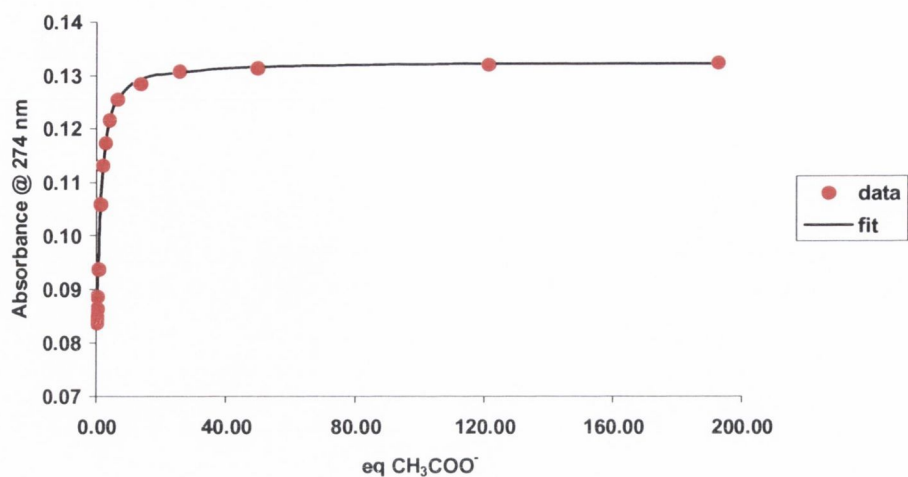


Figure 13: Experimental binding isotherm for the UV-Visible titration of **72** ($4 \mu\text{M}$) with CH_3COO^- and corresponding fit from SPECFIT. Data represented by the red circles, while the fit is represented by the solid black line.

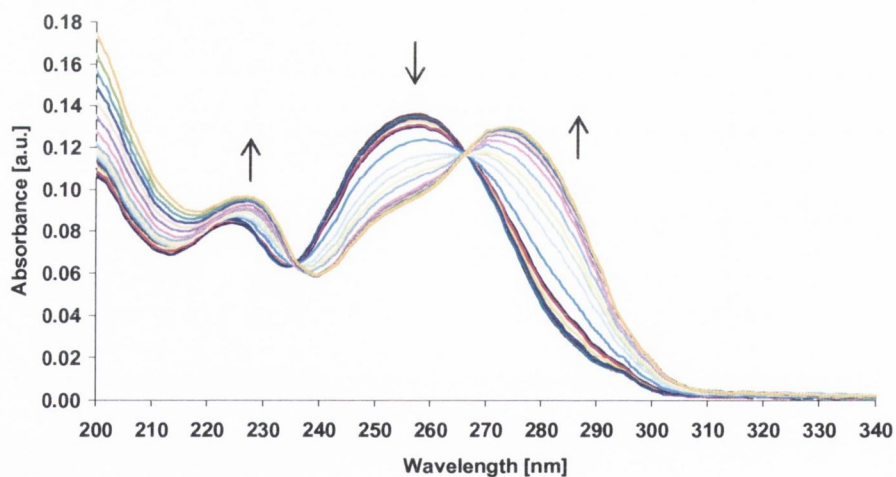


Figure 14: UV-Visible spectra showing the changes in absorbance of receptor **72** ($4 \mu\text{M}$) upon gradual additions of F^- ($0 \rightarrow 245 \mu\text{M}$) in CH_3CN .

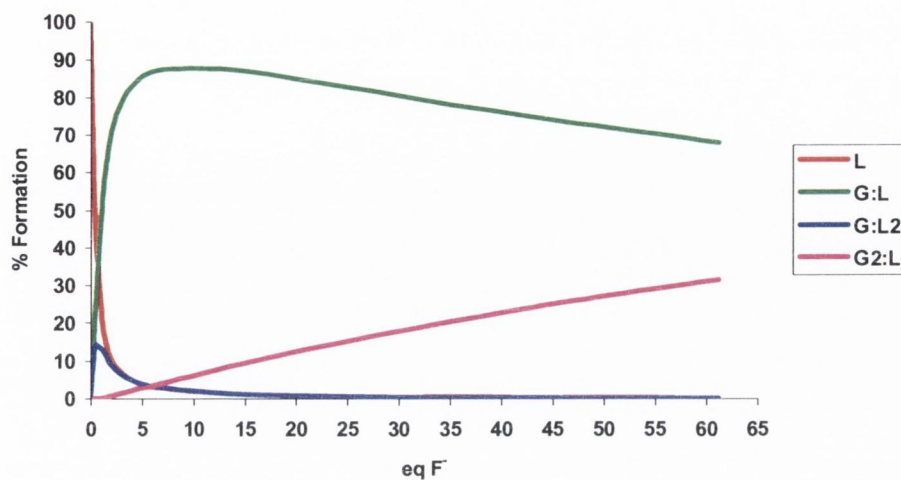


Figure 15: Speciation diagram for the UV-Visible titration of **72** (L) with F^- (G) in CH_3CN . Speciation is shown relative to the number of equivalents of F^- .

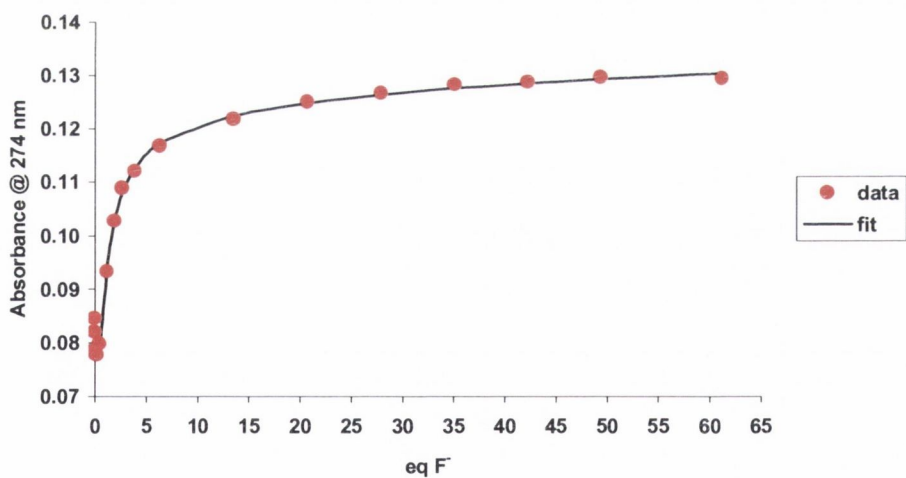


Figure 16: Experimental binding isotherm for the UV-Visible titration of **72** ($4 \mu M$) with F^- and corresponding fit from SPECFIT. Data represented by the red circles, while the fit is represented by the solid black line.

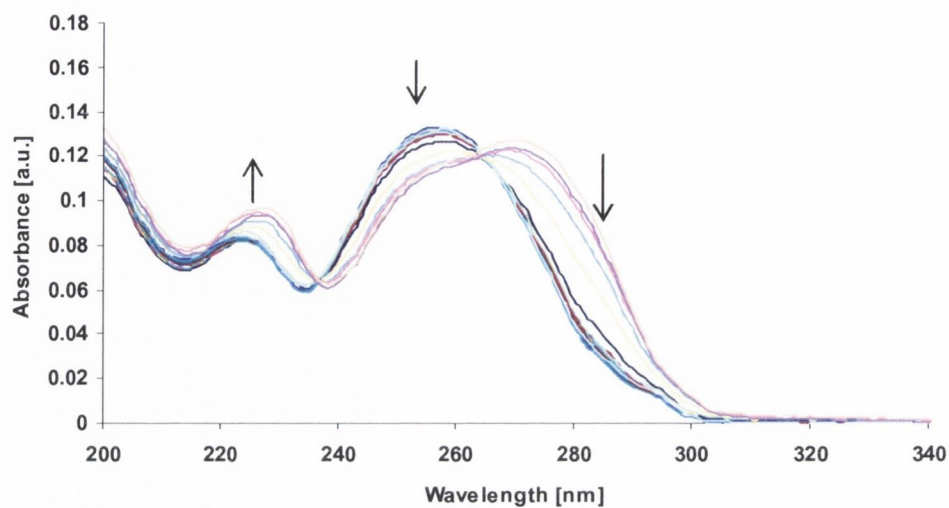


Figure 17: UV-Visible spectra showing the changes in absorbance of receptor **72** ($4 \mu\text{M}$) upon gradual additions of $\text{H}_2\text{P}_2\text{O}_7^{2-}$ ($0 \rightarrow 0.92 \text{ mM}$) in CH_3CN .

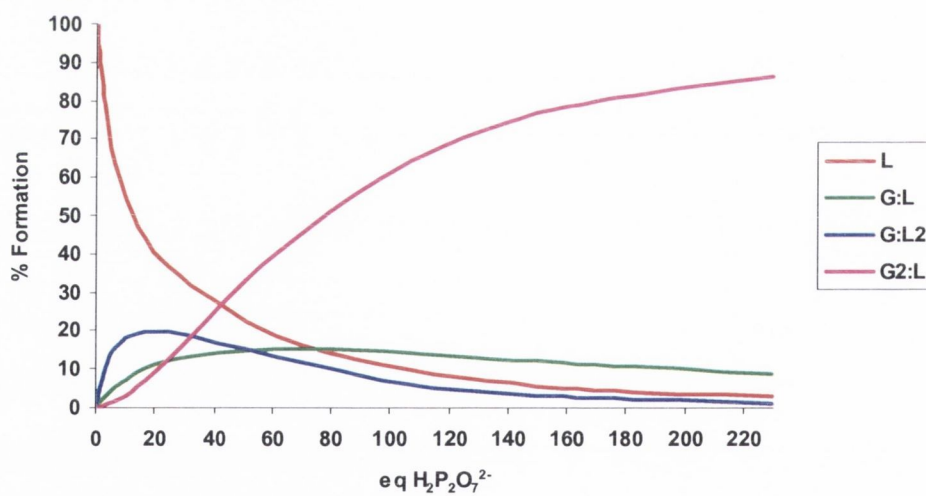


Figure 18: Speciation diagram for the UV-Visible titration of **72** (L) with $\text{H}_2\text{P}_2\text{O}_7^{2-}$ (G) in CH_3CN . Speciation is shown relative to the number of equivalents of $\text{H}_2\text{P}_2\text{O}_7^{2-}$.

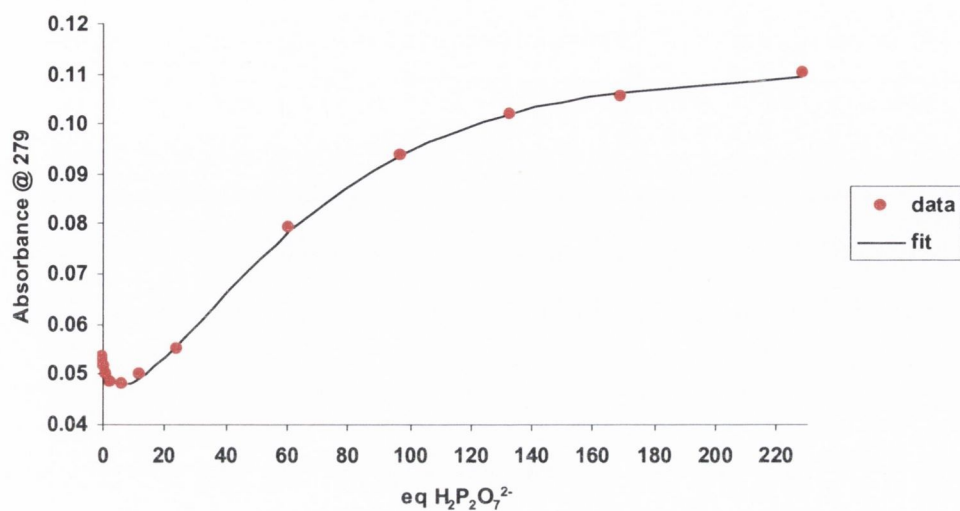


Figure 19: Experimental binding isotherm for the UV-Visible titration of **72** ($4 \mu\text{M}$) with $\text{H}_2\text{P}_2\text{O}_7^{2-}$ and corresponding fit from SPECFIT. Data represented by the red circles, while the fit is represented by the solid black line.

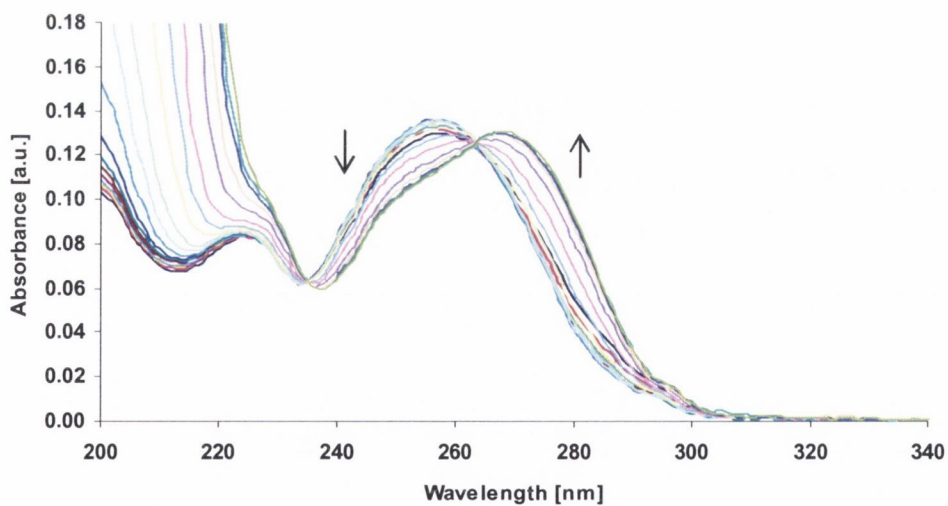


Figure 20: UV-Visible spectra showing the changes in absorbance of receptor **72** ($4 \mu\text{M}$) upon gradual additions of Cl^- ($0 \rightarrow 2.38 \text{ mM}$) in CH_3CN .

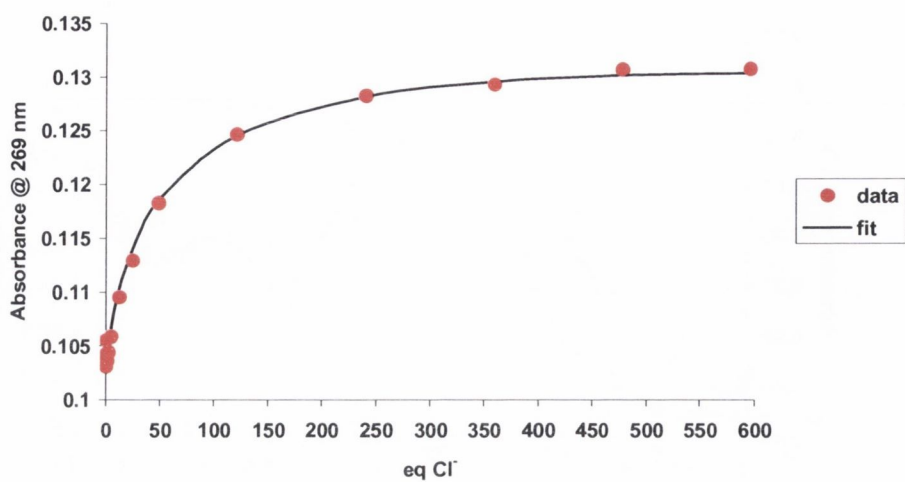


Figure 21: Experimental binding isotherm for the UV-Visible titration of 72 (4 μM) with Cl^- and corresponding fit from SPECFIT. Data represented by the red circles, while the fit is represented by the solid black line.

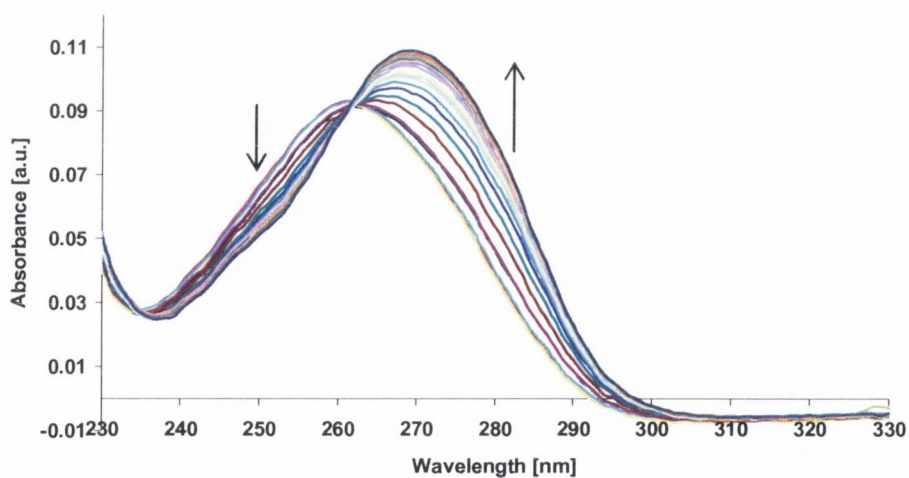


Figure 22: Absorption spectra showing the changes in absorbance of model receptor 73 (4 μM) upon gradual additions of H_2PO_4^- (0 \rightarrow 40.10 μM) in CH_3CN .

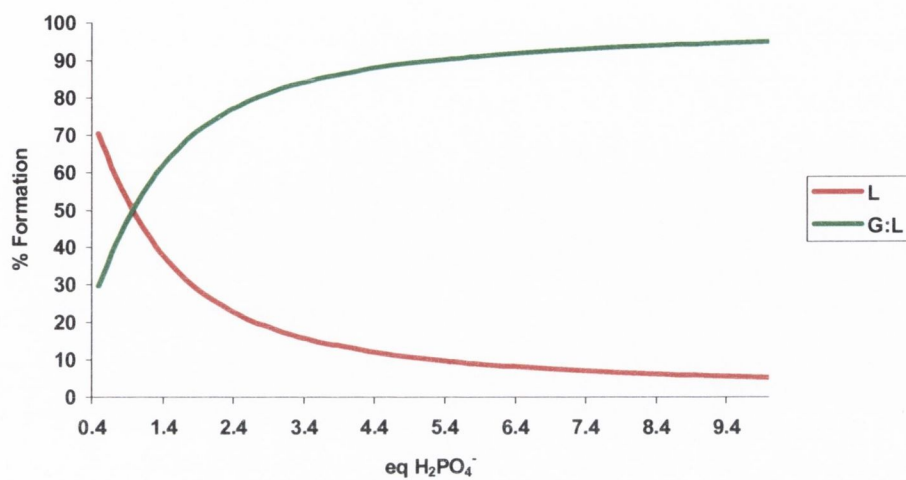


Figure 23: Speciation diagram for the UV-Visible titration of **73** (L) with H_2PO_4^- (G) in CH_3CN . Speciation is shown relative to the number of equivalents of H_2PO_4^- .

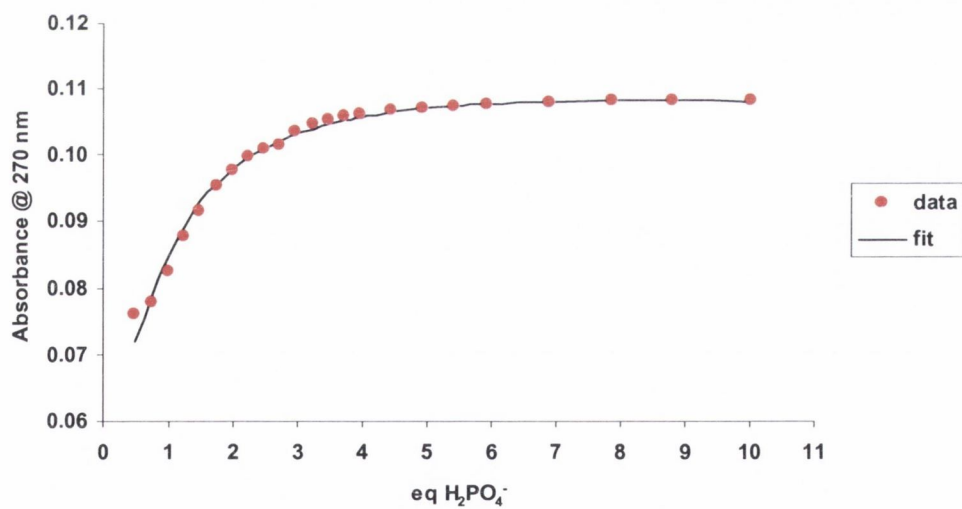


Figure 24: Experimental binding isotherm for the UV-Visible titration of **73** ($4 \mu\text{M}$) with H_2PO_4^- and corresponding fit from SPECFIT. Data represented by the red circles, while the fit is represented by the solid black line.

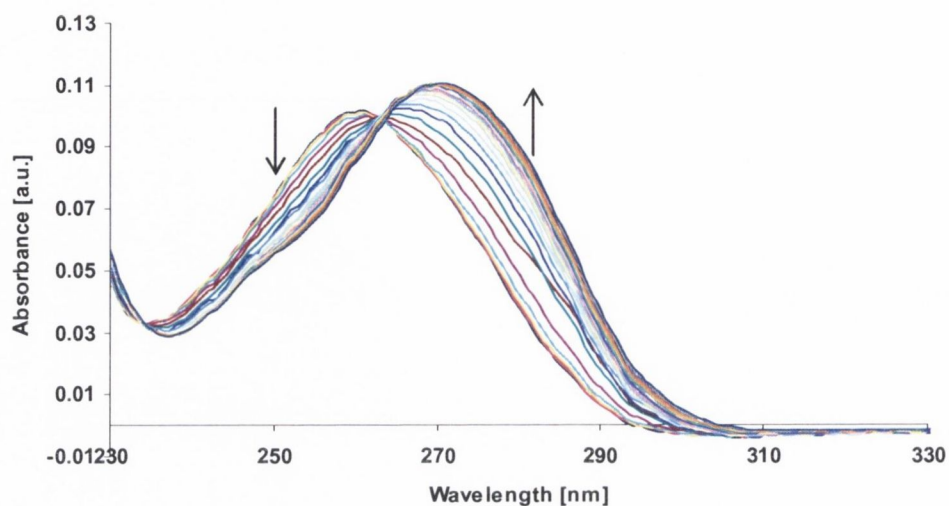


Figure 25: Absorption spectra showing the changes in absorbance of model receptor 73 ($4 \mu\text{M}$) upon gradual additions of F^- ($0 \rightarrow 40.1 \mu\text{M}$) in CH_3CN .

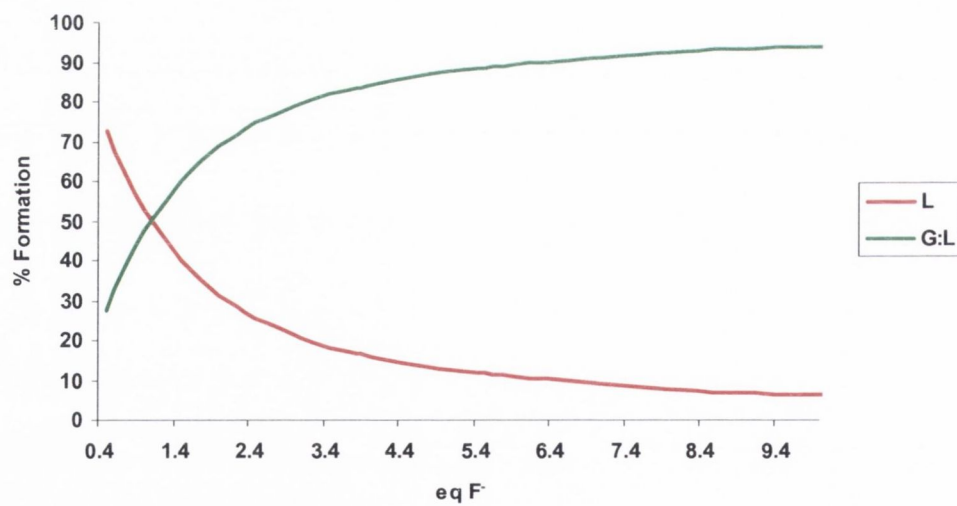


Figure 26: Speciation diagram for the UV-Visible titration of 73 (L) with F^- (G) in CH_3CN . Speciation is shown relative to the number of equivalents of F^- .

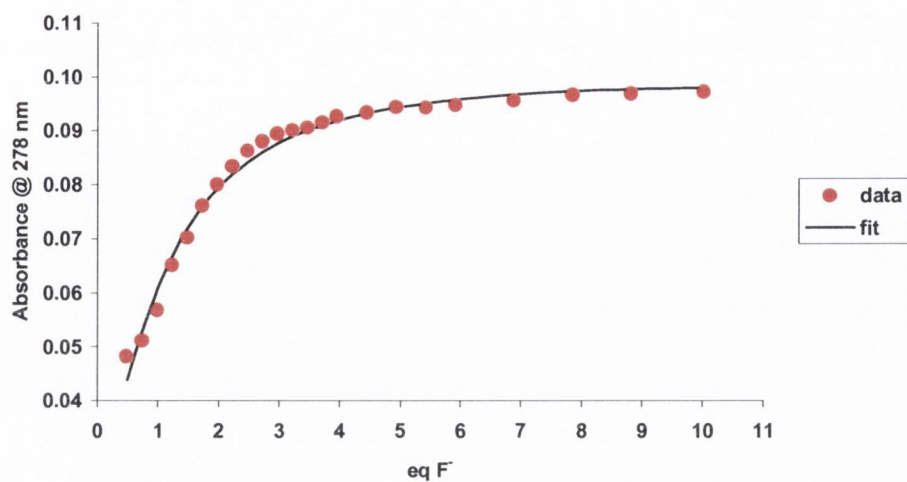


Figure 27: Experimental binding isotherm for the UV-Visible titration of **73** ($4 \mu\text{M}$) with F^- and corresponding fit from SPECFIT. Data represented by the red circles, while the fit is represented by the solid black line.

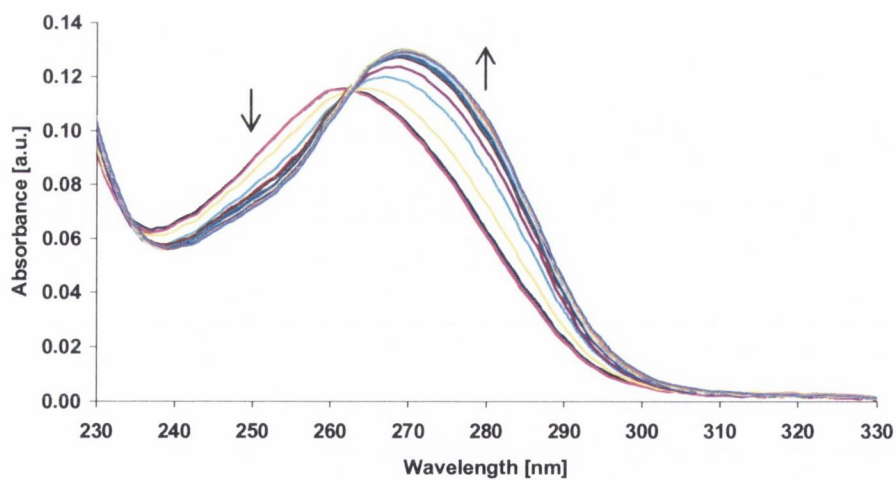


Figure 28: Absorption spectra showing the changes in absorbance of model receptor **73** ($4 \mu\text{M}$) upon gradual additions of $\text{H}_2\text{P}_2\text{O}_7^{2-}$ ($0 \rightarrow 40.1 \mu\text{M}$) in CH_3CN .

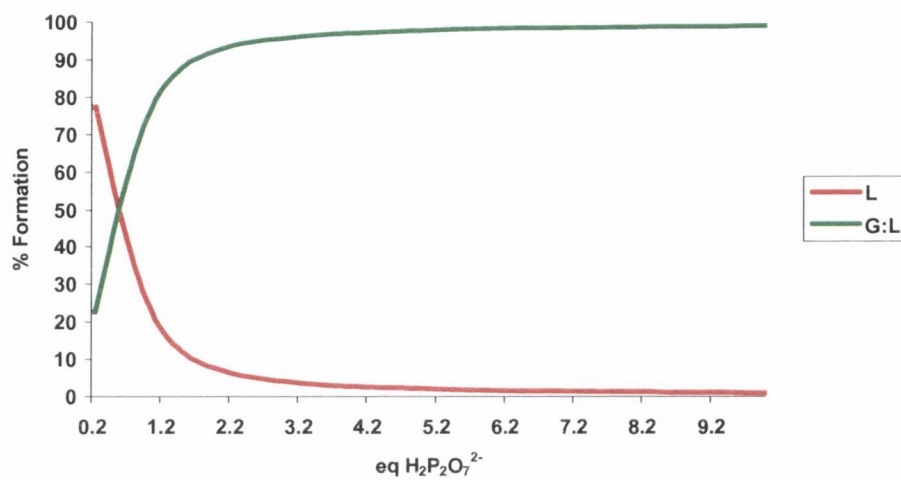


Figure 29: Speciation diagram for the UV-Visible titration of **73** (L) with $\text{H}_2\text{P}_2\text{O}_7^{2-}$ (G) in CH_3CN . Speciation is shown relative to the number of equivalents of $\text{H}_2\text{P}_2\text{O}_7^{2-}$.

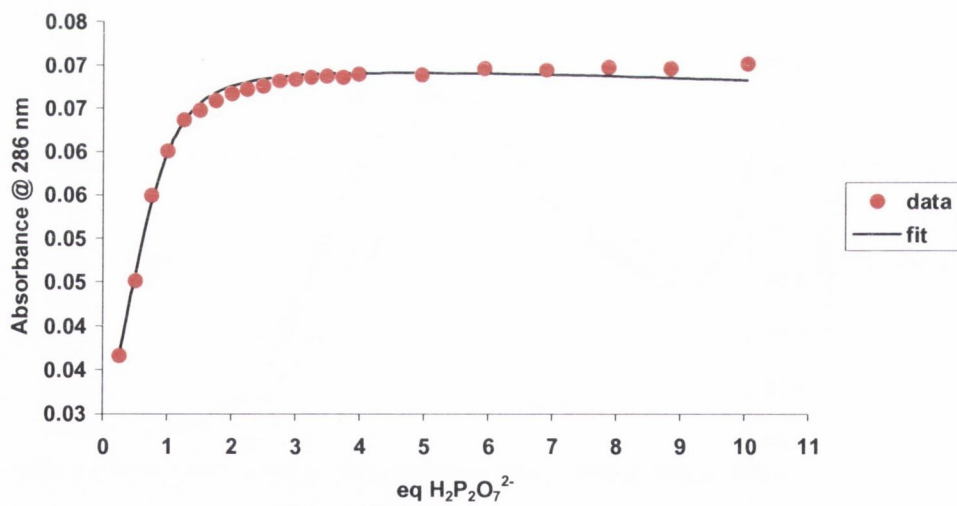


Figure 30: Experimental binding isotherm for the UV-Visible titration of **73** ($4 \mu\text{M}$) with $\text{H}_2\text{P}_2\text{O}_7^{2-}$ and corresponding fit from SPECFIT. Data represented by the red circles, while the fit is represented by the solid black line.

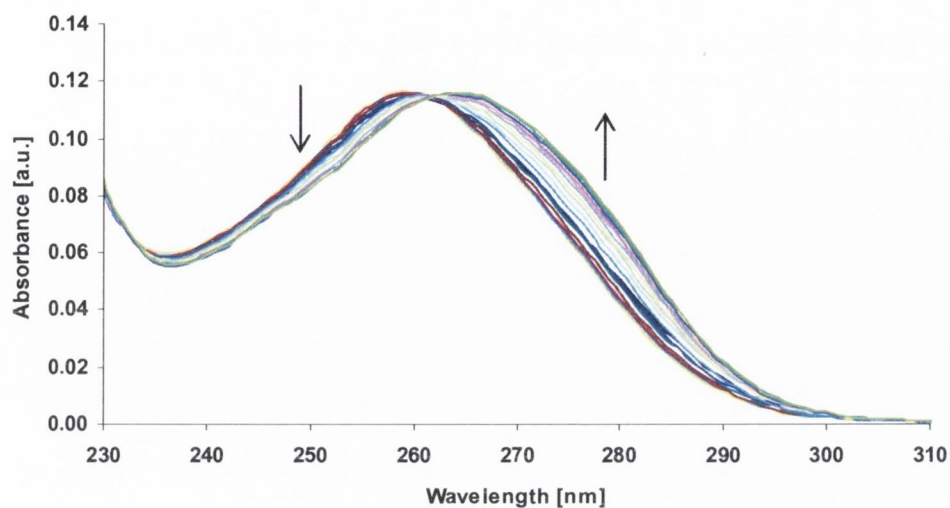


Figure 31: Absorption spectra showing the changes in absorbance of model receptor 73 (4 μM) upon gradual additions of Cl⁻ (0 → 261 μM) in CH₃CN.

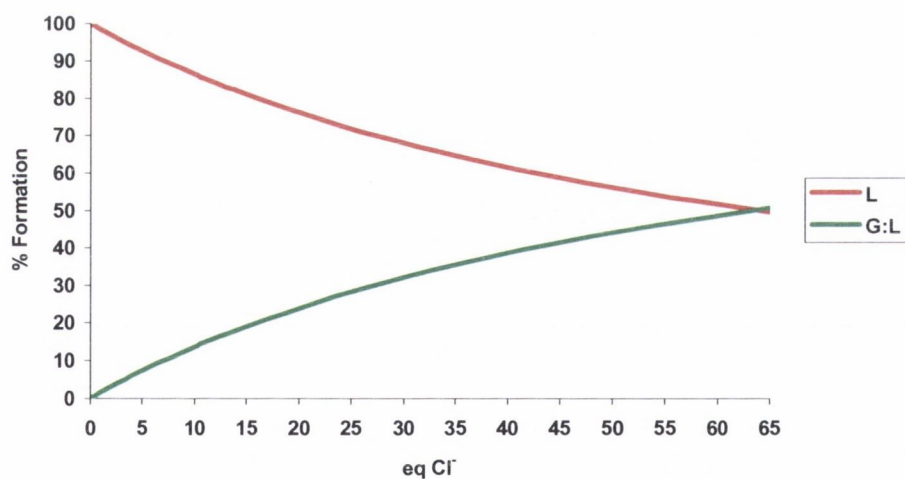


Figure 32: Speciation diagram for the UV-Visible titration of 73 (L) with Cl⁻ (G) in CH₃CN. Speciation is shown relative to the number of equivalents of Cl⁻.

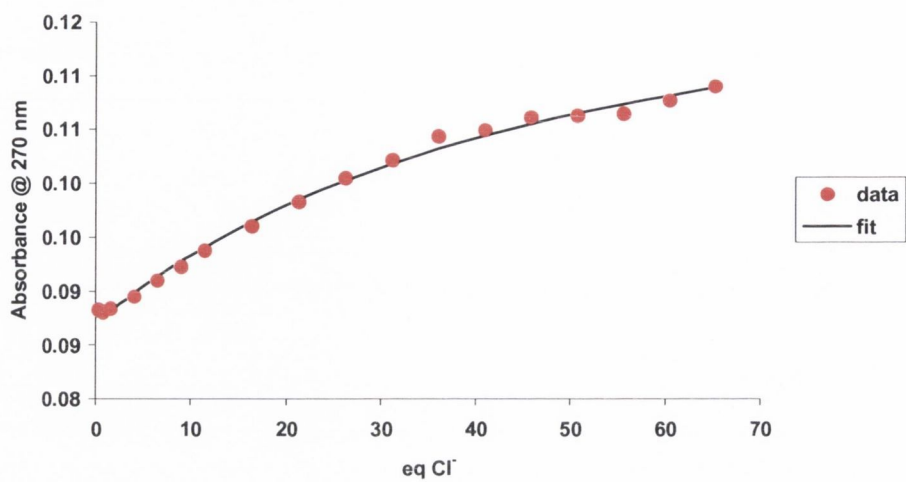


Figure 33: Experimental binding isotherm for the UV-Visible titration of 73 (4 μM) with Cl^- and corresponding fit from SPECFIT. Data represented by the red circles, while the fit is represented by the solid black line.

Appendix 3-Absorption, fluorescence, and speciation data for Chapter 4

A3.1 Titration of 87 with anions

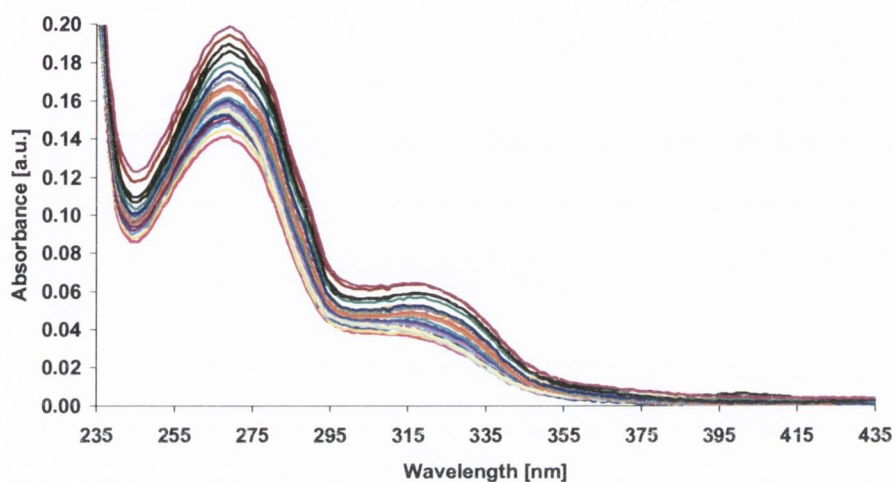


Figure A3.1.1: Absorption spectra of **87** (4.8 μM) upon gradual additions of H₂PO₄⁻ (0 → 3.49 mM) in CH₃CN.

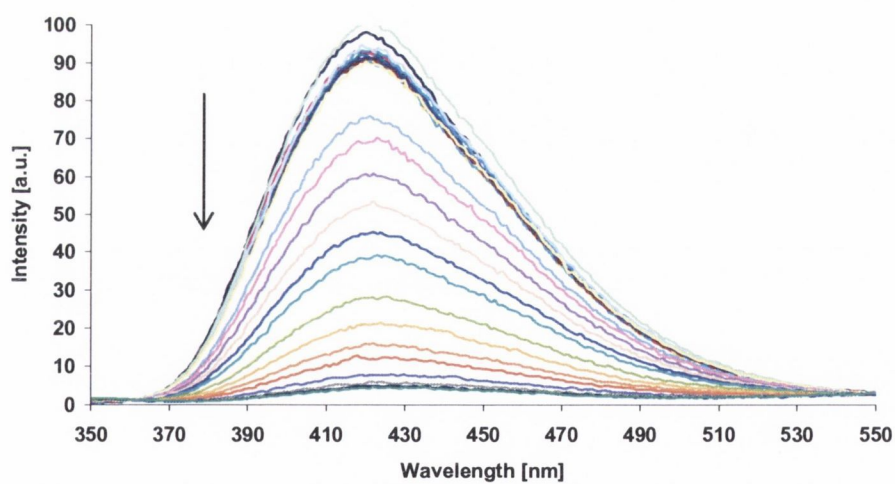


Figure A3.1.2: Fluorescence emission spectra of **87** (4.8 μM) upon gradual additions of H₂PO₄⁻ (0 → 3.49 mM) in CH₃CN.

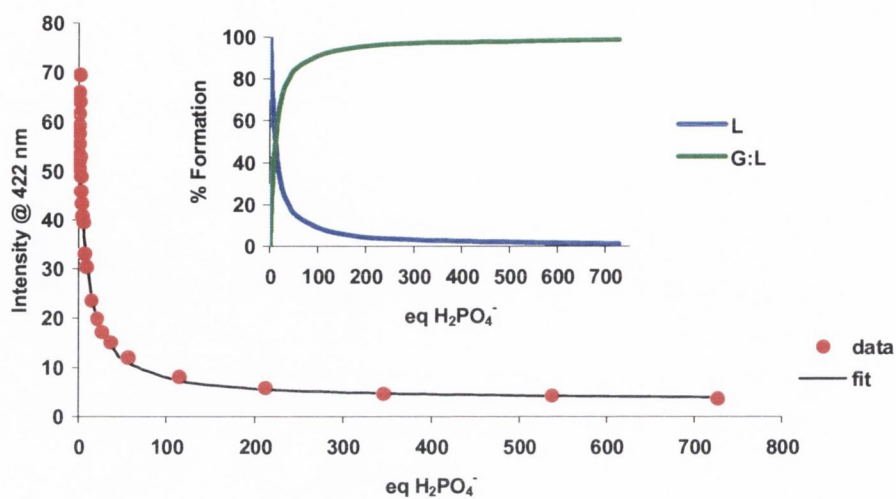


Figure A3.1.3: Experimental binding isotherm and corresponding fit at 422 nm for the fluorescence titration of **87** (L) with H_2PO_4^- (G) (0 \rightarrow 3.49 mM) in CH_3CN . Insert: Speciation diagram showing the formation of the 1:1 (G:L) complex.

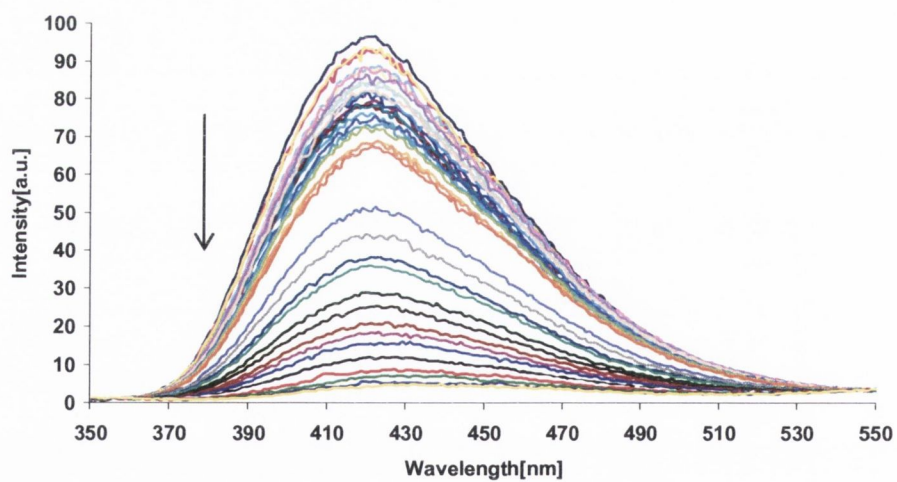


Figure A3.1.4: Fluorescence emission spectra of **87** (4.8 μM) upon gradual additions of F^- (0 \rightarrow 2.95 mM) in CH_3CN .

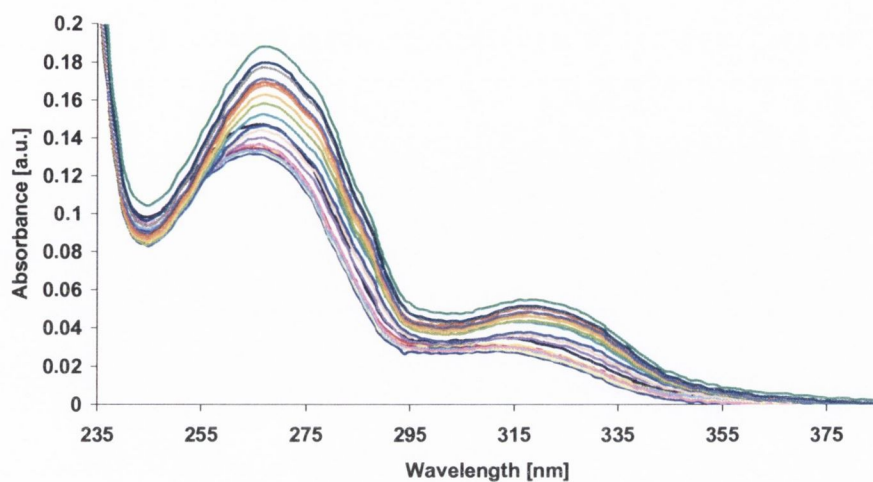


Figure A3.1.5: Fluorescence emission spectra of **87** ($4.8 \mu\text{M}$) upon gradual additions of Cl^- ($0 \rightarrow 17.50 \text{ mM}$) in CH_3CN .

A3.2 Speciation diagrams for the titration of **87** with Cu(II)

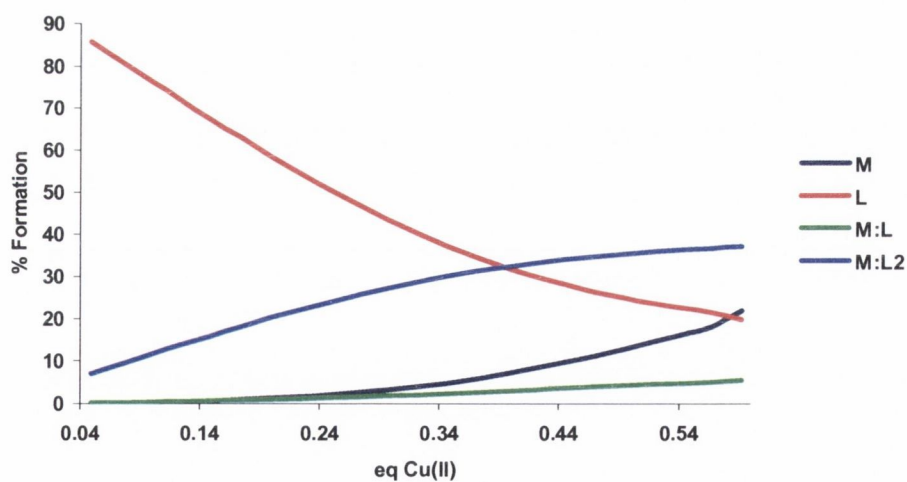


Figure A3.2: Speciation distribution diagram for the UV-visible titration of **87** (L) with Cu(II) (M), in CH_3CN .

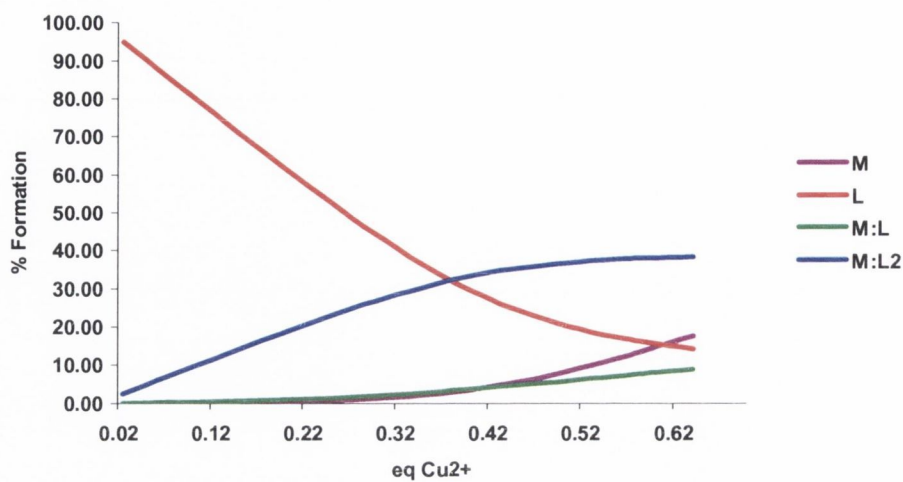


Figure A3.2.1: Speciation distribution diagram for the fluorescence emission titration of **87** (L) with Cu(II) (M), in CH₃CN.

A3.3 Titration of Fe:**87**₂ with anions

A3.3.1 Absorption titrations of Fe:**87**₂ with anions

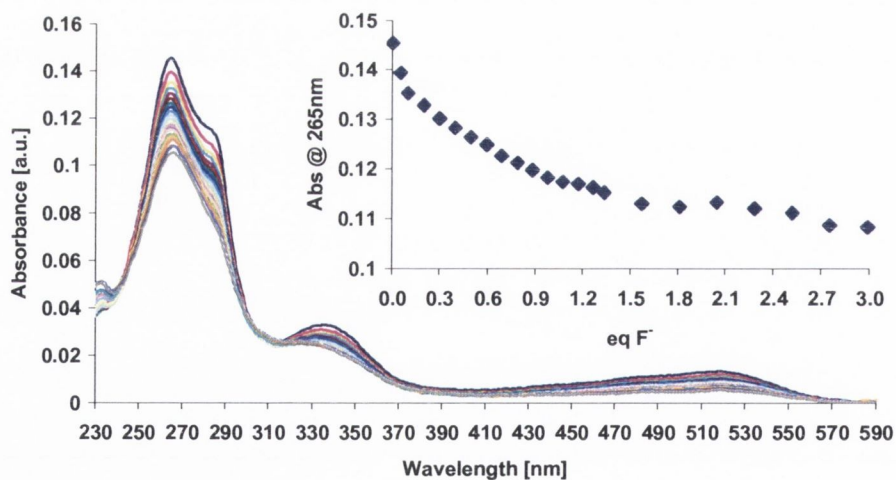


Figure A3.3.1: Absorption spectra of the Fe(II) complex of **87** (4 μM) upon gradual additions of F⁻ (0 → 12.90 μM) in CH₃CN. Insert: The changes in the absorbance at 265 nm as a function of the number equivalents of F⁻.

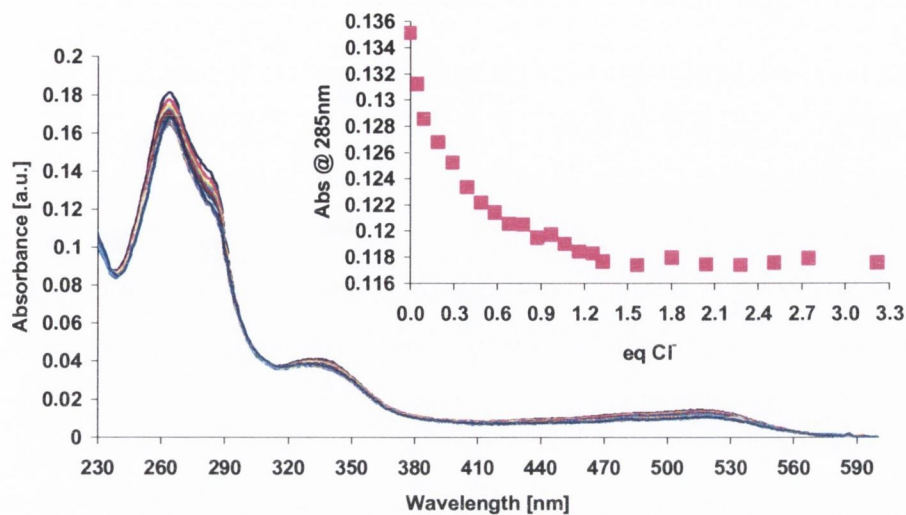


Figure A3.3.1.1: Absorption spectra of the Fe(II) complex of **87** (4 μM) upon gradual additions of Cl^- (0 \rightarrow 16.60 μM) in CH_3CN . Inset: The changes in the absorbance at 285 nm as a function of the number equivalents of Cl^- .

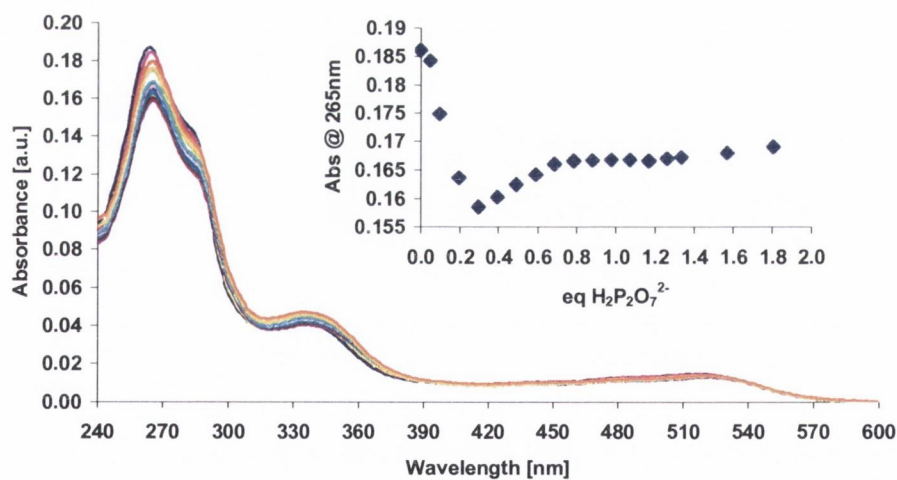


Figure A3.3.1.2: Absorption spectra of the Fe(II) complex of **87** (4 μM) upon gradual additions of $\text{H}_2\text{P}_2\text{O}_7^{2-}$ (0 \rightarrow 11.00 μM) in CH_3CN . Inset: The changes in the absorbance at 265 nm as a function of the number equivalents of $\text{H}_2\text{P}_2\text{O}_7^{2-}$.

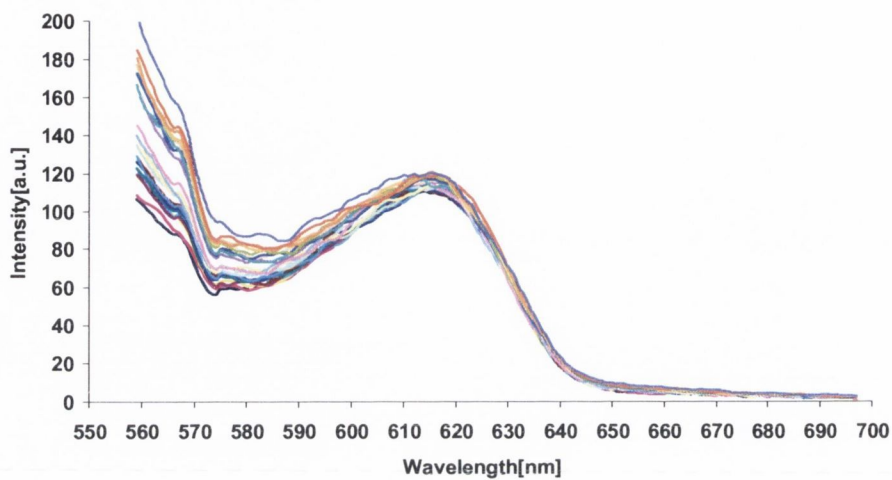
A3.3.2 Fluorescence emission titrations of Fe:87₂ with anions

Figure A3.3.2: Fluorescence emission spectra of the Fe(II) complex of **87** ($4 \mu\text{M}$) upon gradual additions of F^- ($0 \rightarrow 12.90 \mu\text{M}$) in CH_3CN , when exciting at 520 nm.

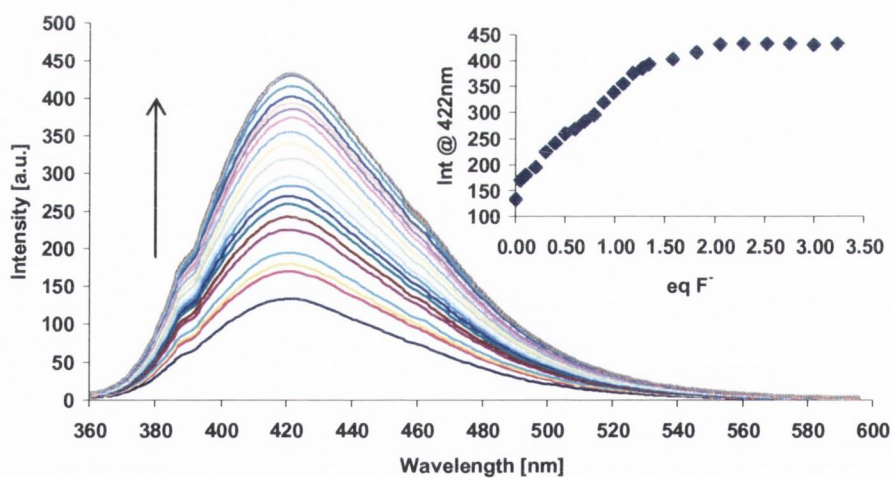


Figure A3.3.2.1: Fluorescence emission spectra of the Fe(II) complex of **87** ($4 \mu\text{M}$) upon gradual additions of F^- ($0 \rightarrow 12.90 \mu\text{M}$) in CH_3CN . Insert: The changes in the fluorescence intensity at 422 nm as a function of the number equivalents of F^- .

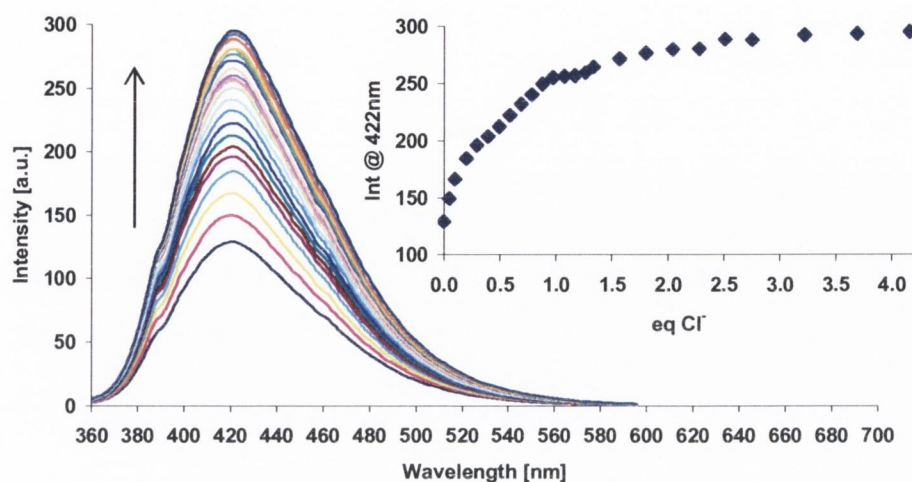


Figure A3.3.2.2: Fluorescence emission spectra of the Fe(II) complex of **87** ($4 \mu\text{M}$) upon gradual additions of Cl^- ($0 \rightarrow 16.60 \mu\text{M}$) in CH_3CN . Insert: The changes in the fluorescence intensity at 422 nm as a function of the number equivalents of Cl^- .

A3.4 Titration of $\text{Cu}:\mathbf{87}_2$ with anions

A3.4.1 Absorption titrations of $\text{Cu}:\mathbf{87}_2$ with anions

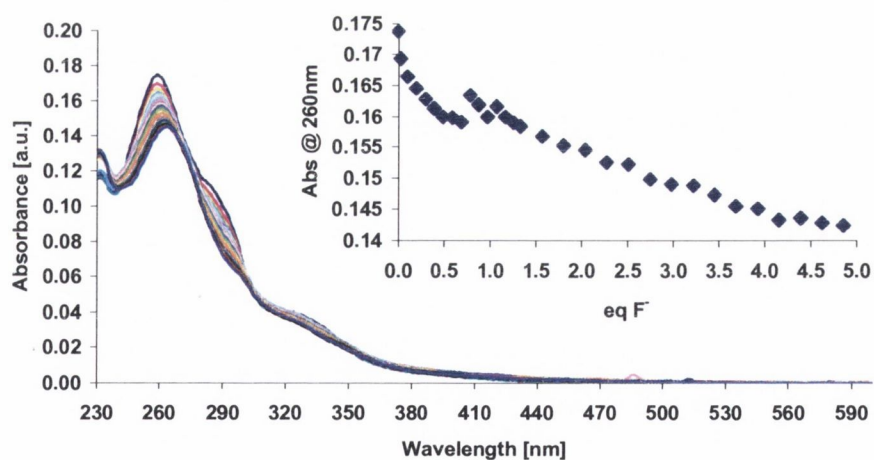


Figure A3.4.1: Absorption spectra of the Cu(II) complex of **87** ($4 \mu\text{M}$) upon gradual additions of F^- ($0 \rightarrow 19.50 \mu\text{M}$) in CH_3CN . Insert: The changes in the absorbance at 260 nm as a function of the number equivalents of F^- .

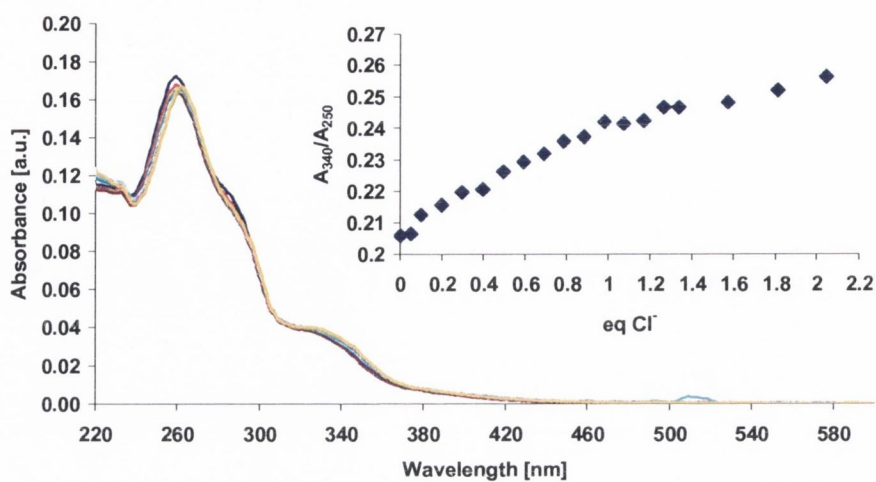


Figure A3.4.1.1: Absorption spectra of the Cu(II) complex of **87** (4 μM) upon gradual additions of Cl⁻ (0 → 9.13 μM) in CH₃CN. Insert: The changes in the ratio of the absorbances at 340 nm and 260 nm (A_{340}/A_{260}) as a function of the number equivalents of Cl⁻.

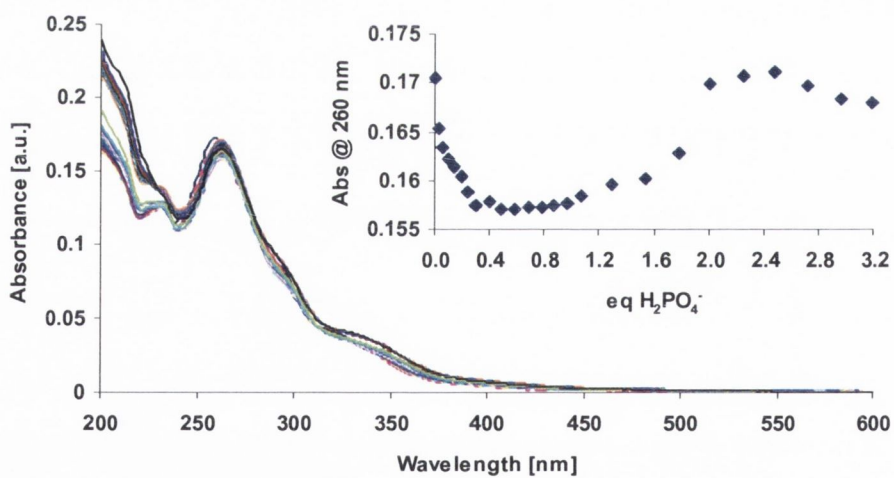


Figure A3.4.1.2: Absorption spectra of the Cu(II) complex of **87** (4 μM) upon gradual additions of H₂PO₄⁻ (0 → 12.70 μM) in CH₃CN. Insert: The changes in the absorbance at 262 nm as a function of the number equivalents of H₂PO₄⁻.

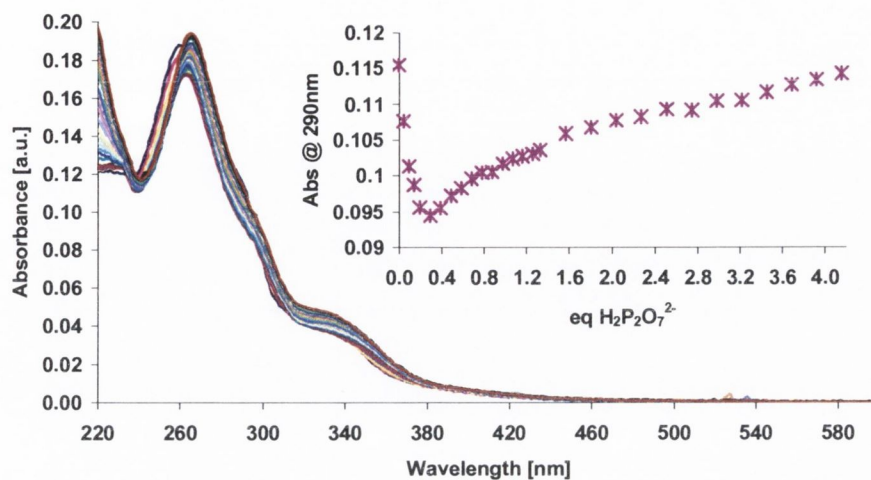


Figure A3.4.1.3: Absorption spectra of the Cu(II) complex of **87** ($4 \mu\text{M}$) upon gradual additions of $\text{H}_2\text{P}_2\text{O}_7^{2-}$ ($0 \rightarrow 16.60 \mu\text{M}$) in CH_3CN . Insert: The changes in the absorbance at 290 nm as a function of the number equivalents of $\text{H}_2\text{P}_2\text{O}_7^{2-}$.

A3.4.2 Fluorescence emission titrations of Cu:87₂ with anions

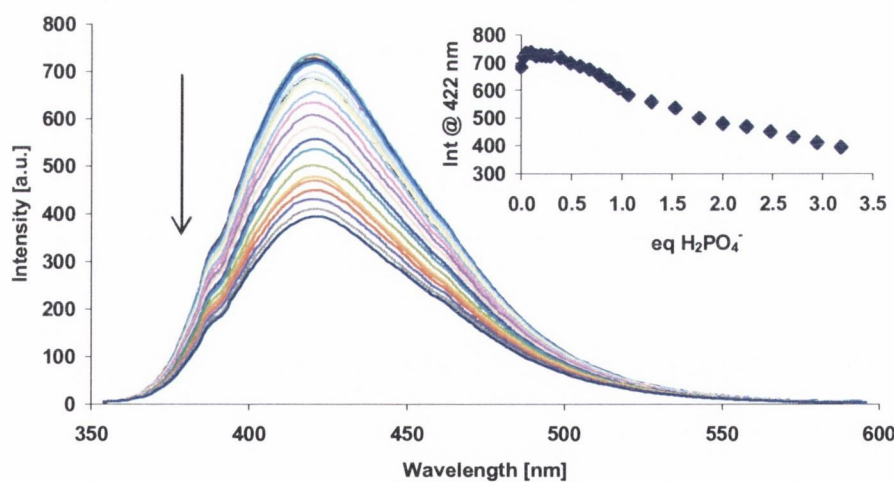


Figure A3.4.2: Fluorescence emission spectra of the Cu(II) complex of **87** ($4 \mu\text{M}$) upon gradual additions of H_2PO_4^- ($0 \rightarrow 12.70 \mu\text{M}$) in CH_3CN . Insert: The changes in the fluorescence intensity at 422 nm as a function of the number equivalents of H_2PO_4^- .

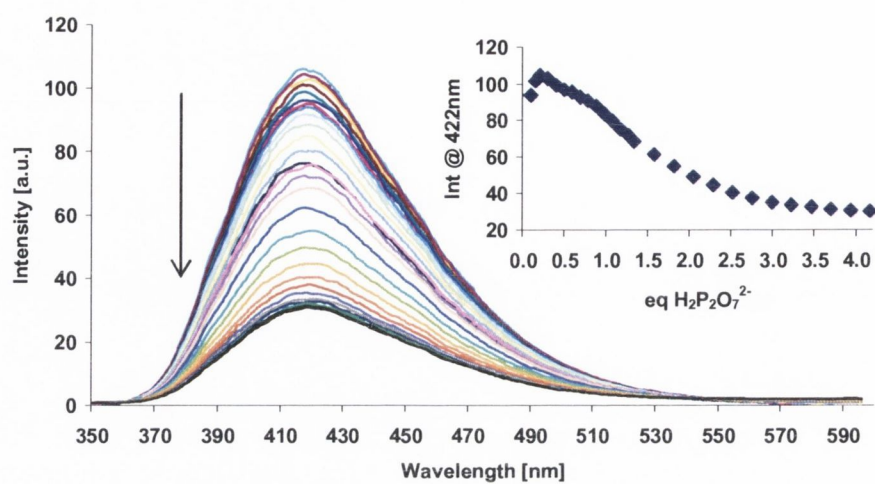


Figure A3.4.2.1: Fluorescence emission spectra of the Cu(II) complex of **87** ($4 \mu\text{M}$) upon gradual additions of $\text{H}_2\text{P}_2\text{O}_7^{2-}$ ($0 \rightarrow 16.60 \mu\text{M}$) in CH_3CN . Insert: The changes in the fluorescence intensity at 422 nm as a function of the number equivalents of $\text{H}_2\text{P}_2\text{O}_7^{2-}$.

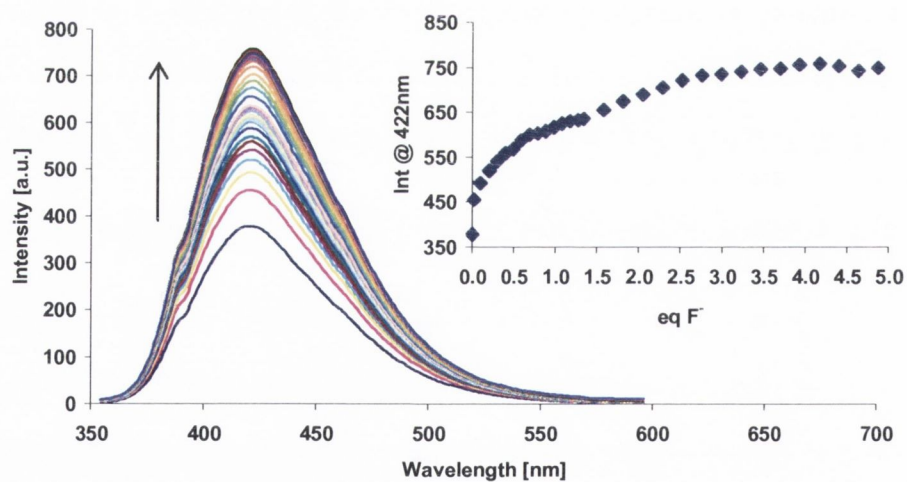


Figure A3.4.2.2: Fluorescence emission spectra of the Cu(II) complex of **87** ($4 \mu\text{M}$) upon gradual additions of F^- ($0 \rightarrow 19.50 \mu\text{M}$) in CH_3CN . Insert: The changes in the fluorescence intensity at 422 nm as a function of the number equivalents of F^- .

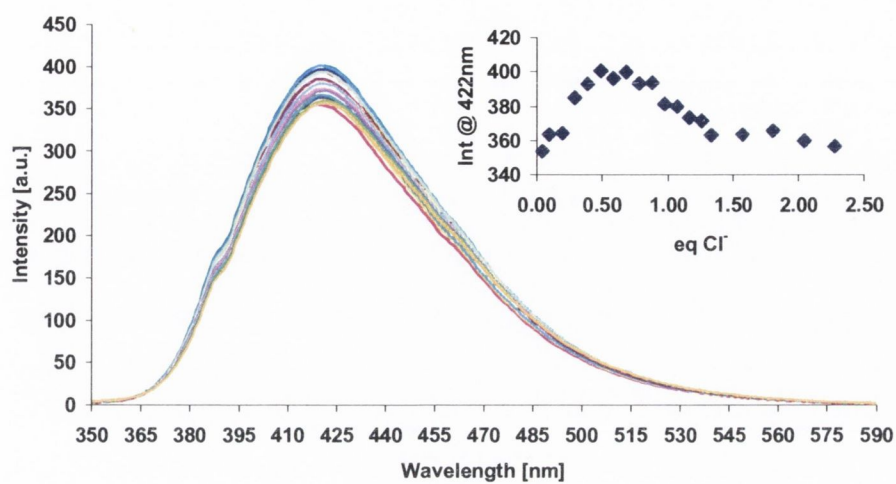


Figure A3.4.2.3: Fluorescence emission spectra of the Cu(II) complex of **87** ($4 \mu\text{M}$) upon gradual additions of Cl^- ($0 \rightarrow 9.13 \mu\text{M}$) in CH_3CN . Insert: The changes in the fluorescence intensity at 422 nm as a function of the number equivalents of Cl^- .

Publications

pH driven self-assembly of a ternary lanthanide luminescence complex: the sensing of anions using a β -diketonate-Eu(III) displacement assay†

Joseph P. Leonard,* Cidalia M. G. dos Santos, Sally E. Plush, Thomas McCabe and Thorfinnur Gunnlaugsson*

Received (in Cambridge, UK) 9th August 2006, Accepted 27th September 2006

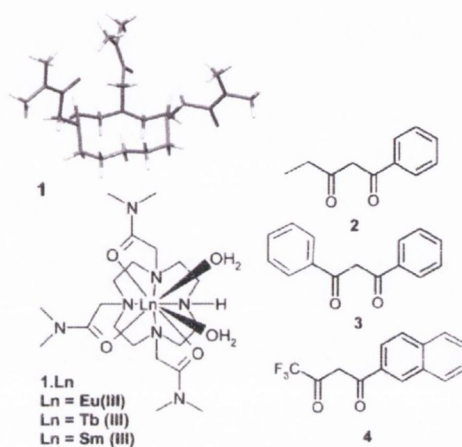
First published as an Advance Article on the web 23rd October 2006

DOI: 10.1039/b611487c

The synthesis and the photophysical evaluation of a novel pH dependent lanthanide luminescent self-assembly in water between a cyclen based europium complex and a β -diketonate is described and its use as a luminescent sensor in displacement assays for anions such as acetate, bicarbonate and lactate, where the Eu(III) emission was quenched upon anion recognition.

The design and synthesis of self-assembly architectures from structurally defined building blocks is at the centre of supramolecular chemistry.¹ Often such structures can be self-assembled, de-assembled, structurally altered or their function modulated by external controls, or inputs, such as light, electrochemistry or by using chemical inputs.^{2,3} We are interested in the formation of such functional self-assemblies from lanthanide ions and we have developed both mixed f-d metal ion self-assemblies as well as luminescent lanthanide ternary complexes using coordinating anions and Tb(III) based cyclen complexes.⁴⁻⁷ In this communication we demonstrate the formation of a new functional luminescent self-assembly ternary complex⁸ between the heptadentate europium complex **1**·Eu and the aromatic based β -diketonate **4**. Moreover, we demonstrate that the self-assembly formation is highly pH dependent and that we can employ this assembly at physiological pH as a luminescent sensor for anions.

The β -diketonates are well known to form stable complexes with lanthanide ions usually in 3 : 1 stoichiometry.⁹ Moreover, such complexes made from aromatic based β -diketonates can be highly luminescent as demonstrated by Tsukube *et al.*, where the β -diketonates acts as a sensitising antenna for the lanthanide ion.^{7,9} However, often such lanthanide complexes have coordinating solvent molecules, such as water, which can quench the lanthanide excited state through O–H vibrational deactivation.¹⁰ Our objective was to take advantage of this quenching process and use coordinatively unsaturated lanthanide complexes, *e.g.* **1**·Ln, which have two metal bound water molecules, and complex these with aromatic β -diketonates such as **2–4**, Scheme 1. This would lead to the formation of ternary self-assembly complexes, provided that the β -diketonates could displace the aforementioned metal bound water molecules, and as such, remove this quenching pathway. We also foresaw that the formation of these self-assemblies could be pH dependent, as both **1**·Ln and the structure of the antennae could be pH dependent.¹⁰ Herein, we present our



Scheme 1 The X-ray crystal structure of the protonated (as the HCl salt) form of **1** (Cl⁻ has been removed for clarity); **1**·Ln and the β -diketonates.

results, which are, to the best of our knowledge, the first examples of such pH driven self-assembly and the use of this ternary complex as a luminescent sensor for anions, where the Eu(III) emission was quenched or 'switched off' upon displacing the β -diketonate antenna by the anions.¹¹

The synthesis of **1** has previously been described by us, which involved the use of cyclen and the *N,N*-dimethyl- α -chloroamide in a single step.¹² The ¹H NMR (400 MHz, CDCl₃) of **1** showed the expected C₂ symmetry. We were also able to grow crystals of **1**, suitable for X-ray crystal structure analysis, Scheme 1, by slow evaporation from a methanol–CH₂Cl₂ solution, which confirmed the structure of **1**·HCl.¹³ The corresponding Eu(III), Sm(III) and Tb(III) complexes of **1**·Eu, **1**·Sm and **1**·Tb, were all formed from the corresponding lanthanide triflate salts. The X-ray crystal structures of **1**·Eu and **1**·Tb showed that the lanthanide ions were coordinating to the four nitrogens of the ring and the oxygen of the three acetamide arms.⁶ In both cases, the remaining two coordination sites were occupied by metal bound water molecules.⁶ By measuring the excited state lifetimes of **1**·Eu and **1**·Tb in H₂O and D₂O, the hydration state (*q*), the number of metal bound water molecules, was also confirmed to be two in solution.^{6,14} We next evaluated the ability of the three antennae, **2–4** to sensitize the lanthanide excited states of **1**·Ln by populating the lanthanide excited states (which under normal conditions is difficult to do directly due to symmetry forbidden f–f transitions)⁷ in pH 7.4 buffered solutions and in the presence of 0.1 M TMACl. As the complexes do not have incorporated antenna themselves,¹⁰ we used the λ_{max} for the three β -diketonates as the excitation

School of Chemistry, Centre for Synthesis and Chemical Biology, Trinity College Dublin, Dublin 2, Ireland. E-mail: gunnlaut@tcd.ie; Fax: +353 1671 2826; Tel: +353 1 608 3459

† Electronic supplementary information (ESI) available: Potentiometric titrations and general experimental. See DOI: 10.1039/b611487c

wavelengths. Excitation of 1·Eu, 1·Sm and 1·Tb at these wavelengths, in the absence of the antennae did not result in any lanthanide luminescence, as expected. We next carried out spectrophotometric titrations, observing the lanthanide emissions for 1·Eu, 1·Sm and 1·Tb, upon increasing concentrations of 2–4. For these titrations, *only* the characteristic Eu(III) emission, occurring at 595, 616, 685 and 700 nm for the deactivation of the 5D_0 excited state to 7F_J ($J = 1, 2, 3$ and 4) was observed.⁷ Moreover, the Eu(III) emission was *only* visible upon forming a complex between 1·Eu and 4 ($\lambda_{\text{max}} = 336$ nm); 1·Eu–4. Here the Eu(III) emission was found to be fully ‘switched on’ after the addition of *ca.* one equivalent of 4, Fig. 1, indicating the formation of a 1 : 1 complex in solution.† These luminescence changes clearly signified that 4 is able to populate the 5D_0 excited state efficiently, which could only occur if the antenna was directly coordinating to the Eu(III) centre, since the efficiency of the energy transfer is distance dependent.^{7,9} For these changes a quantum yield of luminescence, Φ_{Eu} , of 0.028 was determined by a method recently developed by Bünzli *et al.*¹⁵ As neither 2 nor 3 were found to modulate the emissions of 1·Eu, 1·Sm or 1·Tb, this strongly suggests that the structural as well as the physical nature (*e.g.* excited state energy, pK_a , *etc.*) of the β -diketonates is crucial to their ability to coordinate to these ions. The formation of the assembly should only be possible by the displacement of the two metal bound water molecules.⁶ Indeed $q \sim 0$ ($\tau_{\text{H}_2\text{O}} = 0.38$ ms and $\tau_{\text{D}_2\text{O}} = 0.42$ ms upon excitation of 4 at 336 nm) was observed for 1·Eu, in the presence of two *eq.* of 4. The structure of the self-assembly 1·Eu–4 can also be predicted by analysing the changes for the individual transitions in Fig. 1. Here, the hypersensitive $\Delta J = 2$, centred at 616 nm, gave rise to the largest changes in the Eu(III) emission. As $\Delta J = 2$ is sensitive to the change to the local coordination environment we can conclude that 4 is coordinating directly to the ion centre.

We next evaluated formation of the complex as a function of pH, by mixing together in a 1 : 1 stoichiometry 1·Eu and 4, and observing the changes in the Eu(III) emission as a function of pH. Here the emission was found to be highly pH sensitive by titrating an acid solution with base, Fig. 2, where maximum intensity was observed around pH 6.5. As before, the largest emission changes were observed for $\Delta J = 2$ transition. Moreover, the Eu(III) emission changes were also visible under a UV lamp as can be seen in Fig. 3. Here the red Eu(III) emission was only observed upon formation of the self-assembly (recorded at pH 7.5), while in either acid (pH < 4) or alkaline solutions (pH > 9.3), the assembly dissociated and the blue fluorescence emission of 4 was observed.

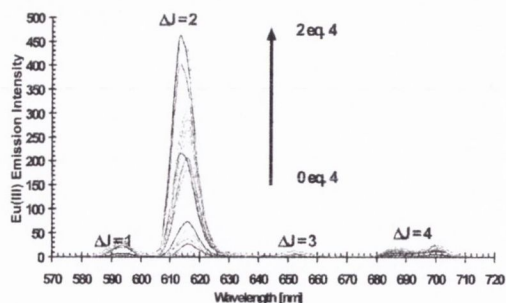


Fig. 1 The changes in the Eu(III) emission of 1·Eu upon titration with 4 at pH = 7.4 (0.1 M HEPES) and in the presence of 0.1 M TMACl.

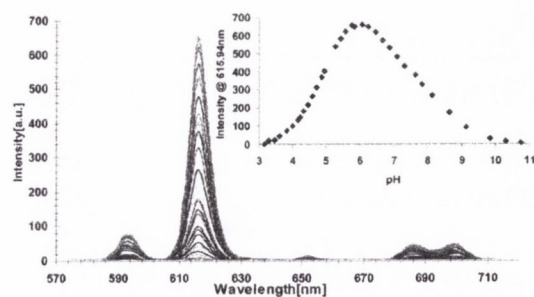


Fig. 2 The changes in the Eu(III) emission of 1·Eu upon titration with 4 as a function of pH, being switched ‘on–off’ upon basification. *Insert:* the changes in the 616 nm transition as a function of pH.

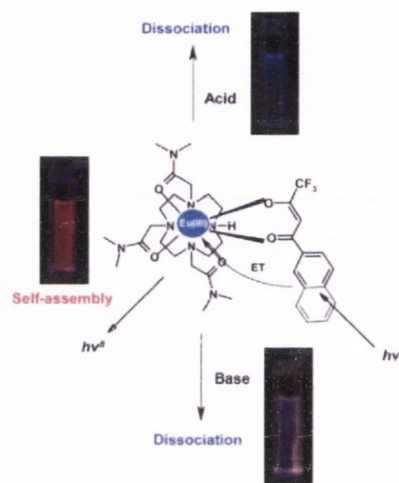


Fig. 3 Schematic representation of the luminescent Eu(III) ternary self-assembly 1·Eu–4 at pH 7.5 (red Eu(III) emission) and the dissociation of the assembly in acid at pH 2 and alkaline solution at pH = 12 (blue emission from the β -diketonate).

We also attempted to determine the hydration state of 1·Eu, in the presence of 4, at both pH 2 and pH 11. While this gave $q = 2.1$ in acid ($\tau_{\text{H}_2\text{O}} = 0.27$ ms and $\tau_{\text{D}_2\text{O}} = 0.59$ ms upon excitation at 395 nm), we were unable to determine q accurately in alkaline solution, possibly because of the deprotonation of the metal bound water molecules at this pH. Nevertheless, these results demonstrate that the formation of the self-assembly is pH driven.

We also observed the changes in the absorption and the fluorescence emission spectra of 4 as a function of pH. On both occasions significant changes were observed where the ground and the excited states were modulated between pH 4–8.† With the aim of gaining further insight into the nature of the Eu(III) complex pH dependence, we carried out potentiometric pH titrations on 1 and 1·Eu† using a glass electrode. From these titrations we can conclude that the complex is highly stable with respect to metal dissociation with stability constant $\log K$ of 17.17 (± 0.02). For 1, we were only able to determine two pK_a 's with the non-linear least squares regression programme HYPERQUAD, these being $pK_{a1} = 8.06$ (± 0.07), $pK_{a2} = 2.33$ (± 0.08).† For 1·Eu, there are three possible sites for protonation; two assigned to the metal bound water molecules [1·EuOH₂ and 1·Eu(OH)₂] and the third one to the pK_a of the secondary amine of the cyclen ring. The latter of these we were unable to determine, as it is expected to be highly

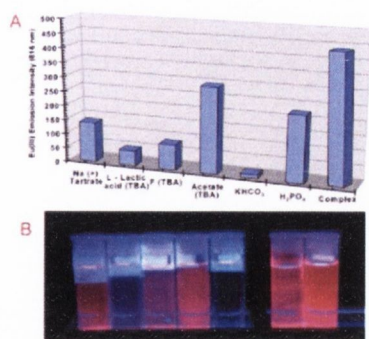


Fig. 4 (A) The changes in the recorded Eu(III) emission at 616 nm at pH 7.4. The tertiary complex is shown for comparison. (B) The changes observed under a UV-Vis lamp clearly showing naked eye intensity changes for the same anions in A. TBA = tetrabutylammonium salts.

acidic due to the presence of the Eu(III) ion. However, we were able to determine two pK_a values of $7.06 (\pm 0.08)$ and $6.53 (\pm 0.02)$, assigned to the deprotonation of the two metal bound water molecules. From the speciation diagram (see ESI†) it can be seen that when the Eu(III) emission is *ca.* 90% enhanced (Fig. 2), the pH is *ca.* 6 and that the most dominant species in solution is in fact the $1\text{-Eu}(\text{OH})_2$. Hence, the binding of **4** to $1\text{-Eu}(\text{OH})_2$ within the pH window of 4–7 is associated with the deprotonation of the α -proton in **4** (*c.f.* ESI for the spectro-photometric pH titration of **4**), and not the metal bound waters. In more alkaline solution the formation of 1-EuOH and $1\text{-Eu}(\text{OH})_2$ prevents the binding of the antenna due to electrostatic repulsion.

The self-assembly ternary complex 1-Eu-4 can also be considered as a potential luminescent sensor, as it should be possible to replace the coordinating antenna with other suitable coordinating ligands such as anions.^{6,8,16} This could possibly give rise to the formation of lanthanide based ‘displacement assays’, complimentary to those developed by Anslyn *et al.*,¹¹ where, the Eu(III) emission would be expected to be reduced upon displacement of **4**, as energy transfer from the antenna would be prevented. To evaluate this hypothesis, we carried out quantitative analysis by adding various anions (~ 1 mM) to a solution of the above ternary complex at pH 7.4 (emission *ca.* 50% ‘switched on’) in the presence of 0.1 M TMACl. Upon addition of anions such as Br^- , ClO_4^- , PF_6^- and NO_2^- to 1-Eu-4 no significant Eu(III) emission changes were observed, while for I^- and H_2PO_4^- the Eu(III) emission at 616 nm was reduced in intensity by 20–40%.† This indicates that some displacement of the antenna had occurred. In contrast to these results, the use of sodium tartarate, lactic acid, F^- , CH_3CO_2^- , KHCO_3 gave more pronounced luminescent changes as can be seen in Fig. 4A for the 616 nm transition. Moreover, these changes were also clearly distinguishable by the naked-eye under a UV lamp, Fig. 4B. We also carried out more detailed anion titrations on 1-Eu-4 using sodium tartarate, lactic acid and NaHCO_3 at pH 7.5, which showed that the Eu(III) emission was gradually reduced.† These results clearly demonstrate that such self-assembly ternary lanthanide complexes can be employed in the sensing of anions in a displacement type assay. To the best of our knowledge, such anion sensing has not been demonstrated before using lanthanide based luminescent ternary complexes.

In summary, we have demonstrated the successful formation of a luminescent Eu(III) ternary complex 1-Eu-4 in water, where the self-assembly is highly pH dependent, and that the resulting complex can be employed as a luminescent sensor for anions (at pH 7.4), where the β -diketonate antenna **4** is displaced with concomitant changes in the Eu(III) emission.

We thank Enterprise Ireland, IRCSET and TCD for financial support.

Notes and references

† Upon addition of excess of **4** to 1-Eu , the Eu(III) emission was significantly reduced. However, no such dissociation occurred when these titrations were carried out in MeOH.

- J. D. Badjic, V. Balzani, A. Credi, S. Silvi and J. F. Stoddart, *Science*, 2004, **303**, 1845; K. S. Chichak, K. S. S. J. Cantirill, A. R. Pease, S. H. Chiu, G. W. V. Cave, J. L. Atwood and J. F. Stoddart, *Science*, 2004, **304**, 1308; P. Thordarson, E. J. A. Bijsterveld, A. E. Rowan and R. J. M. Nolte, *Nature*, 2003, **424**, 915.
- E. R. Schofield, J. P. Collin, N. Gruber and J. P. Sauvage, *Chem. Commun.*, 2003, 188; S. Bonnet, J. P. Collin, J. P. Sauvage and E. R. Schofield, *Inorg. Chem.*, 2004, **43**, 8346.
- J. V. Hernandez, E. R. Kay and D. A. Leigh, *Science*, 2004, **306**, 1532; V. Bermudez, N. Capron, T. Gase, f. G. Gatti, F. Kajzar, D. A. Leigh, F. Zerbetto and S. W. Zhang, *Nature*, 2000, **406**, 608.
- K. S en shal-David, J. P. Leonard, S. E. Plush and T. Gunnlaugsson, *Org. Lett.*, 2006, **8**, 2727.
- T. Gunnlaugsson, J. P. Leonard, K. S en chal and A. J. Harte, *Chem. Commun.*, 2004, 782; T. Gunnlaugsson, J. P. Leonard, K. S en chal and A. J. Harte, *J. Am. Chem. Soc.*, 2003, **125**, 12062.
- T. Gunnlaugsson, A. Harte, J. P. Leonard and M. Nieuwenhuyzen, *Supramol. Chem.*, 2003, **15**, 505; T. Gunnlaugsson, A. Harte, J. P. Leonard and M. Nieuwenhuyzen, *Chem. Commun.*, 2002, 2134.
- T. Gunnlaugsson and J. P. Leonard, *Chem. Commun.*, 2005, 3114; J. P. Leonard and T. Gunnlaugsson, *J. Fluoresc.*, 2005, **15**, 585.
- S. J. A. Pope, B. P. Burton-Pye, R. Berridge, T. Khan, P. J. Skabara and S. Faulkner, *Dalton Trans.*, 2006, 2907; R. S. Dickins, T. Gunnlaugsson, D. Parker and R. D. Peacock, *Chem. Commun.*, 1998, 1643; C. Li and W.-T. Wong, *Chem. Commun.*, 2002, 2034.
- R. K. Mahajan, I. Kaur, R. Kaur, S. Uchida, A. Onimaru, S. Shinoda and H. Tsukube, *Chem. Commun.*, 2003, 2238; H. Tsukube and S. Shinoda, *Chem. Rev.*, 2002, **102**, 2389; H. Tsukube, S. Shinoda and H. Tamiaki, *Coord. Chem. Rev.*, 2002, **226**, 227; P. G. Sammes and G. Yahioğlu, *Nat. Prod. Rep.*, 1996, 1.
- S. Faulkner and B. P. Burton-Pye, *Chem. Commun.*, 2005, 259; M. P. Lowe and D. Parker, *Chem. Commun.*, 2000, 707.
- A. T. Wright and E. V. Anslyn, *Chem. Soc. Rev.*, 2006, **35**, 14; S. L. Wiskur, H. Ait-Haddou, J. J. Lavigne and E. V. Anslyn, *Acc. Chem. Res.*, 2001, **34**, 963.
- T. Gunnlaugsson, J. P. Leonard, S. Mulready and M. Nieuwenhuyzen, *Tetrahedron*, 2003, **59**, 3231.
- SAINT-NT and SHELXTL, Br uker AXS Madison, Wisconsin, 1998, G. M. Sheldrick, University of G ttingen, G ttingen, Germany, 1998; *Crystal data*: $\text{C}_{20}\text{H}_{42}\text{N}_7\text{O}_3\text{Cl}$, $M = 464.06$, monoclinic, $a = 15.1926(14)$, $b = 11.0971(10)$, $c = 15.5763(14)$  , $\beta = 111.215(2)^\circ$, $U = 2448.1(4)$  ³, $T = 123$ K, space group $P2_1/n$, $Z = 4$, $\mu(\text{Mo-K}\alpha) = 0.191$ mm⁻¹, 25078 reflections collected, 6074 unique, ($R_{\text{int}} = 0.0256$), $R = 0.0549$, $wR2 [I > 2\sigma(I)] = 0.1247$. CCDC 616591. Crystallographic data in CIF or other electronic format can be found at 10.1039/b611487c.
- A. Beeby, I. M. Clarkson, R. S. Dickins, S. Faulkner, D. Parker, L. Royle, A. S. de Sousa, J. A. G. Williams and M. Woods, *J. Chem. Soc., Perkin Trans. 2.*, 1999, 493.
- A. S. Chauvin, F. Gumy, D. Imbert and J. C. G. B unzli, *Spectrosc. Lett.*, 2004, **37**, 517.
- P. A. Gale, *Acc. Chem. Res.*, 2006, **39**, 465; P. A. Gale, *Chem. Commun.*, 2005, 3761; T. Gunnlaugsson, P. E. Kruger, P. Jensen, J. Tierney, H. D. P. Ali and G. M. Hussey, *J. Org. Chem.*, 2005, **70**, 10875; T. Gunnlaugsson, H. D. P. Ali, M. Glynn, P. E. Kruger, G. M. Hussey, F. M. Pfeffer, C. M. G. dos Santos and J. Tierney, *J. Fluoresc.*, 2005, **15**, 287.

Selective fluorescent sensing of chloride

Cidália M. G. dos Santos, Thomas McCabe and Thorfinnur Gunnlaugsson*

School of Chemistry, Centre for Synthesis and Chemical Biology, Trinity College Dublin, Dublin 2, Ireland

Received 20 February 2007; revised 27 February 2007; accepted 8 March 2007

Available online 13 March 2007

Abstract—The urea functionalised phenanthroline sensor **1**, which was characterised by several methods, including X-ray crystallography, gives rise to large changes in the fluorescence emission spectra upon interaction with several anions such as acetate, phosphate, fluoride and chloride in CH₃CN. However, only in the presence of Cl[−] was the emission enhanced, as for the other ions photoinduced electron transfer (PET) quenching was observed. Fitting these fluorescence changes, using non-linear regression analysis, showed that these anions bind to **1** in 1:1 (anion:sensor) stoichiometry, with the exception of Cl[−], which was shown to give rise to 1:1 as well as 1:2 binding, as a result of coordination of the chloride to two equivalents of **1**.

© 2007 Elsevier Ltd. All rights reserved.

The recognition and sensing of anions has become a very topical area of research in the field of supramolecular chemistry.^{1–3} Anions play a major function in the environment, industry and importantly, in biology where phosphate, carbonate and chloride are the most commonly found. In particular, Cl[−] which has relatively high extracellular concentrations, is essential to human health and is transported across cell membranes by various Cl[−] proteins, often in conjunction with cation transportation.⁴ Due to its spherical structure and relative large ionic radius, Cl[−] recognition is not trivial, and often requires the use of structurally complex hosts, such as those developed by Davis⁵ and Smith.⁶ Nature often transports Cl[−] in the form of ion pairs and non-peptide based natural transporters are known such as the prodigiosins, which can transport HCl.⁷ A few examples of such transport mimics have recently been published by Sessler et al. and by Gale and co-workers respectively.^{8,9} These examples demonstrate the feasibility of the use of small and hence, structurally simple molecules for such recognition. We are interested in the recognition and sensing of anions^{3,10} using either lanthanide based coordination complexes,¹¹ or charge neutral receptors such as ureas,¹² thioureas¹³ and amidoureas.¹⁴ For these latter examples, the detection of ions such as AcO[−], H₂PO₄[−], pyrophosphate and F[−] has been demonstrated selectively over many other anions such as Cl[−], Br[−] and I[−]. However, in recent work, where we focused our efforts on the development of heteroditopic receptors,

we synthesised the 1,10-phenanthroline (*phen*) based urea ligand **1** (of which the X-ray crystal structure is shown in Fig. 1),¹⁵ and investigated the effect that anion coordination had on the photophysical properties of the *phen* structure. Interestingly, we discovered that while **1** could strongly bind to a series of anions in CH₃CN solution, the sensing of Cl[−] by **1** was particularly interesting being both strong and achieved by the formation of a 2:1 self-assembly complex between **1** and Cl[−]. This is, to the best of our knowledge, the first example of a simple charge neutral fluorescent sensor which demonstrates both strong and good selectivity for Cl[−].¹⁶

The synthesis of **1** was achieved in a few high yielding steps as shown in Scheme 1. The first step involved reduction of commercially available 5-nitro-1,10-phenanthroline, **2**, in refluxing ethanol solution, under argon, using hydrazine monohydrate (N₂H₄) and 10% Pd/C catalyst. A yellow solid was obtained after filtration and removal of the solvent under reduced pressure. This solid was washed twice with diethyl ether to produce **3** as a pale yellow solid in 92% yield. This was then

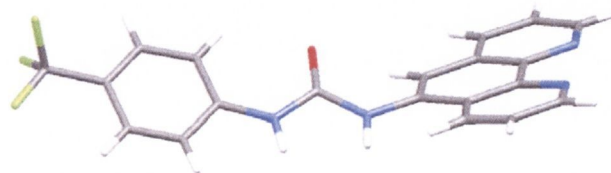
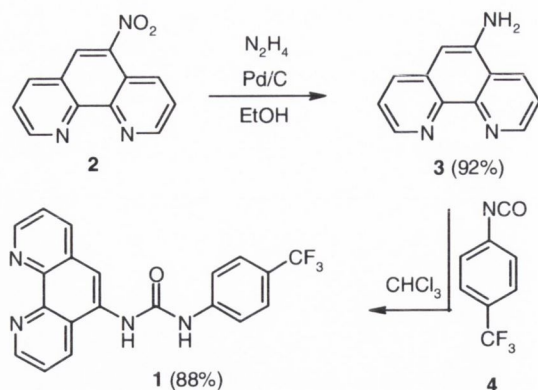


Figure 1. The X-ray crystal structure of **1**.

* Corresponding author. Tel.: +353 1 896 3459; fax: +353 1 671 2826; e-mail: gunnlaut@tcd.ie



Scheme 1. The synthesis of **1**.

reacted with trifluoro-*p*-tolyl isocyanate, **4**, in $CHCl_3$ at room temperature, under an inert atmosphere to yield an off white precipitate, which was filtered and washed with cold $CHCl_3$. This gave an off-white solid which was recrystallised from hot MeOH to yield the desired receptor **1** as a crystalline solid in 88% yield.¹⁷ The 1H NMR spectrum (400 MHz, $DMSO-d_6$) showed the presence of the two urea N–H singlets at 9.55 and 9.12 ppm, respectively, as well as the expected set of doublets for the phenyl aromatic protons. The ^{13}C NMR (100 MHz, $DMSO-d_6$) of **1** showed all the expected 18 signals, with the urea carbonyl quaternary resonance appearing at 152.87 ppm.

The X-ray crystal structure of **1** is presented in Figure 1, and shows that the urea moiety is coplanar with the trifluoro-*p*-tolyl group (torsion angle of -0.26°), while being significantly shifted out of the plane of the *phen* moiety (torsion angle of -35°).¹⁵ The two urea N \cdots H bond lengths were found to be identical at 0.860 Å. As is clear from the crystal structure, the two urea protons are ideally situated for directional hydrogen bonding interactions with anions that can participate in linear interactions such as AcO^- , $H_2PO_4^-$ and F^- . We were unable to produce suitable crystals of **1** in the presence of anions for X-ray crystal structure analysis.

The ability of **1** to sense various anions was evaluated in CH_3CN using the anions as their tetrabutylammonium salts (TBA^+). The absorption spectrum of **1**, in the absence of anions, exhibited a band centred at 266 nm ($\log \epsilon = 4.50$), assigned to the $\pi-\pi^*$ transition of the *phen* moiety and a broad shoulder centred at around 320 nm ($\log \epsilon = 3.85$), which was assigned to the $n-\pi^*$ transitions. When exciting the sample at both of these wavelengths, a broad emission band was observed with λ_{max} at 422 nm. Thus both absorptions were assigned to the *phen* chromophore. Significant changes were observed in the absorption spectra upon titration of **1** with anions such as AcO^- and $H_2PO_4^-$ and interestingly, also for Cl^- .¹⁸ These responses, clearly signify changes in the ground state of the sensor upon hydrogen bonding to these anions as demonstrated for Cl^- in Figure 2. The sensing of Cl^- is unusual as it is typically not observed for such simple urea or amidourea based recep-

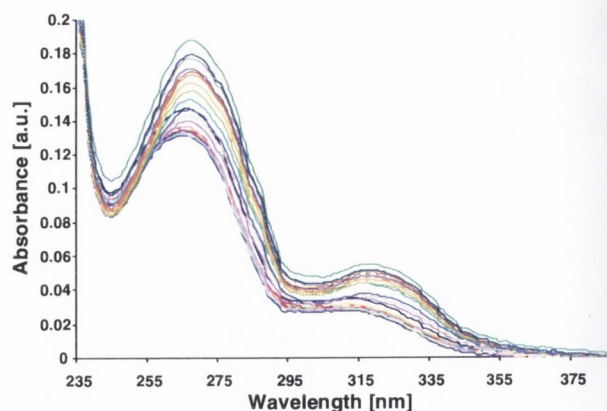


Figure 2. The changes in the absorption spectra of **1** (4.8 μM) upon gradual addition of Cl^- (0–17.50 mM) in MeCN.

tors. As seen in Figure 2, an increase was observed in both the 266 nm and 320 nm transitions upon increasing the concentration of Cl^- , but no other spectral shifts, or the formation of isosbestic points, were observed. For both AcO^- and $H_2PO_4^-$ similar changes were observed, where the absorption was enhanced by ca. 20–30%. However, more structural changes were observed in the absorption spectra in the case of F^- , where the 266 nm band was shifted to 270 nm, while the 320 nm band was shifted to 325 nm, with the formation of concomitant isosbestic points. These changes demonstrate the ability of F^- to (i) bind to the urea moiety, and (ii) potentially deprotonate the urea moiety.¹⁹ In contrast to these results, minor changes were observed for Br^- at very high anion concentrations.

The fluorescence emission spectra were also monitored upon addition of anions following excitation at both the 265 nm and 320 nm transitions. Upon addition of AcO^- , $H_2PO_4^-$ and F^- , the fluorescence emission was considerably quenched (98%, 94%, and 93%, respectively), or 'switched off', as shown in Figure 3 for the changes observed with AcO^- . This clearly demonstrates the ability of **1** to function as a luminescent 'on-off' switch for these anions. It is worth pointing out that no other spectral changes occurred in the fluorescence

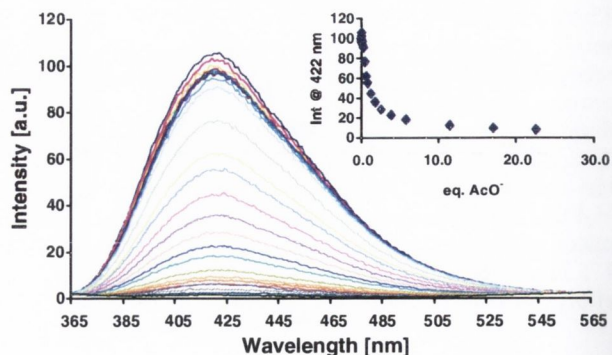


Figure 3. The changes in emission intensity of **1** (4.8 μM) upon gradual addition of AcO^- ($[AcO^-] = 0-1.53$ mM), in MeCN upon excitation at 265 nm. Inset: The changes in the emission intensity at 422 nm as a function of AcO^- equivalents.

emission spectra, that is, no shifts in λ_{\max} or the formation of long wavelength emitting species were observed. Hence, we propose that upon anion recognition, the urea moiety is twisted out of the plane of the *phen* fluorophore which gives rise to the slight enhancement in the $\pi \rightarrow \pi$ nature of the fluorophore (as seen in the absorption spectra). At the same time, electron transfer quenching of the *phen* excited state, from the electron rich anion receptor, is activated, causing the emission to 'switch off'. Hence, this can be considered as being an anion modulated photoinduced electron transfer (PET) quenching, even though no formal covalent spacer separates the fluorophore from the urea receptor.^{12,20} From these changes, binding constants of $\log \beta_{11} = 5.19 (\pm 0.03)$ and $\log \beta_{11} = 4.35 (\pm 0.06)$ were observed for $\text{AcO}^- \cdot \mathbf{1}$ and $\text{H}_2\text{PO}_4^- \cdot \mathbf{1}$, respectively, using the nonlinear least-squares fitting programme SPEC-FIT. These values indicate strong binding of $\mathbf{1}$ for these anions in CH_3CN . The fact that AcO^- is bound more strongly than H_2PO_4^- reflects the ability of this anion to bind to the receptor in a more linear 'Y' shape hydrogen bonding manner. Hence, on all occasions the best fit for the above changes was observed for the 1:1 binding stoichiometry. The changes in the emission intensity of $\mathbf{1}$ upon titration with F^- were, however, best fitted to 2:1 binding (anion:sensor) interactions. This is in agreement with the findings from the absorption data, where a two-step equilibrium was observed. These can be viewed as involving the initial interaction of the anion with $\mathbf{1}$ through hydrogen bonding to give the $\text{F}^- \cdot \mathbf{1}$ complex, followed by binding and subsequent deprotonation by the second F^- to give bifluoride HF_2^- , in a manner previously postulated by ourselves and Gale et al.^{19,21} From these changes $\log \beta_{11} = 4.75 (\pm 0.26)$ and $\log \beta_{21} = 4.73 (\pm 0.21)$ values were determined for $\text{F}^- \cdot \mathbf{1}$ and $\text{F}_2^- \cdot \mathbf{1}$ (the formation of HF_2^-), respectively. As in the ground state investigation above, titrations using Br^- did not give rise to any significant luminescent quenching except at high concentrations, which could be due to a heavy atom effect rather than binding of this anion to the receptor.

However, the most interesting results were observed for the fluorescence titration of $\mathbf{1}$ with Cl^- , Figure 4. Here

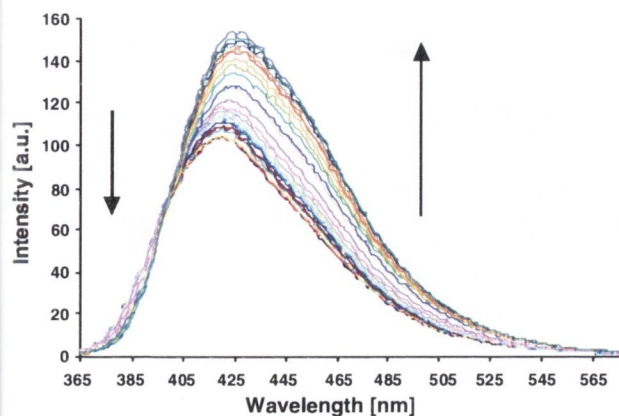


Figure 4. Changes in the emission spectra of $\mathbf{1}$ ($4.8 \mu\text{M}$) upon titration with Cl^- (0 – 17.50 mM) in MeCN , upon excitation at 265 nm .

the quenching of the singlet excited state was not observed as in the above cases, but a fluorescence enhancement. Here, the *phen* emission was enhanced by ca. 45%, with a concomitant shift towards longer wavelengths ($\lambda_{\max} 422 \text{ nm} \rightarrow 428 \text{ nm}$), with the formation of an iso-emissive point at 399 nm . This is the first time that we have observed such luminescent behaviour for such structurally simple receptors. Furthermore, it is clear that these changes are of a different nature to those observed for the AcO^- or H_2PO_4^- titrations above, and thus cannot be assigned to an enhancement in PET quenching. We therefore propose that upon recognition of Cl^- , the aforementioned anion induced twisting of the urea moiety (from the *phen* ligand) is minor and the spherical anion reduces the effect of the PET quenching from the trifluoro-*p*-tolyl group to the *phen* fluorophore, by 'blocking' the pathway of the electron transfer. Such 'intervening media' has been proposed to influence energy transfer quenching in several electron-donor-acceptor systems, such as in those developed by Shimidzu et al.²² where a cation was employed, and in supramolecular systems designed to mimic the nature of the electron transfer in the photosynthetic reaction centre.²³

Plotting the changes at 422 nm as a function of $-\log[\text{Cl}^-]$ gave rise to changes occurring over ca. 4 logarithmic units, indicating more than a simple 1:1 binding process. By fitting the changes observed in Figure 4 for 1:1 type complex formation, $\text{Cl}^- \cdot \mathbf{1}$, a binding constant of $\log \beta_{11} = 3.84 (\pm 0.14)$ was determined. While this shows that $\mathbf{1}$ has high affinity for Cl^- , we and others, have demonstrated that usually such simple urea based receptors do not bind to large spherical anions³ but rather through multiple binding interactions.^{4,24} Consequently, we considered an alternative binding mode for $\mathbf{1}$, where two sensors self-assemble around the anion to give a $\text{Cl}^- \cdot \mathbf{1}_2$ complex. Fitting the above changes to such stoichiometry, gave a strong binding constant of $\log \beta_{12} = 5.94 (\pm 0.16)$. Analysis of the speciation distribution diagram, shown in Figure 5, clearly shows that the initial addition of Cl^- gives rise to the formation of a self-assembly (blue line) of two molecules of $\mathbf{1}$ and Cl^- , and that up to 27% of the species in solution

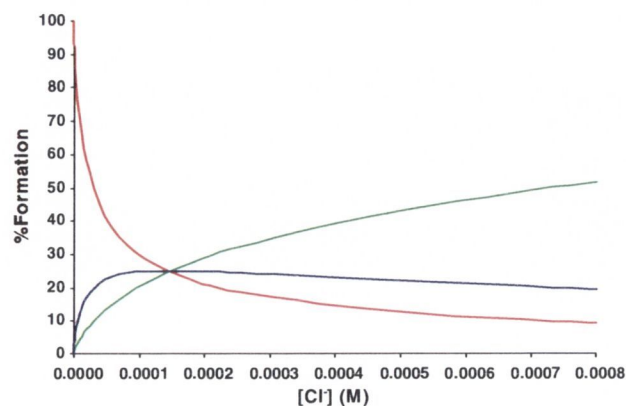


Figure 5. The speciation distribution plot for the binding of $\mathbf{1}$ ($4.8 \mu\text{M}$) to Cl^- : — = $\mathbf{1}$; — = $\text{Cl}^- \cdot \mathbf{1}$; — = $\text{Cl}^- \cdot \mathbf{1}_2$. Only part of the concentration range is shown.

from $[Cl^-] = 0 \rightarrow 0.8$ mM is in the form of the $Cl^- \cdot 1_2$ complex. However, the formation of the 1:1 complex begins to dominate after 0.2 mM (green line), eventually being the most stable species in solution.^{25,26} With the aim of demonstrating the selectivity of **1** for Cl^- , the luminescence of **1** was recorded in the presence of one equivalent of AcO^- , which quenched the fluorescence. However, upon addition of increased concentrations of Cl^- , the emission was restored, giving rise to a red shifted emission, as observed in Figure 4. These results demonstrate that Cl^- can be sensed selectively by **1**, through (a) the formation of a self-assembly, and (b) by the fact that only for Cl^- was the fluorescence of **1** increased, while being quenched by other competitive ions such as AcO^- , $H_2PO_4^-$ and F^- .

In summary, we have developed **1** as a selective fluorescence sensor for Cl^- . While only minor changes were observed in the absorption spectra of **1** upon anion recognition, the fluorescence emission spectra were dramatically affected. Nevertheless, only for the sensing of Cl^- was the fluorescence of **1** enhanced. For other competitive ions the emission was either quenched or not modulated. We are currently evaluating the anion binding of **1** in the presence of both transition and lanthanide ions.

Acknowledgements

We would like to thank TCD and IRCSET for financial support, Dr. John E. O'Brien for assisting with NMR and Dr. Sally E. Plush and Dr. Susan Quinn for their help. We particularly would like to thank Dr. Joseph P. Leonard for his assistance at the start of this investigation.

References and notes

- Sessler, J. L.; Gale, P. A.; Cho, W. S., *Anion Receptor Chemistry*; Royal Society of Chemistry: Cambridge, UK, 2006; Steed, J. W. *Chem. Commun.* **2006**, 2637; Gale, P. A. *Acc. Chem. Res.* **2006**, *39*, 465; Martínez-Máñez, R.; Sancenón, F. *Chem. Rev.* **2003**, *103*, 4419; Suksai, C.; Tuntulani, T. *Chem. Soc. Rev.* **2003**, *32*, 192.
- Wu, F. Y.; Li, Z.; Guo, L.; Wang, X.; Lin, M. H.; Zhao, Y. F.; Jiang, Y. B. *Org. Biomol. Chem.* **2006**, *4*, 624; Ghosh, K.; Adhikari, S. *Tetrahedron Lett.* **2006**, *47*, 8165; Evans, L. S.; Gale, P. A.; Light, M. E.; Quesada, R. *Chem. Commun.* **2006**, 965; Pfeffer, F. M.; Seter, M.; Lewcenko, N.; Barnett, N. W. *Tetrahedron Lett.* **2006**, *47*, 5251; Jun, E. J.; Swamy, K. M. K.; Bang, H.; Kim, S. J.; Yoon, J. Y. *Tetrahedron Lett.* **2006**, *47*, 3103; Liu, B.; Tian, H. *Chem. Lett.* **2005**, *34*, 686; Wel, L. H.; He, Y. B.; Wu, J. L.; Wu, X. J.; Meng, L.; Yang, X. *Supramol. Chem.* **2004**, *16*, 561.
- Gunnlaugsson, T.; Glynn, M.; Tocci (née Hussey), G. M.; Kruger, P. E.; Pfeffer, F. M. *Coord. Chem. Rev.* **2006**, *250*, 3094.
- Davis, A. P.; Sheppard, D. N.; Smith, B. D. *Chem. Soc. Rev.* **2007**, *36*, 348.
- Davis, A. P.; Joos, J. B. *Coord. Chem. Rev.* **2003**, *240*, 143; Boon, J. M.; Smith, B. D. *Curr. Opin. Chem. Biol.* **2002**, *6*, 749.
- McNally, B. A.; Koulov, A. V.; Smith, B. D.; Joos, J.-B.; Davis, A. P. *Chem. Commun.* **2005**, 1087.
- Ohkuma, S.; Sato, T.; Okamoto, M.; Matsuya, H.; Arai, K.; Kataoka, T.; Nagai, K.; Wasserman, H. H. *Biochemistry* **1998**, *334*, 731.
- Sessler, J. L.; Elleer, L. R.; Cho, W. S.; Nicolaou, S.; Aguilar, A.; Lee, J. T.; Lynch, V. M.; Magda, D. J. *Angew. Chem., Int. Ed.* **2005**, *44*, 5989.
- Gale, P. A.; Light, M. E.; McNally, B.; Navakhun, K.; Sliwinski, K. E.; Smith, B. D. *Chem. Commun.* **2005**, 3773.
- Gunnlaugsson, T.; Ali, H. D. P.; Glynn, M.; Kruger, P. E.; Hussey, G. M.; Pfeffer, F. M.; dos Santos, C. M. G.; Tierney, J. J. *Fluoresc.* **2005**, *15*, 287.
- Leonard, J. P.; dos Santos, C. M. G.; Plush, S. P.; McCabe, T.; Gunnlaugsson, T. *Chem. Commun.* **2007**, 129; Harte, A. J.; Jensen, P.; Plush, S. E.; Kruger, P. E.; Gunnlaugsson, T. *Inorg. Chem.* **2006**, *45*, 9465; Gunnlaugsson, T.; Leonard, J. P. *Chem. Commun.* **2005**, 3114; Gunnlaugsson, T.; Leonard, J. P. *J. Fluoresc.* **2005**, *15*, 585; Harte, A. J.; Leonard, J. P.; Nieuwenhuyzen, M. *Supramol. Chem.* **2003**, *15*, 505; Gunnlaugsson, T.; Harte, A. J.; Leonard, J. P.; Nieuwenhuyzen, M. *Chem. Commun.* **2002**, 2134.
- Pfeffer, F. M.; Buschgens, A. M.; Barnett, N. W.; Gunnlaugsson, T.; Kruger, P. E. *Tetrahedron Lett.* **2005**, *46*, 6579; Gunnlaugsson, T.; Davis, A. P.; O'Brien, J. E.; Glynn, M. *Org. Biomol. Chem.* **2005**, *3*, 48; Pfeffer, F. M.; Gunnlaugsson, T.; Jensen, P.; Kruger, P. E. *Org. Lett.* **2005**, *7*, 5375; Gunnlaugsson, T.; Davis, A. P.; O'Brien, J. E.; Glynn, M. *Org. Lett.* **2002**, *4*, 2449; Gunnlaugsson, T.; Davis, A. P.; Hussey, G. M.; Tierney, J.; Glynn, M. *Org. Biomol. Chem.* **2004**, *2*, 1856; Gunnlaugsson, T.; Davis, A. P.; Glynn, M. *Chem. Commun.* **2001**, 2556.
- dos Santos, C. M. G.; Glynn, M.; McCabe, T.; Seixas de Melo, J. S. Burrows, H. D.; Gunnlaugsson, T. *Supramol. Chem.*, **2007**, *19*, in press.
- Quinlan, E.; Matthews, S. E.; Gunnlaugsson, T. *Tetrahedron Lett.* **2006**, *47*, 9333; Gunnlaugsson, T.; Kruger, P. E.; Jensen, P.; Tierney, J.; Ali, H. D. P.; Hussey, G. M. *J. Org. Chem.* **2005**, *70*, 10875.
- The data were collected on a Bruker Smart Apex Diffractometer*. The crystal was mounted on a 0.35 mm quartz fibre and immediately placed on the goniometer head in a 150 K N₂ gas stream. The data were acquired using Smart Version 5.625 software in multi-run mode and 2400 frames in total, at 0.3° per frame, were collected. Data integration and reduction was carried out using Bruker SAINT+ Version 6.45 software and corrected for absorption and polarization effects using SADABS Version 2.10 software. Space group determination, structure solution and refinement were obtained using Bruker Shelxtl Ver. 6.14 software. *SMART Software Reference Manual, version 5.625, Bruker Analytical X-ray Systems Inc., Madison, WI, 2001. Sheldrick, G. M. SHELXTL, An Integrated System for Data Collection, Processing, Structure Solution and Refinement, Bruker Analytical X-ray Systems Inc., Madison, WI, 2001. *Crystal data*: C₈₀H₅₂F₁₂N₁₆O₄, Monoclinic, space group P2₁/c, $a = 13.1965(14)$, $b = 11.8685(12)$, $c = 11.0189(11)$ Å, $\beta = 91.320(2)^\circ$, $U = 1725.4(3)$ Å³, $T = 150$ K, μ (Mo-K α) = 0.117 mm⁻¹, $Z = 4$, a total of 13251 reflections were measured for $4 < 2\theta < 57$ and 3031 unique reflections were used in the refinement, $[R(\text{int}) = 0.0288]$, the final parameters were $wR2 = 0.1693$ and $R1 = 0.0648$ [$I > 2\sigma(I)$]. CCDC 637076.
- We have previously demonstrated the sensing of such halides using heavy atom affect quenching: Gunnlaugsson, T.; Bichell, B.; Nolan, C. *Tetrahedron* **2004**, *60*, 5799; Chloride has also been elegantly detected by NMR using catechols: Smith, D. K. *Org. Biomol. Chem.* **2003**, *1*, 3874; and recently by using acridone fluorescence sensing:

- Blázquez, M. T.; Muñoz, F. M.; Sáez, S.; Simón, L. M.; Alonso, A.; Raposo, C.; Lithgow, A.; Alcázar, V.; Morán, J. R. *Heterocycles* **2006**, *69*, 73.
17. Sensor **1** was obtained as an off-white solid in 88% yield (1.38 g). Mp decomposes above 290 °C; Calculated for $C_{20}H_{14}N_4OF_3$ $[M+H]^+$ $m/z = 383.1120$. Found $m/z = 383.1107$. 1H NMR (400 MHz, DMSO- d_6) δ_H : 9.55 (br s, 1H, NH), 9.16 (d, 1H, PhenCH, $J = 4$ Hz), 9.12 (br s, 1H, NH), 9.00 (d, 1H, PhenCH, $J = 4.04$ Hz), 8.65 (d, 1H, PhenCH, $J = 8.52$ Hz), 8.43 (d, 1H, PhenCH, $J = 8.04$ Hz), 8.39 (s, 1H, PhenCH), 7.89 (dd, 1H, PhenCH, $J = 8.52$ Hz), 7.72 (m, 5H, PhenCH + ArCH); ^{13}C NMR (100 MHz, DMSO- d_6) δ_C : 152.87, 149.87, 148.74, 145.89, 143.34, 143.13, 135.61, 132.08, 130.44, 128.50, 126.25, 126.22, 123.77, 123.68, 122.95, 122.21, 118.01, 116.07; ^{19}F NMR (376 MHz, DMSO- d_6): -60.58 (CF₃).
18. Chloride has recently been used as a template for the formation of anion pseudocryptands and directed self-assemblies: Nabeshima, T.; Masubuchi, S.; Taguchi, N.; Akina, S.; Saiki, T.; Sato, S. *Tetrahedron Lett.* **2007**, *48*, 1595; Goetz, S.; Kruger, P. E. *Dalton Trans.* **2006**, 1277; Beer, P. D.; Sambrook, M. R.; Curiel, D. *Chem. Commun.* **2006**, 2105; Keegan, J.; Kruger, P. E.; Nieuwenhuyzen, M.; O'Brien, J.; Martin, N. *Chem. Commun.* **2001**, 2192.
19. Gunnlaugsson, T.; Kruger, P. E.; Lee, T. C.; Parkesh, R.; Pfeffer, F. M.; Hussey, G. M. *Tetrahedron Lett.* **2003**, *44*, 6575; Gunnlaugsson, T.; Kruger, P. E.; Jensen, P.; Pfeffer, F. M.; Hussey, G. M. *Tetrahedron Lett.* **2003**, *44*, 8909.
20. It is possible that the anion sensing also contributes to the formation of a twisted internal charge transfer (TICT) excited state in **1**. de Silva, A. P.; Gunaratne, H. Q. N.; Gunnlaugsson, T. *Tetrahedron Lett.* **1998**, *39*, 5077; Letard, J.-F.; Lapouyade, R.; Retting, W. *Pure Appl. Chem.* **1993**, *65*, 1705.
21. Evans, L. S.; Gale, P. A.; Light, M. E.; Quesada, R. *New J. Chem.* **2006**, *30*, 1019; Camiolo, S.; Gale, P.; Hursthouse, M. B.; Light, M. E. *Org. Biomol. Chem.* **2003**, *1*, 741.
22. Iyoda, T.; Morimoto, M.; Kawasaki, N.; Shimidzu, T. *J. Chem. Soc., Chem. Commun.* **1991**, 1480.
23. de Silva, A. P.; Rice, T. E. *Chem. Commun.* **1999**, 163; Harriman, A.; Heitz, V.; Sauvage, S.-P. *J. Phys. Chem.* **1993**, *97*, 5940.
24. Davis, A. P. *Coord. Chem. Rev.* **2006**, *250*, 2939; Schatzmann, B.; Alhashimy, N.; Diamond, D. *J. Am. Chem. Soc.* **2006**, *128*, 8606; Bai, Y.; Zhang, B.-G.; Xu, J.; Duan, C.-Y.; Dang, D.-B.; Liu, D.-L.; Meng, Q.-J. *New J. Chem.* **2005**, *29*, 777.
25. Without X-ray crystallographic data for the $Cl^- \cdot 1_2$ complex it is difficult to predict its structure. However, we propose that the two sensors hydrogen bond to the anion in a head-to-tail fashion, where the two *phen* moieties would be facing away from each other. See also Ref. 26.
26. During the course of our work, a ditopic receptor was found to bind Cl^- upon addition of Cu(I) in a semi-helical fashion: Amendola, V.; Boiocchi, M.; Colasson, B.; Fabbrizzi, L. *Inorg. Chem.* **2006**, *45*, 6138.

Lanthanide luminescent anion sensing: evidence of multiple anion recognition through hydrogen bonding and metal ion coordination†

Cidália M. G. dos Santos, Pablo Barrio Fernández, Sally E. Plush, Joseph P. Leonard and Thorfinnur Gunnlaugsson*

Received (in Austin, TX, USA) 12th April 2007, Accepted 18th May 2007

First published as an Advance Article on the web 15th June 2007

DOI: 10.1039/b705560a

The delayed lanthanide luminescence of the terbium [Tb(III)] diaryl-urea complex **1**·Tb is significantly enhanced upon sensing of dihydrogenphosphate (H_2PO_4^-) in CH_3CN , which occurs through multiple anion binding through hydrogen bonding interactions and potential metal ion coordination to Tb(III).

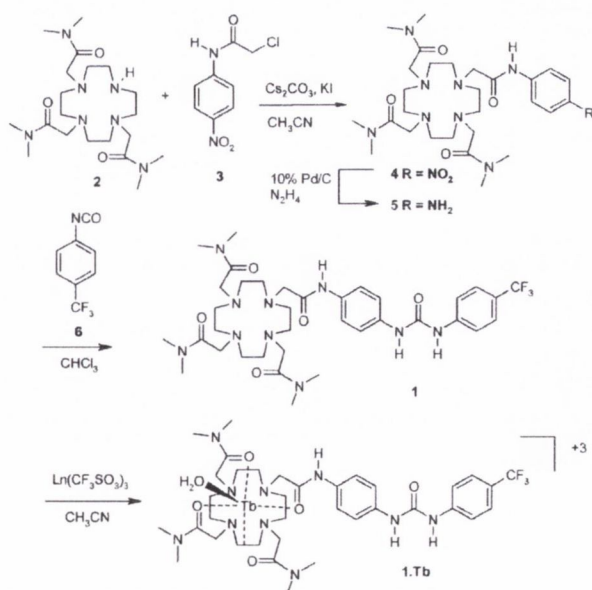
The luminescent and colorimetric sensing of anions is both a challenging and highly topical area of research.^{1–3} The most common methods for achieving such anion recognition has been *via* the use of: (i) transition metal ion coordination complexes;⁴ (ii) ammonium or guanidinium moieties,⁵ and (iii) charge neutral hydrogen bonding moieties, such as amides, ureas, thiourea, *etc.*⁶ Using heptadentate tri-arm cyclen (1,4,7,10-tetraazacyclododecane) Tb(III) and Eu(III) complexes, we and others have recently demonstrated the sensing of both aliphatic and aromatic carboxylates, *via* the formation of ternary complexes in buffered solution, where the emission was either enhanced or reduced upon coordination of these anions to the f-metal ions.^{7,8} Similarly, using chromophores, based on charge neutral receptors, we have developed numerous examples of both fluorescent and colorimetric anion sensors, which can function in both organic and aqueous solutions.^{9,10} Nevertheless, the combination of these two anion binding interactions in a single molecule, with the aim of achieving maximum luminescent ‘output’ coupled with high anion affinity, has not been demonstrated to date using members of the f-metal ion family. However, such sensing has recently been shown to work well using d-metal ions.¹¹ With the objective of demonstrating such dual sensing interactions using f-metal ions, we synthesised the Tb(III) complex **1**·Tb from **1**. Herein, we demonstrate the results from this investigation and prove that this design gives rise to: (a) high anion binding affinity, (b) multiple binding interactions and (c) large Tb-luminescence enhancements.

The Tb(III) $^5\text{D}_4$ transition is Laporte-forbidden and direct excitation of Tb(III) is often difficult.¹² Nevertheless, excitation *via* the use of ligand or antennae, gives rise to sensitised emission.^{12–14} In **1**, the aryl-urea has a dual role, it can function as both the sensitizing antenna¹² and the hydrogen bonding anion receptor.² Therefore, we anticipated that anion binding at the urea moiety would modulate the sensitization process to the lanthanide excited state, and hence, the Tb(III) emission.

The synthesis of **1** (Scheme 1), involved the coupling of the tri-arm acetamide cyclen **2**¹⁵ and chloro-*N*-(nitro-phenyl) acetamide,

3,¹⁶ in dry CH_3CN in the presence of Cs_2CO_3 and KI at 85 °C for 72 h. This gave **4**, which was purified by column chromatography on alumina. This was followed by the reduction of the nitro group, using N_2H_4 in ethanol at 90 °C, in the presence of 10% Pd/C catalyst, to yield **5**, which was reacted with trifluoro-*p*-tolyl isocyanide, **6**, in dry CHCl_3 at room temperature, giving **1** in 80% yield. The $^1\text{H-NMR}$ (CDCl_3) spectrum of **1**† showed the presence of three characteristic N–H resonances at 9.61, 9.38 and 9.01 ppm. The complex, **1**·Tb, was finally formed in 51% yield by refluxing **1** with one equivalent of $\text{Tb}(\text{CF}_3\text{SO}_3)_3$ in CH_3CN under argon, followed by precipitation from diethyl ether. The ESMS of **1**·Tb showed the expected isotopic distribution pattern and the ^1H NMR (CD_3OD) spectrum showed the shifted resonance for the equatorial and the axial protons of the cyclen and the $\alpha\text{-CH}_2$ due to the presence of the paramagnetic metal ion. Analysis of the excited state lifetimes of the Tb(III) emission in D_2O and H_2O , respectively, gave the hydration state^{12,13} ~ 1 , indicating a single metal bound water molecule.

The absorption spectra of **1**·Tb showed a broad band centred around 280 nm in CH_3CN , assigned to the urea antenna moiety. The changes in the spectra were monitored as a function of added anions such as AcO^- , H_2PO_4^- , F^- and Cl^- (as their TBA salt solutions). The addition of ions such as AcO^- and H_2PO_4^- caused the absorption maximum to shift towards the red, with concomitant $\sim 20\%$ reduction in the absorption, showing the



Scheme 1 Synthesis of **1** and the Tb(III) sensors **1**·Tb.

School of Chemistry, Centre for Synthesis and Chemical Biology, Trinity College Dublin, Dublin 2, Ireland. E-mail: gunnlaui@tcd.ie; Fax: +353 1 671 2826; Tel: +353 1 896 3459

† Electronic supplementary information (ESI) available: Synthesis and figures 1–14. See DOI: 10.1039/b705560a

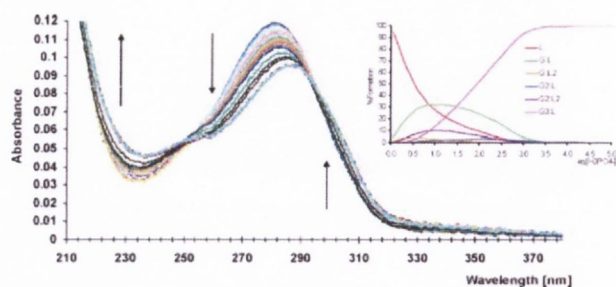


Fig. 1 The changes observed in the absorption spectra of **I**·Tb (4 μ M) upon addition of H_2PO_4^- (0–57.3 μ M) in MeCN. Arrows indicate the changes upon increasing concentration of H_2PO_4^- . Inset: The speciation distribution diagram for the binding of H_2PO_4^- .

binding of the anions to the receptor, as demonstrated for H_2PO_4^- in Fig. 1. The titration profile obtained from plotting the absorption changes in Fig. 1, suggested that the anion binding was more complex than a simple 1 : 1 stoichiometry (see ESI†). Fitting these changes, using the nonlinear least squares regression program SPECFIT (see ESI†), gave several binding constants, reflecting that the anions were bound through the proposed ‘multiple’ binding interactions. These results are summarised in Table 1, for H_2PO_4^- and AcO^- . Here, the stoichiometry (shown as the guest : **I**·Tb ratio $G_n : L_n$) and binding values ($\log K$) clearly shows that **I**·Tb initially binds both of these anions with large 1 : 1 binding affinity, where H_2PO_4^- is bound marginally stronger than AcO^- . We assign such a strong anion binding affinity to the neighbouring lanthanide ion, which, being a strong Lewis acid makes the urea protons stronger hydrogen bonding donors.

From these changes, the speciation distribution diagram was also determined (shown as insert for H_2PO_4^- in Fig. 1), which demonstrated that initially the 1 : 1 binding event (shown as a green line) dominates, but is then replaced at higher anion concentrations with higher order stoichiometries such as $G_3 : L_1$. Similarly, for AcO^- , both the $G_1 : L_1$ and $G_2 : L_1$ binding stoichiometries were observed. The binding of Cl^- was also observed in the absorption spectra. However, in comparison to the results in Table 1, it was weak and spectral changes only occurred at high anion concentrations. The titration of F^- gave rise to significant changes in the absorption spectra assigned to multiple F^- binding interactions as well as the deprotonation of the urea moiety by F^- , to give HF_2^- .¹⁷ However, the binding constants for F^- were significantly lower than those observed for H_2PO_4^- and AcO^- in Table 1 (see ESI†).

With the aim of further investigating these multiple binding interactions, both the fluorescence and the Tb(III) emission were monitored upon anion titration. For the former, the emission from the antenna ($\lambda_{\text{ex}} = 280$ nm) gave rise to a broad band centred at 340 nm (see ESI†), that was both weak and significantly polluted by the contribution from the Tb(III) emission, which occurs at longer wavelength. However, upon titration with either H_2PO_4^- or AcO^- the emission was significantly modulated. Even though, the spectra were of poor quality (see ESI†), we were able to obtain binding constants from these changes. These are in reasonable agreement with those obtained for the changes in the ground state, Table 1, further supporting the determined anion binding stoichiometries. However, in contrast to these results, the most significant findings from these investigations were observed in the lanthanide emission, which showed striking changes for the

Table 1 Results from the binding constant evaluation of H_2PO_4^- and AcO^- , upon binding to **I**·Tb in CH_3CN ^a

Anion	Technique	Stoichiometry	LogK	Std deviation
H_2PO_4^-	UV-Vis	G : L	7.07 ^b	0.23
		G : L ₂	4.87	0.47 ^c
		G ₂ : L	5.64	0.95 ^c
		G ₂ : L ₂	6.79	0.37
		G ₃ : L	7.94 ^b	0.21
H_2PO_4^-	Fluorescence	G : L	6.86	0.21
		G : L ₂	5.15	0.25 ^c
		G ₂ : L	5.34	0.94 ^c
		G ₂ : L ₂	6.84	0.53 ^c
		G ₃ : L	7.95 ^b	0.20
H_2PO_4^-	Tb(III) emission	G : L	7.04 ^b	0.14
		G : L ₂	4.59	0.24 ^c
		G ₂ : L	4.90	0.82 ^c
		G ₂ : L ₂	7.20	0.18 ^c
		G ₃ : L	8.04 ^b	0.12
AcO^-	UV-Vis	G : L	6.27	0.116
		G ₂ : L	5.84	0.087
AcO^-	Fluorescence	G : L	5.78	0.302
		G ₂ : L	5.11	0.511
AcO^-	Tb(III) emission	G : L	6.87	0.475
		G ₂ : L	5.12	0.497

^a Obtained by fitting the spectroscopic data using SPECFIT.

^b Binding constant is large and consequently SPECFIT has difficulties giving accurate determination for $\log \beta$. ^c Species present in less than 10%.

deactivation of the Tb(III) excited state [$^5\text{D}_4 \rightarrow ^7\text{F}_j$ ($J = 6-3$)] upon titration with H_2PO_4^- and excitation at 280 nm.[‡]

The overall Tb(III) luminescence changes for titrations of H_2PO_4^- are shown in Fig. 2. These results were fully reproducible and clearly demonstrate that the Tb-emission is significantly more sensitive to the anion recognition than seen in either the ground or the singlet excited states. Furthermore, the Tb(III) emission, and hence, the Tb(III) excited state lifetimes (ESI†), are modulated in a two ‘step’ process, where the initial addition of H_2PO_4^- leads to *ca.* 70% quenching in the Tb(III) emission (insert Fig. 2). This is subsequently followed by over *ca.* 90% luminescent enhancement between *ca.* 1 \rightarrow 3 eq. of H_2PO_4^- . This is, to the best of our knowledge, the first time that a lanthanide luminescence is modulated in this manner by an anion.

Moreover, by further analysing the changes in the 546 nm transition vs. the number of eq. of H_2PO_4^- , it was found that the

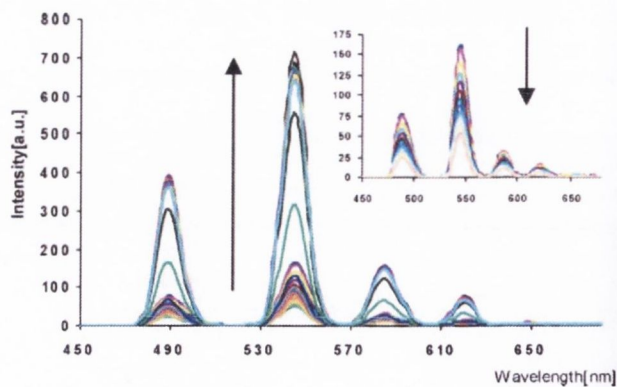


Fig. 2 The Tb(III) emission spectra showing the changes in the intensity of **I**· (4 μ M) upon titration with H_2PO_4^- (0 \rightarrow 57.3 μ M) in MeCN. Inset: The changes observed upon addition of 0 \rightarrow 1 eq. of H_2PO_4^- , which caused quenching in the Tb(III) emission.

Tb(III) emission enhancements also occurred in a two step process; where the major contribution to these changes took place within the 2 → 3 eq. range of H₂PO₄⁻. The changes in the 546 nm transition were fitted using the SPECFIT programme. This gave an excellent fit as shown in the ESI†,‡ from which several binding constants were determined. Again, the results from the fitting of the binding isotherm clearly indicated that 1·Tb senses these anions through multi-step binding interactions and that the binding constants correlate well with that observed from the changes in both the absorption and the fluorescence spectra, Table 1. The speciation distribution diagram obtained from the changes in the Tb(III) emission upon titration with H₂PO₄⁻ is shown in the ESI† and clearly demonstrates that initially the 1 : 1 stoichiometry is formed with a high binding constant of logK = 7.0. However, after the addition of ca. one eq. of anion the G₃ : L₁ binding begins to dominate. Interestingly, the 2 : 1 complex only formed in small quantities. In contrast to these results, the titration of 1·Tb with AcO⁻ only gave rise to luminescent quenching. Furthermore, only two stoichiometries were determined; namely the G₁:L₁ and G₂:L₁, Table 1 (see ESI†). These results also showed that 1·Tb selectively sensed H₂PO₄⁻ over AcO⁻. This was confirmed by titrating H₂PO₄⁻ to a quenched solution of 1·Tb bound AcO⁻. On both occasions, the Tb-emission was 'switched on' in the same manner as seen above for the titration of H₂PO₄⁻ in Fig. 2 (See ESI†).

So what binding interactions constitute to this complex multiple anion recognition? We propose that the initial anion recognition is due to binding of the anion at the urea moiety of the antenna. This is then followed by a second binding event between these anions and the amide bridge, through anion...H-N hydrogen bonding interactions. We have confirmed this by carrying out UV-vis titrations of an acetamide analogue of the receptor/antenna part of 1·Tb, which also gave rise to both G₁:L₁ and G₂:L₁ binding for these anions (cf. 7 in ESI†). However, the binding constants are lower than observed for 1·Tb. In the case of binding of H₂PO₄⁻ to 1·Tb, the third binding interaction, G₃:L₁ is more difficult to determine without the aid of X-ray crystallography. However, this binding, clearly giving rise to the largest changes in the Tb(III) emission, is most likely taking place through a more direct interaction with the metal ion (and possibly *via* contribution from one of the aryl protons.¹⁸ Contribution from simple electrostatic interactions between the complex and the anion cannot be ruled out either). This may be occurring through the displacement of the aforementioned axial metal bound water molecule. Water is an effective quencher of the ⁵D₄ excited state and displacement of the water generally gives rise to luminescence enhancements.^{7,8} These changes are also observed in the ground state, which suggests that the Tb(III) ion also affects the electronic properties of the antenna.

In summary, we have developed a novel lanthanide luminescent sensor for anions by incorporating a hydrogen bonding receptor into a sensitizing antenna. Analysis of the ground state, and the emission from the singlet and the Tb(III) excited states, clearly demonstrated the formation of multiple species and hence multiple binding interactions in solution. It also showed that the Tb(III) is extremely sensitive to the changes in the local coordination environment. Furthermore, the selective detection of H₂PO₄⁻ over AcO⁻ by 1·Tb was also observed, with the H₂PO₄⁻ forming both 1 : 1 and 3 : 1 complexes with 1·Tb, in CH₃CN. These results represent, to the best of our knowledge, the first examples of the

use of a combination of hydrogen bonding anion receptors and f-metal ion coordination for luminescent anion sensing.

We thank Enterprise Ireland, IRCSET and TCD for financial support and Dr John E. O'Brian for running NMR.

Notes and references

† The Eu(III) complex of 1, 1·Eu, was also formed. However, the emission was very weak in comparison to that of 1·Tb, as the Eu(III) excited state is quenched by photoinduced electron transfer (*cf.* ESI†).

§ As these measurements are carried out in less competitive CH₃CN solvent the emission enhancement might even be more striking.

- J. L. Sessler, P. A. Gale and W. S. Cho, *Anion Receptor Chemistry*, Royal Society of Chemistry, Cambridge, UK, 2006.
- T. Gunnlaugsson, M. Glynn, G. M. Tocci (née Hussey), P. E. Kruger and F. M. Pfeffer, *Coord. Chem. Rev.*, 2006, **250**, 3094.
- S. E. Garcia-Garrido, C. Caltagirone, M. E. Light and P. A. Gale, *Chem. Commun.*, 2007, 1450; J. W. Steed, *Chem. Commun.*, 2006, 2637; P. A. Gale and R. Quesada, *Coord. Chem. Rev.*, 2006, **250**, 3219; P. A. Gale, *Chem. Commun.*, 2005, 3761; R. Martínez-Mañez and F. Sanconón, *Chem. Rev.*, 2003, **103**, 4419.
- E. J. O'Neil and B. D. Smith, *Coord. Chem. Rev.*, 2006, **250**, 3068; M. H. Filby and J. W. Steed, *Coord. Chem. Rev.*, 2006, **250**, 3200; S. Goetz and P. E. Kruger, *Dalton Trans.*, 2006, 1277.
- E. Garcia-España, P. Díaz, J. M. Linares and Antonio Bianchi, *Coord. Chem. Rev.*, 2006, **250**, 3004; E. A. Katayev, Y. A. Ustynuk and J. L. Sessler, *Coord. Chem. Rev.*, 2006, **250**, 2952.
- C. Lin, V. Simov and D. G. Drueckhammer, *J. Org. Chem.*, 2007, **72**, 1742; C. M. G. dos Santos, T. McCabe and T. Gunnlaugsson, *Tetrahedron Lett.*, 2007, **48**, 3135; F. M. Pfeffer, M. Seter, N. Lewcenko and N. W. Barnett, *Tetrahedron Lett.*, 2006, **47**, 5251; D. R. Turner, M. J. Paterson and J. W. Steed, *J. Org. Chem.*, 2006, 1598; E. Quinlan, S. E. Matthews and T. Gunnlaugsson, *Tetrahedron Lett.*, 2006, **47**, 9333; K. Bowman-James, *Acc. Chem. Res.*, 2005, **38**, 671; S. J. Brooks, P. A. Gale and M. E. Light, *Chem. Commun.*, 2005, 4696.
- S. Pandya, J. Yu and D. Parker, *Dalton Trans.*, 2006, 2757; S. J. A. Pope, B. P. Burton-Pye, R. Berridge, T. Khan, P. J. Skabara and S. Faulkner, *Dalton Trans.*, 2006, 2907; J. H. Yu and D. Parker, *Eur. J. Org. Chem.*, 2005, 4249; T. Gunnlaugsson, A. Harte, J. P. Leonard and M. Nieuwenhuyzen, *Chem. Commun.*, 2002, 2134.
- S. E. Plush and T. Gunnlaugsson, *Org. Lett.*, 2007, **9**, 1919; J. P. Leonard, C. M. G. dos Santos, S. E. Plush, T. McCabe and T. Gunnlaugsson, *Chem. Commun.*, 2007, 129; A. J. Harte, P. Jensen, S. E. Plush, P. E. Kruger and T. Gunnlaugsson, *Inorg. Chem.*, 2006, **45**, 9465.
- T. Gunnlaugsson, H. D. P. Ali, M. Glynn, P. E. Kruger, G. M. Hussey, F. M. Pfeffer, C. M. G. dos Santos and J. Tierney, *J. Fluoresc.*, 2005, **15**, 287.
- T. Gunnlaugsson, P. E. Kruger, P. Jensen, J. Tierney, H. D. P. Ali and G. M. Hussey, *J. Org. Chem.*, 2005, **70**, 10875; T. Gunnlaugsson, A. P. Davis, G. J. E. O'Brein and M. Glynn, *Org. Biomol. Chem.*, 2005, **3**, 48; T. Gunnlaugsson, A. P. Davis, G. M. Hussey, J. Tierney and M. Glynn, *Org. Biomol. Chem.*, 2004, **2**, 1856; T. Gunnlaugsson, A. P. Davis, J. E. O'Brien and M. Glynn, *Organic Lett.*, 2002, **4**, 2449.
- P. Plitt, D. E. Gross, V. M. Lynch and J. L. Sessler, *Chem.-Eur. J.*, 2007, **13**, 1374; T. Mizuno, W. H. Wei, L. R. Eller and J. L. Sessler, *J. Am. Chem. Soc.*, 2002, **124**, 1134.
- T. Gunnlaugsson and J. P. Leonard, *Chem. Commun.*, 2005, 3114; J. P. Leonard and T. Gunnlaugsson, *J. Fluoresc.*, 2005, **15**, 585.
- D. Parker, R. S. Dickins, H. Puschmann, C. Cosland and J. A. K. Howard, *Chem. Rev.*, 2002, **102**, 1977; D. Parker and J. A. G. Williams, *J. Chem. Soc., Dalton Trans.*, 1996, 316.
- T. Gunnlaugsson and J. P. Leonard, *Dalton Trans.*, 2005, 3204; T. Gunnlaugsson, A. J. Harte, J. P. Leonard and K. Senechal, *Chem. Commun.*, 2004, 782; T. Gunnlaugsson and J. P. Leonard, *Chem. Commun.*, 2003, 2424; T. Gunnlaugsson, A. J. Harte, J. P. Leonard and K. Senechal, *J. Am. Chem. Soc.*, 2003, **125**, 12062.
- T. Gunnlaugsson, J. P. Leonard, S. Mulready and M. Nieuwenhuyzen, *Tetrahedron*, 2004, **60**, 105.
- A. J. Harte and T. Gunnlaugsson, *Tetrahedron Lett.*, 2006, **47**, 6575.
- T. Gunnlaugsson, P. E. Kruger, T. Clive Lee, R. Parkesh, F. M. Pfeffer and G. M. Hussey, *Tetrahedron Lett.*, 2003, **44**, 6575.
- V. S. Bryantsev and B. P. Hay, *J. Am. Chem. Soc.*, 2005, **127**, 8282.